UNIVERSITAT DE BARCELONA

Definition and validation of targets associated with the metabolic reprogramming of haematological malignancies

Miriam Guadalupe Contreras Mostazo

Doktorand:

Miriam Guadalupe Contreras Mostazo

Titel:

Definition and validation of targets associated with the metabolic reprogramming of haematological malignancies

Betreuer:

Prof. Marta Cascante (UB), Dr. Silvia Marín Martínez (UB), Prof. Harald Schwalbe (GUF)

Einleitung und Ziele dieser Arbeit

Krebszellen, einschließlich leukämische Zellen, können auf eine therapeutische Behandlung reagieren, indem sie ihren metabolischen Phänotyp verändern und letztendlich resistent werden, um ihren beschleunigten Proliferationszustand zu erhalten. Dieses Phänomen der Veränderung der zellulären Bioenergetik von Tumoren, und der dadurch verursachten Veränderungen des Zellstoffwechsels und der metabolischen Anpassung ist als "metabolische Reprogrammierung" bekannt und wurde als ein relevantes Kennzeichen von Krebs anerkannt. Dementsprechend gibt es immer mehr Hinweise darauf, dass die metabolische Reprogrammierung einer der Schlüsselmechanismen der Resistenz von Krebszellen ist. Darüber hinaus wurden in den letzten Jahrzehnten mehrere metabolische Studien zur Leukämie und insbesondere zur akuten myeloischen Leukämie (AML) und zur chronisch-myeloischen Leukämie (CML) durchgeführt. Die Forschung zum Verständnis der metabolischen Eigenschaften von AML und CML und die Entdeckung neuer und wirksamer Behandlungsmethoden für Patienten, im Besonderen für AML-Patienten, bleibt jedoch eine Herausforderung für Mediziner. Daher ist das Hauptziel dieser Arbeit die Untersuchung der Anpassungen des Zellstoffwechsels, die im Prozess der Resistenzbildung gegenüber verschiedenen konventionellen therapeutischen Behandlungen bei AML- und CML-Erkrankungen auftreten. Durch die Erforschung dieser neuen metabolischen Anpassungen wollten wir potenzielle metabolische und nicht-metabolische Angriffspunkte aufzeigen, die für eine neuartige Kombination genutzt werden könnten.

Um das Hauptziel dieser Arbeit zu erreichen, wurden die folgenden konkreten Ziele bearbeitet:

1) Charakterisierung des initialen metabolischen Phänotyps von parentalen Zellen bei akuter myeloischer Leukämie (AML).

2) Charakterisierung des metabolischen Profils von parentalen Zellen der akuten myeloischen Leukämie (AML) und von Cytarabin- und Doxorubicin-resistenten Zelllinien.

3) Definition und Validierung von Targets, die mit der metabolischen Reprogrammierung parentaler und resistenter AML-Zelllinien verbunden sind.

4) Generierung einer Imatinib-resistenten CML-Zelllinie KU812 und Charakterisierung des metabolischen Profils von parentalen CML- und Imatinib-resistenten Zellen.

5) Definition und Validierung von Targets, die im Zusammenhang mit der metabolischen Reprogrammierung von Imatinib-resistenten CML-Zellen stehen.

Forschungstätigkeiten

Um das erste konkrete Ziel dieser Arbeit zu erreichen, führten wir eine umfassende metabolische Charakterisierung von parentalen AML-Zellen (THP-1 und HL-60 parental, auch THP-1 und HL-60 P genannt) durch, die uns großzügiger Weise von Prof. Jindrich Cinatl (Institut für Medizinische Virologie, Universitätsklinikum Frankfurt, Goethe-Universität Frankfurt, Deutschland) und Prof. Martin Michaelis (Centre for Molecular Processing and School of Biosciences, University of Kent, Canterbury, UK) zur Verfügung gestellt wurden. Unsere Ergebnisse zeigen ein völlig unterschiedliches metabolisches Profil, mit wichtigen Unterschieden zwischen THP-1- und HL-60 P-Zellen hinsichtlich des Verbrauchs von Metaboliten, die Zellen zur Gewinnung von Energie und Vorläuferelementen für die Zellproliferation verwenden. Diese Ergebnisse machen deutlich, wie wichtig es ist, den anfänglichen Phänotyp der Zellen zu untersuchen, um die metabolischen Veränderungen vorherzusehen, die durch die Resistenzbildung in diesen AML-Zelllinien entstehen können.

Um die zweite Zielsetzung zu verwirklichen, wurde eine umfangreiche metabolische Charakterisierung unter normoxischen und hyperoxischen Inkubationsbedingungen von AML-Zellen und ein anschließender Vergleich der resistenten Zellen mit ihren jeweiligen parentalen Gegenstücken durchgeführt. Die AML-Zellen, die von Prof. Jindrich Cinatl und Prof. Martin Michaelis zur Verfügung gestellt wurden, sind parental oder resistent gegen die konventionellen AML-Chemotherapeutika AraC und Dox.

Für die präzise metabolische Charakterisierung wurden verschiedene experimentelle Ansätze verwendet. Zum einen wurden metabolische Messungen unter normoxischen und hypoxischen

Inkubationsbedingungen mit zwei verschiedenen Methoden durchgeführt: 1) mittels Spektrophotometer, das sogenannte Cobas Mira Plus (Horiba ABX), das in der Lage ist, Stoffwechselraten (z.B. Glukose- und Glutaminverbrauch und Laktatproduktion) aus Zellkulturmedien zu messen, indem die Produktion von NAD(P)H in spezifischen Reaktionen für jeden Metabolit bei einer Wellenlänge von 340 nm ermittelt wird; und 2) mittels des Absolute IDQ p180-Kits von Biocrates, welches eine quantitative Analyse von Aminosäuren, biogenen Aminen, Glycerophospholipiden, Sphingolipiden und Acylcarnitinen unter Verwendung einer Flüssigchromatographie-Tandem-Massenspektrometrie- (LC-MS/MS) und Fließinjektions-Massenspektrometrie-Analyse (FIA- MS/MS) ermöglicht. Zum anderen wurden die extrazelluläre Ansäuerungsrate und die Sauerstoffverbrauchsrate unter Normoxie in parentalen und resistenten AML-Zellen, die zuvor unter normoxischen und hypoxischen Inkubationsbedingungen inkubiert worden waren, mit einem Seahorse XF96 Extracellular Flux Analyser gemessen. Schließlich wurden alle hier durchgeführten metabolischen Assays durch die Untersuchung des Proteinexpressionsprofils mittels SILAC-basierter Protein-Massenspektrometrie-Experimente ergänzt, um Änderungen der Metabolitenkonzentrationen direkt mit Änderungen des enzymatischen Repertoires resistenter AML-Zelllinien korrelieren zu können. Zusammenfassend zeigten die Ergebnisse dieser Multi-OMIC-Studie, dass der Erwerb von AraC-Resistenz die Reprogrammierung des Glukosestoffwechsels von THP-1- und HL-60-AML-Zellen, sowohl unter normoxischen, als auch unter hypoxischen Bedingungen durch Erhöhung des glykolytischen Flusses verursacht, während er nicht mit einer Veränderung der mitochondrialen Atmung assoziiert ist. Darüber hinaus beobachteten wir eine mögliche Fehlfunktion des ETC-Komplex I sowie Veränderungen im Glutamin- und Serin-Glycin-1C-Metabolismus in AML-Zellen, die einen aktiveren mitochondrialen Stoffwechsel aufweisen (z.B. THP-1 AraC Zellen).

Hingegen zeigen die Ergebnisse des Erwerbs der Dox-Resistenz Veränderungen im Glukose- und Aminosäuremetabolismus durch Verringerung des glykolytischen Flusses von THP-1- und HL-60-AML-Zellen und die Verringerung des Aminosäureverbrauchs von HL-60 Zellen unter normoxischen Bedingungen. Darüber hinaus hebt die Multi-OMIC-Studie den Polyamin-Stoffwechsel als eine wichtige metabolische Quelle von THP-1 Dox-Zellen unter hypoxischen Bedingungen hervor. Zudem verringert der Erwerb einer Dox-Resistenz dramatisch die mitochondriale Atmungskapazitäz von AML-Zellen unter normoxischen und hypoxischen Bedingungen, welche einen aktiven mitochondrialen Stoffwechsel besitzen. Allerdings ist die

Mehrzahl der mit dem mitochondrialen Metabolismus assoziierten Proteine signifikant hochreguliert. Daher wurden diese metabolischen Veränderungen im mitochondrialen Stoffwechsel und die metabolischen Veränderungen im Zusammenhang mit dem Polyaminstoffwechsel in dieser Arbeit als potenzielle Schwachstellen hervorgehoben, die für die Behandlung von Dox-Chemotherapeutika resistenten AML-Patienten genutzt werden können.

Um das vierte konkrete Ziel dieser Arbeit zu erreichen, generierten wir zunächst aus parentalen KU812 Zellen eine Imatinib-resistente CML-Zellmodelllinie (hier als KU812 ImaR bezeichnet) durch verlängerte Exposition gegenüber subletalen Dosen von Imatinib. Basierend auf den Ergebnissen der metabolischen Charakterisierung von AML-Zellen und mit dem Ziel, das metabolische Profil der parentalen und Imatinib-resistenten CML-Zellen zu charakterisieren, haben wir den gleichen experimentellen Ansatz (eine Multi-OMIC-Studie) für AML-Zellen verfolgt, diesmal jedoch für das hier untersuchte Modell der parentalen und resistenten CML-Zellen. Es ist erwähnenswert, dass diese metabolische Charakterisierung im Vergleich zur metabolischen Charakterisierung von AML-Zellen eine größere Menge und neueste experimentelle Ansätze einschließt, darunter Enzymaktivitäts-Assays, Glutathion, ROS-Messungen und Messungen der mitochondrialen Atmung durch das hochauflösende Respirometer Oroboros. Die Ergebnisse der CML-Multi-OMIC-Studie zeigten, dass der Erwerb einer Imatinib-Resistenz die Neuprogrammierung des Glukosestoffwechsels durch eine Verbesserung des glykolytischen Flusses, des Pentosephosphatwegs und des Glykogenstoffwechsels bewirkt. Diese Veränderungen heben diese Stoffwechselwege als potenzielle metabolische Schwächen der KU812-ImaR-Zellen hervor. Darüber hinaus zeigten unsere Ergebnisse auch eine hohe metabolische Plastizität der KU812 ImaR-Zellen, was die Orchestrierung vieler mit dem Aminosäurestoffwechsel verbundener Stoffwechselwege einschließt. Schließich zeigten die Ergebnisse der Multi-OMIC-Studie mit KU812 ImaR-Zellen eine erhöhte mitochondriale Atmungskapazität, was den mitochondrialen Stoffwechsel dieser Zellen als eine weitere potenzielle Schwachstelle hervorhebt, die zur Überwindung der Imatinib-Resistenz genutzt werden kann.

Die in dieser Arbeit verwendete Multi-OMIC-Studie, die mit Modellen der parentalen und resistenten AML- und CML-Zellen durchgeführt wurde, ist ein zuverlässiger Ansatz zur Identifizierung potenzieller metabolischer und nicht-metabolischer Targets, die für die Behandlung der AML und CML genutzt werden können. Diese Multi-OMIC-Studie hat es uns

ermöglicht, verschiedene Targets vorzuschlagen und/oder zu validieren, die mit Stoffwechselwegen wie Serin-Glycin-1C, Pentosephosphatweg, Glutaminolyse, Glykogenolyse usw. assoziiert sind, und damit die beiden letzten konkreten Zielsetzungen dieser Arbeit zu erreichen, "die Definition und Validierung von Targets, die mit der metabolischen Reprogrammierung von parentalen und resistenten AML-Zellen einerseits, und von parentalen und resistenten CML-Zelllinien andererseits, assoziiert sind".

Abschließend zielt diese Arbeit auf eine umfassende Charakterisierung der metabolischen Profile von parentalen und resistenten AML- und CML-Zellen ab. Die oben genannten Ergebnisse sind Teil dieses Ansatzes und erlauben die Identifizierung potentieller metabolischer und nicht-metabolischer Targets, die in neuartigen Kombinationsbehandlungen zur Verbesserung der Behandlungseffizienz und zur Überwindung von Behandlungsresistenzen genutzt werden könnten. Die Auswahl von Single-Hit-Hemmungen ermöglicht die Zellüberlebensfähigkeit sowohl der parentalen als auch der resistenten AML- und CML-Zellen zu reduzieren. Wenngleich die Nutzung von Medikamenten zu einem neuen Zweck ein vielversprechendes Feld in der Arzneimittelforschung darstellt, und gleichzeitig ein sehr anspruchsvoller Ansatz ist, wurde die Nutzung des Chemotherapeutikums Dox (ein konventionelles AML-Chemotherapeutikum) zur Bekämpfung der Imatibib-Resistenz in KU812-ImaR-Zellen in dieser Doktorarbeit identifiziert.

Definition and validation of targets associated with the metabolic reprogramming of haematological malignancies

Miriam Guadalupe Contreras Mostazo

Doctoral Thesis

2020

UNIVERSITAT DE BARCELONA

GOETHE UNIVERSITÄT FRANKFURT AM MAIN

Doctoral Program in Biotechnology

Department of Biochemistry and Molecular Biomedicine

Faculty of Biology

Definition and validation of targets associated with the metabolic reprogramming of haematological malignancies

Doctoral Thesis submitted by Miriam Guadalupe Contreras Mostazo to obtain the Ph.D degree from the University of Barcelona and Goethe University of Frankfurt in the frame of dual degree agreement

Prof. Marta Cascante Serratosa
Co-supervisor and tutor

Prof. Harald Schwalbe
Co-supervisor

Prof. Dr. Harald Schwalbe

Dr. Silvia Marín Martínez
Co-supervisor

Miriam Guadalupe Contreras Mostazo
Doctoral student, 2020

To Fran, my family, my best friends Patri and Irene and my "Amanitas muscarias" to support me and tolerate all my "peculiar" moments. Without them, these last years could not have been so fantastic.

My sincere thanks to Prof. Marta Cascante, Prof. Harald Schwalbe, Dr. Silvia Marín, Dr. Roldán Cortés, Dr. Frank Schnütgen and Dr. Nina Kurrle for their support, knowledge, and time to make this Ph.D. possible.

My honest gratitude and appreciation to Dr. Marta Casado, Dr. Hubert Serve, Dr. Bernhard Brüne and Dr. Dominik Fuhrmann for giving me the opportunity to work in their labs and for the great advices.

Special thanks to my lab group "BQI" for the continuous help, laughs and moviemaker skills. Also, thanks to Dr. Irene Reyes, to the people of Frankfurt lab and to all my colleagues of the HaemMetabolome project for the continuous help and the great moments that we have lived together.

Finally, but not less important, I would like to express my gratitude to the people of my new lab group (IBIS, Seville) and to Dr. Jose Antonio Pérez Simón for supporting and motivating me this last year of Ph.D. I could not be happier in this new work atmosphere.

INDEX

INDEX

1. ABBREVIATIONS

1 ABBREVIATIONS

α-KG	α-ketoglutarate
1-C	One-carbon
2-DG	2-deoxyglucose
2-HG	2-hydroxyglutarate
3-PG	3-phosphoglycerate
AA	Antimycin A
ABC	ATP-binding cassette
AC	Acylcarnitine
ALL	Acute lymphoblastic leukaemia
AML	Acute myeloid leukaemia
AP	Accelerated phase
APL	Acute promyelocytic leukaemia
AraC	Cytarabine
AraCDP	AraC diphosphate
AraCMP	AraC monophosphate
AraCTP	AraC triphosphate
BCAA	Branched-chain amino acid
BM	Bone marrow
BP	Blast phase
BPTES	Bis-2-[5-phenylacetamido-1,2,4-thiadiazol-2-yl] ethyl sulfide
CAR	Chimeric antigen receptor
CCCP	Carbonyl cyanide m-chlorophenylhydrazone
CML	Chronic myeloid leukaemia
CP	Chronic phase
CLP	Common lymphoid progenitor
CMP	Common myeloid progenitor
CR	Complete remission
DAB	1,4-dideoxy-1,4-imino-d-arabinitol
dCTP	Deoxycytidine triphosphate
DHEA	Dehydroepiandrosterone
dNTP	Deoxynucleotide triphosphate
DRI	Drug resistant index
Dox	Doxorubicin
EAA	Essential amino acid
ECAR	Extracellular acidification rate
ECM	Extracellular matrix
ELISA	Enzyme-linked immunosorbent assay
ETC	Electron transport chain
F6P	Fructose-6-phosphate
FA	Fatty acid
FACS	Fluorescence-activated cell sorter
FAO	Fatty acid oxidation
FDA	Food and Drug Administration
FBS	Fetal bovine serum
G1P	Glucose-1-phosphate
3-phosphate	
GFP	Green fluorescent protein
GMP	Granulocyte-monocyte progenitor
GO	Gene ontology
Gp	Glycerol-3-phosphate
GSA	Glutamate-γ-semialdehyde
H^+	Proton

HBP pathway	Hexosamine biosynthesis
HIF	Hypoxia-inducible factors
HSC	Hematopoietic stem cell
HSCT transplantation	Hematopoietic stem cell
Hyp	Hypoxia
IC50 concentration	Half maximal inhibitory
ICAT	Isotope-coded affinity tag
IMM	Inner mitochondrial membrane
iTRAQ absolute quantification	isobaric tag for relative and
KO	Knock-out
LC-MS-MS	Liquid chromatography-MS
MALDI-TOF desorption/ionization	Matrix-assisted laser time-of-flight
MDS	Myelodysplastic syndrome
MEPs progenitor	Megakaryocyte-erythroid
MPN	Myeloproliferative neoplasm
MPPs	Multipotent progenitor cells
MS	Mass spectrometry
MTORC rapamycin complex	Mammalian target of
NEAA	Non-essential amino acid
NMR	Nuclear magnetic resonance
Norm	Normoxia
NTC	Non-target control
O_2	Oxygen
OCR	Oxygen consumption rate
OXPHOS	Oxidative phosphorylation
P	Parental
Pyr	Pyruvate
R5P	Ribose-5-phospahte
RCS	Reactive chloride species
Ru5P	Ribulose-5-phosphate
Redox	Reduction-oxidation
ROS	Reactive oxygen species
Rot	Rotenone
RNS	Reactive nitrogen species
RSS	Reactive sulfur species
s-AML leukaemia	secondary-Acute myeloid
SILAC amino acids in cellular culture	Stable isotope labelling with
SSP	Serine synthesis pathway
t-AML leukaemia	Therapy-related acute myeloid
TCA	Tricarboxylic acid cycle
TCGA	The Cancer Genome Atlas
TCPA	The Cancer Protein Atlas
TMT	Tandem mass tags
TKI	Tyrosine kinase inhibitor
UDP	Uridine diphosphate
VEGF factor	Vascular endothelial growth
WBC	White blood cell
WHO	World Health Organization

PROTEIN/ENZYMES ABBREVIATIONS

6-PGD/PGD dehydrogenase	6-phosphogluconate
6-PGL	Phosphogluconolactonase
ACACA	Acetyl-CoA carboxylase alpha
ACAT	Acetyl-CoA-acetyltransferase
ACC	Acetyl-CoA carboxylase
ACLY	ATP-citrate lyase
ACO	Aconitase
ACSS short-chain family member	Acetate acyl-CoA synthetase
ADPGK glucokinase	ADP dependent isoform of
AGP	Alpha-1-acid glycoprotein
APP	Amyloid Beta Precursor Protein
ARG	Arginase
ASCT transporter	Alanine/serine/cysteine
ASL	Argininosuccinate lyase
ASNS	Asparagine synthetase
ASS1	Argininosuccinate synthetase
ATG	Autophagy-related protein
ATP5	ATP synthase
BCAT Transaminase	Branched Chain Amino Acid
BCKD dehydrogenase	Branched-chain keto acid
CA	Carbonic anhydrase
CACT translocase	Carnitine acylcarnitine
CAT	Catalase
CDA	Cytidine deaminase
CDK	Cyclin dependent kinase
COX	Cytochrome oxidase
CPT	Carnitine palmitoiltransferase
CMPK kinase	Cytidine monophosphate
CS	Citrate synthase
CTBP	C-Terminal Binding Protein
CYCS	Cytochrome c
dCK	Deoxycytidine kinase
DHFR	Dihydrofolate reductase
ECHS	Enoyl-CoA hydratase
FASN	Fatty acid synthase
FBP	Fructose 1,6-bisphosphatase
FDFT1	Squalene synthase
FH	Fumarate hydratase
FLT3	Fms related tyrosine kinase 3
G6PDH dehydrogenase	Glucose-6-phosphate
GAPDH dehydrogenase	Glyceraldehyde-3-phosphate
GBE	1,4-alpha-glucan-branching
GCL	Glutamate–cysteine ligase
GDH	Glutamate dehydrogenase
GFPT phosphate aminotransferase	Glutamine-fructose-6-
GK	Glucokinase
GLUD	Glutamate dehydrogenase
GLS	Glutaminase
GLUT	Glucose transporter
GP/PYG	Glycogen phosphorylase
GPD dehydrogenase	Glycerol-3-phosphate
GPx	Glutathione peroxidase

GNPNAT	Glucosamine-6-phosphate N-acetyltransferase
GS	Glycogen synthase
GS	Glutamine synthetase
GSH	Glutathione
GSR	Glutathione reductase
GST	Glutathione S-transferase
GYG	Glycogenin
GYS	Glycogen synthase
HK	Hexokinase
HSF	Heat shock transcription factor
IDH	Isocitrate dehydrogenase
IGF2BP	Insulin-like growth factor-2 mRNA-binding protein
IRS	Insulin receptor
INSR	Insulin receptor precursor
KGDH	α-ketoglutarate dehydrogenase
OAT	Ornithine aminotransferase
OGDH	Oxoglutarate dehydrogenase
P4H	Prolyl 4-hydroxylase
P5CDH	Pyrroline-5-carboxylate dehydrogenase
P5CS	Pyrroline-5-carboxylate synthase
PDC	Pyruvate dehydrogenase complex
PDH	Pyruvate dehydrogenase
PDK	Pyruvate dehydrogenase kinase
PDP	Pyruvate dehydrogenase phosphatase
PDPR	Pyruvate dehydrogenase phosphatase regulatory subunit
PFK	Phosphofructokinase
P-gp	P-glycoprotein
PGM	Phosphoglucomutase
PHGDH	Phosphoglycerate dehydrogenase
PI3K	Phosphatidylinositol 3-kinase
PK	Pyruvate kinase
PKC	Protein kinase C
PKM	Pyruvate kinase muscle isoenzyme
PRODH	Proline dehydrogenase
proT	Proline transporter
PSAT	Phosphoserine aminotransferase
PSPH	Phosphoserine phosphatase
PYCR	Pyrroline-5-carboxylate reductase
LDH	Lactate dehydrogenase
MDH	Malate dehydrogenase
ME	Malic enzyme
MRP	Multidrug-resistance related protein
MTHFD1L	Methylenetetrahydrofolate dehydrogenase 1 like
NDPK	Nucleoside diphosphate kinase
NDUF	NADH:Ubiquinone oxidoreductase
NOS	Nitric oxide synthase
NOX	NADPH oxidase
NQO1	NAD(P)H quinone oxidoreductase

Nrf2	Factor erythroid 2-related factor 2
RRM2	Ribonucleotide reductase regulatory subunit M2
SAMHD	SAM domain and HD domain-containing protein
SUCLG	Succinyl-CoA ligase [GDP-forming] subunit beta
SDH	Succinate dehydrogenase
SFK	Src family kinase
SHMT	Serine hydromethyltransferase
SLC	Solute carrier family
SMO	Spermidine oxidase
SOAT	Sterol O-acyltransferase
SUCLA	Succinyl-CoA synthetase
TALDO	Transaldolase
THBD	Thrombomodulin
TKT	Transketolase
TKTL	Transketolase like
TOMM20	Translocase of outer mitochondrial membrane
Topo/TOP	Topoisomerase II
TYMS	Thymidylate synthetase
UAP	UDP-N- acetylhexosamine pyrophosphorylase

2. INTRODUCTION

2 INTRODUCTION

2.1 Cancer overview

Cancer is a broad term that comprises a collection of diseases in which cellular changes cause the uncontrolled growth and division of abnormal cells. Some cancers result in an abnormal mass of tissue, called solid tumours. However, other cancers (e.g. leukaemia) generally do not form these solid tumours. Cancer is a major public health problem worldwide responsible for an estimated 9.6 million deaths in 2018, hence, 1 in 6 deaths worldwide. In the specific case of leukaemia, the global cancer observatory reported more than 400,000 new cases and 309,006 deaths due to leukaemia in 2018[1].

In the past decades, the understanding of factors that influence the development of cancer has become important. In this line, the influence of the environment, the genetic endowment, and their interactions have been reported to explain the cancer incidence[2]. The World Health Organisation (WHO) established that the transformation of normal cells into tumour cells is the result of the interaction between the genetic conditions and external agents such as physical carcinogens (ultraviolet and ionising radiation), chemical carcinogens (tobacco, food contamination, etc.) and biological carcinogens (infections from virus, bacteria or parasites).

2.2 Haematopoiesis and Leukaemia

Haematopoiesis is a tightly regulated process that gives rise to the different lineages of mature blood cells including lymphocytes, erythrocytes, and monocytes throughout normal life. The origin of the haematopoietic differentiation tree is called the hematopoietic stem cells (HSC)[3,4], which are thus responsible for the regeneration of all the cellular components of the haematopoietic system. In particular, HSCs initiate this differentiation by evolving into multipotent progenitor cells (MPPs) which can further generate common lymphoid or myeloid progenitors (CLPs and CMPs, respectively). Next, CLPs and CMPs differentiate into

mature blood cells (e.g. red blood cells, megakaryocytes, myeloid cell, and lymphocytes) (**Fig. 2.1**). Moreover, HSCs are regulated by protein niche factors such as cytokines, chemokines, extracellular matrix protein; and by non-protein niche factors including high extracellular concentration of calcium ion and low oxygen (O_2) concentration (hypoxia)[5]. Interestingly, Schofield (1978) first proposed the HSC niche as a possible explanation of the the self-renewal capability of HSCs[6]. In mammals, HSCs are retained in the bone marrow (BM) niche, which is known to be a hypoxic organ. In this hypoxic niche of the BM, hypoxia-inducible factors (HIFs), characterised as stress sensor proteins, play important roles in the cells of the HSC niche, including the HSCs.

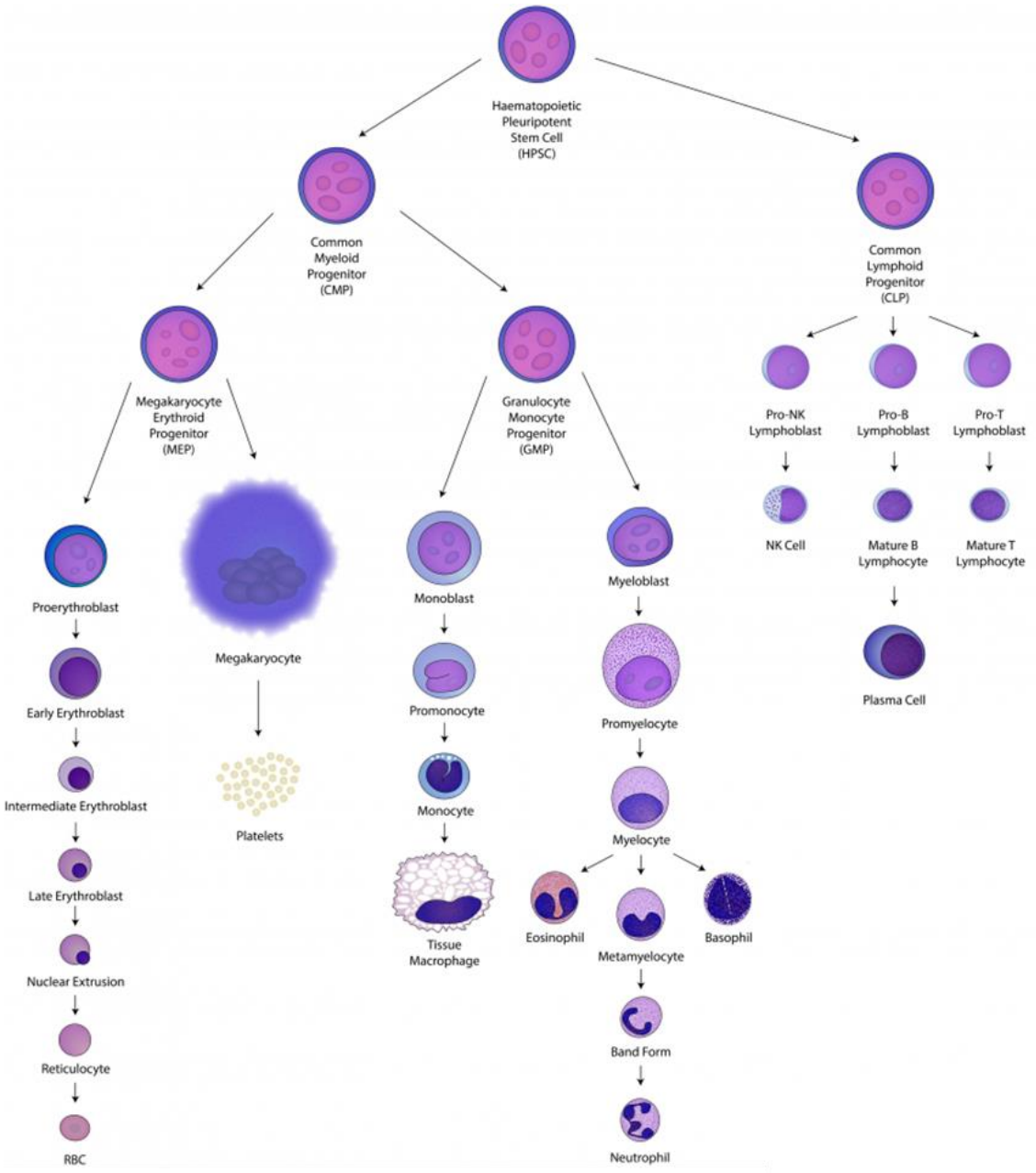

Figure 2.1 Haematopoiesis. "The haematopoietic stem cell (HSC) differentiates into common myeloid progenitor (CMP) or common lymphoid progenitor (CLP) cells. CMPs can generate all mature myeloid cells while granulocyte-monocyte progenitors (GMPs) or megakaryocyte-erythroid progenitors (MEPs) produce only myeloid/monocytic and megakaryocytic/erythroid lineage cells, respectively. B and T lymphocytes and NK cells differentiate from the common lymphoid progenitor (CLP)". Taken from http://learnhaem.com/courses/anaemia/lessons/normal-haematopoiesis/topic/haematopoiesis/.

Abnormalities in this system produce many hematological disorders including leukaemia, which is a malignant clonal proliferation of HSCs in the BM that occurs in children and adults. The diagnosis is confirmed by the examination of the BM and peripheral blood[7] and lymph nodes and spleen.

Leukaemia can be divided into two main groups, myeloid and lymphoid, based on the origin of the cell type affected. Furthermore, each group subdivides into acute or chronic leukaemia depending on how mature the cells are. Therefore, there are four broad subtypes: acute lymphoid, acute myeloid, chronic lymphoid and chronic myeloid leukaemias. In this thesis, only the acute myeloid (AML) and chronic myeloid leukaemia (CML) were specifically addressed.

2.2.1 Acute myeloid leukaemia

2.2.1.1 Definition, epidemiology and risk factors

Acute myeloid leukaemia (AML) is characterised by an aggressive and fast growth of abnormal myeloid blasts in the BM, peripheral blood or extramedullary tissues, leading to BM failure and death. It is a cytogenetically and molecularly[8] very heterogeneous disease. AML is mainly a disease of older adults and the median age of diagnosis is 67 years[9].

Furthermore, the American Cancer Society established in 2018 that the principal risk factors are the age of the patient (higher occurrence in older people), the gender (more common in males than in females), lifestyle-related (e.g. smoking), chemical (e.g. benzene, formaldehyde) and radiation exposure, certain chemotherapeutic treatments, blood-disorder predisposition (e.g. myelodysplastic syndrome [MDS]), and genetic syndromes (e.g. anaemia)[10].

2.2.1.2 Classification and gene mutations

AML can be classified into three distinct categories based on clinical ontogeny: i) *de novo* AML, which arises in the absence of an identified exposure or prodromal stem cell disorder, ii) secondary AML (s-AML), which represents a transformation from previous myelodysplastic syndrome (MDS) or myeloproliferative neoplasm (MPN); and iii) therapy-related AML (t-AML), which develops as a late complication in patients with prior exposure to leukemogenic therapies[11]. In addition, sequencing of AML genomes has been performed in order to study the genetic basis of AML ontogeny. In this regard, many different leukemogenic mutations have been identified. For instance, mutations in proteins necessary for RNA splicing (e.g. serine/arginine-rich splicing factor 2, SRSF2), in proteins necessary for DNA methylation and demethylation (e.g. DNA methyltransferases, DNMTs, or methylcytosine dioxygenase, TET2), in chromatin modification (e.g. polycomb group protein, ASXL1), in genes encoding myeloid transcription factors (e.g. runt-related transcription factor 1, RUNX1 or CCAAT/enhancer-binding protein alpha, CEBPA), or in signal transduction proteins (Fms related tyrosine kinase 3, FLT3)[11,12].

2.2.1.3 Diagnosis

The primary diagnosis of AML depends on the morphological identification of leukemic myeloblasts in preparations of peripheral blood and BM[13]. Thereby, a marrow or blood blast count of ≥20%, including myeloblasts, monoblasts and megakaryoblasts, is a prerequisite for the definitive diagnosis of AML[14]. Moreover, other methodologies including immunophenotyping, cytogenetic, and molecular genetic analysis have been incorporated into the diagnosis criteria. Regarding immunophenotyping, Béné *et al.* published a list of markers (e.g. myeloperoxidase, MPO) helpful for establishing the diagnosis of AML[15]. In addition, the accomplishment of cytogenetic analysis is mandatory in the evaluation of AML. In this case, the WHO category known as “AML with recurrent genetic abnormalities” was described and includes eight balanced translocations and inversions, and their

variants[16]. Furthermore, AML diagnosis should include screening for: a) mutations in NPM1, CEBPA, and RUNX1 genes; b) mutations in FLT3; and c) mutations in TP53 and ASXL1[14].

2.2.1.4 Treatment

Standard treatment

The general approach to AML therapy has not changed substantially in the last decades. It mainly consists of induction of remission and post-remission therapy which contains certain chemotherapies and/or hematopoietic stem cell transplantation (HSCT) [17]. In regard to the induction therapy, for adult patients (<60 years), the "7 + 3" therapy, 7 days standard-dose cytarabine (AraC) and 3 days of anthracycline (e.g. doxorubicin, Dox; or daunorubicin) is recommended[17]. However, this chemotherapy is not used for elderly patients (>60 years). Moreover, in terms of post-remission treatment, high-dose of AraC is recommended for adult patients with favourable prognosis, whereas allogenic HSCT is performed in the first remission for patients with adverse prognosis [17]. For elderly patients with favourable risk, consolidation therapy should contain AraC and anthracycline, while nonmyeloablative HSCT should be considered for patients with unfavourable risk. Indeed, for relapsed or refractory AML population, allogeneic HSCT is the selected treatment [17].

AraC is a pyrimidine nucleoside analogue. As shown in **Fig. 2.2.A**, AraC is transported into cells through a nucleoside transporter, the solute carrier family 29 member 1 (SLC29A1). Next, AraC is phosphorylated to obtain AraC monophosphate (AraCMP) by a deoxycytidine kinase (dCK), and then to AraC diphosphate (AraCDP) by cytidine monophosphate kinase 1 (CMPK1). Finally, AraCDP is converted to AraC triphosphate (AraCTP) by one of several nucleoside diphosphate kinases (NDPKs)[18]. Thereafter, AraCTP competes with deoxycytidine triphosphate (dCTP), causing cell death by interfering with DNA synthesis. In fact, AraC is known for its cell-phase-specific cytotoxicity, primarily in the S phase during the DNA synthesis process. However, AraC can occasionally block the progression of cells from G1 phase to the S phase and it can also inhibit DNA polymerases.

Dox, an anthracycline given as the second drug in standard therapy in addition to AraC, is one of the most important anti-cancer chemotherapy drugs used for the treatment of solid tumours and acute leukaemias[19,20]. Dox enters into the cells through the plasmatic membrane or via the solute carrier family 22 member 16 (SLC22A16)[20] (**Fig. 2.2.B**). Despite the extensive usage for treatment, the molecular mechanisms by which Dox causes cell death are still unclear. A number of mechanisms have been described in the last decades: i) topoisomerase II poisoning, ii) DNA adduct formation, iii) oxidative stress, and iv) ceramide overproduction[21–24] (**Fig. 2.2.B**). Intercalation of doxorubicin into DNA causing torsional stress and nucleosome destabilisation have been proposed as the basic mechanism of anthracycline, and specifically Dox, causing cell death[21]. However, the oxidative stress mechanism and, more specifically, the role of Dox reduction-oxidation (redox) biology in the cancer cell death has been also recognised[25]. As depicted in **Fig. 2.2.B**, both the cytochrome P450 enzyme system and the electron transport chain (ETC) complexes carry out the one-electron reduction of dox quinone to dox-semiquinone, leading to NAPDH consumption, redox cycle and generation of superoxide anion radical (i.e. reactive oxygen species [ROS] generation).

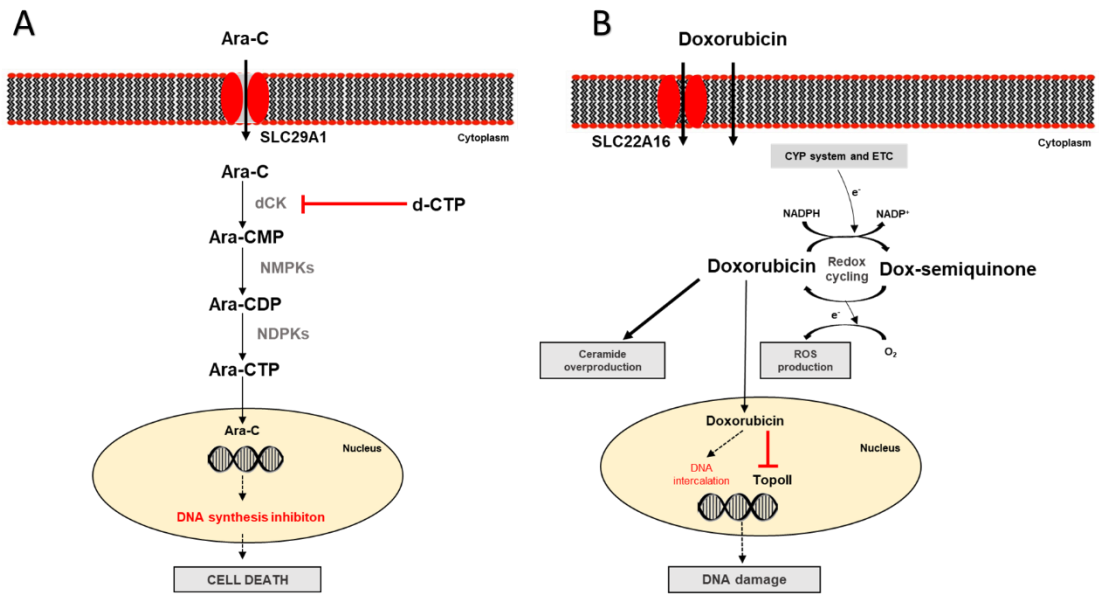

Figure 2.2 Schematic representation of AraC and Dox transport and effects on cancer cells. A) Representation of the mechanism of action of AraC chemotherapeutic drug. AraC chemotherapeutic drug causes cell death by DNA synthesis inhibition. **B)** Representation of the mechanism of action of Dox chemotherapeutic drug. Dox treatment causes cell death either by DNA damage via topoisomerase II (TopoII) inhibition, ROS production, or ceramide overproduction. Abbreviations: Cytarabine, AraC; AraCytidine-5'-monophosphate, AraCMP; AraCytidine-5'-diphosphate, AraCDP; AraCytidine-5'-triphosphate, AraCTP; cytochrome 450, CYP; deoxycytidine kinase, dCK; electron transport chain, ETC; nucleoside analogue; NDPK; nucleoside diphosphate kinase; NMPK; oxygen, O_2; solute carrier family 29 member 1, SLC29A1; and solute carrier family 22 member 16, SLC22A16.

Mechanism of resistance: AraC and Dox chemotherapeutics

Multiple clinical trials have demonstrated complete remission (CR) rates after the administration of the standard treatment (AraC + Dox) of 60-80% in young adults and 40%-60% in older adults (>65 years old). However, most of patients rapidly relapse resulting in treatment failure[14,26–28]. Recent studies have underlined drug resistance as a key to this treatment failure. Tumour drug resistance can be divided into: i) primary drug resistance, defined as the absence of drug response; and ii) acquired resistance, characterised by the loss of the previous drug response which results in drug resistance[29]. Zhang and collaborators reviewed the three main mechanisms of drug resistance in AML[29]: i) drug

resistance-related protein or enzyme, ii) miRNAs alterations, and iii) autophagy. The first mechanism is formed by proteins or enzymes such as P-glycoprotein (P-gp)[30], topoisomerase[31], protein kinase C (PKC), glutathione S-transferase (GST), or multidrug-resistance related protein (MRP1)[32]. Thus, P-gp is an organic ion pump with ATP-dependent drug ejection function[33] and its upregulation has been associated with the drug-resistant variant of AML cell lines[34]. Particularly, it has been shown that PKC could enhance P-gp activity through phosphorylation, thus favouring the acquisition of drug resistance[35]. Additionally, the amplification of topoisomerase 2α (TOP2A) has been determined as a mechanism of Dox resistance[36]. Moreover, GST enzymes, which catalyse the binding of glutathione to chemical drugs[37], has been also found to be related to drug resistance in leukaemia[38,39]. Finally, the inhibition of MRP1, known as a glutathione (GSH) transport pump which mediates the ATP-dependent transmembrane efflux of multiple anticancer drugs as well as other xenobiotics[40], has been demonstrated to reverse drug resistance by decreasing intracellular ATP[41].

miRNAs alterations constituted the second mechanism of drug resistance. miRNAs are a family of small 18-24 bp noncoding double-stranded RNAs, which are able to suppress protein expression and play an important role in drug resistance[42]. miRNAs may also prove to be relevant in AML, but very few studies have been reported to date. However, a downregulation of miRNA-181a has been reported in AraC resistant AML cells[43].

Regarding autophagy (third mechanism of resistance), a process of phagocytosis of the cell's own cytoplasmic proteins and organelles, likewise contributes to the acquisition of AML chemotherapeutics resistance via heat shock transcription factor 1 (HSF1)[44] or the proto-oncogene Met[45]. For instance, HSF1 is known to promote drug resistance in leukaemia by upregulating the expression of an autophagy-related protein named autophagy related 7 (ATG7)[46].

Furthermore, two novel mechanisms of resistance have been described for AraC: overexpression of SAM domain and HD domain-containing protein 1 (SAMHD1) and cytidine deaminase (CDA). SAMHD1 is a deoxynucleotide triphosphate (dNTP) hydrolase responsible

of dNTPs cleavage into deoxyribonucleosides and inorganic triphosphate[47]. Importantly, Schneider *et al.* showed its capacity of reducing AraC cytotoxicity in AML cells by hydrolysing AraCTP, thus resulting in a reduction of AraCTP concentration in leukemic cells[48]. On the other hand, the AraC deactivation function of CDA[49], an enzyme of the pyrimidine salvage pathways, has been also determined and is considered as an AraC resistance factor in AML treated patients[50].

Novel targets

In the last two years, several novel therapies, mainly small molecules and antibodies, emerged and started to be considered for AML treatment[51]. However, exploration of new targets is urgently needed to achieve accurate therapy for AML. Some of the developed treatments are based on FLT3, IDH and nuclear exporter (chromosome region maintenance 1, CRM1) inhibitors (**Table 2.1**); and based on immune therapies. The novel FLT3 inhibitors, G-749 and gilteritinib, acting against both FLT3 ITD and D835 mutations, have been shown to inhibit FLT3 phosphorylation, and thereby increase the ability to overcome midostaurin drug resistance in pre-clinical trials[52–54]. The IDH1 and IDH2 inhibitors (AG-120 and AG-221, respectively) also showed promising response rates in AML patients[55]. Thus, Food and Drug Administration (FDA) has conceded these inhibitors to be utilised as AML treatment. Moreover, CRM1, a major nuclear exporter protein, plays a role in the export and inactivation of several tumour suppressors, such as p53, p73, FOXO1, RB1, and p21[56]. Interestingly, preclinical studies indicate that treatment of AML cell lines, patient samples and AML xenografts with novel CRM1 inhibitors (Selinexor) induces strong anti-leukemic effects [52,56].

Furthermore, immune therapies have changed the therapeutic landscape of AML. Monoclonal antibodies in AML therapy include antibodies against AML surface antigens such as CD33 (e.g. lintuzumab), antibodies conjugated to toxins in various anti-CD33 (gemtuzumab, ozogamicin, SGN33A, IMGN779) and anti-CD123 (SL-401, SGN-CD123A) formulations, and antibodies conjugated to radioactive particles such as 131I or 225Ac-

labeled anti-CD33 or anti-CD45 antibodies[57]. In addition, important progress has been made with adoptive cellular therapies using autologous or allogeneic T cells engineered with synthetic chimeric antigen receptors (CARs) redirected against tumour antigens[58].

Table 2.1 Novel therapies of AML including inhibitors and immune therapies. Treatments based on inhibitors and immune therapies are described. Information obtained from Yang, X. & Wang (2018), and Assi et al. (2018)[17,57]. Abbreviations: FLT3 Fms-like tyrosine kinase 3; and IDH, isocitrate dehydrogenase.

Type of treatment	Target	Drug
Inhibitor	FLT3	Sorafenib Midostaurin Quizartinib Crenolanib Gilteritinib Lestaurtinib G-749
Inhibitor	IDH1	AG-120
Inhibitor	IDH2	AG-221
Inhibitor	CRM1	Selinexor
Immune therapy	CD33	Lintuzumab Gentuzumab ozogamicin SGN-33A IMGN779
Immune therapy	CD38	Daratumumab
Immune therapy	CD123	SL-401 SGN-CD123A
Immune therapy	CART-cells	CD33

2.2.2 Chronic myeloid leukaemia

2.2.2.1 Definition, epidemiology and risk factors

Differently from AML which results in an increase of abnormal myeloid blasts, CML is a malignant clonal disorder of HSCs that leads to an aberrant increase of normal myeloid blast, in addition to an increase of erythroid cells and platelets in peripheral blood[59]. In CML, a translocation between chromosomes 9 and 22, known as Philadelphia (Ph) chromosome, is found in 95% of patients[59] resulting in the formation of BCR-ABL1 fusion gene that disrupts the normal cell regulatory process in the BM. The remaining 5% of patients have diverse translocations involving additional chromosomes but still forming the BCR-ABL1 fusion gene.

Reports from several European CML registries showed an annual incidence of 0.7-1.0 per 100,000 people. Concerning the risk factors, CML is not a hereditary disease and no clear evidence of risk factors are known. However, different studies have manifested that environmental factors, such as radiation, benzene or pesticides, can increase the risk of CML development [60,61].

2.2.2.2 Disease progression and diagnosis

The median age of CML patients diagnosis is 57-60 years [62]. For diagnosis, the most common sign of CML is an abnormal white blood cell count (more than 5% of blasts in the BM), which can be detected by peripheral blood and bone marrow cell analysis.

Regarding disease progression, CML can be classified into three phases: chronic phase

CP), accelerated phase (AP) and blast phase (BP). Common signs and symptoms of CP-CML is anaemia, splenomegaly, fatigue, weight loss, malaise, etc.[63]. CP-CML can evolve to AP-

CML, characterised by an increase in the number of leucocytes or white blood cells (WBCs), a more-pronounced splenomegaly and, occasionally, resistance to treatment[64]. Following AP-CML, or in 20% of patients[63] immediately after CP-CML, CML can progress to BP-CML, characterised by worsening symptoms, bleeding, fever, infections, resistance to therapy and >20% of WBCs in the BM [63,65]. Regarding to the diagnosis, BM aspiration is mandatory for all patients with CML suspicion to confirm the diagnosis, thus providing information that is needed for staging in terms of blast and basophil percentages[63]. Of note, due to the fact that Ph chromosome is present in more than 90% of CML patients, the diagnosis also relies on the detection of this abnormal chromosome, performed by cytogenetic analysis of BM samples.

2.2.2.3 Treatment

Imatinib, the gold standard CML treatment

The treatment of CML has substantially evolved throughout the years. The use of arsenic was first reported as CML therapy[66]. Next, radiotherapy and chemotherapeutic treatment using busulfan and hydroxyurea remained as standard therapy for long time[67,68]. However, due to the inefficiency of these treatments, in 1993 the allogeneic stem cell transplantation became the treatment of choice for CML[69]. Moreover, the discovery of the BCR-ABL1 protein in 1986 enabled the development of a new drug with the ability to inhibit the activity of this oncoprotein[70]. This new drug imatinib was approved by the FDA in 2001 and became the standard CML treatment. Imatinib is today the prime example of a success story in cancer research. Imatinib belongs to the first generation of tyrosine kinase inhibitors (TKIs), and acts via competitive inhibition at the ATP-binding site of the BCR-ABL1 fusion protein, resulting in the inhibition of the tyrosine kinase activity of BCR-ABL1 protein. Subsequently, Hochhaus *et al*. revealed that the overall survival for CML patients treated with imatinib was 95%[71]. However, the best outcomes of imatinib treatment are

determined for patients with CP-CML, because patients with AP-CML or BC-CML poorly respond to imatinib treatment[72].

Mechanism of resistance to Imatinib

The terms of primary and acquired resistance (explained in **Section 2.2.1.4**) can be also applied for imatinib treatment. In particular, it has been determined that primary resistance occurs in approximately 3% of CP-CML patients and acquired resistance in 20% of CP-CML patients [73].

The molecular mechanisms of imatinib resistance development are heterogeneous. At least there are six well-described mechanism of resistance: 1) lower oral bioavailability[74], 2) increase of plasma protein binding[75], 3) overexpression of multidrug resistance genes (e.g. P-gp)[76], 4) BCR-ABL1 point mutations[77,78], and 5) BCR-ABL1 gene amplification[79]. Regarding the first mechanism of resistance, drug efficiency is subject to the gastrointestinal absorption due to the oral administration of imatinib. Moreover, imatinib is known to be 89-96% bound to serum proteins, mainly albumin[80], but also to alpha-1-acid glycoprotein (AGP) [81], a hepatic acute-phase protein, thus interfering with the imatinib therapeutic effect (mechanism 2). As mechanism 3, drug transporters can play a part in resistance to imatinib either by transporting the drug out of the target cell or by releasing the drug out of cells of the gastrointestinal tract[80]. Proteins of the ATP-binding cassette (ABC) transporter family (e.g. P-gp, also called ATP-binding competitor B1 [ABCB1]), which were already mentioned above (**Section 2.2.1.4**), have been shown to be responsible for the loss of drug response in many malignancies. In fact, Mahon *et al*. suggested that overexpression of P-gp as a possible mechanism of imatinib resistance [82], and this has been additionally implicated in the lack of cytogenic response with imatinib[76]. Moreover, mechanism 5 comprises point mutations in the ABL tyrosine kinase site, is considered to be one of the principal causes of acquired resistance. To date, more than 50 mutations have been described. Among them, 15 amino-acid substitutions account for more than 85% of the mutations, and the mutations responsible for 66% of reported cases occur at seven sites (G250, Y253, E255, T315, M351,

F359, and H396) [80]. Finally and confirming mechanism 5, cells with higher expression of BCR-ABL1 showed to be much less sensitive to imatinib[83]. Of note, this mechanism of imatinib resistance was suggested as the most frequent cause of resistance identified in cell lines that were modified to develop resistance[82]. In contrast, in a study of 66 patients with primary or acquired imatinib resistance, only two patients showed BCR-ABL1 genomic amplification[84]. Thus, in practice, imatinib resistance is more likely to be due to point mutations than to BCR-ABL1 overexpression.

Treatment approaches to overcome imatinib resistance

Despite the reported high efficiency of imatinib against Philadelphia chromosome-positive CML, there is an urgent need for additional treatment options for patients who acquired resistance. As a consequence, second-generation TKIs were developed and characterised for their activity against resistant BCR-ABL1 mutations [63].

Several second-generation TKIs have been developed as alternative treatment approaches to inhibit wild-type and mutant forms of BCR-ABL1 (e.g. dasatinib and nilotinib) and have been approved for clinical use in CML patients that are intolerant or resistant to imatinib. Dasatinib is an oral TKI exhibiting a higher in vitro activity than imatinib *in vitro*[85]. Mechanistically, this drug blocks both the activity of BCR-ABL1 and that of the Src family kinases (SFKs)[86]. But in addition, it also inhibits most of the mutated BCR-ABL1 variants, with the exception of the T3151L mutation, and, hence, induces cell death in leukemic cells resistant to imatinib. Due to this success, Dasatinib is therefore nowadays first-line therapy for CP-CML patients[85,87]. Nilotinib, a structurally related drug to imatinib is 20–50-fold more potent against BCR-ABL1 fusions [88] and additionally exhibits high activity against point mutant BCR-ABL1, again with the exception of T3151L mutant. Like dasatinib, nilotinib initially demonstrated the ability to induce hematologic cytogenetic response in patients who failed imatinib treatment[63]. However, no obvious differences in efficacy between dasatinib and nilotinib have been detected[89]. Up to now, CML patients have a wide CML therapeutic armamentarium, including the mentioned above plus other TKIs (bosutinib,

ponatinib), omacetaxine, and several agents (hydroxyurea, interferon-alpha, busulfan, AraC, etc.)[63]. Nevertheless, it is important to continue CML research in order to find new strategies to overcome such drug resistance for CML patients in whom therapy still fails and who show signs of drug resistance.

2.3 Cancer metabolism and tumour metabolic reprogramming

Metabolism is the group of all the chemical reactions occurring in a living organism to maintain life. Two types of metabolic reactions are described: catabolism, which comprises the breakdown of molecules to obtain energy; and anabolism, which is described as the synthesis of all compounds that cells require to grow. Metabolic pathways use available nutrients to generate metabolites that can be further utilised as energy sources for important functions such as cell maintenance, biosynthesis processes or to control redox balance in the cell[90].

The development of cancer depends on genetic alterations that either modify signalling pathways or result in a dysregulation of pathways controlling proliferation processes and metabolism. To explain the tumour's acquired skills during the development of cancer, the commonly known "hallmarks of cancer" were defined. In brief, cancer is characterised by complex phenotypic and molecular changes including uncontrolled and sustained proliferation, which evade growth suppressors, resist cell death, and induce angiogenesis and metastasis [91].

In contrast to normal cells, cancer cells are also characterised by a hypoxic microenvironment, to which they need to adapt. In this line, different studies have demonstrated that cancer cells coordinate and change different metabolic processes such as glycolysis, glutaminolysis, pentose phosphate pathway (PPP), glycogenolysis, mitochondrial biogenesis, lipid synthesis and fatty acid oxidation (FAO) in order to support cellular biogenesis of macromolecules and energy production (reviewed in [92]). These metabolic changes in tumour cells are commonly known as "metabolic reprogramming",

which is also recognised as a cancer hallmark[91]. Furthermore, cancer cells have developed mechanisms that influence these pathways and modify them in order to meet their purposes.

The activation of oncogenes (genes that support cell proliferation and survival) and/or the inactivation of tumour suppressor genes (genes that slow down cell proliferation, promote DNA repair and trigger apoptosis) are examples of the molecular mechanisms developed by cancer cells mentioned above[93]. Oncogenes comprise transcription factors (e.g. c-MYC), growth factors signalling molecules (e.g. EGFR, RAS, PI3K), serine-threonine protein kinases (e.g. Akt and mTOR), and apoptosis inhibitors such as Bcl-2. On the other hand, tumour suppressor genes are classified into three classes of proteins: i) cell cycle and proliferation inhibitors (e.g. RB, p53, and PTEN), ii) apoptosis inducers (e.g. caspase 8 and p53), and iii) proteins that participate in the DNA repair (e.g. MSH2, MSH6, ATM, and ATR).

2.3.1 Glucose metabolism and biosynthetic pathways

2.3.1.1 Glucose uptake, glycolysis, and pyruvate metabolism

Glucose uptake constitutes the first step of glucose metabolism and is regulated and facilitated by glucose transporters (GLUTs). Based on their sequence similarity, there are 14 GLUT proteins classified into 3 classes (Class I, II and III)[94]. However, GLUT1-4 are the four most studied isoforms. Noteworthily, unlike other members of class I, GLUT4 is sequestered in intracellular compartments, and redistributed to the plasma membrane upon insulin response via the insulin signalling pathway [95,96] (**Fig. 2.3**). In addition to glucose, fructose can also be transported into cells and be further utilised in glycolysis by fructose kinase through GLUT5 transporter[97].

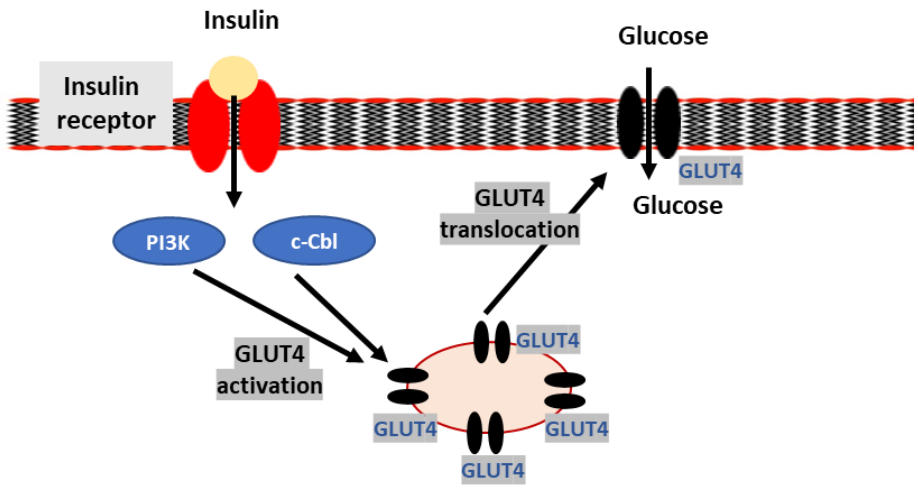

Figure. 2.3 Insulin-regulated GLUT4 translocation. This process occurs through two signaling pathways: one involving the lipid kinase phosphatidylinositol 3-kinase (PI3K) and the other involving proto-oncoprotein c-Cbl. Both pathways take part in GLUT4 translocation from the intracellular GLUT4-containing vesicles to the cell membrane, allowing glucose to enter the cell.

In the context of cancer, the upregulation of GLUT1 transporters has been reported in the majority of cancers [98,99], and correlated with poor cancer prognosis and chemoresistance, for example in AML[100]. Moreover, Chen *et al.* revealed that AML cells can compensate low glucose levels by upregulating the gene for the transporter GLUT5. Indeed, they showed that high expression of GLUT5 is associated with poor AML patient prognosis and that the AraC cytotoxic effect *in vitro* was enhanced upon GLUT5 inhibition[101].

Cancer cells predominantly produce energy through glycolysis. Glycolysis is the first step in the breakdown of glucose and involves nine reactions catalysed by different enzymes (illustrated in **Fig. 2.4**). From these enzymes, there are three rate-limiting enzymes which are known to control glycolytic flux depending on the conditions: hexokinase (HK), phosphofructokinase (PFK), and pyruvate kinase (PK). Normal cells catabolise glucose through glycolysis to pyruvate, which is transported to the mitochondria. There, pyruvate is oxidatively decarboxylated by pyruvate dehydrogenase complex (PDC), releasing CO_2, producing NADH, and converting pyruvate into acetyl-CoA. Thus, constituting the step

between glycolysis and tricarboxylic acid (TCA) cycle. PDC activity is modulated by reversible phosphorylation which is catalysed by pyruvate dehydrogenase kinases (PDKs) and pyruvate dehydrogenase phosphatases (PDPs). Moreover, acetyl-CoA fuels the TCA cycle and the ETC, where oxidative phosphorylation (OXPHOS) occurs and O_2 is the final electron acceptor. On the other hand, cancer cells divergently convert much of the pyruvate into lactate via lactate dehydrogenase (LDH) even in the presence of O_2[102]. This phenomenon is referred as aerobic glycolysis or Warburg effect[103]. Remarkably, several groups have shown an effective prevention of cancer cell proliferation when knocking down LDHA isoform, thus preventing the pyruvate to lactate conversion[98,104].

2.3.1.2 Pentose phosphate pathway

Even tough glycolysis is the central energy-producing pathway, cancer cells also rely on PPP, thus providing an alternative pathway for glucose metabolism. PPP diverts G6P from glycolysis to biosynthesise NADPH, ribose-5-phosphate (R5P) and various glycolytic intermediates[105]. Like glycolysis, this pathway takes place in the cytosol. Moreover, PPP is composed of two branches (illustrated in **Fig. 2.4**): the oxidative branch, which generates NADPH and ribose for subsequent ribonucleotides production, and the nonoxidative branch. The oxidative branch has three irreversible reactions. It starts with the dehydrogenation of G6P to 6-phosphogluconolactone, performed by the enzyme glucose-6-phosphate dehydrogenase (G6PDH). Then, it is hydrolysed by phosphogluconolactonase (6-PGL) into 6-phosphogluconate. In the last reaction 6-phosphogluconate dehydrogenase (6-PGD) catalyses the oxidative decarboxylation of 6-phosphogluconate to ribulose-5-phosphate (Ru5P), which is further converted to R5P serving as a nucleotide precursor or being metabolised via the nonoxidative branch to produce fructose-6-phosphate (F6P) and glyceraldehyde-3-phosphate (G3P) by transketolase (TKT) and transaldolase (TALDO) 1[105,106]. In the oxidative branch, $NADP^+$ acts as electron acceptor, hence, NAPDH is generated. NADPH plays a crucial role in both reductive biosynthesis and in the protection

of cells from ROS, which can cause cell death. The other important molecule, generated in the oxidative and nonoxidative phases, is R5P, which constitutes an important precursor to biomolecules such as DNA, RNA, and ATP.

The role of PPP in cancer cell processes such as proliferation, survival, tumour invasion, angiogenesis, and responses to chemotherapeutics has become of general interestengaging in the recent years. Indeed, overexpression of the main PPP genes has been shown in different cancers types including gastric, colorectal and kidney cancers and leukaemia[107–109]. Of note, Jing *et al.* reviewed that the activity of G6PDH, which is the first rate-limiting enzyme in the PPP, directly reflects the flux of oxidative PPP and determines the flux preference between glycolysis and the PPP[110]. In fact, G6PDH has been suggested as a potential therapeutic target of human cancer due to its role in PPP flux and NADPH production[106] .

On the other hand, TKT and TALDO1 are the two major enzymes of the non-oxidative branch. They are able to determine the direction of metabolite flux in PPP due to the reversible metabolic link between the non-oxidative branch of PPP and glycolysis[105]. Up to now, one TKT and two transketolase-like genes (TKTL1 and TKTL2) have been identified[111]. Several studies demonstrated that specifically TKTL1 is upregulated in many different cancers including gastric[112], colon and urothelial cancer[108] and chronic myeloid leukaemia[113], resulting in an enhanced non-oxidative glucose degradation via the PPP. In contrast, TKT and TKTL2 have not been described to be upregulated in cancer cells[114]. In agreement, our group and others have previously described the role of TKTL1 in major metabolic reprogramming processes of cancer cells[115]. Additionally, it has been recently demonstrated that high TKTL1 induces accumulation of R5P, thus facilitating nucleotide and DNA synthesis as well as cell cycle progression[116]. It is for these reasons that TKTL1 has been suggested as a promising target for new anti-cancer therapies by substrate limitation[108,117] or DNA synthesis inhibition[116].

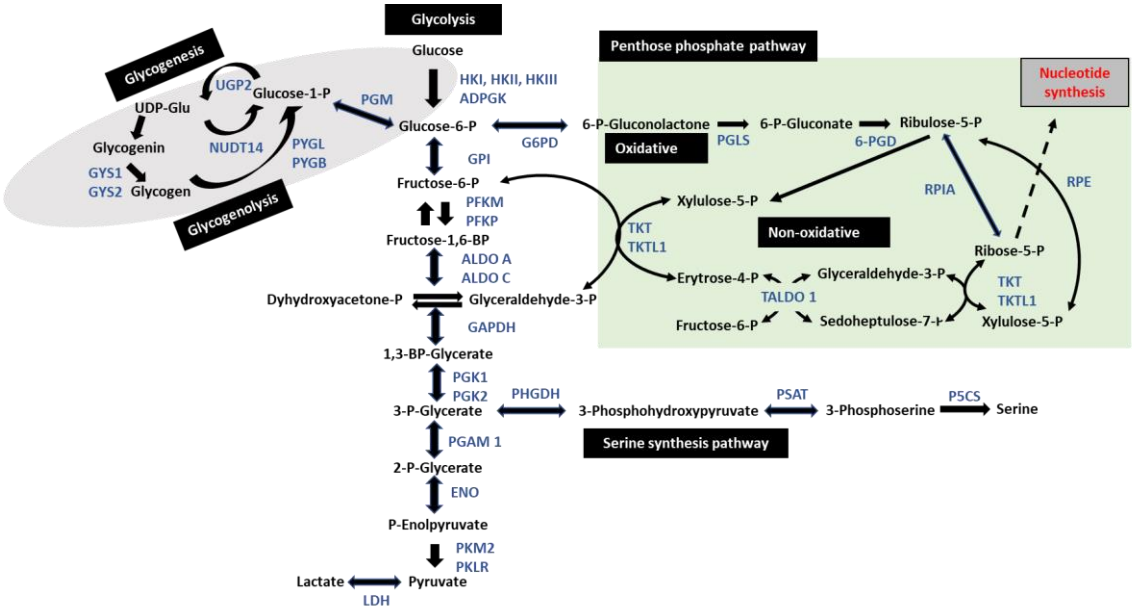

Figure 2.4 Glycolysis pathway, glycogen metabolism, pentose phosphate pathway and serine synthesis pathway. Schematic representations of the metabolites and enzymes involved in these metabolic processes. Abbreviations: HK, hexokinase; G6PD, glucose-6-phosphate dehydrogenase; 6-PGD, phosphogluconate dehydrogenase; TKT, transketolase; PK, pyruvate kinase; LDH, lactate dehydrogenase; GK, glucokinase; PGK, phosphoglycerate kinase; ENO, enolase; PFKM, phosphofructokinase muscle; PFKP, phosphofructokinase platelet; PSPH, phosphoserine phosphatase; ALDO, aldolase; GAPDH, glyceraldehyde-3-phosphate dehydrogenase; PGAM, phosphoglycerate mutase; PK, pyruvate kinase; PYGL, glycogen phosphorylase L; PYGB, glycogen phosphorylase B; PGM,phosphoglucomutase; NUDT14, nudix hydrolase 14; GYS, glycerol synthetase; UGP2, UDP-glucosa pyrophosphorylase 2; PGLS, 6-phosphogluconolactonase ; RPIA, ribose 5-phosphate isomerase A RPE, ribulose-5-phosphate-3-epimerase; TKTL-1, transketolase like 1; and TALDO 1, transaldolase 1.

2.3.1.3 Glycogen metabolism

Glycogen is a cellular energy source and storage for cells. As illustrated in **Fig. 2.4,** glycogen synthesis is performed in the cytosol starting with the phosphorylation of glucose by glucokinase (GK), in the liver, or by hexokinase, in muscle and other tissues, thus obtaining G6P. In the second step, G6P is converted into glucose-1-phosphate (G1P) by the enzyme

phosphoglucomutase (PGM) and further converted into uridine diphosphate (UDP)-glucose by the reaction with uridine triphosphate (UTP), catalysed by G1P uridylyltransferase. Next, UDP-glucose is converted into glycogenin, which is finally elongated by glycogen synthase (GS) to obtain glycogen. On the other hand, glycogen breakdown requires the coordinated activities of glycogen phosphorylase (GP or PYG) and the bifunctional glycogen debranching enzyme. GP takes care of the cleavage of glucose residues from the glycogen chain, producing G1P[118]. Moreover, the rates of glycogen synthesis and breakdown depend on the rates of phosphorylation/dephosphorylation of the key enzymes which are controlled, for instance in liver and muscle cells, by hormones such as glucagon, insulin, and epinephrine[119]. Regarding the regulation of glycogen metabolism, it is mainly regulated by GS and GP, which are the rate-limiting enzymes of glycogen synthesis and degradation, respectively.

Large quantities of glycogen have been described in a variety of cancer entities including breast, kidney, uterus, bladder, ovary, skin and brain cancer[120–123]. In agreement, cancer genomic data has shown that glycogenic synthase (GYS) enzymes 1 and 2, and 1,4-alpha-glucan-branching (GBE1) enzymes are upregulated in 18% of the AML patients with significantly poor survival outcome[124].

Taken all the facts mentioned above and due to the fact that some anti-cancer therapies in clinical trials have shown crucial changes in glycogen metabolism within the tumour (reviewed by Jayaraman[125]), glycogen metabolism has been suggested as a novel and potential therapeutic target for cancer treatment. In this line, several GP inhibitors have been developed targeting either the allosteric site binding AMP (e.g. AVE5688, AVE2865, and AVE9423)[126], the inhibitor sites binding purine nucleotides (e.g. Flavopiridol)[127], or the catalytic sites binding glucose, G1P and inorganic phosphate (e.g. 1,4-dideoxy-1,4-amino-D-arabinitol, DAB)[128].

2.3.2 Amino acid metabolism

Amino acids are crucial for the formation of cellular proteins and serves as intermediate molecules in different metabolic processes such as a lipids and nucleic acid biosynthesis. There are twenty defined amino acids, nine of them (histidine, isoleucine, leucine, lysine, methionine, phenylalanine, threonine, tryptophan, and valine) are known as essential amino acids (EEAs), as they need to be supplied by diet due to the fact that humans cannot synthesise them. The rest of amino acids (alanine, aspartate, asparagine, arginine, cysteine, glutamate, glutamine, glycine, proline, serine, and tyrosine) are called non-essential amino acids (NEAAs), as humans can synthesise them. Furthermore, there are many interconnected pathways of NEAA synthesis[129]. For instance, glutamate can be utilised to generate alanine, aspartate, serine or proline. Aspartate is also used to generate asparagine and to generate arginine via the urea cycle. Serine is another example and it is known to serve as a substrate for the glycine generation by donating methyl groups for one-carbon (1C) metabolism and additionally functions as a substrate for the transsulfuration pathway generating cysteine. Contrarily, tyrosine is the only NEAA which is not directly connected to the other NEAAs, but it is synthesised from the essential amino acid (EAA) phenylalanine.

Regarding cancer metabolism, NEAAs support relevant cell processes including biosynthesis of the TCA cycle and NADPH generation and participate in other metabolic pathways such as the urea cycle and one carbon (1-C) metabolism (summarised in **Fig. 2.5**). Consequently, the interest of targeting NEAA metabolism for cancer therapy has gained importance in the last years and, thus, several NEAA-targeted therapies have been already revealed and use for cancer treatment (reviewed in [130]).

2.3.2.1 Glutamine

Glutamine is a non-essential amino acid, known to be the most studied in the context of cancer metabolism[98,131]. It is the most abundant amino acid in human plasma. However, under rapid proliferation or stress conditions, glutamine can become conditionally essential

(i.e. glutamine needs to be obtained through other pathways such as diet). Glutamine can be uptaken via different amino acid transporters, being ASCT2 (alanine/serine/cysteine transporter 2, coded by the SLC1A5 gene) the most known[132]. Then, glutamine is catabolised through a process called glutaminolysis and it is converted into many important metabolites such as glutamate, citrate, pyruvate, lactate, aspartate, alanine and CO_2[98]. Glutamine plays important biological roles within the cell, due to its ability to provide both carbon and nitrogen for many biosynthetic reactions (**Fig. 2.5**). For example, carbons from glutamine, as α-ketoglutarate (αKG), support the biosynthetic functions of TCA cycle[133], while glutamine derived nitrogens are required for the biosynthesis of molecules such as hexosamines, nucleotides, and other NEAAs[129,134,135]. Furthermore, glutaminolysis is critical for cancer cell proliferation and survival. It has been shown that high concentrations of extracellular glutamine fuel cancer cell growth and survival[136] and that mitochondrial enzymes relevant to glutamine/glutamate oxidation are also elevated in tumour cells[137]**.** Additionally, glutaminolysis also helps to regulate redox balance, mTOR signalling, apoptosis, and autophagy[98]. Due to all these facts, numerous approaches targeting glutamine metabolism in cancer have already been proposed and tested[138,139]. For example, the inhibition of glutamine catabolism by glutaminase (GLS) has gained the major focus of both academic and pharmaceutical cancer metabolism research. GLS can be inhibited by several small molecules, such as bis-2-[5-phenylacetamido-1,2,4-thiadiazol-2-yl] ethyl sulfide (BPTES)[140], CB-839[141], and compound 968[142]. Of note, CB-839 is currently being tested in multiple phase II trials alone or in combination with other drugs (e.g. everolimus and paclitaxel), showing positive clinical responses in renal cell carcinoma and AML[98].

On the other hand, glutamine is produced by glutamine synthetase (GS), an enzyme that catalyses the condensation of glutamate and ammonia in an ATP-dependent manner[143]. Despite that the emphasis on glutamine metabolism in cancer has been focused on glutamine catabolism, glutamine synthesis is also crucial because it serves as an essential component in the synthesis of proteins[144]. However, cells can overcome glutamine deficiency using asparagine for proliferation and protein synthesis. In addition to the synthesis of protein, glutamine synthesis plays an important role in the transport of EAAs,

balancing pH and detoxifying NH_3 and glutamate[145]. Finally, it is worth mentioning that the exposure of hypoxia increases both GS enzymatic activity[146], and GS mRNA and protein levels[147].

2.3.2.2 Glutamate

Glutamate is a nonessential amino acid that can be synthesised through different metabolic pathways. Contrarily to glutamine, glutamate is not an essential amino acid for cancer cells and cannot be found at higher concentrations in human plasma either. In fact, most of the intracellular glutamate is coming from glutamine via GLS[148]. In addition, glutamate can also be synthesised from branched-chain amino acids (BCAAs) and αKG through transferases (Branched Chain Amino Acid Transaminase 1 and 2, BCAT1/2). Regarding glutamate catabolism, glutamate can be converted to αKG via glutamate dehydrogenase (GDH), or via transaminases.

Furthermore, glutamate plays a relevant role in the biosynthesis of proline, ornithine, aspartate, alanine, and serine, which can be further used for the synthesis of cysteine, glycine, asparagine and arginine[129,149], and in the synthesis of glutathione[150] (**Fig. 2.5**). Of note, inhibition of GDH, alone or combined with other treatments, has been shown to inhibit tumour growth in different cancers such as pancreatic and lung cancer[151,152].

2.3.2.3 Aspartate and asparagine

Aspartate metabolism is known for its role in the transfer of electrons between the cytosol and the mitochondria through the malate-aspartate shuttle in rapidly proliferating cells (e.g. cancer cells)[153] . Moreover, the transport of aspartate via the aspartate-glutamate carrier has also been described to support cell proliferation and cell redox homeostasis in low-glutamine environments[154]. Similar to other amino acid inhibitors, aspartate

aminotransferases inhibitors have been suggested as potential cancer therapeutics, whose inhibition can either decrease or inhibit tumour growth[151].

On the other hand, asparagine is required for DNA synthesis in cancer cells. Noteworthy, asparaginase is a good example of a current cancer therapy used against paediatric acute lymphoblastic leukaemia (ALL) that directly targets NEAA metabolism[155]. In this therapy, patients are injected with asparaginase preparations resulting in hydrolysis of serum asparagine into aspartic acid and ammonia.

2.3.2.4 Arginine, ornithine and urea cycle

Arginine, an NEAA, and ornithine, a non-protein amino acid, can be trafficked into cells. Arginine can be further converted into ornithine through arginase (ARG1 and ARG2). Both are intermediate metabolites of the urea cycle, a metabolic pathway that converts the toxic ammonia to urea to be excreted via urine (**Fig. 2.5**). Argininosuccinate synthetase 1 (ASS1), responsible for converting aspartate and citrulline into arginosuccinate, and argininosuccinate lyase (ASL), which catalyses the breakdown of arginosuccinate to arginine and fumarate, are relevant urea cycle genes. A study performed by Rabinovich *et al.* revealed that ASS1 and ASL suppression in tumours shows to be beneficial for tumour growth by increasing the availability of aspartate for nucleotide synthesis[156].

Furthermore, arginine is also the precursor of polyamines, small organic cations which are essential for normal cell growth and development in eukaryotes[157]. A study performed by Nowotarski *et al.* demonstrated that polyamines are essential for the proliferation and differentiation of the blood cells as the metabolites of L-arginine[158]. Interestingly, polyamine catabolism has been associated with carcinogenesis. Specifically, spermidine oxidase (SMO) protein, which is a FAD-dependent enzyme that oxidises spermine to produce spermidine, 3- aminopropanal and H_2O_2, has been determined in colon and lung cancers[159,160]. Of note, an inhibitor of SMO, known as MDL 72,527, was reported to efficiently inhibit SMO in a valid model for colon carcinogenesis[159].

2.3.2.5 Serine, glycine and one-carbon metabolism

Serine is the third most consumed metabolite by cancer cells after glucose and glutamine[161]. Like glutamine, serine can be taken by the transporter ASCT2[132], but it can also synthesised *de novo* through the serine synthesis pathway (SSP) via the glycolytic intermediate 3-phosphoglycerate (3-PG)[129], as illustrated in **figure 2.4**. Moreover, serine can be converted into glycine via the activity of cytosolic or mitochondrial serine hydromethyltransferases (SHMT1 and SHMT2). This conversion provides 1-C units, which are further utilised by the folate and methionine cycles, metabolic pathways known as 1C-metabolism.

Serine itself is an EAA in cancer cells due to its participation in purine biosynthesis, mitochondrial protein translation, lipid biosynthesis, and glycolysis regulation (**Fig. 2.5**). Certain tumours depend on the environmental serine uptake[162], thus the limitation of serine availability in plasma has been categorised as beneficial for patients with serine-sensitive cancers. Regarding the enzymes associated with serine synthesis and cancer metabolism, PHGDH has been shown to increase in multiple cancers[163–165] and, consequently, PHGDH inhibitors such as CBR-5884, NCT-502, NCT-503 and indole amines are currently under preclinical studies[166–168].

Furthermore, 1-C metabolism has been suggested to benefit cancer survival due to its fundamental role in multiple pathways such as nucleotide synthesis[169], NADPH production[170], redox homeostasis[170] and epigenetic modifications[171]. For this reason, methotrexate and 5-FU have been used as antifolate chemotherapeutics targeting 1- C metabolism[172].

2.3.2.6 Proline

Proline is a proteogenic amino acid that can be synthesised i) from glutamate by the enzyme pyrroline-5-carboxylate (P5C) synthase (P5CS, so-called ALDH18A1) and P5C reductase

(PYCR) with P5C as the main intermediate or ii) from ornithine via ornithine aminotransferase (OAT) and PYCR (summarised in **Fig. 2.6**). The breakdown of proline back to glutamate occurs strictly in mitochondria and is catalysed by the mitochondrial enzymes proline dehydrogenase (PRODH) and P5C dehydrogenase (P5CDH, so-called ALDH4A1). This proline-P5C cycle is responsible for the transfer of the reducing equivalents from cytosolic NADPH into the mitochondrial respiratory chain when the reductive step occurs outside mitochondria[173], and it is also involved in other relevant functions such as OXPHOS, pyridine nucleotide levels maintenance, and ROS generation[174].

Besides these functions, proline can be also stored in collagen, the main protein component of the extracellular matrix (ECM), during proline oversupply[175]. Therefore, proline can be further released from collagen degradation upon metabolic stress in order to serve as a source of energy, amino acid synthesis, and redox signalling (**Fig. 2.6**).

Furthermore, enzymes associated with proline metabolism including PYCR and PRODH has been linked to cancer cell metabolism. It has been demonstrated that PYCR enzyme generates excess of $NADP^+$, which is further utilised by the oxidative branch of PPP, thus supporting nucleotide synthesis and, in turn, activating biomass production [176]. In agreement, Cai *et al.* showed that PYCR1 knockdown/knockout impairs cell proliferation in different cancers such as lymphoma and breast cancer[177]. On the other hand, PRODH has been shown to increase and promote metastasis[178] and cell survival under hypoxic conditions[151].

Glutamine	Glutamate	Aspartate	Asparagine	Arginine	Serine	Glycine	Proline
Nucleotide synthesis Hexoamines NEEAs synthesis Redox balance	Glutathione NEEAs synthesis	Nucleotide synthesis NAPDH generation Redox homeostasis Urea cycle	Amino acid exchanges	Nucleotide synthesis inhibition Urea cycle	Nucleotide synthesis 1C-metabolism Lipid biosynthesis	Nucleotide synthesis 1C-metabolism Glutathione	Collagen synthesis OXPHOS enhance ROS generation Nucleotide maintenance

Figure 2.5 Functional roles of amino acids in cancer metabolism. Abbreviations: non-essential amino acids, NEAAs; and reactive oxygen species, ROS.

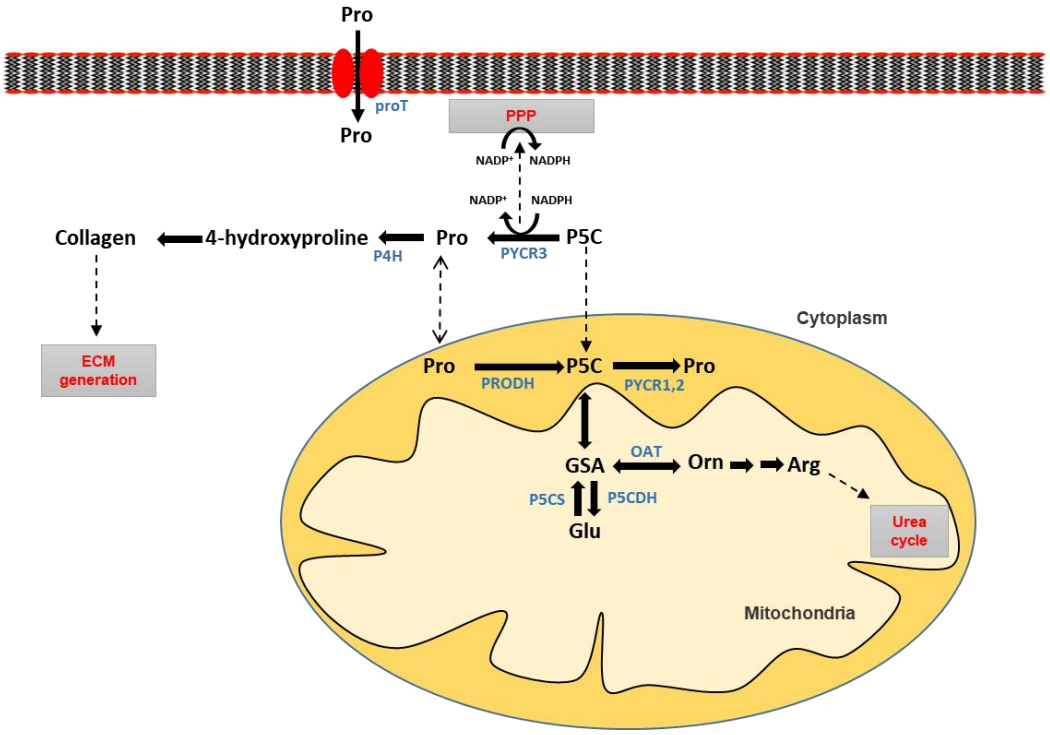

Figure 2.6 Summary of reactions and enzymes involved in proline metabolism. Abbreviations: Arg, arginine; ECM, extracellular matrix; GSA, glutamic semialdehyde; Glu, glutamate; NADP, Nicotinamide adenine dinucleotide phosphate; OAT, ornithine aminotransferase; Orn, ornithine; P4H, prolyl 4-hydroxylase; P5C, delta-1-pyrroline-5-carboxylate; P5CDH, delta-1-pyrroline-5-carboxylate dehydrogenase; P5CS, delta-1-pyrroline-5-carboxylate synthetase; PPP, pentose phosphate pathway; Pro, proline; PRODH, proline dehydrogenase; proT, proline transporter; and PYCR, pyrroline-5-carboxylate reductase.

2.3.3 Mitochondrial metabolism

It is widely accepted that the elevated uptake of glucose and the increase of glycolysis, known as “the Warburg effect”, increase bioenergetics and anabolic growth in cancer cells[180]. Otto Warburg also suggested that cancer cells maintain these elevated glycolytic rates at the expense of primary mitochondrial defects[181]. However, it is now well-known that cancer cells are able to orchestrate the reprogramming of glycolysis and mitochondrial metabolism in order to adapt to the tumour microenvironment, which is characterised by hypoxia, pH changes, and metabolite deprivation, thus conferring a high metabolic plasticity

to cancer cells[182]. Last but not less important, mitochondria also plays a role in tumour anabolism, redox control, calcium homeostasis, transcriptional regulation and cell death[182–185].

2.3.3.1 Tricarboxylic acid cycle and oxidative phosphorylation

TCA cycle is one of the cellular processes of mitochondrial metabolism. In brief, the TCA cycle involves a group of reactions that take place in the mitochondrial matrix and, finally, releases two CO_2 molecules, three NADH, one $FADH_2$ and one GTP. During this process reducing power is stored via NADH, and $FADH_2$ electron carriers and further reoxidised in the ETC to obtain ATP (**Fig. 2.7**). From the biochemical point of view, the TCA cycle has been divided into two stages: i) decarboxylative, in which citrate is converted to succinyl-CoA realising two CO_2 molecules, and ii) reductive, including the successive oxidation of succinate to oxaloacetate[186]. Moreover, the dual compartmentalisation (cytosolic and mitochondrial) of TCA cycle reactions and metabolites allows cells to respond to metabolic changes and sustain anabolic reactions. Another important characteristic of the TCA cycle is the metabolite interconversion. For instance, citrate can be exported to the cytoplasm and cleaved to obtain acetyl-CoA for fatty acid (FA) synthesis; and other TCA metabolites can indeed provide substrates for amino acid synthesis by transamination or gluconeogenesis.

OXPHOS is the mitochondrial metabolic pathway responsible for ATP synthesis via nutrients oxidation. NADH and $FADH_2$ are known as electron donors, which transfers the electrons to the final electron acceptor (O_2). As shown in **Fig. 2.7,** these reactions take place in the ETC. Three of the carriers are cytochromes, and two are small mobile electron carriers. The first large carrier is NADH dehydrogenase (complex I), which receives reducing power NADH and then oxidises it to NAD^+. Complex I transfers its electrons to the small mobile electron carrier known as coenzyme Q or ubiquinone through the NAD dehydrogenase. Next, ubiquinone transfers the electrons to cytochrome c reductase (complex III), which then

passes its electrons to cytochrome c, and subsequently to the cytochrome c oxidase (complex IV). Finally, these electrons are transferred to O_2, which is reduced to water. Additionally, these three big electron carriers pump the protons from the matrix into the intermembrane space, generating an important proton gradient, which is further used by the ATP synthase (complex V) to obtain ATP.

Several studies have shown that mutations or dysregulations of multiple enzymes belonging to the TCA cycle and OXPHOS are correlated with disease transformation and progression (reviewed in [187]). In this line, succinate dehydrogenase (SDH) and fumarate hydratase (FH) inhibitors have been reported even though the development is still in early stages[188,189]. Mutated-IDH2 inhibitors (e.g. AGI-6780, bromodomain-containing protein 4 (BRD4), or AG-221) have been interestingly highlighted as therapeutic agents for AML[190–192].

Regarding OXPHOS metabolism, its role in the understanding of cancer development and cancer drug resistance has gained more interest[193–195]. Several studies have determined OXPHOS upregulation in diverse cancers such as breast cancer[196], AML[197], and pancreatic ductal adenocarcinoma[198]. For instance, OXPHOS inhibitors such as metformin, VLX600, and ME-344 treatment, which are complex I inhibitors, have shown to cause cancer cell death[199–202]. Complex II inhibitors (lonidamine and vitamin E analog α–tocopheryl succinate) have been evaluated as anti-tumour drugs and showed to be therapeutically effective for some cancers[203,204]. Moreover, the antiproliferative effect of arsenic trioxide (a complex IV inhibitor) has been determined in human myeloid leukemia[205], in addition to other cancer such as prostate and ovarian cancers[206,207]. Likewise, OXPHOS downregulation has been also associated with poor clinical outcomes in all cancer types and suggested as a key metabolic signature in melanoma and renal cancer[208].

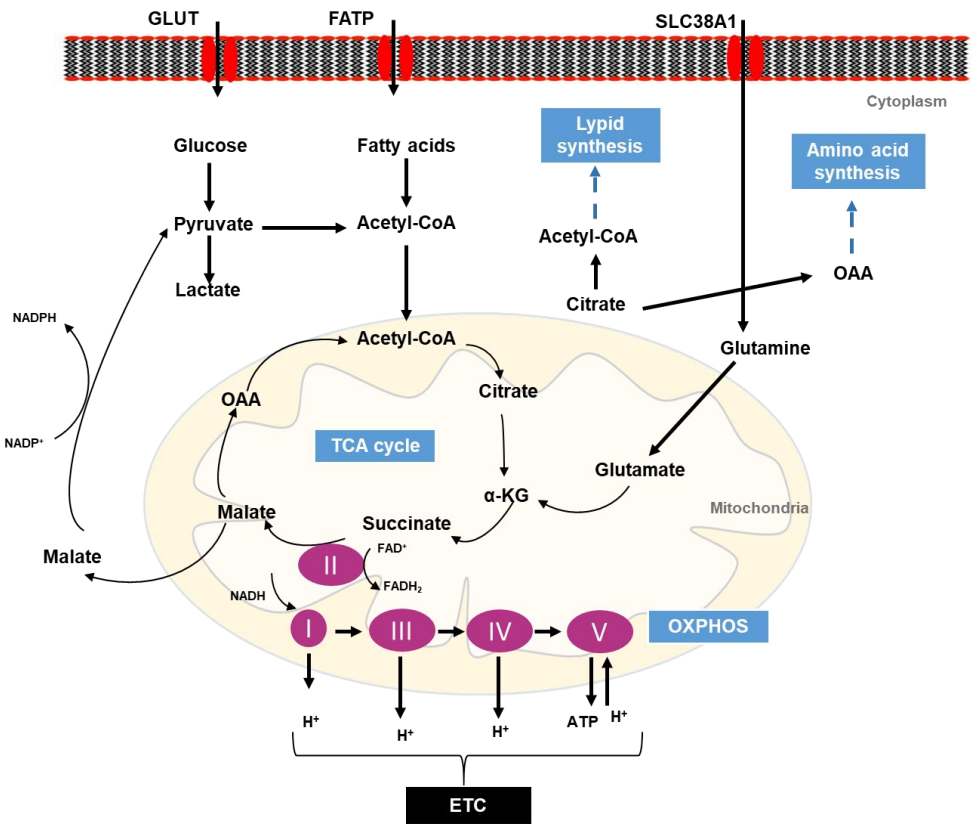

Figure 2.7 Biochemical and biosynthetic reactions driving tricarboxylic acid cycle and oxidative phosphorylation. TCA cycle and OXPHOS reactions and derived biosynthetic pathways are illustrated. Abbreviations: α-ketoglutarate, α-KG; electron transport chain, ETC; fatty acid transporter, FATP; glucose transporter, GLUT; oxaloacetate, OAA; and solute carrier family 38 member 1, SLC38A1.

2.3.3.2 Glycerol-phosphate shuttle

The glycerol-3-phosphate (GP) shuttle is a mechanism that transports electrons to the mitochondrial carrier in the OXPHOS pathway. In this shuttle, dihydroxyacetone phosphate (DHAP) is converted to GP by a cytoplasmic glycerol-3-phosphate dehydrogenase 1 (GPD1 or cGPDH), oxidising one molecule of NADH to NAD^{+}[209]. GP can be converted back to DHAP by a mitochondrial glycerol-3-phosphate dehydrogenase 2 (GPD2 or mGPDH), thus transferring 2 electrons and 2 H^{+} onto FAD, forming $FADH_2$ in the mitochondrial

intermembrane. In the next step, a ubiquinone molecule in the core of the inner membrane collects the two 2 electrons and 2 H^+, thereby reducing ubiquinone to ubiquinol with concurrent oxidation of $FADH_2$ to FAD. Finally, ubiquinol transfers electrons to complex III allowing mitochondria to produce ATP independently of complex I and II activities[210] (**Fig. 2.8**).

There are three main metabolic roles in the GP shuttle: i) the reoxidation of cytosolic NAD in glycolytic cells; ii) the bypassing of complex I during cytosolic NADH oxidation; and iii) the regulation of cytosolic GP as metabolite connecting glycolysis, lipogenesis and OXPHOS[210]. Another important role of the GP shuttle is ROS generation[211,212]. Moreover, a study carried out by Saheki *et al.* highlighted the metabolic role of GPD2 in glycolysis, gluconeogenesis, glycerol, and lipid metabolism[213]; and anti-proliferative effects of GPD2 inhibitors have been accordingly reported on thyroid[214] and pancreatic cancer cells[215].

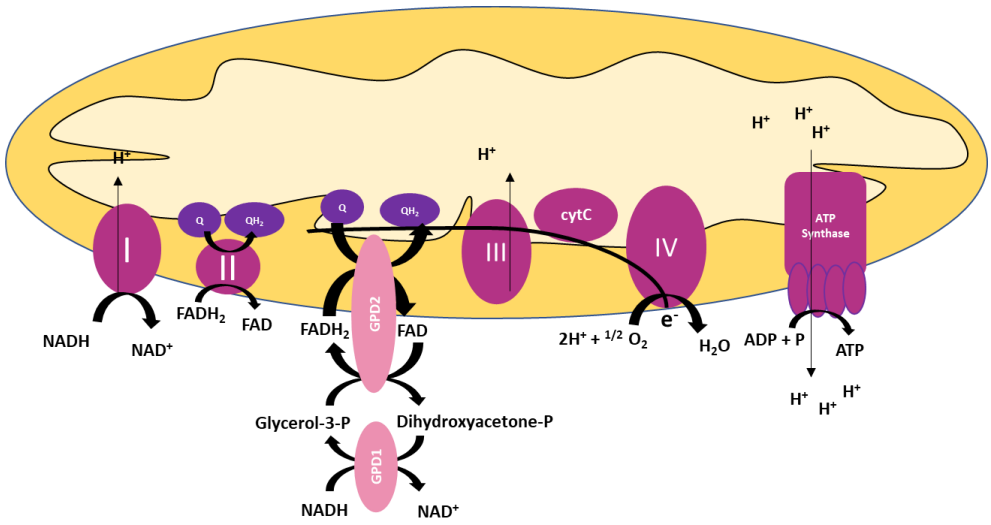

Figure 2.8 Diagram of the oxidative phosphorylation and glycerol-3-phosphate shuttle. Abbreviations: flavin adenine dinucleotide, FAD; Glycerol-3-Phosphate Dehydrogenase 1 and 2, GPD1 and 2; nicotinamide adenine dinucleotide, NAD; and coenzyme Q, Q.

2.3.4 Fatty acid metabolism

Fatty acids (FAs) are essential for cell membrane synthesis and energy storage and production. Cells can increase the amount of FAs by "*de novo* lipogenesis" and decrease it by FAO, lipolysis (increase the released of FAs from storage), and re-esterification (decrease of FAs flux towards storage) (**Fig. 2.9**).

FA synthesis starts with the transport of citrate, which is obtained from the TCA cycle or from glutaminolysis by reductive carboxylation. Then, cytosolic citrate via ATP-citrate lyase (ACLY) or acetate acyl-CoA synthetase short-chain family member 2 (ACSS2) generate cytosolic acetyl-CoA. Acetyl-CoA is further carboxylated by acetyl-CoA carboxylase (ACC), thus generating malonyl-CoA. Ultimately, a series of condensation processes catalysed by fatty acid synthase (FASN) produce palmitate using NAPDH, which is further used for FA elongation, desaturation and lipid synthesis[216] (**Fig. 2.9**).

On the other hand, FAO involves a repeated sequence of four enzyme activities resulting in the release of an acetyl-CoA molecule, one molecule of $FADH_2$ and NADH. The final product, acetyl-CoA, then enters the TCA cycle and is used to generate ATP. There are three components participating in this transporting system: carnitine palmitoiltransferase 1 (CPT1), the carnitine acylcarnitine translocase (CACT) and CPT2[217]. CPT1 is located in the outer mitochondrial membrane and converts acyl-CoA to acyl-carnitine. Then, CACT, which is located in the IMM, shuttles acylcarnitine into the mitochondrial matrix, where CTP2 reconverts acyl-carnitine to acyl-CoA[218]. Once acyl-CoA is inside the mitochondria, FAO takes place. (**Fig. 2.9**).

Regarding the relation between FA metabolism and cancer, a crucial role of FA metabolism for cancer cell survival, proliferation, differentiation, and metastasis has been reported[218,219]. The metabolic reprogramming of cancer cells involves an increased FA metabolism due to their high metabolic demand. To this end, both essential lipogenic enzymes (e.g.FASN, ACLY, and ACC), and FAO enzymes (e.g. CPT1) are upregulated in cancer

cells[216,220]. Of note, CPT1 upregulation has been correlated with poor patient outcomes in AML[221]

Furthermore, FA metabolism is also related to chemoresistance of cancer cells. To this end, both the FASN inhibition by siRNA and the CPT1A inhibition by etomoxir sensitise breast and ovarian resistant cancer cells to cisplatin[222,223], and leukemic cells to AraC[224], respectively.

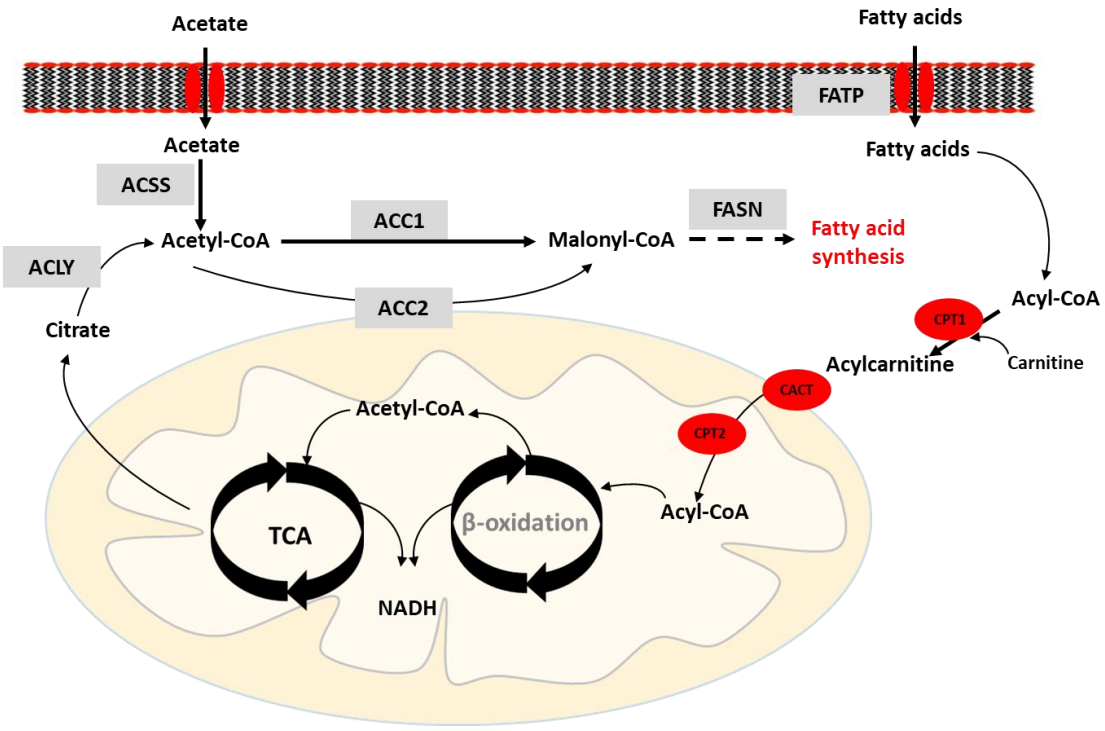

Figure 2.9 Illustration of fatty acid metabolism. Key enzymes involved in fatty acid metabolism. Abbreviations: acetyl-CoA carboxylase, ACC; ATP citrate lyase, ACLY; acyl-CoA synthetase short-chain family member, ACSS; carnitine acylcarnitine translocase, CACT; carnitine/palmitoyl-transferase (CPT), fatty acid synthase, FASN; fatty acid transporter protein, FATP; nicotinamide adenine dinucleotide , NADH; and tricarboxylic acid cycle, TCA.

2.3.5 Maintenance of redox homeostasis: ROS mitigation

Redox balance changes and redox signalling deregulation are common hallmarks of general cancer progression and resistance to treatment. Reactive species are responsible for the

oxidative stress and can be divided into four groups: ROS, reactive nitrogen species (RNS), reactive sulfur species (RSS) and reactive chloride species (RCS). From them, ROS is the most abundantly reactive species produced. Low concentration of ROS promotes cell proliferation and survival, whereas intermediate concentration promotes a momentary or permanent cell cycle arrest and can induce cell differentiation. On the other hand, high concentrations of ROS produce oxidative DNA damage and subsequent occurrence of mutations[225]. Regarding ROS production, cellular enzymes (such as OXPHOS enzymes, NADPH oxidases (NOX), nitric oxide synthases, cyclooxygenases, xanthine oxidase, lipoxygenases and organelles (mitochondria, peroxisomes, endoplasmic reticulum) are the primary sources of ROS in cancer cells (reviewed in [226]). In particular, mitochondria, which consumes approximately 80% of molecular O_2 during OXPHOS, is the one contributing most prominently. Additionally, peroxisomes are also another source of high ROS generation. In this case, superoxide and H_2O_2 are generated by xanthine oxidase.

Excessive ROS production promotes an oxidative imbalance that could harm or kill cancer cells. In consequence, cancer cells develop an immense antioxidant system. They use what is known as the first line of defence against ROS, which includes glutathione peroxidase (GPx), peroxiredoxins, catalases (CATs) and superoxide dismutase enzymes, to transform free radicals into stable and less damaging molecules. Interestingly, decreased levels of SOD, CAT and GPx enzymes have been detected in subtypes of leukaemia including AML and ALL[227]. Moreover, other important mechanisms of oxidative stress protection in cancer cells are related to the nuclear factor erythroid 2-related factor 2 (Nrf2), and glutathione.

2.3.6 Glutathione: The roles in ROS mitigation and xenobiotic detoxification

Glutathione is a crucial antioxidant molecule and a detoxifying agent in cells. It also maintains the thiol status of proteins and plays an important role in cellular proliferation and differentiation. There are two forms of glutathione: reduced form (GSH) and oxidised

form (GSSG). Under normal conditions, reduced GSH is the major form in cells[228]. However, GSH is reduced under oxidative stress due to its contribution to the H_2O_2 detoxification via GPx enzyme, generating GSSG. Then, GSSG can be recycled to GSH by glutathione reductase (GSR). This mechanism is activated in organelles where H_2O_2 detoxification by CATs is absent (e.g. mitochondria) or overloaded[229].

Lately, studies have targeted the role of GPx and GSR in cell survival and chemotherapeutic resistance[230–232]. For instance, the increase of GPx4 level was revealed to promote cancer cell survival and resistance to ferroptosis in drug-tolerant cancer cells[230].

Xenobiotic detoxification is another function of GSH. However, the main responsible for this function is the family of enzymes known as GST, which catalyse the conjugation of GSH to a wide range of substrates (e.g. carcinogens, anticancer drugs, metabolites, etc.) and further secrete the conjugates extracellularly[233] . There are three types of GST described: cytosolic, mitochondrial, and nuclear. As mentioned in **Section 2.2.2.4,** GST proteins catalyse the binding of glutathione to AML drugs, thereby reducing the cytotoxic effect of the chemotherapeutic[37–39]. Indeed, recently developed GST inhibitors have been suggested to overcome therapeutic resistance and it has become a current field of interest[234].

2.3.7 Hypoxia: its influence in cancer and in leukaemia

Hypoxia is defined as the reduced availability of O_2 to cells, tissues or organisms and is known to induce metabolic and proteomic changes[235]. Solid tumours, for instance, are often characterised by hypoxic regions, as a consequence of aberrant vascularisation and a poor blood supply[236]. Moreover, organs such as thymus, kidney, and BM are characterised by a hypoxia of ≤1% of O_2 partial pressure due to their atypical blood vessel networks[237].

Hypoxic stress is mainly regulated by HIFs. The HIF family of transcription factors includes HIF1, HIF2, and HIF3 and all contain an oxygen-sensitive HIF-α subunit, which dimerises with the constitutively expressed HIF1-β subunit[238,239]. Of the three isoforms, HIF-1 is the most

studied and is frequently overexpressed in tumour cells[240]. Under normoxic conditions, HIF-α subunits have a very short half-life due to its rapid degradation. However, HIF-α is stabilised under hypoxia. Moreover, HIF regulates transcriptional responses in normal and cancer cells[239]. This regulation is mediated by transcriptional activity of HIFs, secretion of signalling molecules, and metabolic rewiring from oxygen-dependent catabolism to glycolysis. Indeed, over 100 genes implicated in numerous cell functions (angiogenesis, erythropoiesis, cell growth and proliferation, invasion/metastasis and metabolic adaptation) are regulated directly and indirectly by HIF, and some of them showed to increase their expression in tumours compared to normal cells[241,242].

Tumour cells can adapt to conditions such as nutrition deprivation, and hostile microenvironment, which would typically lead to cell death of normal cells. For instance, tumour cells can overcome proliferation limitations due to stressful microenvironment by stimulating the production of new blood vessels via vascular endothelial growth factor (VEGF)[243]. Additionally, the upregulation of genes including VEGF and P-gp by tumour-associated hypoxia has been associated with poor cancer prognosis[244] and chemotherapeutic resistance[245].

Remarkably, hypoxia is of pathophysiologic importance in solid tumours, but it does not seem to be as crucial in haematological malignancies. As mentioned in **Section 2.2,** haematopoiesis occurs in the stem cell niche, which is characterised by reduced partial pressure of O_2 (pO_2) (<1% of O_2). Upon cell differentiation, hematopoietic cells are constantly facing changes in pO_2, ranging from maximum 12% O_2 in arterial blood to 1% or lower in tissues far from vessels as they circulate throughout the human body[246]. Haematological malignancies such as AML and CML are characterised by an intensified blast cell proliferation and it is assumed that this fact is linked with a decrease of O_2 availability by high consumption, thus leading to a hypoxic microenvironment[247]. Despite some studies suggest no role of real hypoxia in AML due to its usual low O_2 within the BM[246,248,249], there are several studies challenging this view. An example is the observations of Jesen *et al.,*

highlighting an increasing level of hypoxia during leukemic progression, similar to the one observed in solid tumour progession[250]. Moreover, overexpression of HIF-1α has been reported in several studies targeting subtypes of leukaemia including AML, Acute promyelocytic leukaemia (APL), ALL and CML[251–253], and has been additionally selected as a marker of cancer poor prognosis and chemotherapy outcome[247,254,255].

2.4 Metabolism in leukaemia

HSCs are responsible for the maintenance of the blood system. Its metabolism is known to be a key player in processes such as proliferation, differentiation or quiescence. Consequently, HSCs are highly dependent on their metabolic flexibility to accomplish these processes and maintain survival in their niche, which is known to be hypoxic[256]. However, this metabolic adaptation is sufficient to fulfilll the low energy demand of HSCs. Another metabolic pathway responsible for the HSCs maintenance is the FAO pathway[257]. Moreover, HIF1-α also stimulates PDK 2 and 4 activities, thus decreasing pyruvate dehydrogenase (PDH) activities in HSCs and preventing pyruvate contribution to TCA cycle and OXPHOS[258]. Nevertheless, recent studies have reported that leukemic cells do not only reprogram the metabolism for cell proliferation but also for the acquisition of drug resistance[194,259–261].

2.4.1 Metabolism of AML cells

AML cells exhibit a high glucose uptake[262] and a high-glycolytic profile, which has been additionally associated with favourable outcomes regarding the diagnosis[263]. For instance, serum samples of AML patients and healthy controls were compared and a different glucose metabolic signature was found, where high levels of metabolites including lactate, 2-oxoglutarate, pyruvate, 2-hydroxyglutarate (2-HG) and GP were negatively associated with survival[264]. AML also exhibit activation of the central cellular signalling complex mammalian target of rapamycin complex 1 (mTORC1), known to promote glycolysis and high-glucose flux through the PPP, contributing to glucose supply[265,266] and emphasising dependence on

PPP for AML cell proliferation and survival. Thus, inhibition of mTORC1 induces a switch towards oxidative metabolism and a glucose-independent survival of AML cells[267]. Moreover, overexpression of G6PD has been demonstrated to correlate with an adverse AML prognosis[267] and, interestingly, *in vitro* and *in vivo* inhibition of G6PD and 6-PDG revealed antileukemic activities and AraC synergies[259,267].

The switch from aerobic glycolysis towards mitochondrial respiration has been suggested to interfere with AML cell growth. In fact, Wang *et al.* showed that deletions of the two glycolytic enzymes pyruvate kinase muscle isoenzyme (PKM)2 and LDHA, inhibit leukaemia initiation and maintenance in AML mice models[268]. However, Škrtić *et al.* revealed that AML cells have higher mitochondrial mass and an increased OCR relative to normal hematopoietic progenitors[269]. Likewise, a less efficiency of ETC complexes, thus increasing ROS production, has been additionally shown in AML compared to normal cells[270]. Therefore, targeting the TCA cycle and OXPHOS could potentially impact AML cell proliferation. Noteworthily, CPI-613, which is known to compromise the mitochondrial function by inhibiting PDH and α-ketoglutarate dehydrogenase (KGDH) enzymes, is an example of a chemotherapeutic approach targeting mitochondrial functioning in AML patients[271].

Furthermore, AML cells are also characterised by alterations in glutamine, arginine and BCAAs metabolism. Glutamine supports redox control by providing glutathione and fuelling the TCA cycle via αKG in AML cells (reviewed in [272]). Interestingly, knockout (KO) or inhibition of GLS by CB-839 inhibitor was determined to reduce OXPHOS, arrest proliferation and induce apoptosis in AML cells[273]. Moreover, the dependence of AML cells on arginine and its lack of ASS1 enzyme is well-known[274]. Regarding to BCAAs, BCAT1 enzyme has been found to be overexpressed in AML cells[275] and, additionally, its inhibition by gabapentin (BCAT1 inhibitor) shows to suppress clonal growth of AML cell lines and primary AML cells[276].

Lipid metabolism constitutes an additional metabolic pathway highly reprogrammed in leukaemia for energy production. Kreitz *et al.* reviewed that FAs are a crucial requirement

for cell growth, therapeutic resistance and apoptosis induction in AML cells[272]. Therefore, AML cells depend on high FAO rates and low FAS activity. In fact, the increase of FAO has been associated with AML poor prognosis and chemotherapeutic resistance[260]. Besides lipid metabolism, diverse studies have pointed to sterol metabolism and the beneficial effect of its inhibition via statins drugs on AML proliferative attenuation[277–279].

2.4.2 Metabolism of CML cells

Targeting metabolism of AML cells for cancer therapy has been the subject of diverse studies; however, much less effort has been made for CML cells. To our knowledge, there is a study comparing $CD34^+$ CML cells and $CD34^+$ normal cells where mitochondrial respiration, glucose oxidation, and anaplerosic reactions were found to be upregulated in $CD34^+$ CML cells when compared to $CD34^+$ normal cells[280,281]. Particularly, $CD34^+$ CML cells also showed to have an increase in mitochondrial content and mitochondrial membrane potential, thus increasing mitochondrial oxidative functions. Moreover, transcriptome data analysis determined an overall gene overexpression associated with OXPHOS and glycolysis processes in $CD34^+$ CML cells[282]. Finally, $CD34^+$ CML cells also enhance the FAO pathway when compared to $CD34^+$ normal cells, similarly to AML cells.

2.4.3 Metabolism of AML and CML resistant cells

Resistance of leukemic cells to chemotherapy drugs is acknowledged to be the main obstacle in AML and CML treatment[29,283]. To date, biomarker predictions by genetic and genomic analyses to identify resistance factors against AML and CML treatments have not been fully established due to the complexity of the information. This problem might be resolved using phenotypic data, such as metabolic profiling[284]. However, it is equally important to understand the metabolic reprogramming by which AML and CML cells become resistant to chemotherapy drugs (e.g. AraC, Dox, and imatinib).

Some of the general metabolic changes of AML cells treated with AraC chemotherapeutic include the decrease of extracellular acidification and oxygen consumption rates (ECAR and OCR, respectively) (i.e. glycolysis and mitochondrial respiration, respectively)[285]. Moreover, Farge *et al.* showed by *in vitro* and *in vivo* experiments that residual AML cells resistant to AraC chemotherapeutic drug (i.e. innately resistant to AraC) additionally increase ROS, mitochondrial mass and activity, and mitochondrial respiration[260]. Interestingly, these cells also showed a high OXPHOS phenotype dependent on an increased TCA cycle activity and FAO, and not on glutamine consumption.

On the other hand, there are no metabolic studies conducted with Dox resistant cells to our knowledge. Nevertheless, Stäubert *et al.* showed that HL-60 cells resistant to daunorubicin, a chemotherapy drug similar to Dox chemotherapeutic drug, are more dependent on glycolysis and FAO, and contrarily less dependent on exogenous glutamine[285].

Regarding the imatinib chemotherapy drug, imatinib exposure leads to alterations in glucose uptake, and in the *de novo* nucleic acid and/or FA synthesis of myeloid leukemic cells[286–288]. Indeed, dose-dependent metabolic changes in the TCA cycle have been additionally revealed. For instance, low doses of imatinib lead to an induction of this cycle, whereas high doses leads to downregulation[289]. As mentioned in **Section 2.2.1.4**, there are several mechanisms of imatinib resistance including BCR-ABL1 overexpression and BCR-ABL1 mutations in CML cells. Consequently, different metabolic changes are defined depending on these mechanisms of resistance. Therefore, BCR-ABL1-overexpressing CML cells resistant to imatinib enhance glycolysis and non-oxidative PPP[117] whereas the accumulation of TCA cycle intermediates, NADH/NAD+ increase, ETC alterations, and low O_2 consumption is determined in BCR-ABL1-mutated CML resistant cells[194]. It is worth mentioning that, to date, there has been less exploration of the metabolic rewiring associated with BCR-ABL1-independent imatinib-resistant CML cells. However, Noe *et al.* showed that TKI resistant CML cells, which are characterised by a positive but not overexpressed or mutated BCR-ABL1 protein, route their metabolism through glycolysis and PPP, and additionally disrupt their mitochondrial metabolism[261].

2.5 Multi-OMIC approach in cancer

In order to investigate the capabilities acquired during the development of cancer, the investigation of the alterations in the cellular machinery at different levels including genome, epigenome, transcriptome, proteome, and metabolome is required. OMIC technologies are characterised by high-throughput interfaces that facilitate the investigation of these cellular alterations, thus allowing the comprehension of biological systems and uncovering the molecular signatures of cancer cells[290]. In addition, while the study of a single type of OMICS can provide great knowledge at a unidirectional level, multi-OMIC study enables a deeper understanding and a more complete picture of the complex link between the cancerous genotype and phenotype. One example of a multi-OMIC approach is the one proposed by Yugi *et al.*, in which transcriptomic, proteomics and metabolomics datasets in addition to the newest datasets such as phosphoproteomics, protein-protein interactions, DNA-protein interactions and allosteric regulation, were included[291].

2.5.1 Proteomics

Proteomics is used to quantify protein abundance in addition to protein modification and interaction. The complexity and dynamic range of the proteome, when compared to the transcriptome, is higher, thus hindering its identification and quantification. Aslam *et al.* reviewed that protein technologies can be divided depending on their applications into: i) protein purification techniques, also called chromatography-based techniques; ii) protein analysis techniques, which comprises protein microarrays, enzyme-linked immunosorbent assay (ELISA), and western blotting; iii) protein characterisation techniques including gel-based approaches and mass spectrometry (MS), iv) protein quantification techniques, which comprise isotope-coded affinity tag (ICAT) labelling, stable isotope labelling with amino acids in cell culture (SILAC), isobaric tag for relative and absolute quantification

(iTRAQ) techniques, and tandem mass tags (TMT); and v) protein structural analysis (e.g. X-ray crystallography and nuclear magnetic resonance [NMR] spectrometry).

Liquid chromatography-MS (LC-MS-MS) or matrix-assisted laser desorption/ionisation time-of-flight (MALDI-TOF) characterisation have revolutionised the field of proteomics and are currently the central mass spectrometry techniques used in proteomics[292]. However, the proteomic field is also moving forward to protein quantification techniques such as SILAC. SILAC is an MS-based approach developed to study regulation of gene expression, cell signalling, and post-translational modifications. In this technique, the proteome of the cells in culture are labelled with "light", "medium" or "heavy" form of amino acids and differentiation is performed via MS[293,294]. Indeed, one advantage of SILAC, when compared to other labelling strategies such as iTRAQ or TMT, is the direct-handle provision to fundamental cellular processes and proteomes[295].

Although proteomics is under continuous development, advance in the understanding of biomedical research such as diagnosis, protein-based biomarkers, and therapeutics has been achieved. The recent development of a new version of The Cancer Protein Atlas (TCPA) called "The Cancer Genome Atlas (TCGA) Pan-cancer Analysis", which provides comprehensive protein-centric analyses that integrate protein expression data and other TCGA data across cancer types, constitutes an example of a valuable resource for cancer research[296].

2.5.2 Metabolomics

Metabolomics quantifies small molecules types such as sugars, lipids, amino acids, nucleotides, and steroids from a myriad of sample types including primary cells, cell lines, tissues, biofluids or entire organisms. Metabolite levels reflect metabolic function, and changes of these levels can be used as disease indicative[297]. In fact, metabolomics is now known to provide biological insights of metabolic pathways and fluxes in diseases[298] and has been suggested to be an effective tool in the discovery of biomarkers for cancer

diagnosis and progression[290]. For instance, the identification of five metabolites (bilirubin, LysoPC(17:0), n-oleoyl threonine, 12- hydroxydodecanoic acid, and tetracosahexaenoic acid) has recently been identified as biomarkers for cervical cancer[299].

Metabolomics, when compared to the other OMIC approaches, present several advantages: i) the cell metabolome is the final downstream product of the genome and is the closest to the functional phenotype of the cell or organism studied; ii) cell metabolome is also closer to the environment and more susceptible to external perturbations, thus contributing with additional and valuable information; and iii) metabolomic studies are less costly than the other OMIC studies[300]. However, there are also challenges regarding metabolite identification such as the enormous diversity regarding the chemical nature and concentration of metabolites. These facts make the identification, quantification, and analysis difficult, thus complicating the reproducibility that must be overcome to improve this OMIC efficiency[290].

Metabolomics can be classified into targeted or non-targeted studies. Targeted studies quantitatively measure a selected group of metabolites for metabolic pathways investigation or for biomarkers validation[301], and require *a priori* knowledge of metabolites of interest and known compounds[302]. On the other hand, non-targeted studies involve profiling of the metabolome, thus achieving global coverage. This approach is commonly used for studies of biomarker discovery[303]. Besides targeted and untargeted metabolomics, tracer-based metabolomics has been widely used. It is considered a special form of targeted metabolomics in which the distribution of ^{13}C from a labelled precursor among various metabolic intermediates is determined, helping to define the redistribution of the isotope tracer among metabolic intermediates[304,305]. Depending on the application and instrumentation, metabolomics can obtain information of small molecules in solid (through solid-state NMR), liquid (through liquid chromatography MS [LC-MS], capillary electrophoresis MS [CE-MS]), or gas phase (e.g. gas chromatography MS [GC-MS]) using spectroscopy (e.g. NMR) and MS (e.g. LC/GC-MS or tandem MS)[306].

To sum up, the utilisation of proteins and metabolites through the different OMIC approaches is essential not only to decode the complex phenotype of biological systems but also to identify targets for therapeutic purposes. For this reason, the OMIC approach followed in our study utilised SILAC analysis, as a proteomic technology, and targeted metabolomics.

3. OBJECTIVES

3 OBJECTIVES

Despite the understanding of the metabolic and molecular etiology of both AML and CML haematological malignancies and the development of novel therapeutic strategies, the effective treatment of patients remains a challenge for clinicians. In fact, one of the main obstacles in the treatment of leukaemia is the resistance of leukemic cells to chemotherapeutics and, consequently, research on the mechanism of drug resistance in leukaemia has been accordingly very active. The phenomenon of changes of tumour cellular bioenergetics, where cells experience cell metabolism alterations and metabolic adaptation, is known as "metabolic reprogramming", and it has been recognised as a relevant cancer hallmark. Over the last decades, several metabolic studies targeting leukaemia and specifically AML and CM have been conducted. Indeed, there is an increasing amount of evidence indicating that metabolic reprogramming is one of the key mechanisms of resistance by cancer cells[307]. Therefore, it is our main objective to investigate the rewiring of cell metabolism occurring in the process of resistance acquisition to different conventional therapeutic treatments in AML and CML diseases. In consequence, by revealing this metabolic rewiring, we plan to highlight potential metabolic and non-metabolic targets that could be exploited in novel combination treatments to improve treatment efficiency and to overcome resistance to treatment.

In order to achieve the main objective of this thesis, the following specific objectives will be assessed:

1. Characterisation of the initial metabolic phenotype of acute myeloid leukaemia (AML) parental cells (**Chapter 1**).
2. Characterisation of the metabolic profile of acute myeloid leukaemia (AML) parental and cytarabine and doxorubicin-resistant cell lines (**Chapter 1**).

3. Definition and validation of targets associated with the metabolic reprogramming of parental and resistant AML cell lines (**Chapter 1**).
4. Generation of an imatinib-resistant KU812 CML cell line (**Chapter 2**) and characterisation of the metabolic profile of CML parental and imatinib-resistant cells (**Chapter 2**).
5. Definition and validation of targets associated with the metabolic reprogramming experienced by imatinib-resistant CML cells (**Chapter 2**).

4. MATERIALS AND METHODS

4 MATERIALS AND METHODS

4.1 Cell culture

AML cell lines (THP-1 and HL-60 parental; cytarabine [AraC] resistant and doxorubicin [Dox] resistant) were generously provided by Prof. Jindrich Cinatl (Institute of Medical Virology, University Hospital Frankfurt, Goethe University Frankfurt, Germany) and Prof. Martin Michaelis (Centre for Molecular Processing and School of Biosciences, University of Kent, Canterbury, UK). The KU812 cell line (CML cell line) was purchased from the American Type Culture Collection (ATCC, Manassas, Virginia, USA). All the cell lines were cultured in RPMI-1640 medium supplemented with 10% fetal bovine serum (FBS), 4mM glutamine and 1% penicillin and streptomycin at 37°C in a humidified incubator with 5% CO2. For hypoxia incubations, cells were kept in a hypoxia chamber so-called SciTive Workstation (Baker Ruskinn, Leeds, UK) at 1% O2 and 5% CO2 during 5 to 7 days. Particularly, AraC and Dox resistant cells were maintained with 8µM of AraC or20pM of Dox, respectively.

4.2 Generation of the imatinib-resistant KU812 cells

To generate imatinib resistant cells, KU812 cells were treated with increasing concentration of imatinib (0.074-1µM). KU812 cells (parental) were also maintained without imatinib at the same passage. Cell viability and proliferation were tested every 24 hours by cell counting using a Scepter TM Handheld Automated Cell Counter (Merck Millipore, Billerica, MA, USA) and the Countess II FL Automated Cell Counter (Thermo Fisher Scientific Inc., Waltham, MA, USA). Furthermore, they were passaged using an increase of 0.017µM imatinib approximately every week. Of note, drug increase was postponed depending on the state of cell viability. When their doubling time in the presence of 1µM imatinib was almost the same as that of the parental cells in the absence of imatinib, cells were considered resistant to imatinib. Acquisition of resistance was also verified every 3 weeks until resistance was obtained. For that, both parental and “imatinib resistant” cells were incubated during 72 hours with the following imatinib concentrations: 0.02, 0.08, 0.2, 0.8, 2, 8, 20, 80 and 200

µM and cell viability was measured using Cell Titer-Glo® Luminescent Cell Viability Assay (Promega, Madison, USA). Imatinib resistant cells (KU812 ImaR) were finally maintained with additional supplementation of 0.2 µM imatinib. Finally, for KU812 imatinib treated cells, KU812 parental cells were treated with the half maximal inhibitory concentration (IC50, 0.08 µM) of imatinib during 72 hours before the experiments were performed.

4.3 Cell characterisation and cell viability assay

To assess the characterisation of the cell, cell size was determined using a Scepter TM Handheld Automated Cell Counter (Merck Millipore, Billerica, MA, USA) at different time periods. In addition, protein content differences between the different cell lines (AML and CML parental and resistant cell lines) were further analysed by i) collecting in Eppendorf tubes different number of cells (from 250.000 cells/ml to $2x10^6$ cells/ml), ii) counting cell number of each Eppendorf, and iii) lysing cells and measuring the total protein content in all the conditions by Bicinchoninic acid (BCA) assay (Thermo Fisher Scientific, Waltham, MA USA).

Cell viability was measured using Cell Titer-Glo® Luminescent Cell Viability Assay. For the cell viability testing after drug incubation, 16000 cells/well were seeded in 96-well plates using 100µl suspension cell volume. Fresh media (100µl) containing the desired concentration of drug, the combination of drugs under study, or vehicle was added, and cells were incubated 72h. For Hoechst stain assay, cells were washed with PBS before adding 100µl of 0.01% SDS per well. Plates were then stored frozen at -20°C. To analyse the samples, plates were thawed at 37°C until fully liquid and 100µL of 4µg/ml HO33342 in stain solution buffer (1M NaCl, 1mM EDTA, 10mM Tris-HCl pH 7.4) added to each well. Tinfoil-covered plates were placed on a shaker and incubated at 37°C for 1h. Fluorescence was quantified on a FLUOstar OPTIMA Microplate Reader (BMG LABTECH GmbH, Ortenberg, Germany) at 355nm excitation and 460nm emission. For Cell Titer-Glo® Luminescent Cell Viability Assay, the same incubation was performed but using 96-well opaque-walled plates and measurements were made according to manufacturer's instructions. Briefly, plates

were removed from the incubator, allowed to equilibrate at room temperature 30 minutes and 100µl of Cell Titer-Glo reagent was added directly to the wells. Content was mixed for 2 minutes on an orbital shaker and plater were allowed to incubate at room temperature for 10 minutes to stabilise the luminescent signal. Luminescence was determined using a Mithras LB 940 reader (Berthold Technologies, DLReady, Germany), which allows the integration of the signals detected in the short-wavelength filter at 485nm and the long-wavelength filter at 530nm. Cell viability was assessed and represented as a percentage of viability relative to untreated control cells. IC50 values were calculated using GraphPad Prism 6 software (La Jolla, CA, USA).

4.4 Cell cycle analysis

Cell cycle analysis was performed after 72h imatinib treatment only using CML cells. 1×10^6 cells of KU812 Parental, treated and resistant cells were collected, centrifuged, resuspended in 0.5ml PBS and added dropwise to 4.5ml 70% (v/v) cold ethanol. Samples were stored at -20°C overnight. Then, cells were centrifuged, washed with PBS and resuspended in PBS containing 0.2mg/ml DNAse free RNAse A (Roche, Basel, Switzerland) and incubated for 1h at 37°C shaking. Prior to analysis, 0.05µg/ml propidium iodide (PI) was added. Fluorescence-activated cell sorter (FACS) analysis was accomplished at 488 nm in an Epics XL flow cytometer (Coulter Corporation, Hialeah, GL, USA). Data of $1x10^6$ cells were collected and analyses using the software FlowJo® Percentage of cells in G1, S and G2 was determined from the calculated area below the respective gates. Experiments were performed in triplicates and independently repeated twice.

4.5 Intracellular glutathione quantification

Total glutathione content was determined by the glutathione reductase enzymatic method. $5x10^6$ cells of KU812 parental and ImaR cells were lysed with 5% 5-sulfosalicylic acid solution, vortexed and disrupted by two freezing/thawing cycles in liquid nitrogen and 37 °C

water bath. For each sample, 50µl of cell lysate were taken for subsequent protein quantification by BCA assay. Cell extracts were incubated at 4°C for 10min and centrifuged at 10,000g for 10min. For glutathione quantification, a working solution containing 15U/ml of glutathione reductase and 40µg/ml of 5,5'-Dithiobis (2-nitrobenzoic acid) was prepared in assay buffer (100mM K_2HPO_4/KH_2PO_4, 1mM EDTA, pH 7.0). Glutathione standards were prepared from a 50mM oxidised glutathione (GSSG) stock solution. The reaction was initiated by mixing 150µl working solution with 10µl cell extract (diluted 1:5 or 1:10) or 10µl GSSG standard (final concentrations from 0 to 12.5µM). Next, 50µl 0.16mg/ml NADPH solution were added to the samples and the absorbance was recorded at 340nm. Total glutathione concentration was normalised for protein content and cell number.

4.6 Intracellular reactive oxygen species (ROS) levels

400.000 KU812 Parental and ImaR cells were seeded in separated 60cm plates and incubated for 72 hours. Next, approximately $1.5x10^6$ cells were collected and washed once with warm PBS. They were further incubated with 5µM 2'-7'-dichlorodihydrofluorescein diacetate (DCFDA, Invitrogen) in PBS supplemented with 4mM glutamine and 10mM glucose. After 5min at 37°C, cells were centrifuged and supernatant was discarded. Next, cells were resuspended 5µM DCFDA + PBS + 4mM glutamine + 10mM glucose + PI (20µg/ml). Finally, the emitted fluorescence was recorded by flow cytometry at 520nm Data for DCF fluorescence intensity using an Epics XL flow cytometer (Coulter Corporation, Hialeah, FL, USA). For negative controls, the same protocol was performed using identical number of cells but without addition of DCFDA and IP. For positive control, the same protocol was followed using identical number of cells but cells were previously incubated with 250µl of 50µM phorbol-12-myristate-13-acetate (PMA) + PBS for 10min at 37°C.

4.7 Measurement of extracellular metabolites

Glucose, lactate, glutamate and glutamine concentrations were determined by spectrophotometry (COBAS Mira Plus, Horiba ABX) from cell culture media by monitoring the production of NAD(P)H in specific reactions for each metabolite at 340nm wavelength [308]. Glucose concentration was measured using hexokinase (HK) and glucose-6-phosphate dehydrogenase (G6PD) coupled enzymatic reactions (ABX Pentra Glucose HK CP, HORIBA ABX, Montpellier, France). Lactate concentration was determined by lactate dehydrogenase (LDH) reaction at 37°C by mixing the media samples with 1.55mg/ml NAD+ and 87.7U/ml LDH (Roche) in 0.2M hydrazine 12mM EDTA buffer (pH 9). Glutamate concentration was assessed by its conversion to α-ketoglutarate through glutamate dehydrogenase (GLDH) reaction in the presence of ADP. This reaction was performed at 37°C by adding media sample to a cuvette containing 2.41mM ADP, 3.9mM NAD and 39U/ml of GLDH in 0.5M glycine/0.5M hydrazine buffer, pH 9. Glutamine was determined by its conversion first to glutamate through glutaminase (GLS) reaction and subsequently quantification of glutamate concentration as described above. GLS reaction was performed by adding media sample to a cuvette containing a mixture consisted of 90mU/ml GLS in 111mM acetate buffer, pH 5. Reaction was carried out for 90min at 37°C in agitation.

In order to calculate the consumption/production rate of each metabolite, media samples at the beginning and at the end of the experiment were taken and frozen for subsequent analysis. At the same time points, cell numbers were determined for normalisation. All biochemical assays were carried out under exponential growth conditions. All results are expressed in micromol or nanomol of metabolite consumed or produced per hour and per million cells. Moreover, ratios between the different metabolites were calculated.

4.8 Metabolites extracellular flux and intracellular content analysis

Samples collection

Media samples were used to measure metabolites consumption and production rates measurements. THP-1 and HL-60 parental, AraC and Dox resistant cells; and KU812 Parental and ImaR cells were incubated with RPMI-1640 medium supplemented with 10% FBS, 4mM glutamine and 1% penicillin and streptomycin for 96 hours and media samples were collected at 0h and at specific incubation time points (**Table 4.1**), depending on the cell line and condition.

Table 4.1. Incubation times for all the AML and CML cell lines

Cell line	Incubation time points	
	Normoxia	Hypoxia
THP-1 Parent	72h	24h
THP-1 AraC	48h	24h
THP-1 Dox	72h	24h
HL-60 Parental	72h	48h
HL-60 AraC	48h	48h
HL-60 Dox	48h	48h
KU812 Parental	96h	72h
KU812 ImaR	48h	48h

For metabolites intracellular concentration measurements, cell pellets were used. All the cell lines were incubated for 24 hours and cell pellets were collected, washed 3 times with ice-cold-PBS and snap-freeses using liquid nitrogen until cell pellet preparation.

Samples processing

Right before measuring, cell pellets were thawed at room temperature and resuspended in 70µl of 85:15 EtOH:PBS solution. Cells were disrupted by two

sonication/freezing/defreezing cycles using titanium probe (VibraCell, Sonics & Materials Inc., Tune: 50, Output: 25), liquid N2 and a 95˚C heat block. Cell lysates were then centrifuged at 20,000rcf for 5 minutes at 4˚C. Supernatants were transferred into new tubes and total protein content was determined by BCA assay. In addition, media samples were defrosted.

The sample preparation and measurements were performed according to the manufacturers' manual of the Biocrates AbsoluteIDQ p180 kit (UM-P180). In detail, internal standards for the LC method were applied to the filter inserts of the 96-well kit plate, which already contained the internal standards (ISTD) for the FIA method. Standards, internal standards, quality controls and media samples (10µl of each) and pellets samples (50µl each) were added onto the filter inserts and dried for 30min under a nitrogen stream. Amino acids and biogenic amines were derivatised for 20min with an excess of 5% phenylisothiocyanate in ethanol/water/pyridine (ratio 1/1/1, v/v/v), and subsequently dried for 45min under a nitrogen stream. Metabolites and internal standards were then extracted with 300µl methanol containing 5mM ammonium acetate by shaking for 30min, and eluted by centrifugation for 5min at room temperature and 500×g. One-half of the eluate was diluted with water (50/50, v/v) for the LC-MS/MS analysis, and the second half of the eluate was diluted with the kits' running solvent (1/3, v/v) for FIA-MS/MS analysis.

4.9 Glycogen content analysis

For the quantification of the glycogen content, $10x10^6$ millions of KU812 Parental and ImaR cells were collected, centrifuged and washed twice with ice-cold PBS. 400µl of 0.1M NaOH was added and samples were heated to 100°C for 15min for protein denaturation. Samples were sonicated for 5 min 2x3X using a titanium probe (VibraCell, Sonics & Materials Inc., Tune: 50, Output: 30). The pH of the samples was adjusted to pH 6-7 and afterwards 5µl of [U-^{13}C-D7]-glucose was added as an internal standard for all of them. Then 200µl of 1,25mg/ml α–amyloglucosidase in 0.4M acetate buffer was added to digest the glycogen and incubated overnight at 37°C under agitation. Both the glucose released from glycogen

and the glucose internal standard were isolated using Dowex 1x8/Dowex-50WX8 ion-exchange columns, eluting with water. The eluted samples were then dried overnight under airflow. After drying, the glucose was derivatised (explained below). The GC/MS analysis was carried out under chemical ionisation. Ions were monitored by SIM recording the ion abundance for C1-C6 glucose in the range of 327-334m/z and of [U-^{13}C-D7]-glucose in the range of 339-345m/z.

Sample derivatisation

Isolated metabolites were derivatised by first heating to 100°C with 2% (v/v) hydroxylamine hydrochloride in pyridine for 30min and then with acetic anhydride for 60min. Next, samples were evaporated under N_2 gas flow and the final derivative was dissolved with ethyl acetate.

Calibration curve

For calibration curve of the glycogen quantification, the same quantity of the internal standard [U-^{13}C-D7]-glucose used for the samples was added to varying quantities of ^{12}C-glucose. The calibration solutions were derivatised as explained above. Estimation of glycogen content was performed using the calibration curve and data was normalised by cell number.

4.10 Nuclear magnetic resonance (NMR) analysis

Samples preparation

30x10^6 millions of KU812 Parental and ImaR cells were plated 24 hours before the experiment in glucose/glutamine-free media and supplemented with 11mM uniformly 13C-labelled glucose for the glucose tracers or 2mM uniformly 13C-labelled glutamine for the glutamine tracers. Cells were harvested, washed with 37°C phosphate buffer saline (PBS) and spun down for 20 seconds at 16000g. PBS was removed, and cells were vortexed for 10 seconds after adding 400µl pre-chilled methanol. 325µl dH2O and 400 µl pre-chilled

chloroform were added to each sample and vortexed for 40 seconds. Cells were placed on ice for 10 minutes and then centrifuged at 5000g for 10min at 4°C in a swingout rotor. 500µl were taken from the upper (polar) layer and then dried using a vacuum dryer for 4h.

NMR measurements

190µl of NMR buffer (100mM phosphate, 100% D2O and 0.5mM TMSP (reference compound), pH 7) was added to each sample (dried cell extracts) and then sonicated for 10min. 190µl of each sample was loaded in the NMR tubes (3mm tubes, Norell, HT version or the new 96-tubes racks). Samples were measured on a 600MHz DRX HD Bruker spectrometer at 25°C, TD: 32K, 512 scans using (zgesgp) pulse program for the 1D measurements. 2D experiments were measured using (hsqcetgpsp.2.cl) pulse program, 298K, TD (1024, 4096) with 14% NUS and 64 scans.

Data analysis and normalisation

Metabolites identification was performed using Chenomx software. Quantification and label incorporation analysis was performed in 'NMRLab'[309]. Metabolites intensities were normalised to TMSP peak and to million cells. Statistics was performed in GraphPad Prism 6 software using Welch's t-test or Student's t-test.

4.11 Enzymatic activities of CML cell lines

10x 10^6 cells were collected for each cell line (KU812 Parental and ImaR) and washed with PBS. Pellets were resuspended into 1ml of lysis buffer (20mM TrisHCl, pH 7.5, 1mM dithiothreitol, 1mM EDTA, 0.02% (v/v) Triton X-100, 0.02% (v/v) sodium deoxycholate) supplemented with protease inhibition cocktail (Sigma-Aldrich). Cell lysates were disrupted by sonication using titanium probe (VibraCell, Sonics & Materials Inc., Tune: 50, Output: 25) and immediately centrifuged at 12000×g for 20min at 4 °C. The supernatant was separated and used for the determination of specific enzyme activities by spectrophotometric using a COBAS Mira Plus chemistry analyser. The supernatant was also used to quantify protein content by BCA. All enzymatic activities were determined by monitoring NAD(P)H increment

or decrement at 340nm wavelength. Finally, enzymatic activities were normalised by protein content.

Hexokinase (HK, EC 2.7.1.1)

HK specific activity was determined by coupling HK and G6PD reactions in the following conditions: 3.3mM NADP+ , 14.8mM ATP, 14.8mM MgCl2, 2.8U/ml G6PD and 50mM Tris-HCl, pH 7.6, at 37°C. Reactions were initiated by the addition of glucose up to a final concentration of 10mM.

Glucose-6-phosphate dehydrogenase (G6PD, EC 1.1.1.49.)

G6PD activity was measured by adding samples to a cuvette containing 0.5mM NADP+ in 50mM Tris-HCl, pH 7.6, at 37°C. Reaction was initiated by the addition of G6P up to a final concentration of 2mM.

6-Phosphogluconate dehydrogenase (6-PGD, EC 1.1.1.44.)

G6PD activity was measured by adding samples to a cuvette containing 0.5mM NADP+ in 50mM Tris-HCl, pH 7.6, at 37°C. Reaction was initiated by the addition of G6P up to a final concentration of 2mM.

Transketolase (TKT, EC 2.2.1.1.)

TKT specific activity was determined by adding samples to a cuvette containing 5mM MgCl2, 0.2U/ml triose phosphate isomerase, 0.2mM NADH, 0.1mM thiamine pyrophosphate in 50mM Tris-HCl, pH 7.6, at 37°C. The reaction was initiated by the addition of a substrate mixture prepared by dissolving 50mM R5P in 50mM Tris-HCl, pH 7.6, in the presence of 0.1U/ml ribulose-5-phosphate-3-epimerase and 1.7mU/ml phosphoriboisomerase. The substrate mixture was continuously stirred and held at 37°C for 1h and then kept at -20°C until use.

Pyruvate kinase (PK, EC 2.7.1.40)

PK specific activity was determined by coupling PK and LDH reactions in the following conditions: 0.8mM NADH, 1.6mM ADP, 12.1mM MgCl2, 36.8mM KCl and 5.2U/ml LDH in

20mM KH2PO4/K2HPO4 buffer, pH 7.2, at 37°C. Reactions were initiated by the addition of PEP up to a final concentration of 3.5mM.

Lactate Dehydrogenase (LDH, EC 1.1.1.42)

LDH specific activity was measured by adding sample extracts to a cuvette containing 0.2mM NADH in 100mM KH2PO4/K2HPO4, pH 7.4, at 37°C. Reaction was initiated by the addition of pyruvate up to a final concentration of 0.2mM.

4.12 Oxygen consumption rate (OCR) and extracellular acidification rate (ECAR)

Oxygen consumption rate (OCR) and the extracellular acidification rate (ECAR) were analysed using a Seahorse 96 extracellular flux analyser (Agilent, Waldbronn, Germany). XF96 sensor cartridges (Agilent, Waldbronn, Germany) were hydrated overnight in XF Calibrant Solution (Agilent, Waldbronn, Germany) at 37°C in a non-CO_2 incubator. Stress test reagents (Agilent, Waldbronn, Germany) were re-constituted in appropriate media. A total of $1{,}5x10^5$ for THP-1, $3x10^5$ for HL-60, and $2x10^5$ for KU812 cells previously incubated under normoxic or hypoxic conditions (also referred as normoxia and hypoxia) in 200µl of KHB Buffer were plated in Seahorse 96-well cell culture plates and equilibrated for 30min before recordings. Oxygen and proton measurements together with were carried out over 110min, following the programmed protocol; hence, basal O_2 consumption rate and basal ECAR were determined under normoxia. In addition, suspension cells for each condition were collected and protein concentration was measured by Lowry protein assay kit (Bio-Rad, Munich, Germany). Data of CML parental and resistant cells were normalised by protein due to fact that protein content was the same in both cell line models. With regard to AML parental and resistant cells, data were normalised by cell number due to the fact that cell protein content varies between cell line models.

Mitostress test

Mitochondrial function was analysed by sequential injections of 2.5µM oligomycin, to block ATP-coupled respiration; 0,2µM carbonyl cyanide m-chlorophenylhydrazone (CCCP) for HL-

60 cell lines and 0.3µM of CCCP for THP-1 and KU812 cell lines, to uncouple the respiratory chain; 0.2µM of CCCP for HL-60 cell lines and 0.3µM of CCCP for THP-1 and KU812 cell lines together with 2mM of Pyruvate, to assure complete maximal respiration; and 1µg/ml antimycin A together with 1µM rotenone, to block mitochondrial respiration. For this test, Krebs Henseleit buffer (111mM NaCl, 4.7mM KCl, 1.25mM CaCl2, 2mM MgSO4, 1.2mM Na2HPO4) supplemented with 10mM L-glucose and 4mM L-glutamine was used. An example of OCR profile is shown in **figure 4.1.A.**

Glycolysis stress test

For the glycolytic stress test, cells were treated with sequential injections of 5mM glucose and another 5mM glucose (10mM in total), to drive the cell to perform glycolysis; 2.5µM oligomycin; and 100mM 2-deoxyglucose (2-DG), to inhibit glycolysis. For this test, Krebs Henseleit buffer (111mM NaCl, 4.7mM KCl, 1.25mM CaCl2, 2mM MgSO4, 1.2mM Na2HPO4) supplemented with 4mM L-glutamine was used. An example of OCR profile is shown in **figure 4.1.B.**

Mito Fuel Flex test

Briefly, the Mito Fuel Flex Test determines the dependency of mitochondrial respiration on three major metabolic substrates, for instance fuel pathways (pyruvate, FAs, and glutamine). The substrate dependency is calculated as one fuel substrate relative to all pathways. For the dependence towards glucose cells were treated with 2mM UK5099, to inhibit the mitochondrial pyruvate transporter, followed by 4mM etomoxir, to block carnitine palmitoyl transferase 1 A together with 3mM BPTES, to antagonise GLS. Finally, 2.5µM oligomycin was used to inhibit total respiration. To determine glutamine dependence, BPTES was added, followed by etomoxir and UK5099. FA dependency was assayed by adding etomoxir, followed by BPTES together with UK5099. For these assays DMEM D5030 supplemented with 10mM L-glucose and 4mM L-glutamine was used. An example of the FA Mito Fuel Flex test is shown in **figure 4.1.C.**

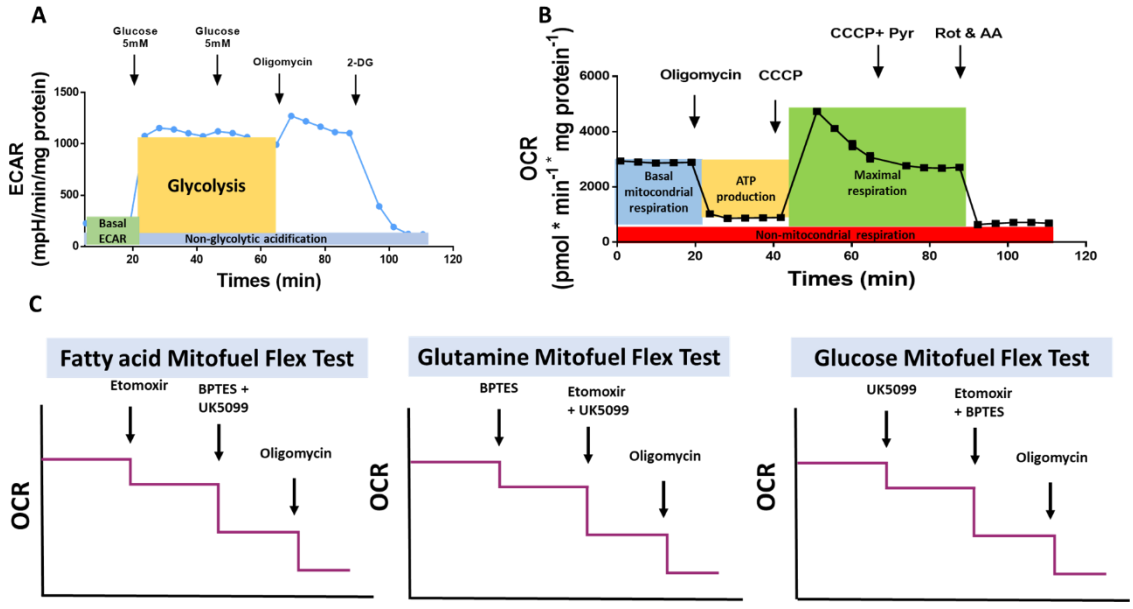

Figure 4.1. Schematic OCR and ECAR profiles of the Glycolysis stress test, Mitostress test and Mito Fuel Flex tests. A) Schematic ECAR profile after glucose 5mM, glucose 5mM (10mM), oligomycin and 2-deoxyglucose (2-DG) sequential injections. ECAR values for basal ECAR, glycolysis and non-glycolytic acidification are illustrated. **B)** Schematic OCR profile after oligomycin, CCCP, CCCP+Pyruvate (Pyr), and rotenone+antimycin A (Rot & AA) sequential injections. OCR rates for basal mitochondrial respiration, ATP production, Maximal respiration and non-mitochondrial respiration are illustrated. **C)** Schematic OCR profile after inhibitors (Etomoxir, BPTES and UK5099) and oligomycin sequential injections. The different Mito Fuel Flex tests are illustrated.

Test calculations

Calculations of parameters coming from the **Mitostress test**:

- **Basal mitochondrial respiration =** the subtraction of the non-mitochondrial respiration (OCR value after the infection of rotenone+antimycin A) to the baseline OCR.
- **ATP production =** the subtraction of the baseline OCR to the OCR rate after the injection of oligomycin.
- **Maximal respiration without pyruvate** = the subtraction of the non-mitochondrial respiration to the OCR rate after the CCCP injection.

- **Maximal respiration with pyruvate** = = the subtraction of the non-mitochondrial respiration to the OCR rate after the CCCP+Pyruvate injection.

Calculations of parameters coming from the **Glycolysis stress test**:

- Basal ECAR = baseline ECAR without any injections and considering the 4mM of glutamine supplemented in the KHB buffer.

-Total ECAR= the ECAR value after the second injection of 5mM glucose (i.e. 10mM of glucose) and considering the 4mM of glutamine supplemented in the KHB Buffer.

- Glycolysis rate = the subtraction of the basal ECAR to the ECAR value after the second injection of 5mM glucose (i.e. 10mM glucose).

- Crabtree effect = the subtraction of the baseline OCR to the OCR rate after the second injection of 5mM glucose (i.e. 10mM glucose) divided by the baseline OCR. Next, the fold difference (log_2) of the resulting value was calculated.

Calculations of parameters coming from the **Mito Fuel Flex test**:

-**Contribution of each substrate to the mitochondrial respiration:** the subtraction of the OCR rate after the target inhibitor injection to the OCR baseline divided by the subtraction of the OCR rate after oligomycin injection to the OCR baseline, and multiply by 100 to obtain the percentage.

-**Contribution of all the inhibitors to the mitochondrial respiration:** the subtraction of the OCR rate after the injection of all the inhibitors to the OCR baseline divided by the subtraction of the OCR rate after oligomycin injection to the OCR baseline, and multiply by 100 to obtain the percentage.

4.13 Oximetry for KU812 parental and resistant cell lines

OXPHOS flux in KU812 Parental, treated (treatment procedure explained above) and ImaR cells was determined using a high-resolution respirometer (Oxygraph-2k, Oroboros

Instruments, Innsbruck, Austria) following the protocol described in ([310]). In brief, $2x10^6$ millions of cells were collected and washed one in phosphate buffered saline (PBS), centrifuge and finally resuspended in MiR05 (3mmol/l MgCl2, 0.5mmol/l EGTA, 20mmol/l taurine, 10mmol/l KH2PO4, 60mmol/l K-lactobionate, 110mmol/l sucrose, 20mmol/l HEPES, and 1g/l bovine serum albumin) for permeabilised-cell approaches and in RPMI-1640 for intact-cell approach. Then, respiratory oxygen consumption was assessed in real time as pmol of O_2 per second per million cells in 2ml Oxygraph chambers. Routine cellular respiration rate was first measured before the addition of any substrate or inhibitor and it was further measured after the addition of substrates and inhibitors of interest following the required protocols for each approach explained as follows:

Cell intact approach

Substrates and inhibitors were sequentially added as follows: 5mM pyruvate, 2.5µM oligomycin, stepwise titration of CCCP uncoupler in 0.05µM increment as needed, 0.5µM rotenone, and 2.5µM antimycin A. KU812 Parental, treated and ImaR cells were used for this approach.

Complex I activity measurement

Firstly, basal respiration was measured before cells were permeabilised using 15µg digitonin. Then, substrates and inhibitors were sequentially added as follows: 10mM glutamate, 2mM malate, 5mM ADP, 10µM cytochrome c (mitochondrial membrane integrity was verified by the addition of cytochrome c and the changes observed in OCR were always lower than 10%), 5mM pyruvate.

Complex II activity measurement

Basal respiration was first measured and then cells were permeabilised using 15µg digitonin. The following sequential injections were performed: 10mM glycerol-3-phosphate, 5mM ADP and 10mM succinate.

Complex IV activity measurement

Respiration was measured after the addition of 5mM ascorbate plus 0.5mM tetramethyl-phenylenediamine dihydrochloride (TMPD) and after the addition of 100mM azida, which inhibit complex IV activity. Subtracting the second respiration measurement to the first, complex IV activity was addressed.

Fatty acid approach

Firstly, basal respiration was measured before cells were permeabilised using 15µg digitonin. Then, substrates and inhibitors were sequentially added as follows: 0.04mM palmitoyl-CoA carnitine plus 0.1mM malate, 5mM ADP and 1.9mM malate. This approach was performed using only KU812 Parental and ImaR cells.

Data analysis

Data was analysed using DatLab7 (Oroboros, Austria) software. Oxygen consumption rates (OCRs), expressed as picomoles (pmol) per second (s) per million of cells (Mill). The O_2 flow in these states was corrected by the subtraction of non-mitochondrial respiration, which was obtained after the addition of antimycin A. All data was normalised by cell number.

4.14 Western blotting

Cells were washed with ice-cold PBS and incubated for 30min on ice with RIPA buffer containing 50mM Tris (pH 8.0), 150mM sodium chloride, 1% Triton X-100, 0.5% sodium deoxycholate, 0.1% sodium dodecyl sulphate (SDS), 1% protease inhibitor cocktail and 1% phosphatase inhibitor cocktail (Thermo Fisher Scientific Inc.). Cells were sonicated and centrifuged at 16,000xg for 20min at 4°C. Supernatants were recovered and the protein content was quantified by the BCA kit (Pierce Biotechnology). Equal amounts of protein per sample were size-separated by electrophoresis on 10% SDS polyacrylamide gels and electroblotted onto polyvinylidene fluoride transfer membranes (PVDF) (BioRad

Laboratories, Hercules, CA, USA). 5% skim milk in PBS 0.1% Tween was used for blocking step (1h at RT) and blots were incubated with the corresponding primary antibodies (**Table 4.2**) overnight at 4°C under agitation according to the conditions indicated below. In order to remove the remaining primary antibody, membranes were rinsed with PBS-Tween (0.1%) and further treated with the appropriate secondary antibody (**Table 4.3**) for 1h at room temperature. Afterward, membranes were washed again with PBS-Tween (0.1%) before the analysis. All blots were treated with Immobilon ECL Western Blotting Detection Kit Reagent (EMD Millipore, Billerica, MA, USA) and developed after exposure to an autoradiography film (VWR International, Radnor, PA, USA) in the darkroom. Expression of all the proteins was finally investigated against the Lamin-B or TATABOX housekeeping proteins, as a loading control.

Table 4.2 Primary antibodies for Western Blotting analysis

Protein	Brand	Dilution for Western Blot
ALDH18A1/P5CS	Santa Cruz Biotechnology	1:1000
HKI	Santa Cruz Biotechnology	1:1000
HK II	Santa Cruz Biotechnology	1:1000
HK III	Santa Cruz Biotechnology	1:1000
P5CRL/PYCR	Santa Cruz Biotechnology	1:1000
GLUL	Santa Cruz Biotechnology	1:1000
Lamin-B	Santa Cruz Biotechnology	1:10000
PRODH	GeneTex	1:1000
GLS2	GeneTex	1:1000
TATABOX	Abcam	1:1000
GLS1	Abcam	1:1000
TKT	Sigma-Aldrich	1:1000
SLC6A7/proT	Quimigen	1:500

Table 4.3 Secondary antibodies for Western Blotting analysis

Protein	Brand	Dilution for Western Blot
Anti-mouse	PO260, Dako	1/10000
Anti-rabbit	NA934V, Amersham Biosciences	1/10000
Anti-goat	Santa Cruz Biotechnology	1/10000

4.15 SILAC-based Proteome Analysis

Stable isotope labelling with amino acids in cellular culture (SILAC)

For SILAC RPMI medium devoid of arginine and lysine (Thermo Fisher, #88365) supplemented with 10% dialysed FBS (Gibco, #26400044), 100U/ml Penicillin, 100µg/ml Streptomycin (Gibco, #15140122) and the respective isotope-labelled amino acids (all from Cambridge Isotopes, Tewksbury, MA) was used. "Light" SILAC medium contained [12C614N4]-L-arginine and [12C614N2]-L-lysine and "heavy" SILAC medium contained [13C615N4]-L-arginine and [13C615N2]-L-lysine.

Both AML and CML cells were grown for at least 5 passages prior sample collection to ensure complete incorporation of the isotopes into proteins.

Sample preparation

Cells were washed with cold 1x PBS and lysed in 0.5% Nonidet P-40 (NP-40) buffer containing 50mM Tris/HCl, pH 7.5, 150mM NaCl, 1mM Na3VO4, 5mM NaF, and protease inhibitors (Complete™, Mini, EDTA-free Protease Inhibitor Cocktail, Roche). For protein expression profiling, lysates of cells labelled differentially during SILAC were mixed in equimolar ratios and separated by SDS-PAGE using precast Bis-Tris minigels (NuPAGE Novex 4–12%, Life Technologies). After protein visualisation by staining with Coomassie Brilliant Blue (Serva) each gel lane was cut into 23 slices. The separated proteins were reduced with DTT (Sigma-Aldrich) and alkylated with iodoacetamide (Sigma-Aldrich). After overnight in-

gel protein digestion with trypsin (Serva), peptides were extracted from the gel matrix and analysed by liquid chromatography / mass spectrometry (LC/MS).

Liquid chromatography and mass spectrometry

The tryptic peptide mixtures were measured on a quadrupole-Orbitrap hybrid mass spectrometer (Q Exactive HF, Thermo Fisher Scientific) coupled to an Ultimate 3000 HPLC system (Thermo Fisher Scientific). The samples were preconcentrated and desalted on a trap column (20×0.1mm, ReproSil-Pur 120 C18-AQ, 5µm, Dr. Maisch GmbH; packed in-house) at 5µl·min−1 in loading buffer [2% (vol/vol) ACN, 0.1% FA]. The peptide samples were separated on an analytical column (320 × 0.075mm, ReproSil-Pur 120 C18-AQ, 1.9µm, Dr. Maisch GmbH; packed in-house) using an 60min linear gradient from 4% to 34% buffer B [95% (vol/vol) ACN, 0.1% FA] versus a decreasing concentration of buffer A (0.1% FA) at a flow rate of 300nl/min. For the analysis of eluting peptides, the mass spectrometer was operated in a data-dependent acquisition mode selecting the 30 most abundant precursor ions (*m/z* 350-1600 range, charge state 2-6) for higher energy collisional dissociation (HCD) with an isolation width of *m/z* 1.6 and a stepped normalised collision energy (NCE) setting of 26-30%. Survey spectra and fragment ion spectra were acquired with are solution setting of 70,000 or 15,000 FWHM at *m/z* 200 in the Orbitrap analyser, respectively. AGC target values and maximum injection times for MS and MS/MS were set to 1×10^6 in 50ms and 1×10^5 in 60ms, respectively. Fragmented precursor ions were dynamically excluded from selection for 30s.

Data processing

Raw data files from LC-MS/MS measurements were processed using the MaxQuant software (version 1.6.0.1, MPI for Biochemistry)[311]. MS/MS spectra were searched against the UniProtKB/Swiss-Prot human database containing 88,993 protein entries (downloaded November 2016) supplemented with 245 frequently observed contaminants with the Andromeda search engine [312]. Precursor and fragment ion mass tolerances were set to 6 and 20ppm after initial recalibration, respectively. Protein N-terminal acetylation and

methionine oxidation were allowed as variable modifications. Cysteine carbamidomethylation was defined as a fixed modification. Minimal peptide length was set to seven amino acids, with a maximum of two missed cleavages. The false discovery rate (FDR) was set to 1% on both the peptide and the protein level using a forward-and-reverse concatenated decoy database approach. For SILAC quantitation, multiplicity was set to two for double labelling (Lys+0/Arg+0, Lys+8/Arg+10) and at least two ratio counts were required for peptide quantitation. Both the "match between runs" and "re-quantify" options of MaxQuant were enabled.

Subsequent evaluation of MaxQuant output data was conducted with the Perseus software (version 1.6.0.7, MPI for Biochemistry) [313]. After removal of hits to the decoy database and potential contaminants, the SILAC ratios were logarithmised and filtered for valid values in each measurement. To assign regulated proteins, ratio thresholds were determined by subjecting the SILAC ratios of the whole population of identified proteins to an outlier analysis based on a FDR < 5% and Benjamini-Hochberg correction for multiple hypothesis testing [314]. Ratios already reflect the $\log_2$ fold change values. Next, $\log_2$ fold change values were filtered according to a threshold of 0.58 $\log_2$ fold change value (fold difference [FD] of 1.50-fold up) and of -0.58 $\log_2$ fold change value (FD=1.5-fold down) to obtain the significantly up or down regulated proteins, respectively. Finally, $\log_2$ fold change values were integrated and visualised in specific pathways using Pathview Web[315] and specific biological processes using PANTHER[316].

4.16 CRISPR/Cas9 technology

Based on the metabolic results, we selected two genes involved in proline metabolism ALDH18A1 [P5CS]; and SLC6A7 [proline transporter, proT]) to be depleted from the CML cell lines KU812 parental and ImaR by CRISPR/Cas9 gene editing. Subsequently, the effect of the depletion regarding imatinib resistance was further evaluated by a competitive cell growth assay and a cumulative growth curve (**Section 4.17**). The CRISPR/Cas9-method, introduced

by Emmanuelle Charpentier and Jennifer Doudna[317], was used to introduce abrogating point mutations into the ALDH18A1 and SLC6A7 coding regions in both KU812 Parental and ImaR cell lines. Therefore, three different guide RNAs (gRNAs) were designed using the benchling software package (http://benchling.com) targeting different exons of the gene to exclude off target effects. The first step to generate a specific KO is to identify an efficient gRNA that guides the Cas9 protein to its target sequence (**Table 4.4**). This guide RNA has to be complementary to the sequence of the target gene and needs to be in direct proximity to a Protospacer Adjacent Motif (PAM; NGG) sequence. The Benchling software package is a freeware tool that aids in this design. The designed gRNAs were cloned into the LentiCRISPRv2-ΔCas9-EGFP vector (kindly provided by F. Schnuetgen, from the department of Medicine, Hematology/Oncology, Goethe-University Frankfurt).

Using the cell line 293T LentiX (Takara), lentiviral particles were produced for each specific gRNA and transduced into spCas9 expressing CML cell lines (spCas9-Blasticidin; generated in the Serve's lab). Subsequently, Cas9 binds to the expressed gRNA and introduces a DNA double strand break (DSB) at the desired target locus. This DSB is repaired by the endogenous cellular DSB repair pathway "non-homologous end joining" (NHEJ), which is an error-prone process causing small insertions or deletions (indels) leading to the KO of the gene.

The success of the KO cell lines was tested by Western blotting through the detection of the target protein in gRNA treated cells versus cells treated with a gRNA non-target control (NTC).

Table 4.4 Sequences of the selected gRNAs.

CR NTC1 s	CACCGttccgggctaacaagtcct
CR NTC1 as	AAACaggacttgttagcccggaaC
CR hALDH18A1 E3 s	CACCGtacccctcagtcgtacaca
CR hALDH18A1 E3 as	AAACtgtgtacgactgaggggtaC
CR hALDH18A1 E4 s	CACCGcgcaagcgttgtttgccaa
CR hALDH18A1 E4 as	AAACttggcaaacaacgcttgcgC
CR hALDH18A1 E5 s	CACCGgtaaacatagcctcataca
CR hALDH18A1 E5 as	AAACtgtatgaggctatgtttacC
CR hSLC6A7 E2 s	CACCGtggactttgctgcacaccg
CR hSLC6A7 E2 as	AAACcggtgtgcagcaaagtccaC
CR hSLC6A7 E3 s	CACCGcatgaggaagtagggcacg
CR hSLC6A7 E3 as	AAACcgtgccctacttcctcatgC
CR hSLC6A7 E4 s	CACCGgtctccaaggacggcaacg
CR hSLC6A7 E4 as	AAACcgttgccgtccttggagacC

Golden Gate cloning

Golden Gate cloning describes a one-step cloning method that combines both restriction and ligation reactions in one tube[318].

Golden Gate reaction mixture	**Cycler program:**	
Vector 150ng	5min 37°C	9cycles
Annealed Oligos 1µl	10min 16°C	
10X ligase buffer 2µl		
T4 DNA ligase 1µl	15min 37°C	
BsmBI 1µl	5min 80°C	
ddH2O ad 20µl		

Transformation of chemically competent DH5α cells

Chemically competent DH5α cells were thawed on ice for 15 minutes. Then 20µl ligation reaction were added and carefully mixed. After incubation of 20 minutes on ice, a short

heat shock was performed for 1 minute at 42°C in a water bath. The cells were immediately placed on ice and then plated on agar plates containing ampicillin (100µg/ml) and incubated over night at 37°C.

Plasmid isolation

➔ Mini-prep

From an overnight culture, 1.5ml were transferred into reaction tubes and centrifuged (14000xg, 5 min, RT). The supernatant was discarded and the cell pellets were resuspended in 100µl P1 buffer. Then 200µl P2 buffer were added and mixed by inverting the reaction tubes. After addition of 150µl P3 buffer and mixing, the reaction tubes were centrifuged (14000xg, 5 min, RT). The supernatant was transferred to a new reaction tube and mixed with 1ml 100% ethanol. After centrifugation (14000xg, 5 min, RT), the DNA pellet was washed with 150µl 70% ethanol. After centrifugation (14000xg, 1 min, RT), the supernatant was discarded and the pellet shortly dried and resuspended in 50µl ddH2O.

➔ Midi-prep

Midi-preps were performed using the "ZyppyTM Plasmid Midiprep"-Kit (Zymo Research) according to the manufacturer's protocol. In short, 50ml of an overnight culture were transferred to a 50ml reaction tube, centrifuged (5000xg, 15 minutes, 4°C) and resuspended in 6ml ddH2O. Then 1ml Lysis Buffer was added and mixed by inverting the tubes. After 5 min incubation time, 3.5ml Neutralisation Buffer were added, mixed and transferred into a combined Zymo-Midi Filter column. After centrifugation (600xg, 5 min, 4°C), the blue Filter was removed and the column placed into a 1.5ml reaction tube. The remaining lysate was removed by another centrifugation step (14000xg, 30sec, RT) and the column was washed with 400µL Endo-Wash Buffer and twice with 400µL Zyppy Wash buffer. The column was transferred onto a new reaction tube, 150µL ddH2O were added, incubated for 1 min and DNA was eluted from the column by centrifugation (14000xg, 1min, RT). DNA concentrations were measured with a NanoDrop spectrometer (Thermo, Wilmington, DE).

➔ Maxi-prep

Maxi-preps were performed using the "NucleoBond PC 500"-Kit (Macherey-Nagel) according to the manufacturer's protocol. In short, 200ml of an overnight culture were transferred to 50ml reaction tubes, centrifuged (5000xg, 15 minutes, 4°C) and resuspended in 12ml P1. Lysis was achieved by addition of 12ml P2 and it was mixed by inverting. Then 12ml P3 were added and the mixture was centrifuged (5000xg, 15 minutes, 4°C). The Filter columns were equilibrated with 6ml N2 and the supernatant transferred onto the columns. After washing with 36ml N3, the column was placed onto a new Reaction tube and DNA was eluted from the column with 15ml N5. Then 11ml isopropanol were added and the mixture was centrifuged (5000xg, 3 h, 4°C). After discarding of the supernatant, the DNA pellet was washed with 3ml 70% ethanol and centrifuged (5000xg, 1 min, 4°C). The supernatant was discarded and the DNA pellet shortly dried. DNA was resuspended in 250µL ddH2O and DNA concentrations were measured with a NanoDrop spectrometer. All Maxi-Prep plasmids were diluted to a concentration of 1µg/µl.

DNA sequencing

DNA sequencing was performed by the Seqlab Company (Göttingen, Germany). DNA samples (1µg plasmid or 0.1µg PCR fragments) were prepared with 30pmol oligonucleotide for sequencing in a total volume of 15µL.

Virus production

Virus production was achieved by transfection of Hek293T cells with lentivirus-encoding plasmids (psPax2: Gag-Pol; pMD2.G: VSV.G Env) and PEI (1µg/µl) together with a transfer plasmid carrying the gene that was incorporated into the virus. On the first day, Hek293T cells were seeded onto 15cm dishes at $1.2x10^7$ cells. On the second day, the plasmid mix was prepared separately from the PEI mix using DMEM without supplements:

16µg transfer plasmid	PEI 1µg/µL 140µl
14µg psPax2	
8µg pMD2.G	
in 1.75ml ØDMEM	in 1.75ml ØDMEM

Both solutions were mixed separately and incubated at RT for 5 min. The solutions were then mixed and incubated at RT for 20 min before addition to the packaging cells dropwise.

On the third day, the medium was changed to new DMEM or RPMI. Two to three days after medium change, the cell supernatant was sterile filtered with a 0,45 µm sterile filter, transferred to 1.5ml cryotubes and stored at -80°C.

4.17 Competition cell growth assay and cumulative growth curve

Proliferation changes of transduced cells were measured by two different approaches: competition cell growth assay and cumulative growth curve. Both proliferation assays were performed after three days of transduction of KU812 parental and ImaR NTC, ALDH18A1 KO, and SLC6A7 KO cells. Cells were FACS-sorted based on green fluorescent protein (GFP) expression.

For the competition cell growth assay, 70% of GFP positive KU812 cells (KU812 Parental and ImaR NTC, ALDH18A1 KO or SLC6A7 KO cells) were mixed with 30% of untransduced cells (KU812 Parental and ImaR wildtype cells) and seeded in 6-well plates at a density of 1×10^5 cells per ml in 2.5ml per well in triplicates. GFP percentage was measured every second day over a period of 26 days to test for competitive growth of the respective cells over wildtype cells. After each measurement, fresh media was added to keep the volume constant (2.5ml). At later times, to avoid confluent cultures, parts of the population were discarded, and the remaining cells were diluted with fresh medium.

In order to generate longer growth curves, cumulative growth assays were performed. Therefore, KU812 Parental and ImaR NTC and KO cells were seeded in 12-well plates at a density of $2.5x10^5$ cells/ml in 2ml per well. Every second day, cells were manually counted and reseeded at the initial concentration in fresh medium. The theoretical cumulative growth curve was calculated from the respective dilution factors.

Both proliferation assays were performed once in triplicates. Regarding data analysis of the competition cell growth assay, the GFP expression percentages of KU812 KO cell lines were normalised by the GFP expression of the KU812 NTC cell lines and percentages were plotted using the GraphPad Prism 6 software (La Jolla, CA, USA). Moreover, cumulative growth counting of the different NTC and KO cell lines were also plotted using the GraphPad Prism 6 software (La Jolla, CA, USA).

Flow cytometry

For FACS-sorted by GFP expression and for GFP expression measurements to test cell proliferation, 100-200µl of cell samples plus 4ml of PBS were added into a FACS tube. Samples were centrifuged at 1200rpm for 5min and supernatant was discarded and 100µl of PBS was added. Then, flow cytometry analyses were performed on a BD LSRFortessa™ Becton Dickinson (Franklin Lakes, USA). Live cells were discriminated from cell debris and dead cells based on physical parameters (forward- and side-0 scatter). Fluorescence background levels were set with untransduced and unstained cells.

4.18 Imatinib-resistant BCR-ABL1 kinase domain mutation analysis

In order to exclude the occurrence of gatekeeper mutations in the production of resistant cells.

Genomic DNA was isolated from 5 x 10^6 cells of the respective cultures by Phenol/Chloroform extraction. Therefore, cells were incubated at 60°C overnight in 400µl PK reaction buffer (50mM Tris/HCl, 5mM EDTA, 150mM NaCl, 0,5% SDS) supplemented

freshly with 100µg/ml Proteinase K. The digested samples were mixed with 400µl Phenol/Chloroform/Isoamylalcohol (25:24:1), carefully mixed by shaking upside down and then centrifuged for 5 min 14.000 rpm. The upper aqueous phase was carefully removed and transferred to a fresh Eppendorf tube. Samples were likewise reextracted using 400µl Chloroform and the aqueous phase was again transferred to a fresh tube. Genomic DNA was precipitated by centrifugation (5min 14,000 rpm) using 1ml ice-cold Ethanol. The DNA pellet was washed using 150µl ice-cold 70% Ethanol and centrifucation (1min, 14,000 rpm) and briefly dried. DNA was dissolved in 0.1mM Tris/HCl pH 8.5 and diluted to a concentration of 200ng/ml.

From these genomic DNA samples exons 4, 5 and 6 of ABL1 were amplified using the following primers (BCR-ABL1 Ex4 s: 5'-AGGCTGTTCCCTGTTTCCTT-3', BCR-ABL1 Ex4 as: 5'-CAGATGCATCGCCTAATGC-3', BCR-ABL1 Ex5 s: 5'-GCTGTCATGGAACCTGTCTG-3', BCR-ABL Ex5 as: ATTCCAACGAGGTTTTGTGC-3', BCL-ABL Ex6 s: GAGCCACGTGTTGAAGTCCT-3', BCR-ABL1 Ex6 as: 5'-AATGTGTTGCCAGCACTGAG-3').

PCR reactions were performed using the following protocol:

5µl DreamTaq buffer

2µl dNTPs (0,2mM each)

2.5µl Sense Primer (10µM)

2.5µl Antisense Primer (10µM)

200ng genomic DNA

0.5µl DreamTaq (2.5 U)

to 50µl Water

Moreover, PCRs were performed in a standard PCR cycler using the following protocol: 1 cycle at 98°C for 20 s, 35 cycles of 98°C 20 s, 57°C 30 s, 72°C 1 min and a final elongation step at 72°C for 7 min.

Finally, PCR reactions were separated on an agarose gel and specific amplicons were isolated using the Zymoclean Gel DNA Recovery Kit (Zymoresearch, Freiburg, Germany)

according to the manufacturer's protocol. DNA fragments were Sanger sequenced using the respective sense primers.

5. RESULTS

5 RESULTS

5.1 Resistance mechanism developed by AML cells lines is associated with an important metabolic reprogramming dependent on drug inducer

5.1.1 Introduction and scope

In this chapter, we focus our attention on drug resistance in AML. As mentioned before, the standard treatment for AML involves a combination of cytarabine (AraC) plus anthracycline (e.g. Doxorubicin, Dox)[8]. However, only up to 70% of younger AML patients (aged <65 years), and up to 50% of older AML patients (aged ≥65 years) achieve complete remission with this treatment[319] whereas the other 10–40% of patients fail to respond to the standard treatment due to primary refractory disease (e.g. innate resistance) or treatment failure (e.g. acquired resistance). Therefore, new chemotherapeutics able to both overcome innate and acquired resistance in addition to the standard treatment are urgently needed.

As mentioned in the objectives section, we hypothesise that the rewiring of cell metabolism is a crucial part of the process through which AML cells become resistant to AraC and Dox. Thus, the study of the initial metabolic phenotype and the understanding of the metabolic reprogramming after the acquisition of AraC and Dox resistance in two AML cell lines are the main objectives of this chapter. In order to accomplish the second objective "Characterisation of the metabolic profile of AML parental and cytarabine and doxorubicin-resistant cell lines", THP-1 and HL-60 cell lines resistant to the chemotherapeutic drugs AraC and Dox were obtained (explained in **section 4.1**). Next, different experimental approaches to elucidate consumption and production rates of metabolites including oxygen, and to determine the intracellular concentrations of these metabolites, were performed to thoroughly characterise the metabolic profile of the THP-1 and HL-60 parental cells, as well as the metabolic reprogramming that underlies the acquisition of resistance to AraC and Dox in both AML cell lines. This metabolic characterisation was performed both under

normoxia (21% O_2), as these cell lines were developed under normoxic, and under hypoxic (1% O_2) incubation conditions, as these hypoxic incubation conditions prevail in the physiological environment of AML cell lines within the bone marrow.

All the metabolic assays conducted here were complemented with the study of the protein expression profile via SILAC-based protein mass spectrometry experiments, to be able to correlate changes in metabolite concentrations directly with changes in enzymatic equipment of resistant AML cell lines. Additionally, this protein expression profiling was also used to analyse other metabolic pathways which could not be measured otherwise because of the limited measurability of their metabolites.

Once a comprehensive analysis of the metabolome and proteome was performed, we addressed the second objective of this chapter, which is the "Definition and validation of targets associated with the metabolic reprogramming of parental and resistant AML cell lines". In this line, metabolic and additionally non-metabolic proteins were selected and/or validated as potential therapeutic targets for AraC- and Dox-resistant AML cells.

5.1.2 Results

5.1.2.1 Metabolic characterisation of THP-1 and HL-60 AML cell lines

Prior to characterising of the metabolic reprogramming induced by Ara-C and Dox resistance in THP-1 and HL-60 AML cell lines, we characterised the metabolic profile of the two parental AML cell lines. Therefore, we initially measured glucose consumption, glutamine consumption and lactate production rates in both AML cell lines incubated under both normoxic and hypoxic conditions (also referred as normoxia and hypoxia). Our results showed no differences in the consumption and production rates of the aforementioned metabolites between THP-1 and HL-60 parental cells (from here on named THP-1 P and HL-60 P, respectively) under normoxia (**Fig. 5.1.1.A**). With regard to the hypoxic incubation conditions, only THP-1 P cells displayed a significant increase in glucose consumption and lactate production, and a decrease in glutamine consumption compared to normoxia, thus

suggesting that THP-1 P cells may be more sensitive than HL-60 P cells to the hypoxic-mediated effect.

Moreover, the ratio between lactate production and glucose consumption ($ratio_{lactate/glucose}$) was calculated. The $ratio_{lactate/glucose}$, which denotes the molecules of lactate generated from each glucose consumed, constitutes an indicator of glycolytic flux. Briefly, when $ratio_{lactate/glucose}$ equals 2 it means that all glucose molecules may have been used for lactate production, exclusively. However, when this ratio is lower than 2, this means that part of glucose carbons has not been converted into lactate but were used for other purposes different to lactate production (e.g. lipid synthesis, or pyruvate for TCA cycle). On the other hand, when this ratio is above 2, this means that the cells produce lactate from other sources different than glucose. **Fig. 5.1.1.B** shows that $ratio_{lactate/glucose}$ was significantly higher for HL-60 P than for THP-1 P cells under normoxia. Moreover, the fact that this ratio was 2.4 ± 0.1 for HL-60 P but 1.8±0.1 for THP-1 P indicates that at least HL-60 P cells may have upregulated other pathways apart from glycolysis to fuel lactate production. On the other hand, no differences were obtained for the $ratio_{lactate/glucose}$ between AML parental cells incubated under hypoxic conditions.

Furthermore, the ratio between glucose and glutamine consumptions ($ratio_{glucose/glutamine}$), indicative of how many molecules of glutamine are consumed per molecule of glucose, was unchanged for both AML parental cells under normoxia (**Fig. 5.1.1.C**). Nevertheless, under hypoxic incubation conditions, both THP-1 P and H-60 P cells increased the $ratio_{glucose/glutamine}$ by 6 and 2 times, respectively. This increase in the $ratio_{glucose/glutamine}$ indicates that both AML parental cell lines decreased glutamine consumption relative to glucose consumption under hypoxia.

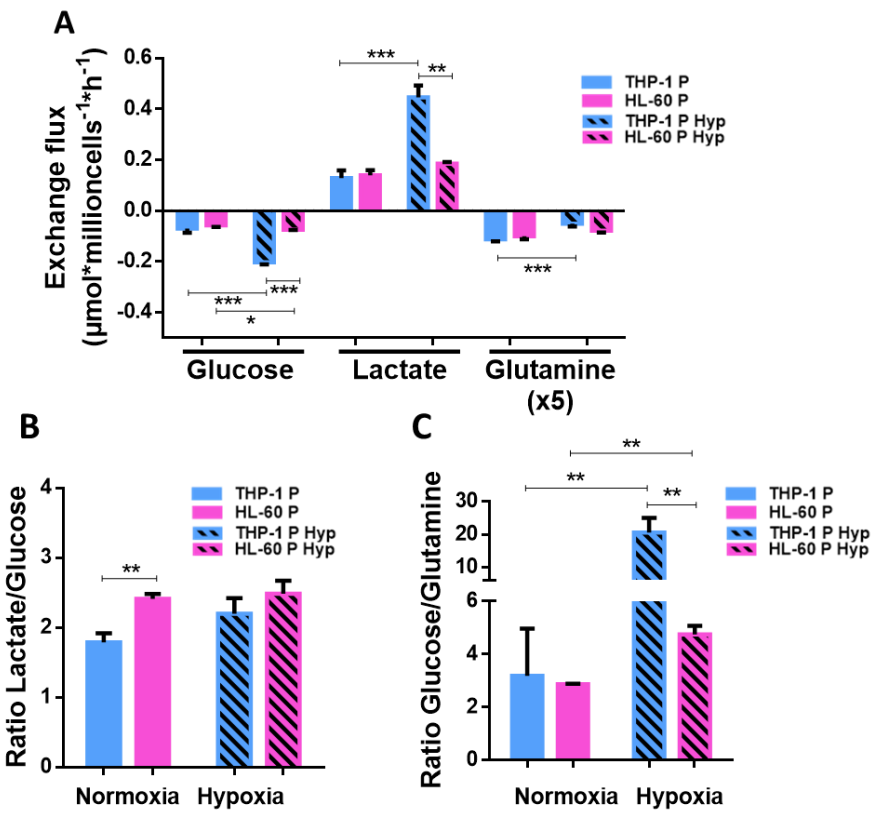

Figure 5.1.1 Metabolic differences between THP-1 and HL-60 parental AML cell lines. A) Exchange fluxes for THP-1 parental (P) and HL-60 P under normoxia and under hypoxia (Hyp). Glucose and glutamine consumption, and lactate production rates were determined as described in **Section 4.7**. Data were normalised to cell number and incubation time. **B)** The ratio lactate/glucose was determined by dividing lactate production flux rates by glucose consumption flux rates. **C)** The ratio glucose/glutamine was determined by dividing the glucose consumption flux rate by glutamine consumption flux rates. Data are provided as mean ± SD of n = 2 and significance was determined by two-tailed independent sample Welch's t-test. Statistically significant between THP-1 P vs. HL-60 P cells under normoxia or under hypoxia, and between THP-1 P or HL-60 under normoxia vs. hypoxia are indicated as $p<0.05$ (*), $p<0.01$ (**), and $p<0.001$ (***).

In order to complement the metabolic profiles of the AML parental cells incubated under normoxic and hypoxic conditions (normoxic or hypoxic-AML cells), ECAR and OCR were determined under normoxia using the XF96 Extracellular Flux Analyser (Seahorse) (**Fig. 5.1.2**). On one hand, ECAR quantifies the total protons produced and excreted by cells which

are mainly attributed to lactic acid produced in glycolysis and to the carbonic anhydrase (CA)-mediated hydration of the CO_2 ($CO_2 + H_2O$ --> $HCO_3^- + H^+$) produced in the TCA cycle. On the other hand, OCR provides information of the mitochondrial respiration, another energy-yielding pathway in cells. Our results show that HL-60 P cells incubated under normoxic conditions (normoxic-HL-60 P cells) displayed higher ECAR values than THP-1 P cells incubated under normoxic conditions (normoxic-THP-1 P cells) (**Fig. 5.1.2.A**). Moreover, normoxic-THP-1 P cells exhibited 11.6 higher OCR values than normoxic-HL-60 P cells (**Fig. 5.1.2.B**), thus indicating that normoxic-THP-1 P cells exploits more efficiently the mitochondrial respiration capacity for energy production than normoxic-HL-60 P cells. In fact, the elevated OCR of the normoxic-THP-1 P cells is an indicator of higher mitochondrial activity, which is also associated with an increase of CO_2 production from TCA cycle. Thus, the lower ECAR values found in normoxic-THP-1 P cells suggests that these cells should have extra mechanisms (e.g. proton neutralisation) to compensate the high proton production originating from CA-mediated hydration, or that they may reroute the CO_2 to citrate through glutamine-dependent reductive carboxylation.

Regarding AML cells incubated under hypoxic conditions (hypoxic-AML cells), hypoxic-THP-1 P cells) exhibited the same ECAR values than normoxic-THP-1 P cells although lactate production was dramatically increased under hypoxia. On the contrary, ECAR, in HL-60 P cells incubated under hypoxic conditions (hypoxic-HL-60 P cells), decreased although hypoxic-HL-60 P cells showed the same lactate production under normoxic and hypoxic incubation conditions (**Fig. 5.1.2.A**). Thus, these results suggest that glycolysis may not be the only contributor to ECAR value. It is worth mentioning that lactate production measurements were performed under hypoxic incubation conditions but ECAR values were measured in hypoxic-adapted cells under normoxic conditions (reoxygenation conditions). Therefore, even though the aforementioned results still suggest that the changes in the ECAR values are explained by the fact that glycolysis may not be the only contributor to ECAR value, further experiments measuring ECAR values of hypoxic-AML cells under hypoxic conditions (hypoxia) should be conducted. Furthermore, OCR decreased for hypoxic-THP-1 P cells, but it increased for hypoxic-HL-60 P cells (**Fig. 5.1.2.B**). As OCR increased for hypoxic-

HL-60 cells, a higher proton production (and thus higher ECAR) in hypoxic-adapted cells than normoxic cells would have been expected. Therefore, we hypothesise that the lower ECAR value in hypoxic-HL-60 cells could be due to the neutralisation of proton production occurring inside the hypoxic-HL-60 P cells or to an increase of the CO_2 rerouting to citrate through the glutamine-dependent reductive carboxylation. However, further studies to elucidate this fact would be needed.

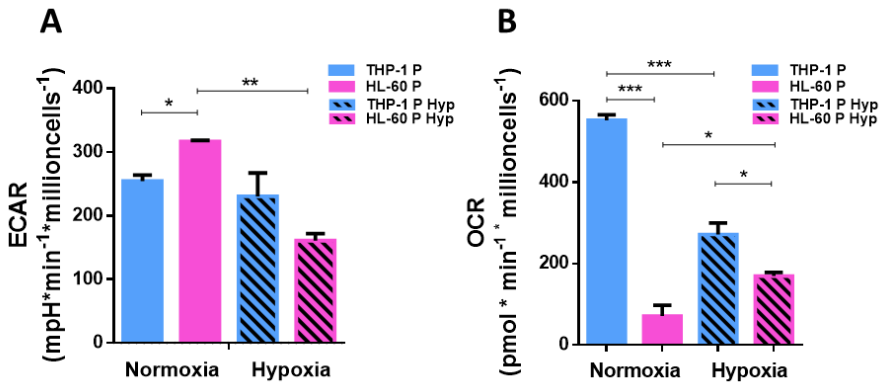

Figure 5.1.2 Extracellular acidification (ECAR) and basal mitochondrial oxygen consumption (OCR) rates of THP-1 and HL-60 cell line models. A) ECAR was measured under normoxia in THP-1 and HL-60 Parental (P) cells incubated in KHB buffer with 4mM glutamine and 10mM glucose under normoxic and hypoxic (Hyp) incubation conditions. **B)** Basal mitochondrial OCR levels measured under normoxia in THP-1 and HL-60 P cells incubated in KHB buffer with 4mM glutamine and 10mM glucose under normoxic and hypoxic (Hyp) incubation conditions. The basal mitochondrial OCR was determined by measuring OCR during sequential injections of oligomycin, CCCP, CCCP+Pyruvate, and Rotenone+Antimycin, and was calculated as described in **section 4.12**. Both ECAR and OCR were measured using a XF96 Extracellular Flux Analyser. Data were normalised by cell number. Data are provided as mean ± SD of n = 3 and significance was determined by two-tailed independent sample Student's t-test. Statistically significant between THP-1 P vs. HL-60 P cells incubated under normoxic or hypoxic incubation conditions, and between THP-1 or HL-60 P cells incubated under normoxic incubation conditions vs. THP-1 or HL-60 P cells incubated under hypoxic incubation conditions are indicated as $p<0.05$ (*), $p<0.01$ (**), and $p<0.001$ (***).

Since previous results showed metabolic differences between both AML cell lines at the level of mitochondrial metabolism, proton neutralisation, lactate and glutamine synthesis, we decided to perform a more accurate metabolic profiling by analysing the exchange flux rates of all amino acids and of polyamines in both cell lines under normoxia and hypoxia. The full list of exchange flux rates of both AML cell lines under normoxia is provided in **Table 1 from Appendix 1,** while **Figure 5.1.3** depicts the exchange fluxes that were significantly different between THP-1 P and HL-60 P cells. Particularly, higher consumption rates for histidine, isoleucine, leucine, lysine, phenylalanine, threonine, tryptophan, tyrosine, valine and glutamine, and higher production rate for glutamate were determined for THP-1 P when compared to HL-60 P cells. On the other hand, HL-60 P cells exhibited higher production rates of alanine and proline than THP-1 P cells. With regard to the exchange fluxes measured under hypoxia, all the exchange fluxes, with the exception of alanine that was produced more in HL-60 P than in THP-1 P cells, were non-significantly different between both AML cell lines (**Table 2 from Appendix 1**).

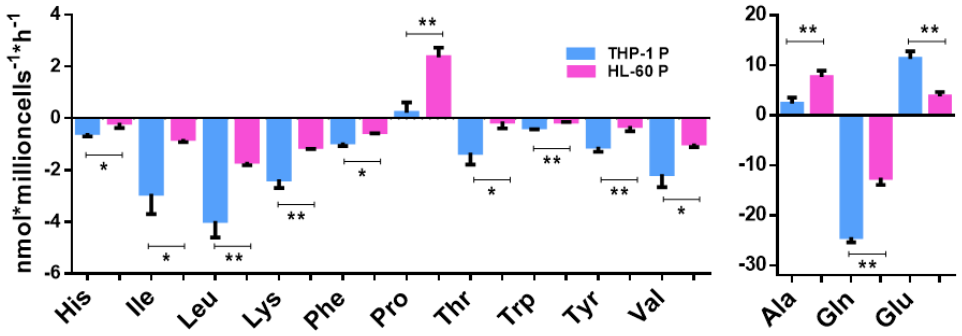

Figure 5.1.3 Exchange fluxes of amino acids for THP-1 parental and HL-60 parental AML cell line models under normoxia. Amino acids consumption and production rates in THP-1 parental (P) and HL-60 P cells obtained under normoxia were estimated after measuring the concentration of amino acids using the Absolute p180 Biocrates kit in incubation, as described in **Section 4.8.** Data were normalised to cell number and incubation time. Only exchanges fluxes of amino acids that were significantly different between cells lines were plotted. Data are provided as mean ± SD of n = 3 of one representative experiment and significance was determined by two-tailed independent sample Student's t-test. Statistically significant differences between THP-1 P and HL-60 P cells are indicated as p<0.05 (*), p<0.01 (**), and p<0.001 (***). Abbreviations: Alanine, Ala; glutamate, Glu; glutamine, Gln; histidine, His; isoleucine, Ile; leucine, Leu; Lysine, Lys; parental, P; phenylalanine, Phe; proline, Pro; threonine, Thr; tryptophan, Trp; tyrosine, Tyr; and valine, Val.

All together, these results suggest that THP-1 P and HL-60 P AML cell lines exhibited completely different metabolic profiles, with important differences in the consumption of metabolites that cells use to obtain energy and precursor units for cell proliferation. Although both cell lines exhibited a similar glycolytic flux under normoxia, THP-1 cells have much higher activity of OXPHOS than HL-60 cells. Moreover, THP-1 cells showed a ratio lactate/glucose lower than 2, indicating that part of pyruvate coming from glucose carbons might enter into TCA cycle. In this line, THP-1 cells also presented higher consumption of amino acids such as isoleucine, leucine, lysine, valine or threonine, among others, whose catabolism produces pyruvate, acetyl-coA or succinyl-coA, thus fuelling the TCA cycle and, thereby, increasing OXPHOS activity. On the other hand, HL-60 cells have increased proline and alanine synthesis, that are processes involved in the redirection of pyruvate and glutamate out of the TCA cycle. This fact together with the lower consumption of other

amino acids could explain the low OXPHOS activity observed in this cell line. Despite these different metabolic profiles, both cell lines proliferate under normoxia with a similar duplication time (49±5.1 and 41±7.4 for THP-1 P and HL-60P, respectively).

5.1.2.2 Resistance validation, cell volume and protein content comparison between cytarabine and doxorubicin resistant and parental AML cell lines

In order to achieve the first objective of this thesis ("to determine the metabolic changes developed by the different AML cell lines after the acquisition of AraC or Dox resistance and compare them to the parental counterparts"), we worked with four resistant AML cell line models generously obtained by Prof. Jindrich Cinatl (Institute of Medical Virology, University Hospital Frankfurt, Goethe University Frankfurt, Germany) and Prof. Martin Michaelis (Centre for Molecular Processing and School of Biosciences, University of Kent, Canterbury, UK): THP-1 resistant to AraC (here named as THP-1 AraC), HL-60 resistant to AraC (HL-60 AraC), THP-1 resistant to Dox (THP-1 Dox), and HL-60 resistant to Dox (HL-60 Dox). Firstly, we confirmed resistance against AraC or Dox by cell viability assay, thus determining the half maximal inhibitory concentrations (IC50) of the different cell models versus the sensitive parental (THP-1 P and HL-60 P) counterparts. All the resistant cell models presented higher IC50 values than their parental counterparts (**Fig. 5.1.4**).

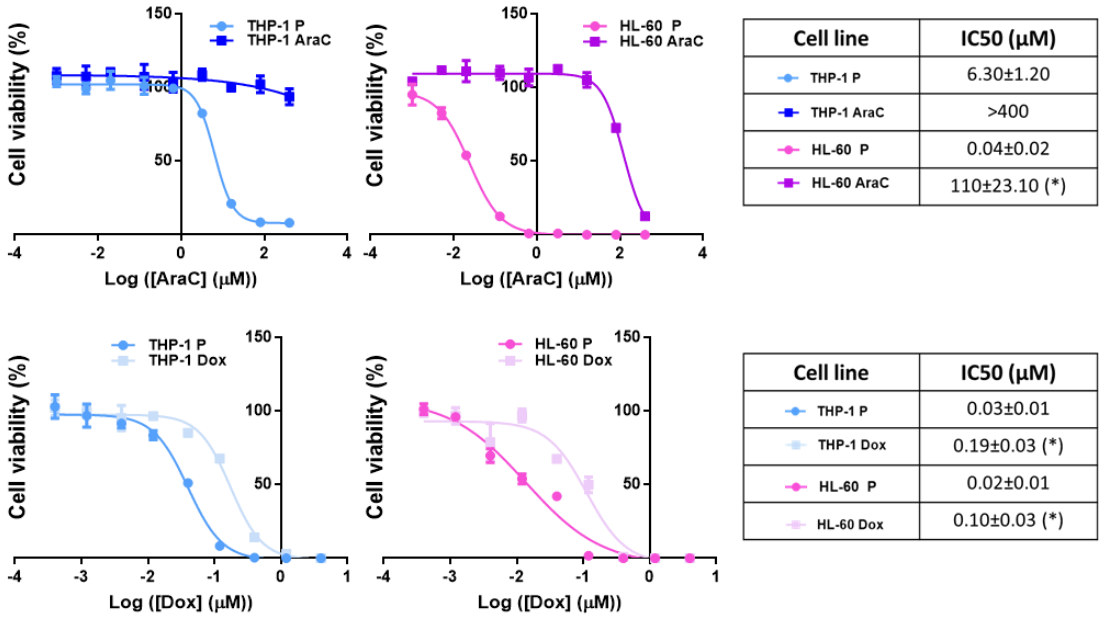

Cell line	IC50 (μM)
THP-1 P	6.30±1.20
THP-1 AraC	>400
HL-60 P	0.04±0.02
HL-60 AraC	110±23.10 (*)

Cell line	IC50 (μM)
THP-1 P	0.03±0.01
THP-1 Dox	0.19±0.03 (*)
HL-60 P	0.02±0.01
HL-60 Dox	0.10±0.03 (*)

Figure. 5.1.4 Cell viability of THP-1 and HL-60 cells parental or resistant to AraC and Dox after incubation with AraC or Dox. Cells were incubated 72 hours with DMSO (vehicle control) or different concentrations of the corresponding drug (AraC or Dox). Cell viability was determined and the half maximal inhibitory concentration (IC50) was calculated as described in **Section 4.3**. Data are provided as mean ± SD of n=2 and significance was determined by two-tailed independent sample Welch's t-test. Statistically significant differences between the THP-1/HL-60 resistant cells and their parental (P) cell lines are indicated as $p<0.05$ (*).

Furthermore, cell volume and protein content of all the AML cells were determined. Whereas development of resistance to AraC did not affect cell volume, both THP-1 and HL-60 cells that developed Dox resistance experienced shrinkage of 34% and 30%, respectively **(Fig. 5.1.5.A**). Moreover, both THP-1 AraC and Dox cell lines showed a 17% and 33% decrease in protein content compared to THP-1 P cells, respectively (**Fig. 5.1.5.B**). However, development of resistance to AraC or Dox did not induce any significant change in protein content in HL-60 cells.

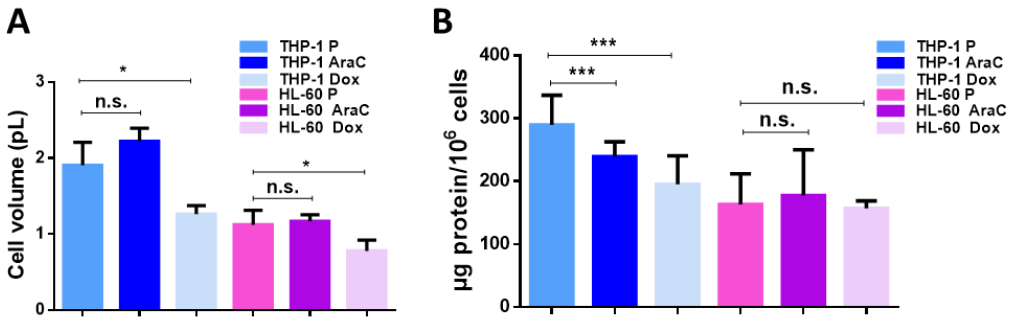

Figure 5.1.5 Cell volume and protein content of THP-1 and HL-60 parental and AraC and Dox resistant cells. Cell volume (**A**) and protein content (**B**) of THP-1 and HL-60 Parental (P), and AraC and Dox resistant cells determined under normoxia. Cell volume was determined by Scepter™ 2.0 Cell Counter. For protein content, samples from the different cell lines were collected and counted, and protein content of lysates of these samples were measured by BCA assay. Data are provided as mean ± SD of n = 5 for **panel A** and mean ± SD of n = 3 for **panel B**. Significance was determined by two-tailed independent sample Student's t-test. Statistically significant differences between resistant and their parental cells are indicated as $p \geq 0.05$ (n.s.), $p < 0.05$ (*), and $p < 0.001$ (***).

5.1.2.2.1 AML cells resistant to cytarabine and doxorubicin preferentially express proteins associated with cellular and metabolic processes

Since proteomic analysis, by analysing differentially altered protein concentrations, provides an understanding of the molecular signatures of the disease, we decided to evaluate the effect of AraC and Dox resistance acquisition on the protein profile of THP-1 and HL-60 cells. Therefore, SILAC-based protein mass spectrometry experiments with parental and resistant cells incubated under normoxic and hypoxic conditions were performed.

The results of the protein profiles indicated that from a total of 3461 proteins identified in all THP-1 cell lines under normoxic incubation conditions, 12% were upregulated and 14% downregulated in THP-1 AraC cells; whereas 10% were upregulated and 13%

downregulated in THP-1 Dox cells when compared to THP-1 P cells (**Tables 3-6 from Appendix 1**). On the other hand, differences between the different HL-60 cell lines under normoxic incubation conditions were not as strong as between THP-1 cell lines. From 3486 identified proteins, 11% were upregulated and 9% downregulated in HL-60 AraC cells; and 3% were upregulated and 3% downregulated in HL-60 Dox cells (**Tables 7-10 from Appendix 1**). Unfortunately, the technical replicates of the quantitative proteomic analyses performed for parental and resistant cell lines under hypoxic incubation conditions demonstrated a high variability. So, they could not be statistically evaluated (data not shown). For this reason, we only focussed on the quantitative analysis of the obtained proteomics data of AML cells incubated under normoxic conditions.

Furthermore, differentially regulated proteins under normoxia were clustered into biological processes using the gene ontology classification system so-called PANTHER database system. This analysis of the biological processes revealed that cellular processes (30%), considering any process that is carried out at the cellular level but not necessarily restricted to a single cell, and metabolic processes (21%) were the most altered in the acquisition of the four resistant phenotypes (**Fig. 5.1.6**). Thus, this analysis indicated that reprogramming of metabolism plays a key role in the acquisition of AraC and Dox resistance of THP-1 and HL-60 AML cells.

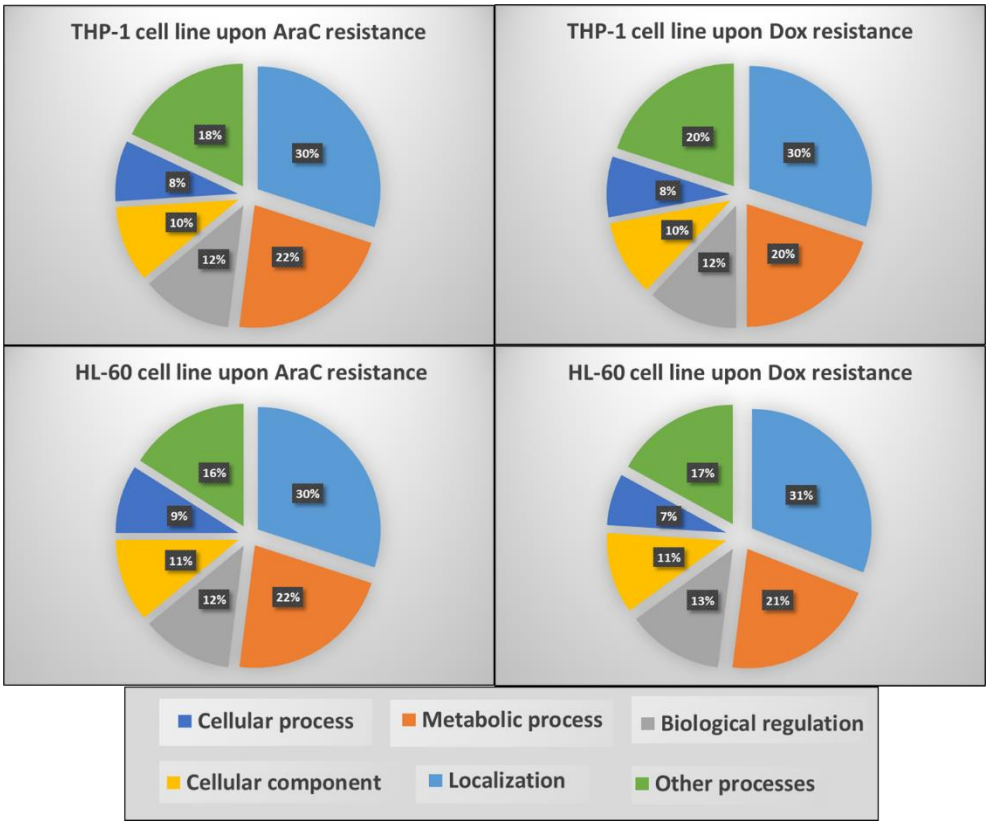

Figure 5.1.6. Clustering into biological processes, based on the gene ontology classification system, of differentially regulated proteins from the SILAC protein profiles of AraC and Dox resistant vs. parental cells incubated under normoxic conditions. The pie chart shows the biological process enrichment analysis of the regulated proteins. The pie chart shows the distribution of biological processes enrichment into subcategories. On-web analysis was performed using the PANTHER database system as described in **Section 4.15.** Only biological processes enriched in more than 7.3% appear in the plot. Data are provided as mean ± SD of n=2.

5.1.2.2.2 Cytarabine resistance induces an enhancement of glycolysis whereas the effect of doxorubicin resistance in glycolysis is cell line and oxygen level dependent

Considering that protein expression analysis revealed that metabolic changes plays an important role in the acquisition of AraC and Dox resistance, we further conducted a more complete analysis of the metabolic reprogramming induced by the acquisition of Ara-C and Dox resistance in THP-1 and HL-60 AML cell lines.

Firstly, glucose consumption and lactate production rates of the AML resistant cells were measured under normoxia and hypoxia as described in **Section 4.7**. Under normoxia, both AraC resistant cells increased their glucose consumption when compared to their parental counterparts **(Figs. 5.1.7.A and B**). Regarding the production of extracellular lactate, both AraC resistant cell lines showed a tendency towards an increase of lactate production, although it was only significantly different from its parental counterpart for THP-1 AraC cells. Moreover, the $ratio_{lactate/glucose}$ in the AML cells did not change upon AraC resistance acquisition (**Figs. 5.1.7.C and D**), indicating that the increase of the glucose and lactate rates in AraC resistant cells was of the same order to those of the parental cell lines. On the contrary, Dox resistant cells exhibited lower glucose consumption (THP-1 Dox by 50% and HL-60 Dox by 29%) and lactate production (THP-1 Dox by 75% and HL-60 Dox by 36%) rates relative to their parental cells **(Figs. 5.1.7.A and B**). Furthermore, the $ratio_{lactate/glucose}$ in THP-1 Dox resistant cells was decreased by 51% compared to THP-1 P cells, although this ratio was not affected in the development of Dox resistance in HL-60 cells (**Figs. 5.1.7.C**).

With regard to the extracellular glucose consumption and lactate production under hypoxia, AraC and Dox resistant cells overall exhibited almost the same pattern of changes described under normoxia (**Figs. 5.1.8.A and B**). Contrary to the results under normoxia, both glucose and lactate fluxes were increased in Dox resistant cells under hypoxia. These results suggest that Dox resistant cells may become more glycolytic upon the hypoxic-mediated effect. In parallel to what was observed under normoxia, the $ratio_{lactate/glucose}$ was only affected in THP-1 Dox resistant cells, which showed a decrease of 24% compared to THP-1 P cells (**Figs. 5.1.8.C-D**).

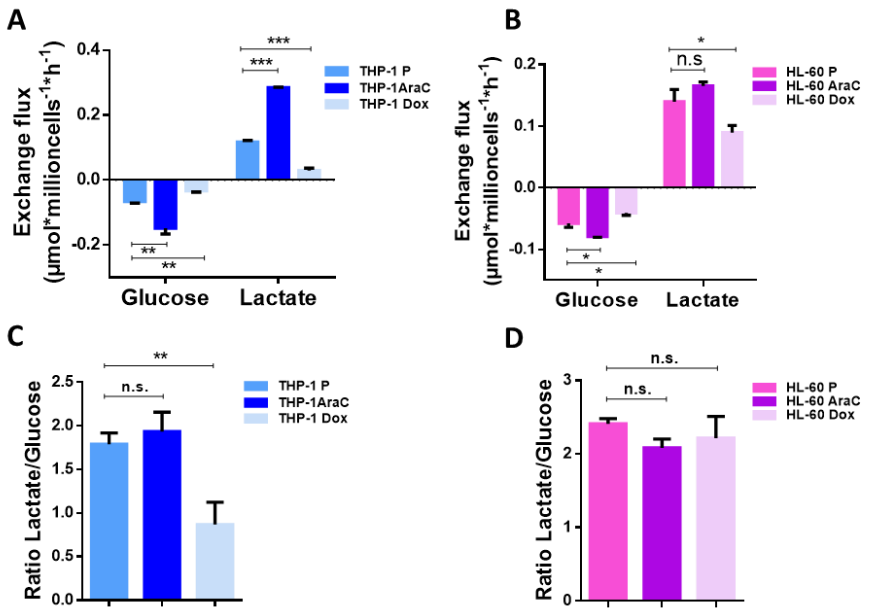

Figure 5.1.7 Effect of AraC and Dox resistance on glucose and lactate exchange fluxes under normoxia. A and B) Exchanges fluxes of THP-1 parental (P) and resistant cells (**panel A**) and of HL-60 P and resistant cells (**panel B**). Glucose consumption and lactate production rates were obtained under normoxia as described in **Section 4.7**. Data were normalised to cell number and incubation time. **C and D**) Ratio lactate/glucose determined by dividing lactate production rates by glucose consumption flux rates measured under normoxia. **Panel C** illustrates THP-1 cell lines and **panel D,** HL-60 cell lines. Data are provided as mean ± SD of n=2 and significance was determined by two-tailed independent sample Welch's t-test. Statistically significant differences between THP-1/HL-60 resistant cells and their parental (P) cells are indicated as $p \geq 0.05$ (n.s.), $p < 0.05$ (*), $p < 0.01$ (**), and $p < 0.001$ (***).

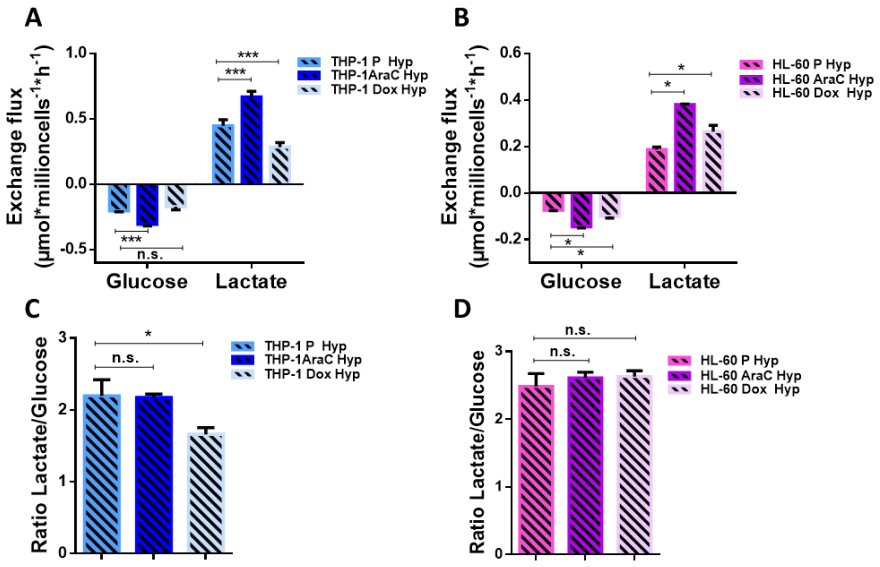

Figure 5.1.8 Effect of AraC and Dox resistance on glucose and lactate exchange fluxes under hypoxia. A and B) Exchange fluxes of THP-1 parental (P) and resistant cells (**panel A**) and of HL-60 P and resistant cells (**panel B**). Glucose and glutamine consumption, and lactate production rates were obtained under hypoxia as described in **Section 4.7**. Data were normalised to cell number and incubation time. **C and D**) Ratio lactate/glucose determined by dividing lactate production rates by glucose consumption flux rates measured under hypoxia. **Panel C** illustrates THP-1 cell lines and **panel D** HL-60 cell lines. Data are provided as mean ± SD of n=2 and significance was determined by two-tailed independent sample Welch's t-test. Statistically significant differences between THP-1/HL-60 resistant cells and their parental (P) cells, are indicated as $p \geq 0.05$ (n.s.), $p < 0.05$ (*), and $p < 0.001$ (***).

All together, these results suggest that development of resistance to Ara-C induced an increase of glycolytic flux in both cell models both under normoxic and hypoxic conditions. With regard to the development of resistance to Dox, our results show that its effect on the glycolytic flux was dependent on the cell line and on the oxygen conditions to which cells were exposed. Thus, when AML cells were under normoxic conditions, Dox resistant cells decreased glycolytic flux, while under hypoxic conditions the effect depended on the cell line.

We further assessed the total ECAR value under normoxia in all the AML resistant cell lines previously incubated under normoxic or hypoxic conditions (**Fig. 5.1.9**). ECAR values did not increase in any of the AraC resistant cells neither in normoxic nor in hypoxic incubation conditions (**Fig. 5.1.9**). Similar to what was above observed in THP-1 P cells (shown in **section 5.1.2.1**), the fact that THP-1 AraC cells incubated under hypoxic conditions increased lactate production (**Figs. 5.1.7-8**) but non-significant differences were observed regarding the ECAR values suggest that glycolysis is not the only contributor to ECAR value in THP-1 AraC cells. However, as already mentioned in **section 5.1.2.1**, further experiments should be conducted, but this time measuring ECAR values of hypoxic-AML resistant cells under hypoxic conditions (hypoxia), to clarify this suggestion.

Furthermore and considering that CA2 decreased dramatically (10.1-fold down) and that the electroneutral sodium bicarbonate cotransporter (SLC4A7) increased (2.24-fold up), we confirm the relevance of the CA-mediated hydration of the CO_2 as an important contributor to the ECAR values contrary to the generalised assumption that ECAR is a read-out of glycolytic flux. Taking together these results, the fact that no changes were observed in ECAR can be explained by the decrease of CA activity that compensate the increase in glycolytic flux. In addition, the increase in SLC4A7 also must be considered as a key player in the proton efflux balance. On the contrary, CA2 protein expression was increased by 1.92-fold and non-significant differences were observed regarding SLC4A7 protein expression in HL-60 AraC cells when compared to HL-60 P cells (**Fig. 5.1.10**), suggesting that glycolysis and not CA2 is the main contributor to the observed ECAR values in HL-60 AraC cells. Therefore, these results led to the hypothesis that both the decreased contribution of CA2 to the ECAR value and the compensatory mechanisms of intracellular bicarbonate balance may take place in cells highly dependent on mitochondrial respiration (e.g. THP-1 cells).

Regarding the Dox resistant cells, the ECAR value only decreased significantly for HL-60 Dox resistant cells incubated under normoxia (**Figs. 5.1.9.A-B**). Similar to the results observed in HL-60 AraC, the proteomic profiles showed a strong increase of CA2 (9.23-fold up) (**Fig. 5.1.10**), thus again highlighting glycolysis as the main contributor to the observed ECAR values. However, the fact that the protein expression of SLC4A7 protein decreased in these

cells (2.17-fold down) suggests that the enhanced bicarbonate transport could also play a role in the proton balance.

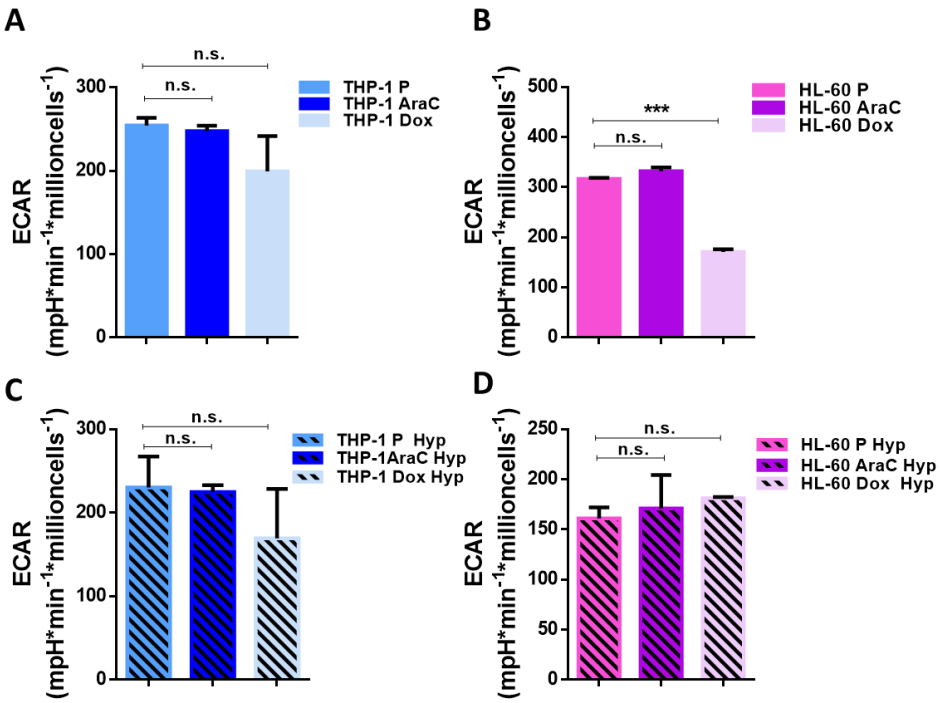

Figure 5.1.9 Extracellular Acidification Rate (ECAR) of THP-1 and HL-60 AraC and Dox resistant, and parental cells incubated under normoxic and hypoxic conditions. ECAR was measured under normoxia using a XF96 Extracellular Flux Analyser in THP-1 and HL-60 parental (P) and resistant cells incubated in KHB Buffer with 4mM glutamine and 10mM glucose under normoxic and hypoxic conditions. Total ECAR value was calculated as explained in **Section 4.12.,** and illustrated in **panel A,** for THP-1 cell lines incubated under normoxic conditions; **panel B**, for HL-60 cell lines incubated under normoxic conditions; **panel C**, for THP-1 cell lines incubated under hypoxic conditions; and **panel D**, for HL-60 cell lines incubated under hypoxic conditions. Data were normalised by cell number. Data are provided as mean ± SD of n = 3 and significance was determined by two-tailed independent sample Student's t-test. Statistically significant differences THP-1/HL-60 resistant cells and their parental (P) cells are indicated as $p \geq 0.05$ (n.s.), and $p < 0.001$ (***).

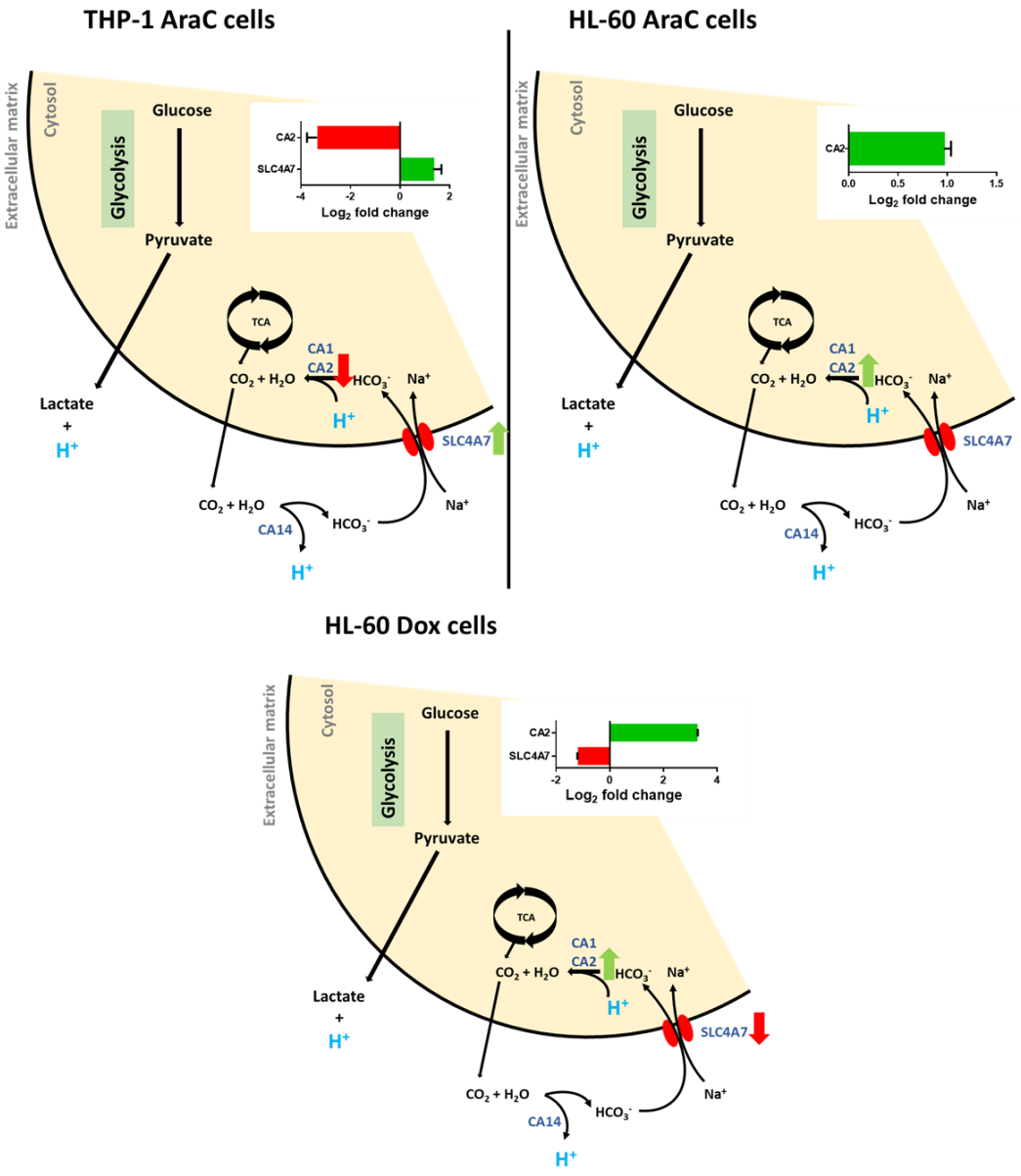

Figure 5.1.10 Protein profile differences of proteins associated with H^+ production, neutralisation, and bicarbonate buffering in THP-1 AraC, HL-60 AraC and HL-60 Dox resistant cells vs. THP-1 and HL-60 parental cells. The protein expression profile of the carbonic anhydrase 2 (CA2), and the sodium bicarbonate cotransporter (SLC4A7) under normoxia were obtained using SILAC-based proteomic experiments described in **section 4.15**. Log_2 fold change values were calculated as explained in **section 4.15** and represented by green colour= protein upregulation; and red= protein downregulation. Data are provided as mean ± SD of n=2 of one representative experiment.

In order to complement the analysis of the effect of resistance acquisition in glycolysis under normoxia, protein profiles regarding the glycolytic enzymes were analysed (shown in **tables 3-10 from Appendix 1**). Firstly, non-significant changes were observed in most of the proteins associated with glycolysis between Dox resistant and their respective parental AML cells. With regard to AraC resistant cells, the increase in glucose consumption observed in HL-60 AraC cells was supported by a slight upregulation of the glucose transporter GLUT1 (1.54-fold up) and a high increase on PGM1 (3.39-fold up) and PGM2 (3.06-fold up) (**Fig. 5.1.11**). On the other hand, THP-1 AraC cells exhibited a downregulation of several proteins associated with glycolysis (see **table 4 from Appendix 1**), including hexokinase 1 (HK1), glyceraldehyde-3-phosphate dehydrogenase (GAPDH), and PKM (**Fig. 5.1.11**), indicating that the observed increase of glucose consumption must be due to mechanisms independent from the overexpression of key glycolytic enzymes (e.g. HK and PKM) or the glucose transporters. In this line, proteins associated with the insulin-dependent glucose uptake via translocation of GLUT4 to the membrane such as insulin-like growth factor-2 mRNA-binding proteins (IGF2BPs) 1, 2 and 3 were upregulated in THP-1 AraC cells compared to THP-1 P cells (1.79, 2.31 and 2.50-fold up, respectively). Moreover, fructose 1,6-bisphosphatase (FBP1), which is a key player of gluconeogenesis and a potent negative regulator of glycolysis, was strongly downregulated (3.65-fold down) (**Fig. 5.1.11**). Of note, it has been reported that the decrease of FBP1 protein expression in glioblastoma cells[320] or the knockdown of FBP1 in HSCs[321] substantially increases glucose uptake and extracellular acidification or glycolysis, respectively. Therefore, we hypothesise that THP-1 AraC cells may counteract the downregulation of glycolytic proteins and enhance glycolytic flux via the downregulation of FBP1. However, this hypothesis would require further experimental substantiation.

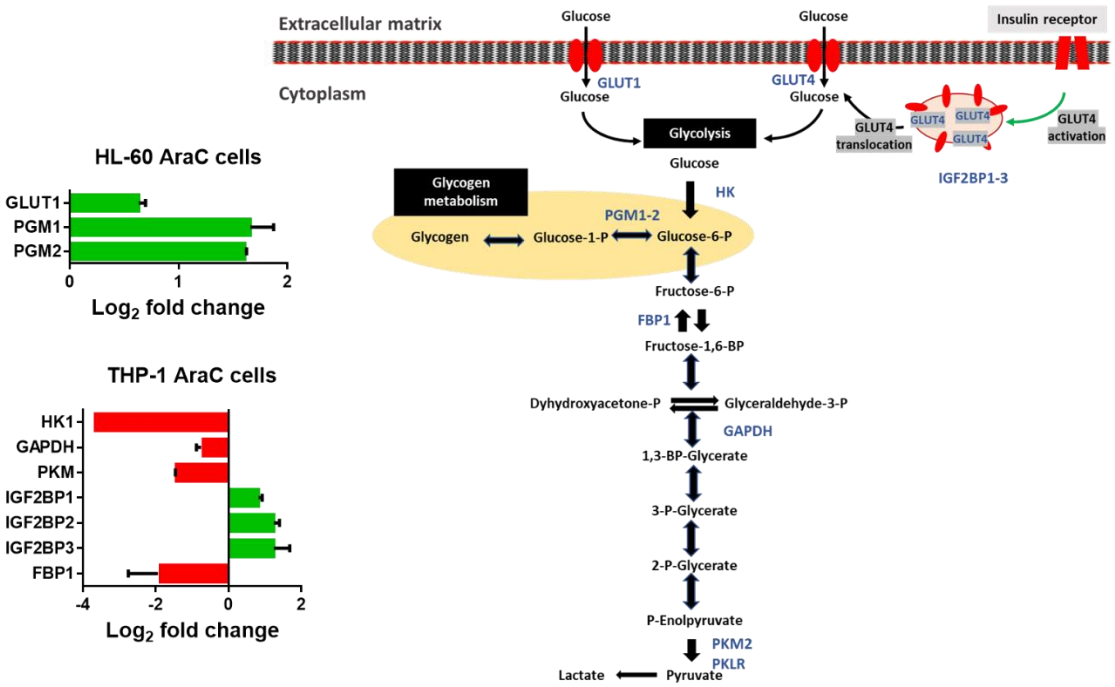

Figure 5.1.11. Differences in the protein profile of enzymes of the glucose metabolism in THP-1 and HL-60 cells upon AraC resistance. The protein expression profile of proteins associated with glucose uptake and transporters, glycolysis, and glycogen metabolism under normoxia was obtained using SILAC-based proteomic experiments described in **section 4.15**. Log_2 fold change values were calculated as explained in **section 4.15** and represented by green colour= protein upregulation; and red= protein downregulation in THP-1 and HL-60 AraC-resistant cells compared to their parental counterparts. Data are provided as mean ± SD of n = 2. Abbreviations: fructose-biphosphate 1, FBP1; glyceraldehyde-3-phosphate dehydrogenase, GAPDH; glucose transporter, GLUT; hexokinase 1 (HK1); insulin like growth factor 2 mRNA binding protein, IGF2BP; phosphoglucomutase, PGM; and pyruvate kinase, PK.

5.1.2.2.3 Doxorubicin resistance reduces mitochondrial respiration capacity in AML cells with high OXPHOS activity, while Cytarabine resistance does not affect mitochondrial respiration capacity in AML cells

Recent studies have revealed the crucial role of mitochondrial metabolism regarding chemotherapeutic treatment and resistance[322]. Therefore, we decided to explore the mitochondrial metabolism of AML resistant cells incubated under normoxia using a

Seahorse XF96 Extracellular Flux Analyser. Briefly, AML parental and resistant cells were incubated in the absence of glucose and sequential injections of oligomycin, CCCP, CCCP+Pyruvate (Pyr), and Rotenone+Antimycin were performed under normoxic conditions in order to measure OCR values and estimate: i) basal mitochondrial respiration, and ii) maximal mitochondrial respiration without and with Pyr.

Figs. 5.1.12.A and B illustrate a significant decrease of basal (87% decrease) and maximal mitochondrial respiration without and with Pyr (83% and 85% decrease, respectively) in THP-1 Dox cells under normoxia compared to their parental counterpart. On the contrary, no differences in basal and maximal mitochondrial respiration were found in HL-60 Dox cells (**Figs. 5.1.12.C and D**). On the other hand, THP-1 AraC resistant cells exhibited the same basal and maximal mitochondrial respiration that THP-1 P cells, while maximal mitochondrial respiration when pyruvate was present was 76% higher in HL-60 AraC resistant cells than in HL-60 P cells (**Fig. 5.1.12.D),** suggesting that pyruvate may constitute an important carbon source for mitochondrial respiration in HL-60 AraC cells. In fact and as explained above, basal mitochondrial respiration was much lower in HL-60 P than in THP-1 P cells. Moreover, the basal OCR exhibited by THP-1 Dox cells was of the same level as the observed in all the HL-60 cell lines. This result suggests that HL-60 Dox cells did not decrease the OCR because its metabolism may not be based on mitochondrial respiration.

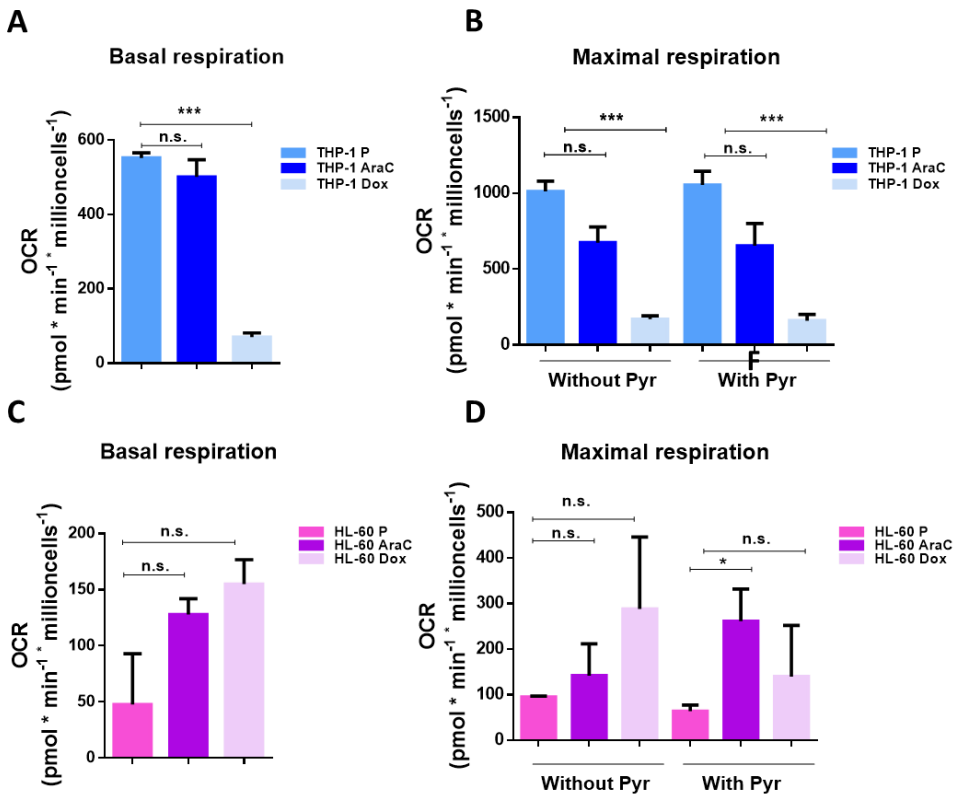

Figure 5.1.12 Basal and maximal mitochondrial respiration of THP-1 and HL-60 cells resistant to AraC or Dox compared to parental cells incubated and measured under normoxic conditions. Oxygen consumption rate (OCR) was measured under normoxia during sequential injection of oligomycin, CCCP, CCCP + Pyruvate and Rotenone + Antimycin in THP-1 and HL-60 parental and resistant cells incubated under normoxic conditions using a XF96 Extracellular Flux Analyser to illustrate basal mitochondrial respiration of THP-1 cells (**panel A**) and of HL-60 cells (**panel C**), maximal mitochondrial respiration without and with pyruvate (Pyr) of THP-1 cells (**panel B**) and HL-60 cells (**panel D**). Data were normalised by cell number. Data are provided as mean ± SD of n = 3 and significance was determined by two-tailed independent sample Student's t-test. Statistically significant differences between THP-1/HL-60 resistant cells and their parental (P) cells are indicated as $p \geq 0.05$ (n.s.), $p < 0.05$ (*), and $p < 0.001$ (***).

Since we only observed differences regarding mitochondrial respiration capacity in THP-1 cell lines incubated under normoxic conditions, we also explored the OCR profile of these cells incubated under hypoxic conditions but measure under normoxic conditions (normoxia) (**Figs. 5.1.13.A-B**). Our results showed that the acquisition of resistance to AraC did not affect the mitochondrial respiration capacity of THP-1 cells neither under normoxic nor under hypoxic incubation conditions. However, as observed under normoxic incubation

conditions, THP-1 Dox cells incubated under hypoxic conditions decreased basal (94% decrease) and maximal mitochondrial respiration rates without and with Pyr (85% decrease for both). These results, on one hand, indicate that THP-1 Dox cells previously incubated under hypoxic conditions maintain the low mitochondrial respiration profile produced by the hypoxic adaptation despite the reoxygenation suffered during the OCR measurement process and, on the other hand, confirm our suspicion that the development of Dox resistance induces an important reprogramming of the mitochondrial function in those cell lines which show an active mitochondrial activity.

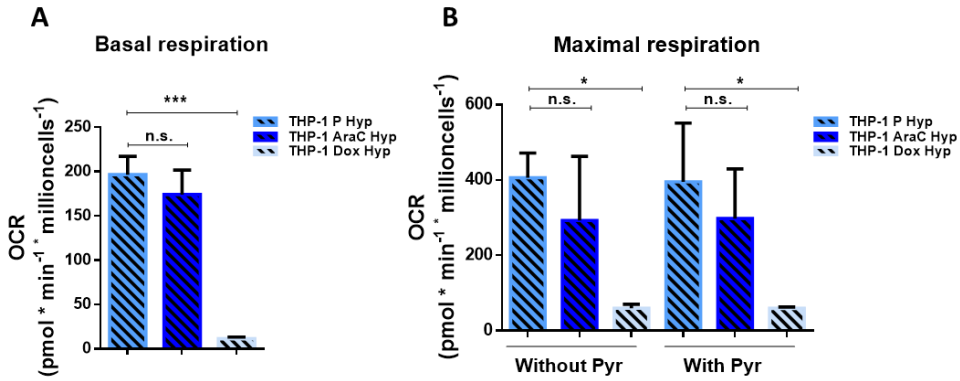

Figure 5.1.13 Basal and maximal mitochondrial respiration measurements of THP-1 resistant to AraC or Dox compared to THP-1 parental (P) cells incubated under hypoxic conditions. Oxygen consumption rate (OCR) measured under normoxia during sequential injection of oligomycin, CCCP, CCCP + Pyruvate and Rotenone + Antimycin in THP-1 parental and resistant cells previously incubated under hypoxic conditions using a XF96 Extracellular Flux Analyser to illustrate basal mitochondrial respiration (**panel A**), and maximal mitochondrial respiration without and pyruvate (Pyr) (**panel B**). Data were normalised by cell number. Data are provided as mean ± SD of n = 3 and significance was determined by two-tailed independent sample Student's t-test. Statistically significant differences between THP-1 resistant cells and THP-1P cells are indicated as $p \geq 0.05$ (n.s.), $p < 0.05$ (*), and $p < 0.001$ (***).

To better understand the changes in the mitochondrial metabolism upon the acquisition of AraC or Dox resistance, we examined the protein expression profile of proteins associated with the TCA cycle and OXPHOS (**Tables 3-10 from Appendix 1**). Results of THP-1 AraC cells

showed a significant upregulation of PDHA1 (1.59 fold) and PDHB (1.55 fold) and a downregulation of the mitochondrial succinate-CoA ligase [ADP-forming] subunit beta (a subunit of ATP-specific succinyl-CoA synthetase, SUCLA2, 1.60-fold). (**Fig. 5.1.14**). With regard to the differences in OXPHOS proteins in THP-1 AraC cells, proteins associated with complex I, including NADH:Ubiquinone oxidoreductase (NDUF) subunits A2, A9, A10, A12, B4, B8 and S1, were significantly downregulated; whereas other complex I proteins (e.g. NDUFB5, NDUFB6, and NDUFS6), were upregulated when compared to THP-1 P cells (**Fig. 5.1.14**), thus suggesting a possible complex I dysfunction (or reorganisation). Moreover, SDHA)which in addition to its role in the TCA cycle is a catalytic subunit of complex II, and the cytochrome oxidase (COX) 5A, 6B1, and 7A2L subunits, which are important for complex IV activity, were also upregulated when compared to THP-1 P cells. Therefore, THP-1 AraC cells seem to counteract the dysfunction of complex I by increasing complex II and complex IV protein expression.

On the other hand, HL-60 AraC cells displayed a downregulation of the mitochondrial aconitate hydratase (ACO2) (1.54-fold down) and an upregulation of mitochondrial succinyl-CoA ligase [GDP-forming] subunit beta (SUCLG2) (2.03-fold up), when compared to HL-60 P cells (**Fig. 5.1.14**). Moreover, the mitochondrial glutamate dehydrogenase (GLUD1) was strongly downregulated (2.65-fold down). All these proteomic changes suggest that TCA cycle activity was decreased in HL-60 AraC cells, while the increase of SUCLG2 could be related to the need of regenerating GTP from GDP. Moreover, a downregulation of proteins associated with complex I (e.g. NDUFA5, NDUFA9, NDUFS2, NDUFS3, and NDUFS8) and complex IV (e.g. COX5B and COX14, COX5B) was observed in HL-60 AraC relative to HL-60 P cells. It is worth mentioning that no changes were observed in complex V (ATPase) proteins in any of the AML cells resistant to AraC (**Fig. 5.1.14**).

Regarding Dox resistant cells, **Fig. 5.1.14** illustrates changes in the TCA cycle and OXPHOS proteins in THP-1 Dox cells. Despite the much lower OCR levels observed in THP-1 Dox relative to THP-1 P cells, THP-1 Dox cells exhibited a general upregulation of proteins associated with TCA cycle, such as citrate synthase (CS), ACO2, oxoglutarate dehydrogenase

(OGDH), SUCLG2 and malate dehydrogenase 2 (MDH2), but also associated with OXPHOS. With regard to OXPHOS, we have observed upregulation of proteins associated with complex I (NDUFA4 and NDUFB6), complex III (cytochrome c, CYCS), and complex IV (COX7C and COX7A2L), although no significant changes were found in proteins associated with complex II and complex V. On the other hand, no changes in proteins associated with TCA cycle and a decrease of two complex I proteins (MT-ND4 and 5) were observed in HL-60 Dox relative to HL-60 P cells.

Taken together, all the results from this section indicate that the development of resistance to AraC may be causing a complex I dysfunction that may be compensated by an enhancement of complex II activity both in THP-1 and in HL-60 cells. Indeed, the total mitochondrial respiration of AraC resistance cells was not affected by the AraC resistance acquisition. Regarding the development of Dox resistance, our results suggest that the acquisition of Dox resistance affects the mitochondrial metabolism especially of cells highly dependent on mitochondrial respiration (i.e. THP-1 cells) (explained in **Section 5.1.2.1**). However, the decrease observed in the mitochondrial respiration of these cells was not accompanied by a decrease in the levels of proteins associated with the TCA cycle and the OXPHOS. In fact, we obtained the opposite result. These results suggest that Dox may be probably affecting the mitochondrial respiration through other processes, thus conditioning the mitochondrial functionality such as the mitochondrial membrane integrity, the mitochondrial dynamic, or the mitochondrial membrane potential. Further studies should be conducted in order to better understand the effect of Dox in the mitochondria of these cells.

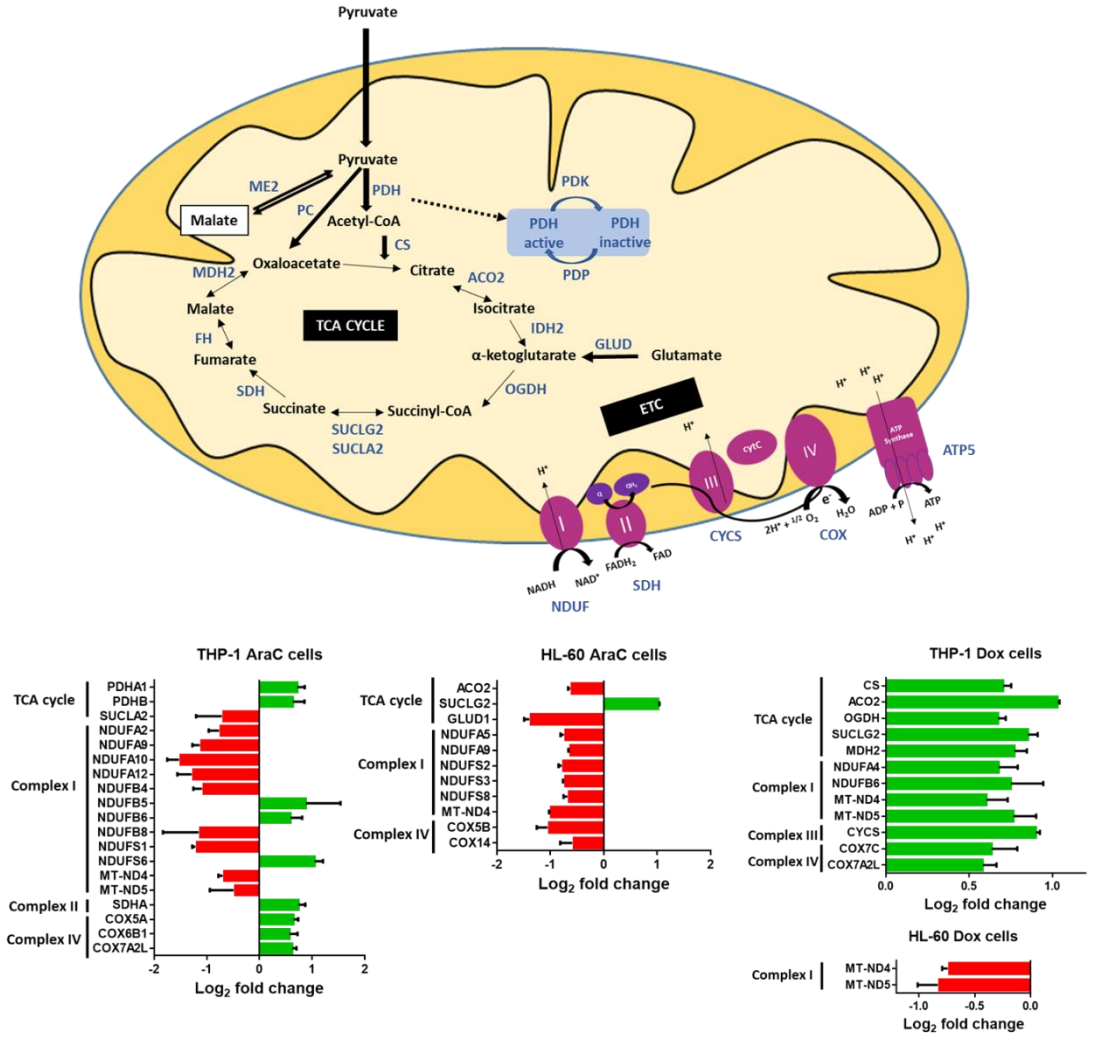

Figure 5.1.14 Differences in the protein profile of THP-1 and HL-60 AML resistant vs. their parental cells regarding TCA cycle and the ETC complexes. Protein expression profiling was obtained using SILAC-based protein mass spectrometry experiments described in **Section 4.15.** Log_2 fold change values were calculated as explained in **Section 4.15** and represented by green color= protein upregulation; and red= protein downregulation. Data are provided as mean ± SD of n=3 of one representative experiment. Abbreviations: aconitase, ACO; ATP synthase, ATP5; citrate synthase, CS; cytochrome C oxidase, COX; cytochrome C, CYCS; electron transport chain, ETC; fumarate hydratase, FH; glutamate dehydrogenase, GLUD; isocitrate dehydrogenase, IDH; malate dehydrogenase, MDH; malic enzyme, ME; mitochondrially encoded NADH:ubiquinone oxidoreductase core subunit, MT-ND; NADH:ubiquinone oxidoreductase, NDUF; oxoglutarate dehydrogenase, OGDH; pyruvate carboxylase, PC; pyruvate dehydrogenase, PDH; pyruvate dehydrogenase kinase, PDK; pyruvate dehydrogenase phosphatase, PDP; succinate-CoA ligase ADP-forming subunit beta, SUCLA2; succinate-CoA ligase GDP-forming subunit beta, SUCLG2; succinate dehydrogenase, SDH; and tricarboxylic acid, TCA.

5.1.2.2.4 Development of resistance to both Cytarabine and Doxorubicin impairs glutamine metabolism

Once glycolytic flux and mitochondrial metabolism were studied, differences in glutamine metabolism between AML parental and resistant cells were determined. As shown in **figure 5.1.15.A**, AraC resistant THP-1 cells significantly increased glutamine consumption by 91% when compared to THP-1 P cells. Regarding to Dox resistance, glutamine consumption was decreased by 40% in HL-60 Dox cells. Glutamine consumption for THP-1 Dox and HL-60 AraC resistant cells did not differ from the glutamine consumption of their parental cells. Therefore, results under normoxia highlighted a pattern of cell line-dependent changes regarding glutamine consumption. With regard to hypoxia, THP-1 resistant cells displayed higher glutamine consumption than THP-1 P cells, whereas THP-1 Dox and both HL-60 resistant cells consumed the same glutamine than their parental counterparts (**Fig. 5.1.15.B**).

To further analyse the alteration in the glutamine metabolism of AML resistant cells, intracellular content of glutamine was measured by HPLC-MS/MS according to the methodology described in **section 4.8.** Only THP-1 AraC cells showed a significantly higher glutamine content when compared to THP-1 P cells under normoxia (**Fig. 5.1.15.C**), whereas all resistant cells displayed the same glutamine intracellular content when compared to parental cells in hypoxia (**Fig. 5.1.15.D**).

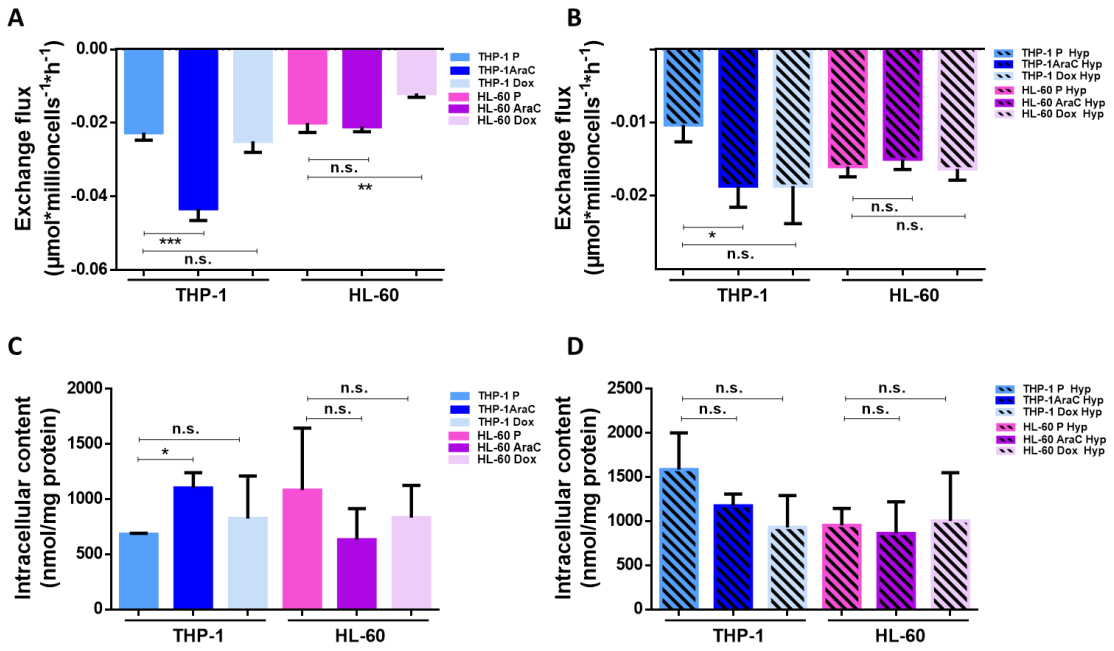

Figure 5.1.15 Effect of AraC and Dox resistance on glutamine metabolism of THP-1 and HL-60 AML cells in normoxic and hypoxic conditions. A and B) Glutamine exchange fluxes of THP-1 and HL-60 parental (P) and AraC or Dox resistant cells under normoxia (**panel A**) and hypoxia (**panel B**). Glutamine consumption rates were obtained under normoxia and hypoxia as described in **section 4.7**. Data were normalised to cell number and incubation time. **C and D)** Glutamine intracellular content of THP-1 and HL-60 P and AraC or Dox resistant cells under normoxia (**panel C**) and hypoxia (**panel D**). Cell pellets were collected to measure the intracellular content of glutamine as described in **section 4.8**. Data were normalised by the extracted protein**.** Data are provided as mean ± SD of n=2 for **panels A and B**, and as mean ± SD of n = 3 of one representative experiment for **panels C and D.** Significance was determined by two-tailed independent sample Student's t-test. Statistically significant differences between THP-1/HL-60 resistant cells and their parental (P) cells are indicated as p≥0.05 (n.s.), p<0.05 (*), p < 0.01 (**), and p < 0.001 (***).

The balance between glutamine anabolism and catabolism depends on the activity of two important enzymes: glutaminase (GLS) and glutamine synthetase (GS). The analysis of the SILAC-based protein mass spectrometry experiments revealed that the protein expression level of GLS was upregulated in both THP-1 AraC (1.51-fold up) and THP-1 Dox cells (3.04-fold up), and the protein expression level of GLUL was also upregulated in THP-1 Dox cells (1.78-fold up) (**Tables 3 and 5 from Appendix 1**). Therefore, the higher glutamine consumption observed in THP-1 AraC but not in THP-1 Dox could be explained by the fact

that the protein expression of GLUL is not upregulated in THP-1 AraC, suggesting that THP-1 AraC compared to THP-1 Dox cells may rely more on external glutamine. With regard to HL-60 resistant cells, no changes were observed in the protein expression of GLS protein while GLUL was downregulated in both resistant cell lines, by a 1.54-fold down for HL-60 AraC and 2.05-fold down for HL-60 Dox. The observed downregulation of GLUL together with the decrease of not only glutamine but also glucose consumption and lactate production suggest that HL-60 Dox cells may slow down its energetic metabolism upon the Dox treatment.

Alltogether, our results reveal that glutamine metabolism was altered in all AML resistant cells, although the changes in protein expression levels did not directly correlate with the glutamine exchange flux. This suggests that there should be other players beyond the expression levels of these two proteins that are taking part in the regulation of the glutamine metabolism. Moreover, the effects on glutamine metabolism were cell line and drug dependent.

5.1.2.2.5 Development of resistance to Cytarabine and Doxorubicin alters the amino acid metabolism of AML cells in a cell line-dependent manner

Since glutamine metabolism was altered in all the AML resistant cells, we decided to explore if the metabolism of the rest of amino acids was also affected upon the acquisition of drug resistance. Therefore, we determined the exchange fluxes and intracellular content of the rest of amino acids and polyamines under normoxia and hypoxia. Results are provided in **tables 11-18 from Appendix 1. Figures 5.1.16 and 5.1.17** illustrate the exchange fluxes and intracellular contents with significant differences between resistant and parental cells under normoxia. We observed that THP-1 AraC cells consumed more asparagine, lysine, methionine, phenylalanine and serine, and produced more glycine and ornithine than THP-1 P cells (**Fig. 5.1.16.A**) whereas HL-60 AraC cells only increased tryptophan consumption when compared to HL-60 P cells (**Fig. 5.1.16.B**) under normoxia. It is worth to note that THP-1 AraC cells also showed a dramatic upregulation of asparagine synthetase (ASNS) (2.3-fold

up) which together with the increased of asparagine consumption is indicative of an increased need of this amino acid by these cells.

Regarding Dox resistant cells, THP-1 Dox cells consumed proline (contrary to the THP-1 P cells that produce it) and consumed less serine than THP-1 P cells (**Fig. 5.1.16**.**A**) whereas HL-60 Dox cells showed a decrease in the consumption of isoleucine, leucine, methionine and phenylalanine, and a decrease in the production of alanine, glutamate, ornithine and proline when compared to HL-60 P cells (**Fig. 5.1.16**.**B**). These results highlighted the fact that the metabolic reprogramming which takes place during the acquisition of resistance to a drug is totally dependent on the original metabolic state of the tumour cells.

Regarding the intracellular content of these metabolites, no differences were found between THP-1 resistant and parental cells (**Table 15 from Appendix 1**). On the other hand, results of HL-60 cells revealed that the intracellular content of methionine, phenylalanine, tyrosine and valine was lower in HL-60 AraC relative to HL-60 P cells whereas no differences were observed between HL60 Dox and HL60 P cells (**Fig. 5.1.17**).

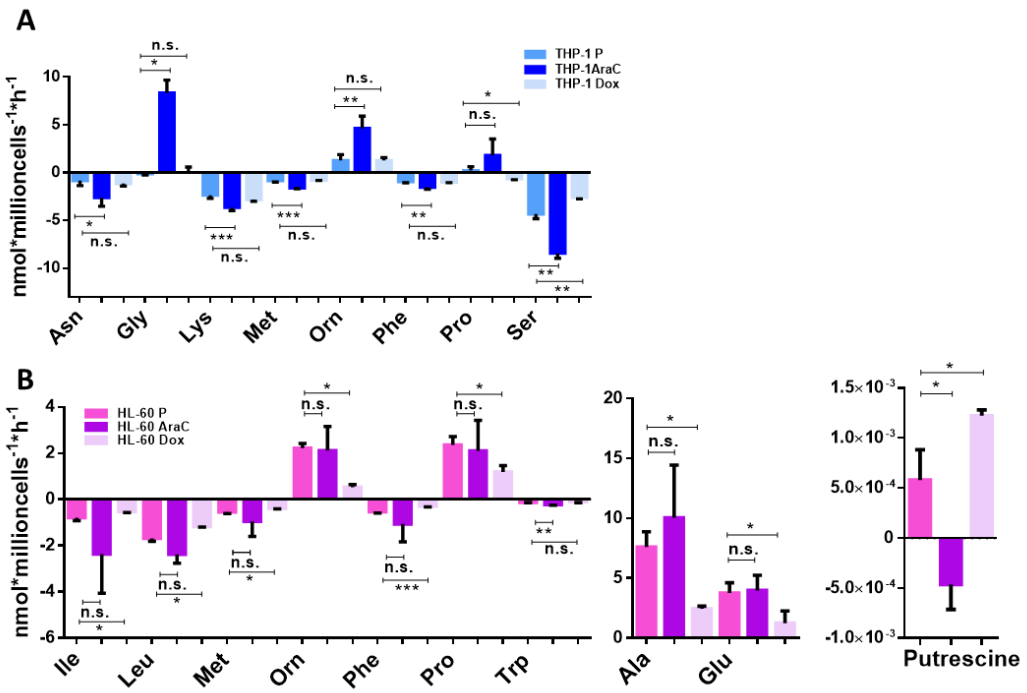

Figure 5.1.16 Exchange fluxes of amino acids and polyamines in THP-1 and HL-60 AML cell lines resistant to AraC and Dox compared to parental cells under normoxic conditions. Amino acids consumption and production rates of THP-1 parental (P) versus THP-1 resistant cells (**panel A**) and of HL-60 P versus resistant cells (**panel B**) under normoxia were estimated by measuring the concentration of amino acids in incubation media using the Absolute IDQ p180 Biocrates kit, as described in **Section 4.8.** Data were normalised to cell number and incubation time. Only amino acids whose exchange flux was significantly different between cells lines were plotted. Data are provided as mean ± SD of n = 3 of one representative experiment and significance was determined by two-tailed independent sample Student's t-test. Statistically significant differences between THP-1/HL-60 resistant cells and their parental (P) cells are indicated as $p \geq 0.05$ (n.s.), $p < 0.05$ (*), $p < 0.01$ (**), and $p < 0.001$ (***). Abbreviations: alanine, Ala; asparagine, Asn; glutamate, Glu; glycine, Gly; isoleucine, Ile; leucine, Leu; lysine, Lys; methionine, Met; ornithine, Orn; parental, P; phenylalanine, Phe; proline, Pro; serine, Ser; and tryptophan, Trp.

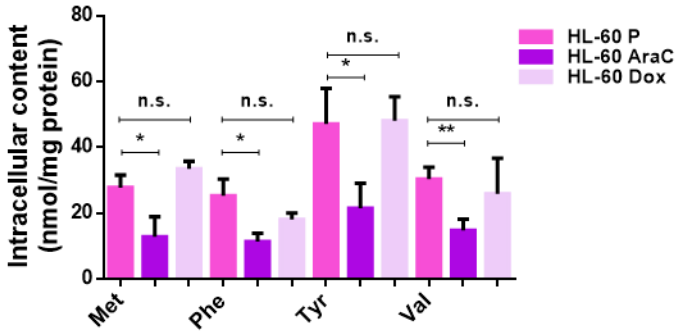

Figure 5.1.17 Intracellular content of amino acids in HL-60 cells resistant to AraC and Dox compared to parental cells under normoxic conditions. Cell pellets were collected to measure the intracellular content of amino acids as described in **Section 4.8**. Data were normalised by the extracted protein. Only amino acids whose content was significantly different between resistant and parental cell lines were plotted. Data are provided as mean ± SD of n = 3 of one representative experiment and significance was determined by two-tailed independent sample Student's t-test. Statistically significant differences between HL-60 resistant and P cells are indicated as $p \geq 0.05$ (n.s.), $p < 0.05$ (*), and $p < 0.01$ (**). Abbreviations: methionine, Met; parental, P; phenylalanine, Phe; tyrosine, Tyr; and valine, Val.

The observed increase in serine consumption and glycine production in THP-1 AraC cells suggests that 1-C metabolism needed for purine synthesis could be enhanced. In fact, the protein profiling results of THP-1 AraC relative to THP-1 P cells showed an upregulation of 1.5-fold in methylenetetrahydrofolate dehydrogenase 1 like (MTHFD1L), which is the mitochondrial isoform responsible of the synthesis of 1-carbon derivatives of tetrahydrofolate involved in the *de novo* synthesis of purine and thymidylate. Furthermore, the increase of asparagine would also increase the production of aspartate, thus allowing the synthesis of carbamoyl aspartate needed in the pyrimidine synthesis. These results suggest that AraC resistant THP-1 cells may be compensating the toxic effect of AraC chemotherapeutic drug by increasing other processes essential for the DNA synthesis. Nevertheless, this hypothesis would require further investigation.

Beyond the increase of components associated with DNA synthesis, it is noteworthy to mention that the anabolism/catabolism of the other amino acids, whose consumption or

production has been increased (i.e. lysine, ornithine, and phenylalanine), implies a NADPH consumption. Moreover, we observed in the protein profiles (**Table 4 from Appendix 1**) that protein levels of G6PD, PGD, malic enzyme (ME) 1 and IDH1, which play an important role in NADPH synthesis, were significantly downregulated by a 1.85, 2.70, 2.14, and 2.51-fold down, respectively) in THP-1 AraC cells when compared to THP-1 P cells. Only the above mentioned MTHFD1L, that produces NADPH together with the 1-C derivative of tetrahydrofolate, was upregulated. Thus, these results suggest that THP-1 AraC cells may have lower NADPH levels. However, this also requires further validation. On the other hand, none of these effects in DNA components or NADPH balance processes were observed in HL-60 AraC cells. Instead, HL-60 AraC cells downregulated MTHFD1L (1.83-fold down) and upregulated IDH1 (1.67-fold up). Therefore, due to the fact that THP-1 P cells had a more active mitochondrial metabolism when compared to HL-60 P cells, we hypothesise that the metabolic changes induced by AraC in our both AML cell lines were dependent on the mitochondrial activity.

Regarding Dox resistant cells, the decrease in the anabolic/catabolic pathways consuming NADPH (i.e. decrease in ornithine and proline synthesis and in phenylalanine catabolism) was the most remarkable alteration among the affected amino acids metabolic pathways in HL-60 Dox cells. In fact, the protein profile (shown in **table 9 from Appendix 1**) showed a significant upregulation of the IDH1 protein level (1.54-fold up) but not in the others NADPH-producer enzymes. With regard to THP-1 Dox cells, the huge decrease in OCR observed in these cells did not have an effect on the amino acid metabolism, although many of them are TCA cycle intermediates precursors. Curiously, proline was consumed instead of being produced, so that a reduction of proline synthesis from glutamate with a concomitant lower NADPH consumption would be expected. Ultimately, THP-1 Dox cells experienced a decrease in the protein expression levels of PGD (2.35-fold down), ME1 (1.85-fold down) and IDH1 (1.96-fold down), contrary to what was observed in HL60 Dox cells.

Regarding the results of exchange fluxes and intracellular content of amino acids and polyamines under hypoxia, both THP-1 resistant cells exhibited an increase of alanine production, thus indicating that there may be an increase of the production of α-

ketoglutarate for TCA cycle fuelling without release of ammonia to the cytosol (**Fig. 5.1.18.A**). In this sense, the intracellular content of alanine was higher in THP-1 resistant when compared to THP-1 P cells (**Fig. 5.1.18.B**). Moreover, the consumption of isoleucine, lysine and serine was higher in THP-1 AraC cells than in THP-1 P cells. In brief, the catabolism of these amino acids generates acetyl-CoA from isoleucine and lysine, and pyruvate from serine. Thus, these results suggest that THP-1 AraC cells may be fuelling the TCA cycle through the synthesis of acetyl-coA, pyruvate and α-ketoglutarate. In the case of THP-1 Dox cells, a higher ornithine production, and putrescine and spermidine consumptions were observed (**Fig. 5.1.18.A**), suggesting that ornithine decarboxylase (ODC) may be degraded in THP-1 Dox cells under the effect mediated by hypoxia. In fact, the results of the protein profile highlighted a downregulation of 1.56-fold down in the enzyme NAD(P)H quinone oxidoreductase 1 (NQO1), which binds and stabilises the ODC enzyme[323]. Finally, we observed that phenylalanine intracellular content was higher in THP-1 AraC cells and lower in THP-1 Dox cells when compared to parental cells (**Fig 5.1.18.B**). Unfortunately, we do not have any plausible explanation for this last result, and specific studies would be needed to properly understand the role of phenylalanine under hypoxia in these resistant cells.

On the other hand, no differences were observed in the exchange fluxes of amino acids and polyamines of HL-60 resistant compared with HL-60 P cells (**Table 14 from Appendix 1**). However, the intracellular levels of arginine, asparagine and lysine were lower in HL-60 AraC cells, and only arginine content was lower in HL-60 Dox cells, both when compared to HL-60 P cells (**Fig. 5.1.18.C**). In this case, specific studies would be also needed to better understand the role that these amino acids play in the metabolism of our HL-60 resistant cells under hypoxia.

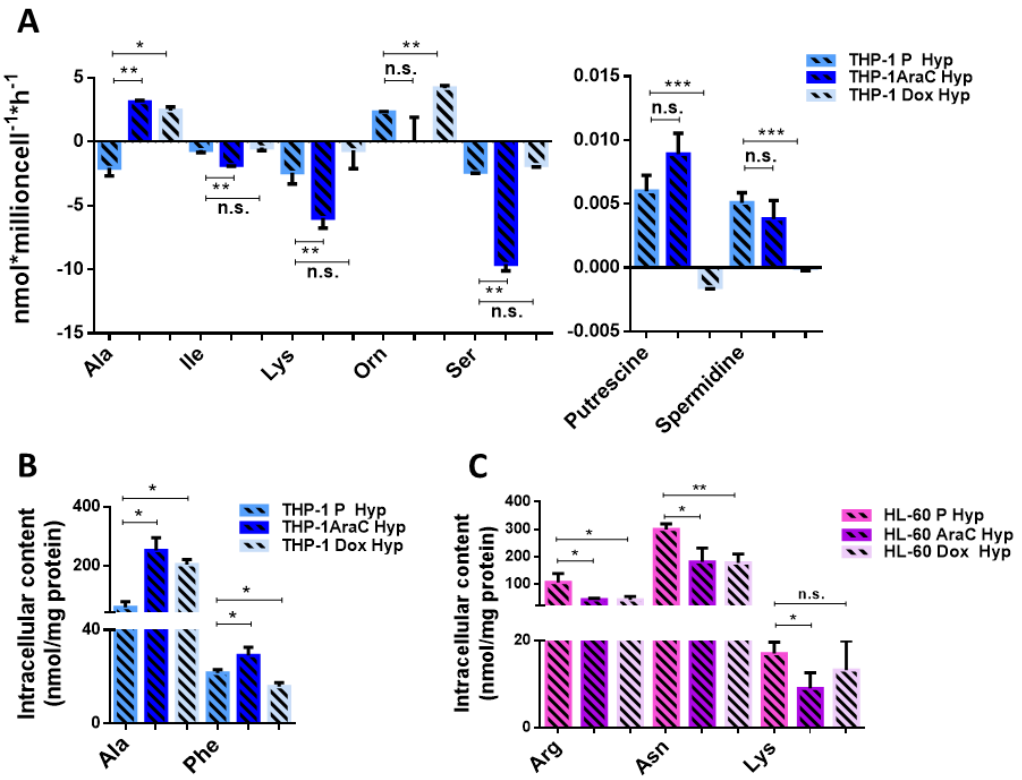

Figure 5.1.18 Exchange fluxes and intracellular content of amino acids and polyamines in THP-1 and HL-60 AML cell lines resistant to AraC or Dox compared to parental cells under hypoxic conditions. A) Amino acids consumption and production rates of THP-1 parental (P) versus THP-1 resistant cells in hypoxia estimated after measuring the concentration of amino acids using the Absolute IDQ p180 Biocrates kit in incubation media, as described in **Section 4.8.** Data were normalised to cell number and incubation time. **B and C)** Intracellular content of amino acids and polyamines between THP-1 P and its resistant cells (**panel A**) and between HL-60 P and its resistant cells (**panel B**) in hypoxia. Cell pellets were collected to measure the intracellular content of amino acids as described in **Section 4.8**. Data were normalised by the extracted protein. Only amino acids whose exchange fluxes or intracellular content were significantly different between resistant and their parental cells were plotted. Data are provided as mean ± SD of n = 3 of one representative experiment and significance was determined by two-tailed independent sample Student's t-test. Statistically significant differences between THP-1/HL-60 resistant cells and their parental (P) cells are indicated as p≥0.05 (n.s.), p<0.05 (*), p<0.01 (**), and p<0.001 (***). Abbreviations: alanine, Ala; arginine, Arg; asparagine, Asn; isoleucine, Ile; lysine, Lys; ornithine, Orn; phenylalanine, Phe; and serine, Ser.

5.1.2.2.6 Development of Cytarabine resistance enhances 1C-metabolism and serine synthesis pathway in AML cell lines

As pointed out above, a significant increase in serine and methionine consumption and glycine production was observed in THP-1 AraC cells. Moreover, an upregulation of MTHFD1L responsible of the synthesis of 1-C derivatives of tetrahydrofolate involved in the *de novo* synthesis of purine and thymidylate was also observed. For this reason, we hypothesised that both the SSP and 1-C metabolisms could be upregulated due to the acquisition of AraC resistance. In order to confirm this hypothesis, the protein expression profile of proteins involved in these pathways was further analysed in THP-1 and HL-60 AraC cells (see **Tables 3-4 from Appendix 1**).

Interestingly, proteins involved in the SSP including phosphoglycerate dehydrogenase (PHGDH) and phosphoserine aminotransferase 1 (PSAT1) were significantly upregulated in THP-1 AraC cells by a of 1.72 and 2.03-fold up, respectively (**Fig. 5.1.19**). Moreover, thymidylate synthetase (TYMS), a protein involved in 1-C metabolism and DNA synthesis, was also upregulated (2.01-fold up). Moreover, other proteins associated with SSP and 1-C metabolisms such as phosphoserine phosphatase (PSPH), SHMT2 and dihydrofolate reductase (DHFR) were slightly upregulated (1.38, 1.37 and 1.39-fold up, respectively) (**data not shown**), although their upregulation was not considered as significant due to the fact that protein expression values were below the threshold selected for SILAC data analysis (FD≥1.5) (explained in **Section 4.15**). Regarding HL-60 AraC cells, only TYMS expression was upregulated by a 2.24-fold when compared to HL-60 P cells (**Fig. 5.1.19**).

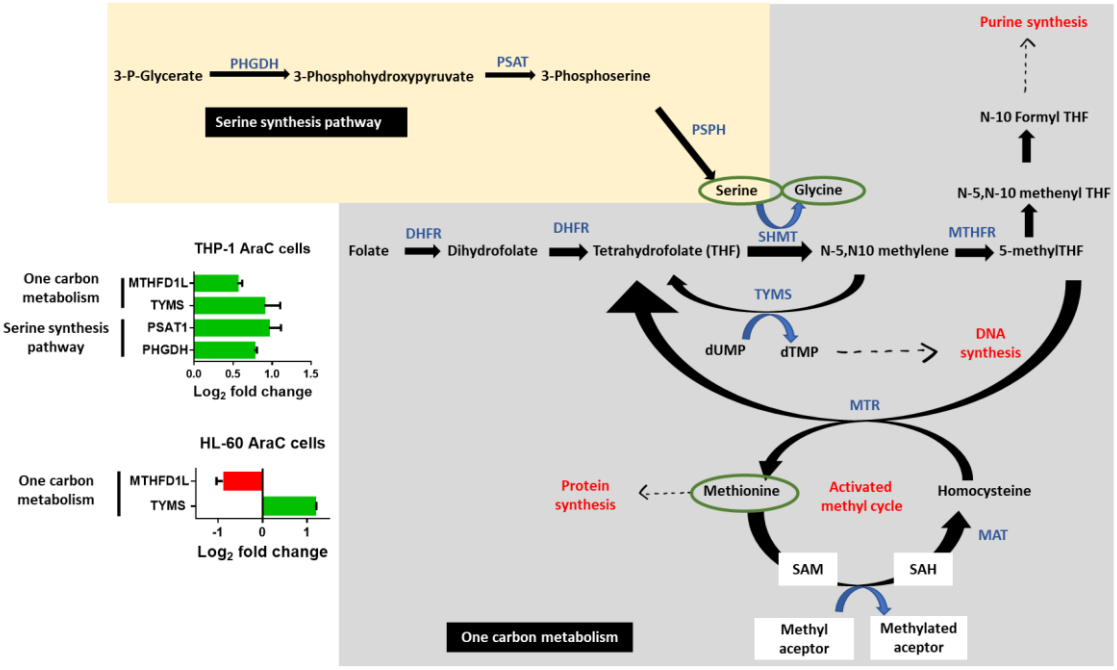

Figure 5.1.19 Protein profiles of THP-1 AraC and HL-60 AraC compared to their parental counterparts regarding serine synthesis pathway and 1-C metabolism. Protein expression profiling was obtained using SILAC-based protein mass spectrometry experiments described in **Section 4.15.** Log_2 fold change values were calculated as explained in **Section 4.15.** Significant proteins changed were represented by green color= protein upregulation. Data are provided as mean ± SD of n=3 of one representative experiment. Abbreviations: dihydrofolate reductase, DHFR; methionine adenosyltransferase, MAT; methylenetetrahydrofolate reductase, MTHFR; 5-methyltetrahydrofolate-homocysteine methyltransferase, MTR; phosphoglycerate dehydrogenase, PHGDH; phosphoserine aminotransferase 1, PSAT1; phosphoserine phosphatase, PSPH; S-adenosylhomocysteine, SAH; S-adenosylmethionine, SAM; serine hydroxymethyltransferase 2, SHMT; and thymidylate synthetase, TYMS.

According to these results, we next studied if the inhibition of enzymes involved 1-C metabolism could be used as a therapeutic strategy. Therefore, we conducted a cell viability assay after the incubation of AML parental and AraC resistant cells with methotrexate (DHFR inhibitor) and pemetrexed (TYMS and DHFR inhibitor). As shown in **Fig. 5.1.20,** both parental and AraC resistant cells were similarly sensitive to the presence of these inhibitors, indicating that these inhibitors do not have a higher effect in AraC resistant cells. Moreover, it is worth mentioning that IC50 concentrations were indeed inside the concentration range

to be used for AML treatment, especially for THP-1 cells, where the obtained IC50 values were 2500 and 10 times lower than for HL-60 cells for methotrexate and pemetrexed, respectively. Although specific studies should be conducted to confirm this hypothesis, it is possible that the higher effect of methotrexate in THP-1 P and AraC resistant cells might be related to their higher mitochondrial activity.

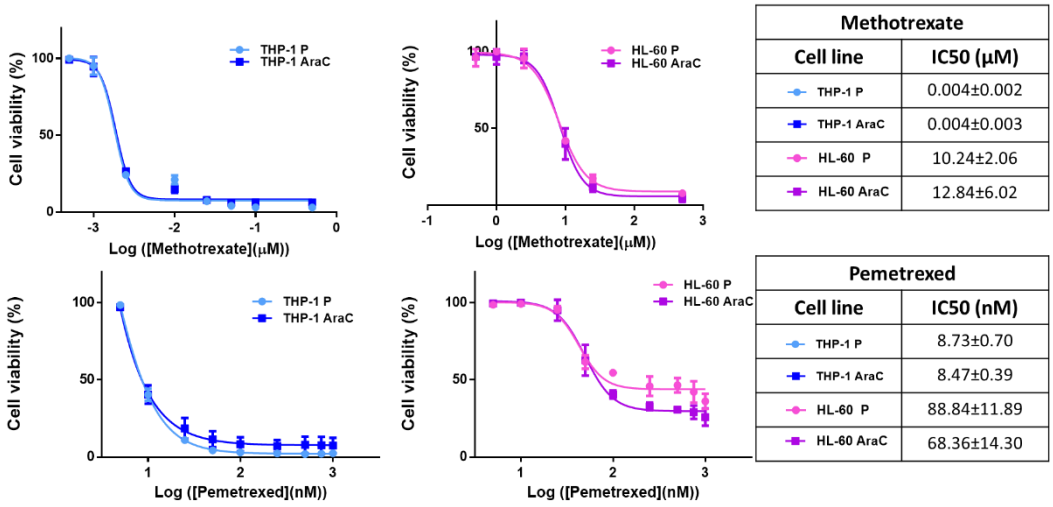

Methotrexate	
Cell line	IC50 (μM)
THP-1 P	0.004±0.002
THP-1 AraC	0.004±0.003
HL-60 P	10.24±2.06
HL-60 AraC	12.84±6.02

Pemetrexed	
Cell line	IC50 (nM)
THP-1 P	8.73±0.70
THP-1 AraC	8.47±0.39
HL-60 P	88.84±11.89
HL-60 AraC	68.36±14.30

Figure 5.1.20 Effect of Methotrexate and Pemetrexed on the cell viability of THP-1 and HL-60 AML cells parental and resistant to AraC. Cells were incubated for 72 hours with DMSO (vehicle control) or with increasing concentrations of the corresponding inhibitor. IC50s are on the left side of the figure and were calculated as described in **Section 4.3**. Data are provided as mean ± SD of n=3.

5.1.2.2.7 Development of drug resistance modifies the intracellular content of acylcarnitines in AML cell lines without showing correlation with fatty acid oxidation-dependent mitochondrial respiration

It has been recently described that FA metabolism influences relevant aspects of AML biology including acclimatisation to the microenvironment and response/resistance to chemotherapeutics[260]. Previous studies have supported the idea that higher intracellular levels of acylcarnitines (ACs) correlate with a more active FAO[324]. Therefore, intracellular levels of ACs were examined between AML parental and resistant cells under normoxic and hypoxic conditions in order to study the potential differences regarding FAO (shown in **Tables 19-22 from Appendix 1**). No differences in the ACs intracellular content were found for THP-1 P and resistant cells under normoxic conditions. However, under hypoxia, THP-1 cells resistant to AraC and Dox showed a lower intracellular content of 25 and 30% of the forty analysed ACs, respectively (**Fig. 5.1.21**). Regarding HL-60 resistant cell lines under normoxia, HL-60 AraC cells showed a decrease in the intracellular content (28% of the analysed ACs), whereas HL-60 Dox cells increased 20% of the analysed ACs, both compared to HL-60 P cells (**Fig. 5.1.22.A**). Moreover, both HL-60 resistant cell lines displayed an overall decrease of the intracellular content of the analysed ACs under hypoxia (**Fig. 5.1.22.B**). Specifically, HL-60 AraC cells exhibited a much bigger reduction of ACs intracellular content (from 28% of the analysed ACs under normoxia to 98% under hypoxia), and HL-60 Dox cells decreased the intracellular content of the ACs that were found to be increased under normoxia (from 20% increased ACs under normoxia to 15% decreased ACs under hypoxia) (**Fig. 5.1.22.B**). These results indicate a less reliance on FAO of HL-60 Dox cells when compared to HL-60 P cells under normoxia. With regard to hypoxia, all our resistant AML cell lines are less reliant on FAO than their parental counterparts.

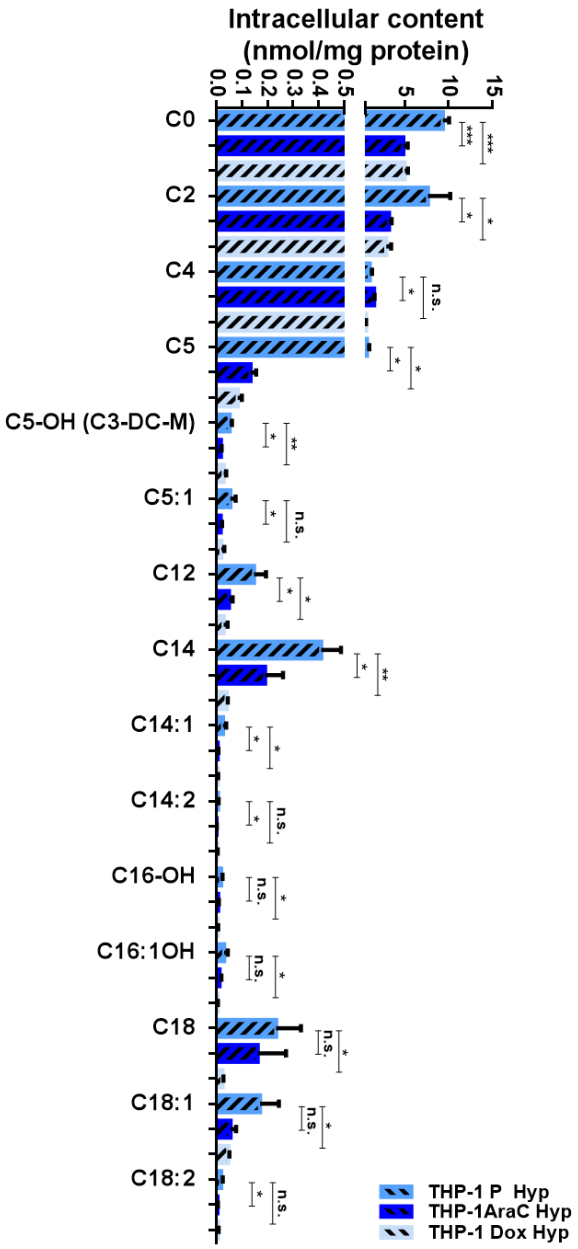

Figure 5.1.21 Intracellular content of acylcarnitines in THP-1 AraC and Dox resistant cell lines compared to THP-1 parental cells under hypoxic conditions. Cell pellets were collected to measure the intracellular content of acylcarnitines as described in **Section 4.8**. Data were normalised by the extracted protein. Data are provided as mean ± SD of n = 3 of one representative experiment and significance was determined by two-tailed independent sample Student's t-test. Statistically significant differences between THP-1 resistant and parental (P) cells are indicated as $p \geq 0.05$ (n.s.), $p < 0.05$ (*), $p < 0.01$ (**), and $p < 0.001$ (***).

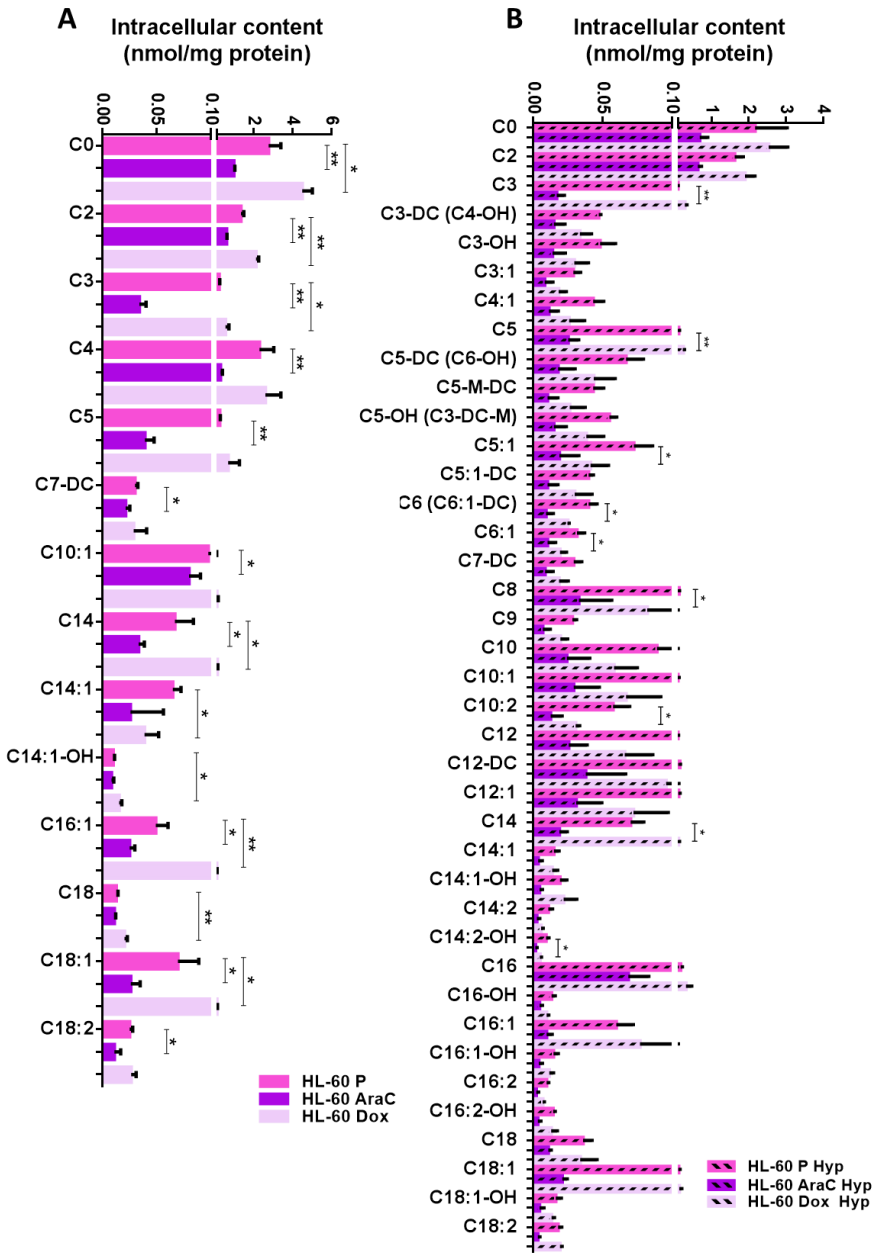

Figure 5.1.22 Intracellular content of acylcarnitines in HL-60 AraC and Dox resistant cell lines compared to HL-60 parental cells under normoxic and hypoxic conditions. Cell pellets were collected to measure the intracellular content of acylcarnitines under normoxia (**panel A**) and hypoxia (**panel B**). as described in **Section 4.8**. Data were normalised by the extracted protein. Data are provided as mean ± SD of n = 3 of one representative experiment and significance was determined by two-tailed independent sample Student's t-test. Only statistically significant differences between HL-60 resistant and parental (P) cells are indicated as p<0,05 (*), p<0.01 (**), and p<0.001 (***).

Next, we decided to investigate the mitochondrial respiration dependency on FAO of AML parental and resistant cells by using the Mito Fuel Flex Test (described in **Section 4.12**). Despite the differences observed in ACs, **Fig. 5.1.23** shows that non-significant differences were observed regarding the mitochondrial respiration dependency on FAO for any of the AML resistant cell lines when compared to their parental ones, neither under normoxic nor in hypoxic incubation conditions.

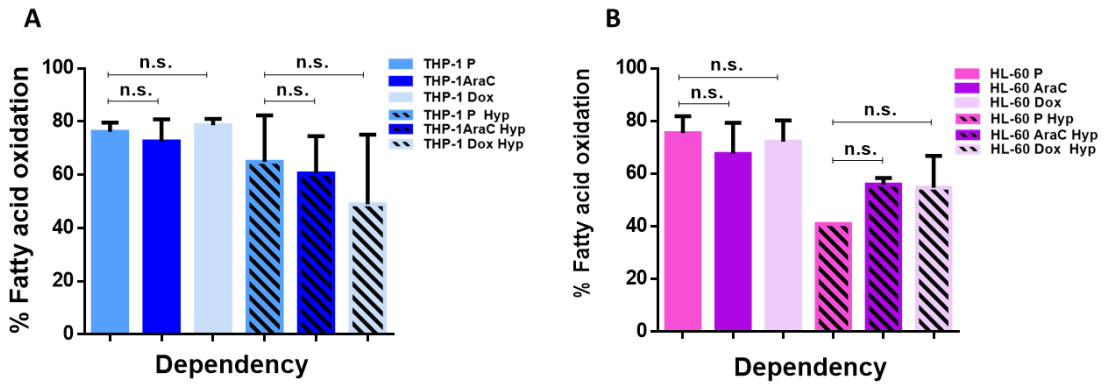

Figure 5.1.23 Fatty acid contribution to mitochondrial respiration of THP-1 and HL-60 AML cell lines resistant to AraC or Dox relative to their parental (P) counterparts. Oxygen consumption rate (OCR) measured under normoxia during sequential injection of Etomoxir, BPTES + UK5099, and oligomycin in THP-1 and HL-60 parental and resistant cells incubated under both normoxic or hypoxic incubation conditions using a Seahorse XF96 Extracellular Flux Analyser. Cells were first incubated with DMEM media in the presence of glucose and glutamine. Data normalised to protein concentration. Data are provided as mean± SD of n = 3 and significance was determined by two-tailed independent sample Student's t-test. Statistically significant differences between THP-1/HL-60 resistant cells and their parental (P) cells are indicated as p≥0.05 (n.s.).

Furthermore, protein profiles under normoxia were analysed using the data of the **tables 3-10 from Appendix 1** in order to ensure the correlation between the intracellular levels of ACs and protein levels of proteins related to FAO process. Unfortunately, we could not observe any correlation between the intracellular levels of ACs and protein changes under normoxia. As an example, HL-60 AraC cells showed upregulation of proteins associated with FAO such as the two isoforms of the enzyme acetyl-CoA-acetyltransferase (ACAT1 and 2), although these cells had lower intracellular content of ACs, thus suggesting a less active FAO

of HL-60 AraC compared to HL-60 P cells. Therefore, these results together with the results obtained from the Mito Fuel Flex Test lead us to question whether a correlation between ACs intracellular levels and FAO exists.

5.1.2.2.8 Potential metabolic and non-metabolic targets identified by protein expression analysis (SILAC)

We decided to follow the same approach proposed by Ong *et al.* and use the SILAC proteomic data of our AraC and Dox resistant cells under normoxia to identify new putative targets that could be exploited to treat AML disease when AraC and Dox resistance has emerged[325]. In fact, we focus our attention on those upregulated proteins that can be further inhibited to reduce the cell viability of AML resistant cells. Therefore, an analysis of which pathways showed the highest number of upregulated proteins, in terms of drug-specific (common for both AraC or Dox resistant AML cells) or cell-line-specific (common for both THP-1 or HL-60 resistant cell lines) , was further accomplished using PANTHER database system and selecting the pathway gene ontology.

From the total list of pathways containing the most upregulated proteins in the AML resistant versus parental cells (shown in **tables 23-26 from Appendix 1**), Wnt signaling pathway, an ancient pathway that regulates development and stemness, was the most upregulated regarding the altered AraC resistance-specific pathways (18% of proteins upregulated in THP-1 AraC and 6% in HL-60 AraC cells) (**Table 5.1.1**). Next, p53 pathway was the second most upregulated pathway (19 and 9% of proteins upregulated in THP-1 and HL-60 AraC cells, respectively). It is noteworthy to mention that the only proteins associated with p53 pathway that were upregulated in both AraC resistant cells were the C-Terminal Binding Protein 1 (CTBP1) in regard to Wnt signaling pathway, and cyclin dependent kinase 1 (CDK1) and ribonucleotide reductase regulatory subunit M2 (RRM2) for p53 pathway. However, we could not find any pathway with upregulated proteins that was specific for the acquisition of Dox resistance.

Regarding the cell line-specific pathways with upregulated proteins, we found blood coagulation and *de novo* purine biosynthesis to be specific for THP-1 resistant cell lines (**Table 5.1.1**). In this case, the only common upregulated proteins were the thrombomodulin (THBD) and the Amyloid Beta Precursor Protein (APP), both related with blood coagulation, and non-common upregulated proteins were found for the *de novo* purine biosynthesis pathway.

Finally, cholesterol biosynthesis and androgen/estrogen/progesterone biosynthesis processes emerged to be specific for HL-60 resistant cells. In addition, both HL-60 resistant cell lines showed a common upregulation of squalene synthase (FDFT1) involved in cholesterol biosynthesis process, and the sterol O-acyltransferase 1 (SOAT1) related with the androgen/estrogen/progesterone biosynthesis.

Considering the resultant proteins from the pathway gene ontology PANTHER analysis (**Table 5.1.1**), we chose to study the antiproliferative effect of YM-63501, an inhibitor of FDFT1 (that should be specific for HL-60 resistant cell lines), in all the AML resistant and parental cells. For instance, a reduction of cell viability was found for all the resistant and parental cells by inhibiting the FDFT1 protein (**Fig. 5.1.24**). However, we could not observe the expected selective effect on HL-60 resistant cells, and even THP-1 Dox cells showed the lowest IC50 value among all the cell lines. Unfortunately, we could not perform studies inhibiting the rest of the highlighted proteins (shown in **Table 5.1.1**). Therefore, these studies would be required to validate if their inhibitions could selectively inhibit the proliferation of AML resistant cells.

Table 5.1.1 Main drug resistance or cell line -specific pathways upregulated under normoxia. Upregulated proteins with a FD≥1.5 (log_2 fold change=0.58) obtained from proteomic profiling (SILAC) data of THP-1 and HL-60 resistant relative to parental cells were analysed using Panther classification systems for pathways selection. Data are provided as mean ± SD of n=2. Abbreviations: Non-detected (N.D.).

	PATHWAYS	COMMON PROTEINS	CELL LINES			
			THP-1 AraC		HL-60 AraC	
			Mean Log2 fold change	SD Log2 fold change	Mean Log2 fold change	SD Log2 fold change
AraC-resistance specific	Wnt signalling pathway	C-Terminal Binding Protein 1 (CTBP1)	0.83	N.D.	0.83	0.07
	p53 pathway	Cyclin dependent kinase 1 (CDK1)	0.72	0.26	1.02	0.04
		Ribonucleotide reductase regulatory subunit M2 (RRM2)	1.39	0.01	0.70	0.12
THP-1-cell line specific			THP-1 AraC		THP-1 Dox	
			Mean Log2 fold change	SD Log2 fold change	Mean Log2 fold change	SD Log2 fold change
	Blood coagulation	Amyloid Beta Precursor Protein (APP)	2.15	N.D.	0.94	N.D.
		Thrombomodulin (THBD)	2.69	1.40	0.68	0.39
	de novo purine biosynthesis	Non-common proteins				
HL-60-cell line specific			HL-60 AraC		HL-60 Dox	
			Mean Log2 fold change	SD Log2 fold change	Mean Log2 fold change	SD Log2 fold change
	Cholesterol biosynthesis	Squalene synthase (FDFT1)	1.36	0.07	0.68	0.02
	Androgen/estrogen/progestorene byosinthesis	Sterol O-acyltransferase 1 (SOAT1)	0.79	N.D.	0.93	N.D.

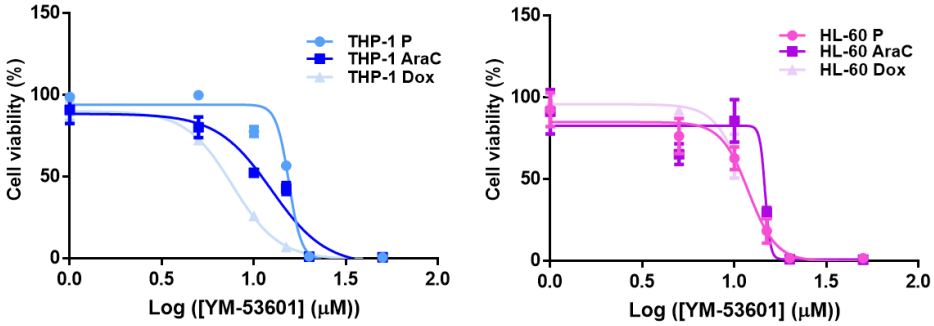

Cell line	IC50 (μM)
THP-1 P	15.7±1.3
THP-1 AraC	11.0±2.4
THP-1 Dox	7.2±0.5 (*)

Cell line	IC50 (μM)
HL-60 P	11.2±1.9
HL-60 AraC	15.1±5.8
HL-60 Dox	11.3±0.9

Figure 5.1.24 Effect of YM-53601 inhibitor on the cell viability of AML parental and resistant cells. Cells were incubated for 72 hours with DMSO (vehicle control) or with increasing concentrations of the inhibitor YM-3601. IC50s were calculated as described in **Section 4.3**. Data are provided as mean ± SD of n=3 and significance was determined by two-tailed independent sample Student's t-test.

5.2 Unveiling metabolic remodelling associated with BCR-ABL1-independent imatinib resistance in chronic myeloid leukaemia (CML) KU812 cells

5.2.1 Introduction and scope

Chronic myeloid leukaemia (CML) is a clonal bone marrow stem cell cancer characterised by an increased proliferation of myeloid cells within the bone marrow. This disease progresses typically in three phases, chronic phase, accelerated phase and blast crisis, which behaves like an acute myeloid leukaemia and eventually leads to death of the patient. From all the newly diagnoses of leukaemia in adults, CML accounts for 15% of the cases[63]. As mentioned above, four TKIs (imatinib, nilotinib, dasatinib and bosutinib) constitute the first line of CML treatment[63] in chronic phase and, especially, imatinib has proven to be highly effective. However, up to 25% of CML patients develop TKI resistance during therapy despite initial complete remission[326]. Hence, there is an urgent need for additional treatment strategies for patients who acquired resistance. Previous studies have reported the link between metabolic reprogramming and drug resistance acquisition in the BCR-ABL1-dependent CML cells resistant to imatinib[195,286–288,327]. However, to date, only few studies have investigated the metabolic rewiring associated with BCR-ABL1- independent imatinib resistant CML cells.

This chapter focuses on understanding the metabolic reprogramming of CML cells during acquisition of BCR-ABL1-independent imatinib resistance. To this end, we first generated from KU812 parental cells (here referred as KU812 P) an imatinib-resistant CML cell model line (here referred as KU812 ImaR) by prolonged exposure to sub-lethal doses of imatinib. Next, similarly to **Chapter I**, a multi-OMIC characterisation and comprehensive comparison of the metabolic phenotype of KU812 ImaR cells and KU812 P cells, both under normoxic and hypoxic conditions, was performed in order to achieve the main objectives of this chapter: i) a better knowledge of the metabolic adaptation underlying BCR-ABL1-independent imatinib resistance in CML, and ii) the identification of metabolic

vulnerabilities associated with resistance development that can be further validated and exploited for new therapies in CML treatment.

5.2.2 Results

5.2.2.1 Development and characterisation of imatinib-resistant KU812 cell line

In order to investigate the metabolic rewiring underlying BCR-ABL1-independent imatinib resistance in CML, an imatinib-resistant cell line (here referred as KU812 ImaR or TKI-resistant) was developed using KU812 cell line (here referred as KU812 parental or KU812 P), as described in detail in **section 4.2.** The process of developing the KU812 ImaR is illustrated in **figure 5.2.1**.

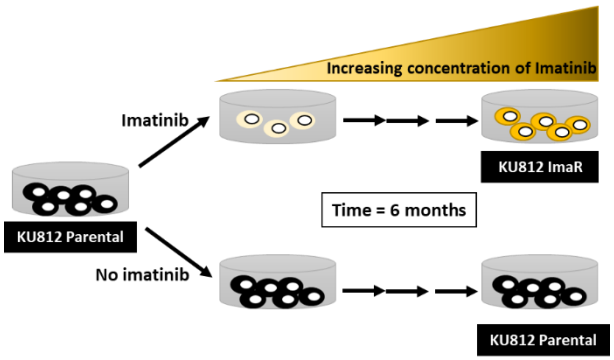

Figure 5.2.1 Graphical description of the generation of an imatinib-resistant KU812 cell line (KU812 ImaR) under normoxia by exposure to increasing concentrations of imatinib. For details regarding the concentrations used see Materials and Methods (**section 4.2**). Viability was controlled every second day. Acquisition of resistance was verified every 3 weeks until resistance was obtained.

The antiproliferative effect of imatinib resistance was verified as described in **section 4.3** and the IC_{50} values of imatinib for both KU812 P and KU812 ImaR were determined (**Fig. 5.2.2**). Results showed that KU812 ImaR cells enhanced their tolerance to imatinib by more than two orders of magnitude when compared to KU812 P cells (drug resistance index (DRI)=350). The IC_{50} values for KU812 P and KU812 ImaR cells were also determined for

dasatinib and nilotinib (TKIs of second generation). Likewise, KU812 ImaR cells showed to be also resistant to these second generation TKIs when compared to the parental counterpart ($DRI_{Dasatinib}$>8300 and $DRI_{Nilotinib}$=1280) (**Fig. 5.2.2**).

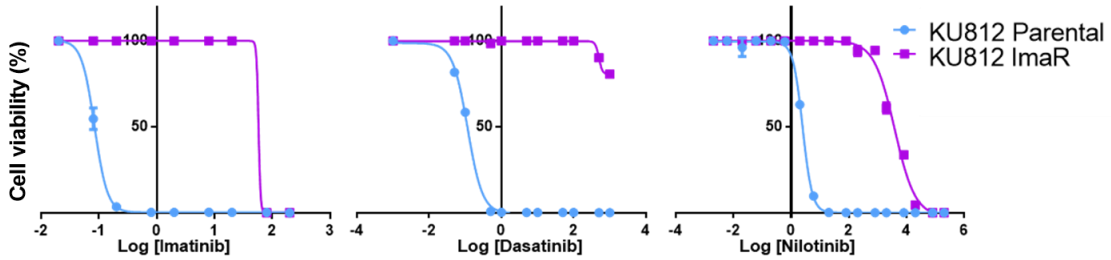

Cell line	Imatinib (µM)	Dasatinib (nM)	Nilotinib (nM)
KU812 P	0.08±0.01	0.12±0.01	2.50±0.45
KU812 ImaR	28.00±8.61	>1000	3200±494

Figure 5.2.2 Effect of three different clinically relevant tyrosine kinase inhibitors (TKIs) on the viability of KU812 parental and KU812 imatinib-resistant cells. KU812 Parental (P) and Imatinib-resistant (ImaR) cells were incubated 72 hours with DMSO (vehicle control) or increasing concentrations of the corresponding inhibitor. Viability of the cells at each concentration was determined and the half-maximal inhibitory concentrations (IC_{50}) were calculated as described in **section 4.3.** Data are provided as mean±SD of n=3.

In order to exclude the involvement of gatekeeper BCAR-ABL1 mutations during the generation of KU812 ImaR cells, relevant exons of ABL1 were sequenced as described in **section 4.18.** No sequence changes were detected in any of the relevant exons (covering the loci of the known gatekeeper mutations G250, Y253, E255, D276, F311, T315, F317, M351 and F359) (**Fig. 5.2.3**). Moreover, an upregulation of BCR-ABL1 expression as a potential resistance mechanism of the KU812 ImaR cell line could be precluded by SILAC-based protein mass spectrometry as KU812 ImaR cells show a downregulation of BCR-ABL1 expression compared to the parent cell line (4-fold down). All together, these results indicate that a resistant cell line was successfully generated, KU812 ImaR cells show significantly increased IC_{50} concentrations for to different TKIs and that the resistance

developed was neither associated with a mutation in the kinase domain nor with BCR-ABL1 protein overexpression.

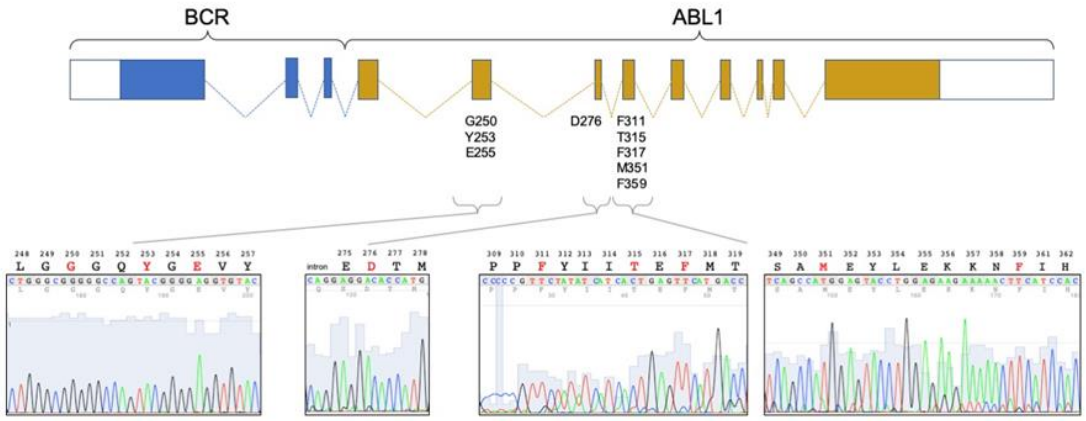

Figure 5.2.3 BCR-ABL1 mutation analysis. The nine indicated mutations account for 60% to 70% of all mutations causing imatinib-resistance [328]. Exon 4, 5 and 6 of ABL1 were amplified as explained in **section 4.18** and Sanger sequenced.

To further characterise KU812 ImaR cells, the growth rate, cell cycle and morphology was assessed and compared to the KU812 P cell line. Although there were no significant differences in the cell proliferation between KU812 ImaR and KU812 P cells under normoxic or hypoxic conditions (**Fig. 5.2.4.A**), both cell lines showed a reduced growth behaviour under hypoxic conditions. With regard to the cell cycle, KU812 ImaR cells showed a small but significant increase in S phase and a corresponding decrease in G0-G1 phase (**Fig. 5.2.4.B**). Moreover, although protein content was equal for KU812 P and KU812 ImaR cells (**Fig. 5.2.4.C**), cell size (cell diameter and cell volume) was increased in KU812 ImaR cells (1.79±0.08pL) compared to KU812 P cells (1.11±0.04pL). Of note, KU812 ImaR underwent a 38±4 % increase in cell volume with respect to KU812 P (**Fig. 5.2.4.D**).

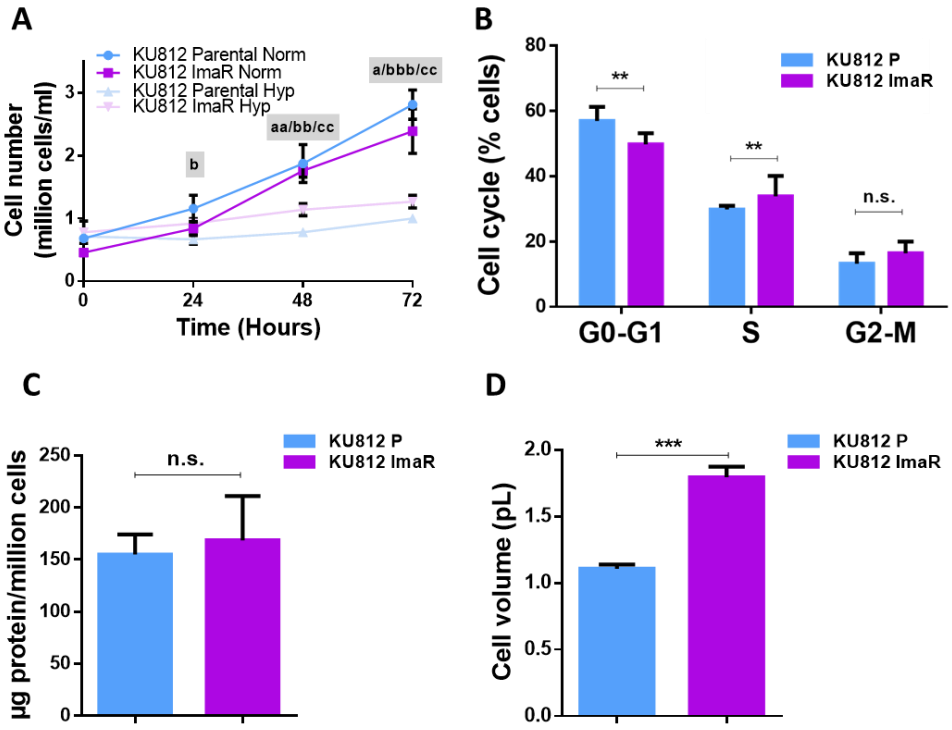

Figure 5.2.4 Characterisation of Parental and ImaR KU812 CML cells. A) Growth curve of KU812 Parental (P) and KU812 ImaR cells under normoxia (Norm) and hypoxia (Hyp). **B)** Cell cycle distribution of KU812 P and KU812 ImaR cells determined by flow cytometry. **C)** Protein content differences between KU812 ImaR relative to parental cells. Cells from the different cell lines were collected and counted, and protein content of these samples was measured by BCA assay**. D)** Cell volume of KU812 P and KU812 ImaR cells under normoxia measured with the Scepter™ Handheld Automated Cell Counter. Data are provided as mean ± SD of n = 2. Significance was determined by two-tailed independent sample Welch's t-test of 2 independent experiments. In **panel A,** the statistically significant differences between KU812 P and KU812 ImaR in hypoxia (**a)**, KU812 P under normoxia vs. hypoxia (**b**) or KU812 ImaR under normoxia vs. hypoxia (**c**) are indicated as p<0.05 (a, b or c), p<0.01 (bb, cc or dd), p<0.001 (aaa,bbb or ccc). In **panel B, C and D** the statistical differences between KU812 P and ImaR are indicated as p≥0.05 (n.s.), p<0.01 (**), and p<0.001 (***).

Ultimately, to better understand the effect of BCR-ABL1-independent imatinib resistance in CML, we followed SILAC-based protein mass spectrometry experiments to quantify changes in protein expression between KU812 P and ImaR cells under normoxia and hypoxia. From a total of approximately 3,200 identified proteins in the cell lines, 26.6% were upregulated and 26.0% were downregulated in the KU812 ImaR compared to the KU812 P cells under

normoxia (**Tables 1-2 from Appendix 2**). Unfortunately, technical replicates of quantitative proteomic analyses performed for KU812 ImaR and KU812 P under hypoxia demonstrated a high variability and, thus, could not be statistically evaluated (**data not shown**). For this reason, we focussed the quantitative analysis of the obtained proteomics data to normoxia only. From the identified proteins, a total of 850 were upregulated and a total of 831 were downregulated in KU812 ImaR compared to KU812 P cells, respectively (**Tables 1-2 from Appendix 2)**. Moreover, clustering of the differentially expressed proteins into biological processes, based on the gene ontology (GO) classification system using PANTHER database system, revealed that the GO terms associated with cellular processes (29%) and metabolic processes (20%) were the most enriched (**Fig. 5.2.5**). A more detailed analysis on these metabolic processes showed that the up/down regulated proteins are significantly associated with the GO terms “organic substance metabolic processes” and “cellular metabolic processes”. Thus, this analysis indicates that reprogramming of metabolism plays a key role in the acquisition of imatinib resistance of KU812 cells.

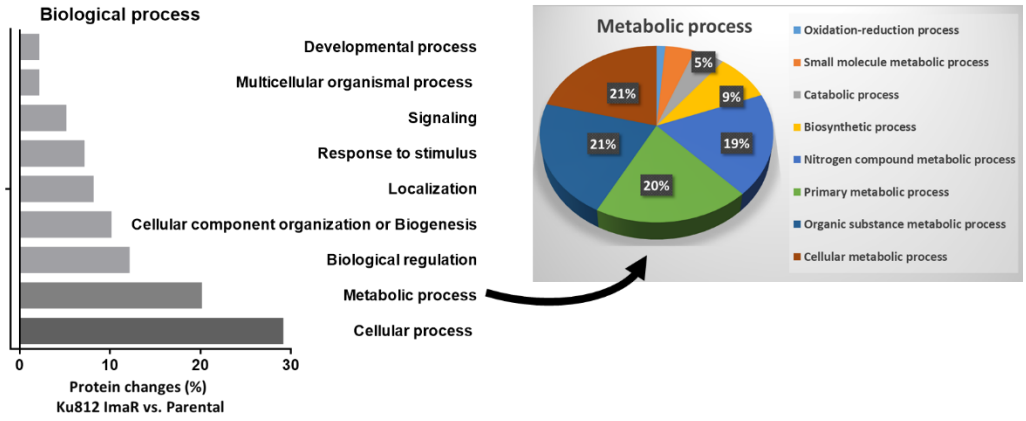

Figure 5.2.5. Pathway analysis of differentially expressed proteins identified by SILAC-based proteomics analysis of KU812 ImaR vs. KU812 P under normoxia. The bar chart shows biological processes enrichment analysis, based on the gene ontology classification system, of the up/down regulated proteins using the log_2fold change for the analysis. The pie chart shows the distribution of metabolic processes enrichment into subcategories. On-web analysis was performed using the PANTHER database system as described in **section 4.15.** Only biological processes enriched in more than 1% appear in the plot. Data are provided as mean ± SD of n = 2.

5.2.2.2 Development of imatinib-resistance is associated with increased glycolysis as well as rewired glucose to pentose phosphate pathway, glycogen synthesis, and serine-glycine-1C metabolism

The observation that around 20% of the proteins up/down regulated were associated with metabolic processes prompted us to further analyse the rewiring of the main pathways of central carbon metabolism underlying acquired BCR-ABL1-independent imatinib resistance. Since glycolysis was shown to be affected by BCR-ABL1-mutation-dependent acquisition of imatinib-resistance[117] and glucose is together with glutamine one of the two major sources of energy in cancer cells, we aimed to first evaluate if BCR-ABL1-independent resistance acquisition was also accompanied by altered glucose metabolism. Therefore, we measured glucose consumption and lactate production rates in KU812 P and ImaR cells. A proportional enhancement of both glucose consumption and lactate production was observed in KU812

ImaR cells compared to KU812 P cells both under normoxia (60% higher) and under hypoxia (70% higher) (**Fig. 5.2.6.A)**. Moreover, the ratio between lactate production and glucose consumption was the same for both cell lines under normoxia and hypoxia (**Fig. 5.2.6.B**).

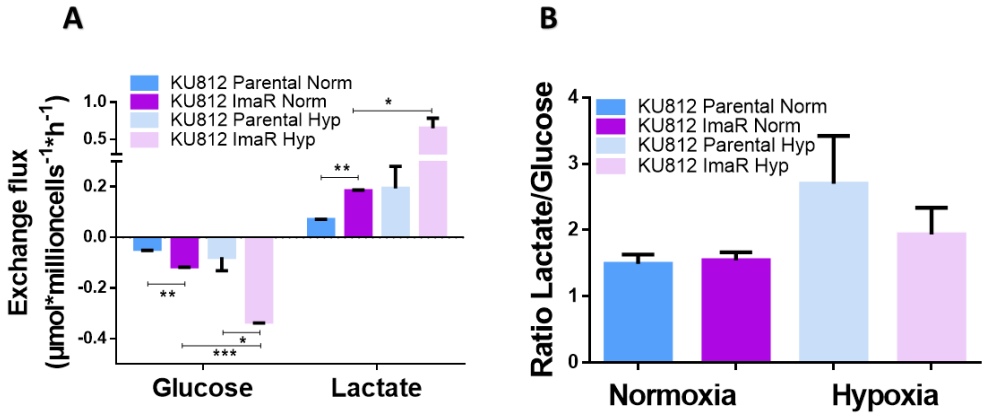

Figure 5.2.6 Glucose consumption and lactate production rates of KU812 imatinib-resistant relative to KU812 Parental cells. A) Exchange fluxes of KU812 Parental (P) and imatinib-resistant (ImaR) cells. Glucose and lactate production rates were obtained under normoxia (Norm) and hypoxia (Hyp) (1% O_2) as described in **section 4.7**. Data were normalised to cell number and incubation time. **B)** Ratio lactate/glucose using glucose and lactate flux rates under normoxia and hypoxia. Data are provided as mean ± SD of n=3 and significance was determined by two-tailed independent sample Student's t-test. Statistical differences between KU812 P vs. ImaR cells under normoxia and hypoxia, KU812 P cells under normoxia vs. hypoxia, and KU812 ImaR cells under normoxia vs. hypoxia are indicated as $p<0.05$ (*), $p<0.01$ (**), and $p<0.001$ (***).

We further investigated if the enhanced lactate production observed in KU812 ImaR cells contributes to the ECAR value. Results obtained using the XF96 Extracellular Flux Analyser (Seahorse) showed no significant differences between KU812 P and ImaR cells previously incubated under normoxic and hypoxic conditions regarding the ECAR value under normoxia (**Fig. 5.2.7)**. As shown above for THP-1 AraC cells (**Section 5.1.2.2.2**), these results also suggest that the contribution to ECAR of CA mediated TCA-derived CO_2 hydration is lower in KU812 ImaR than in KU812 P cells. Indeed, the downregulation of the CA1 and CA2 protein expressions (13.59 and 15.65- fold down , respectively) together with the

upregulation of SLC4A7 transporter (3.45-fold) again confirmed a decreased contribution of CAs to the ECAR value and a compensatory mechanisms of intracellular bicarbonate balance through extracellular HCO_3^- import in KU812 ImaR cells (illustrated in **Fig. 5.2.8**).

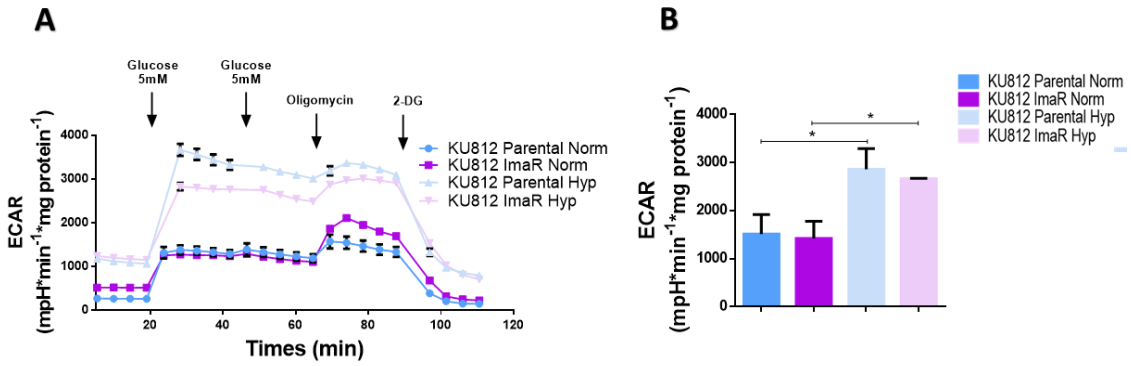

Figure 5.2.7 Glycolytic profile of KU812 Imatinib resistant compared to KU812 Parental cells. A) Extracellular acidification rate (ECAR) measured under normoxia using a XF96 Extracellular Flux Analyser during sequential injection of glucose, oligomycin and 2-DG in KU812 Parental (P) and imatinib-resistant (ImaR) cells previously incubated under normoxic (Norm) and hypoxic (Hyp) conditions. Cells were first incubated in the absence of glucose. **B)** ECAR after glucose addition (Total ECAR) in KU812 P and ImaR previously incubated under normoxic and hypoxic conditions were calculated as explained in **section 4.12** using ECAR values of **panel A**. Data were normalised by protein. Data are provided as mean ± SD of n = 3 and significance was determined by two-tailed independent sample Student's t-test. Statistical differences between KU812 P vs. ImaR cells incubated under normoxic and hypoxic conditions, KU812 P cells incubated under normoxic vs. hypoxic conditions, and KU812 ImaR cells incubated under normoxic vs. hypoxic conditions are indicated as $p<0.05$ (*).

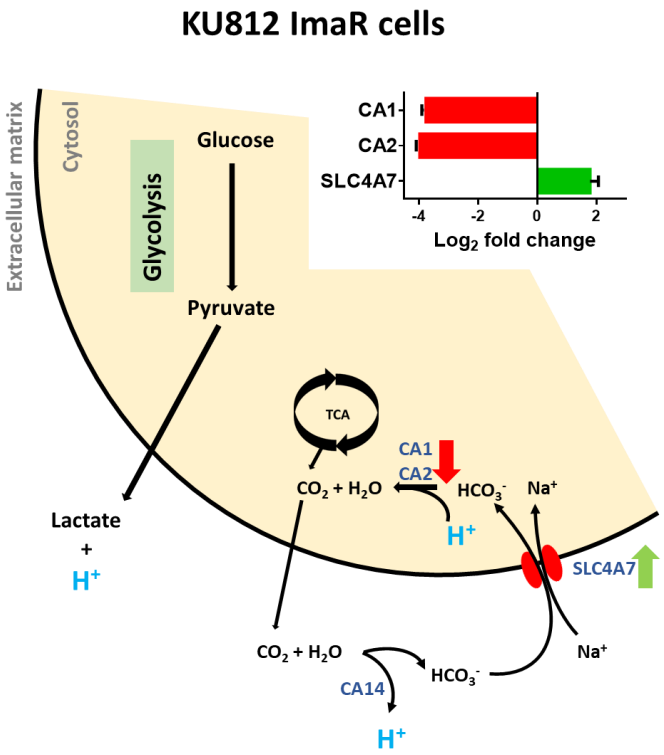

Figure 5.2.8 Protein profile differences of protein associated with H+ production and neutralisation, and bicarbonate buffering in KU812 ImaR. vs. KU812 P cells upon imatinib resistance. The protein expression profiling of the carbonic anhydrase (CA) 1 and 2, and the sodium bicarbonate cotransporter (SLC4A7) under normoxia were obtained using SILAC proteomic experiments described in **section 4.15**. Log_2 fold change values were calculated as explained in **section 4.15** and represented by green colour= protein upregulation; and red= protein downregulation. Data are provided as mean ± SD of n=2 of one representative experiment.

In parallel to ECAR measurements, the Crabtree effect was analysed by measuring the OCR changes after glucose addition under normoxia in KU812 P and ImaR cells previously incubated under normoxic and hypoxic conditions, in order to analyse the dependence on glucose as a source of energy. In brief, the Crabtree effect involves the inhibition of the mitochondrial respiration capacity in the presence of a high concentration of glucose. Results showed that the OCR rate decreased dramatically after glucose addition in KU812 P cells incubated under normoxic conditions and measured under normoxia (**Fig. 5.2.9**). On the contrary, the basal OCR in the absence of glucose was maintained after glucose addition in KU812 ImaR cells incubated under normoxic conditions and measured under normoxia,

indicating a total absence of the Crabtree effect. Under hypoxic incubation conditions, the Crabtree effect measured under normoxia was also significantly lower in KU812 ImaR when compared to KU812 P cells. It is well known that cells displaying the Crabtree effect have a reduced need for OXPHOS and higher dependence on glycolysis, thereby having less susceptibility to drugs targeting mitochondria[329]. The fact that the acquisition of imatinib resistance results in the loss of Crabtree effect in CML cells highlighted that KU812 ImaR cells may be more dependent on OXPHOS and more sensitive to mitochondrial toxicants, thus opening new avenues to be explored in the treatment of imatinib resistance.

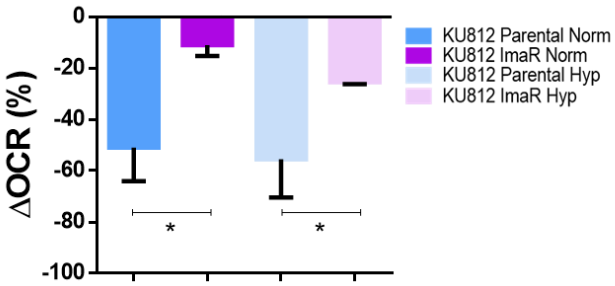

Figure 5.2.9 The Crabtree effect of KU812 Parental versus imatinib-resistant cells incubated under normoxic and hypoxic conditions. OCR rates of both cell lines in both incubation conditions was evaluated under normoxia by adding 10mM of glucose to glucose-deprived media. The Crabtree effect was calculated as described in **section 4.12** and the percentage of ΔOCR was represented. Data are provided as mean ± SD of n=3 and significance was determined by two-tailed independent sample Student's t-test. Statistical differences between KU812 P vs. ImaR cells under normoxic and hypoxic incubation conditions, KU812 P cells under normoxic vs. hypoxic incubation conditions, and KU812 ImaR cells under normoxic vs. hypoxic incubation conditions are indicated as $p<0.05$ (*).

To further analyse differences in glucose metabolism between KU812 P and ImaR cells under normoxia, the protein profile of a subset of proteins related with glucose metabolism was analysed (see data in **tables 1-2 from Appendix 2**). The expression of most of the proteins involved in glycolysis was upregulated in KU812 ImaR cells under normoxia (**Fig. 5.2.10**). However, HK isoforms I and II (HK1 and HK2) and the liver/red blood cell isoform of PK (PKLR) were downregulated. Moreover, the ADP dependent isoform of glucokinase

(ADPGK) was strongly upregulated (3.98-fold up). Taking into account that it has been reported that the Km of ADPGK for glucose is similar to HK2 (0.3 mM and 0.4 mM respectively) and higher than HK1 (0.03 mM)[330], it is reasonable to assume that ADPGK plays an important role in the conversion of glucose to glucose-6-P in KU812 ImaR cells. Moreover, it is well known that HK1 and HK2 can bind to the mitochondrial membrane and these mitochondrial-bound hexokinases preferentially use mitochondrial generated-ATP[331]. These facts lead to the hypothesis that the use of cytosolic ADP to phosphorylate glucose could be an advantage to save mitochondrial ATP for other purposes. Nevertheless, this hypothesis would require further experimental confirmation.

It is also noteworthy to mention the dual role of HK1 and HK2 in binding to mitochondria, protecting cells from apoptosis through the antagonisation of pro-apoptotic BCL2 proteins (e.g. Bak and Bax) at the mitochondrial membrane, and that this additional function cannot be compensated by ADPGK, which is localised in the endoplasmic reticulum. The fact that the protein profile showed an increase in BCL2 protein (4.43-fold up), which is a well-known antiapoptotic protein, lead us to hypothesise that this could be a compensatory mechanism in the loss of apoptosis protection due to the lower HK1 and HK2 protein expression. Moreover, we believe that this BCL2 protein upregulation could result in an increased sensitivity of KU812 ImaR cells towards BCL2 inhibitors. To validate this hypothesis, we treated KU812 P and KU812 ImaR with venetoclax (BCL2 inhibitor). Results showed that venetoclax was effective in reducing cell viability of both KU812 P and ImaR cells at micromolar concentrations without significant differences in the respective obtained IC_{50} values (**Fig. 5.2.11**).

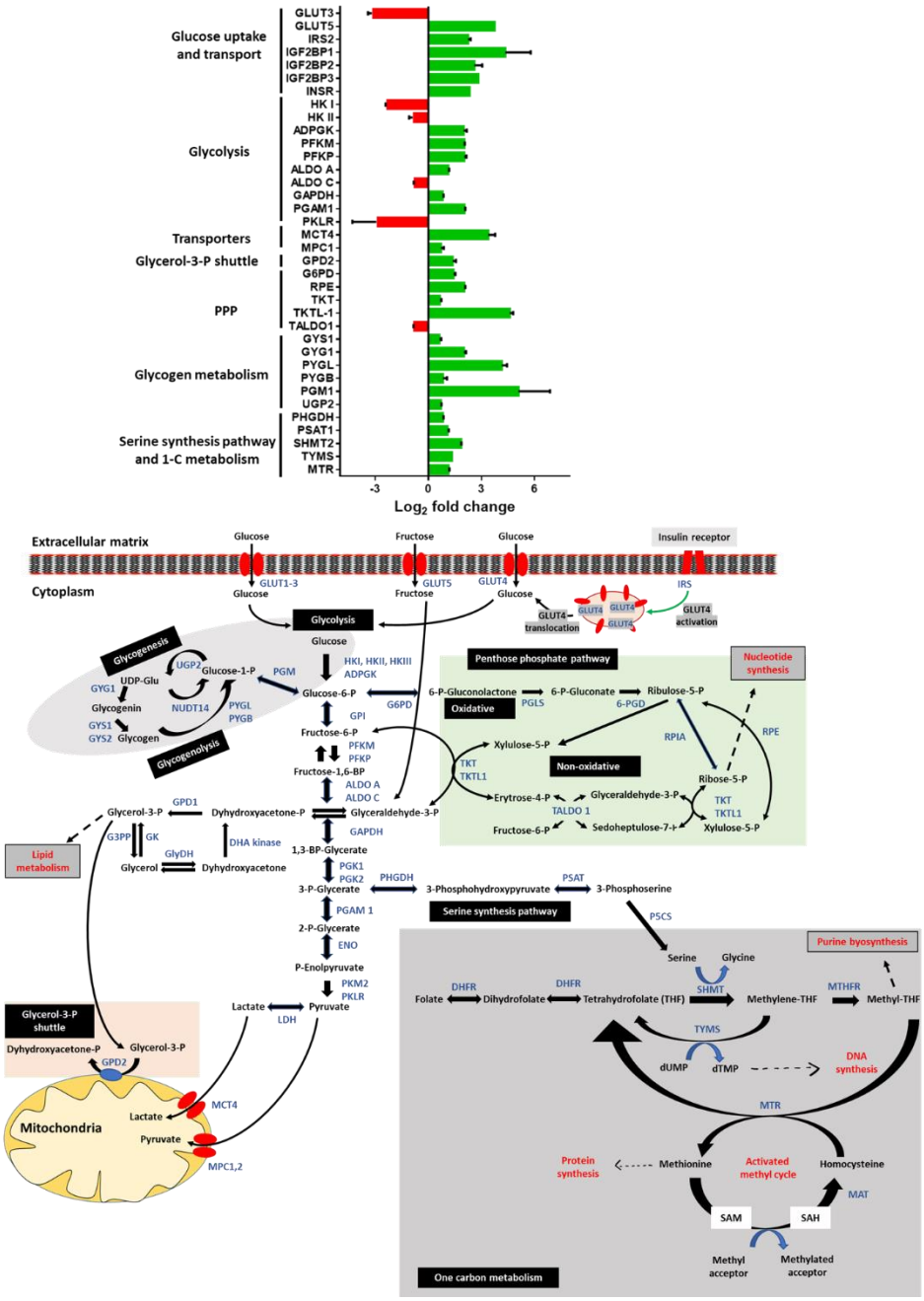

Figure 5.2.10. Protein profile differences of glucose metabolism and its rewiring in KU812 cells upon imatinib resistance. The protein expression profiling of proteins associated with glucose uptake and transporters, glycolysis, glycerol-3-P shuttle, glycogen metabolism, PPP, serine synthesis and 1-C metabolism under normoxia was obtained using SILAC-based proteomic experiments described in **section 4.15**. Log_2 fold change values were calculated as explained in **section 4.15** and represented by green colour= protein upregulation; and red= protein downregulation in KU812 imatinib-resistant cells compared to KU812 parental cells. Data are provided as mean ± SD of n = 2.

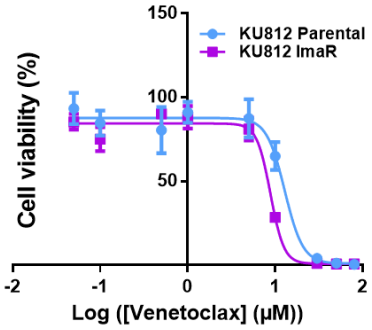

Cell line	Venetoclax (µM)
KU812 P	14.3±5.3
KU812 ImaR	7.9±1.4

Figure 5.2.11 Effect of venetoclax on the cell viability of KU812 Parental and imatinib-resistant cells. KU812 Parental (P) and imatinib-resistant (ImaR) cells were incubated 72 hours with DMSO (vehicle control) or increasing concentrations of venetoclax. IC_{50} values were calculated as explained in **section 4.3**. Data are provided as mean ± SD of n=2 and significance was determined by two-tailed independent sample Welch's t-test.

Regarding the expression of glucose transporters, we observed that GLUT3 was downregulated (8.66-fold down) in the protein profile of KU812 ImaR cells and that the expression of GLUT1, 2 and 4 did not show any significant differences between KU812 P and ImaR cells, indicating that the observed increase of glucose consumption must be due to mechanisms independent from the overexpression of the HK enzyme or the canonical glucose transporters. In this regard, protein expression of GLUT5, known for its role in fructose transport and its lower capacity to transport glucose into the cell[97], was highly upregulated (12.13-fold up). Likewise, proteins associated with the insulin-dependent glucose uptake via translocation of GLUT4 to the membrane such as insulin receptor 2 (IRS2); IGF2BP 1 and 2; and the insulin receptor precursor (INSR) were also upregulated in KU812 ImaR compared to KU812 P cells (4.76, 20.39, 6.08 and 5.04-fold up, respectively). Therefore, KU812 ImaR cells may counteract the downregulation of GLUT3 via GLUT5 and insulin-dependent glucose uptake upregulation via GLUT4 translocation.

In order to confirm the lower expression of the different HK isoforms as described above, we next performed Western blot analysis to validate these proteomics results. HKI, II and III showed a reduced expression in KU812 ImaR relative to KU812 P cells (**Figure 5.2.12.A)**.

Moreover, enzyme activities were determined by enzyme activity assays (described in **section 4.11**) to verify if the changes on protein level regarding the enzymes catalysing the rate-limiting steps of glycolysis affected the respective enzymatic activity. In agreement, HK and PK enzyme activities were significantly reduced in KU812 ImaR compared to KU812 P cells (**Fig. 5.2.12.B**). Thus, enzyme activity results corroborated what was determined in the protein profile.

The fact that the increase of glucose consumption and lactate production in KU812 ImaR cells was proportional, in addition to the observed increase in lactate flux, leads to the hypothesis that other branches of glucose metabolism such as oxidative and non-oxidative PPP, glycogen metabolism, serine-glycine-1C metabolism, glycerol metabolism and pyruvate/lactate transport to mitochondria, could be enhanced.

The protein profile showed that all PPP related proteins are upregulated (**Fig. 5.2.10**), with the exception of TALDO1. Interestingly, G6PD, which is the main enzyme controlling the oxidative branch of PPP, TKT, which is known to control the non-oxidative PPP, and transketolase like 1 (TKTL1), a minority isoenzyme of transketolase, were the most upregulated (2.68, 1.57 and 24.23-fold up, respectively). In order to validate the increase of transketolase and G6PD expression, enzyme activities were measured. In agreement with the observed changes at protein levels, enzyme activities were significantly increased in KU812 ImaR relative to KU812 P cells (**Fig. 5.2.12.B**).

To study if the differences observed in G6PD resulted in an increased sensitivity of resistant cells to G6PD inhibitors, we next incubated KU812 P and ImaR cells with dehydroepiandrosterone (DHEA), an uncompetitive inhibitor of G6PD. Noteworthy, even though the inhibition of the activity of G6PD by DHEA reduced the cell viability of both KU812 P cells (IC_{50} = 8.1µM) and KU812 ImaR cells (IC_{50} = 11.6µM) (**Fig. 5.2.13)**, the inhibitory effect of DHEA was not significantly higher in KU812 ImaR relative to KU812 P cells, thus suggesting that this inhibitor may not be a good candidate to target specifically the KU812 ImaR cells.

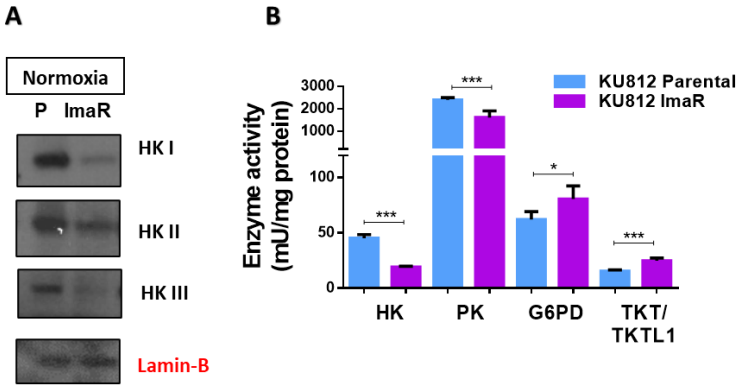

Figure 5.2.12. Correlation of HK protein expression and enzyme activities with imatinib resistance. A) Western blot analysis of differential HK protein expression between KU812 Parental (P) and imatinib-resistant (ImaR) cells under normoxia. **B)** Hexokinase (HK), pyruvate kinase (PK), glucose-6-phosphate dehydrogenase (G6PD) and transketolase (TKT) + transketolase like 1 (TKTL1) specific enzyme activities measured under normoxia. Data are provided as mean ± SD of n = 2 and significance was determined by two-tailed independent sample Welch's t-test. Statistically significant differences between KU812 P and ImaR cells are indicated as $p<0.05$ (*), and $p<0.001$ (***).

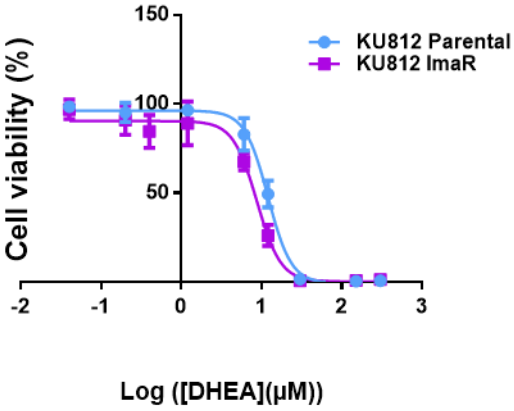

Cell line	DHEA (µM)
KU812 P	11.66±1.24
KU812 ImaR	8.12±1.33

Figure 5.2.13. Effect of the G6PD inhibition on the cell viability of KU812 Parental and imatinib-resistant cells by the dehydroepiandrosterone (DHEA) inhibitor. KU812 Parental (P) and imatinib-resistant (ImaR) cells were incubated 72 hours with DMSO (vehicle control) or different concentrations of DHEA. Data are provided as mean ± SD of n=2 and significance was determined by two-tailed independent sample Welch's t-test.

Another pathway, where glucose carbons can be rerouted, is the glycogen metabolism. To explore this possibility, we measured the differences on glycogen content between KU812 P and ImaR cells. Results showed a 2.6-fold increase in glycogen content in KU812 ImaR

relative to KU812 P cells (**Fig. 5.2.14.A**). Consistently, the protein profile also showed that GYS1 and glycogenin-1 (GYG1), which play a role in glycogen synthesis and maximal glycogen level attainment, were upregulated by a 1.54 and 4.02-fold, respectively, in KU812 ImaR relative to KU812 P cells. In agreement with the glycogen accumulation observed, PGM1, the enzyme which indirectly regulates glycogen and pentose-phosphate synthesis by fine tuning of the glucose-1-P and glucose-6-P balance, was also strongly upregulated (34.15-fold up) in KU812 ImaR cells (**Fig. 5.2.10**). Besides, glycogen phosphorylase liver (PYGL) and brain (PYGB) isoenzymes, responsible of glycogen degradation and identified as relevant enzymes for the optimal function of PPP[332], were upregulated (17.81 and 1.78-fold up, respectively) in KU812 ImaR cells. All together, these results suggest that an enhanced glycogen synthesis/degradation cycle is necessary to simultaneously sustain glycogen accumulation and to support PPP activity in KU812 ImaR cells. Next, we decided to explore the impact of glycogenolysis inhibitors on KU812 P and ImaR cells by using three different inhibitors (1,4-dideoxy-1,4-imino-d-arabinitol [DAB]; CP-320626; and CP-91149). **Figure 5.2.14.B** illustrates that glycogenolysis inhibitors reduced cell viability of both parental and ImaR cells. However, we could not observe a higher inhibitory effect in KU812 ImaR relative to KU812 P cells for any of the three inhibitors, suggesting that these inhibitors may not be the best therapeutic approach to overcome imatinib resistance.

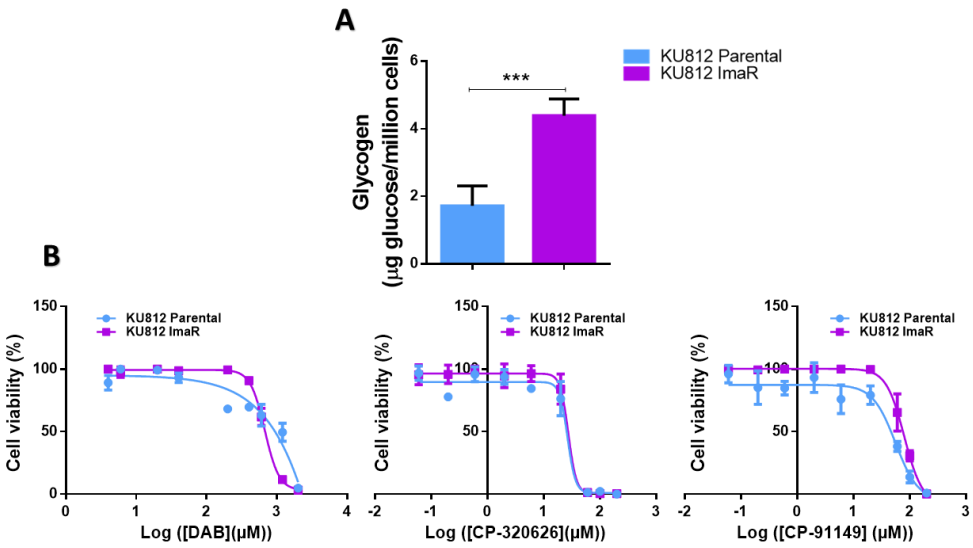

Cell line	DAB (µM)	CP-320626 (µM)	CP-91149 (µM)
KU812 P	868±218	33±17	46±15
KU812 ImaR	588±116	32±14	76±7

Figure 5.2.14 Comparison of glycogen content between KU812 Parental and imatinib-resistant (ImaR) cells (A) and effect of glycogenolysis inhibitors on KU812 Parental and ImaR cell viability (B). A) GC-MS was used to assess the glycogen content of parental (P) and ImaR cells. Measurement of the glycogen content was carried out using [U-^{13}C-D$_7$]-glucose as recovery standard and internal standard quantification procedures. Glucose from glycogen was corrected by millions of cells. **B)** Effect of 1,4-dideoxy-1,4-imino-d-arabinitol (DAB), CP-320626, and CP-91149 inhibitors on the cell viability of KU812 P and ImaR cells. Cells were incubated 72 hours with DMSO (vehicle control) or increasing concentrations of the corresponding inhibitor. Data are provided as mean ± SD of n = 2 and significance was determined by two-tailed independent sample Welch's t-test. Statistically significant differences between KU812 P and ImaR cells in **panel A** are indicated as p<0.001 (***).

Finally, we explored the glucose carbons rerouting at the level of 3-carbon molecules. Firstly, we cultured KU812 P and ImaR cells in the presence of uniformly ^{13}C labelled [U-^{13}C]-glucose and subsequently analysed the incorporation of ^{13}C into serine and glycine by NMR. **Figure 5.2.15.A** illustrates that ^{13}C incorporation from [U-^{13}C]-glucose into the C2 position of glycine and C3 position of serine was 3.4 and 2.6-fold increased, respectively, in KU812 ImaR cells when compared to KU812 P cells. Moreover, protein profiling results were analysed in order to examine the changes in key protein levels involved in SSP and 1-C

metabolism. In brief, upregulation of PHGDH and PSAT (key players of SSP), and SHMT2, TYMS and MTR (key players of 1-C metabolism) in KU812 ImaR relative to KU812 P cells were observed (**Fig. 5.2.10**). These results indicate that the SSP and 1C-metabolism are also crucial pathways influencing glucose metabolism of KU812 ImaR cells.

Since the above results indicate an enhancement of serine and 1C-metabolism through rerouting carbons from glycolytic intermediates, such as 3-P-glycerate, we hypothesise that KU812 ImaR cells could additionally increase the uptake of serine, glycine, and methionine to fuel these pathways. In order to explore this possibility, we measured the exchange fluxes and intracellular contents of serine, glycine, and methionine by using the Biocrates AbsoluteIDQ p180 Kit (described in **section 4.8**) (data shown in **Tables 3-6 from Appendix 2**). A higher serine and methionine consumption, as well as a higher glycine intracellular content were observed in KU812 ImaR cells under normoxia (**Fig. 5.2.15 B-C**), suggesting a higher flux of those metabolic pathways in KU812 ImaR relative to KU812 P cells. Likewise, serine consumption and glycine intracellular content were also higher in KU812 ImaR under hypoxia. However, we could not determine any significant differences between both cell lines regarding methionine consumption in hypoxia.

Considering these results, which suggest an enhanced SSP and 1-C metabolism in KU812 ImaR relative to KU812 P cells, we determined the cell viability of both parental and ImaR cells after the treatment with several 1-C metabolism inhibitors including methotrexate (DHFR inhibitor), pemetrexed (TYMS and DHFR inhibitor), and SHIN2 (SHMT1 and 2] inhibitor). A reduction of cell viability was found for both cell lines (KU812 P and ImaR) but a selective effect on KU812 ImaR relative to KU812 P cells was not observed (**Fig. 5.2.15 D)**, indicating that 1-C metabolism is important for both resistant and non-resistant cells.

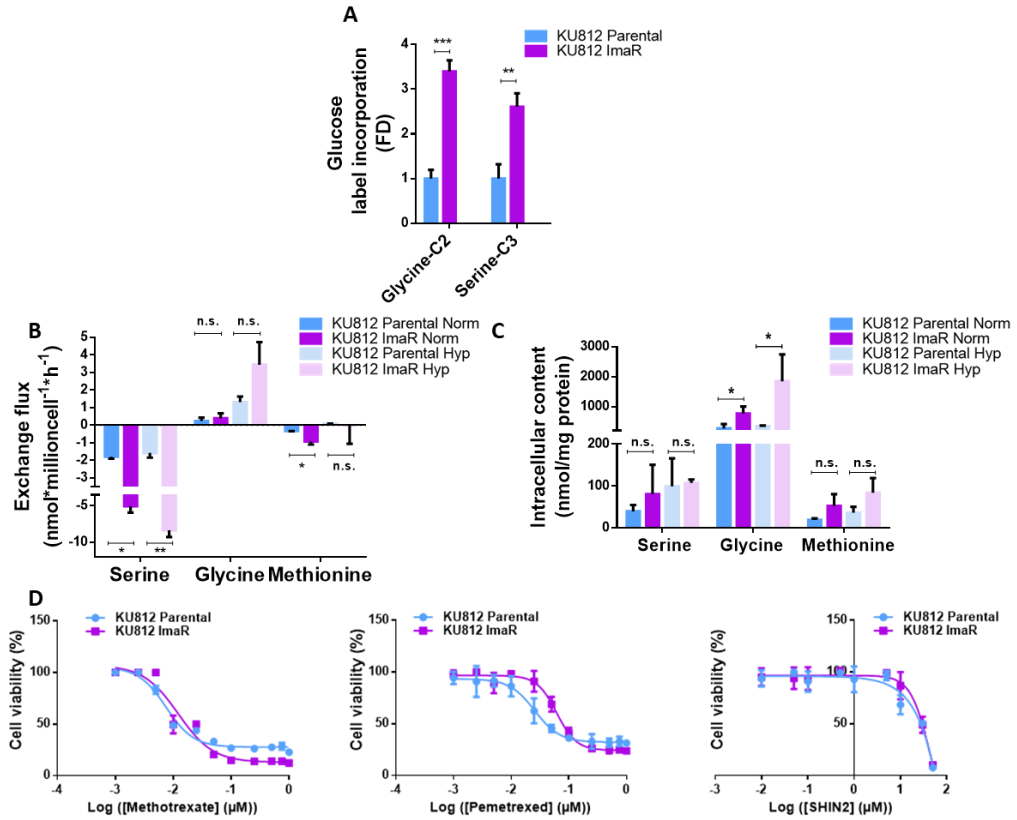

Cell line	Methotrexate (nM)	Pemetrexed (nM)	SHIN2 (μM)
KU812 P	12.66±2.96	41.96±14.28	33.76±4.65
KU812 ImaR	17.04±5.34	79.28±15.46	40.32±2.06

Figure 5.2.15 Differences in glycine, serine and methionine metabolism between KU812 Parental and imatinib-resistant cells and the effect of the inhibition of 1-C metabolism. A) ^{13}C Glucose label incorporation into glycine and serine metabolites in KU812 imatinib-resistant (ImaR) compared to KU812 parental (P) cells under normoxia, determined by NMR analysis**. B and C)** Exchange fluxes (**B**) and intracellular content (**C**) of serine, glycine, and methionine between KU812 P and ImaR cells measured by HPLC-MS/MS as described in **section 4.8**. **D)** Effect of methotrexate, pemetrexed and SHIN2 inhibitors on KU812 P and ImaR cell viability. Cells were incubated 72 hours with DMSO (vehicle control) or increasing concentrations of the respective inhibitor. Data are provided as mean ± SD of n = 3 of one representative experiment for **panel A, B and C,** and as mean ± SD of n=2 for **panel D.** Significance was determined by two-tailed independent sample Welch's or Student's t-test. Statistically significant differences between KU812 P and ImaR cells are indicated as p≥0.05 (n.s.), p<0.05 (*), p<0.01 (**), and p<0.001 (***).

To further explore the glucose metabolism network at the level of 3-carbon molecules, we analysed the proteomic changes associated with the glycerol metabolism and pyruvate/lactate mitochondrial transporters. Results show that GPD2) the mitochondrial pyruvate carrier MPC1, as well as the monocarboxylate carriers MCT4 (SLC16A3) were upregulated in KU812 ImaR cells (**Fig. 5.2.10**). It is worth mentioning that MCT4 has been described to be localised within the plasmatic and mitochondrial membranes and to be able to import/export lactate/pyruvate between mitochondria and cytosol in symport with a H^+ [333]. These changes in pyruvate and monocarboxylate carrier are indicative of an increased flux of pyruvate/lactate into the mitochondria, further suggesting a stronger dependence on pyruvate to support mitochondrial respiration. Moreover, the increase of GPD2 observed in KU812 ImaR cells indicates a stronger dependence on GP shuttle, thus additionally suggesting an altered mitochondrial respiration capacity that will be further explored in **section 5.2.1.2.9**.

5.2.2.3 Development of resistance to imatinib enhances glutamine transport and rewires glutamine metabolism

We next investigated differences associated with the acquisition of imatinib resistance with regard to the transport and metabolism of glutamine, another major energy and carbon source that additionally provides nitrogen to biosynthetic pathways. Therefore, exchange fluxes of glutamine and glutamate under normoxia were determined by using the Biocrates AbsoluteIDQ p180 Kit (described in **section 4.8**). The obtained results showed a higher glutamine consumption and glutamate production in KU812 ImaR when compared to KU812 P cells. (**Fig. 5.2.16 A**)**.**

To elucidate if the increase of glutamine consumption and glutamate production observed in KU812 ImaR cells was due to an increase of the GLS isoenzymes or a decrease in GS (the main enzymes involved in glutaminolysis and glutamine synthesis, respectively), the expression of these proteins were quantified by Western blot analysis and by protein profile (SILAC) analysis. Overall, KU812 ImaR cells showed lower levels of GLS isoenzymes (GLS1

and GLS2) in the Western blot results and a slightly downregulation (1.69-fold down) of the total protein concentration (**Table 2 from Appendix 2**). Moreover, no differences were observed regarding GS protein levels**.** Furthermore, the increased of glutamine consumption observed in KU812 ImaR cells was consistent with the dramatic increase observed at protein level of the two main glutamine transporters SLC38A1 (SNAT1) (15.11-fold up) and SLC38A2 (SNAT2) (5.00-fold up). Other amino acids transporters such as LAT1 were also upregulated (1.73-fold up) in KU812 ImaR cells, indicating that these cells not only have a stronger dependence on glutamine but also on other amino acid metabolic pathways **(Fig. 5.2.17**). All together, these results demonstrate that the observed changes in the glutamine consumed, and the glutamate produced in KU812 ImaR cells are not due to an increase in glutaminolysis despite the fact that glutamine import is upregulated in KU812 ImaR cells.

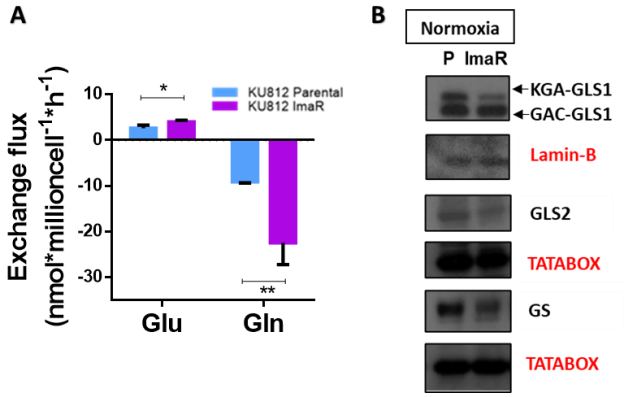

Figure 5.2.16 Characterisation of glutamine metabolism in KU812 imatinib-resistant compared to KU812 parental cells. A) Exchanges fluxes of glutamate and glutamine of KU812 Parental (P) and imatinib-resistant (ImaR) cells. Glutamine consumption and glutamate production were obtained under normoxia as described in **section 4.7.** Data were normalised to cell number and incubation time. **B)** Western blotting analysis of total protein fractions related to glutamine metabolism of KU812 P and ImaR cells under normoxia. Data are provided as mean ± SD of n=3 for **panel A** and significance was determined by two-tailed independent sample Student's t-test. Statistically significant differences between KU812 P and ImaR cells are indicated as $p<0.05$ (*), and $p<0.01$ (**). Abbreviations: Kidney-type glutaminase 1, KGA-GLS1; glutaminase C, GAC-GLS1; glutaminase 2, GLS2; and glutamine synthetase, GS.

To further investigate the metabolic fate of glutamine in KU812 ImaR cells, the protein profile of enzymes that use glutamine as substrate were analysed using the data from **Tables 1-2 from Appendix 2**. Glutamine-fructose-6-phosphate aminotransferase 1 (GFPT1), the first and rate limiting enzyme in hexosamine biosynthesis pathway (HBP)[334], was one of the enzymes significantly upregulated (5.68-fold up), indicative of the glutamine and glucose rewiring towards HBP in KU812 ImaR cells (**Fig. 5.2.17**). Nevertheless, the other non-rate-limiting enzymes involved in the HBP such as the glucosamine-6-phosphate N-acetyltransferase (GNPNAT1), the PGM3, and the UDP-N- acetylhexosamine pyrophosphorylase 1 (UAP1) were significantly downregulated. In brief, HBP produces uridine diphosphate N-acetylglucosamine (UDP-GlcNAc) from glucose and glutamine and plays an important role in the biosynthesis of glycoproteins[335]. Proteomic profiling also unveiled an important increase in another important glutamine consuming enzyme, the ASNS (4.40-fold up), which converts glutamine and aspartate into glutamate and asparagine.

All together, these results prompted us to investigate the exchange fluxes and intracellular content alterations of amino acids upon imatinib resistance generation, specially alterations of proline, an important end product of glutamine metabolism, and its precursors ornithine, aspartate and arginine, due to its close relation with the glutamine metabolism.

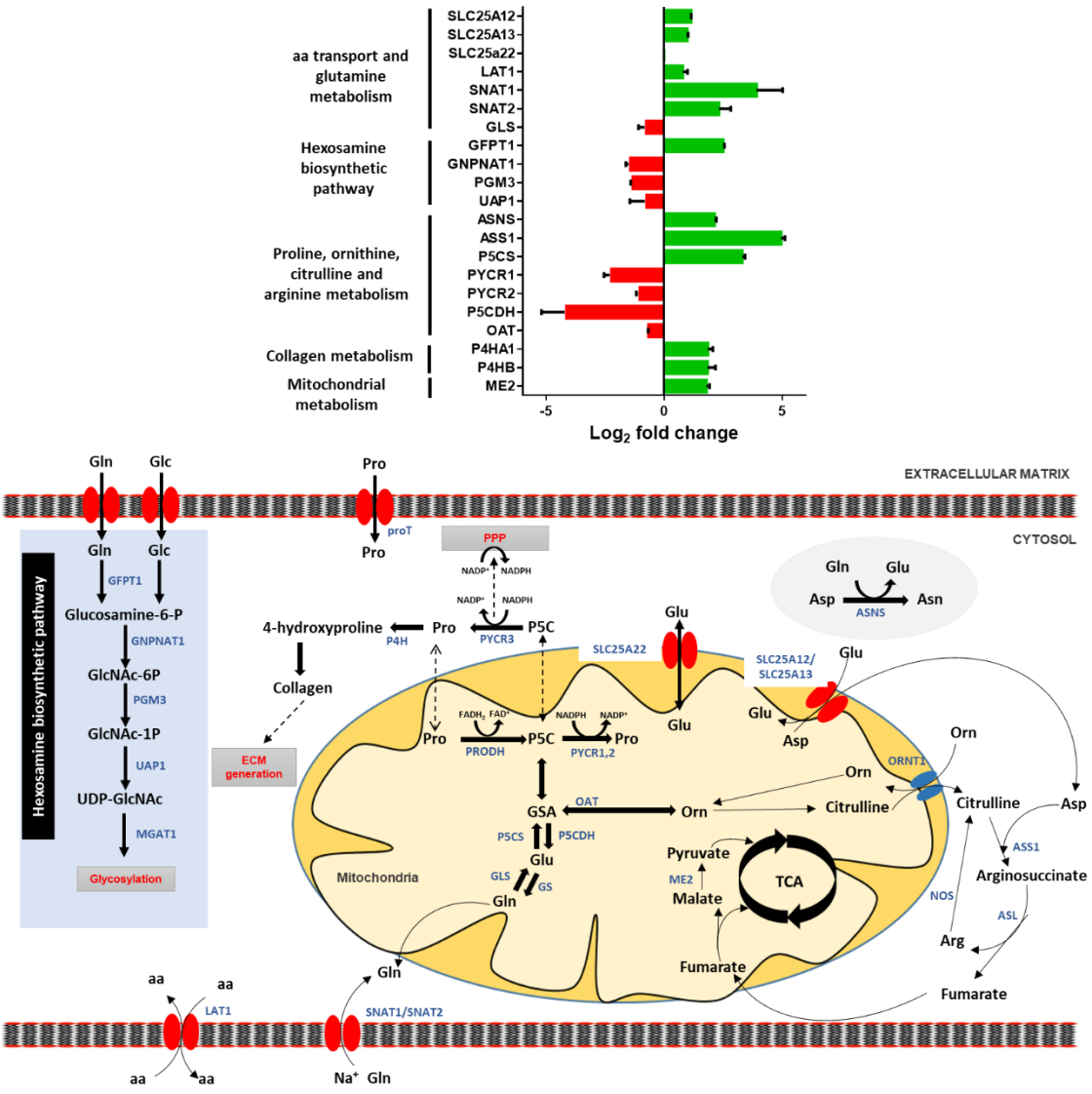

Figure 5.2.17 Protein profile of the rewiring of glutamine metabolism in KU812 imatinib-resistant when compared to KU812 parental cells. The protein expression profiling of proteins related to amino acid transporters, glutamine, hexosamine, proline, ornithine, citrulline, arginine and collagen metabolism under normoxia was obtained using SILAC-based proteomic experiments described in **section 4.15**. Log_2 fold change values were calculated as explained in **section 4.15** and represented by green colour = protein upregulation; and red = protein downregulation. Data are provided as mean ± SD of n = 2.

5.2.2.4 Development of resistance to imatinib rewires the metabolism of proline and its related metabolic precursors

To further unveil the metabolic rewiring associated with the acquisition of imatinib resistance, we next investigated differences in proline metabolism and its related precursors including ornithine and glutamate. As shown in **Fig. 5.2.18 A,** KU812 ImaR cells exhibited an enhanced production of proline (13-fold increase) and ornithine (3-fold increase) compared to KU812 P cells. Regarding the intracellular content of these amino acids, we observed that proline and ornithine intracellular contents were sixteen and seven times higher, respectively, in KU812 ImaR compared to KU812 P cells (**Fig. 5.2.18 B**).

Considering that both proline and ornithine can be synthesised from glutamate through glutamate-γ-semialdehyde (GSA) synthesis, but ornithine can also be synthesised from other carbon sources such as arginine, we next cultured KU812 P and ImaR cells in the presence of either uniformly ^{13}C labelled [U-^{13}C]-glucose or [U-^{13}C]–glutamine and subsequently analysed the incorporation of ^{13}C into glutamate, proline and ornithine metabolites by NMR (data shown in **Tables 7-8 from Appendix 2**). No ^{13}C incorporation originating from [U-^{13}C]-glucose was observed in proline or in ornithine in both KU812 P and ImaR cells (**Fig. 1 from Appendix 2**). On the other hand, ^{13}C incorporation from [U-^{13}C]-glutamine in the carbons C3, C4 and C5 of proline was 45, 39 and 33-fold higher, respectively, in KU812 ImaR than in KU812 P cells (**Fig. 5.2.18.C**), indicating a dramatic increase of proline synthesis from glutamine in KU812 ImaR cells. Likewise, ^{13}C incorporation originating from [U-^{13}C]-glutamine in the carbons C3 of glutamate was also higher (3.0-fold up) in KU812 ImaR cells. In contrast, ^{13}C incorporation originating from [U-^{13}C]-glutamine in C2 and C4 of glutamate and in C5 of ornithine were not significantly different in KU812 ImaR when compared to KU812 P cells. The uniformly labelled glutamate coming from [U-^{13}C]-glutamine can be transformed into α-ketoglutarate that can be metabolised through the TCA cycle, generating again a new α-ketoglutarate that will have less ^{13}C atoms. Thus, the new α-ketoglutarate molecules will have lost the ^{13}C in C4 and C5.

Thus, the higher ^{13}C label incorporation in C3 than in C4 is indicative of a higher activity of the TCA cycle in KU812 ImaR than in P cells.

To better elucidate the metabolic role of proline in KU812 ImaR cells, the protein profile of proteins associated with proline metabolism and amino acids closely related to proline metabolism was revisited. The rate limiting enzyme of proline and ornithine synthesis, pyrroline-5-carboxylate synthase (P5CS, also called ALDH18A1), was highly upregulated in KU812 ImaR cells (9.91-fold up). This upregulation was accompanied by the downregulation of the enzyme that catalyses the reverse reaction, the delta-1-pyrroline-5-carboxylate dehydrogenase (P5CDH or ALDH4A1) (17.63-fold down) and of the two isoforms of PYCR 1 and 2 (4.70-fold up and 2.04-fold down). (**Figs. 5.2.17**). Moreover, the downregulation of P5CS and PYCR at protein levels was also validated by Western blot analysis **(Fig. 5.2.18.D**). In addition, PRODH, which is the enzyme that catalyses the reverse reaction of PYCR, was also analysed by Western blot analysis due to the fact that it was not observed in the protein profiles. Results showed a downregulation of this enzyme in KU812 ImaR when compared to KU812 P cells (**Fig. 5.2.18.D).** Therefore, we hypothesise that these enzyme changes observed at mitochondrial level could result in a large increase of the mitochondrial P5C pool. It is also worth mentioning that the enzyme responsible for collagen synthesis, prolyl 4-hydroxylase (P4H), was also upregulated (3.63-fold up) in KU812 ImaR compared to KU812 P cells, suggesting that KU812 ImaR cells may be additionally utilising proline for collagen synthesis purpose.

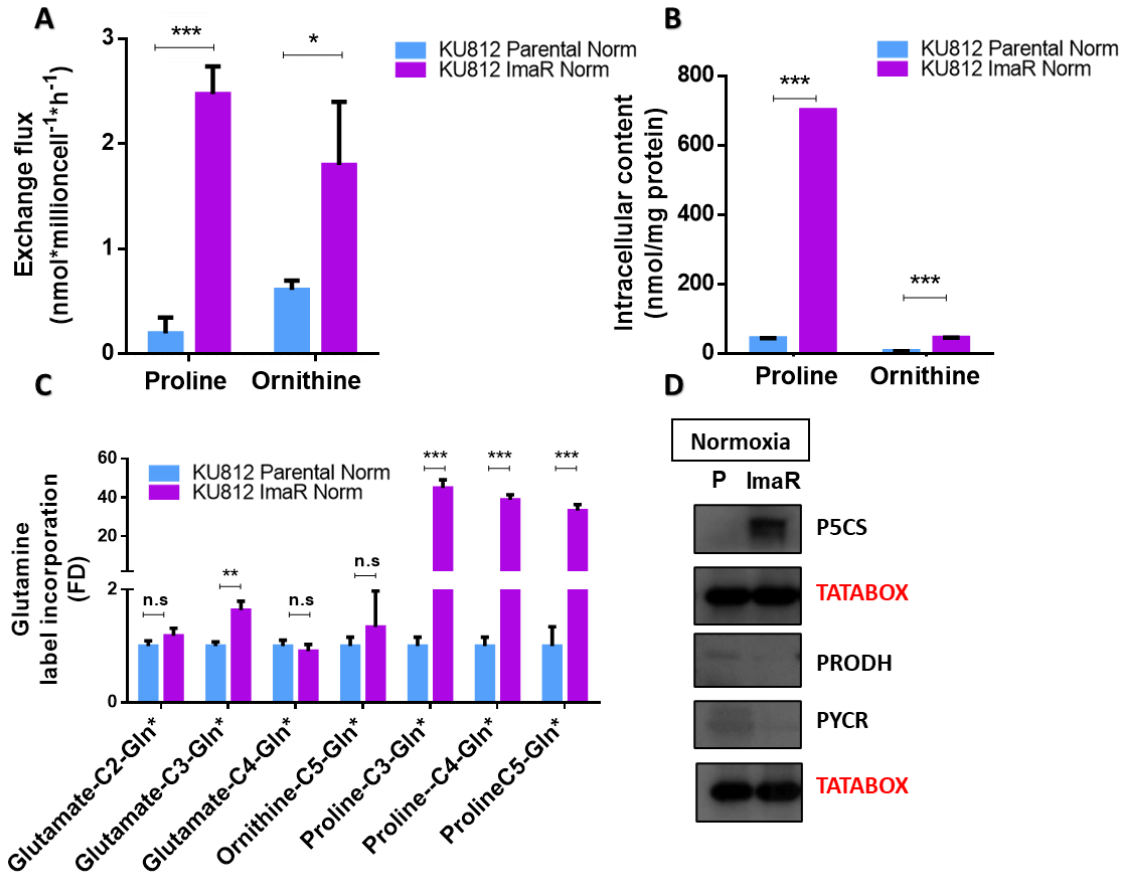

Figure 5.2.18 Glutamine rewiring to proline metabolism in KU812 cells upon imatinib resistance development. A) Exchange flux differences of proline and ornithine between KU812 parental (P) and imatinib-resistant (ImaR) cells were measured under normoxia as described in **section 4.8**. Data was normalised to cell number and incubation time. **B)** Intracellular concentrations of proline and ornithine in KU812 Parental and ImaR cells under normoxia. Data was normalised by the extracted protein**. C)** ^{13}C Glutamine label incorporation in different carbons of glutamate, ornithine and proline in KU812 ImaR compared to KU812 Parental cells under normoxia, determined by NMR analysis**. D)** Western blot analysis of enzymes related to proline metabolism of KU812 Parental and ImaR cells under normoxia. Data are provided as mean ± SD of n = 3 of one representative experiment for **panel A, B and C.** Significance was determined by two-tailed independent sample Student's t-test. Statistically significant differences between KU812 P and ImaR cells are indicated as p≥0,05 (n.s.), p<0.05 (*), p<0.01 (**) and p<0.001 (***).

Furthermore, we examined the protein expression of the mitochondrial amino acid transporters by using protein profile analysis (**Tables 1-2 from Appendix 2**). SLC25A12 and SLC25A13 transporters, which are involved in the exchange of mitochondrial aspartate for cytosolic glutamate across the inner mitochondrial membrane, showed an upregulation in KU812 ImaR compared to KU812 P cells (**Fig. 5.2.17**). Consistent with the observed increase of ASNS, the upregulation of these transporters in KU812 ImaR cells indicates an enhanced aspartate/glutamate transport, which can be driven by an increased demand of cytosolic aspartate for asparagine synthesis. Moreover, KU812 ImaR cells also exhibited a dramatic upregulation of ASS1 (31.07-fold up), the rate-limiting enzyme of arginine synthesis, which catalyses the synthesis of arginosuccinate from citrulline and aspartate (**Fig. 5.2.17**). This fact together with the observed upregulation of the SLC25A12 and SLC25A13 transporters suggests an increased requirement of aspartate in the cytosol to serve the need of aspartate-dependent biosynthetic reactions in KU812 ImaR cells. On the other hand, the upregulation of ASS1 observed in KU812 ImaR cells also suggests an enhancement of the pathway producing arginine and fumarate through the sequential reactions of ASS1 and ASL. In brief, arginine generated through this pathway can be utilised for protein synthesis or be converted again to citrulline through nitric oxide synthase (NOS). Moreover, the resulting fumarate can enter the mitochondria to be converted into malate and pyruvate, thereby fuelling the mitochondrial respiration. Therefore, we hypothesise that KU812 ImaR cells utilise the arginine generated to synthesise both proteins or citrulline via NOS, and the fumarate to fuel mitochondrial respiration. It is also worth mentioning that the mitochondrial ME2, which converts malate into pyruvate within the mitochondria, was also upregulated (3.46-fold up) in KU812 ImaR compared to KU812 P cells, thus reinforcing this hypothesis.

Finally, KU812 ImaR cells exhibited a decrease in the expression of the mitochondrial glutamate/H+ symporter (SLC25A22) (1.66-fold down, which is involved in the glutamate transport across the inner mitochondrial membrane providing glutamate to mitochondrial glutamate dehydrogenase for its conversion to α-ketoglutarate and NADPH. It has been

reported that SLC25A22 knockdown results in lack of ETC functioning and NADPH formation[336].

5.2.2.5 Targeting transport and biosynthesis of proline to investigate the essentiality of proline for the survival of imatinib-resistant cells

The results described in the previous section highlighted proline synthesis as a potential metabolic target that could be further exploited to specifically target imatinib-resistant cells. To this end, we used CRISPR/Cas9 technology (described in **section 4.16**) to individually knockout two important proteins of the proline metabolism, the first enzyme in the proline biosynthesis pathway (P5CS/ALDH18A1) and the sodium-dependent proline transporter (proT/SLC6A7). Next, a competitive growth assay was conducted in order to determine the differential effects on cell proliferation between KU812 P and ImaR non-targeted control (NTC) and KO cells. As depicted in **Fig. 5.2.19**, KU812 P and ImaR KO cells including P5CS and proT KOs slightly reduce the cell proliferation when compared to KU812 P and ImaR NTC cells. Moreover, the decrease of cell proliferation induced by these KOs was significantly higher in KU812 ImaR when compared to KU812 P cells. However, we did not observe a decrease of cell proliferation exceeding 65%.

In order to elucidate the effect of P5CS and proT KOs on proline metabolism in KU812 P and ImaR cells, the proline exchange flux was measured by using the Biocrates AbsoluteIDQ p180 Kit (described in **section 4.8**). Consistent with results mentioned above, KU812 ImaR NTC cells produced proline instead of consuming it as observed in KU812 NTC P cells (**Fig. 5.2.19**). However, the differences between both cell models were not as dramatic as the differences observed between KU812 P and KU812 ImaR cells. Moreover, whereas non-significant differences were obtained regarding the proT KO, KU812 ImaR cells showed to stop producing proline upon the P5CS KO, indicating a significant effect of P5CS KO in the KU812 ImaR proline metabolism.

All together, these results suggest that even though proline metabolism was altered, at least upon P5CS KO, both P5CS and proT KOs will not serve as feasible strategies to overcome TKI resistance.

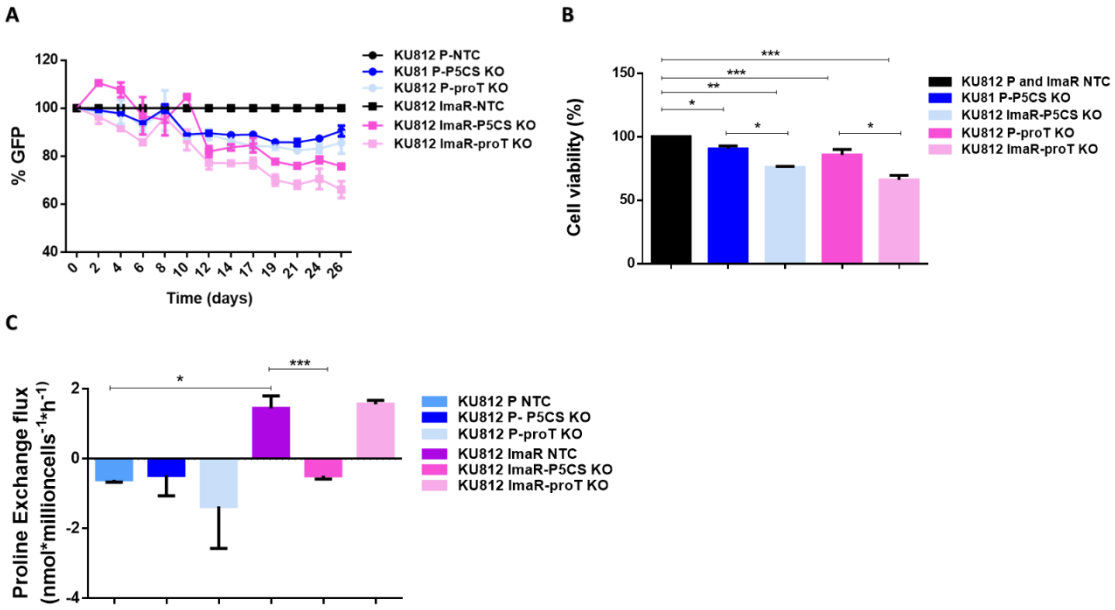

Figure 5.2.19 Effect of the knockout of proteins involved in proline synthesis and transportation in KU812 Parental vs. imatinib-resistant cells. A) The percentage of GFP in KU812 Parental (P) and KU812 imatinib-resistant (ImaR) non-targeted control (NTC) and knockout (KO) cells was measured every second day by flow cytometry as described in **section 4.17. B)** Cell viability of KU812 P and ImaR NTC and KO cells was illustrated by using the percentage of GFP expression. **C)** The exchange flux of proline was measured by HPLC-MS/MS as described in **section 4.8.** Data were normalised by cell number. Data are provided as mean ± SD of n = 2 (**panel A** and **B**) and as mean ± SD of n = 3 (**panel C**) of one representative experiment. Significance was determined by two-tailed independent sample Welch's t-test or Student's t-test and statistical differences between KU812 P and ImaR-NTC vs. KU812 P and ImaR-KO cells, and between KU812 P-KO cells vs. KU812 ImaR-KO cells for **panel A** and **B**, and between KU812 P NTC vs. KU812 ImaR NTC cells, and KU812 ImaR NTC vs. KU812 ImaR-P5CS KO cells for **panel C** are indicated as $p<0.05$ (*), $p<0.01$ (**), and $p<0.001$ (***).

5.2.2.6 Development of imatinib resistance results in the overexpression of key proteins in ROS and xenobiotics detoxification related pathways

Another metabolite directly linked to glutamate (and consequently to glutamine) metabolism and associated with drug resistance is glutathione[39,230]. Thus, we investigated if glutamine metabolism was rewired to glutathione synthesis in KU812 ImaR cells. Results showed that total glutathione levels as well as ^{13}C incorporation (coming from [U-^{13}C]-glutamine) into GSH were lower in KU812 ImaR than in KU812 P cells (**Figs. 5.2.20.A-B**). We next analysed the protein profile of proteins associated with *de novo* glutathione synthesis in KU812 ImaR compared to KU812 P cells. Protein levels of glutamate–cysteine ligase (GCL), both the catalytic and regulatory subunits, were reduced in KU812 ImaR (9.04 and 2.62-fold down, respectively) compared to KU812 P cells (**Fig. 5.2.21.A**). Altogether, these results indicate that the *de novo* glutathione synthesis does not contribute to the increase of glutamine consumption observed in KU812 ImaR cells.

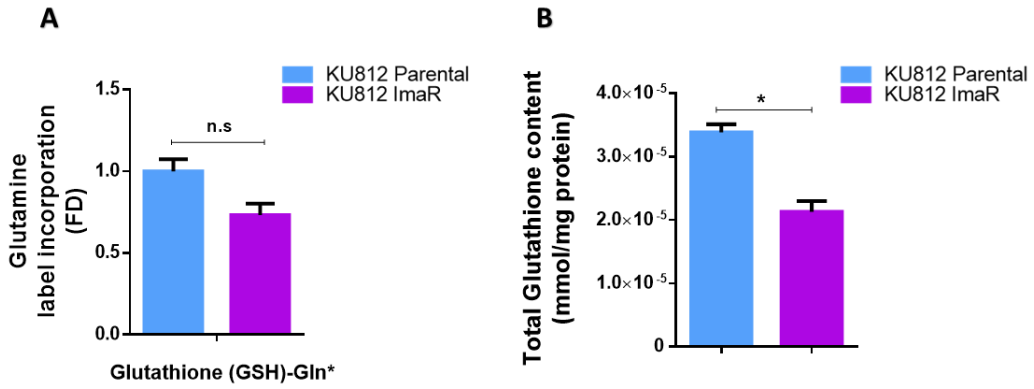

Figure 5.2.20 Differences of glutathione metabolism between KU812 imatinib-resistant and KU812 Parental cells. A) ^{13}C Glutamine label incorporation into glutathione metabolite in KU812 imatinib-resistant (ImaR) compared to KU812 Parental cells under normoxia, determined by NMR analysis**. B)** Total glutathione levels in KU812 Parental and ImaR cells under normoxia determined as described in **section 4.5**. Data are provided as mean ± SD of n=3 of one representative experiment for **panel A** and mean ± SD of n=2 for **panel B**. Significance was determined by two-tailed independent sample Welch's t-test or Student's t-test. Statistically significant differences between KU812 Parental and ImaR cells are indicated as $p<0.05$ (*). Abbreviations: Fold differences, FD.

Regarding the protein levels of other proteins associated with glutathione metabolism, glutathione peroxidases (GPx1, GPx4 and GPx7) as well as glutathione-S-transferases including (GSTP1, GSTM1, and GSTM3) were strongly upregulated in KU812 ImaR cells (**Fig. 5.2.21.A**). Of note, it has been described that GPx enzymes play an important role in ROS detoxification[337] and GSTs have been also recognised as key players in the detoxification of ROS and xenobiotics such as drugs[338]. Moreover, ROS levels were further analysed to verify our hypothesis. Consistently, a decrease of 18% in the ROS levels of KU812 ImaR was determined when compared to KU812 P cells (**Fig 5.2.21.B**)**.** Therefore, these results highlighted an important role of glutathione in the detoxification reactions in KU812 ImaR cells despite the reduced *de novo* synthesis of glutathione described above. In addition, glutathione uptake has been described in different tissues and cells such as brain cells even though the transporters have not been fully elucidated[339]. Thus, we hypothesise that KU812 ImaR cells take up glutathione from the cell media (RPMI-1640 contains 3.3 µM of reduced glutathione) in order to accomplish the detoxification reactions mentioned above. Nevertheless, this hypothesis would require further experimental investigation.

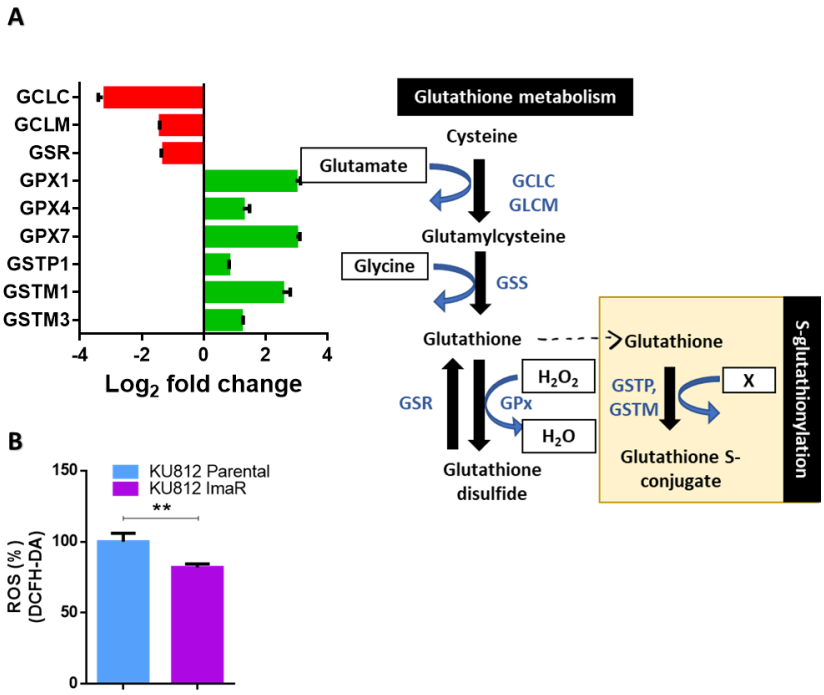

Figure 5.2.21 Protein profile of glutathione metabolism and ROS levels differences in KU812 imatinib-resistant compared to KU812 Parental cells. A) The protein expression profiling of proteins related to glutathione metabolism in KU812 imatinib-resistant (ImaR) and Parental cells under normoxia was obtained using SILAC-based proteomic experiments described in **section 4.15**. Log2 fold change values (ImaR *vs* Parental) were calculated as explained in **section 4.15** and represented by green colour = protein upregulation; and red = protein downregulation. **B)** Intracellular ROS levels in KU812 Parental and ImaR cells measured under normoxia as explained in **section 4.6.** Data are provided as mean ± SD of n = 2. Significance was determined by two-tailed independent sample Welch's t-test. Statistically significant differences between KU812 Parental and ImaR cells are indicated as $p<0.01$ (**).

According to the results above, we next studied if the inhibition of ROS scavenging and detoxification processes, by using the inhibitors RSL-3 (GPx4 inhibitor) and Ezatiostat (GSTP1 inhibitor), could be a good strategy to selectively kill the KU812 ImaR cells. Both inhibitors show antiproliferative effects in KU812 P and ImaR cells (**Fig. 5.2.22**). However, we could not find any significant differences between KU812 P and KU812 ImaR cells with regard to IC_{50} values.

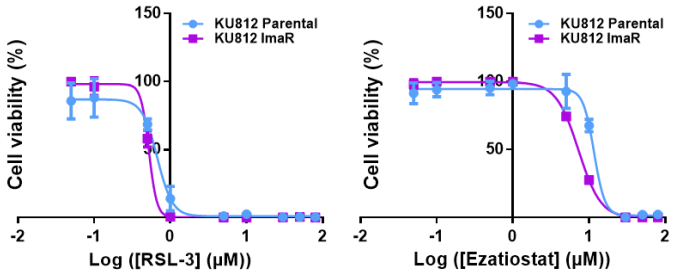

Cell line	RSL-3 (µM)	Ezatiostat (µM)
KU812 P	0.64±0.09	14.48±5.83
KU812 ImaR	0.58±0.10	7.20±0.22

Figure 5.2.22 Effect of RSL-3 and Ezatiostat inhibitors on the cell viability of KU812 parental and imatinib-resistant cells. KU812 parental (P) and imatinib-resistant (ImaR) cells were incubated 72 hours with DMSO (vehicle control) or the increasing concentrations of the corresponding inhibitor. Data are provided as mean ± SD of n=2 and significance was determined by two-tailed independent sample Welch's t-test.

5.2.2.7 Development of resistance to imatinib implied a reorganisation of mitochondrial metabolism and electron transport chain activities to increase mitochondrial respiration capacity

In order to start exploring the mitochondrial metabolism changes upon imatinib resistance in KU812 CML cells incubated under normoxic and hypoxic conditions, a thorough study of the mitochondrial respiration capacity under normoxia using the Seahorse XF96 Extracellular Flux Analyser was performed (described in **section 4.12**). As shown in **Figs. 5.2.23.A-B**, KU812 ImaR cells exhibited higher basal and maximal respiration capacity compared to KU812 P cells, both after normoxic and hypoxic incubation conditions. Indeed, ATP production was also increased upon imatinib resistance acquisition under normoxic incubation conditions (**Figure 5.2.23.C**). With regard to the ATP production capacity of cells incubated under hypoxic conditions, we also observed an increase tendency of ATP production capacity that was not significantly different due to the high variability of the replicates.

As mentioned above, KU812 ImaR relative to KU812 P cells increased the cell volume by 38% during the acquisition of imatinib resistance, so it could be that the increase of mitochondrial respiration capacity observed above could be due to the increase of KU812 ImaR cell volume. The translocase of outer mitochondrial membrane 20 (TOMM20) has been shown to correlate with mitochondrial mass and function[340] and, interestingly, TOMM20 protein expression was 2.3-fold higher in KU812 ImaR relative to KU812 P cells (**Table 1 from Appendix 2**). For this reason, the mitochondrial respiration capacity results were additionally normalised to the $\log_2$ fold change of the protein TOMM20 (**Fig. 3 from Appendix 2**). Results showed that both the basal and maximal respiration and the ATP production per mitochondrial mass were significantly higher in KU812 ImaR than in KU812 P cells.

We next assessed the contribution of different metabolic sources including glutamine, pyruvate (from glucose or other carbon sources) and FAO to mitochondrial respiration capacity in both cell lines incubated in both normoxic and hypoxic conditions. As depicted in **Fig. 5.2.23.C,** these substrates entailed more than 80 % of the O_2 consumption in KU812 P cells incubated in both normoxic and hypoxic conditions, but they contributed to a much lower extent to O_2 consumption in KU812 ImaR cells (36 % under normoxic incubation conditions and 54 % under hypoxic incubation conditions). Thus, results suggest that KU812 ImaR cells may be utilising other sources rather than pyruvate, glutamine or FAO to perform mitochondrial respiration.

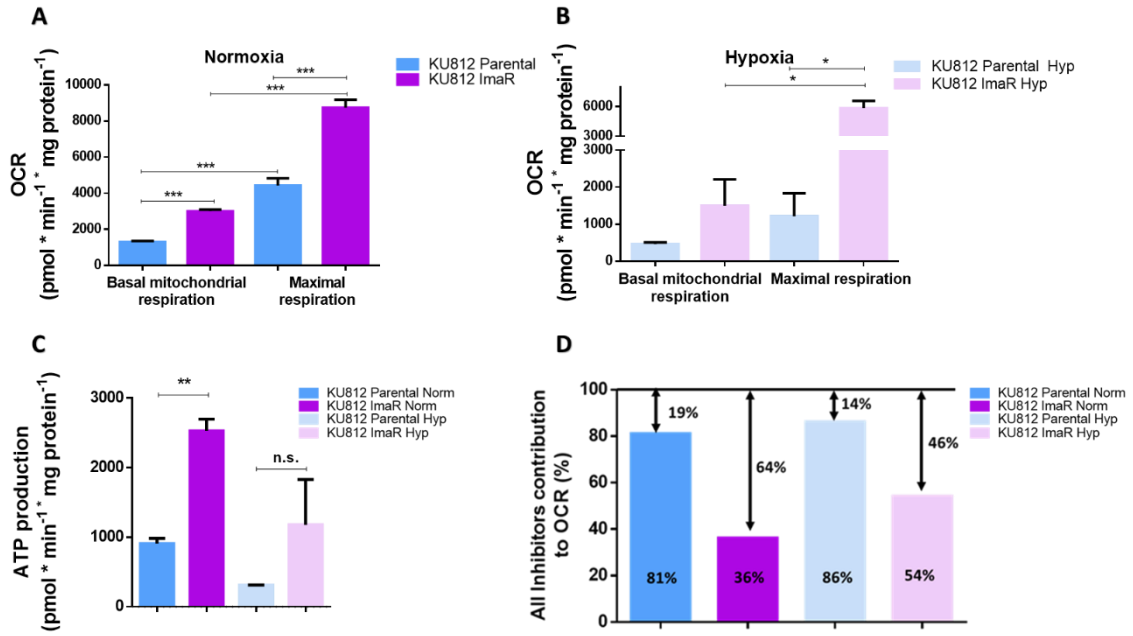

Figure 5.2.23 Characterisation of mitochondrial respiration in KU812 imatinib-resistant vs. KU812 Parental cells. A, B and C) OCR values were measured under normoxia during sequential injection of oligomycin, CCCP, and Rot+Ama in KU812 Parental and imatinib-resistant (ImaR) cells previously incubated under normoxic and hypoxic conditions. Basal and maximal respiration of cells incubated under normoxic (**panel A**) and hypoxic (**panel B**) conditions were calculated as described in **section 4.12.** ATP production-associated respiration of KU812 Parental vs. ImaR cells previously incubated under normoxic and hypoxic conditions (**panel C**) were calculated as explained in **section 4.12**. **D)** Fatty acid, glutamine and glucose/pyruvate contributions to mitochondrial respiration in KU812 Parental and ImaR cells previously incubated under normoxic and hypoxic conditions were determined by measuring OCR under normoxia during sequential injections of Etomoxir, BPTES, UK5099 and Oligomycin inhibitors. For **panel A, B and C** cells were first incubated with KHB Buffer in the presence of glucose and glutamine. For **panel D,** cells were first incubated with DMEM media in the presence of glucose and glutamine. Data were normalised by protein. Data are provided as mean ± SD of n=3**.** Significance was determined by two-tailed independent sample Student's t-test. Statistically significant differences between KU812 P and ImaR cells incubated under normoxic or hypoxic incubation conditions are indicated as p≥0.05 (n.s.), p<0.05 (*), p<0.01(**), and p<0.001(***).

To complete the characterisation of the mitochondrial metabolism, we further looked at the protein profile of proteins involved in the mitochondrial metabolism. Results exhibited higher expression of several proteins of the TCA cycle including CS, ACO2, OGDH, SDH, and

MDH in KU812 ImaR compared to KU812 P cells (**Fig. 5.2.24**). Regarding the pyruvate metabolism, the pyruvate carboxylase, which catalyses the conversion of pyruvate to oxaloacetate, was downregulated by a fold of 8.70-fold down KU812 ImaR compared to KU812 P cells, suggesting that pyruvate entrance into TCA cycle occurs via pyruvate PDH. In agreement, even though non-significant differences were found with regard to PDH or PDP in KU812 ImaR cells, we did observe an 2.6-fold increase of the regulatory subunit of pyruvate dehydrogenase phosphatase regulatory subunit (PDPR), which plays a role in PDH activation. Moreover, KU812 ImaR cells also showed a 3.5-fold increase in the NAD-dependent mitochondrial isoform of ME2, suggesting that KU812 ImaR cells can redirect mitochondrial malate to form pyruvate.

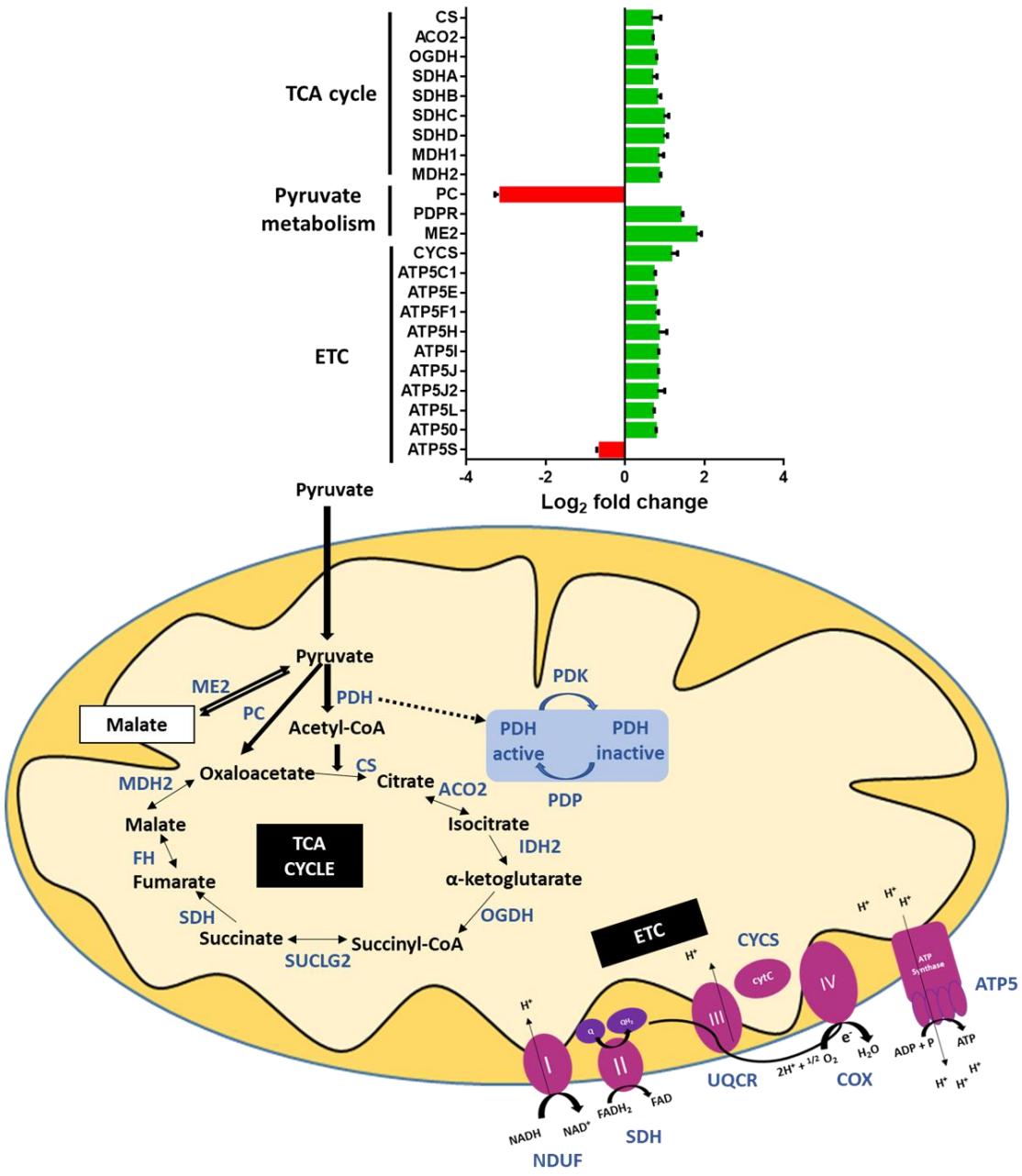

Figure 5.2.24 Protein profile differences of KU812 imatinib-resistant when compared to KU812 Parental regarding its mitochondrial metabolism and mitochondrial-complementary metabolic pathways. The protein abundances of proteins related to pyruvate and mitochondrial metabolism under normoxia were obtained using SILAC-based proteomic experiments described in **section 4.15**. Log_2 fold change values were calculated as explained in **section 4.15** and represented by green colour = protein upregulation; and red = protein downregulation. Data are provided as mean ± SD of n=2.

The mitochondrial network is characterised by the final ATP production through the coupled integration of the ETC with oxidative phosphorylation. In our study, we have demonstrated that KU812 cells increased mitochondrial respiration capacity upon the acquisition of imatinib resistance. For that, we next examined the protein profile data (shown in **Tables 1-2 from Appendix 2**) of proteins involved in the ETC function. **Fig. 5.2.24** depicted an overall upregulation of proteins associated with the ETC in KU812 ImaR relative to KU812 P cells. In particular, KU812 ImaR exhibited a higher protein expression of the SDH (complex II), CYCS, and the ATP synthase (ATP5) subunits (complex V) including ATP5C1, ATP5E, ATP5F1, ATP5H, ATP5I, ATP5J, ATP5J2, ATP5L, and ATP50, when compared to KU812 P cells. On the other hand, non-significant differences were observed in catalytic protein subunits associated with complex I, III and IV between KU812 P and ImaR cells.

In light of the upregulation of key proteins for ETC function, we next investigated the differences in ETC complex activities associated with imatinib resistance acquisition by using permeabilised cells and measuring OCR using the Oroboros Oxygraph-2k respirometer after the injection of different inhibitors and substrates (approach described in **section 4.13**). **Figure 5.2.25.A** showed that complex I activity was significantly lower in KU812 ImaR relative to KU812 P cells when complex I substrates malate and glutamate were only added. Moreover, complex I activity only increased in KU812 ImaR cells until pyruvate was further added. This result suggests that the complex I activity of KU812 ImaR cells turned out to be dependent on pyruvate, unlike in KU812 P cells, whose mitochondria were able to consume O_2 even with only malate as substrate. Regarding the complex II activity, KU812 ImaR cells exhibited the same activity than KU812 P cells when succinate was added as a substrate (**Fig. 5.2.25.B**). Finally, a lower maximal activity of complex IV was observed in KU812 ImaR cells when compared to KU812 P cells (**Fig. 5.2.25.C**). However, the OCR measured during the sequential activity of either complexes I+III+IV or complexes II+III+IV, was not significantly different between KU812 P and ImaR cells. These results point out that the available complex IV in KU812 ImaR cells has enough capacity to absorb the electrons

coming from previous complexes and that the control of the ETC relies on the previous steps.

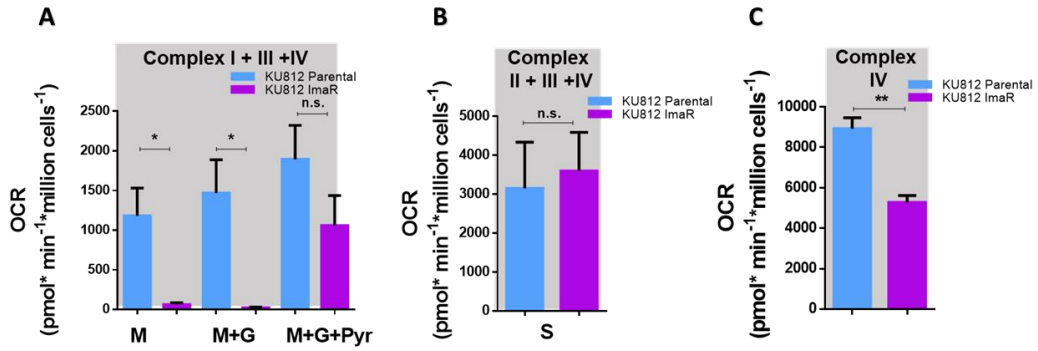

Figure 5.2.25 Activity of the different electron transport chain complexes of KU812 imatinib-resistant vs. KU812 Parental cells. Oxygen consumption rate (OCR) was measured after sequential injections of substrates and inhibitors using a two-channel, high-resolution Oxygraph respirometer under normoxia as indicated in **section 4.13.** Data were analysed using DatLab7 software. For **A (approach to study of complex I activity**): 2mM malate + 5mM ADP (M), 10mM glutamate (G), and 5mM pyruvate (P). For **B (approach to study complex II activity)**: 10mM succinate + 5mM ADP (S). For **C (approach to study complex IV activity):** 5mM Ascorbate + 5mM ADP + 0.5mM tetramethyl-p-phenylendiamine dihydrochloride (TMPD). Data were normalised by cell number. Data are provided as mean ± SD of n = 3 and significance was determined by two-tailed independent sample Student's t-test. Statistically significant differences between KU812 P and ImaR cells are indicated as $p \geq 0.05$ (n.s.), $p < 0.05$ (*), and $p < 0.01$(**). Abbreviations: glutamate, G; malate, M; pyruvate, Pyr; and succinate, S.

Next, we intended to address whether the differences of complex I and IV activities observed in KU812 ImaR when compared to KU812 P cells were due to the imatinib-resistance acquisition or merely to the imatinib treatment. Therefore, complex I, II and IV activities were measured in KU812 P cells treated for 72h with imatinib (from here named KU812 Treated). As shown in **Figs. 5.2.26.A-B**, acute drug exposure to imatinib did not induce complex I pyruvate dependency and neither reduce complex IV activity in KU812 P cells. Moreover, no significant differences were found regarding complex II activity (**Fig. 5.2.26.C**). Thus, we confirmed that the mitochondrial phenotype exhibited in this study by KU812 ImaR cells was due to the imatinib resistance acquisition.

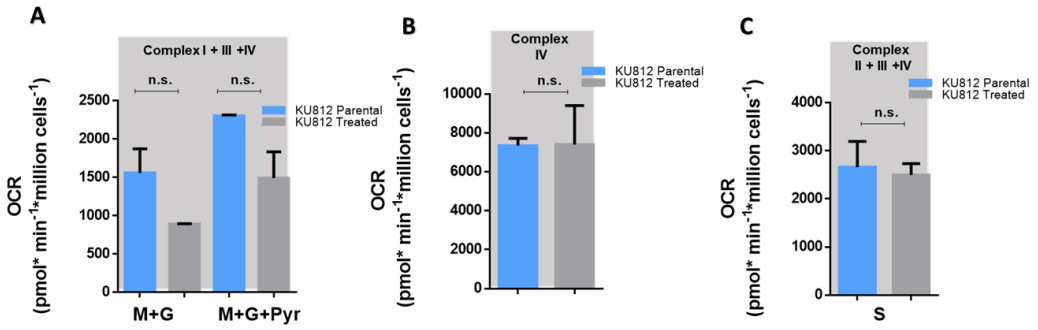

Figure 5.2.26 Activity of the different electron transport chain complexes of KU812 Imatinib-treated vs. KU812 Parental cells. OCR measurements of KU812 Parental and Treated (KU812 Parental cells treated with 80nM imatinib for 72 hours) were determined by Oroboros Oxygraph-2k respirometer under normoxia. OCR were measured after sequential injections of substrates and inhibitors. For **A (approach to study complex I activity**): 2mM malate + 5mM ADP + 10mM glutamate (M+G), and 5mM pyruvate (P). For **B (complex IV activity):** 5mM Ascorbate + 5mM ADP + 0.5mM tetramethyl-p-phenylendiamine dihydrochloride (TMPD). For **C (approach to study complex II activity)**: 10mM succinate + 5mM ADP (S). Data were normalised by cell number. Data are provided as mean ± SD of n = 2 and significance was determined by two-tailed independent sample Welch's t-test. Statistically significant differences between KU812 P and Treated cells are indicated as p≥0.05 (n.s.).

5.2.2.8 Development of resistance to imatinib enhance mitochondrial Glycerol-3-phosphate dehydrogenase expression and branched-chain amino acids metabolism

Since we observed an increase of mitochondrial respiration capacity in KU812 ImaR cells together with the above-mentioned alterations in the mitochondrial metabolism, we further investigated alternative fuelling pathways of mitochondrial respiration. It has been already explained that the GP shuttle plays an important role in bypassing the complex I during cytosolic NADH oxidation[210]. Therefore, we hypothesised that GP shuttle could contribute to the higher mitochondrial respiration capacity observed in KU812 ImaR cells. Differences in the expression profiling of proteins involved in this pathway between KU812 P and ImaR cells were firstly examined. As mentioned in **section 5.2.2.2**, there was a significant upregulation (FD=1.8) of the mitochondrial isoform GPD2 (**Fig. 5.2.10**).

Furthermore, OCR rates were measured by Oroboros Oxygraph-2k respirometer in both permeabilised KU812 P and ImaR cells after the addition of GP. **Fig. 5.2.27.A** shows that there was an increase of mitochondrial respiration when GP was added in KU812 ImaR relative to KU812 P cells, thus confirming a correlation between GPD2 upregulation and its contribution to mitochondrial respiration capacity in KU812 ImaR cells.

Next, we examined if the GPD2-dependent mitochondrial respiration observed in KU812 ImaR cells was due to imatinib resistance acquisition or to imatinib treatment by comparing OCR measurements of KU812 P versus KU812 Treated cells. We observed that KU812 Treated cells were not able to increase mitochondrial respiration after GP addition (**Fig. 5.2.27.B**), thus confirming that the mitochondrial phenotype exhibited by KU812 ImaR cells regarding GP shuttle was due to the acquisition of resistance to imatinib. Nevertheless, when GPD2 was inhibited in both parental and ImaR cells by adding iGP-1 inhibitor[341], only 60% of decrease of KU812 ImaR and P cells viability was obtained (**Fig. 5.2.27.C**) even though concentrations up to 1mM were added.

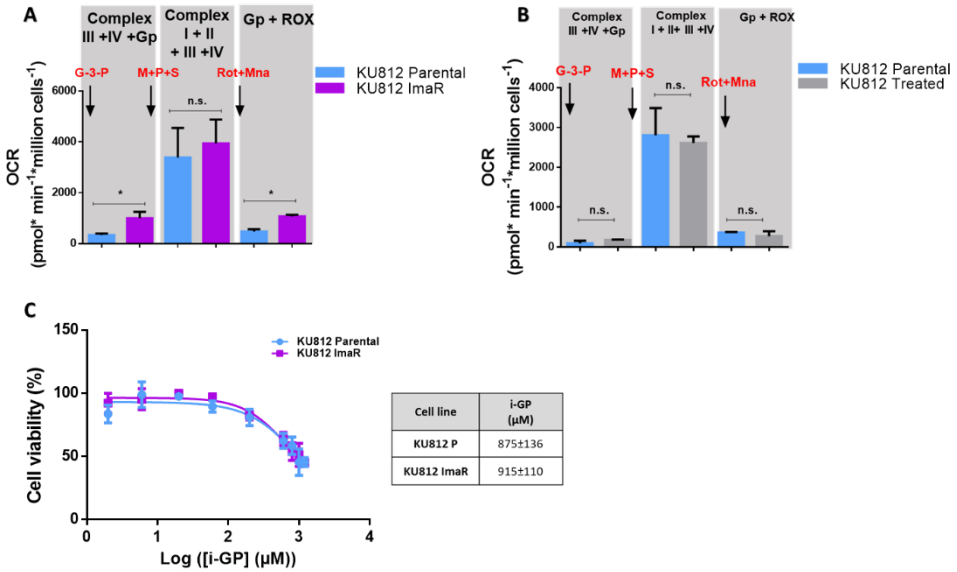

Figure 5.2.27 Contribution of glycerol-3-phosphate shuttle to the mitochondrial respiration of KU812 imatinib-treated or KU812 imatinib-resistant vs. KU812 Parental cells. A and B) OCR measurements of KU812 imatinib-resistant (ImaR) vs. KU812 Parental (P) (**Panel A**), and KU812 Treated (KU812 P cells treated with 80nM imatinib for 72 hours) vs. KU812 P cells (**panel B**) previously incubated under normoxic conditions determined under normoxia by Oroboros Oxygraph-2k respirometer. OCR were measured after sequential injections of 10mM Gp + 5mM ADP, 10mM succinate + 5mM pyruvate + 2mM malate, 5mM malonic acid, and 0.5µM rotenone + 2.5µM antimycin. Data were normalised by cell number and recorded parameters were calculated as explained in **section 4.13. C)** Effect of iGP-1 inhibitor on the cell viability of KU812 P and ImaR cells. Cells were incubated for 72 hours with DMSO (vehicle control) or different concentrations of iGP-1. Data are provided as mean ± SD of n = 2 and significance was determined by two-tailed independent sample Welch's t-test. Statistically significant differences between KU812 P and Treated cells**,** and KU812 P and KU812 ImaR are indicated as p≥0.05 (n.s.) and p<0.05 (*).

As BCAAs catabolism has also been described to fuel the TCA cycle, thus contributing to the mitochondrial respiration, we decided to further study their metabolism. First, we determined the exchange fluxes and the intracellular content of isoleucine, leucine, and valine under normoxia and hypoxia. **Figure 5.2.28.A** depicts that there was a higher consumption of BCAAs in KU812 ImaR than in parental cells under normoxia. However, non-significant differences were determined regarding BCAAs exchange fluxes under hypoxia. Moreover, a higher intracellular content of isoleucine and leucine was observed in KU812

ImaR cells under normoxia and hypoxia, while there were no significant differences regarding the intracellular content of valine (**Fig. 5.2.28.B**).

In parallel, the intracellular content of the BCAA degradation products C3, C4 and C5 ACs was determined in KU812 P and ImaR cells under normoxia. As shown in **Fig. 5.2.28.C**, KU812 ImaR cells showed higher intracellular levels of this three ACs when compared to KU812 P cells, indicative of a higher BCAAs catabolism in KU812 ImaR relative to KU812 P cells.

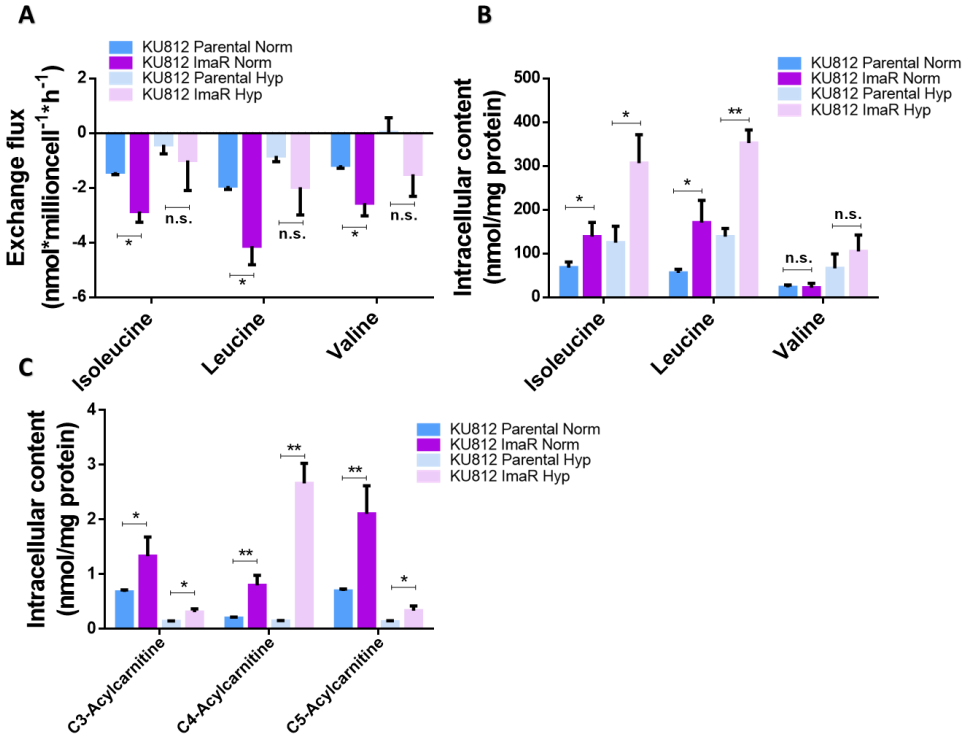

Figure 5.2.28 Exchange fluxes and intracellular content of BCAAs and acylcarnitines in KU812 Parental and imatinib-resistant cells. A and B) Exchange fluxes (**A**) and intracellular content (**B**) of isoleucine, leucine and valine in KU812 Parental and imatinib-resistant (ImaR) cells under normoxia (Norm) and hypoxia (Hyp) were measured by HPLC-MS/MS as described in **section 4.8**. **C)** Intracellular content of C3, C4 and C5 acylcarnitines in KU812 Parental and ImaR cells were measured by HPLC-MS/MS. Data are provided as mean ± SD of n = 3 of one representative experiment. Significance was determined by two-tailed independent sample Student's t-test. Statistically significant differences between KU812 Parental and ImaR cells are indicated as $p \geq 0.05$ (n.s.), $p < 0.05$ (*), and $p < 0.01$ (**).

Given that KU812 ImaR cells exhibited a higher consumption of BCAAs under normoxia, we also analysed the protein profile of proteins associated with the transport and catabolism of BCAAs in KU812 ImaR relative to KU812 P cells under normoxia. Consistent with the higher flux of BCAAs observed above, two main BCAA transporters SLC7A5 (also referred as LAT1) and SLC3A2 were significantly upregulated by a FD of 1.73 and 1.84, respectively, in KU812 ImaR cells (**Fig. 5.2.29**). Moreover, BCAT 1 and 2 and branched-chain keto acid dehydrogenase (BCKD) HA and HB were significantly downregulated in KU812 ImaR cells. It is worth mentioning that the enoyl-CoA hydratase (ECHS1), which is an essential enzyme involved in valine catabolism but not in leucine and isoleucine catabolism[342], was significantly upregulated by a FD of 1.9 in KU812 ImaR relative to KU812 P cells. Of note, the end-product of isoleucine and leucine oxidation is acetyl-CoA (metabolic fuel of ETC-complex I), whereas succinyl-CoA (metabolic fuel of ETC-complex II substrate) is the end product of valine oxidation. Altogether, these results suggest that even though the higher flux of the three BCAAs observed in KU812 ImaR cells, they may be prioritising the oxidation of valine to fuel the TCA cycle through succinyl-CoA, while isoleucine and leucine were accumulated as fuel reserve.

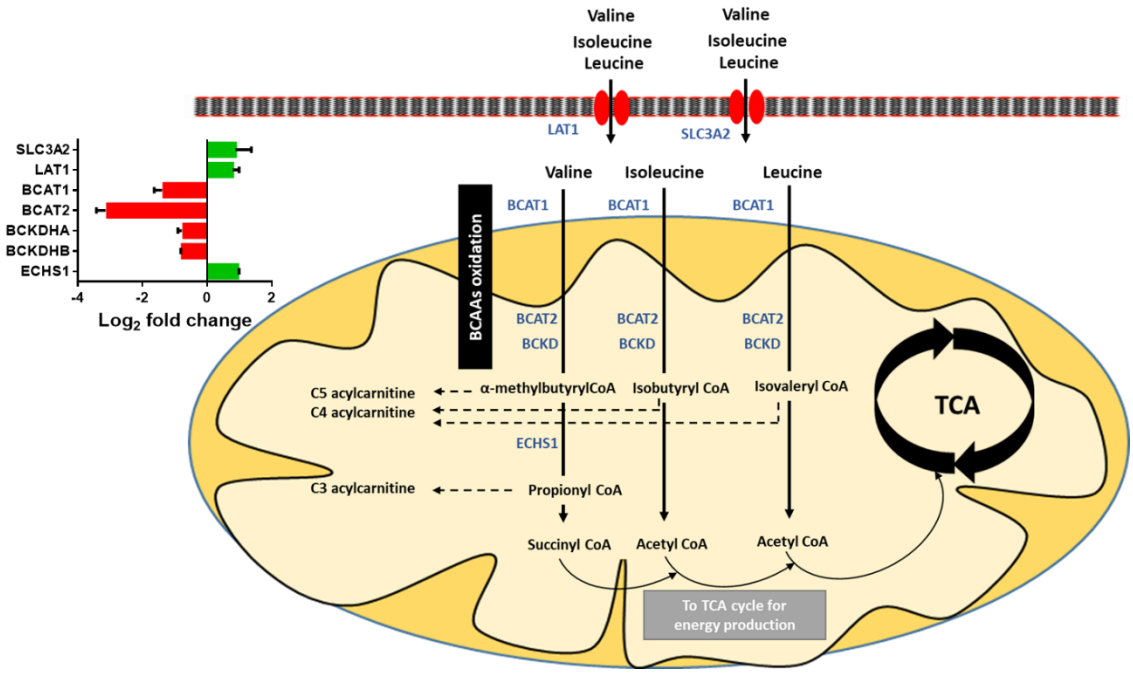

Figure 5.2.29 Protein profile of BCAAs transport and catabolism in KU812 imatinib-resistant vs. KU812 Parental cells. The protein expression profiling of proteins related to BCAAs catabolism under normoxia was obtained for KU812 Parental and imatinib-resistant (ImaR) cells using SILAC-based proteomic experiments described in **section 4.15**. Log_2 fold change values (ImaR vs Parental cells) were calculated as explained in **section 4.15** and represented by green colour = protein upregulation; and red = protein downregulation. Data are provided as mean ± SD of n=2.

5.2.2.9 The acquisition of imatinib resistant alters the fatty acid metabolism of KU812 cells

The oxidation of FAs provides Acetyl-CoA to be used in the TCA cycle, and NADH and $FADH_2$ coenzymes to be used in the ETC, whereas FA synthesis provides building blocks for cellular structures[343]. In order to examine FAO and FA synthesis upon the acquisition of imatinib resistance, we firstly analysed the protein profile of proteins involved in these pathways. Secondly, we explored the FAO dependency as another alternative pathway fuelling the mitochondrial respiration of KU812 ImaR relative to KU812 P cells incubated under normoxic conditions by performing a FA Mitofuel test under normoxia using the Seahorse

XF96 Extracellular Flux Analyser (described in **section 4.12)**. As depicted in **Figure 5.2.30,** key controlling enzymes involved in FAO (CPT1A; and ACAT1) were significantly upregulated by a 1.76 and 3.61-fold down, respectively, in KU812 ImaR cells. Moreover, mitochondrial respiration capacity of KU812 ImaR was much less dependent on FAO than for KU812 P cells (**Fig. 5.2.31**). Altogether, these results suggest that FAO may not be the cause of the increase of mitochondrial respiration capacity in KU812 ImaR cells observed above. On the other hand, proteins associated with FA synthesis such as the mitochondrial citrate transporter (SLC25A1) and the acetyl-CoA carboxylase alpha (ACACA) proteins were significantly upregulated (2.06 and 3.46-fold up, respectively) in KU812 ImaR compared to KU812 P cells, thereby indicating an alteration of FA synthesis in KU812 cells upon the imatinib resistance acquisition.

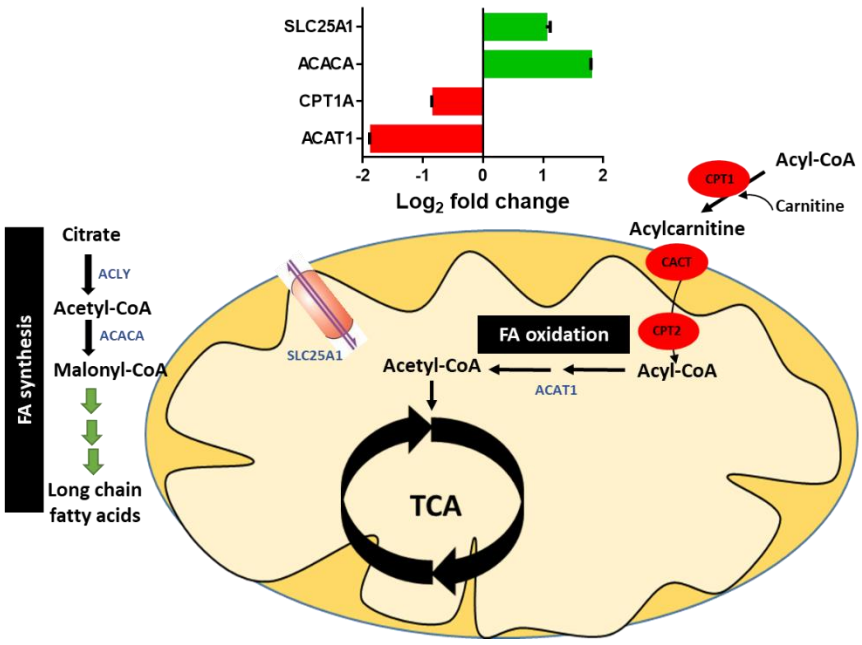

Figure 5.2.30 Protein profile differences of KU812 imatinib-resistant cells when compared to KU812 Parental cells regarding fatty acid metabolism. The protein expression profiling of proteins related to fatty acid metabolism in KU812 imatinib-resistant (ImaR) and parental cells was obtained using SILAC-based proteomic experiments described in **section 4.15**. Fold Differences (log_2FC) between KU812 ImaR and Parental cells were calculated as explained in **section 4.15** and represented by green colour = protein upregulation; and red = protein downregulation. Data are provided as mean ± SD of n=2.

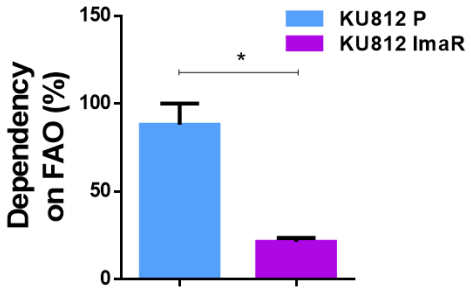

Figure 5.2.31 Fatty acid contribution to mitochondrial respiration of KU812 imatinib-resistant vs. KU812 Parental cells. Dependency of mitochondrial respiration to fatty acid oxidation of KU812 Parental (P) and imatinib-resistant (ImaR) cells incubated under normoxic conditions was calculated by measuring under normoxia the OCR value during sequential injections of Etomoxir, BPTES, UK5099 and Oligomycin inhibitors. Cells were first incubated with DMEM in the presence of glucose and glutamine. Data were normalised by protein. The percentage of dependency to fatty acid oxidation was calculated as explained in **section 4.12**. Data are provided as mean ± SD of n=3 and significance was determined by two-tailed independent sample Student's t-test. Statistically significant differences between KU812 P and KU812 ImaR are indicated as $p<0.05$ (*). Abbreviations: fatty acid oxidation, FAO.

5.2.2.10 The repurposing of Doxorubicin showed to be an effective strategy to overcome TKI resistance in KU812 cells

In **Chapter 1**, we have shown that exposure to Dox significantly reduced the mitochondrial respiration capacity of cells with high mitochondrial activity. Moreover, previous studies also reported that Dox treatment alter the mitochondrial respiration of B-lymphocytes[344]. The fact that our results unveiled that KU812 ImaR cells exhibit a higher mitochondrial respiration capacity that is less dependent from canonical carbon sources (e.g. amino acids, glutamine and glucose) than KU812 P cells prompted us to hypothesise that Dox treatment could reduce the cell viability of KU812 ImaR stronger than of KU812 P cells. The results obtained when treating KU812 P and ImaR cells with Dox validated our hypothesis. Thus, we obtained a 13-fold lower IC_{50} value in KU812 ImaR relative to KU812 P cells after Dox treatment (**Fig. 5.2.32**), indicating that Dox treatment could be a suitable treatment approach to overcome imatinib resistance in CML cells.

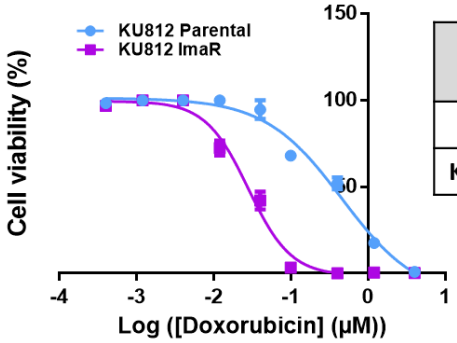

Cell line	Doxorubicin (µM)
KU812 P	0.36±0.09
KU812 ImaR	0.03±0.01 (*)

Figure 5.2.32 Effect of Doxorubicin chemotherapeutic on the cell viability of KU812 Parental and imatinib-resistant cells. KU812 Parental (P) and imatinib-resistant (ImaR) cells were incubated 72 hours with DMSO (vehicle control) or different concentrations of Doxorubicin. Data are provided as mean ± SD of n = 2 and significance was determined by two-tailed independent sample Welch's t-test. Statistically significant differences between KU812 P and KU812 ImaR are indicated as $p<0.05$ (*).

6. DISCUSSION

6 DISCUSSION

Despite the great achievements made during the past decades, resistance to chemotherapeutic drugs continues to be a major problem in leukaemia treatment[345]. The mechanisms of drug resistance in leukaemia are still not clear. Indeed, many studies have revealed that drug resistance acquisition may be a result of multiple factors. For instance, Zhang et al. reviewed the three common mechanisms of drug resistance in AML cells including drug resistance-related protein and enzymes, miRNAs alterations, and autophagy[29]. On the other hand, similar and additional mechanisms of resistance have been revealed regarding the acquisition of resistance to imatinib in CML cells (e.g. lower oral bioavailability, increase of plasma protein binding, overexpression of multidrug resistance genes, BCR-ABL1 point mutations, and BCR-ABL1 gene amplification) (reviewed in [346]). In the last years, it has emerged that metabolic rewiring may play a relevant role in the development of resistance in leukemic cells[285,347]. Moreover, we postulate that this rewiring entails new vulnerabilities in leukaemia that can be exploited for the development of new chemotherapeutic drugs.

In this thesis, we have unveiled the importance of the metabolic changes in the process of the acquisition of resistance to common chemotherapeutic drugs in AML and CML. To this end, we have performed a comprehensive metabolic characterisation of AML cells sensitive or resistant to the conventional AML chemotherapeutic drugs, AraC and Dox (**Chapter 1**); and of CML cells sensitive or resistant to TKIs, and particularly to imatinib which is the standard drug of CML treatment (**Chapter 2**). These studies were performed both under normoxic and hypoxic incubation conditions.

Our results revealed that, upon the acquisition of drug resistance, leukaemic cells remodel many of the main metabolic pathways, and that this metabolic rewiring is not unique. Thus, most of the here studied metabolic pathways have shown a reprogramming that is in some cases associated with the chemotherapeutic drug (drug-dependent) while for others depend on the initial metabolic phenotype of the leukemic cells (cell-line dependent).

Leukaemia parental cell lines display different metabolic phenotypes

Glycolysis and mitochondrial respiration are two major energy-yielding pathways. In this thesis, we have demonstrated that AML parental cell lines can display completely opposite metabolic profiles. Although our THP-1 and HL-60 parental AML cell lines exhibited a similar glycolytic phenotype under normoxic and hypoxic conditions, THP-1 P cells presented a greater mitochondrial respiration capacity than HL-60 P cells. And most importantly, this greater mitochondrial respiration capacity seems to be related with a higher consumption and metabolism of some amino acids, especially those that are precursors of TCA cycle intermediates. The observed differences regarding the initial metabolic phenotypes in AML cells provided the answer to the first specific objective of this thesis and, additionally, raised the fact that the metabolic reprogramming derived from the acquisition of AraC and Dox resistance exhibit differences that are dependent on the initial metabolic phenotype of the AML cell line of study (cell-line dependent).

In the case of CML, we have only used a cell line (KU812) so we cannot conclude if there are distinct metabolic profiles among CML cell lines. In any case, our results showed that KU812 P cell model exhibited a similar metabolic profile to the THP-1 cell model at the level of glycolysis and mitochondrial respiration capacity. Moreover, the metabolic alterations observed upon the acquisition of imatinib resistance including the increase of glycolytic flux and mitochondrial respiration capacity were overall similar to the observed changes in THP-1 cells upon the acquisition of AraC resistance.

Reprogramming of metabolism plays a key role in the acquisition of AraC, Dox and imatinib resistance of the studied AML and CML cell models.

Although in literature, there was some evidence of the relevant role of metabolic reprogramming in leukaemia drug resistance acquisition, there were no publications that could demonstrate this conjecture from a systems biology point of view. Therefore, in this thesis we have explored the protein expression levels of our four resistant AML cell lines (**Chapter 1**) and the resistant CML cell line (**Chapter 2**) under normoxic conditions using

SILAC-based protein mass spectrometry experiments. The analysis of the most enriched biological processes has revealed that both cellular processes and metabolic processes were overall the most altered biological processes during the acquisition of AML and CML resistance to common chemotherapeutic drugs. These findings reinforce the idea to carry out the main objective of our thesis "to investigate the rewiring of cell metabolism occurring in the process of resistance acquisition to different conventional therapeutic treatments in AML and CML haematological malignancies" and encouraged us in the subsequent search for similarities and differences in metabolic changes associated with the acquisition of resistance to the different drug studied in the different cell models.

Hereafter, the results obtained and discussed in the context of each cell model are globally examined to highlight the major features observed in terms of metabolic reprogramming that are common for all the resistant cell lines (i.e. due to the drug resistance acquisition), or that are cell line or drug dependent.

Glycolytic flux: The effects of the drug resistance

It is well-known that cancer cells rewire their metabolism to promote cell proliferation and survival. Indeed, one of the common metabolic alterations in the majority of cancers including AML and CML is increased glycolysis[263,280,282,348,349]. To our knowledge, few metabolic studies have been conducted for AML cells resistant to AraC and Dox chemotherapeutic drugs[260,285,350]. In the case of CML cells, it has been shown that glycolysis is even more increased in CML cells resistant to imatinib when compared to CML cells non-resistant to imatinib[117,261]. It is worth noting that these studies were only performed under normoxia. For all these reasons, we decided to carry out two of the specific objectives of this thesis, the characterisation of the metabolic profiles of (1) two different AML cell models and (2) a CML model, under two different oxygen incubation conditions (normoxia and hypoxia).

Our results are unique in that they reveal that AML cells, which are characterised by a very dissimilar initial metabolic phenotype (described in **Chapter 1, section 5.1.2.1**), are both

able to acquire a more glycolytic phenotype upon AraC resistance under both normoxic and hypoxic incubation conditions. With regard to Dox resistance acquisition in AML cells, our results unveiled that the acquisition of Dox resistance correlates with a lower glycolytic phenotype under normoxia. However, the effect of Dox resistance on the glycolytic flux under hypoxia is less evident. Thus, the effect of Dox resistance on the glycolytic flux varies depending on the AML cell line and on the oxygen conditions to which cells were exposed.

Furthermore, the metabolic characterisation of KU812 CML cells resistant to imatinib, showed that the resistant cells increase the glycolytic flux upon the acquisition of imatinib resistance under both normoxic and hypoxic incubation conditions. This metabolic phenotype is similar to the one observed for the AML cells (THP-1 and HL-60) upon the acquisition of AraC resistance, a fact that encourages us to further study possible phenotypic links between the acquisition of AraC and imatinib resistance. Noteworthy, a similar metabolic phenotype has been described for K562 CML cell line resistant to imatinib under normoxia[261]. And, to our knowledge, CML cell's metabolic reprogramming associated with imatinib resistance under hypoxic incubation conditions has not been previously reported in the literature.

The analysis of the protein expression changes upon the acquisition of AraC and imatinib resistance revealed that, even though glycolysis showed to be a metabolic process closely related to the acquisition of AraC and imatinib resistance, the metabolic reprogramming at protein expression level is achieved following a different strategy. In fact, both THP-1 AraC and KU812 ImaR cells showed even a downregulation of some key proteins related to the glycolysis pathway (e.g. GLUTs, HK, PK, etc.). Nevertheless, the data obtained from the protein profile analysis interestingly suggest that both THP-1 AraC and KU812 ImaR cells may be counteracting these observed protein downregulations by upregulating the expression of proteins belonging to alternative pathways associated with glycolysis (as it happens in KU812 ImaR cells) or by dramatically downregulating the FBP protein, the negative regulator of glycolysis[351] (as it happens in THP-1 AraC cells). In brief, we speculate that the main determinants are the increase of GLUT1 glucose transporter in HL-60 AraC cells, the decrease of FBP1 in THP-1 AraC cells, and the increase of GLUT5 and proteins

associated with the insulin-dependent glucose uptake via translocation of GLUT4 in KU812 ImaR cells.

Pentose phosphate pathway and glycogenolysis: key metabolic features and vulnerabilities of KU812 CML cells resistant to imatinib

PPP has been revealed to play a relevant role in proliferation and redox homeostasis of cancer cells, so it was of our interest to explore since which point this pathway may have a relevant role in drug resistance acquisition. In this thesis, this pathway has been deeply studied in Chapter 2, and only protein expression levels were analised in Chapter 1.

In the case of the here studied CML resistant cell model, we have observed that imatinib resistance development has enhanced both the oxidative and non-oxidative branches of the PPP, concurring with the results reported by Noel *et al.* using K562 imatinib-resistant cells[261]. This fact led to the hypothesis that KU812 ImaR cells may require more R5P, which plays a vital role for nucleotide synthesis, and NADPH, which is essential for fatty acid and proline synthesis, redox homeostasis and ROS scavenging[105]. In fact, all these processes are significantly upregulated in KU812 ImaR cells (discussed in more detail below). As an example, the protein profile results of CML resistant vs. parental cells highlighted an overall upregulation in the expression of proteins associated with FA synthesis (shown in **Chapter 2, section 5.2.2.9**). Moreover, our group and others have previously described the role of TKTL1 in major metabolic reprogramming processes of cancer cells[115]. Interestingly, TKTL1 was one of the most upregulated proteins in the protein profile results. A study performed by Zhao *et al.* (2010) revealed that the inhibition of TKTL1 by oxythiamine enhanced imatinib sensitivity in hematopoietic cells[117]. Therefore, we propose TKTL1 inhibition as a possible strategy for TKI resistance overcoming.

With regards to AML resistant cells, we have observed a downregulation of proteins of the oxidative PPP in THP-1 AraC cells, whereas non significative changes were observed in the other resistant AML cell lines compared with their parental controls. All together, we can

conclude that the reprogramming of PPP depends on both drug and cell line, and its role in drug resistance should be studied individually attending to specific needs of each cell line.

Furthermore, our results revealed that KU812 ImaR cells ensure an enhanced PPP flux thanks in part to an activation of glycogen synthesis and glycogenolysis, similarly to the results shown in a study performed with T-cells[352]. These results underlined the inhibition of glycogenolysis as a possible therapeutic strategy to overcome imatinib-resistant in this CML-resistant cell model. The inhibition of glycogenolysis by DAB, CP-320626, or CP-91149 did not substantially affect more the cell viability of KU812 ImaR cells but it decreased the cell viability of both KU812 P and ImaR cells. Thus, the inhibition of glycogenolysis may be a good therapeutic strategy in CML patients whose initial metabolic phenotype is similar to the CML parental and resistant cell models here studied. It is worth noting that no changes in glycogen phosphorylase were observed in any of our AML resistant cell models.

Mitochondrial metabolism: a key metabolic player in the acquisition of resistance to leukemic chemotherapeutic drugs

The metabolic studies conducted throughout this thesis have pointed out the importance of the mitochondrial metabolism in the metabolic reprogramming associated with the drug resistance acquisition in AML and CML leukaemic cells. Mitochondrial metabolism is not only involved in energy production but also in ROS homeostasis regulation, which are essential processes for cancer cell growth and spreading. Our results highlight the importance of knowing the mitochondrial metabolic state of each sensitive/parental AML cell models to understand and anticipate the mechanisms by which these cells will evade/adapt the mitochondrial effects of the specific drugs.

Specifically, in the AML cell models used here, the acquisition of AraC resistance did not induce changes regarding the mitochondrial respiration capacity, opposite to previous studies performed in residual AML cells resistant to AraC (i.e. innately resistant to AraC) that reported an elevation of mitochondrial activity, mitochondrial respiration and a high OXPHOS[260]. This result has shed light on the metabolic differences between innate and

acquired resistant cell lines to AraC chemotherapeutic drug. Moreover, the protein profile analysis underlined a possible dysfunction of complex I in AraC resistant cells that seemed to be counteracted with an increase in the expression of proteins associated with complex II and IV protein expressions. However, this counteraction was only found in THP-1 AraC cells, thus reinforcing the hypothesis that mitochondrial alterations are more noticeable in cells with a more active mitochondrial metabolism. However, this fact needs experimental substantiation (e.g. measurement of the ETC complex specific activities).

On the other hand, the mitochondrial studies of Dox resistance unveil dramatic alterations in the mitochondrial metabolism of AML cells characterised by a remarkably active mitochondrial respiration capacity (i.e. THP-1 Dox cells). Regarding the protein profile analysis of Dox resistant vs. parental AML cells, our results exhibited an overall upregulation of proteins associated with the TCA cycle and OXPHOS in the THP-1 cell line (mitochondrially more active) but not in the HL-60 cell line (mitochondrially less active). A recent study performed by Wallace *et al.* unveiled that Dox treatment causes a phenomenon called "induction of the mitochondrial permeability transition" in cardiac cells, which is the mitochondrial ability to develop and maintain electrochemical gradients across the IMM through the opening of mitochondrial permeability transition pores[353]. This finding led us to speculate that the same phenomenon may have occurred in THP-1 Dox cells, thus explaining the decrease in mitochondrial respiration capacity observed in this cell line. In this line, we also speculate that THP-1 Dox may have upregulated the entire mitochondrial machinery to compensate for the dramatic effect of Dox treatment on mitochondrial permeability. Regarding HL-60 Dox cells, we hypothesise that the effect of Dox treatment on the mitochondrial permeability is also occurring but, on the contrary, it has not affected the mitochondrial respiration capacity because HL-60 cells themselves have low mitochondrial activity. Nevertheless, this hypothesis needs further experimental validations, for example, measuring mitochondrial membrane potential in both AML parental and Dox-resistant cell models.

The same experimental approaches and analysis conducted in **Chapter 1** were performed for the here studied CML parental and resistant cell models (KU812 P and ImaR cell lines).

Our results highlight the fact that the metabolic phenotype determined for KU812 P cells is similar to the one obtained for THP-1 P cells in that they exhibit a remarkably active mitochondrial metabolism (shown in **Section 5.2.2.7**). This fact together with the above results encouraged us to explore the mitochondria as a potential vulnerability in the here studied CML resistant cell model. As shown in **Section 5.2.2.7**, we did find a striking shift to a more mitochondrial-dependent phenotype in KU812 ImaR cells relative to KU812 P cells both at mitochondrial respiration and protein expression levels and both under normoxic and hypoxic incubations conditions, which is opposite to the mitochondrial metabolism disruptions recently described in another CML cell model (K562 cell line) resistant to imatinib[261]. Considering this finding together with what we observed in the AML study conducted in this thesis (**Chapter 1**), we speculate that the metabolic reprogramming occurring upon the acquisition of imatinib resistance may vary depending on the initial metabolic phenotype of the cell model of study.

Furthermore, in the case of the CML resistant cell we conducted a more thorough study of mitochondrial function, including ETC complex specific activities. Our results showed that despite the mitochondrial respiration capacity was higher in KU812 ImaR relative to KU812 P cells, the specific activity of complexes I and IV were lower in KU812 ImaR than in KU812 P cells. This finding prompted our next question: How did KU812 ImaR cells acquire a more mitochondrial capable phenotype upon imatinib resistance despite the lower specific activities of the ETC complexes?

Interestingly, we proved that KU812 ImaR cells can utilise the GP shuttle as an alternative contributor to mitochondrial respiration. In brief, although NADH oxidation by GP shuttle is energetically less efficient than NADH oxidation by complex I due to the lack of proton pumping activity by GPD2, it still contributes to the OXPHOS for the ATP generation[210]. Therefore, we theorise that KU812 ImaR cells may be counteracting the lower efficiency of complex I and IV activities via GP shuttle and, thereby, contributing to the increased mitochondrial respiration capacity observed in these cells when compared to its parental counterpart. Likewise, the higher flux of BCAAs determined in KU812 ImaR relative to KU812 P cells together with protein profile results of proteins associated with BCAAs transport and

catabolism (shown in **Section 5.2.2.8**) also suggest that KU812 ImaR may be fuelling the TCA cycle via valine but not via isoleucine and leucine, thus additionally contributing to the increased mitochondrial respiration.

The compensation of the extracellular acidification contribution via mitochondrial respiration constitutes a common feature for AraC and Imatinib resistant cells

Acidic extracellular pH is a well-known feature of cancer cells. Cancer cells have successfully controlled proton production and excretion in order to maintain their own cellular activation, increase drug resistance and become more aggressive[354]. In fact, it has been reported that extracellular acidic pH increases the proliferation and reduces the Dox-induced apoptosis in ALL[355].

Despite the fact that the glycolytic production of lactate is considered the major component of extracellular acidification (i.e. extracellular H^+ production), lately it has been reported that the CO_2 produced during mitochondrial respiration also contributes to the extracellular acidification rate (ECAR)[356]. Moreover, this CO_2-derived contribution has been described to differ between cell types[356]. In this thesis, we have demonstrated the importance of the CA enzymes and the SLC4A7 transporter in the contribution to the extracellular acidification associated with CO_2, that appears to be relevant for acidification control both in AML and CML resistant cells. In particular, our results suggest that both THP-1 AraC and KU812 ImaR cells may be compensating the ECAR contribution via mitochondrial respiration through two mechanisms: the decreased contribution of CAs to the ECAR rate and the increased contribution of intracellular bicarbonate balance through extracellular HCO_3^- import, both inducing a decrease of intracellular H^+ levels. However, these common features for THP-1 AraC and KU812 ImaR resistant cells were not found in the HL-60 AraC resistant cells. Due to this, we hypothesise that this proton regulator mechanism is dependent on mitochondrial activity and CO_2 production, being especially relevant in cell models with high mitochondrial respiration capacity. Nevertheless, this hypothesis would require further experimental validation.

The important role of amino acid metabolism in the acquisition of resistance to AML and CML common chemotherapeutic drugs

Cancer cells, including AML and CML cells, require amino acids to fulfil their needs of synthesising proteins for cell proliferation. Besides the role of amino acids in protein synthesis, they are also precursors of metabolic intermediates that replenish glycolysis, TCA cycle, one-carbon metabolism, lipid synthesis and urea cycle, among others. Moreover, in their catabolism and anabolism, there are many redox reactions that participate in the NADH and NADPH homeostasis. In this thesis, we have focused on the role of amino acids metabolism in the resistant leukaemic cells and how this fulfils other metabolic roles (e.g. nucleic acid biosynthesis and NADH redox maintenance) that take part in the metabolic reprogramming associated with chemotherapeutic drug resistance including AraC, Dox and imatinib.

Glutamine and glutamate metabolism: key metabolic players, especially in KU812 ImaR cells

Glutamine is by far the main amino acid consumed by tumour cells. Its metabolism is determinant for tumour growth and survival[136]. The importance of glutamine in tumor survival lies in its participation in many synthetic pathways. As depicted in **figure 6.1**, glutamine serves as substrate for different metabolic reactions (e.g. HBP and transaminases reactions), which are independent of glutaminolysis. Moreover, glutamine can also be converted to glutamate via glutaminolysis. Glutamine-derived glutamate is involved in different transaminase reactions but, most importantly, is well-known for its contribution to the anaplerotic and non-anaplerotic reactions. In light of this complexity of glutamine metabolism, the alterations of glutamine metabolism upon AML and CML chemotherapeutic drug resistance were explored throughout this thesis. With regard to AML cells, our results indicate that glutamine consumption was enhanced upon the acquisition of AraC resistance in AML cells whereas a decrease of the total glutamine consumed was associated with the acquisition of Dox resistance (i.e. drug-dependent metabolic changes). However, these differences in glutamine metabolism showed to be dependent on the mitochondrial-respiration phenotype (i.e. cell line-dependent metabolic

changes) and on the oxygen conditions in which AML cells were incubated. Moreover, as THP-1 cells exhibited a metabolic phenotype with a highly active mitochondrial respiration capacity, we thus theorise that THP-1 cells may have a higher dependency on glutamine to fuel the TCA cycle and obtain TCA cycle intermediates for energetic purposes. All these findings, first, underline the importance of studying the metabolic reprogramming of distinct cell models upon the acquisition of drug resistance; and second and more importantly, highlight the glutaminase reaction as a possible vulnerability of AML cells resistant to AraC, especially of THP-1 AraC cells. In this regard, we propose that the inhibition of the glutaminase reaction, for instance via its inhibition with GLS inhibitor BPTES[357] or CB-839[98], could reduce the viability of AML cells resistant to AraC. However, further validation studies are needed.

On the other hand, the analysis of the glutamine consumption and glutamate production profiles revealed a more active glutamine metabolism in the CML cell model used in our thesis upon the acquisition of imatinib resistance despite the downregulation determined for the protein expression of the key enzyme in the glutaminolysis process, GLS. This result was partially attenuated by the upregulation of the specific glutamine transporters (SNAT1-2) in addition to other amino acids transporters (e.g. LAT1). These findings suggest that KU812 ImaR cells may be using glutamine through reactions and processes that are independent of glutaminolysis. In this regard, our protein profile results showed an upregulation of proteins associated with the HBP, which has a crucial role in many cancer processes including signalling, metabolism, gene regulation and epithelial-mesenchymal transition[335]. Glutamine transaminase reactions are also independent of glutaminolysis and, more importantly, are key players in the synthesis of DNA and RNA (shown in **Fig. 6.1**).

As aforementioned, glutamine participates in metabolic reactions that are dependent on glutaminolysis. Therefore, we explored the metabolic fates of glutamine-derived glutamate to elucidate the increased glutamine consumption observed in the CML resistant cells. Considering the protein profile results, the glutamate-dependent transamination reactions did not explain the increase on glutamine consumption. Moreover, our data showed that glutamine-derived glutamate contributes in a lower extent to the mitochondrial respiration

of KU812 ImaR cells (**Chapter 2, section 5.2.2.7**). This finding together with the downregulation of the glutamate/H^+ symporter SLC25A22 observed in KU812 ImaR cells, whose knockdown has been reported to result in a lack of ETC functioning in astrocytes[336], suggest that glutamine-derived glutamate should contribute to metabolic pathways other than TCA cycle anaplerosis in the CML resistant cell model used in this thesis. Accordingly, these results showed that glutamine-derived glutamate is rewired to other non-anaplerotic reactions such as synthesis of proline, ornithine, arginine, citrulline and collagen in KU812 ImaR cells (**depicted schematically in Fig. 6.1.B** and further discussed below).

The contribution of glutamine-derived glutamate in proline synthesis was the most significant alteration in the here studied CML resistant cells. KU812 ImaR cells exhibited both a substantial increase of proline synthesis (13-fold up) and a significant upregulation of the proteins involved in the proline synthesis. Proline synthesis has been shown to fuel protein production for cell proliferation[174]. Indeed, other studies have demonstrated that the knockdown of proline synthesis enzymes significantly reduces cell proliferation in different tumour cells including lymphoma, lung, breast, melanoma and prostate cancer cells[176]. Thus, we hypothesised that proline metabolism, and particularly its synthesis, could constitute a vulnerability for CML cells resistant to TKIs. However, the inhibition of proline synthesis via P5CS or proT knockouts alone was not sufficient to overcome imatinib resistance in the KU812 ImaR cells.

Related with the observed glutamine rewiring to non-anaplerotic reactions, our results have accordingly unveiled an upregulation of the enzyme ASS1 in KU812 ImaR cells. This result together with the higher intracellular content of ornithine (shown in **Chapter 2, section 5.2.2.4**) led us to hypothesise that KU812 ImaR cells may be in part rewiring the glutamine-derived ornithine and the aspartate to the urea cycle to obtain arginine and fumarate. These two metabolites would be further used to synthesise proteins and to replenish the TCA cycle, respectively. It is worth mentioning that ASS1 has been additionally described as a metabolic regulator in colorectal cancer and its inhibition has been suggested as a novel therapeutic approach[358]. Therefore, we propose ASS1 inhibition as a suitable therapeutic approach to revert TKI resistance, and particularly imatinib resistance, in CML resistant cells.

Another non-anaplerotic reaction in which the glutamine-derived glutamate participates is the synthesis of glutathione, which is the main redox buffer in a cell[359]. However, there was no correlation between the observed increase of glutamine consumption and transport in KU812 ImaR cells, and the increase of the *de novo* glutathione synthesis. Besides, we did find a significant upregulation of glutathione peroxidases (GPX1, GPX4 and GPX7) and glutathione-S-transferases including (GSTP1, GSTM1, and GSTM3), which are involved in the processes of ROS scavenging and xenobiotic detoxification[337,338] (**Chapter 2, section 5.2.2.6**). In this line, previous studies revealed that GSTP1 is a drug-resistance associated protein in leukaemia[360], and that GPX4 may represent a therapeutic strategy to prevent acquired drug resistance in cancer cells[230]. Interestingly, our data highlighted GSTP and GPX4 enzymes as potential targets to counteract TKI resistance, due to their upregulation at protein expression levels. The inhibitory effect of Ezatiostat (a GSTP1 inhibitor), and RSL-3 (a GPX4 inhibitor) on the cell viability of both KU812 P and ImaR cells was not sufficient to overcome TKI resistance. However, they did decrease the cell viability of both KU812 P and ImaR cells and, more importantly, IC_{50} values were within the pharmacological concentration range[361]. Therefore, we speculate that these inhibitors could be a suitable alternative or combinatory choice for the treatment of CML patients.

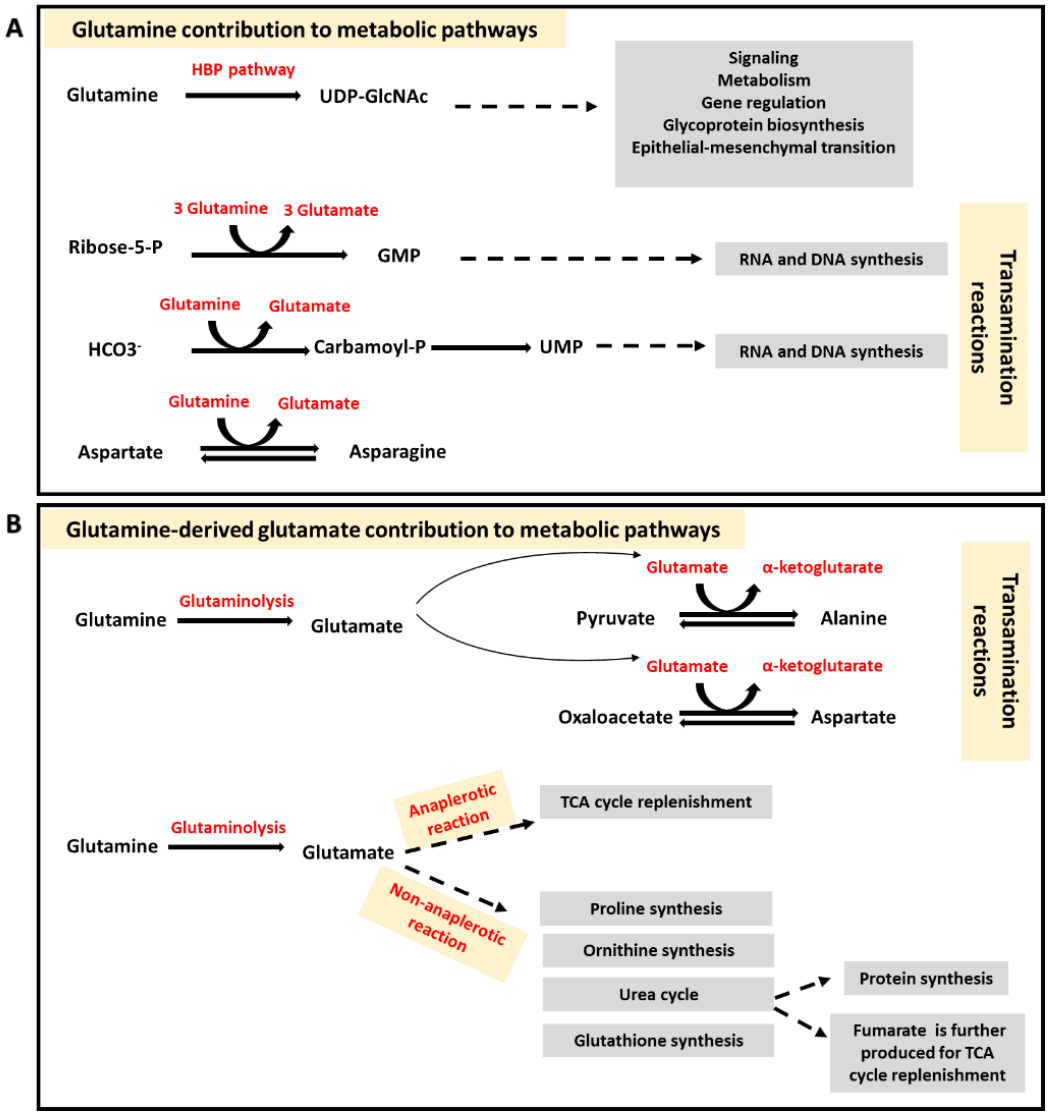

Figure 6.1 Schematic representation of the role of glutamine and glutamine-derived glutamate in different metabolic pathways. Glutamine has its own specific functions (panel A) but it can also be converted to glutamate to exert other functions (panel B). **A)** Glutamine can be converted into UDP-GlcNac through the hexosamine biosynthetic pathway (HBP) and, thereby, contribute to the functioning of different cancer cell processes. Moreover, glutamine can be used in different transamination reactions, thus contributing to the synthesis of either asparagine or purine and pyrimidine (essential metabolites for DNA and RNA synthesis). **B)** Glutamine-derived glutamate can be used in transamination reaction or in anaplerotic and non-anaplerotic reactions as indicated. Regarding the anaplerotic and non-anaplerotic reactions, the first contribute to the TCA cycle replenishment whereas the non-anaplerotic reactions have as a result the synthesis of crucial metabolites that have key roles in the indicated metabolic processes. Abbreviations: guanosine monophosphate, GMP; uridine monophosphate, UMP; and tricarboxylic acids, TCA.

The link between serine-glycine-1C metabolism and DNA synthesis: a phenotypic commonality of THP-1 AraC and KU812 ImaR cells under normoxic conditions

After glutamine, serine is the second most-consumed amino acid by tumour cells. Serine metabolism, including its synthesis and catabolism, plays an important role in the transfer of 1-C units to the tetrahydrofolate, in a metabolic pathway known as the serine-glycine-1C metabolism. The importance of this metabolic pathway was brought to light in some of the here studied resistant cell models, which is an indicator that serine-glycine-1C metabolism may be relevant in the process of drug-resistant acquisition in leukaemic cells.

As shown in **Chapter 1, section 5.1.2.2.5**, THP-1 and HL-60 AraC resistant cells displayed a different pattern of changes regarding the amino acids associated with the serine-glycine-1C metabolism (cell-line dependent phenotype) under normoxic and hypoxic incubation conditions. More specifically, serine and glycine consumption/production profiles together with the protein profile results highlighted that THP-1 AraC cells under normoxia metabolised serine to obtain glycine and 1-C units, which would be further used for purine synthesis (thereby DNA synthesis). Likewise, the protein profile results regarding the CML resistant model under normoxia also underlined a possible need for DNA synthesis (shown in **Chapter 2, section 5.2.2.2**). As it has been described that the decrease of DNA synthesis can be an AraC dose-dependent effect on normal human peripheral blood cells[362], and that imatinib treatment decreases DNA synthesis by inhibiting the cell-cycle progression of T-cells[363], we hypothesise that both THP-1 AraC and KU812 ImaR cells may have enhanced metabolic pathways associated with DNA synthesis to counteract the detrimental effect of the AraC and Imatinib treatments. In this line, we decided to validate if the inhibition of enzymes associated with 1-C metabolism, thus in part DNA synthesis, had an effect on the cell viability of KU812 and THP-1 parental and, especially, on the resistant cells. Even though a more detrimental effect regarding the resistant cells was not observed, our results exhibited a cell viability disadvantage for both parental and resistant cells when cells were treated with these inhibitors. In addition, IC_{50} values were also within the pharmacological concentration range observed in the treatment of other leukaemia such as childhood leukaemia[364], thus we speculate that these inhibitors, similar to Ezatiostat and RSL-3

inhibitors in CML cells, could be a suitable alternative choice for AML and CML patients treatment.

Amino acids alterations of AraC and Dox resistant cells under hypoxic incubation conditions: a cell-line dependent pattern of changes

The here exhibited metabolic reprogramming by AML and CML cells resistant to conventional chemotherapeutic drugs under normoxia has been crucial to better understand how these cells can evade/adapt to drug treatments. However, BM, which is the primary niche of leukaemic cells, is known to be a hypoxic organ. In fact, it has been reported that a hypoxic niche, characterized by a low content of oxygen and drug, plays an important role in the emergence of drug resistance by cell damage elusion[365]. Therefore, we considered that a better knowledge of the amino acid metabolism not only under normoxia but also under hypoxia could be crucial to better understand the metabolic alterations occurring upon drug resistance acquisition in order to better design a therapeutic strategy to kill these resistant leukaemic cells.

As shown in **Chapter 1, section 5.1.2.2.5**), the amino acid fluxes alterations associated with the acquisition of drug resistance under hypoxia were only observed in THP-1 resistant cells (cell-line dependent). As mentioned above, the metabolic phenotype of these cells is characterised by a highly active mitochondrial respiration capacity that also results in higher consumption of several amino acids. Therefore, we speculate that THP-1 resistant cells under hypoxia may have altered the amino acid metabolism to adapt to the reduction of the oxygen levels, and thereby, to the lower possibility to respire.

Regarding the THP-1 Dox cells, polyamine consumption seems to be crucial when THP-1 Dox are under the hypoxic-stress effect. A previous study has shown that the upregulation of the polyamine system promotes the survival of cancer cells, including glioblastoma, prostate and colon cancer cells, during hypoxic stress[366]. Therefore, we propose polyamine metabolism as a possible metabolic target to be inhibited and, thereby, to overcome Dox resistance in AML patients. Interestingly, a recent study has shown that MLD72.527, an inhibitor of polyamine catabolism, re-sensitises THP-1 cells that are infected with the

human cytomegalovirus (HCMV) and that are resistant to Dox chemotherapeutic drug[367]. Thus, we propose that the combination of the doxorubicin and MDL72.527 as an initial treatment in AML patients could avoid the acquisition of Dox resistance in these patients. However, this would need further experimental substantiation.

Finally, even though the amino acid fluxes were not altered in HL-60 resistant cells under hypoxic incubation conditions, the intracellular content of arginine and asparagine did decrease. Nevertheless, further experimental substantiation needs to be performed to better understand the role of amino acid alterations in HL-60 resistant cells under hypoxia.

Metabolic and non-metabolic drug-targets underlined via a comprehensive multi-OMIC approach

The last specific objectives of this thesis are "the definition and validation of targets associated with the metabolic reprogramming of the resistant AML and CML cells". In this regard, the multi-OMIC approach conducted for the AML (**Chapter 1**) and CML (**Chapter 2**) cells in this thesis uncovers both potential weaknesses of metabolic pathways and metabolic and non-metabolic drug-target candidates that could be exploited for leukaemia treatment. As depicted in **figure 6.2**, some of these drug-target candidates were validated and others were proposed for further validation.

Our validation results unveiled that the single-hit inhibition approach by either using specific protein inhibitors of the selected targets or, in the case of proline metabolism, using CRISPR/Cas9 technology, is not a good strategy to efficiently overcome AraC, Dox and imatinib resistance in AML and CML cells. In this regard, we hypothesise that AML and CML resistant cells may be circumventing the inhibition of individual metabolic pathways due to their high metabolically plasticity here described. However, we demonstrated that the majority of these single-hit inhibitions reduce the cell viability of both parental and resistant AML and CML cells with an appropriate concentration range regarding the therapeutic index (i.e. measurement of the relative safety of a drug). In fact, we suggest that inhibitors such as methotrexate or pemetrexed could be potential inhibitors for the treatment of

leukemic cells with high mitochondrial capacity. For all these reasons, we propose that both the single use of the inhibitors their combination with AraC, Dox or imatinib chemotherapeutic drugs could constitute an effective strategy to treat AML and CML patients who initially were resistant or non-resistant to these chemotherapeutic drugs.

Remarkably, in this thesis we have found that the acquisition of Dox resistance negatively alters the mitochondrial metabolism of cells with an active mitochondrial respiration capacity (e.g. THP-1 and KU812 cells). This study has allowed us to propose Dox as a new drug in the treatment of tumours with high mitochondrial activity. In this regard, a very novel proposal which is the repurposing of Dox chemotherapeutic drug (a conventional AML chemotherapeutic drug) to counteract the imatinib resistance in the KU812 ImaR cells has emerged in this thesis. Interestingly, Dox treatment decreased the cell viability of KU812 ImaR cells significantly more than KU812 P cells.

To sum up, the results from the here conducted multi-OMIC study support the conclusion that the resistance mechanisms developed by AML and CML cells lines are associated with an important metabolic reprogramming. Moreover, this study also unveils different metabolic commonalities between both AML and CML parental cells in addition to commonalities in the metabolic reprogramming of AML and CML cells upon the acquisition of chemotherapeutic drug resistance. These metabolic commonalities allow us to associate the effect that drugs have in AML parental and/or resistant cells with the effect that may have in CML parental and/or resistant cells, and vice versa. Finally, the results of this multi-OMIC study pave the way to propose novel and promising therapeutic opportunities for the improvement of AML and CML treatment.

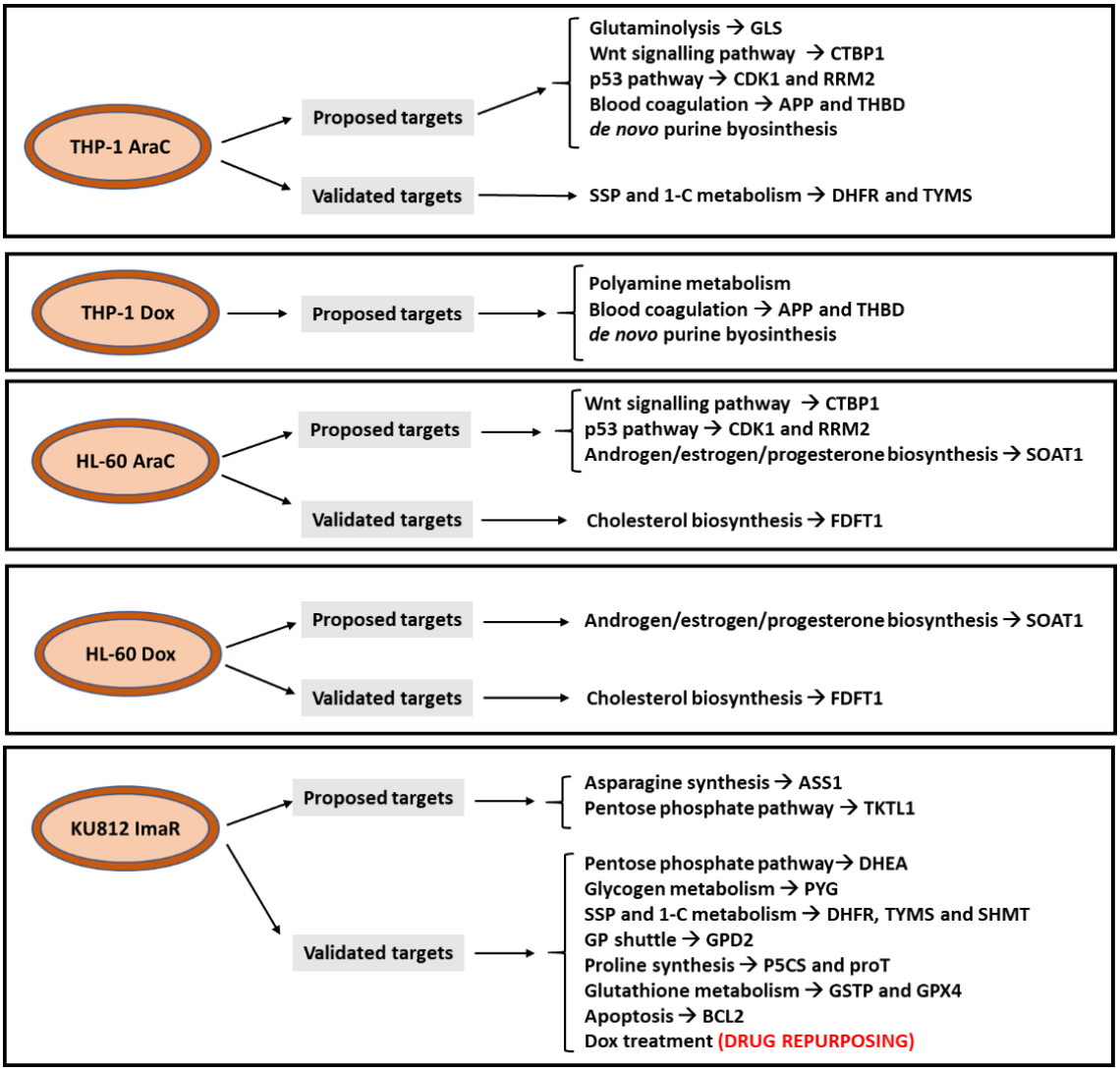

Figure 6.2. Schematic representation of the highlighted drug-targets and metabolic pathways for AML and/or CML treatment. The illustration depicts both the proposed and the validated drug-targets and metabolic pathways that arose from the multi-OMIC approach performed in AML and CML parental and resistant cells. Abbreviations: Amyloid beta precursor protein, APP; cytarabine, AraC; argininosuccinate synthase, ASS1; cyclin dependent kinase 1, CDK1; c-terminal binding protein 1, CTBP1; dehydroepiandrosterone, DHEA; dihydrofolate reductase, DHFR; doxorubicin, Dox; squalene synthase, FDFT1; glutaminase, GLS; glycerol-3-phosphate, GP; glutathione peroxidase 4, GPX4; glutathione s-transferase pi 1, GSTP1; glycerol-3-phosphate dehydrogenase, GPD2; glycogen phosphorylase , PYG; imatinib-resistant, ImaR; pyrroline-5-carboxylate synthase, P5CS; ribonucleotide reductase regulatory subunit M2, RRM2; serine hydroxymethyltransferase, SHMT; sodium-dependent proline transporter, proT; sterol O-acyltransferase 1, SOAT1; thrombomodulin, THBD; transketolase like 1, TKTL1; and thymidylate synthetase, TYMS.

7. CONCLUSIONS

7 CONCLUSIONS

1. The multi-OMIC study conducted for the AML and CML parental and resistant cell models used in this thesis is a reliable approach to identify potential metabolic and non-metabolic targets that can be exploited for AML and CML treatment. The use of this approach has allowed us (1) to find metabolic commonalities in the metabolic reprogramming of AML and CML resistant cells and (2) to propose and/or validate different targets associated with metabolic pathways including serine-glycine-1C, PPP, glutaminolysis, glycogenolysis, among others. Indeed, we found that the single-hit inhibitions reduce the cell viability of both parental and resistant AML and CML cells.

2. The initial metabolic phenotype of AML cells influences the metabolic reprogramming derived from the acquisition of AraC and Dox resistance, which highlights the importance of investigating the initial phenotype of cells to anticipate the metabolic changes that may arise due to the acquisition of resistance.

3. The acquisition of AraC resistance causes the reprogramming of the glucose metabolism of THP-1 and HL-60 AML cells under both normoxic and hypoxic conditions by increasing the glycolytic flux whereas it is not associated with an alteration in the mitochondrial respiration capacity. Nevertheless, we observed a possible disfunction of ETC complex I as well as alterations in glutamine and serine-glycine-1C metabolism in AML cells that display a more active mitochondrial metabolism (i.e. THP-1 AraC cells). These metabolic alterations constitute promising vulnerabilities in AML cells resistant to AraC with these mitochondrial features.

4. The acquisition of Dox resistance causes alterations in the glucose and amino acid metabolism by decreasing the glycolytic flux of THP-1 and HL-60 AML cells as well as the amino acid consumptions of HL-60 AML cells under normoxic conditions. Moreover, we identified the polyamine metabolism as an important metabolic source of THP-1 Dox cells

under hypoxic conditions. On the other hand, the acquisition of Dox resistance dramatically decreases the mitochondrial respiration capacity of AML cells with an active mitochondrial metabolism under normoxic and hypoxic conditions whereas it significantly upregulates the majority of the proteins associated with the mitochondrial metabolism. These metabolic alterations in the mitochondrial metabolism together with the metabolic changes related to the polyamine metabolism constitute potential metabolic vulnerabilities that can be exploited for the treatment of AML patients resistant to Dox chemotherapeutic drugs.

5. The acquisition of imatinib resistance causes the reprograming of glucose metabolism by enhancing the glycolytic flux, PPP, and glycogen metabolism. These changes highlight these metabolic pathways as potential metabolic weaknesses of KU812 ImaR cells. Moreover, the high metabolic plasticity exhibited by KU812 ImaR cells includes the orchestration of many metabolic routes associated with the amino acid metabolism. The enhancement of glutamine, proline, glutathione, serine-glycine-1C metabolism, among others, provides KU812 ImaR cells with high metabolic flexibility that can be used not only for energetic purposes but also to accomplish crucial metabolic processes such as ROS scavenging, xenobiotic detoxification, DNA synthesis or NADPH/NADP balance. Finally, KU812 ImaR cells display enhanced mitochondrial respiration capacity. This metabolic feature underlines mitochondrial metabolism as another potential vulnerability that can be exploited to overcome imatinib resistance. Consequently, we propose the repurposing of Dox treatment as a promising therapy to overcome imatinib resistance in KU812 ImaR cells.

8. REFERENCES

8 REFERENCES

1. Bray, F. *et al.* Global cancer statistics 2018: GLOBOCAN estimates of incidence and mortality worldwide for 36 cancers in 185 countries. *CA. Cancer J. Clin.* **68**, 394–424 (2018).

2. Bansal, R. *Cancer and the Environment*. *IEEE Microwave Magazine* **10**, (National Academies Press, 2002).

3. Ng, A. P. & Alexander, W. S. Haematopoietic stem cells: past, present and future. *Cell Death Discov.* **3**, 17002 (2017).

4. Bonnet, D. Haematopoietic stem cells. *J. Pathol.* **197**, 430–440 (2002).

5. Morikawa, T. & Takubo, K. Hypoxia regulates the hematopoietic stem cell niche. *Pflügers Arch. - Eur. J. Physiol.* **468**, 13–22 (2016).

6. Schofield, R. The relationship between the spleen colony-forming cell and the haemopoietic stem cell. *Blood Cells* **4**, 7–25 (1978).

7. Davis, A. S., Viera, A. J. & Mead, M. D. Leukemia: An overview for primary care. *Am. Fam. Physician* **89**, 731–738 (2014).

8. Döhner, H., Weisdorf, D. J. & Bloomfield, C. D. Acute Myeloid Leukemia. *N. Engl. J. Med.* **373**, 1136–1152 (2015).

9. Noone AM, Howlader N, Krapcho M, Miller D, Brest A, Yu M, Ruhl J, Tatalovich Z, Mariotto A, Lewis DR, Chen HS, Feuer EJ, C. K. SEER Cancer Statistics Review, 1975- 2015, National Cancer Institute. 430–439 (2018).

10. Bray, F. *et al.* Global cancer statistics 2018: GLOBOCAN estimates of incidence and mortality worldwide for 36 cancers in 185 countries. *CA. Cancer J. Clin.* **68**, 394–424 (2018).

11. Lindsley, R. C. *et al.* Acute myeloid leukemia ontogeny is defined by distinct somatic mutations. *Blood* **125**, 1367–1376 (2015).

12. Walter, M. J. What came first: MDS or AML? *Blood* **125**, 1357–1358 (2015).

13. Lowenberg, B., Downing, J. R. & Burnett, A. Acute Myeloid Leukemia. *N. Engl. J. Med.* **341**,

1051–1062 (1999).

14. Dohner, H. *et al.* Diagnosis and management of AML in adults: 2017 ELN recommendations from an international expert panel. *Blood* **129**, 424–448 (2017).

15. Béné, M. C. *et al.* Immunophenotyping of acute leukemia and lymphoproliferative disorders: a consensus proposal of the European LeukemiaNet Work Package 10. *Leukemia* **25**, 567–574 (2011).

16. Arber, D. A. *et al.* The 2016 revision to the World Health Organization classification of myeloid neoplasms and acute leukemia. *Blood* **127**, 2391–405 (2016).

17. Yang, X. & Wang, J. Precision therapy for acute myeloid leukemia. *J. Hematol. Oncol.* **11**, 1–11 (2018).

18. Li, Z. *et al.* Exploring the antitumor mechanism of high-dose cytarabine through the metabolic perturbations of ribonucleotide and deoxyribonucleotide in human promyelocytic Leukemia HL-60 Cells. *Molecules* **22**, (2017).

19. Cortés-Funes, H. & Coronado, C. Role of anthracyclines in the era of targeted therapy. *Cardiovasc. Toxicol.* **7**, 56–60 (2007).

20. Thorn, C. F. *et al.* Doxorubicin pathways: pharmacodynamics and adverse effects. *Pharmacogenet. Genomics* **21**, 440–6 (2011).

21. Yang, F., Teves, S. S., Kemp, C. J. & Henikoff, S. Doxorubicin, DNA torsion, and chromatin dynamics. *Biochim. Biophys. Acta - Rev. Cancer* **1845**, 84–89 (2014).

22. Gewirtz, D. A. A critical evaluation of the mechanisms of action proposed for the antitumor effects of the anthracycline antibiotics adriamycin and daunorubicin. *Biochem. Pharmacol.* **57**, 727–741 (1999).

23. Minotti, G., Menna, P., Salvatorelli, E., Cairo, G. & Gianni, L. Anthracyclines: Molecular Advances and Pharmacologic Developments in Antitumor Activity and Cardiotoxicity. *Pharmacol. Rev.* **56**, 185–229 (2004).

24. Senchenkov, A., Litvak, D. A. & Cabot, M. C. Targeting ceramide metabolism - A strategy for overcoming drug resistance. *J. Natl. Cancer Inst.* **93**, 347–357 (2001).

25. Zhu, H. *et al.* Doxorubicin Redox Biology: Redox Cycling, Topoisomerase Inhibition, and Oxidative Stress. *React. Oxyg. species (Apex, N.C.)* **1**, 189–198 (2016).

26. Kumar, C. C. Genetic abnormalities and challenges in the treatment of acute myeloid Leukemia. *Genes and Cancer* **2**, 95–107 (2011).

27. Döhner, H. *et al.* Diagnosis and management of acute myeloid leukemia in adults: Recommendations from an international expert panel, on behalf of the European LeukemiaNet. *Blood* **115**, 453–474 (2010).

28. Bryan, J. C. & Jabbour, E. J. Management of Relapsed/Refractory Acute Myeloid Leukemia in the Elderly: Current Strategies and Developments. *Drugs and Aging* **32**, 623–637 (2015).

29. Zhang, J., Gu, Y. & Chen, B. Mechanisms of drug resistance in acute myeloid leukemia. *Onco. Targets. Ther.* **12**, 1937–1945 (2019).

30. Hofmann, J. Protein Kinase C Isozymes as Potential Targets for Anticancer Therapy. *Curr. Cancer Drug Targets* **4**, 125–146 (2004).

31. Burgess, D. J. *et al.* Topoisomerase levels determine chemotherapy response in vitro and in vivo. *Proc. Natl. Acad. Sci.* **105**, 9053–9058 (2008).

32. Cole, S. *et al.* Overexpression of a transporter gene in a multidrug-resistant human lung cancer cell line. *Science (80-.).* **258**, 1650–1654 (1992).

33. Germann, U. A. P-glycoprotein—A mediator of multidrug resistance in tumour cells. *Eur. J. Cancer* **32**, 927–944 (1996).

34. Messingerova, L. *et al.* Acute myeloid leukemia cells MOLM-13 and SKM-1 established for resistance by azacytidine are crossresistant to P-glycoprotein substrates. *Toxicol. Vitr.* **29**, 1405–1415 (2015).

35. Hofmann, J. Protein Kinase C Isozymes as Potential Targets for Anticancer Therapy. *Curr. Cancer Drug Targets* **4**, 125–146 (2004).

36. Burgess, D. J. *et al.* Topoisomerase levels determine chemotherapy response in vitro and in vivo. *Proc. Natl. Acad. Sci. U. S. A.* **105**, 9053–9058 (2008).

37. Hatem, E., El Banna, N. & Huang, M. E. Multifaceted Roles of Glutathione and Glutathione-

Based Systems in Carcinogenesis and Anticancer Drug Resistance. *Antioxidants Redox Signal.* **27**, 1217–1234 (2017).

38. Mossallam, G. I., Abdel Hamid, T. M. & Samra, M. A. Glutathione S-transferase GSTM1 and GSTT1 polymorphisms in adult acute myeloid leukemia; its impact on toxicity and response to chemotherapy. *J. Egypt. Natl. Canc. Inst.* **18**, 264—273 (2006).

39. Weich, N. *et al.* GSTM1 and GSTP1, but not GSTT1 genetic polymorphisms are associated with chronic myeloid leukemia risk and treatment response. *Cancer Epidemiol.* **44**, 16–21 (2016).

40. Slot, A. J., Molinski, S. V. & Cole, S. P. C. Mammalian multidrug-resistance proteins (MRPs). *Essays Biochem.* **50**, 179–207 (2011).

41. Ji, Q. & Qiu, L. Mechanism study of PEGylated polyester and β-cyclodextrin integrated micelles on drug resistance reversal in MRP1-overexpressed HL60/ADR cells. *Colloids Surfaces B Biointerfaces* **144**, 203–213 (2016).

42. Gabra, M. M. & Salmena, L. microRNAs and Acute Myeloid Leukemia Chemoresistance: A Mechanistic Overview. *Front. Oncol.* **7**, 255 (2017).

43. Bai, H., Cao, Z., Deng, C., Zhou, L. & Wang, C. miR-181a sensitizes resistant leukaemia HL-60/Ara-C cells to Ara-C by inducing apoptosis. *J. Cancer Res. Clin. Oncol.* **138**, 595–602 (2012).

44. Vydra, N., Toma, A., Glowala-Kosinska, M., Gogler-Piglowska, A. & Widlak, W. Overexpression of heat shock transcription factor 1 enhances the resistance of melanoma cells to doxorubicin and paclitaxel. *BMC Cancer* **13**, 504 (2013).

45. Lin, C. I. *et al.* Autophagy induction with RAD001 enhances chemosensitivity and radiosensitivity through met inhibition in papillary thyroid cancer. *Mol. Cancer Res.* **8**, 1217–1226 (2010).

46. Vydra, N., Toma, A., Glowala-Kosinska, M., Gogler-Piglowska, A. & Widlak, W. Overexpression of heat shock transcription factor 1 enhances the resistance of melanoma cells to doxorubicin and paclitaxel. *BMC Cancer* **13**, 1 (2013).

47. Franzolin, E. *et al.* The deoxynucleotide triphosphohydrolase SAMHD1 is a major regulator

of DNA precursor pools in mammalian cells. *Proc. Natl. Acad. Sci.* **110**, 14272–14277 (2013).

48. Schneider, C. *et al.* SAMHD1 is a biomarker for cytarabine response and a therapeutic target in acute myeloid leukemia. *Nat. Med.* **23**, 250–255 (2017).

49. Ohta, T. *et al.* Impact of cytidine deaminase activity on intrinsic resistance to cytarabine in carcinoma cells. *Oncol. Rep.* **12**, 1115–20 (2004).

50. Fanciullino, R. *et al.* CDA as a predictive marker for life-threatening toxicities in patients with AML treated with cytarabine. *Blood Adv.* **2**, 462–469 (2018).

51. Briot, T., Roger, E., Thépot, S. & Lagarce, F. Advances in treatment formulations for acute myeloid leukemia. *Drug Discov. Today* **23**, 1936–1949 (2018).

52. Saultz, J. N. & Garzon, R. Acute Myeloid Leukemia: A Concise Review. *J. Clin. Med.* **5**, 1–17 (2016).

53. H.K., L. *et al.* G-749, a novel FLT3 kinase inhibitor, can overcome drug resistance for the treatment of acute myeloid leukemia. *Blood* **123**, 2209–2219 (2014).

54. Altman, J. K. *et al.* Antileukemic Activity and Tolerability of ASP2215 80mg and Greater in FLT3 Mutation-Positive Subjects with Relapsed or Refractory Acute Myeloid Leukemia: Results from a Phase 1/2, Open-Label, Dose-Escalation/Dose-Response Study. *Blood* **126**, 321 LP – 321 (2015).

55. Hansen, E. *et al.* AG-120, an Oral, Selective, First-in-Class, Potent Inhibitor of Mutant IDH1, Reduces Intracellular 2HG and Induces Cellular Differentiation in TF-1 R132H Cells and Primary Human IDH1 Mutant AML Patient Samples Treated Ex Vivo; *Blood* **124**, 3734 LP – 3734 (2014).

56. Kojima, K. *et al.* Prognostic impact and targeting of CRM1 in acute myeloid leukemia. *Blood* **121**, 4166–74 (2013).

57. Assi, R., Kantarjian, H., Ravandi, F. & Daver, N. Immune therapies in acute myeloid leukemia: a focus on monoclonal antibodies and immune checkpoint inhibitors. *Curr. Opin. Hematol.* **25**, 136–145 (2018).

58. Tasian, S. K. Acute myeloid leukemia chimeric antigen receptor T-cell immunotherapy: how far up the road have we traveled? *Ther. Adv. Hematol.* **9**, 135–148 (2018).

59. Sawyers, C. L. Chronic myeloid leukemia. *N. Engl. J. Med.* **340**, 1330–40 (1999).

60. Preston, D. L. *et al.* Cancer Incidence in Atomic Bomb Survivors. Part III: Leukemia, Lymphoma and Multiple Myeloma, 1950-1987. *Radiat. Res.* **137**, S68 (1994).

61. Vlaanderen, J., Lan, Q., Kromhout, H., Rothman, N. & Vermeulen, R. Occupational benzene exposure and the risk of chronic myeloid leukemia: A meta-analysis of cohort studies incorporating study quality dimensions. *Am. J. Ind. Med.* **55**, 779–785 (2012).

62. Höglund, M., Sandin, F. & Simonsson, B. Epidemiology of chronic myeloid leukaemia: an update. *Ann. Hematol.* **94**, 241–247 (2015).

63. Jabbour, E. & Kantarjian, H. Chronic myeloid leukemia: 2020 update on diagnosis, therapy and monitoring. *Am. J. Hematol.* **95**, 691–709 (2020).

64. Furtado, V. F. *et al.* Accelerated phase chronic myeloid leukemia: Evaluation of clinical criteria as predictors of survival, major cytogenetic response and progression to blast phase. *Rev. Bras. Hematol. Hemoter.* **37**, 341–347 (2015).

65. Robert S Negrin, MD, Charles A Schiffer, M. Treatment of chronic myeloid leukemia in blast crisis. *Haematologica* **93**, 1765–1769 (2019).

66. Lissauer, H. Zwei Falle von Leucaemie. *Berl Klin Wochenshrift* **2**, 403–404 (1865).

67. Galton, D. A. G. MYLERAN IN CHRONIC MYELOID LEUKÆMIA RESULTS OF TREATMENT. *Lancet* **261**, 208–213 (1953).

68. Rushing, D., Goldman, A., Gibbs, G., Howe, R. & Kennedy, B. J. Hydroxyurea versus busulfan in the treatment of chronic myelogenous leukemia. *Am. J. Clin. Oncol.* **5**, 307–314 (1982).

69. Clift, R. A., Appelbaum, F. R. & Thomas, E. D. Treatment of chronic myeloid leukemia by marrow transplantation. *Blood* **82**, 1954–196 (1993).

70. Druker, B. J. & Lydon, N. B. Lessons learned from the development of an Abl tyrosine kinase inhibitor for chronic myelogenous leukemia. *J. Clin. Invest.* **105**, 3–7 (2000).

71. Hochhaus, A. *et al.* Six-year follow-up of patients receiving imatinib for the first-line treatment of chronic myeloid leukemia. *Leukemia* **23**, 1054–1061 (2009).

72. Hjorth-Hansen, H. *et al.* European LeukemiaNet recommendations for the management of

chronic myeloid leukemia: 2013. *Blood* **122**, 872–884 (2013).

73. Gora-Tybor, J. & Robak, T. Targeted drugs in chronic myeloid leukemia. *Curr. Med. Chem.* **15**, 3036–3051 (2008).

74. Le Coutre, P. *et al.* Pharmacokinetics and cellular uptake of imatinib and its main metabolite CGP74588. *Cancer Chemother. Pharmacol.* **53**, 313–323 (2004).

75. Gambacorti-Passerini, C. Role of alpha1 Acid Glycoprotein in the In Vivo Resistance of Human BCR-ABL+ Leukemic Cells to the Abl Inhibitor STI571. *J. Natl. Cancer Inst.* **92**, 1641–1650 (2000).

76. Illmer, T. *et al.* P-glycoprotein-mediated drug efflux is a resistance mechanism of chronic myelogenous leukemia cells to treatment with imatinib mesylate. *Leukemia* **18**, 401–408 (2004).

77. Branford, S. & Hughes, T. Detection of BCR-ABL mutations and resistance to imatinib mesylate. *Methods Mol. Med.* **125**, 93–106 (2006).

78. Jabbour, E. *et al.* Frequency and clinical significance of BCR-ABL mutations in patients with chronic myeloid leukemia treated with imatinib mesylate. *Leukemia* **20**, 1767–1773 (2006).

79. Gorre, M. E. *et al.* Linking clinical Resistance to STI-571 Cancer Therapy Caused by Gene Mutation or BCR-ABL Amplification. *Adv. Sci.* **293**, 876–880 (2001).

80. Apperley, J. F. Part I: mechanisms of resistance to imatinib in chronic myeloid leukaemia. *Lancet. Oncol.* **8**, 1018–29 (2007).

81. Gambacorti-Passerini, C. B. *et al.* Differences between in vivo and in vitro sensitivity to imatinib of Bcr/Abl+ cells obtained from leukemic patients. *Blood Cells, Mol. Dis.* **28**, 361–372 (2002).

82. Mahon, F. X. *et al.* Selection and characterization of BCR-ABL positive cell lines with differential sensitivity to the tyrosine kinase inhibitor STI571: diverse mechanisms of resistance. *Blood* **96**, 1070–9 (2000).

83. Barnes, D. J. *et al.* Bcr-Abl expression levels determine the rate of development of resistance to imatinib mesylate in chronic myeloid leukemia. *Cancer Res.* **65**, 8912–8919 (2005).

84. Hochhaus, A. *et al.* Molecular and chromosomal mechanisms of resistance to imatinib (STI571) therapy. *Leukemia* **16**, 2190–2196 (2002).

85. Kantarjian, H. *et al.* Dasatinib versus Imatinib in Newly Diagnosed Chronic-Phase Chronic Myeloid Leukemia. *N. Engl. J. Med.* **362**, 2260–2270 (2010).

86. Chan, W. Y., Lau, P. M., Yeung, K. W. & Kong, S. K. The second generation tyrosine kinase inhibitor dasatinib induced eryptosis in human erythrocytes—An in vitro study. *Toxicol. Lett.* **295**, 10–21 (2018).

87. Fujisawa, S. *et al.* Efficacy and safety of dasatinib versus imatinib in Japanese patients with newly diagnosed chronic-phase chronic myeloid leukemia (CML-CP): Subset analysis of the DASISION trial with 2-year follow-up. *Int. J. Hematol.* **99**, 141–153 (2014).

88. Breccia, M. & Alimena, G. Nilotinib: A second-generation tyrosine kinase inhibitor for chronic myeloid leukemia. *Leuk. Res.* **34**, 129–134 (2010).

89. Wei, G., Rafiyath, S. & Liu, D. First-line treatment for chronic myeloid leukemia: Dasatinib, nilotinib, or imatinib. *J. Hematol. Oncol.* **3**, 47 (2010).

90. Vazquez, A. *et al.* Cancer metabolism at a glance. *J. Cell Sci.* **129**, 3367–3373 (2016).

91. Hanahan, D. & Weinberg, R. A. Hallmarks of cancer: The next generation. *Cell* **144**, 646–674 (2011).

92. Phan, L. M., Yeung, S.-C. J. & Lee, M.-H. Cancer metabolic reprogramming: importance, main features, and potentials for precise targeted anti-cancer therapies. *Cancer Biol. Med.* **11**, 1–19 (2014).

93. Tarrado-Castellarnau, M., de Atauri, P. & Cascante, M. Oncogenic regulation of tumor metabolic reprogramming. *Oncotarget* **7**, 62726–62753 (2016).

94. Mueckler, M. *et al.* Sequence and structure of a human glucose transporter. *Science* **229**, 941–5 (1985).

95. Holman, G. D. & Sandoval, I. V. Moving the insulin-regulated glucose transporter GLUT4 into and out of storage. *Trends Cell Biol.* **11**, 173–179 (2001).

96. Bryant, N. J., Govers, R. & James, D. E. Regulated transport of the glucose transporter

GLUT4. *Nat. Rev. Mol. Cell Biol.* **3**, 267–277 (2002).

97. Shepherd, P. R., Gibbs, E. M., Wesslau, C., Gould, G. W. & Kahn, B. B. Human small intestine facilitative fructose/glucose transporter (GLUT5) is also present in insulin-responsive tissues and brain. Investigation of biochemical characteristics and translocation. *Diabetes* **41**, 1360–5 (1992).

98. Counihan, J. L., Grossman, E. A. & Nomura, D. K. Cancer Metabolism: Current Understanding and Therapies. *Chem. Rev.* **118**, 6893–6923 (2018).

99. Wilson, W. R. & Hay, M. P. Targeting hypoxia in cancer therapy. *Nat. Rev. Cancer* **11**, 393–410 (2011).

100. Song, K. *et al.* HIF-1α and GLUT1 Gene Expression is Associated with Chemoresistance of Acute Myeloid Leukemia. *Asian Pacific J. Cancer Prev.* **15**, 1823–1829 (2014).

101. Chen, W.-L. *et al.* Enhanced Fructose Utilization Mediated by SLC2A5 Is a Unique Metabolic Feature of Acute Myeloid Leukemia with Therapeutic Potential. *Cancer Cell* **30**, 779–791 (2016).

102. Bunney, P. E., Zink, A. N., Holm, A. A., Billington, C. J., & Kotz, C. M. Targeting Metabolism for Cancer Therapy. *Physiol. Behav.* **176**, 139–148 (2017).

103. Warburg, O. & Minami, S. Versuche an Überlebendem Carcinom-gewebe. *Klin. Wochenschr.* **2**, 776–777 (1923).

104. Shim, H. *et al.* c-Myc transactivation of LDH-A: Implications for tumor metabolism and growth (oncogenelactate dehydrogenasehypoxiatumorigenicity). *Natl. Institutes Heal.* **94**, 6658–6663 (1997).

105. Patra, K. C. & Hay, N. The pentose phosphate pathway and cancer. *Trends Biochem. Sci.* **39**, 347–354 (2014).

106. Cho, E. S., Cha, Y. H., Kim, H. S., Kim, N. H. & Yook, J. I. The pentose phosphate pathway as a potential target for cancer therapy. *Biomol. Ther.* **26**, 29–38 (2018).

107. Kekec, Y. *et al.* Antioxidant enzyme levels in cases with gastrointesinal cancer. *Eur. J. Intern. Med.* **20**, 403–406 (2009).

108. Langbein, S. *et al.* Expression of transketolase TKTL1 predicts colon and urothelial cancer patient survival: Warburg effect reinterpreted. *Br. J. Cancer* **94**, 578–585 (2006).

109. Xu, S. N., Wang, T. S., Li, X. & Wang, Y. P. SIRT2 activates G6PD to enhance NADPH production and promote leukaemia cell proliferation. *Sci. Rep.* **6**, 1–13 (2016).

110. Jiang, P., Du, W. & Wu, M. Regulation of the pentose phosphate pathway in cancer. *Protein Cell* **5**, 592–602 (2014).

111. Coy, J. F. *et al.* Molecular cloning of tissue-specific transcripts of a transketolase-related gene: Implications for the evolution of new vertebrate genes. *Genomics* **32**, 309–316 (1996).

112. Staiger, W. I. *et al.* Expression of the mutated transketolase TKTL1, a molecular marker in gastric cancer. *Oncol. Rep.* **16**, 657–61 (2006).

113. Philipp, M. *et al.* Expression of transketolase-like gene 1 (TKTL1) depends on disease phase in patients with chronic myeloid leukaemia (CML). *J. Cancer Res. Clin. Oncol.* **140**, 411–417 (2014).

114. Coy, J. F., Dressler, D., Wilde, J. & Schubert, P. Mutations in the transketolase-like gene TKTL1: Clinical implications for neurodegenerative diseases, diabetes and cancer. *Clin. Lab.* **51**, 257–273 (2005).

115. Diaz-Moralli, S. *et al.* A key role for transketolase-like 1 in tumor metabolic reprogramming. *Oncotarget* **7**, 51875–51897 (2016).

116. Li, Y. *et al.* APC/CCDH1 synchronizes ribose-5-phosphate levels and DNA synthesis to cell cycle progression. *Nat. Commun.* **10**, 2502 (2019).

117. Zhao, F. *et al.* Imatinib resistance associated with BCR-ABL upregulation is dependent on HIF-1alpha-induced metabolic reprograming. *Oncogene* **29**, 2962–72 (2010).

118. Zois, C. E. & Harris, A. L. Glycogen metabolism has a key role in the cancer microenvironment and provides new targets for cancer therapy. *J. Mol. Med.* **94**, 137–154 (2016).

119. Berg, J. M., Tymoczko, J. L. & Stryer, L. Glycogen Breakdown and Synthesis Are Reciprocally Regulated. *Biochemistry* 2002 (2002).

120. Rousset, M., Zweibaum, A. & Fogh, J. Presence of glycogen and growth-related variations in 58 cultured human tumor cell lines of various tissue origins. *Cancer Res.* **41**, 1165–70 (1981).

121. Rousset, M., Chevalier, G., Rousset, J. P., Dussaulx, E. & Zweibaum, A. Presence and cell growth-related variations of glycogen in human colorectal adenocarcinoma cell lines in culture. *Cancer Res.* **39**, 531–4 (1979).

122. Rousset, M. *et al.* Kinetics of glycogen levels in asynchronous and synchronous cultures of a human colon carcinoma cell line, HT 29. *Front. Gastrointest. Res.* **4**, 73–9 (1979).

123. Rousset, M., Robine-Leon, S., Dussaulx, E., Chevalier, G. & Zweibaum, A. Glycogen storage in foetal and malignant epithelial cells of the human colon. *Front. Gastrointest. Res.* **4**, 80–5 (1979).

124. Bhanot, H. *et al.* Pathological glycogenesis through glycogen synthase 1 and suppression of excessive AMP kinase activity in myeloid leukemia cells. *Leukemia* **29**, 1555–1563 (2015).

125. Jayaraman, A. Characterization of endothelial cell metabolism under different microenvironmental challenges : exploring therapeutic implications of targeting glycogen degradation Characterization of endothelial cell metabolism under different microenvironmental challen. (2016).

126. Anderka, O. *et al.* Thermodynamic Characterization of Allosteric Glycogen Phosphorylase Inhibitors. *Biochemistry* **47**, 4683–4691 (2008).

127. Oikonomakos, N. G. *et al.* Flavopiridol Inhibits Glycogen Phosphorylase by Binding at the Inhibitor Site. *J. Biol. Chem.* **275**, 34566–34573 (2000).

128. Andersen, B., Rassov, A., Westergaard, N. & Lundgren, K. Inhibition of glycogenolysis in primary rat hepatocytes by 1,4-dideoxy-1,4-imino-D-arabinitol. *Biochem. J.* **342**, 545–550 (1999).

129. Choi, B.-H. & Coloff, J. L. The Diverse Functions of Non-Essential Amino Acids in Cancer. *Cancers (Basel).* **11**, 675 (2019).

130. Lukey, M. J., Katt, W. P. & Cerione, R. A. Targeting amino acid metabolism for cancer therapy. *Drug Discov. Today* **22**, 796–804 (2017).

131. Altman, B. J., Stine, Z. E. & Dang, C. V. From Krebs to clinic: glutamine metabolism to cancer therapy. *Nat. Rev. Cancer* **16**, 619 (2016).

132. Bhutia, Y. D., Babu, E., Ramachandran, S. & Ganapathy, V. Amino acid transporters in cancer and their relevance to 'glutamine addiction': Novel Targets for the design of a new class of anticancer drugs. *Cancer Res.* **75**, 1782–1788 (2015).

133. Hosios, A. M. *et al.* Amino Acids Rather than Glucose Account for the Majority of Cell Mass in Proliferating Mammalian Cells. *Dev. Cell* **36**, 540–9 (2016).

134. Meng, M., Chen, S., Lao, T., Liang, D. & Sang, N. Nitrogen anabolism underlies the importance of glutaminolysis in proliferating cells. *Cell Cycle* **9**, 3921–3932 (2010).

135. Ma, Z. & Vosseller, K. O-GlcNAc in cancer biology. *Amino Acids* **45**, 719–733 (2013).

136. Dang, C. V. Glutaminolysis: Supplying carbon or nitrogen or both for cancer cells? *Cell Cycle* **9**, 3884–3886 (2010).

137. Friday, E., Oliver, R., Welbourne, T. & Turturro, F. Glutaminolysis and glycolysis regulation by troglitazone in breast cancer cells: Relationship to mitochondrial membrane potential. *J. Cell. Physiol.* **226**, 511–519 (2011).

138. Jin, L., Alesi, G. N. & Kang, S. Glutaminolysis as a target for cancer therapy. *Oncogene* **35**, 3619–25 (2016).

139. Matés, J. M., Di Paola, F. J., Campos-Sandoval, J. A., Mazurek, S. & Márquez, J. Therapeutic targeting of glutaminolysis as an essential strategy to combat cancer. *Semin. Cell Dev. Biol.* **98**, 34–43 (2020).

140. Robinson, M. M. *et al.* Novel mechanism of inhibition of rat kidney-type glutaminase by bis-2-(5-phenylacetamido-1,2,4-thiadiazol-2-yl)ethyl sulfide (BPTES). *Biochem. J.* **406**, 407–414 (2007).

141. Gross, M. I. *et al.* Antitumor activity of the glutaminase inhibitor CB-839 in triple-negative breast cancer. *Mol. Cancer Ther.* **13**, 890–901 (2014).

142. Wang, J. *et al.* Targeting mitochondrial glutaminase activity inhibits oncogenic transformation. *Cancer Cell* **18**, 207–19 (2010).

143. Clancy, K. P. *et al.* Localization of the L-Glutamine Synthetase Gene to Chromosome 1q23. *Genomics* **38**, 418–420 (1996).

144. Jepson, M. M., Bates, P. C., Broadbent, P., Pell, J. M. & Millward, D. J. Relationship between glutamine concentration and protein synthesis in rat skeletal muscle. *Am. J. Physiol. Metab.* **255**, E166–E172 (1988).

145. Bott, A. J., Maimouni, S. & Zong, W.-X. The Pleiotropic Effects of Glutamine Metabolism in Cancer. *Cancers (Basel).* **11**, 1–16 (2019).

146. Vats, P. *et al.* Changes in the activity levels of glutamine synthetase, glutaminase and glycogen synthetase in rats subjected to hypoxic stress. *Int. J. Biometeorol.* **42**, 205–209 (1999).

147. Kobayashi, S. & Millhorn, D. E. Hypoxia regulates glutamate metabolism and membrane transport in rat PC12 cells. *J. Neurochem.* **76**, 1935–1948 (2001).

148. Krebs, H. A. Metabolism of amino-acids: The synthesis of glutamine from glutamic acid and ammonia, and the enzymic hydrolysis of glutamine in animal tissues. *Biochem. J.* **29**, 1951–69 (1935).

149. Jones, M. E. Conversion of Glutamate to Ornithine and Proline: Pyrroline-5-Carboxylate, a Possible Modulator of Arginine Requirements. *J. Nutr.* **115**, 509–515 (1985).

150. Meister, A. & Anderson, M. E. Glutathione. *Annu. Rev. Biochem.* **52**, 711–760 (1983).

151. Son, J. *et al.* Glutamine supports pancreatic cancer growth through a KRAS-regulated metabolic pathway. *Nature* **496**, 101 (2013).

152. Jin, L. *et al.* The PLAG1-GDH1 Axis Promotes Anoikis Resistance and Tumor Metastasis through CamKK2-AMPK Signaling in LKB1-Deficient Lung Cancer. *Mol. Cell* **69**, 87-99.e7 (2018).

153. Birsoy, K. *et al.* An Essential Role of the Mitochondrial Electron Transport Chain in Cell Proliferation Is to Enable Aspartate Synthesis. *Cell* **162**, 540–51 (2015).

154. Alkan, H. F. *et al.* Cytosolic Aspartate Availability Determines Cell Survival When Glutamine Is Limiting. *Cell Metab.* **28**, 706-720.e6 (2018).

155. Knott, S. R. V *et al.* Asparagine bioavailability governs metastasis in a model of breast cancer. *Nature* **554**, 378–381 (2018).

156. Rabinovich, S. *et al.* Diversion of aspartate in ASS1-deficient tumours fosters de novo pyrimidine synthesis. *Nature* **527**, 379–383 (2015).

157. Gerner, E. W. & Meyskens, F. L. Polyamines and cancer: old molecules, new understanding. *Nat. Rev. Cancer* **4**, 781–92 (2004).

158. Nowotarski, S. L., Woster, P. M. & Casero, R. A. Polyamines and cancer: implications for chemotherapy and chemoprevention. *Expert Rev. Mol. Med.* **15**, e3 (2013).

159. Goodwin, A. C. *et al.* Polyamine catabolism contributes to enterotoxigenic Bacteroides fragilis-induced colon tumorigenesis. *Proc. Natl. Acad. Sci.* **108**, 15354–15359 (2011).

160. Babbar, N. & Casero, R. A. Tumor Necrosis Factor- Increases Reactive Oxygen Species by Inducing Spermine Oxidase in Human Lung Epithelial Cells: A Potential Mechanism for Inflammation-Induced Carcinogenesis. *Cancer Res.* **66**, 11125–11130 (2006).

161. Dolfi, S. C. *et al.* The metabolic demands of cancer cells are coupled to their size and protein synthesis rates. *Cancer Metab.* **1**, 20 (2013).

162. Maddocks, O. D. K. *et al.* Modulating the therapeutic response of tumours to dietary serine and glycine starvation. *Nature* **544**, 372–376 (2017).

163. Locasale, J. W. *et al.* Phosphoglycerate dehydrogenase diverts glycolytic flux and contributes to oncogenesis. *Nat. Genet.* **43**, 869–74 (2011).

164. Possemato, R. *et al.* Functional genomics reveal that the serine synthesis pathway is essential in breast cancer. *Nature* **476**, 346–350 (2011).

165. Nowotarski, S. L., Woster, P. M. & Casero, R. A. Polyamines and cancer: implications for chemotherapy and chemoprevention. *Expert Rev. Mol. Med.* **15**, e3 (2013).

166. Mullarky, E. *et al.* Identification of a small molecule inhibitor of 3-phosphoglycerate dehydrogenase to target serine biosynthesis in cancers. *Proc. Natl. Acad. Sci. U. S. A.* **113**, 1778–1783 (2016).

167. Pacold, M. E. *et al.* A PHGDH inhibitor reveals coordination of serine synthesis and 1-carbon

unit fate HHS Public Access Author manuscript. *Nat Chem Biol* **12**, 452–458 (2016).

168. Mullarky, E. *et al.* Inhibition of 3-phosphoglycerate dehydrogenase (PHGDH) by indole amides abrogates de novo serine synthesis in cancer cells. *Bioorg. Med. Chem. Lett.* **29**, 2503–2510 (2019).

169. Tong, X., Zhao, F. & Thompson, C. B. The molecular determinants of de novo nucleotide biosynthesis in cancer cells. *Curr. Opin. Genet. Dev.* **19**, 32–37 (2009).

170. Fan, J. *et al.* Quantitative flux analysis reveals folate-dependent NADPH production. *Nature* **510**, 298–302 (2014).

171. Mentch, S. J. & Locasale, J. W. One-carbon metabolism and epigenetics: understanding the specificity. *Ann. N. Y. Acad. Sci.* **1363**, 91–8 (2016).

172. Newman, A. C. & Maddocks, O. D. K. One-carbon metabolism in cancer. *Br. J. Cancer* **116**, 1499–1504 (2017).

173. Hagedorn, C. H. & Phang, J. M. Catalytic transfer of hydride ions from NADPH to oxygen by the interconversions of proline and Δ1-pyrroline-5-carboxylate. *Arch. Biochem. Biophys.* **248**, 166–174 (1986).

174. Tanner, J. J., Fendt, S. M. & Becker, D. F. The Proline Cycle As a Potential Cancer Therapy Target. *Biochemistry* **57**, 3433–3444 (2018).

175. Phang, J. M., Liu, W., Hancock, C. N. & Fischer, J. W. Proline metabolism and cancer: Emerging links to glutamine and collagen. *Curr. Opin. Clin. Nutr. Metab. Care* **18**, 71–77 (2015).

176. Liu, W., Hancock, C. N., Fischer, J. W., Harman, M. & Phang, J. M. Proline biosynthesis augments tumor cell growth and aerobic glycolysis: Involvement of pyridine nucleotides. *Sci. Rep.* **5**, 1–13 (2015).

177. Cai, F. *et al.* Pyrroline-5-carboxylate reductase 1 promotes proliferation and inhibits apoptosis in non-small cell lung cancer. *Oncol. Lett.* **15**, 731–740 (2018).

178. Elia, I. *et al.* Proline metabolism supports metastasis formation and could be inhibited to selectively target metastasizing cancer cells. *Nat. Commun.* **8**, 1–11 (2017).

179. Liu, W. *et al.* Proline oxidase promotes tumor cell survival in hypoxic tumor microenvironments. *Cancer Res.* **72**, 3677–86 (2012).

180. Danhier, P. *et al.* Cancer metabolism in space and time: Beyond the Warburg effect. *Biochim. Biophys. Acta - Bioenerg.* **1858**, 556–572 (2017).

181. Warburg, O. On the Origin of Cancer Cells. *Science (80-.).* **123**, 309 LP – 314 (1956).

182. Porporato, P. E., Filigheddu, N., Pedro, J. M. B. S., Kroemer, G. & Galluzzi, L. Mitochondrial metabolism and cancer. *Cell Res.* **28**, 265–280 (2018).

183. Collins, Y. *et al.* Mitochondrial redox signalling at a glance. *J. Cell Sci.* **125**, 1837 (2012).

184. Rizzuto, R., De Stefani, D., Raffaello, A. & Mammucari, C. Mitochondria as sensors and regulators of calcium signalling. *Nat. Rev. Mol. Cell Biol.* **13**, 566 (2012).

185. Parsons, M. J. & Green, D. R. Mitochondria in cell death. *Essays Biochem.* **47**, 99–114 (2010).

186. Cardaci, S. & Ciriolo, M. R. TCA Cycle Defects and Cancer: When Metabolism Tunes Redox State. *Int. J. Cell Biol.* **2012**, 1–9 (2012).

187. Lunt, S. Y. & Vander Heiden, M. G. Aerobic glycolysis: meeting the metabolic requirements of cell proliferation. *Annu. Rev. Cell Dev. Biol.* **27**, 441–64 (2011).

188. Kitazawa, S. *et al.* Succinate dehydrogenase B-deficient cancer cells are highly sensitive to bromodomain and extra-terminal inhibitors. *Oncotarget* **8**, 28922–28938 (2017).

189. Takeuchi, T., Schumacker, P. T. & Kozmin, S. A. Identification of fumarate hydratase inhibitors with nutrient-dependent cytotoxicity. *J. Am. Chem. Soc.* **137**, 564–567 (2015).

190. Yen, K. *et al.* AG-221, a First-in-Class Therapy Targeting Acute Myeloid Leukemia Harboring Oncogenic IDH2 Mutations. *Cancer Discov.* **7**, 478–493 (2017).

191. Wang, F. *et al.* Targeted Inhibition of Mutant IDH2 in Leukemia Cells Induces Cellular Differentiation. *Science (80-.).* **340**, 622–626 (2013).

192. Chen, C. *et al.* Cancer-associated IDH2 mutants drive an acute myeloid leukemia that is susceptible to Brd4 inhibition. *Genes Dev.* **27**, 1974–1985 (2013).

193. Viale, A., Corti, D. & Draetta, G. F. Tumors and mitochondrial respiration: a neglected

connection. *Cancer Res.* **75**, 3685–3686 (2015).

194. Kluza, J. *et al.* Exploiting Mitochondrial Dysfunction for Effective Elimination of Imatinib-Resistant Leukemic Cells. *PLoS One* **6**, e21924 (2011).

195. Damaraju, V. L., Kuzma, M., Cass, C. E., Putman, C. T. & Sawyer, M. B. Multitargeted kinase inhibitors imatinib, sorafenib and sunitinib perturb energy metabolism and cause cytotoxicity to cultured C2C12 skeletal muscle derived myotubes. *Biochem. Pharmacol.* **155**, 162–171 (2018).

196. Whitaker-Menezes, D. *et al.* Hyperactivation of oxidative mitochondrial metabolism in epithelial cancer cells in situ. *Cell Cycle* **10**, 4047–4064 (2011).

197. Lagadinou, D. *et al.* BCL-2 inhibition targets oxidative phosphorilation and selectively eradicates quiscent human leukemia stem cells. *Cell Stem Cell* **127**, 358–366 (2012).

198. Wylie, B. J. *et al.* Oncogene ablation-resistant pancreatic cancer cells depend on mitochondrial function. *Nature* **514**, 628–632 (2014).

199. Birsoy, K. *et al.* Metabolic determinants of cancer cell sensitivity to glucose limitation and biguanides. *Nature* **508**, 108–12 (2014).

200. Scotland, S. *et al.* Mitochondrial energetic and AKT status mediate metabolic effects and apoptosis of metformin in human leukemic cells. *Leukemia* **27**, 2129–2138 (2013).

201. Zhang, X. *et al.* Induction of mitochondrial dysfunction as a strategy for targeting tumour cells in metabolically compromised microenvironments. *Nat. Commun.* **5**, 3295 (2014).

202. Lim, S. C., Carey, K. T. & McKenzie, M. Anti-cancer analogues ME-143 and ME-344 exert toxicity by directly inhibiting mitochondrial NADH: Ubiquinone oxidoreductase (Complex I). *Am. J. Cancer Res.* **5**, 689–701 (2015).

203. Guo, L. *et al.* Inhibition of mitochondrial complex II by the anticancer agent lonidamine. *J. Biol. Chem.* **291**, 42–57 (2016).

204. Swettenham, E., Witting, P. K., Salvatore, B. A. & Neuzil, J. α-tocopheryl succinate selectively induces apoptosis in neuroblastoma cells: Potential therapy of malignancies of the nervous system? *J. Neurochem.* **94**, 1448–1456 (2005).

205. Perkins, C., Kim, C. N., Fang, G. & Bhalla, K. N. Arsenic induces apoptosis of multidrug-resistant human myeloid leukemia cells that express Bcr-Abl or overexpress MDR , MRP , Bcl-2 , or Bcl-x L. **95**, 1014–1023 (2019).

206. Maeda, H. *et al.* Tumor growth inhibition by arsenic trioxide (As2O3) in the orthotopic metastasis model of androgen-independent prostate cancer. *Cancer Res.* **61**, 5432–5440 (2001).

207. Bornstein, J., Sagi, S., Haj, A., Harroch, J. & Fares, F. Arsenic Trioxide inhibits the growth of human ovarian carcinoma cell line. *Gynecol. Oncol.* **99**, 726–729 (2005).

208. Gaude, E. & Frezza, C. Tissue-specific and convergent metabolic transformation of cancer correlates with metastatic potential and patient survival. *Nat. Commun.* **7**, 1–9 (2016).

209. Ansell, R., Granath, K., Hohmann, S., Thevelein, J. M. & Adler, L. The two isoenzymes for yeast NAD + -dependent glycerol 3-phosphate dehydrogenase encoded by GPD1 and GPD2 have distinct roles in osmoadaptation and redox regulation. *EMBO J.* **16**, 2179–2187 (1997).

210. Mráček, T., Drahota, Z. & Houštěk, J. The function and the role of the mitochondrial glycerol-3-phosphate dehydrogenase in mammalian tissues. *Biochim. Biophys. Acta - Bioenerg.* **1827**, 401–410 (2013).

211. Sekhar, B. S., Kurup, C. K. R. & Ramasarma, T. Generation of hydrogen peroxide by brown adipose tissue mitochondria. *J. Bioenerg. Biomembr.* **19**, 397–407 (1987).

212. Drahota, Z. *et al.* Glycerophosphate-dependent hydrogen peroxide production by brown adipose tissue mitochondria and its activation by ferricyanide. *J. Bioenerg. Biomembr.* **34**, 105–113 (2002).

213. Saheki, T. *et al.* Effects of supplementation on food intake, body weight and hepatic metabolites in the citrin/mitochondrial glycerol-3-phosphate dehydrogenase double-knockout mouse model of human citrin deficiency. *Mol. Genet. Metab.* **107**, 322–329 (2012).

214. Thakur, S. *et al.* Metformin Targets Mitochondrial Glycerophosphate Dehydrogenase to Control Rate of Oxidative Phosphorylation and Growth of Thyroid Cancer In Vitro and In Vivo. *Clin. Cancer Res.* **24**, 4030–4043 (2018).

215. Singh, G. Mitochondrial FAD-linked glycerol-3-phosphate dehydrogenase: A target for cancer therapeutics. *Pharmaceuticals* **7**, 192–206 (2014).

216. Kuo, C. Y. & Ann, D. K. When fats commit crimes: Fatty acid metabolism, cancer stemness and therapeutic resistance. *Cancer Commun.* **38**, 1–12 (2018).

217. Carracedo, A., Cantley, L. C. & Pandolfi, P. P. Cancer metabolism: fatty acid oxidation in the limelight. *Nat. Rev. Cancer* **13**, 227–32 (2013).

218. Ma, Y. *et al.* Fatty acid oxidation: An emerging facet of metabolic transformation in cancer. *Cancer Lett.* **435**, 92–100 (2018).

219. Yu, X. H., Ren, X. H., Liang, X. H. & Tang, Y. L. Roles of fatty acid metabolism in tumourigenesis: Beyond providing nutrition (Review). *Mol. Med. Rep.* **18**, 5307–5316 (2018).

220. Zaugg, K. *et al.* Carnitine palmitoyltransferase 1C promotes cell survival and tumor growth under conditions of metabolic stress. *Genes Dev.* **25**, 1041–51 (2011).

221. Shi, J. *et al.* High Expression of CPT1A Predicts Adverse Outcomes: A Potential Therapeutic Target for Acute Myeloid Leukemia. *EBioMedicine* **14**, 55–64 (2016).

222. Al-Bahlani, S. *et al.* Fatty acid synthase regulates the chemosensitivity of breast cancer cells to cisplatin-induced apoptosis. *Apoptosis* **22**, 865–876 (2017).

223. Bauerschlag, D. O. *et al.* Fatty acid synthase overexpression: Target for therapy and reversal of chemoresistance in ovarian cancer. *J. Transl. Med.* **13**, 1–12 (2015).

224. Samudio, I. *et al.* Pharmacologic inhibition of fatty acid oxidation sensitizes human leukemia cells to apoptosis induction. *J. Clin. Invest.* **120**, 142–156 (2010).

225. del Río, L. A., Sandalio, L. M., Palma, J. M., Bueno, P. & Corpas, F. J. Metabolism of oxygen radicals in peroxisomes and cellular implications. *Free Radic. Biol. Med.* **13**, 557–580 (1992).

226. Purohit, V., Simeone, D. M. & Lyssiotis, C. A. Metabolic Regulation of Redox Balance in Cancer. *Cancers (Basel).* **11**, 955 (2019).

227. Rasool, M. *et al.* Assessment of circulating biochemical markers and antioxidative status in acute lymphoblastic leukemia (ALL) and acute myeloid leukemia (AML) patients. *Saudi J.*

Biol. Sci. **22**, 106–111 (2015).

228. Wu, G., Fang, Y.-Z., Yang, S., Lupton, J. R. & Turner, N. D. Glutathione Metabolism and Its Implications for Health. *J. Nutr.* **134**, 489–492 (2004).

229. Garcia-Ruiz, C. & Fernandez-Checa, J. C. Mitochondrial glutathione: Hepatocellular survival-death switch. *J. Gastroenterol. Hepatol.* **21**, 3–6 (2006).

230. Hangauer, M. J. *et al.* Drug-tolerant persister cancer cells are vulnerable to GPX4 inhibition. *Nature* **551**, 247–250 (2017).

231. Short, S. P. & Williams, C. S. Selenoproteins in Tumorigenesis and Cancer Progression. *Adv. Cancer Res.* **136**, 49–83 (2017).

232. Zhu, Z. *et al.* Glutathione reductase mediates drug resistance in glioblastoma cells by regulating redox homeostasis. *J. Neurochem.* **144**, 93–104 (2018).

233. Zhang, H., Jay Forman, H. & Choi, J. γ-Glutamyl Transpeptidase in Glutathione Biosynthesis. in *Methods in Enzymology* **401**, 468–483 (2005).

234. Allocati, N., Masulli, M., Di Ilio, C. & Federici, L. Glutathione transferases: substrates, inihibitors and pro-drugs in cancer and neurodegenerative diseases. *Oncogenesis* **7**, 8 (2018).

235. Al Tameemi, W., Dale, T. P., Al-Jumaily, R. M. K. & Forsyth, N. R. Hypoxia-Modified Cancer Cell Metabolism. *Front. Cell Dev. Biol.* **7**, 1–15 (2019).

236. Pouysségur, J., Dayan, F. & Mazure, N. M. Hypoxia signalling in cancer and approaches to enforce tumour regression. *Nature* **441**, 437–443 (2006).

237. Simon, M. C. & Keith, B. The role of oxygen availability in embryonic development and stem cell function. *Nat. Rev. Mol. Cell Biol.* **9**, 285–296 (2008).

238. Wang, G. L., Jiang, B. H., Rue, E. A. & Semenza, G. L. Hypoxia-inducible factor 1 is a basic-helix-loop-helix-PAS heterodimer regulated by cellular O2 tension. *Proc. Natl. Acad. Sci. U. S. A.* **92**, 5510–4 (1995).

239. Petrova, V., Annicchiarico-Petruzzelli, M., Melino, G. & Amelio, I. The hypoxic tumour microenvironment. *Oncogenesis* **7**, 10 (2018).

240. Weidemann, A. & Johnson, R. S. Biology of HIF-1α. *Cell Death Differ.* **15**, 621–627 (2008).

241. Goda, N. & Kanai, M. Hypoxia-inducible factors and their roles in energy metabolism. *Int. J. Hematol.* **95**, 457–463 (2012).

242. Al Tameemi, W., Dale, T. P., Al-Jumaily, R. M. K. & Forsyth, N. R. Hypoxia-Modified Cancer Cell Metabolism. *Front. Cell Dev. Biol.* **7**, 1–15 (2019).

243. Seo, B. R., DelNero, P. & Fischbach, C. In vitro models of tumor vessels and matrix: Engineering approaches to investigate transport limitations and drug delivery in cancer. *Adv. Drug Deliv. Rev.* **69**–**70**, 205–216 (2014).

244. Vaupel, P. Hypoxia and Aggressive Tumor Phenotype: Implications for Therapy and Prognosis. *Oncologist* **13**, 21–26 (2008).

245. Trédan, O., Galmarini, C. M., Patel, K. & Tannock, I. F. Drug resistance and the solid tumor microenvironment. *J. Natl. Cancer Inst.* **99**, 1441–1454 (2007).

246. Rieger, C. T. & Fiegl, M. Microenvironmental oxygen partial pressure in acute myeloid leukemia: Is there really a role for hypoxia? *Exp. Hematol.* **44**, 578–582 (2016).

247. Deynoux, M., Sunter, N., Hérault, O. & Mazurier, F. Hypoxia and hypoxia-inducible factors in leukemias. *Front. Oncol.* **6**, 1–9 (2016).

248. Fiegl, M. *et al.* Physiological hypoxia promotes lipid raft and PI3K-dependent activation of MAPK 42/44 in leukemia cells. *Leukemia* **24**, 1364–7 (2010).

249. Drolle, H. *et al.* Hypoxia regulates proliferation of acute myeloid leukemia and sensitivity against chemotherapy. *Leuk. Res.* **39**, 779–785 (2015).

250. Jensen, P. O. *et al.* Increased cellular hypoxia and reduced proliferation of both normal and leukaemic cells during progression of acute myeloid leukaemia in rats. *Cell Prolif.* **33**, 381–395 (2000).

251. Forristal, C. E. *et al.* Hypoxia inducible factor (HIF)-2α accelerates disease progression in mouse models of leukemia and lymphoma but is not a poor prognosis factor in human AML. *Leukemia* **29**, 2075–2085 (2015).

252. Coltella, N. *et al.* HIF factors cooperate with PML-RARα to promote acute promyelocytic

leukemia progression and relapse. *EMBO Mol. Med.* **6**, 640–50 (2014).

253. Zhang, H., Li, H., Xi, H. S. & Li, S. HIF1α is required for survival maintenance of chronic myeloid leukemia stem cells. *Blood* **119**, 2595–2607 (2012).

254. Deeb, G. *et al.* Hypoxia-inducible factor-1α protein expression is associated with poor survival in normal karyotype adult acute myeloid leukemia. *Leuk. Res.* **35**, 579–584 (2011).

255. Zhe, N. *et al.* Heme oxygenase-1 plays a crucial role in chemoresistance in acute myeloid leukemia. *Hematology* **20**, 384–391 (2015).

256. Ito, K. & Suda, T. Metabolic requirements for the maintenance of self-renewing stem cells. *Nat. Rev. Mol. Cell Biol.* **15**, 243–256 (2014).

257. Ito, K. *et al.* A PML-PPAR-δ pathway for fatty acid oxidation regulates hematopoietic stem cell maintenance. *Nat. Med.* **18**, 1350–1358 (2012).

258. Takubo, K. *et al.* Regulation of glycolysis by Pdk functions as a metabolic checkpoint for cell cycle quiescence in hematopoietic stem cells. *Cell Stem Cell* **12**, 49–61 (2013).

259. Bhanot, H. *et al.* Acute myeloid leukemia cells require 6-phosphogluconate dehydrogenase for cell growth and NADPH-dependent metabolic reprogramming. *Oncotarget* **8**, 67639–67650 (2017).

260. Farge, T. *et al.* Chemotherapy-Resistant Human Acute Myeloid Leukemia Cells Are Not Enriched for Leukemic Stem Cells but Require Oxidative Metabolism. *Cancer Discov.* **7**, 716–735 (2017).

261. Noel, B. M. *et al.* Multiomic Profiling of Tyrosine Kinase Inhibitor-Resistant K562 Cells Suggests Metabolic Reprogramming To Promote Cell Survival. *J. Proteome Res.* **18**, 1842–1856 (2019).

262. Cunningham, I. & Kohno, B. 18 FDG-PET/CT: 21st century approach to leukemic tumors in 124 cases. *Am. J. Hematol.* **91**, 379–384 (2016).

263. Herst, P. M., Howman, R. A., Neeson, P. J., Berridge, M. V. & Ritchie, D. S. The level of glycolytic metabolism in acute myeloid leukemia blasts at diagnosis is prognostic for clinical outcome. *J. Leukoc. Biol.* **89**, 51–55 (2011).

264. Chen, W.-L. *et al.* A distinct glucose metabolism signature of acute myeloid leukemia with prognostic value. *Blood* **124**, 1645–1654 (2014).

265. Xu, Q., Simpson, S.-E., Scialla, T. J., Bagg, A. & Carroll, M. Survival of acute myeloid leukemia cells requires PI3 kinase activation. *Blood* **102**, 972–980 (2003).

266. Tamburini, J. *et al.* Protein synthesis is resistant to rapamycin and constitutes a promising therapeutic target in acute myeloid leukemia. *Blood* **114**, 1618–1627 (2009).

267. Poulain, L. *et al.* High mTORC1 activity drives glycolysis addiction and sensitivity to G6PD inhibition in acute myeloid leukemia cells. *Leukemia* **31**, 2326–2335 (2017).

268. Wang, Y.-H. *et al.* Cell-state-specific metabolic dependency in hematopoiesis and leukemogenesis. *Cell* **158**, 1309–1323 (2014).

269. Skrtić, M. *et al.* Inhibition of mitochondrial translation as a therapeutic strategy for human acute myeloid leukemia. *Cancer Cell* **20**, 674–88 (2011).

270. Sriskanthadevan, S. *et al.* AML cells have low spare reserve capacity in their respiratory chain that renders them susceptible to oxidative metabolic stress. *Blood* **125**, 2120–2130 (2015).

271. Pardee, T. S. *et al.* A phase I study of the first-in-class mitochondrial metabolism inhibitor CPI-613 in patients with advanced hematologic malignancies. Subcategory: *Clin Cancer Res* **20**, 5255–5264 (2013).

272. Kreitz *et al.* Metabolic Plasticity of Acute Myeloid Leukemia. *Cells* **8**, 805 (2019).

273. Parlati, F. *et al.* Antitumor Activity Of The Glutaminase Inhibitor CB-839 In Hematological Malignances. *Blood* **122**, 4226–4226 (2013).

274. Miraki-Moud, F. *et al.* Arginine deprivation using pegylated arginine deiminase has activity against primary acute myeloid leukemia cells in vivo. *Blood* **125**, 4060–4068 (2015).

275. Raffel, S. *et al.* BCAT1 restricts αKG levels in AML stem cells leading to IDHmut-like DNA hypermethylation. *Nature* **551**, 384 (2017).

276. Hattori, A. *et al.* Cancer progression by reprogrammed BCAA metabolism in myeloid leukaemia. *Nature* **545**, 500–504 (2017).

277. Stirewalt, D. L., Appelbaum, F. R., Willman, C. L., Zager, R. A. & Banker, D. E. Mevastatin can increase toxicity in primary AMLs exposed to standard therapeutic agents, but statin efficacy is not simply associated with ras hotspot mutations or overexpression. *Leuk. Res.* **27**, 133–45 (2003).

278. Lishner, M., Bar-Sef, A., Elis, A. & Fabian, I. Effect of Simvastatin Alone and in Combination With Cytosine Arabinoside on the Proliferation of Myeloid Leukemia Cell Lines. *J. Investig. Med.* **49**, 319–324 (2001).

279. Holstein, S. A. & Hohl, R. J. Interaction of cytosine arabinoside and lovastatin in human leukemia cells. *Leuk. Res.* **25**, 651–660 (2001).

280. Kuntz, E. M. An Investigation of Metabolic Vulnerabilities in Chronic Myeloid Leukaemic Stem Cells. (2017).

281. Kuntz, E. M. *et al.* Targeting mitochondrial oxidative phosphorylation eradicates therapy-resistant chronic myeloid leukemia stem cells. *Nat. Med.* **23**, 1234–1240 (2017).

282. Giustacchini, A. *et al.* Single-cell transcriptomics uncovers distinct molecular signatures of stem cells in chronic myeloid leukemia. *Nat. Med.* **23**, 692–702 (2017).

283. Patel, A. B., O'Hare, T. & Deininger, M. W. Mechanisms of Resistance to ABL Kinase Inhibition in Chronic Myeloid Leukemia and the Development of Next Generation ABL Kinase Inhibitors. *Hematol. Oncol. Clin. North Am.* **31**, 589–612 (2017).

284. Ward, P. S. & Thompson, C. B. Metabolic reprogramming: a cancer hallmark even warburg did not anticipate. *Cancer Cell* **21**, 297–308 (2012).

285. Stäubert, C. *et al.* Rewired metabolism in drug-resistant leukemia cells: A metabolic switch hallmarked by reduced dependence on exogenous glutamine. *J. Biol. Chem.* **290**, 8348–8359 (2015).

286. Boren, J. *et al.* Gleevec (STI571) Influences Metabolic Enzyme Activities and Glucose Carbon Flow toward Nucleic Acid and Fatty Acid Synthesis in Myeloid Tumor Cells. *J. Biol. Chem.* **276**, 37747–37753 (2001).

287. Gottschalk, S. *et al.* Imatinib (STI571) -Mediated Changes in Glucose Metabolism in Human Leukemia BCR-ABL-Positive Cells Imatinib (STI571) -Mediated Changes in Glucose

Metabolism in. **10**, 6661–6668 (2004).

288. Breccia, M. & Alimena, G. The metabolic consequences of imatinib mesylate: Changes on glucose, lypidic and bone metabolism. *Leuk. Res.* **33**, 871–5 (2009).

289. Poliaková, M., Aebersold, D. M., Zimmer, Y. & Medová, M. The relevance of tyrosine kinase inhibitors for global metabolic pathways in cancer. *Mol. Cancer* **17**, 27 (2018).

290. Chakraborty, S., Hosen, M. I., Ahmed, M. & Shekhar, H. U. Onco-Multi-OMICS Approach: A New Frontier in Cancer Research. *Biomed Res. Int.* **2018**, 1–14 (2018).

291. Yugi, K., Kubota, H., Hatano, A. & Kuroda, S. Trans-Omics: How To Reconstruct Biochemical Networks Across Multiple 'Omic' Layers. *Trends Biotechnol.* **34**, 276–290 (2016).

292. Aslam, B., Basit, M., Nisar, M. A., Khurshid, M. & Rasool, M. H. Proteomics: Technologies and their applications. *J. Chromatogr. Sci.* **55**, 182–196 (2017).

293. Ong, S.-E. & Mann, M. Stable Isotope Labeling by Amino Acids in Cell Culture for Quantitative Proteomics. in *Journal of Chemical Information and Modeling* **53**, 37–52 (2007).

294. Jakobsen, L., Schrøder, J. M., Larsen, K. M., Lundberg, E. & Andersen, J. S. Centrosome Isolation and Analysis by Mass Spectrometry-Based Proteomics. in *Methods in Enzymology* **525**, 371–393 (Elsevier Inc., 2013).

295. Terzi, F. & Cambridge, S. An Overview of Advanced SILAC-Labeling Strategies for Quantitative Proteomics. in *Methods in Enzymology* **585**, 29–47 (2017).

296. Chen, M.-J. M. *et al.* TCPA v3.0: An Integrative Platform to Explore the Pan-Cancer Analysis of Functional Proteomic Data. *Mol. Cell. Proteomics* **18**, S15–S25 (2019).

297. Hasin, Y., Seldin, M. & Lusis, A. Multi-omics approaches to disease. *Genome Biol.* **18**, 1–15 (2017).

298. Gowda, G. A. N. & Djukovic, D. Overview of mass spectrometry-based metabolomics: opportunities and challenges. *Methods Mol. Biol.* **1198**, 3–12 (2014).

299. Yang, K. *et al.* A Comprehensive Analysis of Metabolomics and Transcriptomics in Cervical Cancer. *Sci. Rep.* **7**, 1–11 (2017).

300. Coene, K. L. M. *et al.* Next-generation metabolic screening: targeted and untargeted metabolomics for the diagnosis of inborn errors of metabolism in individual patients. *J. Inherit. Metab. Dis.* **41**, 337–353 (2018).

301. Roberts, L. D., Souza, A. L., Gerszten, R. E. & Clish, C. B. Targeted Metabolomics. *Curr. Protoc. Mol. Biol.* **98**, 30.2.1-30.2.24 (2012).

302. Zhang, X., Zhu, X., Wang, C., Zhang, H. & Cai, Z. Non-targeted and targeted metabolomics approaches to diagnosing lung cancer and predicting patient prognosis. *Oncotarget* **7**, 63437–63448 (2016).

303. Vinayavekhin, N. & Saghatelian, A. Untargeted Metabolomics. in *Current Protocols in Molecular Biology* **90**, 1–24 (John Wiley & Sons, Inc., 2010).

304. Lee, W.-N. P. & Go, V. L. W. Nutrient-gene interaction: tracer-based metabolomics. *J. Nutr.* **135**, 3027S-3032S (2005).

305. Paul Lee, W.-N., Wahjudi, P. N., Xu, J. & Go, V. L. Tracer-based metabolomics: Concepts and practices. *Clin. Biochem.* **43**, 1269–1277 (2010).

306. Misra, B. B., Langefeld, C. D., Olivier, M. & Cox, L. A. Integrated Omics: Tools, Advances, and Future Approaches. *J. Mol. Endocrinol.* **62**, R21–R45 (2018).

307. DeBerardinis, R. J. & Chandel, N. S. Fundamentals of cancer metabolism. *Sci. Adv.* **2**, e1600200 (2016).

308. De Atauri, P. *et al.* Carbon metabolism and the sign of control coefficients in metabolic adaptations underlying K-ras transformation. *Biochim. Biophys. Acta - Bioenerg.* **1807**, 746–754 (2011).

309. Christian, L. & Ulrich, G. MetaboLab-advanced NMR data processing and analysis for metabolomics. *BMC Bioinformatics* **12**, 366 (2011).

310. Pesta, D. & Gnaiger, E. *Mitochondrial Bioenergetics*. **810**, (Humana Press, 2012).

311. Cox, J. & Mann, M. MaxQuant enables high peptide identification rates, individualized p.p.b.-range mass accuracies and proteome-wide protein quantification. *Nat. Biotechnol.* **26**, 1367–72 (2008).

312. Cox, J. *et al.* Andromeda: A peptide search engine integrated into the MaxQuant environment. *J. Proteome Res.* **10**, 1794–1805 (2011).

313. Tyanova, S. *et al.* The Perseus computational platform for comprehensive analysis of (prote)omics data. *Nat. Methods* **13**, 731–740 (2016).

314. Cox, J. & Mann, M. MaxQuant enables high peptide identification rates, individualized p.p.b.-range mass accuracies and proteome-wide protein quantification. *Nat. Biotechnol.* **26**, 1367–72 (2008).

315. Luo, W., Pant, G., Bhavnasi, Y. K., Blanchard, S. G. & Brouwer, C. Pathview Web: User friendly pathway visualization and data integration. *Nucleic Acids Res.* **45**, W501–W508 (2017).

316. Mi, H. *et al.* Protocol Update for large-scale genome and gene function analysis with the PANTHER classification system (v.14.0). *Nat. Protoc.* **14**, 703–721 (2019).

317. Jinek, M. *et al.* A programmable dual-RNA-guided DNA endonuclease in adaptive bacterial immunity. *Science* **337**, 816–21 (2012).

318. Engler, C., Kandzia, R. & Marillonnet, S. A One Pot, One Step, Precision Cloning Method with High Throughput Capability. *PLoS One* **3**, e3647 (2008).

319. Network, N. C. C. NCCN Clinical Practice Guidelines in Oncology: Acute Myeloid Leukemia. *National Comprehensive Cancer* **1**, 2019 (2019).

320. Son, B. *et al.* Decreased FBP1 expression rewires metabolic processes affecting aggressiveness of glioblastoma. *Oncogene* **39**, 36–49 (2020).

321. Guo, B., Huang, X., Lee, M. R., Lee, S. A. & Broxmeyer, H. E. Antagonism of PPAR-γ signaling expands human hematopoietic stem and progenitor cells by enhancing glycolysis. *Nat. Med.* **24**, 360–367 (2018).

322. Panina, S. B., Baran, N., Brasil da Costa, F. H., Konopleva, M. & Kirienko, N. V. A mechanism for increased sensitivity of acute myeloid leukemia to mitotoxic drugs. *Cell Death Dis.* **10**, (2019).

323. Asher, G., Bercovich, Z., Tsvetkov, P., Shaul, Y. & Kahana, C. 20S Proteasomal Degradation of Ornithine Decarboxylase Is Regulated by NQO1. *Mol. Cell* **17**, 645–655 (2005).

324. Marín de Mas, I. *et al.* Model-driven discovery of long-chain fatty acid metabolic reprogramming in heterogeneous prostate cancer cells. *PLoS Comput. Biol.* **14**, e1005914 (2018).

325. Ong, S. E. *et al.* Identifying the proteins to which small-molecule probes and drugs bind in cells. *Proc. Natl. Acad. Sci. U. S. A.* **106**, 4617–4622 (2009).

326. Flis, S. & Chojnacki, T. Chronic myelogenous leukemia, a still unsolved problem: pitfalls and new therapeutic possibilities. *Drug Des. Devel. Ther.* **13**, 825–843 (2019).

327. Will, Y. *et al.* Effect of the multitargeted tyrosine kinase inhibitors imatinib, dasatinib, sunitinib, and sorafenib on mitochondrial function in isolated rat heart mitochondria and H9c2 cells. *Toxicol. Sci.* **106**, 153–161 (2008).

328. Jones, D. *et al.* Laboratory practice guidelines for detecting and reporting BCR-ABL drug resistance mutations in chronic myelogenous leukemia and acute lymphoblastic leukemia. *J. Mol. Diagnostics* **11**, 4–11 (2009).

329. Kenakin, T. P. Pharmacology. in *Pharmacology in Drug Discovery and Development* 1–20 (Elsevier, 2017).

330. Richter, S. *et al.* Expression and role in glycolysis of human ADP-dependent glucokinase. *Mol. Cell. Biochem.* **364**, 131–45 (2012).

331. Schindler, A. & Foley, E. Hexokinase 1 blocks apoptotic signals at the mitochondria. *Cell. Signal.* **25**, 2685–2692 (2013).

332. Favaro, E. *et al.* Glucose utilization via glycogen phosphorylase sustains proliferation and prevents premature senescence in cancer cells. *Cell Metab.* **16**, 751–764 (2012).

333. Hussien, R. & Brooks, G. A. Mitochondrial and plasma membrane lactate transporter and lactate dehydrogenase isoform expression in breast cancer cell lines. *Physiol. Genomics* **43**, 255–64 (2011).

334. Chiaradonna, F., Ricciardiello, F. & Palorini, R. The Nutrient-Sensing Hexosamine Biosynthetic Pathway as the Hub of Cancer Metabolic Rewiring. *Cells* **7**, 53 (2018).

335. Akella, N. M., Ciraku, L. & Reginato, M. J. Fueling the fire: emerging role of the hexosamine biosynthetic pathway in cancer. *BMC Biol.* **17**, 52 (2019).

336. Goubert, E. *et al.* Inhibition of the Mitochondrial Glutamate Carrier SLC25A22 in Astrocytes Leads to Intracellular Glutamate Accumulation. *Front. Cell. Neurosci.* **11**, 1–15 (2017).

337. Espinosa-Diez, C. *et al.* Antioxidant responses and cellular adjustments to oxidative stress. *Redox Biol.* **6**, 183–197 (2015).

338. Tew, K. D. *et al.* The role of glutathione S-transferase P in signaling pathways and S-glutathionylation in cancer. *Free Radic. Biol. Med.* **51**, 299–313 (2011).

339. Bachhawat, A. K., Thakur, A., Kaur, J. & Zulkifli, M. Glutathione transporters. *Biochim. Biophys. Acta - Gen. Subj.* **1830**, 3154–3164 (2013).

340. Whitaker-Menezes, D. *et al.* Hyperactivation of oxidative mitochondrial metabolism in epithelial cancer cells in situ. *Cell Cycle* **10**, 4047–4064 (2011).

341. Orr, A. L. *et al.* Novel Inhibitors of Mitochondrial sn-Glycerol 3-phosphate Dehydrogenase. *PLoS One* **9**, e89938 (2014).

342. Ferdinandusse, S. *et al.* Clinical and biochemical characterization of four patients with mutations in ECHS1. *Orphanet J. Rare Dis.* **10**, 79 (2015).

343. Maher, M., Diesch, J., Casquero, R. & Buschbeck, M. Epigenetic-Transcriptional Regulation of Fatty Acid Metabolism and Its Alterations in Leukaemia. *Front. Genet.* **9**, 1–9 (2018).

344. Aryal, B. & Rao, V. A. Deficiency in Cardiolipin Reduces Doxorubicin-Induced Oxidative Stress and Mitochondrial Damage in Human B-Lymphocytes. *PLoS One* **11**, e0158376 (2016).

345. Ross, D. Novel mechanisms of drug resistance in leukemia. *Leukemia* **14**, 467–473 (2000).

346. Apperley, J. F. Part II: Management of resistance to imatinib in chronic myeloid leukaemia. *Lancet Oncol.* **8**, 1116–1128 (2007).

347. Zaal, E. A. & Berkers, C. R. The Influence of Metabolism on Drug Response in Cancer. *Front. Oncol.* **8**, 1–15 (2018).

348. Jia, D. *et al.* Elucidating cancer metabolic plasticity by coupling gene regulation with metabolic pathways. *Proc. Natl. Acad. Sci. U. S. A.* **116**, 3909–3918 (2019).

349. Chen, W. L. *et al.* A distinct glucose metabolism signature of acute myeloid leukemia with

prognostic value. *Blood* **124**, 1645–1654 (2014).

350. Henkenius, K. *et al.* Maintenance of cellular respiration indicates drug resistance in acute myeloid leukemia. *Leuk. Res.* **62**, 56–63 (2017).

351. Zhang, B. *et al.* FBP1, A Tumor Suppressor and Negative Regulator of Glycolysis, was Epigenetically Silenced in Pancreatic Cancer. *Curr. Signal Transduct. Ther.* **9**, 156–163 (2015).

352. Olivas, J. & Horng, T. Sugar fuels T-cell memory. *Nat. Cell Biol.* **20**, 2–3 (2018).

353. Wallace, K. B., Sardão, V. A. & Oliveira, P. J. Mitochondrial Determinants of Doxorubicin-Induced Cardiomyopathy. *Circ. Res.* **126**, 926–941 (2020).

354. Kato, Y. *et al.* Acidic extracellular microenvironment and cancer. *Cancer Cell Int.* **13**, 89 (2013).

355. Bohloli, M., Atashi, A., Soleimani, M., Kaviani, S. & Anbarlou, A. Investigating Effects of Acidic pH on Proliferation, Invasion and Drug-Induced Apoptosis in Lymphoblastic Leukemia. *Cancer Microenviron.* **9**, 119–126 (2016).

356. Mookerjee, S. A., Goncalves, R. L. S., Gerencser, A. A., Nicholls, D. G. & Brand, M. D. The contributions of respiration and glycolysis to extracellular acid production. *Biochim. Biophys. Acta - Bioenerg.* **1847**, 171–181 (2015).

357. Seltzer, M. J. *et al.* Inhibition of glutaminase preferentially slows growth of glioma cells with mutant IDH1. *Cancer Res.* **70**, 8981–7 (2010).

358. Bateman, L. A. *et al.* Argininosuccinate Synthase 1 is a Metabolic Regulator of Colorectal Cancer Pathogenicity. *ACS Chem. Biol.* **12**, 905–911 (2017).

359. Schafer, F. Q. & Buettner, G. R. Redox environment of the cell as viewed through the redox state of the glutathione disulfide/glutathione couple. *Free Radic. Biol. Med.* **30**, 1191–1212 (2001).

360. Zeng, D.-F. *et al.* Analysis of drug resistance-associated proteins expressions of patients with the recurrent of acute leukemia via protein microarray technology. *Eur. Rev. Med. Pharmacol. Sci.* **18**, 537–43 (2014).

361. Raza, A. *et al.* A phase 2 randomized multicenter study of 2 extended dosing schedules of oral ezatiostat in low to intermediate-1 risk myelodysplastic syndrome. *Cancer* **118**, 2138–2147 (2012).

362. Vilpo, J. A., Veromaa, T. & Eerola, E. Effect of cytosine arabinoside on the human immunosystem: metabolism and cytotoxicity studied with mitogen-stimulated normal blood lymphocytes in vitro. *Int. J. Immunopharmacol.* **10**, 593–600 (1988).

363. Dietz, A. B. *et al.* Imatinib mesylate inhibits T-cell proliferation in vitro and delayed-type hypersensitivity in vivo. *Blood* **104**, 1094–1099 (2004).

364. Norris, R. E. & Adamson, P. C. Clinical potency of methotrexate, aminopterin, talotrexin and pemetrexed in childhood leukemias. *Cancer Chemother. Pharmacol.* **65**, 1125–1130 (2010).

365. Pérez-Velázquez, J., Gevertz, J. L., Karolak, A. & Rejniak, K. A. Microenvironmental Niches and Sanctuaries: A Route to Acquired Resistance. *Adv. Exp. Med. Biol.* **936**, 149–164 (2016).

366. Svensson, K. J. *et al.* Hypoxia-Mediated Induction of the Polyamine System Provides Opportunities for Tumor Growth Inhibition by Combined Targeting of Vascular Endothelial Growth Factor and Ornithine Decarboxylase. *Cancer Res.* **68**, 9291–9301 (2008).

367. Fedorova, N. E. *et al.* Inhibitor of polyamine catabolism MDL72.527 restores the sensitivity to doxorubicin of monocytic leukemia Thp-1 cells infected with human cytomegalovirus. *Biochimie* **158**, 82–89 (2019).

APPENDIX 1

APPENDIX 1: Supplementary data of results of Chapter 1

EXTRACELLULAR FLUXES NORMOXIA					
Kpc (nmol*millioncell-1*h-1)					
	THP-1 Parental		HL-60 Parental		
	Amino acids				
	Mean	SD	Mean	SD	pvalue
Ala	2.29	1.23	7.60	1.28	0.007
Arg	D	D	D	D	D
Asn	-0.84	0.53	0.41	0.90	0.105
Asp	0.21	0.49	0.26	0.27	0.883
Cit	-0.03	0.04	-0.02	0.01	0.658
Gln	-24.37	1.06	-12.51	1.42	0.002
Glu	11.29	1.48	3.76	0.85	0.005
Gly	0.87	1.71	0.33	0.43	0.626
His	-0.57	0.13	-0.17	0.20	0.044
Ile	-2.91	0.79	-0.80	0.12	0.010
Leu	-3.97	0.63	-1.69	0.12	0.004
Lys	-2.36	0.33	-1.10	0.08	0.003
Met	-0.83	0.17	-0.55	0.06	0.049
Orn	1.27	0.61	2.22	0.20	0.063
Phe	-0.93	0.14	-0.53	0.05	0.010
Pro	0.21	0.39	2.35	0.37	0.002
Ser	-3.91	0.82	-2.73	0.31	0.078
Thr	-1.32	0.46	-0.13	0.26	0.017
Trp	-0.35	0.08	-0.13	0.00	0.009
Tyr	-1.09	0.21	-0.30	0.20	0.009
Val	-2.16	0.51	-0.97	0.14	0.017
Polyamines					
Putrescine	1E-03	7E-04	6E-04	3E-04	0.365
Spermidine	3E-04	2E-04	1E-04	5E-05	0.214
Spermine	D	D	D	D	D

Table 1. Extracellular fluxes result of THP-1 and HL-60 Parental cell lines under normoxia. Non-detected amino acids or polyamines or amino acids and polyamines whose replicates were not reproducible are named as discarded (D).

EXTRACELLULAR FLUXES HYPOXIA					
Kpc (nmol*millioncell-1*h-1)					
	THP-1 Parental		HL-60 Parental		pvalue
	Amino acids				
	Mean	SD	Mean	SD	pvalue
Ala	-1.36	1.27	10.99	4.55	0.011
Arg	D	D	D	D	D
Asn	-0.29	2.64	0.35	0.32	0.698
Asp	-0.14	2.51	0.18	0.98	0.848
Cit	D	D	0.05	0.07	D
Gln	-3.59	10.99	-13.89	8.46	0.268
Glu	0.36	5.33	8.24	3.94	0.109
Gly	3.33	1.95	4.35	2.71	0.623
His	-0.72	0.64	0.47	0.81	0.116
Ile	-0.64	0.20	0.10	0.71	0.156
Leu	-2.41	0.85	-0.28	1.62	0.115
Lys	-2.41	0.90	-0.42	0.85	0.049
Met	-0.70	0.79	-0.33	0.20	0.474
Orn	2.31	0.05	3.13	1.98	0.617
Phe	-0.46	0.42	-0.04	0.11	0.168
Pro	0.76	0.45	2.23	1.05	0.091
Ser	-3.76	2.42	-5.20	1.98	0.471
Thr	0.63	2.73	0.49	0.65	0.935
Trp	0.17	0.22	-0.02	0.10	0.247
Tyr	-0.51	0.41	-0.20	0.10	0.277
Val	-1.90	1.98	-0.25	1.23	0.289
Poliamines					
Putrescine	6E-03	1E-03	3E-03	2E-03	0.077
Spermidine	5E-03	8E-04	4E-03	2E-03	0.401
Spermine	D	D	D	D	0.675

Table 2. Extracellular fluxes result of THP-1 and HL-60 Parental cell lines under hypoxia. Non-detected amino acids or polyamines or amino acids and polyamines whose replicates were not reproducible are named as discarded (D).

UPREGULATED PROTEINS IN THP-1 AraC VS. THP-1 P			
Protein names	**Gene names**	**Mean Log_2 fold change**	**SD Log_2 fold change**
Thrombomodulin	THBD	2.69	1.40
Deoxyribonuclease-2-alpha	DNASE2	2.43	0.71
Protein FAM173B	FAM173B	2.38	0.78
Flavin reductase (NADPH)	BLVRB	2.30	0.13
Unconventional myosin-X	MYO10	2.26	N.D.
Amyloid beta A4 protein	APP	2.15	N.D.
Apoptosis regulator Bcl-2	BCL2	2.11	0.26
Heat shock protein beta-1	HSPB1	2.09	0.28
Kynureninase	KYNU	2.06	0.28
Eukaryotic translation initiation factor 3 subunit C	EIF3C;EIF3CL	2.03	1.16
ADP-ribosylation factor GTPase-activating protein 1	ARFGAP1	2.01	N.D.
Serine/arginine repetitive matrix protein 2	SRRM2	1.99	1.24
Acyl-CoA synthetase family member 2, mitochondrial	ACSF2	1.96	N.D.
Protein AATF	AATF	1.94	N.D.
Protein VPRBP	VPRBP	1.87	1.47
Protein NDRG1	NDRG1	1.75	N.D.
U4/U6.U5 tri-snRNP-associated protein 1	SART1	1.74	0.07
Interferon regulatory factor 2-binding protein 1	IRF2BP1	1.74	N.D.
D-tyrosyl-tRNA(Tyr) deacylase 1	DTD1	1.73	N.D.
N-acetylserotonin O-methyltransferase-like protein	ASMTL	1.63	0.39
Alpha/beta hydrolase domain-containing protein 14B	ABHD14B	1.63	0.15
TBC1 domain family member 1	TBC1D1	1.62	N.D.
Eukaryotic translation initiation factor 4B	EIF4B	1.61	0.35
Protein Red	IK	1.61	0.87
Anoctamin-6	ANO6	1.60	0.08
Bromodomain adjacent to zinc finger domain protein 1A	BAZ1A	1.57	0.85
Very low-density lipoprotein receptor	VLDLR	1.55	0.02
Gametocyte-specific factor 1	GTSF1	1.55	0.56
Leukosialin (CD43)	SPN	1.53	0.17
Serine/threonine-protein kinase WNK1	WNK1	1.53	0.21
Mitochondrial import inner membrane translocase subunit TIM14	DNAJC19	1.51	0.10
Ubiquitin-conjugating enzyme E2 T	UBE2T	1.48	0.24
Ornithine aminotransferase, mitochondrial	OAT	1.45	0.03
Telomere-associated protein RIF1	RIF1	1.45	0.33
Protein O-GlcNAcase	MGEA5	1.44	0.23
Matrin-3	MATR3	1.43	0.70
Nuclear export mediator factor NEMF	NEMF	1.43	0.19
Mycophenolic acid acyl-glucuronide esterase, mitochondrial	ABHD10	1.42	0.20
Vesicle transport through interaction with t-SNAREs homolog 1B	VTI1B	1.41	0.41
Fascin	FSCN1	1.40	0.07
Cyclin-dependent kinases regulatory subunit 1	CKS1B	1.39	0.06
Ribonucleoside-diphosphate reductase subunit M2	RRM2	1.39	0.01
Protein disulfide-isomerase A5	PDIA5	1.39	0.45
mRNA-decapping enzyme 1A	DCP1A	1.37	N.D.
Coiled-coil domain-containing protein 58	CCDC58	1.36	N.D.
Ras GTPase-activating-like protein IQGAP3	IQGAP3	1.35	N.D.
U8 snoRNA-decapping enzyme	NUDT16	1.34	N.D.
ER degradation-enhancing alpha-mannosidase-like protein 1	EDEM1	1.33	N.D.
Insulin-like growth factor 2 mRNA-binding protein 3	IGF2BP3	1.32	0.39
UPF0562 protein C7orf55	C7orf55	1.32	N.D.
MARCKS-related protein	MARCKSL1	1.32	N.D.
DNL-type zinc finger protein	DNLZ	1.32	0.11
Nischarin	NISCH	1.31	0.00
Tripartite motif-containing protein 65	TRIM65	1.31	N.D.
CGG triplet repeat-binding protein 1	CGGBP1	1.31	N.D.
Charged multivesicular body protein 1b	CHMP1B	1.31	N.D.
Pterin-4-alpha-carbinolamine dehydratase	PCBD1	1.30	0.59
Collagen type IV alpha-3-binding protein	COL4A3BP	1.29	N.D.
Proteasome subunit beta type-5	PSMB5	1.28	N.D.
Regulatory-associated protein of mTOR	RPTOR	1.28	N.D.
Metaxin-2	MTX2	1.28	0.23
Ubiquitin-conjugating enzyme E2 G1	UBE2G1	1.28	0.01
Gamma-aminobutyric acid receptor-associated protein-like 2	GABARAPL2	1.27	0.17
Arf-GAP with coiled-coil, ANK repeat and PH domain-containing protein 2	ACAP2	1.25	0.49
Melanoma-associated antigen D2	MAGED2	1.24	0.57
Phosphatidylglycerophosphatase and protein-tyrosine phosphatase 1	PTPMT1	1.23	N.D.
Protein FAM162A	FAM162A	1.23	N.D.
Sulfatase-modifying factor 2	SUMF2	1.23	N.D.
Tyrosine-protein phosphatase non-receptor type 23	PTPN23	1.22	N.D.
Succinate-semialdehyde dehydrogenase, mitochondrial	ALDH5A1	1.21	0.50
Insulin-like growth factor 2 mRNA-binding protein 2	IGF2BP2	1.21	0.22
Asparagine synthetase [glutamine-hydrolyzing]	ASNS	1.20	0.11
5-3 exoribonuclease 1	XRN1	1.20	N.D.
E2/E3 hybrid ubiquitin-protein ligase UBE2O	UBE2O	1.20	0.13
1-phosphatidylinositol 4,5-bisphosphate phosphodiesterase beta-3	PLCB3	1.20	N.D.
GTP cyclohydrolase 1 feedback regulatory protein	GCHFR	1.18	N.D.
NTF2-related export protein 2	NXT2	1.18	0.28
CAP-Gly domain-containing linker protein 1	CLIP1	1.17	0.40
Protein C10	C12orf57	1.17	N.D.
Branched-chain-amino-acid aminotransferase, mitochondrial	BCAT2	1.17	0.21

Aldehyde dehydrogenase, mitochondrial	ALDH2	1,17	0,09
Uncharacterized protein KIAA0930	KIAA0930	1,17	0,67
Ubiquitin carboxyl-terminal hydrolase 4	USP4	1,16	N.D.
Sodium bicarbonate cotransporter 3	SLC4A7	1,16	0,39
G2/mitotic-specific cyclin-B1	CCNB1	1,16	0,14
PERQ amino acid-rich with GYF domain-containing protein 2	GIGYF2	1,15	N.D.
WW domain-binding protein 11	WBP11	1,14	1,98
NADH dehydrogenase [ubiquinone] iron-sulfur protein 6, mitochondrial	NDUFS6	1,14	0,00
Kinetochore protein Spc24	SPC24	1,13	N.D.
Annexin A4	ANXA4	1,13	0,16
Endoplasmic reticulum mannosyl-oligosaccharide 1,2-alpha-mannosidase	MAN1B1	1,13	1,72
Lymphocyte antigen 75	LY75	1,12	0,05
60S ribosomal export protein NMD3	NMD3	1,12	N.D.
Coiled-coil domain-containing protein 124	CCDC124	1,11	0,00
Copper homeostasis protein cutC homolog	CUTC	1,11	N.D.
3-hydroxyisobutyryl-CoA hydrolase, mitochondrial	HIBCH	1,10	0,18
Ras-related protein Rab-31	RAB31	1,10	0,06
DCC-interacting protein 13-alpha	APPL1	1,10	0,05
Single-stranded DNA-binding protein, mitochondrial	SSBP1	1,09	0,00
Fragile X mental retardation syndrome-related protein 1	FXR1	1,09	1,48
DNA mismatch repair protein Mlh1	MLH1	1,08	N.D.
AT-rich interactive domain-containing protein 1A	ARID1A	1,08	0,48
Reactive oxygen species modulator 1	ROMO1	1,07	0,08
E3 ubiquitin-protein ligase CBL	CBL	1,07	0,25
LanC-like protein 1	LANCL1	1,07	0,05
Probable leucine--tRNA ligase, mitochondrial	LARS2	1,07	0,48
Importin subunit alpha-5	KPNA1	1,06	0,51
Putative ATP-dependent RNA helicase DHX30	DHX30	1,06	0,26
Peptidase M20 domain-containing protein 2	PM20D2	1,05	0,08
Bromodomain-containing protein 4	BRD4	1,05	N.D.
Splicing factor, arginine/serine-rich 15	SCAF4	1,05	N.D.
KH domain-containing, RNA-binding, signal transduction-associated protein 1	KHDRBS1	1,04	0,76
Kinetochore protein Spc25	SPC25	1,04	0,94
CD166 antigen	ALCAM	1,04	0,28
Cytochrome c oxidase protein 20 homolog	COX20	1,03	N.D.
CKLF-like MARVEL transmembrane domain-containing protein 6	CMTM6	1,03	0,23
THUMP domain-containing protein 3	THUMPD3	1,03	0,59
Alpha-adducin	ADD1	1,03	0,23
E1A-binding protein p400	EP400	1,03	1,19
Ubiquitin carboxyl-terminal hydrolase 11	USP11	1,02	0,46
Phosphoserine aminotransferase	PSAT1	1,02	0,17
HIG1 domain family member 1A, mitochondrial	HIGD1A	1,02	0,06
Replication protein A 14 kDa subunit	RPA3	1,02	0,10
Ubiquitin carboxyl-terminal hydrolase 19	USP19	1,02	0,40
Mitochondrial import inner membrane translocase subunit TIM16	PAM16	1,01	N.D.
Replication protein A 70 kDa DNA-binding subunit	RPA1	1,01	0,38
Gem-associated protein 5	GEMIN5	1,01	0,60
Sorcin	SRI	1,01	N.D.
Thymidylate synthase	TYMS	1,01	0,01
Microtubule-associated protein 4	MAP4	1,00	0,31
Replication protein A 32 kDa subunit	RPA2	1,00	0,54
Plasminogen activator inhibitor 1 RNA-binding protein	SERBP1	1,00	0,58
Oxygen-dependent coproporphyrinogen-III oxidase, mitochondrial	CPOX	0,99	0,07
Glutathione S-transferase Mu 1 and 4	GSTM1;GSTM4	0,99	0,04
High affinity immunoglobulin epsilon receptor subunit gamma	FCER1G	0,99	0,18
Ubiquitin-conjugating enzyme E2 C	UBE2C	0,99	0,81
Metaxin-1	MTX1	0,99	0,10
Girdin	CCDC88A	0,99	N.D.
Pre-rRNA-processing protein TSR1 homolog	TSR1	0,99	0,13
Spectrin alpha chain, non-erythrocytic 1	SPTAN1	0,98	0,04
Condensin complex subunit 2	NCAPH	0,98	0,18
Myocyte-specific enhancer factor 2D	MEF2D	0,98	0,32
ADP-ribosylation factor-related protein 1	ARFRP1	0,98	N.D.
Protein timeless homolog	TIMELESS	0,98	N.D.
Guanidinoacetate N-methyltransferase	GAMT	0,97	N.D.
WD repeat and FYVE domain-containing protein 1	WDFY1	0,97	0,06
Latrophilin-2	LPHN2	0,97	0,73
Neurotrypsin	PRSS12	0,97	N.D.
Protein CDV3 homolog	CDV3	0,97	0,41
Transferrin receptor protein 1	TFRC	0,97	0,01
Enoyl-CoA delta isomerase 1, mitochondrial	ECI1	0,97	0,22
Transcription initiation factor TFIID subunit 9	TAF9B;TAF9	0,97	N.D.
5-demethoxyubiquinone hydroxylase, mitochondrial	COQ7	0,96	N.D.
Calcium-binding mitochondrial carrier protein Aralar2	SLC25A13	0,96	0,12
Ubiquitin carboxyl-terminal hydrolase 10	USP10	0,96	0,43
Epidermal growth factor receptor substrate 15	EPS15	0,95	0,26
Evolutionarily conserved signaling intermediate in Toll pathway, mitochondrial	ECSIT	0,95	N.D.
DNA repair protein complementing XP-G cells	ERCC5	0,94	1,14
Formin-binding protein 1	FNBP1	0,94	0,50
Lysophosphatidylcholine acyltransferase 1	LPCAT1	0,94	0,14

RNA-binding protein 12	RBM12	0,94	0,29
NADH dehydrogenase [ubiquinone] 1 alpha subcomplex assembly factor 3	NDUFAF3	0,94	0,52
Reticulocalbin-2	RCN2	0,93	N.D.
Plexin-A1	PLXNA1	0,93	0,50
Protein-tyrosine kinase 2-beta	PTK2B	0,93	0,10
Spectrin beta chain, non-erythrocytic 1	SPTBN1	0,93	0,02
Alpha-endosulfine	ENSA	0,93	N.D.
SWI/SNF complex subunit SMARCC1	SMARCC1	0,93	0,24
HEAT repeat-containing protein 1	HEATR1	0,93	0,12
CD2-associated protein	CD2AP	0,92	N.D.
DNA polymerase epsilon catalytic subunit A	POLE	0,92	0,07
Complex I assembly factor TIMMDC1, mitochondrial	TIMMDC1	0,92	0,16
Cyclin-dependent kinase 2	CDK2	0,92	0,06
E3 ubiquitin-protein ligase UHRF1	UHRF1	0,92	0,17
Biorientation of chromosomes in cell division protein 1-like 1	BOD1L1	0,91	N.D.
Mediator of RNA polymerase II transcription subunit 20	MED20	0,91	0,47
WD repeat and HMG-box DNA-binding protein 1	WDHD1	0,91	0,32
DNA mismatch repair protein Msh6	MSH6	0,91	0,00
FAST kinase domain-containing protein 3	FASTKD3	0,91	0,56
Nucleolar protein 56	NOP56	0,90	N.D.
Serpin H1	SERPINH1	0,90	0,02
Endoglin	ENG	0,90	N.D.
Band 4.1-like protein 3;Band 4.1-like protein 3, N-terminally processed	EPB41L3	0,90	0,02
Calcium-binding mitochondrial carrier protein Aralar1	SLC25A12	0,89	0,26
Small integral membrane protein 20	SMIM20	0,89	N.D.
Importin-8	IPO8	0,89	0,00
Inosine-5-monophosphate dehydrogenase 2	IMPDH2	0,89	0,23
Dihydropteridine reductase	QDPR	0,89	0,04
Serine/threonine-protein phosphatase 6 regulatory subunit 1	PPP6R1	0,88	1,36
39S ribosomal protein L12, mitochondrial	MRPL12	0,88	0,30
NADH dehydrogenase [ubiquinone] 1 beta subcomplex subunit 5, mitochondrial	NDUFB5	0,88	N.D.
DNA replication complex GINS protein PSF3	GINS3	0,88	0,10
Protein jagunal homolog 1	JAGN1	0,87	0,92
Mitotic spindle assembly checkpoint protein MAD2A	MAD2L1	0,87	0,08
PEST proteolytic signal-containing nuclear protein	PCNP	0,87	0,11
Coiled-coil-helix-coiled-coil-helix domain-containing protein 2	CHCHD2;CHCHD2P9	0,87	N.D.
Pterin-4-alpha-carbinolamine dehydratase 2	PCBD2	0,87	N.D.
Putative E3 ubiquitin-protein ligase UBR7	UBR7	0,86	N.D.
Nuclear transport factor 2	NUTF2	0,86	0,14
Hypoxanthine-guanine phosphoribosyltransferase	HPRT1	0,86	0,09
Glucosamine 6-phosphate N-acetyltransferase	GNPNAT1	0,86	0,08
Mitochondrial 10-formyltetrahydrofolate dehydrogenase	ALDH1L2	0,85	0,04
Tubulin--tyrosine ligase-like protein 12	TTLL12	0,85	0,19
Protein SCAF11	SCAF11	0,85	N.D.
Cytoplasmic FMR1-interacting protein 2	CYFIP2	0,85	0,48
Serine/arginine repetitive matrix protein 1	SRRM1	0,85	0,04
Lysine-specific demethylase 3B	KDM3B	0,84	1,04
Mitochondrial import inner membrane translocase subunit Tim23 and 23B	TIMM23;TIMM23B	0,84	N.D.
Insulin-like growth factor 2 mRNA-binding protein 1	IGF2BP1	0,84	0,05
Ubiquitin-like modifier-activating enzyme 5	UBA5	0,84	0,49
Hematopoietic lineage cell-specific protein	HCLS1	0,84	0,23
EKC/KEOPS complex subunit LAGE3	LAGE3	0,83	N.D.
Fanconi anemia group D2 protein	FANCD2	0,83	N.D.
Shootin-1	KIAA1598	0,83	N.D.
Eukaryotic translation initiation factor 4H	EIF4H	0,83	0,24
DNA replication licensing factor MCM6	MCM6	0,83	0,02
C-terminal-binding protein 1	CTBP1	0,83	N.D.
Zinc finger CCCH domain-containing protein 15	ZC3H15	0,83	0,25
RILP-like protein 2	RILPL2	0,83	N.D.
Glutathione peroxidase 1	GPX1	0,83	0,08
Arylsulfatase B	ARSB	0,82	0,27
ATP-binding cassette sub-family F member 1	ABCF1	0,82	0,02
Plasma membrane calcium-transporting ATPase 4	ATP2B4	0,82	N.D.
General transcription factor 3C polypeptide 5	GTF3C5	0,82	N.D.
Protein PRRC2A	PRRC2A	0,82	0,00
E3 SUMO-protein ligase RanBP2	RANBP2	0,81	0,13
Ribosomal L1 domain-containing protein 1	RSL1D1	0,81	0,12
Mitochondrial import inner membrane translocase subunit Tim17-B	TIMM17B	0,81	N.D.
G patch domain and KOW motifs-containing protein	GPKOW	0,81	N.D.
LYR motif-containing protein 4	LYRM4	0,81	N.D.
Glycine cleavage system H protein, mitochondrial	GCSH	0,80	N.D.
Rab3 GTPase-activating protein catalytic subunit	RAB3GAP1	0,80	0,04
HIG1 domain family member 2A, mitochondrial	HIGD2A	0,79	0,12
Uncharacterized protein C18orf8	C18orf8	0,79	N.D.
DNA replication complex GINS protein SLD5	GINS4	0,79	N.D.
DNA-directed RNA polymerase, mitochondrial	POLRMT	0,79	0,50
Bone morphogenetic protein 8A;Bone morphogenetic protein 8B	BMP8A;BMP8B	0,79	0,00
NAD(P)H-hydrate epimerase	APOA1BP	0,79	0,03
Acylphosphatase-1	ACYP1	0,78	0,03
Exosome complex component RRP41	EXOSC4	0,78	0,21

E3 ubiquitin-protein ligase HERC2	HERC2	0,78	0,09
Probable ATP-dependent RNA helicase DDX20	DDX20	0,78	N.D.
Succinate dehydrogenase [ubiquinone] flavoprotein subunit, mitochondrial	SDHA	0,78	0,05
D-3-phosphoglycerate dehydrogenase	PHGDH	0,78	0,05
Nucleolar complex protein 2 homolog	NOC2L	0,78	0,49
Lysine-specific demethylase 4A	KDM4A	0,78	N.D.
Queuine tRNA-ribosyltransferase subunit QTRTD1	QTRTD1	0,78	0,24
Glia maturation factor beta	GMFB	0,77	N.D.
Trans-2-enoyl-CoA reductase, mitochondrial	MECR	0,77	N.D.
Receptor-type tyrosine-protein phosphatase F	PTPRF	0,77	0,79
Extended synaptotagmin-2	ESYT2	0,77	0,25
Zinc finger CCCH domain-containing protein 4	ZC3H4	0,77	N.D.
Glucoside xylosyltransferase 1	GXYLT1	0,77	0,35
Protein Niban	FAM129A	0,77	0,03
N(G),N(G)-dimethylarginine dimethylaminohydrolase 2	DDAH2	0,76	0,32
Phosphoenolpyruvate carboxykinase [GTP], mitochondrial	PCK2	0,76	0,12
Calponin-2	CNN2	0,76	0,72
DNA replication licensing factor MCM3	MCM3	0,76	0,16
RNA pseudouridylate synthase domain-containing protein 2	RPUSD2	0,76	0,53
Protein IWS1 homolog	IWS1	0,76	0,02
Dehydrogenase/reductase SDR family member 7	DHRS7	0,76	N.D.
Kinesin-like protein KIF2A	KIF2A	0,76	1,46
Retinoblastoma-binding protein 5	RBBP5	0,75	0,04
Kinase D-interacting substrate of 220 kDa	KIDINS220	0,75	N.D.
Nuclease-sensitive element-binding protein 1	YBX1	0,75	0,14
Cat eye syndrome critical region protein 5	CECR5	0,75	0,23
FK506-binding protein 15	FKBP15	0,75	0,75
Mitochondrial chaperone BCS1	BCS1L	0,75	N.D.
Guanine nucleotide-binding protein G(I)/G(S)/G(O) subunit gamma-10	GNG10	0,75	0,56
GA-binding protein alpha chain	GABPA	0,75	N.D.
Citron Rho-interacting kinase	CIT	0,75	0,47
AT-rich interactive domain-containing protein 3A	ARID3A	0,74	0,04
Cyclin-dependent kinase 4 inhibitor C	CDKN2C	0,74	N.D.
Cystatin-A;Cystatin-A, N-terminally processed	CSTA	0,74	0,04
Pumilio domain-containing protein KIAA0020	KIAA0020	0,73	0,10
Regulator of nonsense transcripts 1	UPF1	0,73	0,21
Sterol O-acyltransferase 1	SOAT1	0,73	0,08
POU domain, class 2, transcription factor 1, 3 and 2	POU2F1;POU2F3;POU2F2	0,73	N.D.
Succinate dehydrogenase assembly factor 2, mitochondrial	SDHAF2	0,73	0,03
RalBP1-associated Eps domain-containing protein 1	REPS1	0,73	N.D.
GMP synthase [glutamine-hydrolyzing]	GMPS	0,73	0,12
Phosphatidylinositol 3,4,5-trisphosphate 5-phosphatase 2	INPPL1	0,73	0,16
Cyclin-dependent kinase 1	CDK1	0,72	0,26
DNA replication licensing factor MCM2	MCM2	0,72	0,01
FH1/FH2 domain-containing protein 1	FHOD1	0,72	N.D.
Inositol 1,4,5-trisphosphate receptor type 1	ITPR1	0,72	0,03
YEATS domain-containing protein 4	YEATS4	0,72	N.D.
Programmed cell death protein 4	PDCD4	0,72	0,08
Small ubiquitin-related modifier 1;Small ubiquitin-related modifier	SUMO1	0,72	0,03
Uncharacterized protein C19orf43	C19orf43	0,72	0,60
PHD finger protein 3	PHF3	0,72	N.D.
Protein BRICK1	BRK1	0,71	0,09
ADP-ribosylation factor-like protein 8A	ARL8A	0,71	N.D.
Sulfhydryl oxidase 2	QSOX2	0,71	0,94
Retinoid-inducible serine carboxypeptidase	SCPEP1	0,71	0,09
2,5-phosphodiesterase 12	PDE12	0,71	0,05
39S ribosomal protein L54, mitochondrial	MRPL54	0,71	N.D.
Glutathione S-transferase P	GSTP1	0,70	0,00
tRNA (cytosine(34)-C(5))-methyltransferase	NSUN2	0,70	0,14
Integrin alpha-L	ITGAL	0,70	0,07
U2 snRNP-associated SURP motif-containing protein	U2SURP	0,70	0,73
F-box-like/WD repeat-containing protein TBL1XR1	TBL1XR1	0,70	0,08
Plasminogen receptor (KT)	PLGRKT	0,70	N.D.
NEDD8-activating enzyme E1 catalytic subunit	UBA3	0,70	0,24
Eukaryotic translation initiation factor 2D	EIF2D	0,70	N.D.
Probable helicase senataxin	SETX	0,69	N.D.
COP9 signalosome complex subunit 7b	COPS7B	0,69	N.D.
Pachytene checkpoint protein 2 homolog	TRIP13	0,69	0,07
N-terminal kinase-like protein	SCYL1	0,69	1,33
Cellular nucleic acid-binding protein	CNBP	0,69	0,15
Tumor necrosis factor receptor type 1-associated DEATH domain protein	TRADD	0,69	N.D.
UPF0609 protein C4orf27	C4orf27	0,68	0,13
Nucleosome-remodeling factor subunit BPTF	BPTF	0,68	N.D.
U6 snRNA-associated Sm-like protein LSm7	LSM7	0,68	0,77
PAX3- and PAX7-binding protein 1	PAXBP1	0,68	N.D.
Cell cycle progression protein 1	CCPG1	0,68	N.D.
Protein phosphatase 1 regulatory subunit 27	PPP1R27	0,68	0,06
Replication factor C subunit 5	RFC5	0,68	0,29
Protein SMG5	SMG5	0,68	0,07
Nucleoporin Nup37	NUP37	0,68	0,20

Obg-like ATPase 1	OLA1	0,68	0,11
Phosphatidylinositide phosphatase SAC1	SACM1L	0,68	0,30
Rho GTPase-activating protein 4	ARHGAP4	0,68	0,07
Polypyrimidine tract-binding protein 3	PTBP3	0,67	N.D.
Tubulin beta-4A chain	TUBB4A	0,67	0,14
DNA replication licensing factor MCM4	MCM4	0,67	0,18
Echinoderm microtubule-associated protein-like 4	EML4	0,67	0,49
Calcium uniporter protein, mitochondrial	MCU	0,67	0,06
Phospholipid hydroperoxide glutathione peroxidase, mitochondrial	GPX4	0,67	0,35
Cytochrome c oxidase assembly factor 6 homolog	COA6	0,67	N.D.
CCA tRNA nucleotidyltransferase 1, mitochondrial	TRNT1	0,67	0,06
Prostaglandin E synthase 2;Prostaglandin E synthase 2 truncated form	PTGES2	0,67	0,19
Elongation factor G, mitochondrial	GFM1	0,67	0,08
Pyruvate dehydrogenase E1 component subunit alpha, somatic form, mitochondrial	PDHA1	0,67	0,04
AP-1 complex subunit sigma-1A	AP1S1	0,67	N.D.
TBC1 domain family member 15	TBC1D15	0,67	N.D.
Nuclear pore complex protein Nup50	NUP50	0,67	0,10
Pre-mRNA-splicing factor ATP-dependent RNA helicase PRP16	DHX38	0,67	0,44
DnaJ homolog subfamily B member 1	DNAJB1	0,66	0,03
Ras GTPase-activating protein-binding protein 1	G3BP1	0,66	0,33
Cleavage and polyadenylation specificity factor subunit 4	CPSF4	0,66	N.D.
Lysophospholipase-like protein 1	LYPLAL1	0,66	0,54
Ubiquitin-conjugating enzyme E2 Z	UBE2Z	0,66	N.D.
Tetraspanin-14	TSPAN14	0,66	N.D.
DNA replication licensing factor MCM5	MCM5	0,66	0,13
Crooked neck-like protein 1	CRNKL1	0,66	0,34
Cleavage and polyadenylation specificity factor subunit 2	CPSF2	0,65	0,22
Aflatoxin B1 aldehyde reductase member 2	AKR7A2	0,65	0,06
Cleavage stimulation factor subunit 2	CSTF2	0,65	N.D.
Cytochrome c oxidase subunit 5A, mitochondrial	COX5A	0,65	0,06
Mortality factor 4-like protein 1	MORF4L1	0,65	N.D.
Peptidyl-prolyl cis-trans isomerase FKBP3	FKBP3	0,64	N.D.
Ubiquitin-like protein 5	UBL5	0,64	0,32
Cytochrome c oxidase subunit 6B1	COX6B1	0,64	0,18
Protein QIL1	QIL1	0,64	0,15
Ubiquitin-conjugating enzyme E2 A	UBE2A	0,64	0,37
Ubiquitin carboxyl-terminal hydrolase 47	USP47	0,64	0,21
Eukaryotic translation initiation factor 5B	EIF5B	0,64	0,01
Pyruvate dehydrogenase E1 component subunit beta, mitochondrial	PDHB	0,64	0,15
Seizure 6-like protein 2	SEZ6L2	0,64	0,37
Golgi membrane protein 1	GOLM1	0,63	0,13
Ubiquitin carboxyl-terminal hydrolase 48	USP48	0,63	N.D.
GRIP and coiled-coil domain-containing protein 2	GCC2	0,63	1,09
TGF-beta-activated kinase 1 and MAP3K7-binding protein 1	TAB1	0,63	N.D.
Serine--tRNA ligase, mitochondrial	SARS2	0,63	0,22
GTP-binding protein 1	GTPBP1	0,63	0,07
Activator of 90 kDa heat shock protein ATPase homolog 1	AHSA1	0,63	0,15
D-beta-hydroxybutyrate dehydrogenase, mitochondrial	BDH1	0,63	0,17
Poly(ADP-ribose) glycohydrolase ARH3	ADPRHL2	0,63	N.D.
Transcriptional repressor protein YY1	YY1	0,63	N.D.
NEDD8-activating enzyme E1 regulatory subunit	NAE1	0,62	0,02
Casein kinase II subunit alpha	CSNK2A1	0,62	0,07
Zyxin	ZYX	0,62	0,17
Glutaryl-CoA dehydrogenase, mitochondrial	GCDH	0,62	0,02
DnaJ homolog subfamily C member 13	DNAJC13	0,62	0,11
Aminoacylase-1	ACY1	0,62	0,28
High mobility group protein B3	HMGB3	0,62	0,33
Tubulin beta-6 chain	TUBB6	0,62	0,14
Transcription elongation factor A protein 1	TCEA1	0,62	0,36
Tyrosyl-DNA phosphodiesterase 1	TDP1	0,61	0,57
Serine/threonine-protein kinase tousled-like 1	TLK1	0,61	N.D.
Uridine 5-monophosphate synthas	UMPS	0,61	0,15
DCN1-like protein 1	DCUN1D1	0,61	0,08
Selenocysteine-specific elongation factor	EEFSEC	0,61	N.D.
Cytochrome c oxidase subunit 7A-related protein, mitochondrial	COX7A2L	0,61	0,05
Mpv17-like protein 2	MPV17L2	0,61	N.D.
Serpin B8	SERPINB8	0,61	0,18
Beta-glucuronidase	GUSB	0,61	0,29
Sjoegren syndrome/scleroderma autoantigen 1	SSSCA1	0,61	0,57
Replication factor C subunit 4	RFC4	0,61	0,13
ATP-binding cassette sub-family F member 3	ABCF3	0,61	0,23
Protein FAM195A	FAM195A	0,61	N.D.
DNA replication licensing factor MCM7	MCM7	0,61	0,18
ATP-dependent RNA helicase DDX50	DDX50	0,61	0,03
NudC domain-containing protein 2	NUDCD2	0,61	0,24
Large neutral amino acids transporter small subunit 1	SLC7A5	0,61	0,02
1,2-dihydroxy-3-keto-5-methylthiopentene dioxygenase	ADI1	0,60	0,04
Rab-like protein 6	RABL6	0,60	0,19
Protein Churchill	CHURC1	0,60	0,39
ADP-ribosylation factor-like protein 8B	ARL8B	0,60	0,19
DnaJ homolog subfamily C member 11	DNAJC11	0,60	0,07

Helicase SKI2W	SKIV2L	0,60	1,04
Oxysterol-binding protein 1	OSBP	0,60	0,09
Glutaminase kidney isoform, mitochondrial	GLS	0,60	1,17
General transcription factor 3C polypeptide 3	GTF3C3	0,60	0,42
39S ribosomal protein L51, mitochondrial	MRPL51	0,60	0,69
Pyruvate dehydrogenase phosphatase regulatory subunit, mitochondrial	PDPR	0,60	1,06
tRNA (guanine(26)-N(2))-dimethyltransferase	TRMT1	0,60	0,20
Alpha-globin transcription factor CP2	TFCP2	0,60	0,23
Condensin-2 complex subunit D3	NCAPD3	0,60	0,07
Small ubiquitin-related modifier 2	SUMO2	0,60	0,32
Mitochondrial import inner membrane translocase subunit Tim8 B	TIMM8B	0,60	0,37
Complement component 1 Q subcomponent-binding protein, mitochondrial	C1QBP	0,59	0,15
Ran-specific GTPase-activating protein	RANBP1	0,59	0,05
Prostaglandin reductase 1	PTGR1	0,59	N.D.
Monofunctional C1-tetrahydrofolate synthase, mitochondrial	MTHFD1L	0,59	0,07
WD repeat-containing protein 3	WDR3	0,59	0,23
Glutamine-dependent NAD(+) synthetase	NADSYN1	0,59	N.D.
CDKN2A-interacting protein	CDKN2AIP	0,59	N.D.
Clathrin interactor 1	CLINT1	0,59	0,28
Importin subunit alpha-7	KPNA6	0,59	N.D.
NADH dehydrogenase [ubiquinone] 1 beta subcomplex subunit 6	NDUFB6	0,59	N.D.
39S ribosomal protein L40, mitochondrial	MRPL40	0,59	N.D.
Replication factor C subunit 2	RFC2	0,59	0,12
L-xylulose reductase	DCXR	0,59	0,02

Table 3. Upregulated proteins in THP-1 AraC compared to THP-1 P cells under normoxia. Proteomic profiling (SILAC) data were used. Significantly upregulated proteins were calculated using the fold difference threshold of 1.5 (log_2 fold change=0.58). Mean±SD for n=2 replicates. Non-detected (N.D.) means less than 2 replicates detected for one protein measured.

DOWNREGULATED PROTEINS IN THP-1 AraC VS. THP-1 P			
Protein names	**Gene names**	**Mean Log_2 fold change**	**SD Log_2 fold change**
Arachidonate 5-lipoxygenase-activating protein	ALOX5AP	-5.07	N.D.
Apolipoprotein B-100;Apolipoprotein B-48	APOB	-5.07	N.D.
Deoxycytidine kinase	DCK	-4.36	N.D.
Desmoplakin	DSP	-4.15	0.77
Thymidine phosphorylase	TYMP	-4.08	0.14
Hexokinase-1	HK1	-3.66	N.D.
Carbonyl reductase [NADPH] 1	CBR1	-3.63	0.51
Glycogenin-1	GYG1	-3.56	0.31
Carbonic anhydrase 2	CA2	-3.33	0.65
Keratinocyte proline-rich protein	KPRP	-3.20	1.17
Conserved oligomeric Golgi complex subunit 8	COG8	-3.11	N.D.
Junction plakoglobin	JUP	-3.08	0.90
Vacuolar protein sorting-associated protein 11 homolog	VPS11	-3.01	N.D.
Phospholipase D3	PLD3	-2.99	0.06
Creatine kinase B-type	CKB	-2.95	0.16
Septin-11	40787	-2.90	0.27
Succinyl-CoA:3-ketoacid coenzyme A transferase 1, mitochondrial	OXCT1	-2.68	0.38
Acetyl-CoA acetyltransferase, cytosolic	ACAT2	-2.59	0.37
Cathepsin G	CTSG	-2.59	0.16
Protein furry homolog	FRY	-2.59	0.64
Engulfment and cell motility protein 1	ELMO1	-2.55	N.D.
Galectin-3	LGALS3	-2.54	N.D.
Receptor expression-enhancing protein 5	REEP5	-2.49	N.D.
Dihydropyrimidine dehydrogenase [NADP(+)]	DPYD	-2.36	0.81
Myeloid cell nuclear differentiation antigen	MNDA	-2.35	1.04
Two pore calcium channel protein 1	TPCN1	-2.33	N.D.
Acylglycerol kinase, mitochondrial	AGK	-2.33	N.D.
Prelamin-A/C;Lamin-A/C	LMNA	-2.33	0.03
Lysozyme C	LYZ	-2.29	0.19
Tripartite motif-containing protein 72	TRIM72	-2.16	N.D.
Unconventional myosin-Ig	MYO1G	-2.15	0.02
Isoamyl acetate-hydrolyzing esterase 1 homolog	IAH1	-2.12	0.47
NAD(P)H dehydrogenase [quinone] 1	NQO1	-2.11	0.09
Junctional adhesion molecule A	F11R	-2.11	0.08
Neurochondrin	NCDN	-2.10	N.D.
RNA-binding motif protein	RBMX	-2.04	0.45
Long-chain-fatty-acid--CoA ligase 3	ACSL3	-2.00	0.06
Histone H1.2	HIST1H1C	-1.95	1.87
Annexin A1	ANXA1	-1.92	0.32
Ribonuclease T2	RNASET2	-1.91	0.44
Cathepsin L1	CTSL	-1.88	0.26
Fructose-1,6-bisphosphatase 1	FBP1	-1.87	N.D.
Ribosome production factor 2 homolog	RPF2	-1.86	2.21
Vimentin	VIM	-1.84	0.12
Cytochrome b-245 heavy chain	CYBB	-1.83	0.47
Glutathione S-transferase Mu 3	GSTM3	-1.81	0.63
Exocyst complex component 1	EXOC1	-1.80	N.D.
Type-1 angiotensin II receptor-associated protein	AGTRAP	-1.78	0.51
BTB/POZ domain-containing protein KCTD12	KCTD12	-1.76	N.D.
Transformer-2 protein homolog alpha	TRA2A	-1.75	0.49
Gamma-glutamylaminecyclotransferase	GGACT	-1.73	0.23
Antigen peptide transporter 1	TAP1	-1.72	0.02
Glutaredoxin-1	GLRX	-1.70	0.30
Carboxypeptidase M	CPM	-1.69	0.28
Tubulin alpha-4A chain	TUBA4A	-1.66	0.02
Plectin	PLEC	-1.66	0.09
V-type proton ATPase 116 kDa subunit a isoform 3	TCIRG1	-1.66	N.D.
Arf-GAP with SH3 domain	ASAP1	-1.64	N.D.
5-nucleotidase domain-containing protein 1	NT5DC1	-1.62	0.16
Methionine aminopeptidase 2	METAP2	-1.62	0.73
Heterogeneous nuclear ribonucleoproteins C1/C2	HNRNPC	-1.62	0.55
RNA-binding protein Raly	RALY	-1.60	0.40
Antigen peptide transporter 2	TAP2	-1.59	0.02
Fumarylacetoacetase	FAH	-1.59	0.01
Polypeptide N-acetylgalactosaminyltransferase 2	GALNT2	-1.58	0.07
Heat shock 70 kDa protein 1B and A	HSPA1B;HSPA1A	-1.56	0.16
Ras-related protein Rab-44	RAB44	-1.56	N.D.
ADP-ribosylation factor-like protein 3	ARL3	-1.56	0.26
Exosome complex exonuclease RRP44	DIS3	-1.56	0.60
Importin subunit alpha-4	KPNA3	-1.55	0.26
Rap guanine nucleotide exchange factor 6	RAPGEF6	-1.54	N.D.
Suppressor of G2 allele of SKP1 homolog	SUGT1	-1.54	0.14
Conserved oligomeric Golgi complex subunit 2	COG2	-1.53	N.D.
DIS3-like exonuclease 2	DIS3L2	-1.53	N.D.
Dipeptidyl peptidase 2	DPP7	-1.52	0.35
Neutrophil cytosol factor 4	NCF4	-1.51	N.D.
Macrosialin	CD68	-1.50	N.D.
Granulins	GRN	-1.50	N.D.
N-acetylgalactosamine-6-sulfatase	GALNS	-1.49	0.48
C-type mannose receptor 2	MRC2	-1.49	0.20

CD70 antigen	CD70	-1,48	0,71
Chromatin target of PRMT1 protein	CHTOP	-1,48	0,09
Synaptic vesicle membrane protein VAT-1 homolog	VAT1	-1,47	0,14
TYRO protein tyrosine kinase-binding protein	TYROBP	-1,47	N.D.
Unconventional myosin-Ic	MYO1C	-1,46	N.D.
Formin-like protein 1	FMNL1	-1,45	0,10
CTP synthase 2	CTPS2	-1,44	0,18
Pyruvate kinase PKM	PKM	-1,44	0,03
Tapasin	TAPBP	-1,44	0,21
6-phosphogluconate dehydrogenase, decarboxylating	PGD	-1,44	0,04
Bifunctional coenzyme A synthase	COASY	-1,43	0,09
Annexin A6	ANXA6	-1,43	0,13
PHD finger protein 6	PHF6	-1,43	N.D.
Protein S100-P	S100P	-1,42	0,17
Hydroxymethylglutaryl-CoA lyase, mitochondrial	HMGCL	-1,42	N.D.
Chitinase-3-like protein 1	CHI3L1	-1,42	0,44
DNA topoisomerase 2-alpha	TOP2A	-1,42	0,37
Acidic fibroblast growth factor intracellular-binding protein	FIBP	-1,41	N.D.
DNA-directed RNA polymerase III subunit RPC2	POLR3B	-1,41	N.D.
Lysosome-associated membrane glycoprotein 1	LAMP1	-1,41	0,67
NADH dehydrogenase [ubiquinone] 1 alpha subcomplex subunit 10, mitochondrial	NDUFA10	-1,41	0,35
Zinc finger ZZ-type and EF-hand domain-containing protein 1	ZZEF1	-1,40	N.D.
ATP-binding cassette sub-family B member 10, mitochondrial	ABCB10	-1,39	0,07
Nuclear receptor coactivator 5	NCOA5	-1,39	N.D.
Protein kinase C beta type	PRKCB	-1,37	0,03
60S ribosomal protein L7-like 1	RPL7L1	-1,37	N.D.
Sortilin-related receptor	SORL1	-1,36	0,44
Synaptophysin-like protein 1	SYPL1	-1,36	N.D.
60S ribosomal protein L26-like 1	RPL26L1	-1,35	N.D.
RNA-binding protein FUS	FUS	-1,35	0,76
1-phosphatidylinositol 4,5-bisphosphate phosphodiesterase beta-2	PLCB2	-1,34	N.D.
Choline/ethanolaminephosphotransferase 1	CEPT1	-1,33	0,21
Isocitrate dehydrogenase [NADP] cytoplasmic	IDH1	-1,33	0,04
DNA topoisomerase 2-beta	TOP2B	-1,32	0,36
Ras GTPase-activating protein 3	RASA3	-1,31	N.D.
Toll-interacting protein	TOLLIP	-1,31	0,00
U1 small nuclear ribonucleoprotein C	SNRPC	-1,30	0,50
Exportin-4	XPO4	-1,30	0,31
Interleukin-1 receptor-associated kinase 3	IRAK3	-1,30	0,42
Stomatin-like protein 2, mitochondrial	STOML2	-1,29	0,38
Titin	TTN	-1,29	1,89
Plastin-2	LCP1	-1,29	0,07
Myotubularin-related protein 6	MTMR6	-1,28	N.D.
N-acylethanolamine-hydrolyzing acid amidase	NAAA	-1,28	0,03
Transcriptional activator protein Pur-alpha	PURA	-1,28	0,29
V-type proton ATPase subunit d 1	ATP6V0D1	-1,28	0,33
Neutrophil elastase	ELANE	-1,27	0,20
ADP/ATP translocase 1	SLC25A4	-1,27	N.D.
Dual specificity protein phosphatase 23	DUSP23	-1,26	N.D.
NADH dehydrogenase [ubiquinone] 1 alpha subcomplex subunit 12	NDUFA12	-1,25	0,21
Gelsolin	GSN	-1,25	0,06
BRO1 domain-containing protein BROX	BROX	-1,24	0,02
Glutamate--cysteine ligase regulatory subunit	GCLM	-1,24	N.D.
Intercellular adhesion molecule 3	ICAM3	-1,23	1,42
Nicotinate phosphoribosyltransferase	NAPRT	-1,22	0,03
Lysosomal alpha-glucosidase	GAA	-1,22	0,24
Glutamate--cysteine ligase catalytic subunit	GCLC	-1,22	0,65
NADH-ubiquinone oxidoreductase 75 kDa subunit, mitochondrial	NDUFS1	-1,22	0,03
Torsin-1A	TOR1A	-1,21	0,75
Serine/arginine-rich splicing factor 10	SRSF10	-1,21	0,24
Cathepsin D;Cathepsin D light chain;Cathepsin D heavy chain	CTSD	-1,20	0,06
Deoxyhypusine hydroxylase	DOHH	-1,19	0,07
Peptidyl-prolyl cis-trans isomerase B	PPIB	-1,19	0,09
HLA class I histocompatibility antigen, A-24 and 23 alpha chain	HLA-A	-1,18	0,05
Prenylcysteine oxidase-like	PCYOX1L	-1,17	0,03
Core histone macro-H2A.1	H2AFY	-1,17	0,79
Sulfide:quinone oxidoreductase, mitochondrial	SQRDL	-1,17	0,07
Thiosulfate sulfurtransferase	TST	-1,17	N.D.
NADH dehydrogenase [ubiquinone] 1 beta subcomplex subunit 4	NDUFB4	-1,16	0,25
Calpain-2 catalytic subunit	CAPN2	-1,16	0,12
Methylcrotonoyl-CoA carboxylase subunit alpha, mitochondrial	MCCC1	-1,16	0,21
Far upstream element-binding protein 1	FUBP1	-1,15	0,14
Unconventional myosin-XVIIIa	MYO18A	-1,14	0,27
Heme-binding protein 2	HEBP2	-1,14	0,26
Tyrosine-protein kinase Lyn	LYN	-1,13	N.D.
NADH dehydrogenase [ubiquinone] 1 alpha subcomplex subunit 7	NDUFA7	-1,13	N.D.
Phosphomevalonate kinase	PMVK	-1,13	0,26
NADH dehydrogenase [ubiquinone] 1 alpha subcomplex subunit 9, mitochondrial	NDUFA9	-1,12	0,24
NADH dehydrogenase [ubiquinone] 1 beta subcomplex subunit 8, mitochondrial	NDUFB8	-1,12	0,71
Ras suppressor protein 1	RSU1	-1,12	0,01

High affinity cationic amino acid transporter 1	SLC7A1	-1,12	0,40
Serine/arginine-rich splicing factor 3	SRSF3	-1,11	0,58
Zinc finger CCCH-type antiviral protein 1-like	ZC3HAV1L	-1,11	0,66
HEAT repeat-containing protein 5B	HEATR5B	-1,11	N.D.
Protein diaphanous homolog 3	DIAPH3	-1,10	0,10
Protein LYRIC	MTDH	-1,10	0,68
NADH dehydrogenase [ubiquinone] flavoprotein 1, mitochondrial	NDUFV1	-1,10	0,31
Laminin subunit gamma-1	LAMC1	-1,10	N.D.
LEM domain-containing protein 2	LEMD2	-1,10	N.D.
Caspase recruitment domain-containing protein 9	CARD9	-1,10	0,16
NADP-dependent malic enzyme	ME1	-1,10	N.D.
Mast cell-expressed membrane protein 1	MCEMP1	-1,09	N.D.
Vesicle-fusing ATPase	NSF	-1,09	0,14
Phosphatidylinositol 4-kinase type 2-alpha	PI4K2A	-1,08	0,19
Ubiquitin-like modifier-activating enzyme 7	UBA7	-1,08	0,01
Aminopeptidase N	ANPEP	-1,08	0,39
Translationally-controlled tumor protein	TPT1	-1,07	0,19
Protein-L-isoaspartate(D-aspartate) O-methyltransferase	PCMT1	-1,07	0,08
Trifunctional enzyme subunit beta, mitochondrial;3-ketoacyl-CoA thiolase	HADHB	-1,07	0,15
6-phosphogluconolactonase	H6PD	-1,06	0,44
Voltage-gated potassium channel subunit beta-2	KCNAB2	-1,06	0,11
28S ribosomal protein S24, mitochondrial	MRPS24	-1,06	N.D.
Erythrocyte band 7 integral membrane protein	STOM	-1,05	N.D.
Gamma-glutamyl hydrolase	GGH	-1,05	0,11
Ras-related protein Rap-2c;Ras-related protein Rap-2a	RAP2C;RAP2A	-1,04	0,41
Cullin-1	CUL1	-1,03	0,40
Sequestosome-1	SQSTM1	-1,03	0,30
Adenosine 3-phospho 5-phosphosulfate transporter 1	SLC35B2	-1,02	0,05
E3 ubiquitin-protein ligase TRIP12	TRIP12	-1,02	0,15
Metallo-beta-lactamase domain-containing protein 2	MBLAC2	-1,02	N.D.
Enoyl-CoA hydratase 2	HSD17B4	-1,02	0,11
Beta-2-microglobulin;Beta-2-microglobulin form pI 5.3	B2M	-1,02	0,08
Arylamine N-acetyltransferase 1	NAT1	-1,02	0,09
Nucleobindin-1	NUCB1	-1,01	0,09
Abhydrolase domain-containing protein 16A	ABHD16A	-1,01	N.D.
Protein disulfide-isomerase A3	PDIA3	-1,01	0,00
Syntaxin-4	STX4	-1,00	N.D.
Protein EVI2B	EVI2B	-1,00	N.D.
Axin interactor, dorsalization-associated protein	AIDA	-1,00	N.D.
Epididymis-specific alpha-mannosidase	MAN2B2	-1,00	N.D.
Protein S100-A6	S100A6	-1,00	0,07
Ubiquitin-fold modifier 1	UFM1	-1,00	0,12
Translocating chain-associated membrane protein 1	TRAM1	-0,99	0,24
Tyrosine-protein phosphatase non-receptor type substrate 1	SIRPA	-0,99	N.D.
DnaJ homolog subfamily C member 3	DNAJC3	-0,99	0,09
Protein phosphatase 1 regulatory subunit 7	PPP1R7	-0,99	0,05
Ovarian cancer-associated gene 2 protein	OVCA2	-0,99	0,07
HLA class I histocompatibility antigen, A-2 and 74 alpha chain	HLA-A	-0,99	0,03
TBC1 domain family member 24	TBC1D24	-0,99	N.D.
HLA class I histocompatibility antigen, B-57 and 58 alpha chain	HLA-B	-0,99	0,00
Peroxiredoxin-2	PRDX2	-0,99	0,20
BET1-like protein	BET1L	-0,98	N.D.
AP-3 complex subunit beta-1	AP3B1	-0,98	0,16
Fatty aldehyde dehydrogenase	ALDH3A2	-0,97	0,67
Major facilitator superfamily domain-containing protein 10	MFSD10	-0,97	0,10
MOB kinase activator 3A	MOB3A	-0,97	0,54
Protein transport protein Sec16A	SEC16A	-0,96	0,07
Myeloid-associated differentiation marker	MYADM	-0,96	0,29
Multidrug resistance-associated protein 4	ABCC4	-0,95	0,32
Protein CutA	CUTA	-0,95	N.D.
Protein disulfide-isomerase A6	PDIA6	-0,95	0,07
Fatty acid-binding protein, epidermal	FABP5	-0,94	0,25
Pirin	PIR	-0,94	N.D.
Caspase-8	CASP8	-0,94	0,20
BRISC complex subunit Abro1	FAM175B	-0,94	0,66
HLA class I histocompatibility antigen, Cw-7 alpha chain	HLA-C	-0,94	0,01
Cytoplasmic aconitate hydratase	ACO1	-0,94	0,07
Forkhead box protein K1	FOXK1	-0,93	0,20
LanC-like protein 2	LANCL2	-0,93	1,16
Vacuolar protein sorting-associated protein 16 homolog	VPS16	-0,92	0,06
Trafficking protein particle complex subunit 1	TRAPPC1	-0,92	N.D.
FAD-AMP lyase (cyclizing)	DAK	-0,92	0,15
Diacylglycerol kinase zeta	DGKZ	-0,92	1,57
Calcineurin B homologous protein 1	CHP1	-0,91	N.D.
UPF0160 protein MYG1, mitochondrial	C12orf10	-0,91	0,39
DNA ligase 4	LIG4	-0,91	N.D.
Integrin alpha-5	ITGA5	-0,91	0,13
Peptidyl-prolyl cis-trans isomerase FKBP8	FKBP8	-0,90	0,63
Guanine nucleotide-binding protein-like 1	GNL1	-0,90	0,09
Heterogeneous nuclear ribonucleoproteins A2/B1	HNRNPA2B1	-0,90	0,01

Protein kinase C alpha type	PRKCA	-0,90	N.D.
Vacuolar protein sorting-associated protein 33A	VPS33A	-0,90	N.D.
YTH domain-containing family protein 3	YTHDF3	-0,89	N.D.
Glucose-6-phosphate 1-dehydrogenase	G6PD	-0,89	0,07
Heat shock protein 105 kDa	HSPH1	-0,89	0,06
40S ribosomal protein S24	RPS24	-0,88	1,09
60S ribosomal protein L13	RPL13	-0,88	0,20
CDP-diacylglycerol--inositol 3-phosphatidyltransferase	CDIPT	-0,88	0,09
Heterogeneous nuclear ribonucleoprotein F	HNRNPF	-0,87	0,06
Protein unc-13 homolog D	UNC13D	-0,87	0,15
Sister chromatid cohesion protein PDS5 homolog B	PDS5B	-0,87	0,22
GTP-binding protein SAR1b	SAR1B	-0,87	0,10
Lysosome-associated membrane glycoprotein 2	LAMP2	-0,87	0,04
Flotillin-2	FLOT2	-0,87	0,54
60S ribosomal protein L24	RPL24	-0,87	0,27
Lysosome membrane protein 2	SCARB2	-0,87	0,15
Chromobox protein homolog 3	CBX3	-0,86	0,16
Astrocytic phosphoprotein PEA-15	PEA15	-0,86	0,02
ATP-binding cassette sub-family D member 3	ABCD3	-0,86	0,01
COP9 signalosome complex subunit 7a	COPS7A	-0,86	N.D.
Lysophospholipid acyltransferase 7	MBOAT7	-0,86	0,03
Bcl-2-associated transcription factor 1	BCLAF1	-0,85	0,03
Apoptosis regulator BAX	BAX	-0,85	0,09
Histone H3.1;Histone H3.1t	HIST1H3A;HIST3H3;H3F3C	-0,85	0,25
Glycogen debranching enzyme	AGL	-0,85	0,20
WW domain-binding protein 2	WBP2	-0,85	0,05
Non-secretory ribonuclease	RNASE2	-0,85	N.D.
Secretory carrier-associated membrane protein 2	SCAMP2	-0,85	0,01
Delta(24)-sterol reductase	DHCR24	-0,85	0,31
Microsomal glutathione S-transferase 1	MGST1	-0,85	0,89
Eukaryotic peptide chain release factor GTP-binding subunit ERF3B	GSPT2	-0,85	N.D.
ATP-dependent RNA helicase A	DHX9	-0,84	0,26
Calnexin	CANX	-0,84	0,16
Transmembrane protein 165	TMEM165	-0,84	0,02
Glycine amidinotransferase, mitochondrial	GATM	-0,84	N.D.
Synaptobrevin homolog YKT6	YKT6	-0,84	0,60
ADP-sugar pyrophosphatase	NUDT5	-0,83	0,19
Dedicator of cytokinesis protein 10	DOCK10	-0,83	0,21
Annexin A2;Putative annexin A2-like protein	ANXA2;ANXA2P2	-0,83	0,10
Ubiquitin carboxyl-terminal hydrolase isozyme L3	UCHL3	-0,83	N.D.
Iron-responsive element-binding protein 2	IREB2	-0,83	N.D.
EH domain-containing protein 1	EHD1	-0,83	0,08
Calcium-binding mitochondrial carrier protein SCaMC-1	SLC25A24	-0,83	0,04
Peroxisomal acyl-coenzyme A oxidase 1	ACOX1	-0,83	0,31
V-type proton ATPase 116 kDa subunit a isoform 2	ATP6V0A2	-0,82	0,72
Protein disulfide-isomerase	P4HB	-0,82	0,06
Nucleophosmin	NPM1	-0,82	0,24
Vacuolar protein-sorting-associated protein 36	VPS36	-0,82	N.D.
NADH dehydrogenase [ubiquinone] 1 alpha subcomplex subunit 2	NDUFA2	-0,81	0,24
Gamma-aminobutyric acid receptor-associated protein	GABARAP;GABARAPL1	-0,81	0,04
UDP-N-acetylhexosamine pyrophosphorylase-like protein 1	UAP1L1	-0,81	0,09
WASH complex subunit strumpellin	KIAA0196	-0,81	0,14
1-phosphatidylinositol 4,5-bisphosphate phosphodiesterase eta-1	PLCH1	-0,81	0,53
5(3)-deoxyribonucleotidase, cytosolic type	NT5C	-0,81	N.D.
Serine/arginine-rich splicing factor 1	SRSF1	-0,81	0,28
GPI transamidase component PIG-T	PIGT	-0,81	0,52
Lysosomal Pro-X carboxypeptidase	PRCP	-0,81	0,09
Golgi-associated plant pathogenesis-related protein 1	GLIPR2	-0,80	0,25
POTE ankyrin domain family member J	POTEJ	-0,80	N.D.
Integrin alpha-M	ITGAM	-0,80	0,58
Inhibitor of nuclear factor kappa-B kinase subunit beta	IKBKB	-0,80	0,18
40S ribosomal protein S27-like	RPS27L	-0,80	0,41
Heterogeneous nuclear ribonucleoprotein K	HNRNPK	-0,80	0,15
Long chain 3-hydroxyacyl-CoA dehydrogenase	HADHA	-0,80	0,04
Probable ATP-dependent RNA helicase DDX47	DDX47	-0,80	0,63
Serine-protein kinase ATM	ATM	-0,79	0,70
General transcription factor 3C polypeptide 2	GTF3C2	-0,79	N.D.
40S ribosomal protein S11	RPS11	-0,79	0,57
Cytochrome b-245 light chain	CYBA	-0,79	0,05
LIM and SH3 domain protein 1	LASP1	-0,79	0,26
EMILIN-2	EMILIN2	-0,79	N.D.
tRNA (guanine-N(7)-)-methyltransferase	METTL1	-0,79	N.D.
Zinc transporter SLC39A7	SLC39A7	-0,79	0,23
UDP-N-acetylglucosamine pyrophosphorylase	UAP1	-0,78	0,00
Heterogeneous nuclear ribonucleoprotein U-like protein 2	HNRNPUL2	-0,78	0,05
Dolichyl-phosphate beta-glucosyltransferase	ALG5	-0,78	1,14
Equilibrative nucleoside transporter 1	SLC29A1	-0,78	0,49
Biliverdin reductase A	BLVRA	-0,78	0,08
60S ribosomal protein L4	RPL4	-0,78	0,15
Apolipoprotein B receptor	APOBR	-0,77	0,42

U4/U6 small nuclear ribonucleoprotein Prp3	PRPF3	-0,77	0,34
Protein transport protein Sec24A	SEC24A	-0,77	N.D.
Staphylococcal nuclease domain-containing protein 1	SND1	-0,77	0,11
S-formylglutathione hydrolase	ESD	-0,76	0,04
2,3-cyclic-nucleotide 3-phosphodiesterase	CNP	-0,76	0,27
Pericentrin	PCNT	-0,76	N.D.
WASH complex subunit 7	KIAA1033	-0,76	0,23
Protein unc-45 homolog A	UNC45A	-0,76	0,14
N-acetylglucosamine-6-sulfatase	GNS	-0,76	0,64
Trafficking protein particle complex subunit 2-like protein	TRAPPC2L	-0,75	N.D.
GPI transamidase component PIG-S	PIGS	-0,75	0,12
Septin-7	39326	-0,75	0,03
Neutral amino acid transporter A	SLC1A4	-0,74	0,20
Leukocyte immunoglobulin-like receptor subfamily B member 4	LILRB4	-0,74	N.D.
60S ribosomal protein L23a	RPL23A	-0,74	0,16
Histone deacetylase complex subunit SAP18	SAP18	-0,74	0,04
Golgin subfamily A member 2	GOLGA2	-0,74	0,09
Mitotic spindle assembly checkpoint protein MAD1	MAD1L1	-0,74	N.D.
Reticulon-4	RTN4	-0,74	0,11
B-cell receptor-associated protein 29	BCAP29	-0,74	0,15
Peptidyl-prolyl cis-trans isomerase-like 3	PPIL3	-0,74	N.D.
Lanosterol synthase	LSS	-0,73	0,03
DNA-directed RNA polymerase I subunit RPA2	POLR1B	-0,73	0,67
Complement factor D	CFD	-0,73	N.D.
TBC1 domain family member 13	TBC1D13	-0,73	0,32
BAG family molecular chaperone regulator 1	BAG1	-0,73	N.D.
Peroxiredoxin-4	PRDX4	-0,73	0,38
DAZ-associated protein 1	DAZAP1	-0,72	0,08
Triple functional domain protein	TRIO	-0,72	N.D.
Alpha-actinin-4	ACTN4	-0,72	0,02
28S ribosomal protein S18b, mitochondrial	MRPS18B	-0,72	N.D.
Mitochondrial fission factor	MFF	-0,72	N.D.
DnaJ homolog subfamily C member 7	DNAJC7	-0,71	0,21
Adenylyl cyclase-associated protein 1	CAP1	-0,71	0,03
Serine/threonine-protein phosphatase 2B catalytic subunit alpha isoform	PPP3CA	-0,71	0,23
CCR4-NOT transcription complex subunit 11	CNOT11	-0,71	N.D.
Endoplasmic reticulum resident protein 44	ERP44	-0,71	0,03
60S acidic ribosomal protein P2	RPLP2	-0,71	0,01
ATP-dependent RNA helicase DDX3X	DDX3X	-0,71	0,17
Isochorismatase domain-containing protein 2, mitochondrial	ISOC2	-0,71	0,20
Amyloid beta A4 precursor protein-binding family B member 1-interacting protein	APBB1IP	-0,70	0,01
Protein S100-A8;Protein S100-A8, N-terminally processed	S100A8	-0,70	0,08
Erlin-2	ERLIN2	-0,70	0,10
DnaJ homolog subfamily C member 5	DNAJC5	-0,70	0,08
Rab GDP dissociation inhibitor beta	GDI2	-0,70	0,02
Alpha-1,3/1,6-mannosyltransferase ALG2	ALG2	-0,70	N.D.
Very-long-chain enoyl-CoA reductase	TECR	-0,70	0,05
Stromal cell-derived factor 2-like protein 1	SDF2L1	-0,70	0,02
2-5A-dependent ribonuclease	RNASEL	-0,70	N.D.
Golgi SNAP receptor complex member 1	GOSR1	-0,69	0,08
Methylmalonyl-CoA mutase, mitochondrial	MUT	-0,69	0,03
AMP deaminase 2	AMPD2	-0,69	N.D.
cAMP-dependent protein kinase catalytic subunit alpha	PRKACA	-0,69	N.D.
Glutathione synthetase	GSS	-0,69	0,15
60S ribosomal protein L32	RPL32	-0,69	0,27
Protein syndesmos	NUDT16L1	-0,69	0,02
Deoxyribose-phosphate aldolase	DERA	-0,69	0,17
Catalase	CAT	-0,69	0,11
Leucine-rich repeat flightless-interacting protein 1	LRRFIP1	-0,69	0,03
Tripeptidyl-peptidase 2	TPP2	-0,68	0,01
NADH-ubiquinone oxidoreductase chain 4	MT-ND4	-0,68	0,06
HBS1-like protein	HBS1L	-0,68	0,07
Succinyl-CoA ligase [ADP-forming] subunit beta, mitochondrial	SUCLA2	-0,68	N.D.
Hepatoma-derived growth factor-related protein 2	HDGFRP2	-0,68	0,49
Alanyl-tRNA editing protein Aarsd1	AARSD1	-0,68	0,28
NADH dehydrogenase [ubiquinone] 1 beta subcomplex subunit 9	NDUFB9	-0,68	0,06
Tyrosine-protein phosphatase non-receptor type 6	PTPN6	-0,68	0,03
Signal transducer and activator of transcription 1-alpha/beta	STAT1	-0,68	0,01
Chloride intracellular channel protein 1	CLIC1	-0,67	0,07
Sarcoplasmic/endoplasmic reticulum calcium ATPase 2	ATP2A2	-0,67	0,15
E3 ubiquitin-protein ligase RNF213	RNF213	-0,67	0,02
NADH dehydrogenase [ubiquinone] iron-sulfur protein 5	NDUFS5	-0,67	0,15
Gamma-soluble NSF attachment protein	NAPG	-0,67	N.D.
Very long-chain specific acyl-CoA dehydrogenase, mitochondrial	ACADVL	-0,67	0,00
Tyrosine-protein kinase SYK	SYK	-0,66	0,06
2,4-dienoyl-CoA reductase, mitochondrial	DECR1	-0,66	0,08
Ethanolamine-phosphate cytidylyltransferase	PCYT2	-0,66	0,11
40S ribosomal protein S8	RPS8	-0,66	0,37
HLA class I histocompatibility antigen, A-68 and 69 alpha chain	HLA-A	-0,66	0,09
Valine--tRNA ligase	VARS	-0,66	0,11

Mitochondrial carrier homolog 1	MTCH1	-0,66	N.D.
Leucine-rich repeat-containing protein 57	LRRC57	-0,66	N.D.
Ubiquitin conjugation factor E4 A	UBE4A	-0,65	0,43
40S ribosomal protein S13	RPS13	-0,65	0,07
Putative RNA-binding protein 15	RBM15	-0,65	N.D.
Lamin-B1	LMNB1	-0,65	0,15
Transmembrane 9 superfamily member 2	TM9SF2	-0,65	0,13
Chromosome alignment-maintaining phosphoprotein 1	CHAMP1	-0,65	0,00
DnaJ homolog subfamily C member 17	DNAJC17	-0,65	N.D.
60S ribosomal protein L34	RPL34	-0,64	0,26
Liver carboxylesterase 1	CES1	-0,64	0,16
Signal transducer and activator of transcription 3	STAT3	-0,64	0,15
Vacuolar protein sorting-associated protein 52 homolog	VPS52	-0,64	N.D.
60S ribosomal protein L21	RPL21	-0,64	0,06
Glyceraldehyde-3-phosphate dehydrogenase	GAPDH	-0,64	0,19
Protein canopy homolog 2	CNPY2	-0,64	0,14
60S ribosomal protein L13a	RPL13A	-0,64	0,16
Annexin A11	ANXA11	-0,64	0,13
PDZ and LIM domain protein 1	PDLIM1	-0,64	N.D.
Proteasome activator complex subunit 4	PSME4	-0,63	0,40
Vesicle transport protein GOT1B	GOLT1B	-0,63	0,05
Protein S100-A9	S100A9	-0,63	0,11
Probable ATP-dependent RNA helicase DDX27	DDX27	-0,63	1,27
DnaJ homolog subfamily B member 11	DNAJB11	-0,63	0,87
60S ribosomal protein L18	RPL18	-0,63	0,07
SH3 domain-containing kinase-binding protein 1	SH3KBP1	-0,63	0,01
Ubiquitin-related modifier 1	URM1	-0,63	N.D.
Nuclear cap-binding protein subunit 1	NCBP1	-0,63	0,01
Neurofibromin;Neurofibromin truncated	NF1	-0,62	N.D.
Decaprenyl-diphosphate synthase subunit 2	PDSS2	-0,62	N.D.
NADH dehydrogenase [ubiquinone] flavoprotein 2, mitochondrial	NDUFV2	-0,62	0,01
Kynurenine--oxoglutarate transaminase 3	CCBL2	-0,62	0,16
Clathrin heavy chain 2	CLTCL1	-0,62	0,11
SRSF protein kinase 1	SRPK1	-0,62	0,62
Serine/threonine-protein kinase N1	PKN1	-0,62	0,19
Egl nine homolog 1	EGLN1	-0,62	0,26
Antigen KI-67	MKI67	-0,62	N.D.
Small integral membrane protein 7	SMIM7	-0,62	N.D.
5-nucleotidase domain-containing protein 3	NT5DC3	-0,62	N.D.
SPRY domain-containing protein 4	SPRYD4	-0,62	N.D.
Cysteine and glycine-rich protein 1	CSRP1	-0,61	0,11
Non-specific lipid-transfer protein	SCP2	-0,61	0,13
Homer protein homolog 3	HOMER3	-0,61	N.D.
General transcription factor IIF subunit 1	GTF2F1	-0,61	0,53
40S ribosomal protein S25	RPS25	-0,61	0,15
Transformer-2 protein homolog beta	TRA2B	-0,61	0,22
Serine/threonine-protein kinase 10	STK10	-0,61	0,24
General transcription factor IIF subunit 2	GTF2F2	-0,61	0,57
Manganese-transporting ATPase 13A1	ATP13A1	-0,61	0,08
COMM domain-containing protein 1	COMMD1	-0,61	N.D.
Carnitine O-palmitoyltransferase 1, liver isoform	CPT1A	-0,61	0,28
60S ribosomal protein L29	RPL29	-0,61	0,60
5-oxoprolinase	OPLAH	-0,61	N.D.
Ras-related protein Rab-4A	RAB4A	-0,60	0,62
Endoplasmin	HSP90B1	-0,60	0,00
Vacuolar protein sorting-associated protein 18 homolog	VPS18	-0,60	0,34
Elongation of very long chain fatty acids protein 5	ELOVL5	-0,60	0,13
Thyroid receptor-interacting protein 11	TRIP11	-0,60	0,38
Proteasome subunit beta type-9	PSMB9	-0,60	0,07
E3 ubiquitin-protein ligase MYCBP2	MYCBP2	-0,60	0,11
NADH dehydrogenase [ubiquinone] 1 beta subcomplex subunit 7	NDUFB7	-0,60	N.D.
Tyrosine-protein phosphatase non-receptor type 1	PTPN1	-0,60	0,44
Signal transducer and activator of transcription 6	STAT6	-0,60	0,42
Ras-related C3 botulinum toxin substrate 1	RAC1;RAC3	-0,60	0,29
Enhancer of rudimentary homolog	ERH	-0,60	0,02
ERO1-like protein alpha	ERO1L	-0,59	0,00
60S ribosomal protein L7a	RPL7A	-0,59	0,50
Platelet-activating factor acetylhydrolase IB subunit alpha	PAFAH1B1	-0,59	0,27
Protein SON	SON	-0,59	0,27
Lamin-B receptor	LBR	-0,59	0,26

Table 4. Downregulated proteins in THP-1 AraC compared to THP-1 P cells under normoxia. Proteomic profiling (SILAC) data were used. Significantly downregulated proteins were calculated using the fold difference threshold of 0.7 (log_2 fold change=-0.58). Mean±SD for n=2 replicates. Non-detected (N.D.) means less than 2 replicates detected for one protein measured.

UPREGULATED PROTEINS IN THP-1 Dox VS. THP-1 P			
Protein names	**Gene names**	**Mean Log_2 fold change**	**SD Log_2 fold change**
Succinate-semialdehyde dehydrogenase, mitochondrial	ALDH5A1	2.40	0.21
Serine/arginine repetitive matrix protein 2	SRRM2	2.23	0.91
Reticulocalbin-2	RCN2	1.98	0.15
Eukaryotic translation initiation factor 3 subunit C	EIF3C;EIF3CL	1.92	0.71
NFX1-type zinc finger-containing protein 1	ZNFX1	1.91	N.D.
DNL-type zinc finger protein	DNLZ	1.84	0.01
Sepiapterin reductase	SPR	1.81	0.19
1,4-alpha-glucan-branching enzyme	GBE1	1.76	0.07
Sorcin	SRI	1.74	N.D.
Protein VPRBP	VPRBP	1.72	0.60
Calcium-binding mitochondrial carrier protein Aralar2	SLC25A13	1.70	0.03
Eukaryotic translation initiation factor 4B	EIF4B	1.68	0.08
5-demethoxyubiquinone hydroxylase, mitochondrial	COQ7	1.63	N.D.
AP-1 complex subunit sigma-1A	AP1S1	1.61	N.D.
Pterin-4-alpha-carbinolamine dehydratase 2	PCBD2	1.61	0.16
Glutaminase kidney isoform, mitochondrial	GLS	1.60	0.29
Coiled-coil domain-containing protein 124	CCDC124	1.59	0.37
Pre-rRNA-processing protein TSR1 homolog	TSR1	1.53	0.33
U4/U6.U5 tri-snRNP-associated protein 1	SART1	1.53	0.27
3-hydroxyisobutyryl-CoA hydrolase, mitochondrial	HIBCH	1.53	0.12
Protein NDRG1	NDRG1	1.50	N.D.
Calcium-binding mitochondrial carrier protein Aralar1	SLC25A12	1.49	0.05
Isochorismatase domain-containing protein 1	ISOC1	1.46	0.24
Matrin-3	MATR3	1.45	0.52
Branched-chain-amino-acid aminotransferase, mitochondrial	BCAT2	1.44	0.12
Fumarylacetoacetate hydrolase domain-containing protein 2A and B	FAHD2A;FAHD2B	1.44	N.D.
Mammalian ependymin-related protein 1	EPDR1	1.44	0.23
Spectrin beta chain, non-erythrocytic 1	SPTBN1	1.40	0.19
2-methoxy-6-polyprenyl-1,4-benzoquinol methylase, mitochondrial	COQ5	1.39	N.D.
Sodium-coupled neutral amino acid transporter 2	SLC38A2	1.38	0.20
1-acyl-sn-glycerol-3-phosphate acyltransferase epsilon	AGPAT5	1.36	0.28
Protein FAM173B	FAM173B	1.36	0.46
Calcium uniporter protein, mitochondrial	MCU	1.35	0.10
Glucosamine 6-phosphate N-acetyltransferase	GNPNAT1	1.34	0.09
Spectrin alpha chain, non-erythrocytic 1	SPTAN1	1.34	0.28
Macrophage migration inhibitory factor	MIF	1.34	0.13
Putative hydroxypyruvate isomerase	HYI	1.32	N.D.
Dehydrogenase/reductase SDR family member 7	DHRS7	1.29	N.D.
UPF0562 protein C7orf55	C7orf55	1.28	N.D.
UDP-N-acetylglucosamine--dolichyl-phosphate N-acetylglucosaminephosphotransferase	DPAGT1	1.28	0.33
Peptidyl-prolyl cis-trans isomerase FKBP4	FKBP4	1.27	0.06
General transcription factor II-I	GTF2I	1.26	0.01
Heat shock protein beta-1	HSPB1	1.23	0.09
Protein disulfide-isomerase A5	PDIA5	1.23	0.16
Protein AATF	AATF	1.23	1.08
Proteasome subunit beta type-5	PSMB5	1.23	N.D.
Pterin-4-alpha-carbinolamine dehydratase	PCBD1	1.22	0.21
Protein SMG5	SMG5	1.22	0.89
Aldehyde dehydrogenase X, mitochondrial	ALDH1B1	1.22	N.D.
Alpha/beta hydrolase domain-containing protein 14B	ABHD14B	1.20	0.18
Zinc finger protein 622	ZNF622	1.20	1.25
Peroxisomal membrane protein PMP34	SLC25A17	1.20	0.42
Probable Xaa-Pro aminopeptidase 3	XPNPEP3	1.19	N.D.
Probable leucine--tRNA ligase, mitochondrial	LARS2	1.19	0.24
PDZ and LIM domain protein 1	PDLIM1	1.19	N.D.
Ferritin light chain	FTL	1.18	0.10
Flavin reductase (NADPH)	BLVRB	1.18	0.13
Serine/threonine-protein kinase PRP4 homolog	PRPF4B	1.17	1.02
3-hydroxyisobutyrate dehydrogenase, mitochondrial	HIBADH	1.17	0.13
Vitamin K epoxide reductase complex subunit 1-like protein 1	VKORC1L1	1.16	0.27
Zinc finger CCCH-type antiviral protein 1-like	ZC3HAV1L	1.16	0.03
Insulin-like growth factor 2 mRNA-binding protein 1	IGF2BP1	1.15	0.02
Serpin B10	SERPINB10	1.15	0.21
Calumenin	CALU	1.15	0.15
Lipopolysaccharide-responsive and beige-like anchor protein	LRBA	1.15	0.44
Complement component 1 Q subcomponent-binding protein, mitochondrial	C1QBP	1.12	0.06
Isovaleryl-CoA dehydrogenase, mitochondrial	IVD	1.12	0.10
D-beta-hydroxybutyrate dehydrogenase, mitochondrial	BDH1	1.12	0.10
Metaxin-2	MTX2	1.11	0.16
Membrane-associated progesterone receptor component 1	PGRMC1	1.09	0.25
Acyl-coenzyme A thioesterase 13	ACOT13	1.08	0.27
Mitochondrial import inner membrane translocase subunit Tim8 A	TIMM8A	1.08	0.09
Ubiquitin-conjugating enzyme E2 G	UBE2G1	1.07	0.02
Survival motor neuron protein	SMN1	1.07	0.15
Iron-sulfur cluster assembly 2 homolog, mitochondrial	ISCA2	1.06	N.D.
Glutathione S-transferase Mu 1;Glutathione S-transferase Mu 4	GSTM1;GSTM4	1.05	0.11
Transferrin receptor protein 1;Transferrin receptor protein 1, serum form	TFRC	1.05	0.13
Ribose-5-phosphate isomerase	RPIA	1.05	0.28
Isochorismatase domain-containing protein 2, mitochondrial	ISOC2	1.05	0.37
Retinol dehydrogenase 13	RDH13	1.04	0.18

Mycophenolic acid acyl-glucuronide esterase, mitochondrial	ABHD10	1,04	0,04
Tripartite motif-containing protein 72	TRIM72	1,04	N.D.
Histidine triad nucleotide-binding protein 1	HINT1	1,03	0,03
Cytochrome c oxidase subunit 1	MT-CO1	1,03	0,17
Aconitate hydratase, mitochondrial	ACO2	1,03	0,01
Putative helicase MOV-10	MOV10	1,02	0,02
Sulfatase-modifying factor 2	SUMF2	1,02	N.D.
Tetraspanin-14	TSPAN14	1,02	N.D.
DNA-directed RNA polymerase III subunit RPC1	POLR3A	1,01	0,53
Aspartate aminotransferase, mitochondrial	GOT2	1,01	0,10
Aminopeptidase N	ANPEP	1,01	0,40
Transmembrane protein 70, mitochondrial	TMEM70	1,00	0,06
Microtubule-associated protein 4	MAP4	1,00	0,05
Elongation of very long chain fatty acids protein 1	ELOVL1	1,00	0,10
Histidine triad nucleotide-binding protein 2, mitochondrial	HINT2	1,00	0,12
Cat eye syndrome critical region protein 5	CECR5	0,99	0,10
Protein CDV3 homolog	CDV3	0,97	0,16
Single-stranded DNA-binding protein, mitochondrial	SSBP1	0,97	0,06
Spermine synthase	SMS	0,96	0,02
Aldose reductase	AKR1B1	0,95	0,10
Annexin A1	ANXA1	0,95	0,13
Scavenger receptor class B member 1	SCARB1	0,95	0,05
Gem-associated protein 5	GEMIN5	0,95	0,09
Protein FAM136A	FAM136A	0,95	N.D.
Cytochrome c oxidase subunit 2	MT-CO2	0,95	0,03
Probable ATP-dependent RNA helicase DDX49	DDX49	0,94	0,47
Amyloid beta A4 protein fragment 50	APP	0,94	N.D.
Evolutionarily conserved signaling intermediate in Toll pathway, mitochondrial	ECSIT	0,94	0,27
Enoyl-CoA hydratase/3,2-trans-enoyl-CoA isomerase	EHHADH	0,94	0,08
Glycine cleavage system H protein, mitochondrial	GCSH	0,94	N.D.
Rho GTPase-activating protein 15	ARHGAP15	0,94	0,08
Apoptosis-inducing factor 1, mitochondrial	AIFM1	0,93	0,05
Dihydropteridine reductase	QDPR	0,92	0,21
Vacuolar protein sorting-associated protein 13A	VPS13A	0,92	0,13
Lipoamide acyltransferase component of branched-chain alpha-keto acid dehydrogenase complex, m.	DBT	0,92	0,36
Glucose-6-phosphate isomerase	GPI	0,92	0,09
Nuclear export mediator factor NEMF	NEMF	0,92	0,55
Ribonuclease UK114	HRSP12	0,91	0,02
Pseudouridylate synthase 7 homolog	PUS7	0,91	0,10
Asparagine synthetase [glutamine-hydrolyzing]	ASNS	0,91	0,10
Nuclear pore complex protein Nup50	NUP50	0,91	0,19
Phosphoribosylformylglycinamidine synthase	PFAS	0,91	0,23
Cytochrome c	CYCS	0,91	0,02
Nicotinamide phosphoribosyltransferase	NAMPT	0,91	0,07
2-oxoisovalerate dehydrogenase subunit alpha, mitochondrial	BCKDHA	0,91	0,03
Transmembrane protein 14C	TMEM14C	0,90	0,42
Tubulin--tyrosine ligase-like protein 12	TTLL12	0,90	0,06
Peptidase M20 domain-containing protein 2	PM20D2	0,90	0,12
CD166 antigen	ALCAM	0,90	0,38
Telomere-associated protein RIF1	RIF1	0,90	0,23
Serglycin	SRGN	0,90	1,41
Stress-70 protein, mitochondrial	HSPA9	0,90	0,08
Cytochrome c oxidase subunit 3	MT-CO3	0,89	0,05
Mitochondrial fission 1 protein	FIS1	0,89	N.D.
Ferritin heavy chain	FTH1	0,89	0,09
DNA mismatch repair protein Mlh1	MLH1	0,89	0,08
N-terminal kinase-like protein	SCYL1	0,88	1,05
Transportin-2	TNPO2	0,88	0,10
CAP-Gly domain-containing linker protein 1	CLIP1	0,88	0,04
N-alpha-acetyltransferase 20	NAA20	0,88	0,30
Succinyl-CoA ligase [GDP-forming] subunit beta, mitochondrial	SUCLG2	0,88	0,06
Glutathione peroxidase 7	GPX7	0,88	0,15
Nuclear receptor 2C2-associated protein	NR2C2AP	0,88	0,14
Transducin beta-like protein 2	TBL2	0,88	0,07
NudC domain-containing protein 3	NUDCD3	0,88	0,24
Dol-P-Man:Man(5)GlcNAc(2)-PP-Dol alpha-1,3-mannosyltransferase	ALG3	0,87	0,27
Regulator of nonsense transcripts 1	UPF1	0,87	0,20
Titin	TTN	0,87	0,48
Integrator complex subunit 7	INTS7	0,87	N.D.
CAD protein	CAD	0,87	0,16
Gamma-glutamyl hydrolase	GGH	0,86	0,23
Prohibitin	PHB	0,86	0,07
Fatty acid-binding protein, epidermal	FABP5	0,86	0,05
NudC domain-containing protein 1	NUDCD1	0,86	0,08
Mitochondrial import inner membrane translocase subunit TIM14	DNAJC19	0,85	0,18
Eukaryotic translation initiation factor 4H	EIF4H	0,85	0,19
Mannosyl-oligosaccharide glucosidase	MOGS	0,85	0,02
tRNA (guanine(26)-N(2))-dimethyltransferase	TRMT1	0,85	0,05
tRNA pseudouridine synthase A, mitochondrial	PUS1	0,85	0,09
Metallo-beta-lactamase domain-containing protein 2	MBLAC2	0,84	N.D.

Receptor expression-enhancing protein 5	REEP5	0,84	N.D.
Zinc phosphodiesterase ELAC protein 2	ELAC2	0,84	0,55
Intraflagellar transport protein 27 homolog	IFT27	0,84	0,09
Glutathione S-transferase P	GSTP1	0,84	0,09
Glutamine synthetase	GLUL	0,83	0,18
Azurocidin	AZU1	0,83	0,08
Prohibitin-2	PHB2	0,83	0,10
Mannose-1-phosphate guanyltransferase beta	GMPPB	0,82	1,13
Deoxyhypusine synthase	DHPS	0,82	0,11
Forkhead box protein K1	FOXK1	0,82	0,17
Aminoacylase-1	ACY1	0,82	0,37
Mitochondrial chaperone BCS1	BCS1L	0,82	0,21
Vesicle transport through interaction with t-SNAREs homolog 1B	VTI1B	0,82	0,51
Cytochrome c oxidase subunit 7A2, mitochondrial	COX7A2	0,82	0,07
Lymphocyte antigen 75	LY75	0,82	0,23
DNA-directed RNA polymerase III subunit RPC2	POLR3B	0,82	1,21
Treacle protein	TCOF1	0,82	0,15
Protein FAM162A	FAM162A	0,81	0,07
SPRY domain-containing protein 4	SPRYD4	0,81	N.D.
ATP-binding cassette sub-family B member 7, mitochondrial	ABCB7	0,81	0,35
Coatomer subunit gamma-2	COPG2	0,81	0,53
ADP/ATP translocase 1	SLC25A4	0,81	N.D.
Zinc finger protein 638	ZNF638	0,81	0,19
DNA repair protein RAD50	RAD50	0,80	0,06
Electron transfer flavoprotein subunit alpha, mitochondrial	ETFA	0,80	0,06
NADPH--cytochrome P450 reductase	POR	0,80	0,14
Acyl-coenzyme A thioesterase 1;Acyl-coenzyme A thioesterase 2, mitochondrial	ACOT1;ACOT2	0,80	0,04
Glutamine-dependent NAD(+) synthetase	NADSYN1	0,80	N.D.
Peptidyl-tRNA hydrolase 2, mitochondrial	PTRH2	0,80	0,11
Tyrosine--tRNA ligase, mitochondrial	YARS2	0,80	0,30
Probable ATP-dependent RNA helicase DDX27	DDX27	0,80	1,42
Microsomal glutathione S-transferase 1	MGST1	0,80	0,29
Eukaryotic translation initiation factor 5B	EIF5B	0,79	0,16
Mitochondrial import inner membrane translocase subunit Tim13	TIMM13	0,79	0,05
Pre-mRNA-splicing factor 38B	PRPF38B	0,79	0,09
Zinc finger CCCH domain-containing protein 15	ZC3H15	0,79	0,29
Glutaryl-CoA dehydrogenase, mitochondrial	GCDH	0,79	0,17
Mitochondrial import inner membrane translocase subunit Tim17-B	TIMM17B	0,78	0,28
Mitochondrial import inner membrane translocase subunit TIM44	TIMM44	0,78	0,02
Elongation factor Ts, mitochondrial	TSFM	0,78	0,37
Serine/threonine-protein kinase tousled-like 1	TLK1	0,78	0,42
pre-mRNA 3 end processing protein WDR33	WDR33	0,78	0,26
Heat shock 70 kDa protein 4L	HSPA4L	0,77	0,17
MICOS complex subunit MIC60	IMMT	0,77	0,02
Thioredoxin domain-containing protein 5	TXNDC5	0,77	0,11
High mobility group protein B2	HMGB2	0,77	0,20
ATP-binding cassette sub-family F member 1	ABCF1	0,77	0,24
Putative E3 ubiquitin-protein ligase UBR7	UBR7	0,76	N.D.
BET1 homolog	BET1	0,76	0,31
Transmembrane protein 261	TMEM261	0,76	0,15
Cell growth-regulating nucleolar protein	LYAR	0,76	0,09
Cell cycle progression protein 1	CCPG1	0,76	0,30
Electron transfer flavoprotein subunit beta	ETFB	0,76	0,20
Ras-related protein Rab-5B	RAB5B	0,76	0,05
Thioredoxin-like protein 4B	TXNL4B	0,76	N.D.
Ribose-phosphate pyrophosphokinase 1	PRPS1	0,76	0,07
Annexin A4	ANXA4	0,75	0,02
Fatty aldehyde dehydrogenase	ALDH3A2	0,75	0,31
Phosphatidylinositol 4-kinase alpha	PI4KA	0,75	1,20
NADH dehydrogenase [ubiquinone] 1 beta subcomplex subunit 6	NDUFB6	0,75	0,19
Voltage-dependent anion-selective channel protein 3	VDAC3	0,75	0,02
Sorting and assembly machinery component 50 homolog	SAMM50	0,75	0,23
ELAV-like protein 1	ELAVL1	0,75	0,16
Tyrosyl-DNA phosphodiesterase 1	TDP1	0,75	0,46
Superoxide dismutase [Cu-Zn]	SOD1	0,75	0,02
Ornithine aminotransferase, mitochondrial	OAT	0,74	0,02
Squamous cell carcinoma antigen recognized by T-cells 3	SART3	0,74	0,68
2,4-dienoyl-CoA reductase, mitochondrial	DECR1	0,74	0,06
Hsc70-interacting protein;Putative protein FAM10A4;Putative protein FAM10A5	ST13;ST13P4;ST13P5	0,74	0,06
Pyridoxine-5-phosphate oxidase	PNPO	0,74	N.D.
Malate dehydrogenase, mitochondrial	MDH2	0,74	0,07
E3 ubiquitin-protein ligase HUWE1	HUWE1	0,74	0,24
Phosphatidylglycerophosphatase and protein-tyrosine phosphatase 1	PTPMT1	0,73	0,24
Collagen type IV alpha-3-binding protein	COL4A3BP	0,73	0,27
Ubiquinone biosynthesis protein COQ9, mitochondrial	COQ9	0,73	0,43
Syntaxin-16	STX16	0,73	0,51
DnaJ homolog subfamily B member 1	DNAJB1	0,72	0,02
Heterogeneous nuclear ribonucleoprotein A/B	HNRNPAB	0,72	0,05
Coiled-coil domain-containing protein 58	CCDC58	0,72	N.D.
NADH-ubiquinone oxidoreductase chain 5	MT-ND5	0,72	0,14

Sigma non-opioid intracellular receptor 1	SIGMAR1	0,72	0,32
Metaxin-1	MTX1	0,72	0,45
RNA pseudouridylate synthase domain-containing protein 2	RPUSD2	0,72	0,07
Phosphatidylethanolamine-binding protein 1;Hippocampal cholinergic neurostimulating peptide	PEBP1	0,71	0,05
Beta-lactamase-like protein 2	LACTB2	0,71	0,04
E2/E3 hybrid ubiquitin-protein ligase UBE2O	UBE2O	0,71	0,06
Nuclease-sensitive element-binding protein 1	YBX1	0,71	0,70
28S ribosomal protein S25, mitochondrial	MRPS25	0,71	0,35
Cell cycle and apoptosis regulator protein 2	CCAR2	0,71	0,05
Protein NipSnap homolog 2	GBAS	0,71	0,08
Citrate synthase, mitochondrial	CS	0,71	0,05
Nuclear pore complex protein Nup214	NUP214	0,71	0,28
Surfeit locus protein 4	SURF4	0,71	0,09
Latrophilin-2	LPHN2	0,71	0,57
High mobility group protein B3	HMGB3	0,70	0,13
Translin	TSN	0,70	0,06
Serine/threonine-protein kinase TAO3	TAOK3	0,70	0,08
WD repeat and HMG-box DNA-binding protein 1	WDHD1	0,70	0,05
Epidermal growth factor receptor substrate 15	EPS15	0,70	0,12
Monocarboxylate transporter 1	SLC16A1	0,70	0,08
Replication protein A 32 kDa subunit	RPA2	0,70	0,08
Oxygen-dependent coproporphyrinogen-III oxidase, mitochondrial	CPOX	0,70	0,04
Isocitrate dehydrogenase [NAD] subunit gamma, mitochondrial	IDH3G	0,69	1,06
DnaJ homolog subfamily A member 3, mitochondrial	DNAJA3	0,69	0,04
Grancalcin	GCA	0,69	0,14
Thyroid hormone receptor-associated protein 3	THRAP3	0,69	0,05
CGG triplet repeat-binding protein 1	CGGBP1	0,69	N.D.
Acylphosphatase-2	ACYP2	0,69	0,21
Activator of 90 kDa heat shock protein ATPase homolog 1	AHSA1	0,69	0,01
Methylcrotonoyl-CoA carboxylase beta chain, mitochondrial	MCCC2	0,69	0,19
DNA replication licensing factor MCM2	MCM2	0,69	0,16
Signal recognition particle receptor subunit beta	SRPRB	0,68	0,15
Thrombomodulin	THBD	0,68	0,39
DNA-directed RNA polymerase I subunit RPA1	POLR1A	0,68	0,29
Arf-GAP with coiled-coil, ANK repeat and PH domain-containing protein 2	ACAP2	0,68	0,39
KDEL motif-containing protein 2	KDELC2	0,68	0,11
DNA mismatch repair protein Msh6	MSH6	0,68	0,04
Peptidyl-prolyl cis-trans isomerase H	PPIH	0,68	0,07
Proteasome assembly chaperone 3	PSMG3	0,68	0,14
AFG3-like protein 2	AFG3L2	0,68	0,10
Serine/threonine-protein phosphatase PGAM5, mitochondrial	PGAM5	0,68	0,18
Protein LSM14 homolog A	LSM14A	0,68	0,06
Protein phosphatase 1 regulatory subunit 14B	PPP1R14B	0,67	N.D.
Ras-related protein Ral-A	RALA	0,67	N.D.
Crk-like protein	CRKL	0,67	0,26
Nucleoside diphosphate kinase A	NME1	0,67	0,04
Queuine tRNA-ribosyltransferase subunit QTRTD1	QTRTD1	0,66	0,23
Cytochrome c oxidase subunit NDUFA4	NDUFA4	0,66	0,11
Nucleolar protein 58	NOP58	0,66	0,03
2-oxoglutarate dehydrogenase, mitochondrial	OGDH	0,66	0,05
Phosphatidylinositol transfer protein beta isoform	PITPNB	0,66	0,01
Apolipoprotein O	APOO	0,65	0,17
Protein Red	IK	0,65	0,25
Double-strand break repair protein MRE11A	MRE11A	0,65	0,14
Proteasome assembly chaperone 4	PSMG4	0,65	0,21
Golgi reassembly-stacking protein 2	GORASP2	0,65	0,20
Cytosolic non-specific dipeptidase	CNDP2	0,64	0,12
Carnitine O-palmitoyltransferase 2, mitochondrial	CPT2	0,64	0,09
Bifunctional UDP-N-acetylglucosamine 2-epimerase/N-acetylmannosamine kinase	GNE	0,64	0,28
Small integral membrane protein 20	SMIM20	0,64	0,04
Voltage-dependent anion-selective channel protein 1	VDAC1	0,64	0,08
Prostaglandin E synthase 2;Prostaglandin E synthase 2 truncated form	PTGES2	0,64	0,17
Transmembrane emp24 domain-containing protein 4	TMED4	0,64	0,12
Cytochrome c oxidase subunit 7C, mitochondrial	COX7C	0,64	0,15
Ras-related protein Rab-21	RAB21	0,63	0,23
NudC domain-containing protein 2	NUDCD2	0,63	0,01
DnaJ homolog subfamily C member 11	DNAJC11	0,63	0,08
E3 SUMO-protein ligase RanBP2	RANBP2	0,63	0,11
Heat shock protein 75 kDa, mitochondrial	TRAP1	0,63	0,15
Ribose-phosphate pyrophosphokinase 2	PRPS2	0,63	0,05
Glutamate--cysteine ligase catalytic subunit	GCLC	0,63	0,29
Probable ATP-dependent RNA helicase DDX20	DDX20	0,63	1,12
NADH-ubiquinone oxidoreductase chain 4	MT-ND4	0,63	0,13
Apoptosis regulator Bcl-2	BCL2	0,63	0,19
Dihydrolipoyl dehydrogenase, mitochondrial	DLD	0,63	0,08
NEDD8 ultimate buster 1	NUB1	0,63	N.D.
Serine/arginine repetitive matrix protein 1	SRRM1	0,62	0,09
5(3)-deoxyribonucleotidase, cytosolic type	NT5C	0,62	N.D.
Mitochondrial fission process protein 1	MTFP1	0,62	N.D.
Zinc finger CCCH domain-containing protein 4	ZC3H4	0,62	0,74

Protein FAM195A	FAM195A	0,62	N.D.
GDP-mannose 4,6 dehydratase	GMDS	0,62	0,70
Myeloperoxidase;Myeloperoxidase	MPO	0,62	0,35
Acid ceramidase	ASAH1	0,62	0,05
Glyoxalase domain-containing protein 4	GLOD4	0,62	0,10
Proliferating cell nuclear antigen	PCNA	0,62	0,05
Acyl-CoA synthetase family member 2, mitochondrial	ACSF2	0,62	0,20
Lon protease homolog, mitochondrial	LONP1	0,62	0,06
tRNA (adenine(58)-N(1))-methyltransferase catalytic subunit TRMT61A	TRMT61A	0,62	0,52
Ras-related protein Ral-B	RALB	0,61	0,07
UBX domain-containing protein 7	UBXN7	0,61	0,08
Replication protein A 70 kDa DNA-binding subunit	RPA1	0,61	0,12
Protein DEK	DEK	0,61	0,38
3-mercaptopyruvate sulfurtransferase	MPST	0,61	0,05
B-cell receptor-associated protein 31	BCAP31	0,61	0,12
Focadhesin	FOCAD	0,61	0,06
DNA replication licensing factor MCM5	MCM5	0,61	0,04
DNA replication licensing factor MCM4	MCM4	0,61	0,02
NAD(P) transhydrogenase, mitochondrial	NNT	0,61	0,06
Selenide, water dikinase 2	SEPHS2	0,61	0,23
Peptidyl-prolyl cis-trans isomerase-like 4	PPIL4	0,61	0,59
Mitochondrial ribonuclease P protein 1	TRMT10C	0,60	0,21
Poly(A)-specific ribonuclease PARN	PARN	0,60	0,33
NADH dehydrogenase [ubiquinone] 1 beta subcomplex subunit 7	NDUFB7	0,60	N.D.
Eukaryotic translation initiation factor 5A-1;Eukaryotic translation initiation factor 5A-1-like	EIF5A;EIF5AL1	0,60	0,11
Hydroxyacyl-coenzyme A dehydrogenase, mitochondrial	HADH	0,60	0,05
DNA replication licensing factor MCM3	MCM3	0,60	0,03
Protein Hikeshi	C11orf73	0,59	0,11
DnaJ homolog subfamily C member 10	DNAJC10	0,59	0,24
Heat shock protein HSP 90-alpha	HSP90AA1	0,59	0,16
Glycogen debranching enzyme;4-alpha-glucanotransferase;Amylo-alpha-1,6-glucosidase	AGL	0,59	0,11
Exportin-7	XPO7	0,59	0,12
Heterogeneous nuclear ribonucleoprotein U	HNRNPU	0,59	0,30
OCIA domain-containing protein 1	OCIAD1	0,59	0,10
Ribosome maturation protein SBDS	SBDS	0,59	0,18
Deoxyguanosine kinase, mitochondrial	DGUOK	0,59	N.D.
Putative pre-mRNA-splicing factor ATP-dependent RNA helicase DHX16	DHX16	0,59	0,24
Putative transferase CAF17, mitochondrial	IBA57	0,59	0,29
NHP2-like protein 1	NHP2L1	0,59	0,14
Ubiquinol-cytochrome-c reductase complex assembly factor 1	UQCC1	0,59	N.D.
Synaptophysin-like protein 1	SYPL1	0,59	N.D.

Table 5. Upregulated proteins in THP-1 Dox compared to THP-1 P cells under normoxia. Proteomic profiling (SILAC) data were used. Significantly upregulated proteins were calculated using the fold difference threshold of 1.5 (log_2 fold change=0.58). Mean±SD for n=2 replicates. Non-detected (N.D.) means less than 2 replicates detected for one protein measured.

DOWNREGULATED PROTEINS IN THP-1 Dox VS. THP-1 P			
Protein names	**Gene names**	**Mean Log_2 fold change**	**SD Log_2 fold change**
Annexin A6	ANXA6	-4.05	0.07
Insulin-like growth factor 2 mRNA-binding protein 3	IGF2BP3	-3.46	N.D.
Leukosialin	SPN	-3.00	2.42
Cathepsin G	CTSG	-2.87	0.44
Angiotensinogen	AGT	-2.78	N.D.
Keratinocyte proline-rich protein	KPRP	-2.67	0.60
Gelsolin	GSN	-2.65	0.43
Vimentin	VIM	-2.63	0.05
HLA class II histocompatibility antigen,	HLA-DRB1	-2.57	0.22
HLA class II histocompatibility antigen	HLA-DRA	-2.44	0.27
TYRO protein tyrosine kinase-binding protein	TYROBP	-2.42	N.D.
Lysozyme C	LYZ	-2.33	0.19
Protein S100-P	S100P	-2.27	0.02
Arachidonate 5-lipoxygenase-activating protein	ALOX5AP	-2.17	N.D.
Prelamin-A/C;Lamin-A/C	LMNA	-2.13	0.07
Apolipoprotein C-II	APOC2	-2.11	0.60
Protein S100-A4	S100A4	-2.10	0.09
Fructose-1,6-bisphosphatase 1	FBP1	-2.06	N.D.
EMILIN-2	EMILIN2	-2.04	N.D.
1-phosphatidylinositol 4,5-bisphosphate phosphodiesterase beta-2	PLCB2	-2.01	0.46
Cystatin-C	CST3	-2.00	0.20
Plectin	PLEC	-1.99	0.14
Putative RNA-binding protein 15	RBM15	-1.95	N.D.
Unconventional myosin-XVIIIa	MYO18A	-1.95	0.30
Protein-methionine sulfoxide oxidase MICAL1	MICAL1	-1.94	0.04
Caspase recruitment domain-containing protein 9	CARD9	-1.92	0.97
Creatine kinase B-type	CKB	-1.92	0.39
Platelet endothelial cell adhesion molecule	PECAM1	-1.90	0.46
Lysosomal alpha-glucosidase;76 kDa lysosomal alpha-glucosidase	GAA	-1.88	0.03
Junction plakoglobin	JUP	-1.81	0.89
Inactive ubiquitin thioesterase FAM105A	FAM105A	-1.81	0.10
Integrin alpha-M	ITGAM	-1.79	0.45
Formin-like protein 1	FMNL1	-1.78	0.29
Granulins	GRN	-1.78	N.D.
Lactoylglutathione lyase	GLO1	-1.73	0.14
IgG receptor FcRn large subunit p51	FCGRT	-1.73	0.27
Conserved oligomeric Golgi complex subunit 8	COG8	-1.69	N.D.
CapZ-interacting protein	RCSD1	-1.69	0.19
Phospholipase D3	PLD3	-1.65	0.17
DNA-binding protein SATB1	SATB1	-1.64	0.39
Plasma membrane calcium-transporting ATPase 4	ATP2B4	-1.64	N.D.
Glutathione S-transferase Mu 3	GSTM3	-1.63	1.21
ADP-ribosylation factor-like protein 3	ARL3	-1.62	0.21
Galectin-9	LGALS9	-1.62	0.40
HLA class I histocompatibility antigen	HLA-C	-1.58	N.D.
Protein unc-13 homolog D	UNC13D	-1.58	0.11
Interferon-induced 35 kDa protein	IFI35	-1.56	0.34
Vacuolar protein sorting-associated protein 11 homolog	VPS11	-1.56	N.D.
Desmoplakin	DSP	-1.55	0.07
Septin-9	40057	-1.54	N.D.
Volume-regulated anion channel subunit LRRC8C	LRRC8C	-1.54	0.23
C-type lectin domain family 11 member A	CLEC11A	-1.53	0.64
Unconventional myosin-VI	MYO6	-1.51	0.48
Protein S100-A10	S100A10	-1.50	0.75
Two pore calcium channel protein 1	TPCN1	-1.50	N.D.
Sperm-associated antigen 5	SPAG5	-1.50	N.D.
Nicotinate phosphoribosyltransferase	NAPRT	-1.49	0.42
DNA topoisomerase 2-alpha	TOP2A	-1.49	0.34
Glutaredoxin-1	GLRX	-1.47	0.14
Iron-responsive element-binding protein 2	IREB2	-1.47	N.D.
CD70 antigen	CD70	-1.45	N.D.
Macrosialin	CD68	-1.43	N.D.
Filamin-A	FLNA	-1.42	0.12
E3 ubiquitin-protein ligase RNF213	RNF213	-1.41	0.11
Egl nine homolog 1	EGLN1	-1.40	N.D.
Acetyl-CoA acetyltransferase, cytosolic	ACAT2	-1.39	0.04
Neurochondrin	NCDN	-1.39	N.D.
Tyrosine-protein kinase HCK	HCK	-1.37	0.58
Annexin A2;Putative annexin A2-like protein	ANXA2;ANXA2P2	-1.36	0.06
Acylglycerol kinase, mitochondrial	AGK	-1.36	0.17
Hydroxymethylglutaryl-CoA synthase, cytoplasmic	HMGCS1	-1.35	0.42
Tropomyosin alpha-4 chain	TPM4	-1.35	1.13
Thymidine kinase, cytosolic	TK1	-1.35	0.12
Thymidylate synthase	TYMS	-1.35	0.09
CCR4-NOT transcription complex subunit 11	CNOT11	-1.34	N.D.
Golgi-specific brefeldin A-resistance guanine nucleotide exchange factor 1	GBF1	-1.33	N.D.
Copine-8	CPNE8	-1.33	0.27
Nesprin-3	SYNE3	-1.32	N.D.
Protein S100-A6	S100A6	-1.31	0.13
High affinity immunoglobulin epsilon receptor subunit gamma	FCER1G	-1.30	1.31

Ribosome production factor 2 homolog	RPF2	-1,30	0,59
Galectin-1	LGALS1	-1,29	0,09
P-selectin glycoprotein ligand 1	SELPLG	-1,29	0,58
Astrocytic phosphoprotein PEA-15	PEA15	-1,29	0,23
Antigen KI-67	MKI67	-1,28	0,09
Protein phosphatase 1 regulatory subunit 27	PPP1R27	-1,27	0,09
Plexin-B2	PLXNB2	-1,27	0,16
SUN domain-containing protein 2	SUN2	-1,26	0,05
Schlafen family member 11	SLFN11	-1,26	0,13
DNA topoisomerase 2-beta	TOP2B	-1,25	0,14
Wiskott-Aldrich syndrome protein	WAS	-1,25	0,27
Fermitin family homolog 3	FERMT3	-1,25	0,19
Myeloid cell nuclear differentiation antigen	MNDA	-1,25	0,22
KIF1-binding protein	KIAA1279	-1,25	0,19
Calpain-2 catalytic subunit	CAPN2	-1,24	0,31
6-phosphogluconate dehydrogenase, decarboxylating	PGD	-1,23	0,13
Ubiquitin-conjugating enzyme E2 T	UBE2T	-1,23	N.D.
Pericentrin	PCNT	-1,22	0,46
DNA ligase 4	LIG4	-1,22	N.D.
BTB/POZ domain-containing protein KCTD12	KCTD12	-1,21	N.D.
SH3 domain-binding glutamic acid-rich-like protein 3	SH3BGRL3	-1,21	0,10
Chloride intracellular channel protein 4	CLIC4	-1,19	0,04
Adenylate kinase isoenzyme 1	AK1	-1,19	0,15
Ubiquitin-like modifier-activating enzyme 7	UBA7	-1,19	0,36
Fatty acid desaturase 1	FADS1	-1,19	N.D.
Pyruvate kinase PKM	PKM	-1,19	0,07
Protein kinase C beta type	PRKCB	-1,18	0,18
Thymidine phosphorylase	TYMP	-1,18	0,20
5-oxoprolinase	OPLAH	-1,17	N.D.
BET1-like protein	BET1L	-1,17	0,12
MMS19 nucleotide excision repair protein homolog	MMS19	-1,17	0,25
Golgi phosphoprotein 3	GOLPH3	-1,15	0,24
Probable methyltransferase TARBP1	TARBP1	-1,15	0,08
Protein furry homolog	FRY	-1,15	0,54
WD repeat- and FYVE domain-containing protein 4	WDFY4	-1,14	0,17
Tapasin	TAPBP	-1,14	0,36
Carboxypeptidase M	CPM	-1,14	0,12
Delta(24)-sterol reductase	DHCR24	-1,13	0,17
Centromere protein F	CENPF	-1,13	0,15
Leukocyte immunoglobulin-like receptor subfamily B member 4	LILRB4	-1,13	1,52
Vesicle-associated membrane protein 3	VAMP3	-1,13	0,23
NmrA-like family domain-containing protein 1	NMRAL1	-1,13	N.D.
Phosphatidylinositol 4,5-bisphosphate 3-kinase catalytic subunit delta isoform	PIK3CD	-1,12	0,15
Interferon regulatory factor 8	IRF8	-1,12	0,33
Polymerase delta-interacting protein 3	POLDIP3	-1,12	0,20
Macrophage-capping protein	CAPG	-1,12	0,04
F-actin-capping protein subunit alpha-2	CAPZA2	-1,12	0,12
Long-chain-fatty-acid--CoA ligase 3	ACSL3	-1,11	0,07
Differentially expressed in FDCP 6 homolog	DEF6	-1,11	0,34
ADP-sugar pyrophosphatase	NUDT5	-1,11	0,23
Dihydrofolate reductase	DHFR	-1,10	0,30
BAG family molecular chaperone regulator 1	BAG1	-1,10	N.D.
Synaptic vesicle membrane protein VAT-1 homolog	VAT1	-1,10	0,05
Translocator protein	TSPO	-1,10	0,09
Piezo-type mechanosensitive ion channel component 1	PIEZO1	-1,10	0,11
Dihydropyrimidinase-related protein 2	DPYSL2	-1,09	0,16
Alpha-N-acetylgalactosaminidase	NAGA	-1,09	0,16
Phosphatidylinositol 3,4,5-trisphosphate-dependent Rac exchanger 1 protein	PREX1	-1,09	0,51
Tensin-3	TNS3	-1,08	N.D.
Aminopeptidase B	RNPEP	-1,08	0,09
Neutrophil cytosol factor 4	NCF4	-1,08	N.D.
Bifunctional coenzyme A synthase	COASY	-1,08	0,04
WD repeat and FYVE domain-containing protein 1	WDFY1	-1,08	0,05
Major vault protein	MVP	-1,08	0,27
DNA repair protein complementing XP-G cells	ERCC5	-1,08	N.D.
Guanine nucleotide exchange factor MSS4	RABIF	-1,07	0,53
Sortilin-related receptor	SORL1	-1,07	0,01
Beta-2-microglobulin;Beta-2-microglobulin form pI 5.3	B2M	-1,07	0,04
Coiled-coil domain-containing protein 88B	CCDC88B	-1,07	0,19
Toll-like receptor 2	TLR2	-1,07	0,13
40S ribosomal protein S4, Y isoform 1	RPS4Y1	-1,06	0,46
Tyrosine-protein phosphatase non-receptor type 6	PTPN6	-1,06	0,08
Cathepsin L1	CTSL	-1,06	0,05
Ethylmalonyl-CoA decarboxylase	ECHDC1	-1,05	0,25
Carbonyl reductase [NADPH] 1	CBR1	-1,05	0,05
Sorting nexin-4	SNX4	-1,05	N.D.
Suppressor of G2 allele of SKP1 homolog	SUGT1	-1,05	0,03
SH3 domain-binding protein 1	SH3BP1	-1,05	0,62
Protein diaphanous homolog 3	DIAPH3	-1,05	0,22
N-myc-interactor	NMI	-1,05	0,34

Serpin B8	SERPINB8	-1.05	0.08
Interferon regulatory factor 5	IRF5	-1.04	0.25
Geranylgeranyl pyrophosphate synthase	GGPS1	-1.04	0.29
Dedicator of cytokinesis protein 10	DOCK10	-1.04	0.25
Ribonuclease inhibitor	RNH1	-1.04	0.07
Dual specificity protein phosphatase 23	DUSP23	-1.03	0.15
Axin interactor, dorsalization-associated protein	AIDA	-1.03	0.27
Transmembrane 9 superfamily member 2	TM9SF2	-1.03	0.09
Cytohesin-3;Cytohesin-1	CYTH3;CYTH1	-1.03	N.D.
Serine/arginine-rich splicing factor 10	SRSF10	-1.02	0.77
Cytochrome b-245 heavy chain	CYBB	-1.02	0.29
Acidic fibroblast growth factor intracellular-binding protein	FIBP	-1.01	N.D.
Diacylglycerol kinase zeta	DGKZ	-1.01	0.25
Vesicle-fusing ATPase	NSF	-1.01	0.15
Tudor domain-containing protein 7	TDRD7	-1.01	0.58
2-5A-dependent ribonuclease	RNASEL	-1.01	0.31
Syntaxin-12	STX12	-1.00	0.46
WAS/WASL-interacting protein family member 1	WIPF1	-1.00	0.16
Fatty acid desaturase 2	FADS2	-1.00	0.12
E3 ubiquitin-protein ligase TRIP12	TRIP12	-1.00	0.32
Pyrroline-5-carboxylate reductase 2	PYCR2	-0.99	0.05
Protein unc-93 homolog B1	UNC93B1	-0.99	0.12
Tubulin alpha-4A chain	TUBA4A	-0.98	0.27
Tyrosine-protein kinase SYK	SYK	-0.98	0.05
Utrophin	UTRN	-0.98	0.02
Vasodilator-stimulated phosphoprotein	VASP	-0.98	0.28
Tetratricopeptide repeat protein 37	TTC37	-0.98	0.22
Dimethyladenosine transferase 1, mitochondrial	TFB1M	-0.98	0.35
SHC SH2 domain-binding protein 1	SHCBP1	-0.97	0.24
Peptidyl-prolyl cis-trans isomerase FKBP8	FKBP8	-0.97	0.31
Isocitrate dehydrogenase [NADP] cytoplasmic	IDH1	-0.97	0.06
Filamin-B	FLNB	-0.97	0.22
Lysophosphatidylcholine acyltransferase 2	LPCAT2	-0.97	0.12
Signal-induced proliferation-associated protein 1	SIPA1	-0.96	0.48
Golgi SNAP receptor complex member 1	GOSR1	-0.96	0.38
Mitotic-spindle organizing protein 1	MZT1	-0.96	N.D.
Inositol 1,4,5-trisphosphate receptor type 3	ITPR3	-0.96	1.81
DIS3-like exonuclease 2	DIS3L2	-0.95	N.D.
Integrin beta-2	ITGB2	-0.95	0.21
Nicotinate-nucleotide pyrophosphorylase [carboxylating]	QPRT	-0.95	0.18
Nucleoside diphosphate kinase 3	NME3	-0.95	N.D.
Leucine-rich repeat-containing protein 57	LRRC57	-0.95	0.21
Nuclear RNA export factor 1	NXF1	-0.94	0.12
Serine/threonine-protein phosphatase 6 regulatory ankyrin repeat subunit B	ANKRD44	-0.94	0.03
Phosphoacetylglucosamine mutase	PGM3	-0.94	0.13
Ras-related protein Rab-44	RAB44	-0.93	N.D.
General transcription factor 3C polypeptide 2	GTF3C2	-0.93	N.D.
Fanconi anemia group I protein	FANCI	-0.93	0.36
Zyxin	ZYX	-0.93	0.25
ATP-binding cassette sub-family B member 10, mitochondrial	ABCB10	-0.93	0.23
Ethanolamine-phosphate cytidylyltransferase	PCYT2	-0.93	0.15
Serine/threonine-protein kinase mTOR	MTOR	-0.93	0.40
Retinoblastoma-associated protein	RB1	-0.93	0.58
Exosome complex exonuclease RRP44	DIS3	-0.93	0.16
HBS1-like protein	HBS1L	-0.92	0.13
tRNA (uracil-5-)-methyltransferase homolog A	TRMT2A	-0.92	0.43
Lymphocyte cytosolic protein 2	LCP2	-0.92	0.05
Heterogeneous nuclear ribonucleoprotein F	HNRNPF	-0.92	0.23
LIM and SH3 domain protein 1	LASP1	-0.92	0.22
Ras GTPase-activating protein 3	RASA3	-0.92	0.41
Diphosphomevalonate decarboxylase	MVD	-0.92	0.22
Mothers against decapentaplegic homolog 2,3 and 9	SMAD2;SMAD3;SMAD9	-0.92	0.35
Calpain small subunit 1	CAPNS1	-0.91	0.14
WD repeat-containing protein 26	WDR26	-0.91	0.02
Synaptosomal-associated protein 23	SNAP23	-0.91	0.21
Protein FAM49B	FAM49B	-0.91	0.02
Nuclear receptor coactivator 5	NCOA5	-0.91	N.D.
1,2-dihydroxy-3-keto-5-methylthiopentene dioxygenase	ADI1	-0.91	0.75
Tyrosine-protein phosphatase non-receptor type 7	PTPN7	-0.90	0.38
X-ray repair cross-complementing protein 5	XRCC5	-0.90	0.09
Deoxynucleoside triphosphate triphosphohydrolase SAMHD1	SAMHD1	-0.90	0.08
Importin-9	IPO9	-0.89	0.38
Parafibromin	CDC73	-0.89	0.13
NADP-dependent malic enzyme	ME1	-0.89	0.08
Mitochondrial import inner membrane translocase subunit Tim17-A	TIMM17A	-0.89	N.D.
Tumor necrosis factor alpha-induced protein 2	TNFAIP2	-0.89	N.D.
Translationally-controlled tumor protein	TPT1	-0.88	0.13
Peroxisomal acyl-coenzyme A oxidase 3	ACOX3	-0.88	0.35
Argininosuccinate synthase	ASS1	-0.88	0.05
Growth factor receptor-bound protein 2	GRB2	-0.88	0.10
Phosphatidylinositol 4-kinase type 2-alpha	PI4K2A	-0.88	0.46
Protein PAXX	C9orf142	-0.88	0.19
Junctional adhesion molecule A	F11R	-0.87	0.08
Protein unc-45 homolog A	UNC45A	-0.87	0.16

Serpin B8	SERPINB8	-1,05	0,08
Interferon regulatory factor 5	IRF5	-1,04	0,25
Geranylgeranyl pyrophosphate synthase	GGPS1	-1,04	0,29
Dedicator of cytokinesis protein 10	DOCK10	-1,04	0,25
Ribonuclease inhibitor	RNH1	-1,04	0,07
Dual specificity protein phosphatase 23	DUSP23	-1,03	0,15
Axin interactor, dorsalization-associated protein	AIDA	-1,03	0,27
Transmembrane 9 superfamily member 2	TM9SF2	-1,03	0,09
Cytohesin-3;Cytohesin-1	CYTH3;CYTH1	-1,03	N.D.
Serine/arginine-rich splicing factor 10	SRSF10	-1,02	0,77
Cytochrome b-245 heavy chain	CYBB	-1,02	0,29
Acidic fibroblast growth factor intracellular-binding protein	FIBP	-1,01	N.D.
Diacylglycerol kinase zeta	DGKZ	-1,01	0,25
Vesicle-fusing ATPase	NSF	-1,01	0,15
Tudor domain-containing protein 7	TDRD7	-1,01	0,58
2-5A-dependent ribonuclease	RNASEL	-1,01	0,31
Syntaxin-12	STX12	-1,00	0,46
WAS/WASL-interacting protein family member 1	WIPF1	-1,00	0,16
Fatty acid desaturase 2	FADS2	-1,00	0,12
E3 ubiquitin-protein ligase TRIP12	TRIP12	-1,00	0,32
Pyrroline-5-carboxylate reductase 2	PYCR2	-0,99	0,05
Protein unc-93 homolog B1	UNC93B1	-0,99	0,12
Tubulin alpha-4A chain	TUBA4A	-0,98	0,27
Tyrosine-protein kinase SYK	SYK	-0,98	0,05
Utrophin	UTRN	-0,98	0,02
Vasodilator-stimulated phosphoprotein	VASP	-0,98	0,28
Tetratricopeptide repeat protein 37	TTC37	-0,98	0,22
Dimethyladenosine transferase 1, mitochondrial	TFB1M	-0,98	0,35
SHC SH2 domain-binding protein 1	SHCBP1	-0,97	0,24
Peptidyl-prolyl cis-trans isomerase FKBP8	FKBP8	-0,97	0,31
Isocitrate dehydrogenase [NADP] cytoplasmic	IDH1	-0,97	0,06
Filamin-B	FLNB	-0,97	0,22
Lysophosphatidylcholine acyltransferase 2	LPCAT2	-0,97	0,12
Signal-induced proliferation-associated protein 1	SIPA1	-0,96	0,48
Golgi SNAP receptor complex member 1	GOSR1	-0,96	0,38
Mitotic-spindle organizing protein 1	MZT1	-0,96	N.D.
Inositol 1,4,5-trisphosphate receptor type 3	ITPR3	-0,96	1,81
DIS3-like exonuclease 2	DIS3L2	-0,95	N.D.
Integrin beta-2	ITGB2	-0,95	0,21
Nicotinate-nucleotide pyrophosphorylase [carboxylating]	QPRT	-0,95	0,18
Nucleoside diphosphate kinase 3	NME3	-0,95	N.D.
Leucine-rich repeat-containing protein 57	LRRC57	-0,95	0,21
Nuclear RNA export factor 1	NXF1	-0,94	0,12
Serine/threonine-protein phosphatase 6 regulatory ankyrin repeat subunit B	ANKRD44	-0,94	0,03
Phosphoacetylglucosamine mutase	PGM3	-0,94	0,13
Ras-related protein Rab-44	RAB44	-0,93	N.D.
General transcription factor 3C polypeptide 2	GTF3C2	-0,93	N.D.
Fanconi anemia group I protein	FANCI	-0,93	0,36
Zyxin	ZYX	-0,93	0,25
ATP-binding cassette sub-family B member 10, mitochondrial	ABCB10	-0,93	0,23
Ethanolamine-phosphate cytidylyltransferase	PCYT2	-0,93	0,15
Serine/threonine-protein kinase mTOR	MTOR	-0,93	0,40
Retinoblastoma-associated protein	RB1	-0,93	0,58
Exosome complex exonuclease RRP44	DIS3	-0,93	0,16
HBS1-like protein	HBS1L	-0,92	0,13
tRNA (uracil-5-)-methyltransferase homolog A	TRMT2A	-0,92	0,43
Lymphocyte cytosolic protein 2	LCP2	-0,92	0,05
Heterogeneous nuclear ribonucleoprotein F	HNRNPF	-0,92	0,23
LIM and SH3 domain protein 1	LASP1	-0,92	0,22
Ras GTPase-activating protein 3	RASA3	-0,92	0,41
Diphosphomevalonate decarboxylase	MVD	-0,92	0,22
Mothers against decapentaplegic homolog 2,3 and 9	SMAD2;SMAD3;SMAD9	-0,92	0,35
Calpain small subunit 1	CAPNS1	-0,91	0,14
WD repeat-containing protein 26	WDR26	-0,91	0,02
Synaptosomal-associated protein 23	SNAP23	-0,91	0,21
Protein FAM49B	FAM49B	-0,91	0,02
Nuclear receptor coactivator 5	NCOA5	-0,91	N.D.
1,2-dihydroxy-3-keto-5-methylthiopentene dioxygenase	ADI1	-0,91	0,75
Tyrosine-protein phosphatase non-receptor type 7	PTPN7	-0,90	0,38
X-ray repair cross-complementing protein 5	XRCC5	-0,90	0,09
Deoxynucleoside triphosphate triphosphohydrolase SAMHD1	SAMHD1	-0,90	0,08
Importin-9	IPO9	-0,89	0,38
Parafibromin	CDC73	-0,89	0,13
NADP-dependent malic enzyme	ME1	-0,89	0,08
Mitochondrial import inner membrane translocase subunit Tim17-A	TIMM17A	-0,89	N.D.
Tumor necrosis factor alpha-induced protein 2	TNFAIP2	-0,89	N.D.
Translationally-controlled tumor protein	TPT1	-0,88	0,13
Peroxisomal acyl-coenzyme A oxidase 3	ACOX3	-0,88	0,35
Argininosuccinate synthase	ASS1	-0,88	0,05
Growth factor receptor-bound protein 2	GRB2	-0,88	0,10
Phosphatidylinositol 4-kinase type 2-alpha	PI4K2A	-0,88	0,46
Protein PAXX	C9orf142	-0,88	0,19
Junctional adhesion molecule A	F11R	-0,87	0,08
Protein unc-45 homolog A	UNC45A	-0,87	0,16

ANK repeat and PH domain-containing protein 1	ASAP1	-0,87	N.D.
HLA class I histocompatibility antigen	HLA-C	-0,87	0,18
Lanosterol 14-alpha demethylase	CYP51A1	-0,86	0,45
Copine-1	CPNE1	-0,86	0,15
C-type mannose receptor 2	MRC2	-0,86	0,22
Cysteine and glycine-rich protein 1	CSRP1	-0,85	0,18
Protein Niban	FAM129A	-0,85	0,20
Serine/threonine-protein kinase Nek7	NEK7	-0,85	0,48
Histone H1.2	HIST1H1C	-0,85	0,85
Golgi membrane protein 1	GOLM1	-0,84	0,10
Lysosomal alpha-mannosidase	MAN2B1	-0,84	0,08
Proto-oncogene vav	VAV1	-0,84	0,14
UDP-N-acetylglucosamine--peptide N-acetylglucosaminyltransferase	OGT	-0,84	0,18
Chromodomain-helicase-DNA-binding protein 1-like	CHD1L	-0,84	0,17
Ubiquitin carboxyl-terminal hydrolase isozyme L5	UCHL5	-0,84	0,06
Unconventional myosin-Ig;Minor histocompatibility antigen HA-2	MYO1G	-0,84	0,15
Protein disulfide-isomerase A3	PDIA3	-0,84	0,09
Ubiquitin-conjugating enzyme E2 A	UBE2A	-0,83	0,06
Trafficking protein particle complex subunit 8	TRAPPC8	-0,83	0,54
Chitinase-3-like protein 1	CHI3L1	-0,83	0,18
Transmembrane protein 165	TMEM165	-0,83	0,20
Isopentenyl-diphosphate Delta-isomerase 1	IDI1	-0,82	0,01
Fructose-2,6-bisphosphatase TIGAR	TIGAR	-0,82	0,09
Polypeptide N-acetylgalactosaminyltransferase 2	GALNT2	-0,82	0,03
Eukaryotic translation initiation factor 4 gamma 3	EIF4G3	-0,81	N.D.
Protein S100-A11	S100A11	-0,81	0,08
Leucine-rich repeat flightless-interacting protein 1	LRRFIP1	-0,81	0,05
Rho guanine nucleotide exchange factor 7	ARHGEF7	-0,81	0,17
Minor histocompatibility protein HA-1	HMHA1	-0,81	0,03
Arf-GAP with Rho-GAP domain, ANK repeat and PH domain-containing protein 1	ARAP1	-0,81	0,19
RNA polymerase-associated protein CTR9 homolog	CTR9	-0,81	0,13
Exocyst complex component 1	EXOC1	-0,81	N.D.
AP-1 complex subunit sigma-2	AP1S2	-0,80	0,30
Triple functional domain protein	TRIO	-0,80	N.D.
mRNA-capping enzyme;Polynucleotide 5-triphosphatase	RNGTT	-0,80	0,15
PCI domain-containing protein 2	PCID2	-0,80	0,11
Mast cell-expressed membrane protein 1	MCEMP1	-0,80	N.D.
Activated RNA polymerase II transcriptional coactivator p15	SUB1	-0,80	0,04
Prolactin regulatory element-binding protein	PREB	-0,80	N.D.
Uncharacterized protein KIAA2013	KIAA2013	-0,80	0,50
Ribonucleoside-diphosphate reductase large subunit	RRM1	-0,80	0,03
Shootin-1	KIAA1598	-0,79	N.D.
Coactosin-like protein	COTL1	-0,79	0,11
X-ray repair cross-complementing protein 6	XRCC6	-0,79	0,05
Putative 60S ribosomal protein L39-like 5	RPL39P5;RPL39	-0,79	0,13
E3 ubiquitin-protein ligase UHRF1	UHRF1	-0,79	0,14
Serine/threonine-protein kinase N1	PKN1	-0,79	0,22
HLA class I histocompatibility antigen, A-24 and 23 alpha chain	HLA-A	-0,79	0,09
Double-strand-break repair protein rad21 homolog	RAD21	-0,79	0,19
Pyridoxal kinase	PDXK	-0,78	N.D.
Alpha-actinin-4	ACTN4	-0,78	0,01
Prenylcysteine oxidase-like	PCYOX1L	-0,78	0,21
Guanine nucleotide-binding protein G(I)/G(S)/G(O) subunit gamma-10	GNG10	-0,78	0,37
Ras-related protein Rab-18	RAB18	-0,78	0,23
Ubiquitin-like protein 5	UBL5	-0,77	0,07
Uridine-cytidine kinase 2	UCK2	-0,77	0,12
Ubiquitin-associated domain-containing protein 2	UBAC2	-0,77	0,14
Chloride intracellular channel protein 1	CLIC1	-0,77	0,03
PHD finger protein 6	PHF6	-0,77	N.D.
Dipeptidyl peptidase 2	DPP7	-0,77	0,22
N(G),N(G)-dimethylarginine dimethylaminohydrolase 2	DDAH2	-0,77	0,16
Protein EVI2B	EVI2B	-0,77	N.D.
GDP-L-fucose synthase	TSTA3	-0,77	0,09
Sorting nexin-3	SNX3	-0,76	0,03
HLA class I histocompatibility antigen, B-58 and 57 alpha chain	HLA-B	-0,76	0,07
Phosphatidylinositol 3,4,5-trisphosphate 5-phosphatase 1	INPP5D	-0,76	0,02
Ubiquitin carboxyl-terminal hydrolase 8	USP8	-0,76	0,32
Neudesin	NENF	-0,76	N.D.
Calcium/calmodulin-dependent protein kinase type II subunit delta	CAMK2D	-0,76	0,72
DnaJ homolog subfamily C member 7	DNAJC7	-0,76	0,08
Golgin subfamily A member 2	GOLGA2	-0,76	0,06
Signal transducer and activator of transcription 5B and A	STAT5B;STAT5A	-0,76	0,18
Importin subunit alpha-4	KPNA3	-0,75	0,08
ER degradation-enhancing alpha-mannosidase-like protein 1	EDEM1	-0,75	0,12
Leucine-rich repeat-containing protein 40	LRRC40	-0,75	0,07
Cytoskeleton-associated protein 4	CKAP4	-0,75	N.D.
Erythrocyte band 7 integral membrane protein	STOM	-0,74	0,56
CD97 antigen	CD97	-0,74	0,27
Tumor necrosis factor alpha-induced protein 8-like protein 2	TNFAIP8L2	-0,74	0,93
Zinc finger ZZ-type and EF-hand domain-containing protein 1	ZZEF1	-0,74	N.D.
BRO1 domain-containing protein BROX	BROX	-0,74	0,13
Endophilin-B1	SH3GLB1	-0,74	0,04
V-type proton ATPase 116 kDa subunit a isoform 3	TCIRG1	-0,74	N.D.
F-actin-capping protein subunit beta	CAPZB	-0,73	0,08
Monoacylglycerol lipase ABHD12	ABHD12	-0,73	N.D.

ATP-dependent (S)-NAD(P)H-hydrate dehydratase	CARKD	-0,73	0,34
Beta-adrenergic receptor kinase 1	ADRBK1	-0,73	0,22
Succinyl-CoA:3-ketoacid coenzyme A transferase 1, mitochondrial	OXCT1	-0,73	N.D.
Importin subunit alpha-1	KPNA2	-0,73	0,12
Myocyte-specific enhancer factor 2D	MEF2D	-0,73	0,13
EH domain-containing protein 1	EHD1	-0,72	0,11
GPN-loop GTPase 1	GPN1	-0,72	0,44
Neuroblast differentiation-associated protein AHNAK	AHNAK	-0,72	0,28
Tripeptidyl-peptidase 2	TPP2	-0,72	0,08
Signal transducer and activator of transcription 3	STAT3	-0,72	0,02
Annexin A11	ANXA11	-0,72	0,09
Twinfilin-1	TWF1	-0,71	0,11
Alpha-actinin-1	ACTN1	-0,71	0,03
Mini-chromosome maintenance complex-binding protein	MCMBP	-0,71	0,15
Gamma-tubulin complex component 3	TUBGCP3	-0,71	0,53
Adenylyl cyclase-associated protein 1	CAP1	-0,71	0,12
Protein syndesmos	NUDT16L1	-0,70	0,09
MORC family CW-type zinc finger protein 3	MORC3	-0,70	N.D.
Fanconi anemia group D2 protein	FANCD2	-0,70	0,80
Rho guanine nucleotide exchange factor 2	ARHGEF2	-0,70	0,08
Valine--tRNA ligase	VARS	-0,70	0,17
TRAF-interacting protein with FHA domain-containing protein A	TIFA	-0,70	0,46
BRISC complex subunit Abro1	FAM175B	-0,69	0,26
60S ribosomal protein L31	RPL31	-0,69	0,05
Dolichyl-phosphate beta-glucosyltransferase	ALG5	-0,69	0,11
Regulation of nuclear pre-mRNA domain-containing protein 1A	RPRD1A	-0,69	0,30
Procollagen galactosyltransferase 1	COLGALT1	-0,69	0,15
Lanosterol synthase	LSS	-0,69	0,10
Beta-1-syntrophin	SNTB1	-0,69	0,32
Receptor-type tyrosine-protein phosphatase C	PTPRC	-0,69	0,09
Gamma-tubulin complex component 2	TUBGCP2	-0,69	0,11
Tubulin gamma-1 chain;Tubulin gamma-2 chain	TUBG1;TUBG2	-0,69	0,09
Galectin-3	LGALS3	-0,69	N.D.
Rho-related GTP-binding protein RhoG	RHOG	-0,69	0,09
Protein misato homolog 1	MSTO1	-0,69	0,13
Protein phosphatase 1 regulatory subunit 7	PPP1R7	-0,69	0,19
ATP-citrate synthase	ACLY	-0,69	0,02
Proteasome subunit beta type-9	PSMB9	-0,68	0,05
Vam6/Vps39-like protein	VPS39	-0,68	N.D.
Trafficking protein particle complex subunit 1	TRAPPC1	-0,68	0,66
Spartin	SPG20	-0,68	0,48
Retinal rod rhodopsin-sensitive cGMP 3,5-cyclic phosphodiesterase subunit delta	PDE6D	-0,68	N.D.
60S ribosomal protein L37a	RPL37A	-0,68	0,04
Cyclin-dependent kinases regulatory subunit 1	CKS1B	-0,68	0,21
Ras-related protein Rab-27A	RAB27A	-0,68	0,07
Protein-glutamate O-methyltransferase	ARMT1	-0,68	0,03
Ribosomal RNA-processing protein 7 homolog A	RRP7A	-0,67	N.D.
2,3-cyclic-nucleotide 3-phosphodiesterase	CNP	-0,67	0,33
Flotillin-2	FLOT2	-0,67	0,27
Farnesyl pyrophosphate synthase	FDPS	-0,67	0,02
Alpha-1,6-mannosyl-glycoprotein 2-beta-N-acetylglucosaminyltransferase	MGAT2	-0,67	0,38
TFIIH basal transcription factor complex helicase XPD subunit	ERCC2	-0,67	0,22
Calponin-2	CNN2	-0,67	0,10
Protein flightless-1 homolog	FLII	-0,67	0,10
Helicase SKI2W	SKIV2L	-0,66	0,60
Alpha- and gamma-adaptin-binding protein p34	AAGAB	-0,66	0,14
Fascin	FSCN1	-0,66	0,12
Actin-related protein 3	ACTR3	-0,66	0,05
Calpastatin	CAST	-0,66	N.D.
WW domain-binding protein 2	WBP2	-0,66	0,13
Maspardin	SPG21	-0,66	0,02
UPF0553 protein C9orf64	C9orf64	-0,66	N.D.
Coiled-coil and C2 domain-containing protein 1A	CC2D1A	-0,65	0,33
Synembryn-A	RIC8A	-0,65	0,15
60S ribosomal protein L4	RPL4	-0,65	0,04
Pre-mRNA-splicing factor SYF1	XAB2	-0,65	0,14
CD99 antigen	CD99	-0,65	N.D.
Actin-related protein 2	ACTR2	-0,65	0,07
Peptidyl-prolyl cis-trans isomerase FKBP5	FKBP5	-0,65	0,12
Condensin-2 complex subunit G2	NCAPG2	-0,65	0,15
Actin-related protein 2/3 complex subunit 2	ARPC2	-0,65	0,02
Basic leucine zipper and W2 domain-containing protein 1	BZW1	-0,64	0,15
Enoyl-CoA hydratase 2	HSD17B4	-0,64	0,15
GPI transamidase component PIG-T	PIGT	-0,64	0,15
NAD(P)H dehydrogenase [quinone] 1	NQO1	-0,64	0,11
Zinc finger protein 217	ZNF217	-0,64	0,25
26S proteasome non-ATPase regulatory subunit 5	PSMD5	-0,64	0,22
60S ribosomal protein L36a-like	RPL36AL	-0,64	0,53
RNA-binding protein NOB1	NOB1	-0,64	N.D.
F-actin-capping protein subunit alpha-1	CAPZA1	-0,64	0,10
Peptidyl-prolyl cis-trans isomerase B	PPIB	-0,64	0,11
Zinc finger CCHC domain-containing protein 3	ZCCHC3	-0,64	0,08
Coiled-coil and C2 domain-containing protein 1B	CC2D1B	-0,63	0,28
Kinesin-like protein KIFC1	KIFC1	-0,63	0,29
Integrin alpha-5	ITGA5	-0,63	0,20

ER degradation-enhancing alpha-mannosidase-like protein 3	EDEM3	-0,63	0,61
Proteasome activator complex subunit 3	PSME3	-0,63	0,05
Plexin-A1	PLXNA1	-0,63	0,22
Dual specificity protein phosphatase 3	DUSP3	-0,62	0,07
Phosphomevalonate kinase	PMVK	-0,62	0,05
Heterogeneous nuclear ribonucleoprotein U-like protein 2	HNRNPUL2	-0,62	0,21
60S ribosomal protein L35a	RPL35A	-0,62	0,11
Transformer-2 protein homolog alpha	TRA2A	-0,62	0,77
Plastin-2	LCP1	-0,62	0,05
Inositol 1,4,5-trisphosphate receptor type 1	ITPR1	-0,62	0,16
Heat shock 70 kDa protein 14	HSPA14	-0,62	0,89
40S ribosomal protein S24	RPS24	-0,62	0,42
Antigen peptide transporter 1	TAP1	-0,62	0,13
Torsin-1A-interacting protein 1	TOR1AIP1	-0,62	0,11
Heterogeneous nuclear ribonucleoproteins C1/C2	HNRNPC	-0,62	0,35
Decaprenyl-diphosphate synthase subunit 2	PDSS2	-0,62	0,14
E3 ubiquitin-protein ligase MYCBP2	MYCBP2	-0,62	0,21
DENN domain-containing protein 3	DENND3	-0,61	0,19
Transgelin-2	TAGLN2	-0,61	0,13
Interferon regulatory factor 2-binding protein 2	IRF2BP2	-0,61	0,10
Atlastin-3	ATL3	-0,61	0,09
Leucine-rich repeat and calponin homology domain-containing protein 4	LRCH4	-0,61	N.D.
Ubiquitin-protein ligase E3C	UBE3C	-0,61	N.D.
FH1/FH2 domain-containing protein 1	FHOD1	-0,61	N.D.
Myotubularin-related protein 14	MTMR14	-0,61	0,44
Wings apart-like protein homolog	WAPAL	-0,61	N.D.
Heterochromatin protein 1-binding protein 3	HP1BP3	-0,61	0,17
Probable global transcription activator SNF2L2	SMARCA2	-0,61	0,37
Tyrosine-protein kinase CSK	CSK	-0,61	0,11
Mitogen-activated protein kinase 3	MAPK3	-0,61	0,16
Actin-related protein 2/3 complex subunit 5	ARPC5	-0,60	N.D.
Syntaxin-binding protein 2	STXBP2	-0,60	0,08
U1 small nuclear ribonucleoprotein C	SNRPC	-0,60	0,09
E3 ubiquitin-protein ligase RBX1	RBX1	-0,60	0,42
Protein-L-isoaspartate(D-aspartate) O-methyltransferase	PCMT1	-0,60	0,06
Charged multivesicular body protein 4a	CHMP4A	-0,60	0,04
Fructose-bisphosphate aldolase C	ALDOC	-0,59	0,55
Homer protein homolog 3	HOMER3	-0,59	0,11
60S ribosomal protein L3	RPL3	-0,59	0,20
60S acidic ribosomal protein P2	RPLP2	-0,59	0,18
Glutamine--tRNA ligase	QARS	-0,59	0,07
Nardilysin	NRD1	-0,59	0,20
Calcineurin B homologous protein 1	CHP1	-0,59	N.D.

Table 6. Downregulated proteins in THP-1 Dox compared to THP-1 P cells under normoxia. Proteomic profiling (SILAC) data were used. Significantly downregulated proteins were calculated using the fold difference threshold of 0.7 (log_2 fold change=-0.58). Mean±SD for n=2 replicates. Non-detected (N.D.) means less than 2 replicates detected for one protein measured.

UPREGULATED PROTEINS IN HL-60 AraC VS. HL-60 P			
Protein names	**Gene names**	**Mean Log_2 fold change**	**SD Log_2 fold change**
N-acetylserotonin O-methyltransferase-like protein	ASMTL	3.71	0.02
Vimentin	VIM	3.10	0.12
Annexin A1	ANXA1	2.73	0.03
Hydroxymethylglutaryl-CoA synthase, cytoplasmic	HMGCS1	2.55	0.01
Histone H1.5	HIST1H1B	2.53	N.D.
Neutrophil defensin 3	DEFA3;DEFA1	2.34	0.04
Alpha-2-macroglobulin receptor-associated protein	LRPAP1	2.21	0.23
Fatty acid desaturase 2	FADS2	2.18	0.03
UDP-N-acetylhexosamine pyrophosphorylase	UAP1	2.17	0.09
Neuroblast differentiation-associated protein AHNAK	AHNAK	2.13	0.12
Zinc finger CCCH-type antiviral protein 1-like	ZC3HAV1L	2.10	0.06
Sepiapterin reductase	SPR	2.02	0.13
RNA polymerase II-associated protein 1	RPAP1	1.93	0.23
Dynein assembly factor 5, axonemal	DNAAF5	1.92	0.67
Fatty acid desaturase 1	FADS1	1.91	0.38
Tumor suppressor p53-binding protein 1	TP53BP1	1.89	0.07
Coiled-coil-helix domain-containing protein 2,mitochondrial	CHCHD2;CHCHD2P9	1.88	0.05
5-nucleotidase domain-containing protein 1	NT5DC1	1.87	0.00
Dihydropteridine reductase	QDPR	1.85	0.03
Protein FAM198B	FAM198B	1.84	0.42
Azurocidin	AZU1	1.79	1.93
Histone H2AX	H2AFX;HIST1H2AA	1.78	0.05
Transmembrane protein 33	TMEM33	1.77	0.02
Cytosol aminopeptidase	LAP3	1.76	0.03
Phosphoglucomutase-1	PGM1	1.76	0.21
Transforming acidic coiled-coil-containing protein 3	TACC3	1.74	0.13
7-dehydrocholesterol reductase	DHCR7	1.72	0.11
Omega-amidase NIT2	NIT2	1.72	0.08
Transmembrane protein 128	TMEM128	1.70	0.14
Hematopoietic lineage cell-specific protein	HCLS1	1.68	0.04
Cytoplasmic FMR1-interacting protein 1	CYFIP1	1.67	0.13
Very long-chain acyl-CoA synthetase	SLC27A2	1.67	0.03
Histone RNA hairpin-binding protein	SLBP	1.67	N.D.
DNA topoisomerase 2-alpha	TOP2A	1.66	N.D.
Tricarboxylate transport protein, mitochondrial	SLC25A1	1.65	0.06
FAD-AMP lyase (cyclizing)	DAK	1.65	0.08
Huntingtin	HTT	1.64	0.03
Ras-related protein Rab-18	RAB18	1.63	0.17
Phosphoglucomutase-2	PGM2	1.61	0.02
Gelsolin	GSN	1.60	0.09
Thymidine kinase, cytosolic	TK1	1.60	0.13
Alpha-adducin	ADD1	1.58	0.12
Transferrin receptor protein 1	TFRC	1.57	0.13
WD repeat-containing protein 1	WDR1	1.55	0.03
Procollagen-lysine,2-oxoglutarate 5-dioxygenase 1	PLOD1	1.54	0.96
C-type lectin domain family 11 member A	CLEC11A	1.54	0.23
Epididymis-specific alpha-mannosidase	MAN2B2	1.53	0.08
Replication factor C subunit 1	RFC1	1.52	0.58
2,4-dienoyl-CoA reductase, mitochondrial	DECR1	1.52	0.11
Bone marrow proteoglycan;Eosinophil granule major basic protein	PRG2	1.52	0.16
Carbonyl reductase [NADPH] 1	CBR1	1.51	0.08
Deoxyuridine 5-triphosphate nucleotidohydrolase, mitochondrial	DUT	1.51	0.03
Helicase-like transcription factor	HLTF	1.51	N.D.
Acetyl-CoA acetyltransferase, cytosolic	ACAT2	1.50	0.03
Nck-associated protein 1-like	NCKAP1L	1.49	0.07
Cytochrome c oxidase copper chaperone	COX17	1.49	N.D.
Small integral membrane protein 20	SMIM20	1.46	N.D.
Cystatin-A;Cystatin-A, N-terminally processed	CSTA	1.45	0.03
CapZ-interacting protein	RCSD1	1.44	N.D.
Kinetochore protein Nuf2	NUF2	1.42	N.D.
Zinc transporter ZIP14	SLC39A14	1.41	N.D.
Mevalonate kinase	MVK	1.40	N.D.
Multidrug resistance-associated protein 1	ABCC1	1.39	0.33
Ubiquitin-conjugating enzyme E2 K	UBE2K	1.38	0.06
Oxygen-dependent coproporphyrinogen-III oxidase, mitochondrial	CPOX	1.37	0.02
Glyoxylate reductase/hydroxypyruvate reductase	GRHPR	1.37	0.09
Protein disulfide-isomerase A5	PDIA5	1.37	0.07
Protein IMPACT	IMPACT	1.36	0.05
Squalene synthase	FDFT1	1.36	0.07
Transformer-2 protein homolog alpha	TRA2A	1.36	N.D.
Sjoegren syndrome/scleroderma autoantigen 1	SSSCA1	1.36	0.07
Heterogeneous nuclear ribonucleoprotein U-like protein 2	HNRNPUL2	1.35	0.08
Ubiquitin carboxyl-terminal hydrolase 8	USP8	1.35	0.17
Niemann-Pick C1 protein	NPC1	1.35	0.19
1,4-alpha-glucan-branching enzyme	GBE1	1.34	0.13
Aminoacylase-1	ACY1	1.34	0.13
DnaJ homolog subfamily C member 17	DNAJC17	1.34	0.05
Ubiquitin-like protein 5	UBL5	1.33	0.11
Serine/threonine-protein kinase N1	PKN1	1.33	0.12
RuvB-like 1	RUVBL1	1.32	0.09

Protein FAM98B	FAM98B	1,29	0,12
NEDD8-activating enzyme E1 catalytic subunit	UBA3	1,27	0,04
OCIA domain-containing protein 1	OCIAD1	1,27	0,06
Cold-inducible RNA-binding protein	CIRBP	1,27	0,05
UDP-glucose 6-dehydrogenase	UGDH	1,27	0,12
UDP-N-acetylglucosamine--peptide N-acetylglucosaminyltransferase	OGT	1,26	0,16
DnaJ homolog subfamily C member 13	DNAJC13	1,25	0,16
Phosphatidylinositol 3,4,5-trisphosphate 5-phosphatase 2	INPPL1	1,25	0,03
LETM1 and EF-hand domain-containing protein 1, mitochondrial	LETM1	1,25	0,12
Derlin-3	DERL3	1,23	0,07
Sulfide:quinone oxidoreductase, mitochondrial	SQRDL	1,23	0,24
Golgin subfamily B member 1	GOLGB1	1,23	0,08
Importin subunit alpha-1	KPNA2	1,22	0,11
Heterogeneous nuclear ribonucleoprotein A3	HNRNPA3	1,21	0,01
Heterogeneous nuclear ribonucleoprotein D-like	HNRNPDL	1,21	0,20
DDB1- and CUL4-associated factor 16	DCAF16	1,20	0,04
RuvB-like 2	RUVBL2	1,19	0,05
Uridine 5-monophosphate synthase	UMPS	1,18	0,05
NEDD8-activating enzyme E1 regulatory subunit	NAE1	1,17	0,05
Heterogeneous nuclear ribonucleoproteins A2/B1	HNRNPA2B1	1,17	0,01
Kinetochore protein Spc24	SPC24	1,17	0,06
CGG triplet repeat-binding protein 1	CGGBP1	1,16	N.D.
Thymidylate synthase	TYMS	1,16	0,03
Cysteine and histidine-rich domain-containing protein 1	CHORDC1	1,15	0,01
Isopentenyl-diphosphate Delta-isomerase 1	IDI1	1,13	0,06
Protein furry homolog-like	FRYL	1,13	0,23
Alpha-mannosidase 2C1	MAN2C1	1,11	N.D.
Dipeptidyl peptidase 3	DPP3	1,11	0,07
Intraflagellar transport protein 25 homolog	HSPB11	1,11	N.D.
Serglycin	SRGN	1,11	N.D.
Equilibrative nucleoside transporter 2	SLC29A2	1,11	0,26
Serine/threonine-protein phosphatase 4 regulatory subunit 3B	SMEK2	1,11	N.D.
Constitutive coactivator of peroxisome proliferator-activated receptor gamma	FAM120B	1,10	N.D.
Leupaxin	LPXN	1,10	N.D.
Alpha-mannosidase 2	MAN2A1	1,09	0,26
Beta-glucuronidase	GUSB	1,09	0,17
Fascin	FSCN1	1,09	0,01
Histone chaperone ASF1B	ASF1B	1,09	N.D.
Oxysterol-binding protein-related protein 9	OSBPL9	1,08	N.D.
N-acylneuraminate cytidylyltransferase	CMAS	1,08	N.D.
Centromere protein F	CENPF	1,06	N.D.
Heterogeneous nuclear ribonucleoprotein H3	HNRNPH3	1,06	0,12
Acetyl-CoA acetyltransferase, mitochondrial	ACAT1	1,06	0,04
Eukaryotic translation initiation factor 2A	EIF2A	1,05	0,12
Peroxisomal acyl-coenzyme A oxidase 3	ACOX3	1,05	0,29
Serine/arginine-rich splicing factor 9	SRSF9	1,05	0,09
Ubiquitin-conjugating enzyme E2 S	UBE2S	1,04	N.D.
Tetratricopeptide repeat protein 9C	TTC9C	1,03	0,06
Cyclin-dependent kinase 1	CDK1	1,02	0,04
Radixin	RDX	1,02	0,26
Protein phosphatase 1 regulatory subunit 12A	PPP1R12A	1,02	N.D.
Succinyl-CoA ligase [GDP-forming] subunit beta, mitochondrial	SUCLG2	1,02	0,02
Retinoid-inducible serine carboxypeptidase	SCPEP1	1,02	0,07
Apoptosis regulator Bcl-2	BCL2	1,02	0,08
Probable dolichyl pyrophosphate alpha-1,3-glucosyltransferase	ALG8	1,01	0,08
Transmembrane protein 126A	TMEM126A	1,00	0,03
Glutamate--cysteine ligase regulatory subunit	GCLM	1,00	N.D.
Signal recognition particle 14 kDa protein	SRP14	1,00	0,12
Protein disulfide-isomerase A3	PDIA3	0,99	0,01
Vacuolar protein sorting-associated protein 51 homolog	VPS51	0,99	0,49
Vinculin	VCL	0,99	0,05
Porphobilinogen deaminase	HMBS	0,99	0,09
Sorbitol dehydrogenase	SORD	0,99	0,08
V-type proton ATPase subunit C 1	ATP6V1C1	0,99	0,11
Transmembrane protein 189	TMEM189	0,99	N.D.
Translation initiation factor eIF-2B subunit beta	EIF2B2	0,99	0,01
Farnesyl pyrophosphate synthase	FDPS	0,98	0,01
Trans-3-hydroxy-L-proline dehydratase	L3HYPDH	0,98	N.D.
Ribonuclease P protein subunit p40	RPP40	0,98	N.D.
Ribonuclease UK114	HRSP12	0,97	0,12
Coiled-coil domain-containing protein 58	CCDC58	0,97	0,06
Girdin	CCDC88A	0,96	0,16
Protein FAM162A	FAM162A	0,95	0,09
Heterogeneous nuclear ribonucleoprotein A0	HNRNPA0	0,95	0,03
Biorientation of chromosomes in cell division protein 1-like 1	BOD1L1	0,95	0,02
Cob(I)yrinic acid a,c-diamide adenosyltransferase, mitochondrial	MMAB	0,95	0,19
Serine-protein kinase ATM	ATM	0,95	0,04
Transformer-2 protein homolog beta	TRA2B	0,95	0,06
E3 ubiquitin-protein ligase CHIP	STUB1	0,95	0,11
Carbonic anhydrase 2	CA2	0,94	0,07

Protein S100-A4	S100A4	0,94	0,17
Cystatin-F	CST7	0,94	0,18
GPI ethanolamine phosphate transferase 2	PIGG	0,94	0,08
cAMP-dependent protein kinase catalytic subunit beta	PRKACB	0,94	0,14
Lymphokine-activated killer T-cell-originated protein kinase	PBK	0,94	N.D.
AH receptor-interacting protein	AIP	0,94	0,05
Transcription termination factor 2	TTF2	0,93	0,07
Delta(3,5)-Delta(2,4)-dienoyl-CoA isomerase, mitochondrial	ECH1	0,93	0,09
182 kDa tankyrase-1-binding protein	TNKS1BP1	0,93	0,03
Heterogeneous nuclear ribonucleoproteins C1/C2	HNRNPC	0,93	0,09
RNA pseudouridylate synthase domain-containing protein 2	RPUSD2	0,92	0,41
Beta-2-microglobulin;Beta-2-microglobulin form pI 5.3	B2M	0,92	0,02
Xaa-Pro dipeptidase	PEPD	0,92	0,06
Peptidyl-prolyl cis-trans isomerase FKBP2	FKBP2	0,92	0,03
Translation initiation factor eIF-2B subunit delta	EIF2B4	0,92	0,05
Sister chromatid cohesion protein PDS5 homolog A	PDS5A	0,92	0,02
Ena/VASP-like protein	EVL	0,92	0,22
Signal recognition particle 9 kDa protein	SRP9	0,91	0,03
Prolyl 4-hydroxylase subunit alpha-1	P4HA1	0,91	0,09
Receptor-type tyrosine-protein phosphatase C	PTPRC	0,91	0,10
FH1/FH2 domain-containing protein 1	FHOD1	0,90	0,58
ELAV-like protein 1	ELAVL1	0,90	0,09
Zinc finger HIT domain-containing protein 2	ZNHIT2	0,89	N.D.
Receptor-type tyrosine-protein phosphatase alpha	PTPRA	0,89	N.D.
Apoptotic chromatin condensation inducer in the nucleus	ACIN1	0,89	0,07
N-acetyltransferase 14	NAT14	0,88	0,26
Acyl-CoA desaturase	SCD	0,88	0,03
V-type proton ATPase catalytic subunit A	ATP6V1A	0,88	0,04
Prolyl 3-hydroxylase 1	LEPRE1	0,88	0,07
Mitochondrial import inner membrane translocase subunit Tim8 B	TIMM8B	0,87	0,07
Interferon-inducible double-stranded RNA-dependent protein kinase activator A	PRKRA	0,87	N.D.
Mycophenolic acid acyl-glucuronide esterase, mitochondrial	ABHD10	0,87	0,09
DNA polymerase alpha subunit B	POLA2	0,87	N.D.
V-type proton ATPase subunit B, brain isoform	ATP6V1B2	0,87	0,22
Armadillo repeat-containing protein 8	ARMC8	0,87	0,14
Protein TFG	TFG	0,86	0,08
Small integral membrane protein 12	SMIM12	0,86	0,18
Glycogen [starch] synthase, muscle	GYS1	0,86	0,09
Proteasome subunit beta type-5	PSMB5	0,86	0,06
WD repeat-containing protein 74	WDR74	0,85	N.D.
Cofilin-1	CFL1	0,85	0,03
Protein phosphatase methylesterase 1	PPME1	0,85	0,10
Chromosome-associated kinesin KIF4A	KIF4A	0,85	0,10
Oligoribonuclease, mitochondrial	REXO2	0,85	0,12
ADP-ribosylation factor-like protein 6-interacting protein 1	ARL6IP1	0,84	0,04
Calpain small subunit 1	CAPNS1	0,84	0,04
Phosphoinositide 3-kinase regulatory subunit 4	PIK3R4	0,84	0,11
Heterogeneous nuclear ribonucleoprotein A1	HNRNPA1;HNRNPA1L2	0,83	0,11
Fanconi anemia group I protein	FANCI	0,83	0,17
Ubiquitin thioesterase OTUB1	OTUB1	0,83	0,06
Cartilage-associated protein	CRTAP	0,83	0,18
FACT complex subunit SSRP1	SSRP1	0,83	0,04
C-terminal-binding protein 1	CTBP1	0,83	0,07
Acyl-CoA dehydrogenase family member 9, mitochondrial	ACAD9	0,83	0,16
Protein CMSS1	CMSS1	0,82	0,03
Ethanolamine-phosphate cytidylyltransferase	PCYT2	0,82	0,05
Chromosome transmission fidelity protein 8 homolog	CHTF8	0,81	0,07
Phosphatidylinositol-binding clathrin assembly protein	PICALM	0,81	N.D.
Serine/arginine-rich splicing factor 10	SRSF10	0,81	0,26
Intron-binding protein aquarius	AQR	0,80	0,09
Probable ergosterol biosynthetic protein 28	C14orf1	0,80	N.D.
Copper transport protein ATOX1	ATOX1	0,80	0,06
Proteasomal ATPase-associated factor 1	PAAF1	0,80	0,06
PRA1 family protein 3	ARL6IP5	0,80	0,15
ATP-binding cassette sub-family D member 2	ABCD2	0,80	N.D.
Lysophospholipid acyltransferase 5	LPCAT3	0,80	0,06
Ribonuclease P protein subunit p14	RPP14	0,79	0,12
Sterol O-acyltransferase 1	SOAT1	0,79	N.D.
Ubiquitin conjugation factor E4 A	UBE4A	0,79	0,12
Destrin	DSTN	0,79	0,02
Ras-related protein Rab-8B	RAB8B	0,79	0,26
Cullin-4A	CUL4A	0,78	0,10
V-type proton ATPase subunit H	ATP6V1H	0,78	0,09
Gamma-glutamyl hydrolase	GGH	0,78	0,09
Transmembrane 9 superfamily member 1	TM9SF1	0,78	0,44
Pre-mRNA-splicing factor 38A	PRPF38A	0,78	0,22
Anaphase-promoting complex subunit 4	ANAPC4	0,78	N.D.
Probable RNA-binding protein EIF1AD	EIF1AD	0,78	N.D.
Ras suppressor protein 1	RSU1	0,77	N.D.
FACT complex subunit SPT16	SUPT16H	0,77	0,05

Pyruvate kinase PKM	PKM	0.77	0.03
Mammalian ependymin-related protein 1	EPDR1	0.77	0.16
DNA-(apurinic or apyrimidinic site) lyase, mitochondrial	APEX1	0.76	0.03
Lysosomal protective protein	CTSA	0.76	0.10
HD domain-containing protein 2	HDDC2	0.76	0.02
Mitochondrial import inner membrane translocase subunit Tim13	TIMM13	0.76	0.21
Thymocyte nuclear protein 1	THYN1	0.76	0.04
COMM domain-containing protein 4	COMMD4	0.75	0.17
V-type proton ATPase subunit E 1	ATP6V1E1	0.75	0.04
DNA replication complex GINS protein PSF2	GINS2	0.75	0.23
GrpE protein homolog 1, mitochondrial	GRPEL1	0.75	0.03
Cyclin-G-associated kinase	GAK	0.75	0.16
RNA-binding protein 3	RBM3	0.75	0.10
ATP-dependent zinc metalloprotease YME1L1	YME1L1	0.75	N.D.
F-actin-capping protein subunit alpha-2	CAPZA2	0.74	0.09
2-deoxynucleoside 5-phosphate N-hydrolase 1	DNPH1	0.74	0.13
Polypeptide N-acetylgalactosaminyltransferase 2	GALNT2	0.74	0.27
Dolichyl-diphosphooligosaccharide--protein glycosyltransferase 48 kDa subunit	DDOST	0.74	0.02
Isocitrate dehydrogenase [NADP] cytoplasmic	IDH1	0.74	0.06
Spermine synthase	SMS	0.74	0.05
Protein tyrosine phosphatase receptor type C-associated protein	PTPRCAP	0.73	N.D.
L-aminoadipate-semialdehyde dehydrogenase-phosphopantetheinyl transferase	AASDHPPT	0.73	0.08
Glucoamylase	MGAM	0.73	0.18
Epidermal growth factor receptor substrate 15-like 1	EPS15L1	0.72	0.33
Mediator of RNA polymerase II transcription subunit 12	MED12	0.72	0.02
Ras-related protein Rab-27A	RAB27A	0.72	0.07
Bromodomain-containing protein 3	BRD3	0.72	0.29
Diphosphomevalonate decarboxylase	MVD	0.72	N.D.
Beta-hexosaminidase subunit beta	HEXB	0.72	0.18
Sterol-4-alpha-carboxylate 3-dehydrogenase, decarboxylating	NSDHL	0.72	0.09
Ras-related protein Rab-4B	RAB4B	0.72	0.10
Death domain-associated protein 6	DAXX	0.72	N.D.
DNA replication licensing factor MCM2	MCM2	0.72	0.03
Mitochondrial import receptor subunit TOM34	TOMM34	0.72	0.24
PCI domain-containing protein 2	PCID2	0.71	0.11
Calpain-1 catalytic subunit	CAPN1	0.71	0.03
Dolichyl-diphosphooligosaccharide--protein glycosyltransferase subunit 1	RPN1	0.71	0.01
Histidine triad nucleotide-binding protein 2, mitochondrial	HINT2	0.71	0.12
ATP-citrate synthase	ACLY	0.71	0.02
N6-adenosine-methyltransferase 70 kDa subunit	METTL3	0.71	N.D.
GH3 domain-containing protein	GHDC	0.71	0.08
PEST proteolytic signal-containing nuclear protein	PCNP	0.71	0.04
Complex I assembly factor TIMMDC1, mitochondrial	TIMMDC1	0.71	0.20
Uridine-cytidine kinase 2	UCK2	0.71	0.13
Transcriptional repressor p66-alpha	GATAD2A	0.70	N.D.
Nardilysin	NRD1	0.70	0.04
Ribonucleoside-diphosphate reductase subunit M2	RRM2	0.70	0.12
DNA replication complex GINS protein PSF3	GINS3	0.70	0.18
Serine/arginine-rich splicing factor 7	SRSF7	0.70	0.06
Selenocysteine-specific elongation factor	EEFSEC	0.70	0.37
RNA-binding protein PNO1	PNO1	0.70	0.03
Queuine tRNA-ribosyltransferase	QTRT1	0.70	0.15
Caseinolytic peptidase B protein homolog	CLPB	0.70	0.10
UDP-N-acetylglucosamine--dolichyl-phosphate N-acetylglucosaminephosphotransferase	DPAGT1	0.70	0.07
Target of EGR1 protein 1	TOE1	0.69	0.14
Beta-arrestin-1	ARRB1	0.69	0.01
Cyclin-dependent kinases regulatory subunit 1	CKS1B	0.69	N.D.
Amyloid beta A4 precursor protein-binding family B member 1-interacting protein	APBB1IP	0.69	0.05
Cathepsin G	CTSG	0.69	0.02
Delta-1-pyrroline-5-carboxylate synthase	ALDH18A1/P5CS	0.69	0.04
Protein CDV3 homolog	CDV3	0.69	0.09
Translation factor GUF1, mitochondrial	GUF1	0.68	N.D.
DNA topoisomerase 2-beta	TOP2B	0.68	0.32
Recombining binding protein suppressor of hairless	RBPJ	0.68	0.23
Trafficking protein particle complex subunit 4	TRAPPC4	0.68	0.18
Calcium-binding mitochondrial carrier protein Aralar1	SLC25A12	0.68	0.04
DNA dC->dU-editing enzyme APOBEC-3C	APOBEC3C	0.68	0.10
Mediator of RNA polymerase II transcription subunit 28	MED28	0.68	N.D.
DNA replication licensing factor MCM7	MCM7	0.68	0.03
Anaphase-promoting complex subunit 2	ANAPC2	0.68	0.17
U3 small nucleolar RNA-associated protein 18 homolog	UTP18	0.68	N.D.
Ras-related protein Rab-32	RAB32	0.68	0.15
RNA-binding protein Raly	RALY	0.68	0.12
Leucine-rich repeat-containing protein 57	LRRC57	0.68	0.26
Histone deacetylase complex subunit SAP18	SAP18	0.68	0.08
DnaJ homolog subfamily C member 10	DNAJC10	0.67	0.18
Pachytene checkpoint protein 2 homolog	TRIP13	0.67	0.07
UPF0160 protein MYG1, mitochondrial	C12orf10	0.67	0.12
ATPase ASNA1	ASNA1	0.67	0.09
Ubiquitin-conjugating enzyme E2 A	UBE2A	0.66	0.07

Pyrroline-5-carboxylate reductase 3	PYCRL	0,66	0,07
COMM domain-containing protein 8	COMMD8	0,66	N.D.
GMP reductase 2	GMPR2	0,66	0,20
Nodal modulator 1	NOMO1	0,66	0,05
Histone-binding protein RBBP7	RBBP7	0,66	0,07
Cellular nucleic acid-binding protein	CNBP	0,66	0,03
Polyadenylate-binding protein 2	PABPN1	0,66	0,05
Ribonuclease P protein subunit p30	RPP30	0,66	0,31
Periodic tryptophan protein 2 homolog	PWP2	0,65	0,01
Nodal modulator 2 and 3	NOMO2;NOMO3	0,65	0,02
Zinc finger protein ZPR1	ZPR1	0,65	0,05
DNA replication licensing factor MCM6	MCM6	0,65	0,03
Ubiquitin-like-conjugating enzyme ATG3	ATG3	0,65	0,07
Torsin-1A-interacting protein 2	TOR1AIP2	0,65	0,35
Brefeldin A-inhibited guanine nucleotide-exchange protein 1	ARFGEF1	0,65	0,32
Beta-hexosaminidase subunit alpha	HEXA	0,65	0,07
All-trans-retinol 13,14-reductase	RETSAT	0,65	0,12
Translation initiation factor eIF-2B subunit gamma	EIF2B3	0,65	0,14
m7GpppX diphosphatase	DCPS	0,65	0,04
Acetyl-CoA carboxylase 1;Biotin carboxylase	ACACA	0,64	0,19
Echinoderm microtubule-associated protein-like 3	EML3	0,64	0,03
Protein dopey-2	DOPEY2	0,64	0,18
Endoplasmic reticulum-Golgi intermediate compartment protein 2	ERGIC2	0,64	0,03
Bifunctional polynucleotide phosphatase/kinase	PNKP	0,64	N.D.
Golgi-associated PDZ and coiled-coil motif-containing protein	GOPC	0,63	N.D.
Fatty acid synthase;[Acyl-carrier-protein] S-acetyltransferase	FASN	0,63	0,01
B-cell receptor-associated protein 29	BCAP29	0,63	N.D.
Ubiquitin-protein ligase E3A	UBE3A	0,63	0,04
Flap endonuclease 1	FEN1	0,63	0,02
Heat shock 70 kDa protein 1-like	HSPA1L	0,63	0,00
DNA replication licensing factor MCM4	MCM4	0,63	0,02
Glutaminyl-peptide cyclotransferase-like protein	QPCTL	0,63	0,11
DNA replication licensing factor MCM5	MCM5	0,63	0,03
V-type proton ATPase subunit G 1	ATP6V1G1	0,62	0,23
Major facilitator superfamily domain-containing protein 10	MFSD10	0,62	0,14
Syntaxin-binding protein 2	STXBP2	0,62	0,07
Cytosolic non-specific dipeptidase	CNDP2	0,62	0,02
E3 ubiquitin-protein ligase BRE1A	RNF20	0,62	0,04
Glycosaminoglycan xylosylkinase	FAM20B	0,62	N.D.
Solute carrier family 2, facilitated glucose transporter member 1	SLC2A1	0,62	0,06
SPRY domain-containing protein 4	SPRYD4	0,62	0,09
CUGBP Elav-like family member 2	CELF2	0,62	0,15
SH3 domain-binding glutamic acid-rich-like protein 3	SH3BGRL3	0,61	0,06
F-box only protein 22	FBXO22	0,61	N.D.
Eukaryotic translation initiation factor 1b	EIF1B	0,61	N.D.
Kinesin-like protein KIFC1	KIFC1	0,61	N.D.
Caspase recruitment domain-containing protein 9	CARD9	0,61	0,04
Histone acetyltransferase type B catalytic subunit	HAT1	0,61	0,02
Condensin-2 complex subunit D3	NCAPD3	0,61	0,12
Lanosterol synthase	LSS	0,61	0,10
Leukocyte elastase inhibitor	SERPINB1	0,61	0,04
Antigen KI-67	MKI67	0,61	0,15
Serine/threonine-protein phosphatase 4 catalytic subunit	PPP4C	0,61	0,10
Epoxide hydrolase 1	EPHX1	0,61	0,11
Calcium-binding mitochondrial carrier protein Aralar2	SLC25A13	0,61	0,10
3(2),5-bisphosphate nucleotidase 1	BPNT1	0,60	0,05
Protein arginine N-methyltransferase 6	PRMT6	0,60	N.D.
Protein transport protein Sec61 subunit gamma	SEC61G	0,60	0,17
Mannose-1-phosphate guanyltransferase alpha	GMPPA	0,60	0,06
Translation initiation factor eIF-2B subunit epsilon	EIF2B5	0,60	0,03
E3 ubiquitin-protein ligase RNF123	RNF123	0,59	N.D.
tRNA (uracil-5-)-methyltransferase homolog A	TRMT2A	0,59	0,15
Ribonuclease H2 subunit C	RNASEH2C	0,59	0,04
HEAT repeat-containing protein 3	HEATR3	0,59	0,20
Serine protease HTRA2, mitochondrial	HTRA2	0,59	0,14
Putative glutathione-specific gamma-glutamylcyclotransferase 2	CHAC2	0,59	N.D.
RNA-binding protein with serine-rich domain 1	RNPS1	0,59	N.D.
Heterogeneous nuclear ribonucleoprotein U	HNRNPU	0,59	0,01
DCN1-like protein 5	DCUN1D5	0,59	0,20
Dolichyl-diphosphooligosaccharide--protein glycosyltransferase subunit DAD1	DAD1	0,59	0,05

Table 7. Upregulated proteins in HL-60 AraC compared to HL-60 P cells under normoxia. Proteomic profiling (SILAC) data were used. Significantly upregulated proteins were calculated using the fold difference threshold of 1.5 (log_2 fold change=0.58). Mean±SD for n=2 replicates. Non-detected (N.D.) means less than 2 replicates detected for one protein measured.

DOWNREGULATED PROTEINS IN HL-60 AraC VS. HL-60 P			
Protein names	**Gene names**	**Mean Log_2 fold change**	**SD Log_2 fold change**
HLA class I histocompatibility antigen, B-57 alpha chain	HLA-B	-4.09	N.D.
Ankyrin repeat domain-containing protein 22	ANKRD22	-4.06	N.D.
Basigin	BSG	-3.22	0.41
Proteasome subunit beta type-8	PSMB8	-3.04	0.11
Argininosuccinate synthase	ASS1	-2.99	0.10
Cation-dependent mannose-6-phosphate receptor	M6PR	-2.44	0.64
Chloride channel CLIC-like protein 1	CLCC1	-1.88	0.11
Very-long-chain 3-oxoacyl-CoA reductase	HSD17B12	-1.80	0.05
DNA-directed RNA polymerase, mitochondrial	POLRMT	-1.67	0.17
Tapasin	TAPBP	-1.59	N.D.
Beta-mannosidase	MANBA	-1.59	1.07
Stromal interaction molecule 1	STIM1	-1.58	N.D.
Phosphoenolpyruvate carboxykinase [GTP], mitochondrial	PCK2	-1.57	0.08
Serpin B8	SERPINB8	-1.56	0.14
Nuclear pore complex protein Nup98-Nup96	NUP98	-1.53	N.D.
Heat shock 70 kDa protein 1B;Heat shock 70 kDa protein 1A	HSPA1B;HSPA1A	-1.50	0.05
Microsomal glutathione S-transferase 2	MGST2	-1.49	0.02
Switch-associated protein 70	SWAP70	-1.46	0.07
Galectin-9	LGALS9	-1.44	0.00
Ferritin light chain	FTL	-1.43	0.05
Cat eye syndrome critical region protein 5	CECR5	-1.43	0.17
Glutamate dehydrogenase 1, mitochondrial	GLUD1;GLUD2	-1.41	0.13
Integrin beta-1	ITGB1	-1.40	0.27
Leucyl-cystinyl aminopeptidase	LNPEP	-1.38	0.20
Lamin-B2	LMNB2	-1.35	0.06
LIM domain and actin-binding protein 1	LIMA1	-1.33	N.D.
Myeloid-associated differentiation marker	MYADM	-1.33	0.08
Drebrin	DBN1	-1.30	0.43
Protein jagged-1	JAG1	-1.29	N.D.
Synaptophysin-like protein 1	SYPL1	-1.28	N.D.
Estradiol 17-beta-dehydrogenase 11	HSD17B11	-1.26	0.02
Nuclear pore complex protein Nup160	NUP160	-1.26	0.19
Proteasome maturation protein	POMP	-1.24	0.03
Golgi apparatus protein 1	GLG1	-1.23	0.70
Mitochondrial carrier homolog 2	MTCH2	-1.23	0.14
CD81 antigen	CD81	-1.23	0.26
2-methoxy-6-polyprenyl-1,4-benzoquinol methylase, mitochondrial	COQ5	-1.22	0.07
Transmembrane protein 41B	TMEM41B	-1.21	N.D.
NADH dehydrogenase [ubiquinone] 1 beta subcomplex subunit 4	NDUFB4	-1.21	N.D.
Leukocyte-associated immunoglobulin-like receptor 1	LAIR1	-1.21	0.75
Protein FAM107B	FAM107B	-1.18	0.09
Apoptosis inhibitor 5	API5	-1.18	0.12
Voltage-dependent anion-selective channel protein 2	VDAC2	-1.16	0.01
Manganese-transporting ATPase 13A1	ATP13A1	-1.15	0.55
Ras-related protein Rab-4A	RAB4A	-1.14	N.D.
High affinity cationic amino acid transporter 1	SLC7A1	-1.13	0.35
Uncharacterized protein NCBP2-AS2	NCBP2-AS2	-1.13	N.D.
Thromboxane-A synthase	TBXAS1	-1.13	0.38
Importin-7	IPO7	-1.12	0.02
Prosaposin	PSAP	-1.11	0.07
Phosphatidylglycerophosphatase and protein-tyrosine phosphatase 1	PTPMT1	-1.11	0.19
60S ribosomal protein L7-like 1	RPL7L1	-1.10	0.10
Histone H1.2	HIST1H1C	-1.10	N.D.
Ras-related protein Rab-3D	RAB3D	-1.10	N.D.
Transaldolase	TALDO1	-1.10	0.03
N-acetyltransferase 10	NAT10	-1.09	0.07
Lysosome-associated membrane glycoprotein 2	LAMP2	-1.08	0.21
MICOS complex subunit MIC19	CHCHD3	-1.08	0.12
Rho-related GTP-binding protein RhoG	RHOG	-1.07	0.08
Uracil-DNA glycosylase	UNG	-1.07	N.D.
L-lactate dehydrogenase A chain	LDHA	-1.05	0.03
Cysteine--tRNA ligase, cytoplasmic	CARS	-1.04	0.15
Receptor-type tyrosine-protein phosphatase epsilon	PTPRE	-1.04	N.D.
Succinyl-CoA ligase [ADP-forming] subunit beta, mitochondrial	SUCLA2	-1.03	0.32
Arf-GAP with coiled-coil, ANK repeat and PH domain-containing protein 1	ACAP1	-1.03	N.D.
UPF0317 protein C14orf159, mitochondrial	C14orf159	-1.03	0.25
Cytochrome c oxidase subunit 5B, mitochondrial	COX5B	-1.02	0.23
Protein MAK16 homolog	MAK16	-1.01	N.D.
Arf-GAP with Rho-GAP domain	ARAP1	-1.01	N.D.
Microsomal glutathione S-transferase 3	MGST3	-1.00	0.17
N(4)-(beta-N-acetylglucosaminyl)-L-asparaginase	AGA	-1.00	0.04
GRAM domain-containing protein 4	GRAMD4	-1.00	0.06
Methylthioribulose-1-phosphate dehydratase	APIP	-0.99	0.05
Ribonuclease inhibitor	RNH1	-0.99	0.11
Alpha-N-acetylgalactosaminidase	NAGA	-0.99	N.D.
MICOS complex subunit MIC60	IMMT	-0.98	0.01
Erlin-1	ERLIN1	-0.98	0.18
Erythrocyte band 7 integral membrane protein	STOM	-0.98	0.06
Metaxin-2	MTX2	-0.97	0.10
Tripeptidyl-peptidase 1	TPP1	-0.97	0.11

Heat shock 70 kDa protein 4L	HSPA4L	-0,97	0,06
Glutaredoxin-1	GLRX	-0,97	0,08
NADH-ubiquinone oxidoreductase chain 4	MT-ND4	-0,97	0,04
Pyruvate dehydrogenase protein X component, mitochondrial	PDHX	-0,97	0,16
ADP-ribosylation factor-like protein 8A	ARL8A	-0,97	N.D.
39S ribosomal protein L30, mitochondrial	MRPL30	-0,96	N.D.
Multifunctional protein ADE2	PAICS	-0,96	0,05
Eukaryotic translation initiation factor 4E	EIF4E	-0,96	0,04
General transcription factor IIH subunit 2-like protein	GTF2H2C;GTF2H2	-0,96	N.D.
Voltage-dependent anion-selective channel protein 1	VDAC1	-0,96	0,05
Amidophosphoribosyltransferase	PPAT	-0,96	0,03
Sorting and assembly machinery component 50 homolog	SAMM50	-0,96	0,07
Retinol dehydrogenase 14	RDH14	-0,95	0,23
Grancalcin	GCA	-0,95	0,14
Ubiquitin-like modifier-activating enzyme 6	UBA6	-0,94	0,10
Nucleolar protein 58	NOP58	-0,94	0,16
Tumor susceptibility gene 101 protein	TSG101	-0,94	0,14
RNA-binding protein 12B	RBM12B	-0,93	0,12
Caspase-6	CASP6	-0,93	N.D.
Histone H1x	H1FX	-0,93	N.D.
Translocator protein	TSPO	-0,92	0,06
Lon protease homolog, mitochondrial	LONP1	-0,92	0,01
LEM domain-containing protein 2	LEMD2	-0,92	N.D.
Protein CEBPZOS	CEBPZOS	-0,92	N.D.
SH3 domain-binding protein 1	SH3BP1	-0,92	0,06
Protein SDE2 homolog	SDE2	-0,91	N.D.
PITH domain-containing protein 1	PITHD1	-0,91	0,07
Coactosin-like protein	COTL1	-0,91	0,01
SUN domain-containing protein 2	SUN2	-0,90	N.D.
Junctional adhesion molecule A	F11R	-0,90	0,66
N-alpha-acetyltransferase 15, NatA auxiliary subunit	NAA15	-0,90	0,05
Cytochrome c oxidase subunit 2	MT-CO2	-0,90	0,02
Nucleosome assembly protein 1-like 4	NAP1L4	-0,89	0,07
Pericentriolar material 1 protein	PCM1	-0,89	0,26
Thymosin beta-4;Hematopoietic system regulatory peptide	TMSB4X	-0,89	0,04
Inorganic pyrophosphatase 2, mitochondrial	PPA2	-0,89	0,04
Type-1 angiotensin II receptor-associated protein	AGTRAP	-0,89	0,05
Peptidyl-prolyl cis-trans isomerase-like 3	PPIL3	-0,89	N.D.
Calcineurin subunit B type 1	PPP3R1	-0,89	0,14
Serine/threonine-protein phosphatase 2B catalytic subunit alpha isoform	PPP3CA	-0,89	0,09
ATPase family AAA domain-containing protein 3B	ATAD3B	-0,89	0,17
39S ribosomal protein L23, mitochondrial	MRPL23	-0,88	0,13
Programmed cell death protein 4	PDCD4	-0,88	0,10
Nucleoprotein TPR	TPR	-0,88	0,04
E3 ubiquitin/ISG15 ligase TRIM25	TRIM25	-0,88	0,05
Lamin-B1	LMNB1	-0,88	0,02
Sodium/potassium-transporting ATPase subunit beta-3	ATP1B3	-0,87	0,28
Nucleolar protein 56	NOP56	-0,87	0,13
Synembryn-A	RIC8A	-0,87	0,19
Lysosome-associated membrane glycoprotein 1	LAMP1	-0,87	0,29
CDGSH iron-sulfur domain-containing protein 2	CISD2	-0,87	0,09
Nuclear pore complex protein Nup107	NUP107	-0,87	0,15
Rho GTPase-activating protein 1	ARHGAP1	-0,87	0,03
Monofunctional C1-tetrahydrofolate synthase, mitochondrial	MTHFD1L	-0,87	0,18
Dol-P-Man:Man(7)GlcNAc(2)-PP-Dol alpha-1,6-mannosyltransferase	ALG12	-0,87	N.D.
Mitotic spindle assembly checkpoint protein MAD1	MAD1L1	-0,87	0,14
Choline/ethanolaminephosphotransferase 1	CEPT1	-0,86	0,05
Protein S100-A8;Protein S100-A8, N-terminally processed	S100A8	-0,86	0,23
Nuclear pore membrane glycoprotein 210	NUP210	-0,86	0,03
CAAX prenyl protease 1 homolog	ZMPSTE24	-0,86	0,14
Voltage-dependent anion-selective channel protein 3	VDAC3	-0,86	0,10
Small ubiquitin-related modifier 1;Small ubiquitin-related modifier	SUMO1	-0,85	0,05
Galectin-1	LGALS1	-0,85	0,06
ATPase family AAA domain-containing protein 3A	ATAD3A	-0,85	0,02
Vacuolar protein sorting-associated protein 45	VPS45	-0,85	0,03
Hydroxyacyl-coenzyme A dehydrogenase, mitochondrial	HADH	-0,84	0,04
Nicastrin	NCSTN	-0,84	0,01
Lysocardiolipin acyltransferase 1	LCLAT1	-0,83	0,10
General vesicular transport factor p115	USO1	-0,83	0,04
Protein FAN	NSMAF	-0,83	N.D.
Battenin	CLN3	-0,82	N.D.
Myotubularin-related protein 5	SBF1	-0,82	N.D.
Isochorismatase domain-containing protein 2, mitochondrial	ISOC2	-0,82	N.D.
Enolase-phosphatase E1	ENOPH1	-0,81	0,15
Plasma membrane calcium-transporting ATPase 4	ATP2B4	-0,81	0,10
Probable rRNA-processing protein EBP2	EBNA1BP2	-0,81	0,46
Neutral amino acid transporter A	SLC1A4	-0,81	0,14
rRNA 2-O-methyltransferase fibrillarin	FBL	-0,81	0,03
Rap1 GTPase-GDP dissociation stimulator 1	RAP1GDS1	-0,81	0,17
HCLS1-associated protein X-1	HAX1	-0,81	0,13

Leucine-rich repeat flightless-interacting protein 1	LRRFIP1	-0,81	0,01
ATP-binding cassette sub-family B member 7, mitochondrial	ABCB7	-0,81	0,08
Mitochondrial-processing peptidase subunit alpha	PMPCA	-0,80	0,01
Double-strand-break repair protein rad21 homolog	RAD21	-0,80	0,09
Sn1-specific diacylglycerol lipase beta	DAGLB	-0,80	0,25
Carboxypeptidase D	CPD	-0,80	0,23
TraB domain-containing protein	TRABD	-0,80	0,01
60S ribosomal export protein NMD3	NMD3	-0,80	0,31
Nucleoporin NUP53	NUP35	-0,79	N.D.
Protein SON	SON	-0,79	0,07
Methionine aminopeptidase 1	METAP1	-0,79	0,02
Unconventional myosin-Ig	MYO1G	-0,79	0,06
Ferritin heavy chain;Ferritin heavy chain, N-terminally processed	FTH1	-0,79	0,04
Nuclear pore complex protein Nup155	NUP155	-0,79	0,04
Plastin-2	LCP1	-0,79	0,02
Ubiquinol-cytochrome-c reductase complex assembly factor 2	UQCC2	-0,79	N.D.
Importin subunit alpha-4	KPNA3	-0,78	0,05
39S ribosomal protein L38, mitochondrial	MRPL38	-0,78	0,18
Mitotic spindle assembly checkpoint protein MAD2A	MAD2L1	-0,78	0,35
RNA exonuclease 4	REXO4	-0,77	N.D.
Inositol 1,4,5-trisphosphate receptor type 1	ITPR1	-0,77	0,12
Egl nine homolog 1	EGLN1	-0,77	N.D.
Unconventional myosin-XVIIIa	MYO18A	-0,77	0,03
Mitochondrial-processing peptidase subunit beta	PMPCB	-0,77	0,22
NADH dehydrogenase [ubiquinone] iron-sulfur protein 2, mitochondrial	NDUFS2	-0,76	0,09
Protein FAM136A	FAM136A	-0,76	0,10
N-alpha-acetyltransferase 10	NAA10	-0,76	0,05
Core histone macro-H2A.1	H2AFY	-0,76	0,00
Brain acid soluble protein 1	BASP1	-0,75	0,06
Transmembrane protein 205	TMEM205	-0,75	0,05
Mitochondrial import inner membrane translocase subunit TIM14	DNAJC19	-0,75	0,10
Exportin-4	XPO4	-0,74	0,05
Sister chromatid cohesion protein PDS5 homolog B	PDS5B	-0,74	0,03
Histidine triad nucleotide-binding protein 3	HINT3	-0,74	N.D.
Long-chain-fatty-acid--CoA ligase 1	ACSL1	-0,74	0,16
39S ribosomal protein L14, mitochondrial	MRPL14	-0,73	0,12
Cyclin-dependent kinase 13	CDK13	-0,73	N.D.
NADH dehydrogenase [ubiquinone] iron-sulfur protein 3, mitochondrial	NDUFS3	-0,73	0,05
Choline transporter-like protein 1	SLC44A1	-0,72	N.D.
Tumor necrosis factor receptor type 1-associated DEATH domain protein	TRADD	-0,72	N.D.
F-box-like/WD repeat-containing protein TBL1XR1	TBL1XR1	-0,72	0,10
Protein lunapark	LNP	-0,72	0,00
Chloride intracellular channel protein 4	CLIC4	-0,72	0,05
CCAAT/enhancer-binding protein zeta	CEBPZ	-0,72	0,01
Docking protein 3	DOK3	-0,71	0,37
Vacuole membrane protein 1	VMP1	-0,71	N.D.
Medium-chain specific acyl-CoA dehydrogenase, mitochondrial	ACADM	-0,71	0,06
DnaJ homolog subfamily C member 3	DNAJC3	-0,71	0,05
Syntaxin-12	STX12	-0,71	0,09
Toll-interacting protein	TOLLIP	-0,71	0,15
Ubiquitin-associated domain-containing protein 2	UBAC2	-0,71	0,02
NADH dehydrogenase [ubiquinone] 1 beta subcomplex subunit 9	NDUFB9	-0,71	N.D.
Translocation protein SEC62	SEC62	-0,71	0,06
Cytochrome c oxidase assembly protein COX14	COX14	-0,70	0,26
Ubiquitin carboxyl-terminal hydrolase 48	USP48	-0,70	0,38
Polycomb protein EED	EED	-0,70	0,16
Pre-B-cell leukemia transcription factor-interacting protein 1	PBXIP1	-0,70	0,18
39S ribosomal protein L28, mitochondrial	MRPL28	-0,70	0,09
NADH dehydrogenase [ubiquinone] 1 alpha subcomplex subunit 5	NDUFA5	-0,70	0,09
UBX domain-containing protein 7	UBXN7	-0,70	0,17
Protein scribble homolog	SCRIB	-0,70	0,19
Cytochrome b-245 light chain	CYBA	-0,70	0,09
Large neutral amino acids transporter small subunit 1	SLC7A5	-0,69	0,05
Protein kinase C iota type	PRKCI	-0,69	0,03
Acid ceramidase;Acid ceramidase subunit alpha;Acid ceramidase subunit beta	ASAH1	-0,69	0,06
GTP-binding protein 10	GTPBP10	-0,69	0,38
39S ribosomal protein L43, mitochondrial	MRPL43	-0,69	0,18
Protein arginine N-methyltransferase 3	PRMT3	-0,69	0,66
Alanine--tRNA ligase, mitochondrial	AARS2	-0,68	0,10
Transmembrane protein 192	TMEM192	-0,68	0,06
Nucleolar pre-ribosomal-associated protein 1	URB1	-0,68	0,09
39S ribosomal protein L47, mitochondrial	MRPL47	-0,68	0,07
Ras-related protein Rab-24	RAB24	-0,67	N.D.
BCL2/adenovirus E1B 19 kDa protein-interacting protein 2;Caytaxin	BNIP2;ATCAY	-0,67	0,16
Serpin B10	SERPINB10	-0,67	0,07
39S ribosomal protein L45, mitochondrial	MRPL45	-0,66	0,06
Cathepsin B	CTSB	-0,66	0,17
Fatty aldehyde dehydrogenase	ALDH3A2	-0,66	0,05
Sorting nexin-27	SNX27	-0,66	0,31
Ribosomal RNA processing protein 1 homolog A	RRP1	-0,66	0,18

Macrophage-capping protein	CAPG	-0,66	0,04
S-formylglutathione hydrolase	ESD	-0,65	0,03
Myeloperoxidas	MPO	-0,65	0,02
Tyrosine--tRNA ligase, mitochondrial	YARS2	-0,65	0,06
Probable phospholipid-transporting ATPase IF	ATP11B	-0,65	0,38
NADH dehydrogenase [ubiquinone] iron-sulfur protein 8, mitochondrial	NDUFS8	-0,65	0,10
Ribosome production factor 2 homolog	RPF2	-0,65	0,10
Protein SDA1 homolog	SDAD1	-0,65	0,31
Centriolin	CNTRL	-0,65	N.D.
Nucleoporin Nup37	NUP37	-0,65	0,34
Nuclear pore complex protein Nup133	NUP133	-0,65	0,17
Diacylglycerol kinase zeta	DGKZ	-0,65	0,43
Retinol dehydrogenase 13	RDH13	-0,65	0,22
Protein CCSMST1	CCSMST1	-0,65	0,23
Diphosphoinositol polyphosphate phosphohydrolase 1	NUDT3	-0,65	0,05
Oligosaccharyltransferase complex subunit OSTC	OSTC	-0,64	0,15
39S ribosomal protein L16, mitochondrial	MRPL16	-0,64	0,06
Zinc finger CCHC domain-containing protein 8	ZCCHC8	-0,64	0,07
Nucleoside diphosphate-linked moiety X motif 19, mitochondrial	NUDT19	-0,64	0,45
39S ribosomal protein L15, mitochondrial	MRPL15	-0,64	0,10
15 kDa selenoprotein	42248	-0,64	0,00
39S ribosomal protein L50, mitochondrial	MRPL50	-0,64	0,21
39S ribosomal protein L41, mitochondrial	MRPL41	-0,64	0,06
39S ribosomal protein L49, mitochondrial	MRPL49	-0,64	0,08
Nucleobindin-2;Nesfatin-1	NUCB2	-0,64	0,15
H/ACA ribonucleoprotein complex subunit 1	GAR1	-0,64	0,11
Histone H1.4;Histone H1.3	HIST1H1E;HIST1H1D	-0,64	0,12
Endoplasmic reticulum aminopeptidase 2	ERAP2	-0,64	N.D.
Transmembrane 9 superfamily member 2	TM9SF2	-0,63	0,07
Pleckstrin	PLEK	-0,63	0,10
ADP-ribosylation factor-like protein 8B	ARL8B	-0,63	0,04
Isoleucine--tRNA ligase, cytoplasmic	IARS	-0,63	0,03
Protein lin-7 homolog A	LIN7A	-0,63	N.D.
Mitochondrial import inner membrane translocase subunit TIM16	PAM16	-0,63	0,05
RNA-binding protein 33	RBM33	-0,63	N.D.
Glutamine synthetase	GLUL	-0,63	0,10
Nucleolar protein 9	NOP9	-0,62	0,21
Importin-5	IPO5	-0,62	0,05
Cytochrome b	MT-CYB	-0,62	N.D.
Alpha-1,6-mannosyl-glycoprotein 2-beta-N-acetylglucosaminyltransferase	MGAT2	-0,62	0,91
Aconitate hydratase, mitochondrial	ACO2	-0,62	0,07
Eukaryotic translation initiation factor 4 gamma 2	EIF4G2	-0,62	0,08
Translationally-controlled tumor protein	TPT1	-0,62	0,03
Mitochondrial fission process protein 1	MTFP1	-0,62	0,13
Multidrug resistance-associated protein 4	ABCC4	-0,61	0,18
NADH dehydrogenase [ubiquinone] 1 alpha subcomplex subunit 9, mitochondrial	NDUFA9	-0,61	0,04
Ras GTPase-activating protein-binding protein 2	G3BP2	-0,61	0,19
39S ribosomal protein L24, mitochondrial	MRPL24	-0,61	N.D.
39S ribosomal protein L1, mitochondrial	MRPL1	-0,61	0,18
39S ribosomal protein L4, mitochondrial	MRPL4	-0,61	0,03
Ras-related protein Rab-7b	RAB7B	-0,61	0,15
Protein VPRBP	VPRBP	-0,61	N.D.
39S ribosomal protein L19, mitochondrial	MRPL19	-0,61	0,05
39S ribosomal protein L27, mitochondrial	MRPL27	-0,61	0,07
Uncharacterized protein C2orf47, mitochondrial	C2orf47	-0,61	0,28
Presenilins-associated rhomboid-like protein, mitochondrial;P-beta	PARL	-0,61	0,10
39S ribosomal protein L22, mitochondrial	MRPL22	-0,60	0,23
Structural maintenance of chromosomes protein 3	SMC3	-0,60	0,07
THUMP domain-containing protein 1	THUMPD1	-0,60	0,06
DnaJ homolog subfamily C member 11	DNAJC11	-0,60	0,08
Pentatricopeptide repeat domain-containing protein 3, mitochondrial	PTCD3	-0,60	0,09
Transmembrane protein 11, mitochondrial	TMEM11	-0,60	0,28
ATP synthase mitochondrial F1 complex assembly factor 2	ATPAF2	-0,60	N.D.
SWI/SNF-related matrix-associated actin-dependent regulator of chromatin subfamily A	SMARCAD1	-0,60	0,24
Tyrosine-protein phosphatase non-receptor type 7	PTPN7	-0,60	0,23
Dolichyl-phosphate beta-glucosyltransferase	ALG5	-0,60	0,06
39S ribosomal protein L17, mitochondrial	MRPL17	-0,60	0,03
Platelet-activating factor acetylhydrolase IB subunit gamma	PAFAH1B3	-0,60	0,04
ADP-ribosylation factor GTPase-activating protein 2	ARFGAP2	-0,60	0,27
Monocarboxylate transporter 1	SLC16A1	-0,60	0,07

E3 SUMO-protein ligase RanBP2	RANBP2	-0,60	0,05
Ragulator complex protein LAMTOR3	LAMTOR3	-0,60	0,06
39S ribosomal protein L33, mitochondrial	MRPL33	-0,60	0,17
NHL repeat-containing protein 2	NHLRC2	-0,59	0,05
Glucosamine-6-phosphate isomerase 1	GNPDA1	-0,59	0,03
Very long-chain specific acyl-CoA dehydrogenase, mitochondrial	ACADVL	-0,59	0,03
39S ribosomal protein L9, mitochondrial	MRPL9	-0,59	0,14
Protein transport protein Sec31A	SEC31A	-0,59	0,07
Unhealthy ribosome biogenesis protein 2 homolog	URB2	-0,59	N.D.
Transcription factor ETV6	ETV6	-0,59	0,25
Trifunctional enzyme subunit beta, mitochondrial;3-ketoacyl-CoA thiolase	HADHB	-0,59	0,04
Neurolysin, mitochondrial	NLN	-0,59	0,13
HIV Tat-specific factor 1	HTATSF1	-0,59	0,04

Table 8. Downregulated proteins in HL-60 AraC compared to HL-60 P cells under normoxia. Proteomic profiling (SILAC) data were used. Significantly downregulated proteins were calculated using the fold difference threshold of 0.7 (log_2 fold change=-0.58). Mean±SD for n=2 replicates. Non-detected (N.D.) means less than 2 replicates detected for one protein measured.

UPREGULATED PROTEINS IN HL-60 Dox VS. HL-60 P			
Protein names	**Gene names**	**Mean Log_2 fold change**	**SD Log_2 fold change**
Carbonic anhydrase 2	CA2	3.21	0.05
Neutrophil defensin 3 and 1	DEFA3;DEFA1	2.98	0.11
Arachidonate 5-lipoxygenase-activating protein	ALOX5AP	1.91	N.D.
Vimentin	VIM	1.60	0.13
Cathepsin B	CTSB	1.47	0.41
Constitutive coactivator of peroxisome proliferator-activated receptor gamma	FAM120B	1.39	N.D.
CapZ-interacting protein	RCSD1	1.38	N.D.
Target of Myb protein 1	TOM1	1.29	N.D.
Kinetochore protein Nuf2	NUF2	1.22	N.D.
F-box only protein 22	FBXO22	1.17	N.D.
Transcriptional activator protein Pur-beta	PURB	1.11	N.D.
Heat shock 70 kDa protein 14	HSPA14	1.07	N.D.
Alpha-adducin	ADD1	1.03	0.11
Beta-glucuronidase	GUSB	1.02	0.10
Brefeldin A-inhibited guanine nucleotide-exchange protein 1	ARFGEF1	1.01	0.32
C-type mannose receptor 2	MRC2	1.00	0.09
Procollagen-lysine,2-oxoglutarate 5-dioxygenase 1	PLOD1	0.98	0.31
MORC family CW-type zinc finger protein 2	MORC2	0.97	N.D.
Sterol O-acyltransferase 1	SOAT1	0.93	N.D.
Gamma-tubulin complex component 3	TUBGCP3	0.93	N.D.
UDP-N-acetylglucosamine--peptide N-acetylglucosaminyltransferase	OGT	0.92	0.06
Protein S100-A8;Protein S100-A8, N-terminally processed	S100A8	0.92	0.01
ATP-dependent zinc metalloprotease YME1L1	YME1L1	0.91	N.D.
Integrin beta-2	ITGB2	0.90	0.16
Endoplasmic reticulum aminopeptidase 2	ERAP2	0.89	N.D.
Histone H1.5	HIST1H1B	0.89	N.D.
Granulins	GRN	0.88	0.11
Thiosulfate sulfurtransferase	TST	0.87	0.19
Ubiquilin-1	UBQLN1	0.84	0.22
Cathepsin D	CTSD	0.84	0.02
RAS guanyl-releasing protein 2	RASGRP2	0.83	0.24
Delta(3,5)-Delta(2,4)-dienoyl-CoA isomerase, mitochondrial	ECH1	0.81	0.07
SPRY domain-containing protein 4	SPRYD4	0.80	0.19
Ubiquitin-like protein ISG15	ISG15	0.79	0.26
Beta-hexosaminidase subunit beta	HEXB	0.78	0.38
Mannosyl-oligosaccharide 1,2-alpha-mannosidase IB	MAN1A2	0.77	N.D.
Rapamycin-insensitive companion of mTOR	RICTOR	0.77	N.D.
Vacuolar protein sorting-associated protein 51 homolog	VPS51	0.77	0.48
N6-adenosine-methyltransferase 70 kDa subunit	METTL3	0.75	N.D.
LEM domain-containing protein 2	LEMD2	0.75	N.D.
All-trans-retinol 13,14-reductase	RETSAT	0.75	0.18
Melanoma-associated antigen D2	MAGED2	0.72	N.D.
RNA polymerase II-associated protein 1	RPAP1	0.71	0.12
Tetratricopeptide repeat protein 39C	TTC39C	0.70	0.45
Pyrroline-5-carboxylate reductase 1, mitochondrial	PYCR1	0.70	0.05
Vacuolar ATPase assembly integral membrane protein VMA21	VMA21	0.70	N.D.
Uncharacterized protein KIAA0930	KIAA0930	0.70	N.D.
Protein dopey-2	DOPEY2	0.69	0.21
AP-2 complex subunit alpha-2	AP2A2	0.69	0.18
Proteasome activator complex subunit 1	PSME1	0.69	0.04
C-type lectin domain family 11 member A	CLEC11A	0.69	0.26
Putative phospholipase B-like 2	PLBD2	0.69	0.22
Squalene synthase	FDFT1	0.68	0.02
Proteasome activator complex subunit 2	PSME2	0.68	0.07
Disco-interacting protein 2 homolog B	DIP2B	0.68	0.03
Tyrosine-protein phosphatase non-receptor type 9	PTPN9	0.67	0.27
Receptor-type tyrosine-protein phosphatase C	PTPRC	0.67	0.01
Serglycin	SRGN	0.67	N.D.
Dynein assembly factor 5, axonemal	DNAAF5	0.67	0.02
WASH complex subunit CCDC53	CCDC53	0.66	N.D.
Leukocyte-associated immunoglobulin-like receptor 1	LAIR1	0.66	0.00
Leucine-rich repeat-containing protein 57	LRRC57	0.66	0.20
Fumarylacetoacetate hydrolase domain-containing protein 2A and B	FAHD2A;FAHD2B	0.66	N.D.
HLA class I histocompatibility antigen, B-58 alpha chain	HLA-B	0.65	0.11
Conserved oligomeric Golgi complex subunit 7	COG7	0.65	0.46
Protein diaphanous homolog 2	DIAPH2	0.65	0.07
Calumenin	CALU	0.65	0.33
Structural maintenance of chromosomes protein 5	SMC5	0.64	N.D.
Transmembrane protein 189	TMEM189	0.64	N.D.
Metallo-beta-lactamase domain-containing protein 2	MBLAC2	0.64	N.D.

N-acetyltransferase 14	NAT14	0,64	0,06
Protein FAM210A	FAM210A	0,63	N.D.
Translational activator GCN1	GCN1L1	0,63	0,16
Cysteine and glycine-rich protein 1	CSRP1	0,63	0,04
Isocitrate dehydrogenase [NADP] cytoplasmic	IDH1	0,62	0,12
Coatomer subunit gamma-2	COPG2	0,62	0,09
Maestro heat-like repeat-containing protein family member 1	MROH1	0,62	N.D.
Coronin-1B	CORO1B	0,61	0,15
Cytochrome b-245 light chain	CYBA	0,61	0,21
WASH complex subunit strumpellin	KIAA0196	0,61	0,24
Beta-hexosaminidase subunit alpha	HEXA	0,61	0,11
Dolichol-phosphate mannosyltransferase subunit 1	DPM1	0,61	0,03
Peptidyl-prolyl cis-trans isomerase FKBP8	FKBP8	0,60	0,15
Fatty acid desaturase 2	FADS2	0,60	0,03
Molybdate-anion transporter	MFSD5	0,60	N.D.
Golgi SNAP receptor complex member 2	GOSR2	0,60	N.D.
Golgi apparatus protein 1	GLG1	0,60	0,06
Coiled-coil-helix-coiled-coil-helix domain-containing protein 2	CHCHD2;CHCHD2P9	0,59	0,05
Very long-chain specific acyl-CoA dehydrogenase, mitochondrial	ACADVL	0,59	0,03
DnaJ homolog subfamily C member 10	DNAJC10	0,59	0,08
Fatty acid desaturase 1	FADS1	0,59	0,14
RELT-like protein 1	RELL1	0,59	N.D.

Table 9. Upregulated proteins in HL-60 Dox compared to HL-60 P cells under normoxia. Proteomic profiling (SILAC) data were used. Significantly upregulated proteins were calculated using the fold difference threshold of 1.5 (log_2 fold change=0.58). Mean±SD for n=2 replicates. Non-detected (N.D.) means less than 2 replicates detected for one protein measured.

DOWNREGULATED PROTEINS IN HL-60 Dox VS. HL-60 P			
Protein names	**Gene names**	**Mean Log_2 fold change**	**SD Log_2 fold change**
DNA topoisomerase 2-beta	TOP2B	-1.35	0.65
V-type proton ATPase 116 kDa subunit a isoform 1	ATP6V0A1	-1.33	N.D.
Probable cysteine--tRNA ligase, mitochondrial	CARS2	-1.29	N.D.
RNA polymerase-associated protein LEO1	LEO1	-1.28	N.D.
Kinesin-like protein KIF15	KIF15	-1.27	0.03
Bridging integrator 2	BIN2	-1.26	0.48
Cathepsin G	CTSG	-1.24	0.10
Sodium bicarbonate cotransporter 3	SLC4A7	-1.12	0.06
Succinate-semialdehyde dehydrogenase, mitochondrial	ALDH5A1	-1.09	0.30
Leucine zipper transcription factor-like protein 1	LZTFL1	-1.07	0.23
DNA topoisomerase 2-alpha	TOP2A	-1.07	N.D.
Reticulon-4	RTN4	-1.07	0.02
CCA tRNA nucleotidyltransferase 1, mitochondrial	TRNT1	-1.05	0.25
MAP kinase-activated protein kinase 3	MAPKAPK3	-1.04	0.34
Glutamine synthetase	GLUL	-1.03	0.07
Glycerol-3-phosphate dehydrogenase 1-like protein	GPD1L	-1.02	0.08
Ras-related protein Rab-3D	RAB3D	-1.01	N.D.
Microtubule-associated protein 4	MAP4	-0.97	0.06
Cytochrome b561 domain-containing protein 2	CYB561D2	-0.96	0.05
Coiled-coil domain-containing protein 12	CCDC12	-0.94	0.38
Phosphatidylinositide phosphatase SAC1	SACM1L	-0.93	0.09
Inosine-5-monophosphate dehydrogenase 2	IMPDH2	-0.91	0.05
Ubiquitin-conjugating enzyme E2 T	UBE2T	-0.90	N.D.
Centriolin	CNTRL	-0.86	N.D.
Programmed cell death 6-interacting protein	PDCD6IP	-0.86	0.03
Cytochrome b	MT-CYB	-0.86	N.D.
Protein VPRBP	VPRBP	-0.85	N.D.
Erythrocyte band 7 integral membrane protein	STOM	-0.85	0.02
tRNA-splicing endonuclease subunit Sen34	TSEN34	-0.84	N.D.
Dolichyl-diphosphooligosaccharide--protein glycosyltransferase subunit STT3B	STT3B	-0.84	0.06
Twinfilin-2	TWF2	-0.84	0.04
Protein RFT1 homolog	RFT1	-0.82	0.10
Peptide-N(4)-(N-acetyl-beta-glucosaminyl)asparagine amidase	NGLY1	-0.82	0.15
Myosin-14	MYH14	-0.82	0.07
NADH-ubiquinone oxidoreductase chain 5	MT-ND5	-0.82	0.19
Beta-arrestin-1	ARRB1	-0.79	0.20
Serine/threonine-protein kinase OSR1	OXSR1	-0.79	0.03
Bone marrow proteoglycan;Eosinophil granule major basic protein	PRG2	-0.78	0.08
Aminopeptidase N	ANPEP	-0.78	0.04
Protein kinase C delta type	PRKCD	-0.77	0.19
NADH dehydrogenase [ubiquinone] 1 beta subcomplex subunit 9	NDUFB9	-0.76	N.D.
NADH-ubiquinone oxidoreductase chain 4	MT-ND4	-0.76	0.06
Myosin-9	MYH9	-0.75	0.02
Antigen KI-67	MKI67	-0.75	0.12
Scaffold attachment factor B2	SAFB2	-0.74	0.10
Guanine nucleotide-binding protein-like 3	GNL3	-0.73	0.06
Mannose-1-phosphate guanyltransferase beta	GMPPB	-0.73	0.21
Azurocidin	AZU1	-0.73	0.80
Filamin-B	FLNB	-0.72	0.26
Acylamino-acid-releasing enzyme	APEH	-0.72	0.08
Guanine nucleotide-binding protein G(i) subunit alpha-2	GNAI2	-0.71	0.04
Protein jagged-1	JAG1	-0.71	N.D.
Serine/threonine-protein kinase tousled-like 1	TLK1	-0.71	N.D.
Inositol 1,4,5-trisphosphate receptor type 1	ITPR1	-0.71	0.12
NEDD8 ultimate buster 1	NUB1	-0.71	N.D.
Voltage-dependent anion-selective channel protein 3	VDAC3	-0.71	0.09
Serine/threonine-protein phosphatase 2A 56 kDa regulatory subunit alpha isoform	PPP2R5A	-0.71	N.D.
THUMP domain-containing protein 3	THUMPD3	-0.70	0.56
Magnesium transporter protein 1	MAGT1	-0.70	0.09
Transketolase	TKT	-0.69	0.02
Cytoplasmic dynein 1 light intermediate chain 1	DYNC1LI1	-0.68	0.14
Cytochrome c oxidase copper chaperone	COX17	-0.68	N.D.
NADH-ubiquinone oxidoreductase 75 kDa subunit, mitochondrial	NDUFS1	-0.67	N.D.
Nucleoside diphosphate-linked moiety X motif 19, mitochondrial	NUDT19	-0.67	0.67
NADH dehydrogenase [ubiquinone] 1 alpha subcomplex subunit 11	NDUFA11	-0.66	N.D.
SWI/SNF complex subunit SMARCC1	SMARCC1	-0.65	0.03
AT-rich interactive domain-containing protein 3A	ARID3A	-0.65	0.14
Golgin subfamily A member 4	GOLGA4	-0.65	0.11
ADP-ribosylation factor-like protein 8B	ARL8B	-0.64	0.04
Protein CCSMST1	CCSMST1	-0.64	0.33

Beta-galactosidase	GLB1	-0,64	0,13
Aspartate--tRNA ligase, mitochondrial	DARS2	-0,63	0,08
Voltage-dependent anion-selective channel protein 2	VDAC2	-0,63	0,08
Ubiquitin carboxyl-terminal hydrolase 48	USP48	-0,63	0,38
Ras-related protein Rab-7b	RAB7B	-0,63	0,11
DNA fragmentation factor subunit alpha	DFFA	-0,63	0,19
PX domain-containing protein kinase-like protein	PXK	-0,63	0,10
Cytoplasmic FMR1-interacting protein 2	CYFIP2	-0,63	0,09
HIG1 domain family member 1A, mitochondrial	HIGD1A	-0,63	N.D.
Nuclear pore membrane glycoprotein 210	NUP210	-0,63	0,01
Pre-mRNA-processing factor 40 homolog A	PRPF40A	-0,63	0,02
Recombining binding protein suppressor of hairless	RBPJ	-0,63	0,21
Pyruvate dehydrogenase E1 component subunit beta, mitochondrial	PDHB	-0,63	0,05
Cystatin-A	CSTA	-0,62	0,19
Very long-chain acyl-CoA synthetase	SLC27A2	-0,62	0,05
Tubulin alpha-4A chain	TUBA4A	-0,62	0,16
Guanine nucleotide-binding protein G(I)/G(S)/G(O) subunit gamma-10	GNG10	-0,62	N.D.
Peptidyl-prolyl cis-trans isomerase FKBP5	FKBP5	-0,61	0,02
Serpin B10	SERPINB10	-0,61	0,05
Cytochrome c oxidase assembly factor 7	COA7	-0,61	0,12
Guanine nucleotide-binding protein subunit beta-4	GNB4	-0,61	0,32
Transmembrane protein 50A	TMEM50A	-0,60	0,09
WD repeat-containing protein 18	WDR18	-0,60	N.D.
NADH dehydrogenase [ubiquinone] 1 subunit C2	NDUFC2	-0,59	0,11
DCC-interacting protein 13-alpha	APPL1	-0,59	0,10

Table 10. Downregulated proteins in HL-60 Dox compared to HL-60 P cells under normoxia. Proteomic profiling (SILAC) data were used. Significantly downregulated proteins were calculated using the fold difference threshold of 0.7 (log_2 fold change=-0.58). Mean±SD for n=2 replicates. Non-detected (N.D.) means less than 2 replicates detected for one protein measured.

EXTRACELLULAR FLUXES NORMOXIA								
	THP-1 P		THP-1 AraC		THP-1 Dox		pvalue	pvalue
	Kpc (nmol*millioncell-1*h-1)							
	Mean	SD	Mean	SD	Mean	SD	(AraC vs. P)	(Dox vs. P)
Amino acids								
Ala	2.29	1.23	3.95	1.17	3.50	0.42	0.230	0.184
Arg	D	D	D	D	D	D	D	D
Asn	-0.84	0.53	-2.62	0.91	-1.14	0.27	0.042	0.441
Asp	0.21	0.49	1.52	1.44	0.42	0.78	0.251	0.716
Cit	-0.03	0.04	-0.07	0.17	0.01	0.01	0.705	0.218
Gln	-24.37	6.09	-10.14	7.75	-20.64	1.28	0.136	0.952
Glu	11.29	4.51	13.31	6.12	10.67	1.97	0.363	0.554
Gly	-0.12	0.13	8.35	1.35	0.01	0.58	0.013	0.481
His	-0.57	0.13	-0.31	0.77	-0.65	0.23	0.622	0.629
Ile	-2.91	0.79	-3.05	0.72	-2.14	0.25	0.825	0.225
Leu	-3.97	0.63	-5.41	1.33	-3.57	0.24	0.194	0.389
Lys	-2.36	0.33	-3.66	0.32	-2.82	0.17	0.008	0.123
Met	-0.83	0.17	-1.61	0.08	-0.78	0.04	0.006	0.627
Orn	1.27	0.61	4.62	1.29	1.27	0.32	0.029	0.992
Phe	-0.93	0.14	-1.53	0.22	-1.00	0.06	0.023	0.473
Pro	0.21	0.39	1.80	1.70	-0.63	0.12	0.191	0.023
Ser	-4.34	0.47	-8.44	0.52	-2.58	0.18	0.001	0.003
Thr	-1.32	0.46	-2.44	0.60	-1.42	0.09	0.069	0.762
Trp	-0.35	0.08	-0.52	0.15	-0.37	0.02	0.170	0.717
Tyr	-1.09	0.21	-0.93	0.18	-0.83	0.11	0.356	0.147
Val	-2.16	0.51	-3.25	0.80	-2.01	0.13	0.130	0.663
Polyamines								
Putrescine	1E-03	7E-04	1E-03	1E-03	7E-05	3E-05	0.642	0.147
Spermidine	3E-04	2E-04	4E-04	4E-04	5E-05	5E-05	0.733	0.119
Spermine	D	D	D	D	D	D	D	D

Table 11. Extracellular fluxes result of THP-1 cell line under normoxia. Non-detected amino acids or polyamines or amino acids and polyamines whose replicates were not reproducible are named as discarded (D).

EXTRACELLULAR FLUXES NORMOXIA								
	HL-60 P		HL-60 AraC		HL-60 Dox		pvalue	pvalue
	Kpc (nmol*millioncell-1*h-1)							
	Mean	SD	Mean	SD	Mean	SD	(AraC vs. P)	(Dox vs. P)
Amino acids								
Ala	7.60	1.28	10.04	4.41	2.44	0.22	0.442	0.017
Arg	D	D	D	D	D	D	D	D
Asn	0.41	0.90	-1.39	3.19	-0.47	0.39	0.433	0.226
Asp	0.26	0.27	-0.25	0.53	-0.05	0.23	0.236	0.216
Cit	-0.02	0.01	0.08	0.12	0.00	0.07	0.296	0.687
Gln	-12.51	1.42	-16.88	14.71	-8.26	1.17	0.658	0.017
Glu	3.76	0.85	3.98	1.27	1.23	1.02	0.818	0.032
Gly	0.33	0.43	0.93	1.45	0.86	0.08	0.556	0.164
His	-0.17	0.20	0.06	0.53	0.04	0.12	0.530	0.194
Ile	-0.80	0.12	-2.37	1.69	-0.53	0.04	0.183	0.021
Leu	-1.69	0.12	-2.38	0.38	-1.18	0.02	0.214	0.018
Lys	-1.10	0.08	-2.26	1.83	-1.16	0.24	0.387	0.736
Met	-0.55	0.06	-0.96	0.64	-0.39	0.02	0.385	0.028
Orn	2.22	0.20	2.11	1.04	0.80	0.48	0.877	0.022
Phe	-0.53	0.05	-1.06	0.77	-0.30	0.02	0.357	0.008
Pro	2.35	0.37	2.11	1.31	1.19	0.27	0.781	0.014
Ser	-2.73	0.31	-4.40	3.39	-2.49	0.08	0.484	0.319
Thr	-0.13	0.26	-1.13	1.30	-0.24	0.20	0.310	0.564
Trp	-0.13	0.00	-0.23	0.02	-0.11	0.03	0.009	0.292
Tyr	-0.30	0.20	-1.26	0.81	-0.12	0.12	0.169	0.262
Val	-0.97	0.14	-1.50	0.86	-0.73	0.03	0.395	0.098
Polyamines								
Putrescine	6E-04	4E-04	-5E-04	8E-04	1E-03	2E-04	0.020	0.010
Spermidine	1E-04	5E-05	2E-04	2E-04	1E-04	7E-05	0.696	0.727
Spermine	D	D	D	D	D	D	D	D

Table 12. Extracellular fluxes result of HL-60 cell line under normoxia. Non-detected amino acids or polyamines or amino acids and polyamines whose replicates were not reproducible are named as discarded (D).

EXTRACELLULAR FLUXES HYPOXIA								
	THP-1 P		THP-1 AraC		THP-1 Dox		pvalue	pvalue
	Kpc (nmol*millioncell-1*h-1)							
	Mean	SD	Mean	SD	Mean	SD	(AraC vs. P)	(Dox vs. P)
Amino acids								
Ala	-2.04	0.64	3.10	0.13	2.44	0.29	0.001	0.033
Arg	D	D	D	D	D	D	D	D
Asn	-0.29	2.64	-1.14	1.49	1.37	1.30	0.659	0.401
Asp	-0.14	2.51	-0.23	1.24	2.65	1.41	0.959	0.188
Cit	-0.10	0.03	-0.03	0.11	0.05	0.15	0.423	0.224
Gln	-3.59	10.99	-8.31	8.85	-15.06	14.83	0.595	0.347
Glu	0.36	5.33	5.81	1.09	8.58	3.41	0.215	0.099
Gly	3.33	1.95	1.42	1.27	0.29	0.49	0.239	0.106
His	-0.72	0.64	-0.76	0.37	-0.84	0.80	0.919	0.843
Ile	-0.64	0.20	-1.83	0.08	-0.45	0.25	0.004	0.464
Leu	-2.41	0.85	-3.96	0.38	-1.10	1.59	0.070	0.295
Lys	-2.41	0.90	-5.95	0.80	-0.65	1.46	0.007	0.165
Met	-0.70	0.79	-1.08	0.53	-0.16	0.54	0.530	0.393
Orn	2.31	0.05	0.01	1.91	4.18	0.20	0.096	0.002
Phe	-0.46	0.42	-1.03	0.42	-0.49	0.22	0.172	0.907
Pro	1.02	0.08	0.70	0.66	0.34	0.65	0.490	0.208
Ser	-2.37	0.10	-9.58	0.52	-1.83	0.15	0.001	0.300
Thr	0.63	2.73	-2.01	0.22	0.73	0.20	0.236	0.952
Trp	0.17	0.22	-0.21	0.10	0.04	0.15	0.076	0.443
Tyr	-0.51	0.41	0.47	0.63	-0.44	0.34	0.099	0.828
Val	-1.90	1.98	-3.13	0.04	-0.74	2.23	0.392	0.540
Polyamines								
Putrescine	6E-03	1E-03	9E-03	2E-03	-2E-03	1E-04	0.075	0.008
Spermidine	5E-03	8E-04	4E-03	1E-03	-6E-05	2E-04	0.273	0.006
Spermine	1E-03	9E-04	3E-03	8E-04	6E-05	5E-05	0.089	0.107

Table 13. Extracellular fluxes result of THP-1 cell line under hypoxia. Non-detected amino acids or polyamines or amino acids and polyamines whose replicates were not reproducible are named as discarded (D).

EXTRACELLULAR FLUXES HYPOXIA								
	HL-60 P		HL-60 AraC		HL-60 Dox		pvalue	pvalue
	Kpc (nmol*millioncell-1*h-1)							
	Mean	SD	Mean	SD	Mean	SD	(AraC vs. P)	(Dox vs. P)
Amino acids								
Ala	10.99	4.55	9.61	2.91	8.15	1.17	0.684	0.394
Arg	D	D	D	D	D	D	D	D
Asn	0.35	0.32	0.39	0.66	0.23	0.72	0.930	0.807
Asp	0.18	0.98	0.42	1.13	0.43	0.55	0.795	0.721
Cit	0.05	0.07	0.02	0.10	0.01	0.11	0.644	0.572
Gln	-13.89	8.46	-6.08	4.19	-15.64	4.42	0.250	0.772
Glu	8.24	3.94	5.46	3.85	4.68	1.01	0.433	0.255
Gly	4.35	2.71	0.75	1.24	3.11	0.54	0.134	0.512
His	0.47	0.81	-0.07	0.34	0.32	0.36	0.371	0.783
Ile	0.10	0.71	-0.38	0.69	0.08	0.26	0.452	0.969
Leu	-0.28	1.62	-1.01	1.25	-0.46	0.31	0.572	0.866
Lys	-0.42	0.85	-1.69	0.41	-1.79	0.84	0.104	0.116
Met	-0.33	0.20	-0.46	0.45	-0.30	0.21	0.680	0.877
Orn	3.13	1.98	1.85	0.57	2.10	0.81	0.381	0.471
Phe	-0.04	0.11	-0.25	0.04	-0.07	0.11	0.062	0.691
Pro	2.23	1.05	1.16	0.92	3.21	0.46	0.255	0.241
Ser	-5.20	1.98	-3.38	0.41	-4.00	0.35	0.250	0.404
Thr	0.49	0.65	-0.32	0.65	0.32	0.03	0.310	0.564
Trp	-0.02	0.10	-0.22	0.11	0.01	0.01	0.080	0.681
Tyr	-0.20	0.10	-0.27	0.34	0.17	0.35	0.752	0.204
Val	-0.25	1.23	-0.33	0.99	-0.67	0.29	0.935	0.621
Polyamines								
Putrescine	3E-03	2E-03	8E-04	1E-03	6E-03	1E-03	0.189	0.077
Spermidine	4E-03	2E-03	2E-03	4E-04	6E-03	3E-04	0.318	0.311
Spermine	2E-03	8E-04	1E-04	1E-04	7E-04	2E-04	0.065	0.154

Table 14. Extracellular fluxes result of HL-60 cell line under hypoxia. Non-detected amino acids or polyamines or amino acids and polyamines whose replicates were not reproducible are named as discarded (D).

INTRACELLULAR CONTENT NORMOXIA								
	THP-1 P		THP-1 AraC		THP-1 Dox			
	nmol/mg protein						pvalue	pvalue
	Mean	SD	Mean	SD	Mean	SD	(AraC vs. P)	(Dox vs. P)
Amino acids								
Ala	114.12	52.86	161.29	67.69	209.29	78.88	0.398	0.168
Arg	53.92	31.04	40.27	4.05	47.58	21.28	0.53	0.79
Asn	170.84	22.21	280.70	72.31	268.20	49.39	0.109	0.058
Asp	D	D	76.47	34.09	D	D	D	D
Cit	D	D	D	D	D	D	D	D
Gln	579.07	178.26	1101.74	139.17	823.74	387.39	0.018	0.398
Glu	D	D	D	D	D	D	D	D
Gly	161.48	63.38	156.86	5.45	243.99	85.06	0.93	0.31
His	26.58	17.36	20.69	10.35	16.95	6.15	0.646	0.444
Ile	55.36	18.21	86.51	23.15	57.51	24.36	0.145	0.909
Leu	71.09	24.96	95.57	17.06	78.28	46.68	0.242	0.829
Lys	16.47	12.31	11.86	7.69	7.33	3.66	0.617	0.327
Met	22.72	6.33	31.49	18.00	22.33	13.91	0.495	0.968
Orn	3.45	1.98	3.29	0.97	3.54	2.28	0.911	0.961
Phe	15.22	4.25	22.46	2.61	15.42	8.41	0.078	0.973
Pro	117.45	40.54	170.89	17.35	100.54	37.09	0.136	0.623
Ser	32.77	17.28	90.23	50.81	118.96	90.41	0.181	0.238
Thr	52.10	15.47	99.92	54.23	57.06	32.23	0.263	0.826
Trp	4.49	0.61	4.47	2.30	3.48	1.81	0.990	0.442
Tyr	29.13	5.60	42.22	10.21	30.76	5.85	0.144	0.744
Val	12.93	5.65	18.75	5.06	16.95	4.06	0.255	0.379
Polyamines								
Putrescine	3.07	2.24	2.59	2.18	2.03	1.79	0.805	0.568
Spermidine	0.06	0.05	0.08	0.07	0.08	0.09	0.629	0.885
Spermine	13.02	2.40	12.10	1.91	13.29	1.82	0.150	0.094

Table 15. Intracellular content fluxes result of THP-1 cell line under normoxia. Non-detected amino acids or polyamines or amino acids and polyamines whose replicates were not reproducible are named as discarded (D).

INTRACELLULAR CONTENT NORMOXIA								
	HL-60 P		HL-60 AraC		HL-60 Dox			
	nmol/mg protein						pvalue	pvalue
	Mean	SD	Mean	SD	Mean	SD	(AraC vs. P)	(Dox vs. P)
Amino acids								
Ala	242.41	74.08	221.33	5.61	128.98	39.32	0.671	0.100
Arg	109.52	44.48	72.68	51.03	78.11	13.04	0.40	0.35
Asn	321.55	10.16	319.60	191.36	441.34	180.38	0.988	0.369
Asp	156.61	151.15	154.95	32.98	83.16	38.51	0.99	0.49
Cit	D	D	D	D	D	D	D	D
Gln	1082.62	561.50	631.87	281.58	832.98	292.72	0.304	0.544
Glu	D	D	D	D	D	D	D	D
Gly	470.10	206.55	260.86	66.81	854.69	572.78	0.22	0.37
His	30.98	1.65	19.31	8.51	25.03	11.30	0.136	0.459
Ile	75.42	13.80	48.03	14.98	74.25	6.51	0.081	0.903
Leu	88.97	20.96	61.89	13.39	98.84	12.18	0.145	0.528
Lys	30.23	12.85	18.59	10.30	24.00	2.02	0.291	0.491
Met	27.77	3.80	12.84	6.03	33.53	2.24	0.030	0.102
Orn	7.06	7.26	4.20	1.41	5.04	3.56	0.568	0.696
Phe	25.22	5.15	11.29	2.62	18.07	1.95	0.025	0.125
Pro	433.48	48.07	386.66	42.81	460.76	55.35	0.277	0.555
Ser	140.00	39.33	171.70	109.34	106.42	51.41	0.675	0.423
Thr	80.08	36.17	56.67	22.83	65.40	14.68	0.406	0.567
Trp	3.67	1.07	2.27	0.93	4.82	1.14	0.166	0.271
Tyr	47.12	10.87	21.51	7.56	48.09	7.35	0.034	0.905
Val	30.38	3.61	14.79	3.38	25.85	10.84	0.006	0.552
Polyamines								
Putrescine	13.70	9.29	9.34	3.58	18.16	11.68	0.512	0.633
Spermidine	23.24	3.94	17.19	0.96	25.00	7.74	0.110	0.748
Spermine	12.18	6.94	8.96	2.14	12.74	6.40	0.512	0.923

Table 16. Intracellular content fluxes result of HL-60 cell line under normoxia. Non-detected amino acids or polyamines or amino acids and polyamines whose replicates were not reproducible are named as discarded (D).

INTRACELLULAR CONTENT HYPOXIA								
	THP-1 P		THP-1 AraC		THP-1 Dox			
	nmol/mg protein						pvalue	pvalue
	Mean	SD	Mean	SD	Mean	SD	(AraC vs. P)	(Dox vs. P)
Amino acids								
Ala	58.37	19.30	252.31	43.25	204.05	17.33	0.029	0.015
Arg	40.13	10.50	105.12	45.95	20.20	7.08	0.13	0.06
Asn	356.90	129.83	212.50	52.55	388.82	277.31	0.185	0.869
Asp	105.98	30.81	43.31	22.89	109.25	13.21	0.05	0.88
Cit	0.00	0.00	0.72	0.73	1.02	0.91	0.23	0.19
Gln	1587.17	414.12	1173.53	134.78	930.00	361.11	0.220	0.108
Glu	D	D	D	D	D	D	D	D
Gly	399.83	224.99	292.34	48.71	305.36	123.49	0.50	0.57
His	35.15	7.18	35.07	8.75	20.28	7.81	0.991	0.073
Ile	77.21	19.25	112.58	5.15	58.54	9.32	0.077	0.231
Leu	90.23	23.01	128.29	10.77	76.73	25.01	0.085	0.530
Lys	11.80	4.88	16.42	3.51	10.82	0.67	0.261	0.762
Met	32.99	9.12	29.55	8.85	24.67	8.13	0.664	0.305
Orn	19.01	0.62	11.43	4.87	15.77	4.82	0.112	0.364
Phe	21.56	1.45	29.14	3.48	15.78	1.74	0.048	0.012
Pro	239.33	67.93	274.90	8.33	167.65	16.62	0.461	0.204
Ser	232.19	131.09	101.53	43.31	77.38	36.95	0.220	0.170
Thr	67.33	34.98	105.53	41.85	58.26	4.82	0.294	0.699
Trp	5.54	0.23	8.71	2.34	3.73	0.88	0.143	0.061
Tyr	29.89	3.98	50.98	10.06	31.97	10.02	0.053	0.763
Val	15.16	6.01	22.94	4.17	15.38	1.11	0.148	0.955
Polyamines								
Putrescine	2.42	0.85	1.92	0.82	2.19	1.02	0.508	0.781
Spermidine	13.55	3.69	8.56	1.11	11.81	3.30	0.134	0.574
Spermine	8.09	2.95	7.45	0.84	7.95	1.01	0.748	0.943

Table 17. Intracellular content fluxes result of THP-1 cell line under hypoxia. Non-detected amino acids or polyamines or amino acids and polyamines whose replicates were not reproducible are named as discarded (D).

INTRACELLULAR CONTENT HYPOXIA								
	HL-60 P		HL-60 AraC		HL-60 Dox			
	nmol/mg protein						pvalue	pvalue
	Mean	SD	Mean	SD	Mean	SD	(AraC vs. P)	(Dox vs. P)
Amino acids								
Ala	183.11	24.54	266.89	93.70	212.04	33.39	0.208	0.293
Arg	105.56	33.00	43.00	5.19	42.57	12.31	0.03	0.04
Asn	298.84	20.37	180.68	50.80	176.72	32.63	0.020	0.005
Asp	63.65	18.72	57.30	23.61	66.53	54.79	0.73	0.94
Cit	D	D	D	D	D	D	D	D
Gln	953.89	191.90	861.80	358.34	1003.52	546.63	0.715	0.889
Glu	D	D	D	D	D	D	D	D
Gly	454.91	205.52	405.82	93.39	724.33	857.76	0.78	0.62
His	25.33	8.82	17.62	9.98	19.86	8.09	0.373	0.473
Ile	51.93	22.82	48.68	10.99	52.77	4.65	0.835	0.953
Leu	45.80	37.27	63.91	14.67	41.85	9.12	0.477	0.867
Lys	16.98	2.64	8.99	3.59	13.17	6.71	0.036	0.412
Met	17.84	4.43	17.21	8.52	18.25	4.58	0.916	0.916
Orn	6.50	0.86	6.25	3.26	6.06	2.21	0.905	0.765
Phe	12.89	2.44	12.83	1.99	11.92	5.12	0.974	0.782
Pro	203.83	137.10	226.32	44.91	240.79	44.61	0.801	0.680
Ser	65.62	41.34	143.96	82.57	68.39	21.64	0.216	0.923
Thr	49.75	8.47	83.74	32.97	44.96	6.82	0.159	0.488
Trp	3.23	0.20	4.32	1.10	4.04	1.41	0.165	0.379
Tyr	32.29	9.93	23.51	6.66	24.80	9.70	0.272	0.403
Val	29.89	17.64	20.14	5.66	20.81	11.54	0.414	0.497
Polyamines								
Putrescine	5.42	3.47	1.49	0.64	5.97	1.94	0.185	0.826
Spermidine	13.38	3.60	7.08	2.30	12.60	2.39	0.074	0.771
Spermine	8.68	2.52	5.82	0.80	7.43	1.44	0.180	0.505

Table 18. Intracellular content fluxes result of HL-60 cell line under hypoxia. Non-detected amino acids or polyamines or amino acids and polyamines whose replicates were not reproducible are named as discarded (D).

INTRACELLULAR CONTENT NORMOXIA								
	THP-1 P		THP-1 AraC		THP-1 Dox			
	nmol/mg protein						pvalue	pvalue
	Mean	SD	Mean	SD	Mean	SD	(AraC vs. P)	(Dox vs. P)
Acylcarnitines								
C0	3.404	1.416	4.004	1.610	4.404	2.364	0.654	0.571
C2	1.370	0.763	0.649	0.315	1.157	0.556	0.239	0.718
C3	0.618	0.264	0.500	0.221	0.610	0.238	0.585	0.970
C3-DC (C4-OH)	0.028	0.019	0.028	0.004	0.033	0.005	0.995	0.676
C3-OH	0.019	0.019	0.020	0.002	0.023	0.006	0.878	0.724
C3:1	0.014	0.013	0.012	0.001	0.016	0.004	0.851	0.816
C4	0.469	0.251	0.516	0.294	0.232	0.093	0.843	0.239
C4:1	0.016	0.012	0.017	0.001	0.020	0.002	0.919	0.596
C5	0.231	0.081	0.325	0.136	0.248	0.109	0.377	0.845
C5-DC (C6-OH)	0.023	0.021	0.024	0.002	0.028	0.005	0.930	0.718
C5-M-DC	0.017	0.016	0.016	0.004	0.018	0.004	0.928	0.953
C5-OH (C3-DC-M)	0.038	0.030	0.031	0.002	0.058	0.007	0.741	0.370
C5:1	0.028	0.024	0.032	0.004	0.037	0.007	0.816	0.616
C5:1-DC	0.016	0.013	0.019	0.002	0.019	0.005	0.733	0.691
C6 (C4:1-DC)	0.018	0.009	0.015	0.002	0.019	0.006	0.658	0.834
C6:1	0.011	0.009	0.012	0.001	0.015	0.002	0.866	0.523
C7-DC	0.012	0.014	0.012	0.001	0.013	0.002	0.917	0.934
C8	0.047	0.046	0.041	0.006	0.057	0.025	0.845	0.773
C9	0.011	0.009	0.011	0.002	0.013	0.003	0.963	0.691
C10	0.032	0.032	0.035	0.002	0.044	0.014	0.901	0.610
C10:1	0.037	0.038	0.038	0.003	0.049	0.010	0.976	0.652
C10:2	0.013	0.010	0.011	0.003	0.013	0.003	0.726	0.929
C12	0.031	0.026	0.030	0.003	0.045	0.014	0.989	0.466
C12-DC	0.043	0.039	0.044	0.007	0.051	0.012	0.953	0.749
C12:1	0.040	0.040	0.036	0.005	0.047	0.011	0.897	0.768
C14	0.047	0.013	0.024	0.002	0.028	0.008	0.091	0.106
C14:1	0.010	0.001	0.015	0.004	0.010	0.004	0.186	0.932
C14:1-OH	0.005	0.002	0.004	0.001	0.005	0.001	0.816	0.739
C14:2	0.004	0.004	0.004	0.000	0.005	0.001	0.913	0.849
C14:2-OH	0.003	0.002	0.003	0.001	0.003	0.000	0.796	0.978
C16	0.048	0.015	0.031	0.007	0.049	0.023	0.160	0.961
C16-OH	0.005	0.003	0.004	0.001	0.006	0.002	0.925	0.550
C16:1	0.025	0.010	0.019	0.004	0.017	0.004	0.444	0.297
C16:1-OH	0.005	0.002	0.005	0.000	0.005	0.001	0.819	0.839
C16:2	0.004	0.001	0.003	0.001	0.003	0.001	0.693	0.776
C16:2-OH	0.003	0.001	0.004	0.001	0.004	0.001	0.631	0.185
C18	0.008	0.004	0.006	0.001	0.010	0.002	0.532	0.421
C18:1	0.055	0.028	0.051	0.021	0.049	0.024	0.875	0.783
C18:1-OH	0.006	0.006	0.007	0.001	0.010	0.002	0.798	0.461
C18:2	0.014	0.006	0.012	0.002	0.009	0.002	0.690	0.235

Table 19. Intracellular content of Acylcarnitines of THP-1 cell line under normoxia. Non-detected amino acids or polyamines or amino acids and polyamines whose replicates were not reproducible are named as discarded (D).

INTRACELLULAR CONTENT NORMOXIA								
	HL-60 P		HL-60 AraC		HL-60 Dox			
	nmol/mg protein						pvalue	pvalue
	Mean	SD	Mean	SD	Mean	SD	(AraC vs. P)	(Dox vs. P)
Acylcarnitines								
C0	2.785	0.632	0.989	0.049	4.513	0.523	0.008	0.022
C2	1.355	0.148	0.616	0.022	2.136	0.137	0.001	0.003
C3	0.229	0.038	0.034	0.006	0.557	0.179	0.001	0.036
C3-DC (C4-OH)	0.056	0.008	0.037	0.016	0.055	0.016	0.140	0.916
C3-OH	0.045	0.007	0.030	0.014	0.044	0.018	0.192	0.970
C3:1	0.032	0.003	0.023	0.010	0.030	0.011	0.173	0.772
C4	2.309	0.743	0.304	0.097	2.620	0.796	0.010	0.647
C4:1	0.046	0.006	0.032	0.007	0.049	0.017	0.065	0.777
C5	0.379	0.209	0.039	0.008	0.694	0.587	0.001	0.430
C5-DC (C6-OH)	0.056	0.003	0.041	0.011	0.058	0.021	0.095	0.863
C5-M-DC	0.033	0.002	0.030	0.004	0.039	0.012	0.254	0.459
C5-OH (C3-DC-M)	0.066	0.013	0.045	0.020	0.078	0.032	0.200	0.567
C5:1	0.062	0.004	0.054	0.013	0.075	0.029	0.348	0.497
C5:1-DC	0.039	0.003	0.029	0.009	0.036	0.015	0.154	0.749
C6 (C4:1-DC)	0.037	0.005	0.028	0.011	0.043	0.012	0.274	0.481
C6:1	0.032	0.007	0.022	0.002	0.033	0.014	0.074	0.925
C7-DC	0.030	0.003	0.022	0.004	0.029	0.012	0.030	0.876
C8	0.108	0.010	0.086	0.019	0.117	0.042	0.138	0.732
C9	0.027	0.003	0.021	0.007	0.027	0.013	0.226	0.966
C10	0.076	0.003	0.066	0.012	0.087	0.036	0.205	0.629
C10:1	0.098	0.002	0.080	0.011	0.120	0.060	0.050	0.563
C10:2	0.038	0.007	0.034	0.010	0.044	0.017	0.559	0.654
C12	0.078	0.002	0.066	0.009	0.107	0.044	0.084	0.326
C12-DC	0.111	0.013	0.094	0.013	0.140	0.056	0.172	0.427
C12:1	0.106	0.005	0.088	0.014	0.140	0.067	0.101	0.424
C14	0.067	0.017	0.033	0.005	0.133	0.030	0.029	0.029
C14:1	0.065	0.008	0.026	0.030	0.039	0.013	0.094	0.038
C14:1-OH	0.010	0.001	0.008	0.002	0.016	0.002	0.352	0.021
C14:2	0.009	0.002	0.007	0.001	0.013	0.006	0.208	0.404
C14:2-OH	0.009	0.001	0.005	0.004	0.007	0.002	0.209	0.267
C16	0.087	0.020	0.103	0.041	0.177	0.057	0.579	0.061
C16-OH	0.009	0.001	0.009	0.001	0.013	0.004	0.834	0.174
C16:1	0.050	0.011	0.025	0.005	0.109	0.011	0.025	0.003
C16:1-OH	0.022	0.007	0.012	0.010	0.010	0.003	0.241	0.056
C16:2	0.010	0.001	0.006	0.003	0.015	0.006	0.057	0.195
C16:2-OH	0.008	0.002	0.007	0.002	0.010	0.001	0.443	0.368
C18	0.013	0.002	0.011	0.001	0.021	0.002	0.323	0.009
C18:1	0.070	0.019	0.026	0.009	0.119	0.022	0.022	0.043
C18:1-OH	0.013	0.005	0.013	0.002	0.019	0.009	0.983	0.410
C18:2	0.026	0.003	0.011	0.006	0.027	0.005	0.017	0.753

Table 20. Intracellular content of Acylcarnitines of HL-60 cell line under normoxia. Non-detected amino acids or polyamines or amino acids and polyamines whose replicates were not reproducible are named as discarded (D).

INTRACELLULAR CONTENT HYPOXIA								
	THP-1 P		THP-1 AraC		THP-1 Dox			
	nmol/mg protein						pvalue	pvalue
	Mean	SD	Mean	SD	Mean	SD	(AraC vs. P)	(Dox vs. P)
Acylcarnitines								
C0	9.376	0.704	4.869	0.506	5.026	0.380	0.001	0.001
C2	7.683	2.525	3.259	0.285	2.943	0.540	0.039	0.034
C3	0.396	0.195	0.147	0.010	0.150	0.019	0.092	0.095
C3-DC (C4-OH)	0.076	0.010	0.059	0.007	0.033	0.009	0.074	0.006
C3-OH	0.021	0.009	0.011	0.004	0.014	0.011	0.171	0.470
C3:1	0.017	0.008	0.007	0.001	0.009	0.005	0.090	0.186
C4	1.054	0.270	1.565	0.054	0.633	0.022	0.033	0.055
C4:1	0.028	0.016	0.010	0.003	0.011	0.007	0.124	0.156
C5	0.741	0.276	0.135	0.021	0.084	0.016	0.002	0.001
C5-DC (C6-OH)	0.045	0.019	0.021	0.003	0.017	0.009	0.099	0.088
C5-M-DC	0.027	0.015	0.009	0.004	0.009	0.005	0.104	0.118
C5-OH (C3-DC-M)	0.053	0.009	0.018	0.003	0.029	0.010	0.003	0.036
C5:1	0.056	0.021	0.018	0.005	0.020	0.012	0.038	0.064
C5:1-DC	0.029	0.012	0.011	0.003	0.013	0.005	0.069	0.100
C6 (C4:1-DC)	0.115	0.025	0.091	0.004	0.022	0.008	0.178	0.004
C6:1	0.020	0.008	0.007	0.001	0.009	0.006	0.058	0.138
C7-DC	0.019	0.010	0.006	0.001	0.009	0.006	0.097	0.195
C8	0.086	0.039	0.028	0.007	0.036	0.027	0.066	0.142
C9	0.017	0.007	0.006	0.001	0.009	0.005	0.046	0.195
C10	0.062	0.030	0.020	0.006	0.024	0.017	0.072	0.127
C10:1	0.063	0.040	0.021	0.008	0.024	0.017	0.153	0.194
C10:2	0.022	0.010	0.007	0.002	0.010	0.008	0.054	0.168
C12	0.148	0.047	0.050	0.015	0.029	0.015	0.026	0.014
C12-DC	0.088	0.049	0.024	0.007	0.039	0.031	0.087	0.214
C12:1	0.073	0.043	0.023	0.007	0.025	0.018	0.120	0.151
C14	0.412	0.077	0.191	0.070	0.041	0.005	0.021	0.001
C14:1	0.027	0.012	0.006	0.002	0.006	0.002	0.047	0.046
C14:1-OH	0.026	0.011	0.010	0.004	0.005	0.002	0.069	0.030
C14:2	0.007	0.003	0.002	0.001	0.003	0.002	0.046	0.195
C14:2-OH	0.006	0.003	0.002	0.001	0.002	0.002	0.083	0.138
C16	0.770	0.268	0.384	0.192	0.091	0.011	0.113	0.012
C16-OH	0.019	0.006	0.008	0.003	0.006	0.002	0.050	0.027
C16:1	0.068	0.034	0.018	0.006	0.015	0.004	0.066	0.054
C16:1-OH	0.031	0.014	0.013	0.007	0.005	0.002	0.119	0.037
C16:2	0.007	0.004	0.002	0.001	0.003	0.002	0.096	0.148
C16:2-OH	0.013	0.006	0.004	0.001	0.004	0.002	0.060	0.065
C18	0.234	0.097	0.162	0.111	0.025	0.004	0.443	0.020
C18:1	0.172	0.074	0.056	0.022	0.047	0.004	0.061	0.044
C18:1-OH	0.018	0.008	0.008	0.004	0.005	0.004	0.119	0.073
C18:2	0.019	0.007	0.005	0.001	0.007	0.002	0.031	0.051

Table 21. Intracellular content of Acylcarnitines of THP-1 cell line under hypoxia. Non-detected amino acids or polyamines or amino acids and polyamines whose replicates were not reproducible are named as discarded (D).

INTRACELLULAR CONTENT HYPOXIA								
	HL-60 P		HL-60 AraC		HL-60 Dox			
	nmol/mg protein						pvalue	pvalue
	Mean	SD	Mean	SD	Mean	SD	(AraC vs. P)	(Dox vs. P)
Acylcarnitines								
C0	2.180	0.864	0.686	0.220	2.543	0.514	0.044	0.566
C2	1.631	0.228	0.635	0.101	1.906	0.267	0.002	0.246
C3	0.105	0.005	0.017	0.006	0.286	0.058	0.000	0.006
C3-DC (C4-OH)	0.047	0.001	0.015	0.008	0.034	0.009	0.002	0.056
C3-OH	0.048	0.011	0.014	0.009	0.030	0.010	0.016	0.109
C3:1	0.029	0.005	0.008	0.006	0.018	0.005	0.011	0.066
C4	0.519	0.336	0.180	0.027	0.999	0.219	0.156	0.107
C4:1	0.043	0.008	0.012	0.007	0.026	0.011	0.006	0.085
C5	0.122	0.020	0.025	0.007	0.245	0.034	0.003	0.005
C5-DC (C6-OH)	0.067	0.013	0.018	0.013	0.044	0.016	0.009	0.117
C5-M-DC	0.043	0.008	0.011	0.007	0.026	0.011	0.006	0.091
C5-OH (C3-DC-M)	0.055	0.005	0.015	0.009	0.039	0.013	0.002	0.109
C5:1	0.072	0.013	0.019	0.014	0.041	0.013	0.008	0.047
C5:1-DC	0.040	0.004	0.010	0.008	0.030	0.012	0.004	0.250
C6 (C4:1-DC)	0.040	0.006	0.009	0.005	0.025	0.001	0.002	0.013
C6:1	0.032	0.005	0.010	0.006	0.019	0.005	0.010	0.043
C7-DC	0.029	0.006	0.008	0.006	0.019	0.007	0.010	0.091
C8	0.133	0.011	0.033	0.024	0.082	0.028	0.003	0.044
C9	0.029	0.003	0.007	0.005	0.020	0.005	0.003	0.056
C10	0.089	0.017	0.025	0.017	0.058	0.017	0.009	0.088
C10:1	0.102	0.033	0.029	0.018	0.067	0.025	0.029	0.214
C10:2	0.058	0.012	0.013	0.008	0.031	0.003	0.005	0.018
C12	0.102	0.016	0.026	0.014	0.066	0.020	0.003	0.074
C12-DC	0.152	0.016	0.038	0.028	0.096	0.031	0.004	0.050
C12:1	0.123	0.035	0.031	0.019	0.072	0.025	0.016	0.107
C14	0.070	0.009	0.019	0.006	0.117	0.027	0.001	0.046
C14:1	0.015	0.004	0.004	0.003	0.013	0.004	0.012	0.615
C14:1-OH	0.019	0.005	0.005	0.002	0.022	0.009	0.012	0.673
C14:2	0.011	0.003	0.003	0.002	0.006	0.001	0.016	0.053
C14:2-OH	0.009	0.002	0.002	0.001	0.005	0.001	0.007	0.045
C16	0.172	0.047	0.069	0.015	0.318	0.152	0.023	0.188
C16-OH	0.013	0.003	0.004	0.002	0.010	0.002	0.010	0.126
C16:1	0.060	0.012	0.010	0.004	0.077	0.035	0.002	0.483
C16:1-OH	0.015	0.004	0.004	0.002	0.012	0.003	0.014	0.352
C16:2	0.010	0.002	0.002	0.001	0.007	0.001	0.003	0.050
C16:2-OH	0.014	0.002	0.003	0.002	0.013	0.004	0.003	0.592
C18	0.036	0.007	0.011	0.002	0.034	0.012	0.004	0.784
C18:1	0.123	0.036	0.021	0.004	0.140	0.064	0.008	0.711
C18:1-OH	0.016	0.004	0.005	0.003	0.013	0.002	0.018	0.312
C18:2	0.018	0.003	0.003	0.002	0.019	0.002	0.001	0.636

Table 22. Intracellular content of Acylcarnitines of HL-60 cell line under hypoxia. Non-detected amino acids or polyamines or amino acids and polyamines whose replicates were not reproducible are named as discarded (D).

THP-1 AraC vs. THP-1 P cells	
Pathway	**Upregulated proteins**
Wnt signaling pathway (P00057)	9
CCKR signaling map (P06959)	6
Inflammation mediated by chemokine and cytokine signaling pathway (P00031)	6
p53 pathway (P00059)	6
DNA replication (P00017)	5
Ubiquitin proteasome pathway (P00060)	5
Huntington disease (P00029)	4
PDGF signaling pathway (P00047)	4
Angiotensin II-stimulated signaling through G proteins and beta-arrestin (P05911)	3
Apoptosis signaling pathway (P00006)	3
De novo purine biosynthesis (P02738)	3
Heterotrimeric G-protein signaling pathway-Gq alpha and Go alpha mediated pathway (P00027)	3
Histamine H1 receptor mediated signaling pathway (P04385)	3
Integrin signalling pathway (P00034)	3
p38 MAPK pathway (P05918)	3
5HT2 type receptor mediated signaling pathway (P04374)	2
5-Hydroxytryptamine degredation (P04372)	2
Alpha adrenergic receptor signaling pathway (P00002)	2
Blood coagulation (P00011)	2
Cell cycle (P00013)	2
Cytoskeletal regulation by Rho GTPase (P00016)	2
De novo pyrimidine deoxyribonucleotide biosynthesis (P02739)	2
Endogenous cannabinoid signaling (P05730)	2
Endothelin signaling pathway (P00019)	2
Formyltetrahydroformate biosynthesis (P02743)	2
Gonadotropin-releasing hormone receptor pathway (P06664)	2
Insulin/IGF pathway-protein kinase B signaling cascade (P00033)	2
Muscarinic acetylcholine receptor 1 and 3 signaling pathway (P00042)	2
Oxytocin receptor mediated signaling pathway (P04391)	2
Parkinson disease (P00049)	2
Serine glycine biosynthesis (P02776)	2
TGF-beta signaling pathway (P00052)	2
Thyrotropin-releasing hormone receptor signaling pathway (P04394)	2
Toll receptor signaling pathway (P00054)	2

Table 23. Upregulated proteins involved in the pathway gene ontology PANTHER analysis in THP-1 AraC compared to THP-1 P cells under normoxia. Proteomic profiling (SILAC) data were used. Mean±SD for n=2 replicates. Pathways selected has >1 protein upregulated.

HL-60 AraC vs. HL-60 P cells	
Pathway	**Upregulated proteins**
Cholesterol biosynthesis (P00014)	6
CCKR signaling map (P06959)	5
Apoptosis signaling pathway (P00006)	4
Huntington disease (P00029)	4
De novo pyrimidine deoxyribonucleotide biosynthesis (P02739)	3
Heterotrimeric G-protein signaling pathway-Gi alpha and Gs alpha mediated pathway (P0	3
Inflammation mediated by chemokine and cytokine signaling pathway (P00031)	3
p53 pathway (P00059)	3
Ubiquitin proteasome pathway (P00060)	3
Wnt signaling pathway (P00057)	3
5HT1 type receptor mediated signaling pathway (P04373)	2
Androgen/estrogene/progesterone biosynthesis (P02727)	2
Cytoskeletal regulation by Rho GTPase (P00016)	2
DNA replication (P00017)	2
FAS signaling pathway (P00020)	2
Gonadotropin-releasing hormone receptor pathway (P06664)	2
Heme biosynthesis (P02746)	2
Pyruvate metabolism (P02772)	2
T cell activation (P00053)	2

Table 24. Upregulated proteins involved in the pathway gene ontology PANTHER analysis in HL-60 AraC compared to HL-60 P cells under normoxia. Proteomic profiling (SILAC) data were used. Mean±SD for n=2 replicates. Pathways selected has >1 protein upregulated.

THP-1 Dox vs. THP-1 P cells	
Pathway	**Upregulated proteins**
Apoptosis signaling pathway (P00006)	4
CCKR signaling map (P06959)	4
TCA cycle (P00051)	3
5-Hydroxytryptamine degredation (P04372)	2
Angiogenesis (P00005)	2
Asparagine and aspartate biosynthesis (P02730)	2
ATP synthesis (P02721)	2
Blood coagulation (P00011)	2
De novo purine biosynthesis (P02738)	2
De novo pyrimidine ribonucleotides biosythesis (P02740)	2
DNA replication (P00017)	2
Gonadotropin-releasing hormone receptor pathway (P06664)	2
Mannose metabolism (P02752)	2
Parkinson disease (P00049)	2
Pentose phosphate pathway (P02762)	2
Pyruvate metabolism (P02772)	2
Ras Pathway (P04393)	2
Ubiquitin proteasome pathway (P00060)	2

Table 25. Upregulated proteins involved in the pathway gene ontology PANTHER analysis in THP-1 Dox compared to THP-1 P cells under normoxia. Proteomic profiling (SILAC) data were used. Mean±SD for n=2 replicates. Pathways selected has >1 protein upregulated.

HL-60 Dox vs. HL-60 P cells	
Pathway	**Upregulated proteins**
Inflammation mediated by chemokine and cytokine signaling pathway (P00031)	2
Androgen/estrogene/progesterone biosynthesis (P02727)	1
Apoptosis signaling pathway (P00006)	1
B cell activation (P00010)	1
Cell cycle (P00013)	1
Cholesterol biosynthesis (P00014)	1
Cytoskeletal regulation by Rho GTPase (P00016)	1
Heterotrimeric G-protein signaling pathway-Gq alpha and Go alpha mediated pathway (P00027)	1
Huntington disease (P00029)	1
Integrin signalling pathway (P00034)	1
JAK/STAT signaling pathway (P00038)	1
Parkinson disease (P00049)	1
Proline biosynthesis (P02768)	1
T cell activation (P00053)	1

Table 26. Upregulated proteins involved in the pathway gene ontology PANTHER analysis in HL-60 Dox compared to HL-60 P cells under normoxia. Proteomic profiling (SILAC) data were used. Mean±SD for n=2 replicates. Pathways selected at least 1 protein upregulated.

APPENDIX 2

APPENDIX 2: Supplementary data of results of Chapter 2

UPREGULATED PROTEINS IN KU812 ImaR VS. KU812 P			
Protein names	**Gene names**	**Mean Log_2 fold change**	**SD Log_2 fold change**
Protein S100-A9	S100A9	8.62	0.90
Protein S100-P	S100P	7.12	0.08
NADH-cytochrome b5 reductase 2	CYB5R2	6.61	N.D.
Protein kinase C delta type	PRKCD	5.65	2.43
Protein lin-28 homolog B	LIN28B	5.51	N.D.
Cytoskeleton-associated protein 4	CKAP4	5.32	1.75
Cysteine-rich protein 1	CRIP1	5.25	0.41
Protein S100-A8;Protein S100-A8, N-terminally processed	S100A8	5.22	0.04
Phosphoglucomutase-1	PGM1	5.09	1.78
Apolipoprotein C-II;Proapolipoprotein C-II	APOC2	5.09	N.D.
Liver carboxylesterase 1	CES1	5.07	0.30
High affinity immunoglobulin epsilon receptor subunit gamma	FCER1G	5.06	0.51
CD166 antigen	ALCAM	5.00	N.D.
Argininosuccinate synthase	ASS1	4.96	0.16
Melanoma-associated antigen B2	MAGEB2	4.93	N.D.
Mitochondrial 10-formyltetrahydrofolate dehydrogenase	ALDH1L2	4.87	2.92
Arachidonate 5-lipoxygenase-activating protein	ALOX5AP	4.80	0.61
Peptidyl-prolyl cis-trans isomerase C	PPIC	4.79	N.D.
Bifunctional 3-phosphoadenosine 5-phosphosulfate synthase 2	PAPSS2	4.70	2.89
Aldehyde dehydrogenase, mitochondrial	ALDH2	4.69	0.89
HLA class II histocompatibility antigen gamma chain	CD74	4.65	N.D.
Myeloblastin	PRTN3	4.65	0.27
Transketolase-like protein 1	TKTL1	4.60	0.19
Cellular retinoic acid-binding protein 1	CRABP1	4.55	1.07
Cathepsin G	CTSG	4.52	0.34
Gametocyte-specific factor 1	GTSF1	4.49	N.D.
Putative hydroxypyruvate isomerase	HYI	4.45	N.D.
CAAX prenyl protease 1 homolog	ZMPSTE24	4.45	0.41
Heat shock protein beta-1	HSPB1	4.45	0.09
Cystatin-A;Cystatin-A, N-terminally processed	CSTA	4.40	0.90
Azurocidin	AZU1	4.36	N.D.
Insulin-like growth factor 2 mRNA-binding protein 1	IGF2BP1	4.35	1.43
HLA class II histocompatibility antigen, DR alpha chain	HLA-DRA	4.28	N.D.
Neutrophil cytosol factor 1;Putative neutrophil cytosol factor 1B	NCF1;NCF1B;NCF1C	4.25	N.D.
Cytochrome b-245 light chain	CYBA	4.23	N.D.
Glycogen phosphorylase, liver form	PYGL	4.15	0.29
Unconventional myosin-VI	MYO6	4.15	0.02
Pleckstrin	PLEK	4.14	0.15
Serglycin	SRGN	4.11	1.28
Ubiquitin-like modifier-activating enzyme ATG7	ATG7	3.97	0.13
Fatty acyl-CoA reductase 1	FAR1	3.94	N.D.
Sideroflexin-2	SFXN2	3.94	N.D.
Chitinase-3-like protein 1	CHI3L1	3.93	0.70
Sodium-coupled neutral amino acid transporter 1	SLC38A1/SNAT1	3.92	1.11
Major facilitator superfamily domain-containing protein 1	MFSD1	3.92	N.D.
Neutrophil elastase	ELANE	3.90	0.14
Prostaglandin reductase 1	PTGR1	3.88	0.88
CD63 antigen	CD63	3.85	N.D.
Myeloperoxidase	MPO	3.84	0.32
Sulfide:quinone oxidoreductase, mitochondrial	SQRDL	3.84	0.49
HLA class I histocompatibility antigen, A-2 alpha chain	HLA-A	3.82	0.75
Leukocyte-associated immunoglobulin-like receptor 1	LAIR1	3.81	1.17
Lymphocyte antigen 75	LY75	3.81	0.25
Myeloid cell nuclear differentiation antigen	MNDA	3.80	N.D.
Integrin beta-2	ITGB2	3.80	0.21
Mast cell-expressed membrane protein 1	MCEMP1	3.78	N.D.
Protein-methionine sulfoxide oxidase MICAL1	MICAL1	3.77	0.11
WD repeat- and FYVE domain-containing protein 4	WDFY4	3.77	0.22
Protein S100-A11;Protein S100-A11, N-terminally processed	S100A11	3.77	0.07
Solute carrier family 2, facilitated glucose transporter member 5	SLC2A5/GLUT5	3.75	N.D.
Coronin-1A	CORO1A	3.74	0.30
Phosphatidylinositol 4,5-bisphosphate 3-kinase catalytic subunit delta isoform	PIK3CD	3.73	0.66
Engulfment and cell motility protein 2	ELMO2	3.69	0.32
Peptidase M20 domain-containing protein 2	PM20D2	3.69	N.D.
Thrombospondin type-1 domain-containing protein 7A	THSD7A	3.62	N.D.
NAD(P)H dehydrogenase [quinone] 1	NQO1	3.61	1.50
Gamma-glutamyltranspeptidase 1, 3P, 2	GGT1;GGT3P;GGT2	3.60	0.18
Nicotinate-nucleotide pyrophosphorylase [carboxylating]	QPRT	3.59	N.D.
Cullin-associated NEDD8-dissociated protein 2	CAND2	3.59	0.72
Dedicator of cytokinesis protein 10	DOCK10	3.59	0.97

Receptor-type tyrosine-protein phosphatase eta	PTPRJ	3,55	0,22
Thyroid receptor-interacting protein 6	TRIP6	3,48	N.D.
Adenylyl cyclase-associated protein 1	CAP1	3,46	0,23
Carboxypeptidase D	CPD	3,45	0,16
Dehydrogenase/reductase SDR family member 9	DHRS9	3,43	0,87
Monocarboxylate transporter 4	SLC16A3/MCT4	3,39	0,39
TYRO protein tyrosine kinase-binding protein	TYROBP	3,38	N.D.
Prolyl 3-hydroxylase 1	LEPRE1	3,37	0,04
Anoctamin-6	ANO6	3,36	0,07
C-type mannose receptor 2	MRC2	3,36	0,64
Inactive ubiquitin thioesterase FAM105A	FAM105A	3,36	N.D.
Synaptic vesicle membrane protein VAT-1 homolog-like	VAT1L	3,35	0,30
CDKN2AIP N-terminal-like protein	CDKN2AIPNL	3,34	0,57
Beta-1,4-galactosyltransferase 1	B4GALT1	3,34	N.D.
Huntingtin-interacting protein 1	HIP1	3,34	1,41
Vesicle-associated membrane protein 8	VAMP8	3,33	0,20
Tubulin beta-4A chain	TUBB4A	3,33	0,24
ER degradation-enhancing alpha-mannosidase-like protein 1	EDEM1	3,33	0,03
AT-rich interactive domain-containing protein 3A	ARID3A	3,33	0,66
Delta-1-pyrroline-5-carboxylate synthase	ALDH18A1/P5CS	3,31	0,12
Myoferlin	MYOF	3,29	0,80
Palmitoyl-protein thioesterase 1	PPT1	3,28	0,18
Fructose-2,6-bisphosphatase TIGAR	TIGAR	3,26	N.D.
PX domain-containing protein kinase-like protein	PXK	3,26	0,29
Tubulin beta-6 chain	TUBB6	3,24	0,33
Cartilage-associated protein	CRTAP	3,24	0,25
1-phosphatidylinositol 4,5-bisphosphate phosphodiesterase gamma-2	PLCG2	3,23	0,11
Laminin subunit beta-1	LAMB1	3,21	N.D.
Interferon-induced GTP-binding protein Mx2	MX2	3,20	N.D.
Calpain-5	CAPN5	3,20	N.D.
Lipoma-preferred partner	LPP	3,19	N.D.
G1/S-specific cyclin-D3	CCND3	3,18	N.D.
Fibrillin-2	FBN2	3,18	0,25
Dynamin-1	DNM1	3,17	0,07
Integrin alpha-L	ITGAL	3,15	0,13
Ras-related protein Rab-32	RAB32	3,14	0,21
Phospholipase D4	PLD4	3,13	0,20
Phosphatidylinositol 3,4,5-trisphosphate 5-phosphatase 1	INPP5D	3,08	0,17
Golgi SNAP receptor complex member 1	GOSR1	3,06	0,20
Apoptosis-associated speck-like protein containing a CARD	PYCARD	3,04	0,11
Ubiquitin-like modifier-activating enzyme 7	UBA7	3,04	0,30
Caspase-7;Caspase-7 subunit p20;Caspase-7 subunit p11	CASP7	3,04	N.D.
Phosphatidylinositol 4-phosphate 3-kinase C2 domain-containing subunit alpha	PIK3C2A	3,02	N.D.
Microtubule-associated protein 1B	MAP1B	3,02	0,08
Protein Niban	FAM129A	3,01	0,11
Annexin A4	ANXA4	3,01	0,14
Beta-1-syntrophin	SNTB1	3,00	0,92
Cell division cycle protein 20 homolog	CDC20	3,00	N.D.
Vesicular integral-membrane protein VIP36	LMAN2	3,00	0,11
Glutathione peroxidase 7	GPX7	2,98	0,12
Glutathione peroxidase 1	GPX1	2,97	0,16
Prolyl endopeptidase-like	PREPL	2,95	0,80
Phosphatidylinositol 3,4,5-trisphosphate-dependent Rac exchanger 1 protein	PREX1	2,95	0,94
Caspase-1	CASP1	2,95	1,38
NACHT, LRR and PYD domains-containing protein 2	NLRP2	2,92	1,11
Acyl-CoA synthetase family member 2, mitochondrial	ACSF2	2,92	0,21
Trans-Golgi network integral membrane protein 2	TGOLN2	2,90	0,50
Uncharacterized protein KIAA0930	KIAA0930	2,87	N.D.
Transmembrane protein with metallophosphoesterase domain	TMPPE	2,86	0,03
Ras GTPase-activating-like protein IQGAP3	IQGAP3	2,86	0,26
Glucocorticoid receptor	NR3C1	2,86	N.D.
Tyrosine-protein kinase HCK	HCK	2,85	2,28
Solute carrier family 35 member B1	SLC35B1	2,84	N.D.
Nuclear pore membrane glycoprotein 210	NUP210	2,84	0,04
E3 ubiquitin-protein ligase CBL	CBL	2,84	0,73
Macrophage-capping protein	CAPG	2,83	0,28
Insulin-like growth factor 2 mRNA-binding protein 3	IGF2BP3	2,83	N.D.
Proteasome subunit beta type-9	PSMB9	2,82	0,05
Ras-related protein Rab-31	RAB31	2,80	0,22
Phospholipase D3	PLD3	2,76	0,04
Sarcoplasmic reticulum histidine-rich calcium-binding protein	HRC	2,76	N.D.
Amyloid beta A4 precursor protein-binding family B member 1-interacting protein	APBB1IP	2,76	0,06
Methionine-R-sulfoxide reductase B2, mitochondrial	MSRB2	2,76	0,36
WD repeat and FYVE domain-containing protein 1	WDFY1	2,75	0,24
STE20/SPS1-related proline-alanine-rich protein kinase	STK39	2,73	N.D.
Mitochondrial peptide methionine sulfoxide reductase	MSRA	2,71	0,06
Golgi-associated plant pathogenesis-related protein 1	GLIPR2	2,71	N.D.
Galectin-3-binding protein	LGALS3BP	2,71	0,86
Transducin-like enhancer protein 3	TLE3	2,70	4,89
HLA class I histocompatibility antigen, B-58 alpha chain	HLA-B	2,67	0,17

Peptidyl-prolyl cis-trans isomerase H	PPIH	2,66	0,05
Sn1-specific diacylglycerol lipase beta	DAGLB	2,64	0,75
CKLF-like MARVEL transmembrane domain-containing protein 6	CMTM6	2,63	0,53
Solute carrier family 12 member 9	SLC12A9	2,62	0,69
Inactive tyrosine-protein kinase 7	PTK7	2,62	N.D.
Proteasome subunit beta type-10	PSMB10	2,61	0,05
Insulin-like growth factor 2 mRNA-binding protein 2	IGF2BP2	2,60	0,44
2-hydroxyacyl-CoA lyase 1	HACL1	2,60	0,67
Beta-2-microglobulin;Beta-2-microglobulin form pI 5.3	B2M	2,58	0,09
DNA helicase B	HELB	2,57	N.D.
CTP synthase 1	CTPS1	2,57	0,03
Tripartite motif-containing protein 59	TRIM59	2,56	N.D.
Unconventional myosin-If	MYO1F	2,56	0,04
Macrosialin	CD68	2,54	N.D.
Glutathione S-transferase Mu 1	GSTM1	2,53	0,26
Coiled-coil domain-containing protein 88B	CCDC88B	2,52	0,09
Glutamine--fructose-6-phosphate aminotransferase [isomerizing] 1	GFPT1	2,51	0,05
Tumor necrosis factor alpha-induced protein 2	TNFAIP2	2,50	N.D.
AT-rich interactive domain-containing protein 2	ARID2	2,50	0,35
Nischarin	NISCH	2,49	0,59
Inositol 1,4,5-trisphosphate receptor type 1	ITPR1	2,48	0,08
Fibronectin type III domain-containing protein 3B	FNDC3B	2,48	0,64
Homologous-pairing protein 2 homolog	PSMC3IP	2,48	N.D.
Transmembrane 9 superfamily member 1	TM9SF1	2,46	N.D.
Cation-independent mannose-6-phosphate receptor	IGF2R	2,46	0,01
Fanconi anemia group D2 protein	FANCD2	2,45	0,66
Cytochrome c oxidase copper chaperone	COX17	2,45	0,06
Extended synaptotagmin-2	ESYT2	2,44	0,00
Liprin-beta-1	PPFIBP1	2,43	N.D.
Protein Churchill	CHURC1	2,42	N.D.
Tumor necrosis factor alpha-induced protein 8	TNFAIP8	2,42	0,64
Alpha-2-macroglobulin receptor-associated protein	LRPAP1	2,42	N.D.
Complement factor D	CFD	2,40	1,89
DNA-binding protein SATB1	SATB1	2,39	N.D.
Ephrin type-A receptor 7	EPHA7	2,39	1,90
Acyl-CoA-binding protein	DBI	2,39	0,01
Apolipoprotein B receptor	APOBR	2,39	0,33
Non-specific lipid-transfer protein	SCP2	2,39	0,06
Phosphoribosyltransferase domain-containing protein 1	PRTFDC1	2,37	0,27
AP-4 complex subunit epsilon-1	AP4E1	2,37	N.D.
Lysosomal-trafficking regulator	LYST	2,37	0,67
Probable ATP-dependent RNA helicase DDX60-like	DDX60L	2,36	0,70
Solute carrier family 22 member 18	SLC22A18	2,35	1,91
ATP synthase mitochondrial F1 complex assembly factor 1	ATPAF1	2,34	0,07
Insulin receptor;Insulin receptor subunit alpha;Insulin receptor subunit beta	INSR	2,33	N.D.
Interferon regulatory factor 5	IRF5	2,33	N.D.
Protein CIP2A	KIAA1524	2,33	N.D.
Microtubule-associated protein 1A	MAP1A	2,33	0,29
Sodium-coupled neutral amino acid transporter 2	SLC38A2/SNAT2	2,32	0,50
Serine dehydratase-like	SDSL	2,32	0,05
Endoplasmic reticulum aminopeptidase 1	ERAP1	2,31	0,14
Shootin-1	KIAA1598	2,31	N.D.
Glycine amidinotransferase, mitochondrial	GATM	2,31	N.D.
Protein SCAF11	SCAF11	2,30	0,01
Serine/threonine-protein phosphatase 6 regulatory ankyrin repeat subunit B	ANKRD44	2,29	0,39
DnaJ homolog subfamily B member 12	DNAJB12	2,29	N.D.
1-acyl-sn-glycerol-3-phosphate acyltransferase beta	AGPAT2	2,29	N.D.
Actin-related protein 2/3 complex subunit 5-like protein	ARPC5L	2,28	0,72
Alpha-1,3-mannosyl-glycoprotein 2-beta-N-acetylglucosaminyltransferase	MGAT1	2,28	N.D.
Ras-related protein Rab-27A	RAB27A	2,27	0,09
Myocyte-specific enhancer factor 2D	MEF2D	2,26	0,21
Peptidyl-prolyl cis-trans isomerase E	PPIE	2,26	0,01
Two pore calcium channel protein 1	TPCN1	2,26	N.D.
Leucine-rich repeat and calponin homology domain-containing protein 4	LRCH4	2,26	0,18
Cyclin-dependent kinase 13	CDK13	2,25	0,40
Protein canopy homolog 2	CNPY2	2,25	0,10
Insulin receptor substrate 2	IRS2	2,25	0,14
Fanconi anemia group I protein	FANCI	2,25	0,04
HLA class I histocompatibility antigen, B-46 alpha chain	HLA-B	2,25	N.D.
Kinesin-like protein KIF15	KIF15	2,24	0,01
Protein dopey-2	DOPEY2	2,24	0,34
DCC-interacting protein 13-alpha	APPL1	2,23	0,11
Arylsulfatase B	ARSB	2,23	0,04
DNA polymerase epsilon catalytic subunit A	POLE	2,22	0,18
Microsomal glutathione S-transferase 3	MGST3	2,22	0,30
N-acetylgalactosamine-6-sulfatase	GALNS	2,22	0,18
Podocalyxin	PODXL	2,22	N.D.
Apoptotic protease-activating factor 1	APAF1	2,21	0,14
Multiple epidermal growth factor-like domains protein 8	MEGF8	2,20	0,57
Scavenger receptor class B member 1	SCARB1	2,19	N.D.

Peroxisome assembly factor 2	PEX6	2,19	N.D.
Bcl-2 homologous antagonist/killer	BAK1	2,18	0,27
Transmembrane and coiled-coil domain-containing protein 1	TMCO1	2,18	0,38
Peptidyl-prolyl cis-trans isomerase B	PPIB	2,17	0,09
Cell division cycle protein 123 homolog	CDC123	2,17	N.D.
TPR and ankyrin repeat-containing protein 1	TRANK1	2,16	0,02
DnaJ homolog subfamily C member 5	DNAJC5	2,16	0,25
Rho guanine nucleotide exchange factor 18	ARHGEF18	2,15	0,46
Vesicle transport protein SFT2B	SFT2D2	2,15	N.D.
Apoptosis regulator Bcl-2	BCL2	2,15	0,43
Uncharacterized protein C1orf50	C1orf50	2,14	0,31
Asparagine synthetase [glutamine-hydrolyzing]	ASNS	2,14	0,07
Transmembrane 9 superfamily member 4	TM9SF4	2,13	0,17
RNA-binding protein 33	RBM33	2,12	N.D.
Protein tyrosine phosphatase type IVA 1	PTP4A1	2,12	N.D.
Melanoma-associated antigen D2	MAGED2	2,12	0,22
Transmembrane protein 41B	TMEM41B	2,12	0,12
ATP-binding cassette sub-family D member 3	ABCD3	2,11	0,09
Phosphopantothenate--cysteine ligase	PPCS	2,10	0,07
SH3 domain-binding protein 1	SH3BP1	2,10	0,02
Guanine nucleotide-binding protein G(I)/G(S)/G(O) subunit gamma-10	GNG10	2,10	N.D.
Probable 2-oxoglutarate dehydrogenase E1 component DHKTD1, mitochondrial	DHTKD1	2,10	N.D.
Catechol O-methyltransferase	COMT	2,09	0,11
COBW domain-containing protein 1	CBWD1	2,09	0,18
Endoplasmic reticulum-Golgi intermediate compartment protein 2	ERGIC2	2,09	N.D.
Sp110 nuclear body protein	SP110	2,08	N.D.
Nesprin-3	SYNE3	2,08	N.D.
Lysophosphatidylcholine acyltransferase 1	LPCAT1	2,06	N.D.
Sodium-dependent multivitamin transporter	SLC5A6	2,06	N.D.
Gamma-parvin	PARVG	2,06	1,15
Utrophin	UTRN	2,06	0,13
Aldose 1-epimerase	GALM	2,06	N.D.
Receptor-type tyrosine-protein phosphatase F	PTPRF	2,05	0,30
Phosphoglycerate mutase 1	PGAM1	2,05	0,04
ATP-dependent 6-phosphofructokinase, muscle type	PFKM	2,04	0,02
Autophagy protein 5	ATG5	2,04	N.D.
GTP-binding protein Rheb	RHEB	2,04	0,03
Bifunctional UDP-N-acetylglucosamine 2-epimerase/N-acetylmannosamine kinase	GNE	2,04	0,54
Glucose-6-phosphate translocase	SLC37A4	2,04	N.D.
ATP-dependent 6-phosphofructokinase, platelet type	PFKP	2,03	0,12
Transport and Golgi organization protein 2 homolog	TANGO2	2,03	N.D.
Formin-binding protein 1	FNBP1	2,03	0,14
Aldose reductase	AKR1B1	2,03	0,04
Ribulose-phosphate 3-epimerase	RPE	2,03	0,07
H(+)/Cl(-) exchange transporter 7	CLCN7	2,02	N.D.
Nucleotide exchange factor SIL1	SIL1	2,02	0,15
Prolactin regulatory element-binding protein	PREB	2,02	0,28
Diacylglycerol kinase zeta	DGKZ	2,02	N.D.
Enoyl-CoA hydratase/3,2-trans-enoyl-CoA isomerase	EHHADH	2,02	0,22
Synaptojanin-1	SYNJ1	2,01	N.D.
Cob(I)yrinic acid a,c-diamide adenosyltransferase, mitochondrial	MMAB	2,01	0,56
Glycogenin-1	GYG1	2,01	0,12
Voltage-gated potassium channel subunit beta-2	KCNAB2	2,00	0,11
tRNA dimethylallyltransferase, mitochondrial	TRIT1	2,00	N.D.
Phosphoglycolate phosphatase	PGP	2,00	0,35
Maspardin	SPG21	2,00	0,39
ADP-dependent glucokinase	ADPGK	1,99	0,18
Dol-P-Man:Man(5)GlcNAc(2)-PP-Dol alpha-1,3-mannosyltransferase	ALG3	1,99	0,52
Beta-galactosidase	GLB1	1,99	0,28
Pterin-4-alpha-carbinolamine dehydratase	PCBD1	1,98	0,09
Ras-related protein Rab-5B	RAB5B	1,98	0,06
Rho-related GTP-binding protein RhoC	RHOC	1,98	0,15
Lysosome-associated membrane glycoprotein 2	LAMP2	1,98	0,22
Peroxisomal membrane protein PMP34	SLC25A17	1,98	0,06
Alkyldihydroxyacetonephosphate synthase, peroxisomal	AGPS	1,97	0,09
Protein TFG	TFG	1,97	0,15
Endoplasmic reticulum resident protein 29	ERP29	1,97	0,02
AP2-associated protein kinase 1	AAK1	1,97	N.D.
Ubiquitin carboxyl-terminal hydrolase 15	USP15	1,97	1,28
Oxidoreductase NAD-binding domain-containing protein 1	OXNAD1	1,97	N.D.
Protein disulfide-isomerase A6	PDIA6	1,96	0,02
Selenoprotein K	SELK	1,96	N.D.
Mesencephalic astrocyte-derived neurotrophic factor	MANF	1,96	0,19
Peptidyl-prolyl cis-trans isomerase F, mitochondrial	PPIF	1,96	0,10
TATA element modulatory factor	TMF1	1,96	N.D.
Zinc finger protein Rlf	RLF	1,95	0,33
IgG receptor FcRn large subunit p51	FCGRT	1,94	0,41
Calcium/calmodulin-dependent protein kinase type 1	CAMK1	1,94	2,37
Nuclear factor of activated T-cells, cytoplasmic 2	NFATC2	1,94	N.D.
Biorientation of chromosomes in cell division protein 1-like 1	BOD1L1	1,94	0,25

HAUS augmin-like complex subunit 6	HAUS6	1,93	N.D.
Endoplasmic reticulum-Golgi intermediate compartment protein 3	ERGIC3	1,93	N.D.
Cofilin-2	CFL2	1,93	N.D.
Epididymis-specific alpha-mannosidase	MAN2B2	1,93	0,37
CLIP-associating protein 2	CLASP2	1,92	0,06
Persulfide dioxygenase ETHE1, mitochondrial	ETHE1	1,92	0,01
Kinetochore-associated protein 1	KNTC1	1,92	0,04
DnaJ homolog subfamily B member 11	DNAJB11	1,91	0,01
Peroxisomal membrane protein PEX16	PEX16	1,91	N.D.
Transcription elongation factor, mitochondrial	TEFM	1,90	N.D.
Protein TMED8	TMED8	1,90	N.D.
GRIP and coiled-coil domain-containing protein 2	GCC2	1,90	0,22
Nucleoside diphosphate kinase 3	NME3	1,90	0,27
Galectin-1	LGALS1	1,90	0,03
Cytoplasmic dynein 2 heavy chain 1	DYNC2H1	1,89	N.D.
Histone deacetylase 4	HDAC4	1,89	N.D.
NFU1 iron-sulfur cluster scaffold homolog, mitochondrial	NFU1	1,89	0,08
Aflatoxin B1 aldehyde reductase member 2	AKR7A2	1,89	0,00
POU domain, class 2, transcription factor 1	POU2F1;POU2F3	1,89	N.D.
Intraflagellar transport protein 25 homolog	HSPB11	1,88	0,09
Condensin-2 complex subunit G2	NCAPG2	1,88	0,64
Charged multivesicular body protein 4b	CHMP4B	1,88	0,70
Hypoxanthine-guanine phosphoribosyltransferase	HPRT1	1,87	0,04
Glycosylphosphatidylinositol anchor attachment 1 protein	GPAA1	1,87	0,26
GPI-anchor transamidase	PIGK	1,87	0,06
Brain acid soluble protein 1	BASP1	1,87	0,22
Leucine-rich repeat-containing protein 20	LRRC20	1,87	0,26
Serine/threonine-protein kinase ATR	ATR	1,87	0,07
Deoxyhypusine synthase	DHPS	1,86	0,05
Protein RFT1 homolog	RFT1	1,86	0,24
Prolyl 4-hydroxylase subunit alpha-1	P4HA1	1,86	0,20
Serine hydroxymethyltransferase, mitochondrial	SHMT2	1,86	0,01
LIM domain and actin-binding protein 1	LIMA1	1,86	N.D.
Protein disulfide-isomerase	P4HB	1,84	0,34
7,8-dihydro-8-oxoguanine triphosphatase	NUDT1	1,84	0,18
Phosphatidylinositol glycan anchor biosynthesis class U protein	PIGU	1,84	0,05
ADP-ribosylation factor-like protein 8B	ARL8B	1,83	0,01
Annexin A6	ANXA6	1,83	0,07
Phosphotriesterase-related protein	PTER	1,83	0,25
Beta-glucuronidase	GUSB	1,82	0,00
Condensin-2 complex subunit D3	NCAPD3	1,81	0,06
Tubulin alpha-4A chain	TUBA4A	1,81	0,29
Adenylate kinase isoenzyme 6	AK6	1,80	0,22
Nucleosome assembly protein 1-like 1	NAP1L1	1,80	0,09
Transmembrane protein 131	TMEM131	1,80	N.D.
Cation-dependent mannose-6-phosphate receptor	M6PR	1,80	0,67
Peroxisomal acyl-coenzyme A oxidase 1	ACOX1	1,80	0,29
Nck-associated protein 1-like	NCKAP1L	1,79	0,02
NAD-dependent malic enzyme, mitochondrial	ME2	1,79	0,13
Acetyl-CoA carboxylase 1;Biotin carboxylase	ACACA	1,79	0,01
Bromodomain adjacent to zinc finger domain protein 1A	BAZ1A	1,79	0,15
Sodium bicarbonate cotransporter 3	SLC4A7	1,79	0,29
Phosphoinositide 3-kinase adapter protein 1	PIK3AP1	1,79	0,45
Actin-related protein 2/3 complex subunit 4	ARPC4	1,78	0,05
Dedicator of cytokinesis protein 8	DOCK8	1,78	0,06
Peroxisomal membrane protein 11B	PEX11B	1,78	0,01
Actin-related protein 2/3 complex subunit 3	ARPC3	1,78	0,33
Zyxin	ZYX	1,77	0,02
Actin-related protein 2/3 complex subunit 5	ARPC5	1,77	0,51
Fumarylacetoacetate hydrolase domain-containing protein 2A	FAHD2A;FAHD2B	1,77	0,20
Lysosomal alpha-glucosidase	GAA	1,77	0,01
Telomere-associated protein RIF1	RIF1	1,77	0,01
T-cell immunomodulatory protein	ITFG1	1,77	N.D.
Sulfhydryl oxidase 2	QSOX2	1,77	0,38
Transmembrane protein 128	TMEM128	1,76	N.D.
Prenylcysteine oxidase-like	PCYOX1L	1,76	0,01
Cytochrome P450 20A1	CYP20A1	1,76	0,27
Actin-related protein 2/3 complex subunit 2	ARPC2	1,75	0,14
GPI transamidase component PIG-S	PIGS	1,75	0,08
Phosphatidylinositol 3-kinase regulatory subunit alpha	PIK3R1	1,75	0,29
LEM domain-containing protein 2	LEMD2	1,74	N.D.
Pleckstrin homology domain-containing family O member 2	PLEKHO2	1,74	N.D.
Golgi apparatus protein 1	GLG1	1,74	0,14
Protein disulfide-isomerase A4	PDIA4	1,74	0,08
Transcription initiation factor TFIID subunit 4	TAF4	1,74	N.D.
Cleft lip and palate transmembrane protein 1-like protein	CLPTM1L	1,73	0,26
GPI transamidase component PIG-T	PIGT	1,73	0,45
Immediate early response 3-interacting protein 1	IER3IP1	1,73	0,05
Ras and Rab interactor 3	RIN3	1,72	N.D.
Transmembrane protein 104	TMEM104	1,72	N.D.

Selenoprotein T	SELT	1,72	N.D.
UPF0690 protein C1orf52	C1orf52	1,72	0,33
Death-inducer obliterator 1	DIDO1	1,71	0,40
Secretory carrier-associated membrane protein 1	SCAMP1	1,71	0,18
Acyl-coenzyme A thioesterase 8	ACOT8	1,71	0,21
Tyrosine-protein kinase BAZ1B	BAZ1B	1,71	0,07
Torsin-1A	TOR1A	1,70	0,03
Lysosomal protective protein	CTSA	1,70	0,51
Ras-related protein Rab-13	RAB13	1,70	N.D.
Protein kish-A	TMEM167A	1,70	0,73
VIP36-like protein	LMAN2L	1,70	0,30
Polyadenylate-binding protein 4	PABPC4	1,70	0,02
4-trimethylaminobutyraldehyde dehydrogenase	ALDH9A1	1,70	0,11
Ras-related protein Rab-7a	RAB7A	1,69	0,03
EH domain-containing protein 4	EHD4	1,69	0,28
Alpha-mannosidase 2	MAN2A1	1,68	0,01
Monoacylglycerol lipase ABHD12	ABHD12	1,68	0,04
Protein OS-9	OS9	1,68	0,10
Retinoblastoma-like protein 1	RBL1	1,67	N.D.
PDZ and LIM domain protein 7	PDLIM7	1,67	0,02
Myc-associated zinc finger protein	MAZ	1,67	N.D.
Dolichyl-diphosphooligosaccharide--protein glycosyltransferase subunit STT3B	STT3B	1,67	0,13
Stromal cell-derived factor 2-like protein 1	SDF2L1	1,67	0,11
Transmembrane protein 41A	TMEM41A	1,67	0,10
Lysosomal alpha-mannosidase	MAN2B1	1,67	0,44
Neutral amino acid transporter A	SLC1A4	1,66	1,04
Deoxynucleoside triphosphate triphosphohydrolase SAMHD1	SAMHD1	1,65	0,25
Dolichyl-diphosphooligosaccharide--protein glycosyltransferase subunit 1	RPN1	1,65	0,21
Bridging integrator 2	BIN2	1,65	0,20
Dedicator of cytokinesis protein 2	DOCK2	1,65	0,31
Sideroflexin-3	SFXN3	1,64	0,13
Type-1 angiotensin II receptor-associated protein	AGTRAP	1,64	0,21
Sorting nexin-27	SNX27	1,63	0,28
Sigma non-opioid intracellular receptor 1	SIGMAR1	1,63	0,17
Putative helicase MOV-10	MOV10	1,63	0,33
Sideroflexin-4	SFXN4	1,63	N.D.
WD repeat and FYVE domain-containing protein 3	WDFY3	1,63	0,14
Spectrin alpha chain, non-erythrocytic 1	SPTAN1	1,62	0,05
DnaJ homolog subfamily C member 1	DNAJC1	1,62	1,61
Zinc finger RNA-binding protein	ZFR	1,61	0,37
Chromosome transmission fidelity protein 8 homolog isoform 2	CHTF8	1,61	N.D.
Lysosomal acid phosphatase	ACP2	1,61	0,30
Protein canopy homolog 3	CNPY3	1,61	0,33
EF-hand domain-containing protein D2	EFHD2	1,61	0,09
Lysine-specific demethylase 4A	KDM4A	1,60	N.D.
GDP-fucose protein O-fucosyltransferase 1	POFUT1	1,60	0,39
Beta-hexosaminidase subunit alpha	HEXA	1,60	0,37
Actin-related protein 3	ACTR3	1,60	0,11
Cysteine protease ATG4B	ATG4B	1,60	2,46
E3 ubiquitin-protein ligase UHRF1	UHRF1	1,60	0,12
Nuclear envelope pore membrane protein POM 121C	POM121C;POM121	1,60	1,33
Serine/threonine-protein kinase 10	STK10	1,59	0,04
Secretory carrier-associated membrane protein 2	SCAMP2	1,59	0,37
Bleomycin hydrolase	BLMH	1,59	0,06
Minor histocompatibility protein HA-1;Minor histocompatibility antigen HA-1	HMHA1	1,58	0,18
Translation machinery-associated protein 7	TMA7	1,57	0,05
Neurolysin, mitochondrial	NLN	1,57	0,00
Nuclear fragile X mental retardation-interacting protein 2	NUFIP2	1,57	N.D.
Stromal cell-derived factor 2	SDF2	1,56	0,08
Acetyl-coenzyme A transporter 1	SLC33A1	1,56	N.D.
Granulins;Acrogranin	GRN	1,56	0,03
Proteasome subunit beta type-8	PSMB8	1,56	0,05
LETM1 domain-containing protein 1	LETMD1	1,56	N.D.
Condensin complex subunit 2	NCAPH	1,56	0,49
Probable 18S rRNA (guanine-N(7))-methyltransferase	WBSCR22	1,55	0,14
Cathepsin S	CTSS	1,55	0,06
Myosin light polypeptide 6	MYL6	1,55	0,09
Mitotic checkpoint serine/threonine-protein kinase BUB1 beta	BUB1B	1,55	N.D.
Long-chain-fatty-acid--CoA ligase 1	ACSL1	1,55	0,08
Phosphatidylinositide phosphatase SAC1	SACM1L	1,55	0,07
Niemann-Pick C1 protein	NPC1	1,54	0,06
Vesicle transport through interaction with t-SNAREs homolog 1A	VTI1A	1,54	0,16
Synaptogyrin-1	SYNGR1	1,54	0,19
Thioredoxin-dependent peroxide reductase, mitochondrial	PRDX3	1,53	0,20
C-myc promoter-binding protein	DENND4A	1,53	0,46
Bloom syndrome protein	BLM	1,53	N.D.
Vesicle transport protein SFT2A	SFT2D1	1,53	0,00
Aldehyde dehydrogenase X, mitochondrial	ALDH1B1	1,53	0,14
Histone H2A type 2-B	HIST2H2AB	1,53	1,05
Ribosome-releasing factor 2, mitochondrial	GFM2	1,52	0,18

Copper transport protein ATOX1	ATOX1	1,52	0,03
Ras-related protein Rab-5A	RAB5A	1,52	0,14
KIF1-binding protein	KIAA1279	1,52	0,22
Antigen peptide transporter 2	TAP2	1,52	0,60
Metalloproteinase inhibitor 1	TIMP1	1,52	N.D.
Hypoxia-inducible factor 1-alpha inhibitor	HIF1AN	1,51	N.D.
High mobility group protein B3	HMGB3	1,51	0,20
Calponin-2	CNN2	1,51	0,06
Peroxisomal biogenesis factor 19	PEX19	1,51	N.D.
Protein FAM3C	FAM3C	1,51	0,30
Presenilins-associated rhomboid-like protein, mitochondrial;P-beta	PARL	1,51	0,20
Small ubiquitin-related modifier 1	SUMO1	1,51	0,14
Phospholipase D1	PLD1	1,50	N.D.
Osteoclast-stimulating factor 1	OSTF1	1,50	0,03
Protein timeless homolog	TIMELESS	1,50	0,14
Isoamyl acetate-hydrolyzing esterase 1 homolog	IAH1	1,50	0,41
MIP18 family protein FAM96A	FAM96A	1,50	0,19
Eukaryotic translation initiation factor 4 gamma 2	EIF4G2	1,50	0,04
GTP-binding protein SAR1a	SAR1A	1,49	0,11
3-ketoacyl-CoA thiolase, peroxisomal	ACAA1	1,49	0,32
Calreticulin	CALR	1,49	0,03
3-phosphoinositide-dependent protein kinase 1	PDPK1;PDPK2P	1,48	0,08
A-kinase anchor protein 1, mitochondrial	AKAP1	1,48	0,19
Protein transport protein Sec61 subunit beta	SEC61B	1,48	0,16
Protein CREG1	CREG1	1,48	0,20
Zinc transporter 5	SLC30A5	1,48	N.D.
Hematopoietic lineage cell-specific protein	HCLS1	1,47	0,61
UDP-glucose:glycoprotein glucosyltransferase 1	UGGT1	1,47	0,04
Microtubule-associated protein RP/EB family member 1	MAPRE1	1,47	0,03
Procollagen-lysine,2-oxoglutarate 5-dioxygenase 3	PLOD3	1,47	0,19
Neurogranin;NEUG(55-78)	NRGN	1,47	N.D.
U8 snoRNA-decapping enzyme	NUDT16	1,47	0,10
Gamma-aminobutyric acid receptor-associated protein	GABARAP	1,46	0,11
Immunity-related GTPase family Q protein	IRGQ	1,46	0,24
Attractin	ATRN	1,46	N.D.
Caspase recruitment domain-containing protein 16	CARD16	1,45	N.D.
Ceramide synthase 6	CERS6	1,45	N.D.
Translationally-controlled tumor protein	TPT1	1,45	0,14
Unconventional myosin-XVIIIa	MYO18A	1,45	0,19
Elongation factor 1-alpha 2	EEF1A2	1,45	N.D.
DnaJ homolog subfamily C member 13	DNAJC13	1,44	0,00
Volume-regulated anion channel subunit LRRC8D	LRRC8D	1,44	0,81
Histidine triad nucleotide-binding protein 2, mitochondrial	HINT2	1,44	0,03
Thioredoxin-related transmembrane protein 1	TMX1	1,44	0,05
Calnexin	CANX	1,44	0,13
CD97 antigen	CD97	1,43	0,47
HLA class I histocompatibility antigen, Cw-7 alpha chain	HLA-C	1,43	0,39
Mitochondrial import receptor subunit TOM5 homolog	TOMM5	1,43	0,10
UDP-glucose:glycoprotein glucosyltransferase 2	UGGT2	1,43	N.D.
Guanidinoacetate N-methyltransferase	GAMT	1,43	0,21
Glucose-6-phosphate 1-dehydrogenase	G6PD	1,42	0,10
PH and SEC7 domain-containing protein 4	PSD4	1,42	0,08
Rho GTPase-activating protein 4	ARHGAP4	1,42	0,08
Rapamycin-insensitive companion of mTOR	RICTOR	1,42	N.D.
Cytospin-A	SPECC1L	1,42	N.D.
Acyl-CoA dehydrogenase family member 9, mitochondrial	ACAD9	1,42	0,06
Sentrin-specific protease 3	SENP3	1,41	N.D.
Dihydrofolate reductase	DHFR	1,41	0,10
Recombining binding protein suppressor of hairless	RBPJ	1,41	0,19
Ubiquitin carboxyl-terminal hydrolase 4	USP4	1,40	0,13
PRA1 family protein 3	ARL6IP5	1,40	0,01
Myosin light chain 6B	MYL6B	1,40	0,41
Ataxin-10	ATXN10	1,39	0,14
Structural maintenance of chromosomes protein 4	SMC4	1,39	0,07
V-type proton ATPase subunit S1	ATP6AP1	1,39	N.D.
Pyruvate dehydrogenase phosphatase regulatory subunit, mitochondrial	PDPR	1,39	0,07
RNA-binding protein 27	RBM27	1,39	1,09
NADH-cytochrome b5 reductase 3	CYB5R3	1,39	0,01
Histone acetyltransferase type B catalytic subunit	HAT1	1,39	0,03
UDP-N-acetylhexosamine pyrophosphorylase-like protein 1	UAP1L1	1,39	N.D.
Ras-related protein Rab-33A	RAB33A	1,39	N.D.
UPF0553 protein C9orf64	C9orf64	1,39	N.D.
Calcium-binding mitochondrial carrier protein SCaMC-1	SLC25A24	1,38	0,05
Serine/threonine-protein kinase WNK1	WNK1	1,38	0,51
Protein VPRBP	VPRBP	1,38	0,18
Ganglioside GM2 activator;Ganglioside GM2 activator isoform short	GM2A	1,38	0,02
Glutamine-rich protein 1	QRICH1	1,38	N.D.
NAD(P)H-hydrate epimerase	APOA1BP	1,38	0,08
Zinc finger E-box-binding homeobox 2	ZEB2	1,38	N.D.
Glycerol-3-phosphate dehydrogenase, mitochondrial	GPD2	1,38	0,18

Retinoblastoma-associated protein	RB1	1,37	0,15
Nicastrin	NCSTN	1,37	0,14
DNA repair protein RAD51 homolog 3	RAD51C	1,37	N.D.
Eukaryotic translation initiation factor 4 gamma 3	EIF4G3	1,37	0,61
tRNA (guanine(10)-N2)-methyltransferase homolog	TRMT11	1,37	N.D.
Phosphatidylinositol 4,5-bisphosphate 3-kinase catalytic subunit beta isoform	PIK3CB	1,36	0,18
Volume-regulated anion channel subunit LRRC8C	LRRC8C	1,36	0,31
Retinal rod rhodopsin-sensitive cGMP 3,5-cyclic phosphodiesterase subunit delta	PDE6D	1,36	N.D.
Ras-related protein Rab-8B	RAB8B	1,36	0,07
Nuclear respiratory factor 1	NRF1	1,36	N.D.
Coiled-coil domain-containing protein 58	CCDC58	1,36	0,01
N-acetylgalactosaminyltransferase 7	GALNT7	1,35	N.D.
Serine racemase	SRR	1,35	N.D.
Ras-related protein Rab-18	RAB18	1,35	0,04
Integrin-linked protein kinase	ILK	1,35	0,35
Syntaxin-16	STX16	1,35	N.D.
Delta(24)-sterol reductase	DHCR24	1,35	0,26
Probable C-mannosyltransferase DPY19L1	DPY19L1	1,35	N.D.
WD repeat-containing protein 62	WDR62	1,35	N.D.
Hippocalcin-like protein 1;Neuron-specific calcium-binding protein hippocalcin	HPCAL1;HPCA	1,34	0,13
Rho GTPase-activating protein 1	ARHGAP1	1,34	0,02
Monocarboxylate transporter 2	SLC16A7/MCT2	1,34	N.D.
Cleft lip and palate transmembrane protein 1	CLPTM1	1,34	0,04
Mitochondrial import inner membrane translocase subunit TIM16	PAM16	1,33	0,01
Centrosomal protein of 170 kDa	CEP170	1,33	0,09
Protein FAM136A	FAM136A	1,33	0,16
5-demethoxyubiquinone hydroxylase, mitochondrial	COQ7	1,33	N.D.
Thymidylate synthase	TYMS	1,33	N.D.
Actin-related protein 2/3 complex subunit 1B	ARPC1B	1,33	0,22
CLIP-associating protein 1	CLASP1	1,32	0,11
Thioredoxin domain-containing protein 12	TXNDC12	1,32	0,29
Thiamin pyrophosphokinase 1	TPK1	1,32	N.D.
Copine-8;Copine-9;Copine-5	CPNE8;CPNE9;CPNE5	1,32	N.D.
Mitochondrial import receptor subunit TOM22 homolog	TOMM22	1,32	0,11
Drebrin-like protein	DBNL	1,32	0,14
Lariat debranching enzyme	DBR1	1,32	0,06
Nuclease EXOG, mitochondrial	EXOG	1,32	0,19
F-box only protein 22	FBXO22	1,31	N.D.
Uncharacterized protein KIAA1143	KIAA1143	1,31	N.D.
Bifunctional epoxide hydrolase 2	EPHX2	1,31	N.D.
Neurofibromin;Neurofibromin truncated	NF1	1,31	0,20
Structural maintenance of chromosomes protein 2	SMC2	1,31	0,12
Probable dolichyl pyrophosphate Glc1Man9GlcNAc2 alpha-1,3-glucosyltransferase	ALG8	1,31	0,06
Arf-GAP with coiled-coil, ANK repeat and PH domain-containing protein 2	ACAP2	1,31	0,16
Succinyl-CoA:3-ketoacid coenzyme A transferase 1, mitochondrial	OXCT1	1,31	0,20
THUMP domain-containing protein 3	THUMPD3	1,30	0,22
78 kDa glucose-regulated protein	HSPA5	1,30	0,07
Ena/VASP-like protein	EVL	1,30	0,01
Nuclear pore complex protein Nup214	NUP214	1,30	0,21
HIV Tat-specific factor 1	HTATSF1	1,30	0,06
SUN domain-containing protein 2	SUN2	1,30	N.D.
Dihydroxyacetone phosphate acyltransferase	GNPAT	1,30	0,17
Golgin subfamily B member 1	GOLGB1	1,29	0,05
WD repeat-containing protein 70	WDR70	1,29	N.D.
GTP-binding protein SAR1b	SAR1B	1,29	0,09
Sterol O-acyltransferase 1	SOAT1	1,29	N.D.
Plexin-B2	PLXNB2	1,29	0,15
Deoxyuridine 5-triphosphate nucleotidohydrolase, mitochondrial	DUT	1,29	0,10
RNA-binding protein 26	RBM26	1,29	0,04
Phostensin	PPP1R18	1,29	N.D.
Mitochondrial import inner membrane translocase subunit TIM14	DNAJC19	1,28	0,02
Forkhead box protein K1	FOXK1	1,28	0,17
Adenylate kinase isoenzyme 1	AK1	1,28	0,05
Nucleoside diphosphate kinase 6	NME6	1,28	0,24
Pterin-4-alpha-carbinolamine dehydratase 2	PCBD2	1,28	0,09
Nuclear autoantigenic sperm protein	NASP	1,28	0,21
Eukaryotic translation initiation factor 2A	EIF2A	1,27	0,03
CAP-Gly domain-containing linker protein 1	CLIP1	1,27	0,24
Lysosome-associated membrane glycoprotein 1	LAMP1	1,27	0,23
Vacuolar ATPase assembly integral membrane protein VMA21	VMA21	1,27	0,07
5-formyltetrahydrofolate cyclo-ligase	MTHFS	1,27	0,30
Phospholipid hydroperoxide glutathione peroxidase, mitochondrial	GPX4	1,27	0,21
Erlin-1	ERLIN1	1,27	0,59
BAG family molecular chaperone regulator 1	BAG1	1,26	N.D.
Stromal membrane-associated protein 2	SMAP2	1,26	0,82
Coiled-coil domain-containing protein 51	CCDC51	1,26	N.D.
Magnesium transporter protein 1	MAGT1	1,26	0,02
Lysine-specific demethylase 3B	KDM3B	1,26	0,05
Growth hormone-inducible transmembrane protein	GHITM	1,25	0,24
FYVE and coiled-coil domain-containing protein 1	FYCO1	1,25	0,48

Guanine nucleotide-binding protein subunit beta-4	GNB4	1,25	0,34
Williams-Beuren syndrome chromosomal region 16 protein	WBSCR16	1,25	N.D.
Ras-related protein Rab-22A	RAB22A	1,25	0,61
Probable serine carboxypeptidase CPVL	CPVL	1,25	0,35
Endoplasmic reticulum resident protein 44	ERP44	1,25	0,07
Chromobox protein homolog 5	CBX5	1,25	0,23
Ubiquitin-like-conjugating enzyme ATG3	ATG3	1,24	0,09
Secretory carrier-associated membrane protein 3	SCAMP3	1,24	0,03
10 kDa heat shock protein, mitochondrial	HSPE1	1,24	0,03
Enhancer of mRNA-decapping protein 4	EDC4	1,24	0,31
Phosphatidylinositol 3,4,5-trisphosphate 5-phosphatase 2	INPPL1	1,23	0,11
Motile sperm domain-containing protein 2	MOSPD2	1,23	N.D.
PAS domain-containing serine/threonine-protein kinase	PASK	1,23	N.D.
Adenosylhomocysteinase	AHCY	1,23	0,20
Signal transducer and activator of transcription 2	STAT2	1,23	0,76
Cullin-2	CUL2	1,22	0,05
G patch domain-containing protein 1	GPATCH1	1,22	0,15
Dual specificity protein phosphatase 3	DUSP3	1,22	0,32
Adenosine deaminase	ADA	1,22	0,88
TBC1 domain family member 13	TBC1D13	1,22	0,30
Mitochondrial import receptor subunit TOM20 homolog	TOMM20	1,22	N.D.
Cathepsin L1;Cathepsin L1 heavy chain;Cathepsin L1 light chain	CTSL	1,22	0,07
Protein PRRC1	PRRC1	1,21	0,41
Sulfatase-modifying factor 2	SUMF2	1,21	0,02
NAD(P) transhydrogenase, mitochondrial	NNT	1,21	0,07
PERQ amino acid-rich with GYF domain-containing protein 2	GIGYF2	1,21	0,22
Ubiquitin-associated protein 2	UBAP2	1,21	0,54
BRI3-binding protein	BRI3BP	1,20	0,26
Pyridoxal-dependent decarboxylase domain-containing protein 1	PDXDC1	1,20	0,23
Kinetochore protein Spc24	SPC24	1,20	0,17
ADP-ribosylation factor GTPase-activating protein 3	ARFGAP3	1,20	N.D.
Glutathione S-transferase Mu 3	GSTM3	1,20	0,07
Heat shock 70 kDa protein 14	HSPA14	1,20	0,17
GDP-fucose protein O-fucosyltransferase 2	POFUT2	1,20	N.D.
Dihydropyrimidinase-related protein 2	DPYSL2	1,20	0,21
Ras-related protein Rab-43	RAB43	1,20	N.D.
Tyrosine-protein phosphatase non-receptor type 6	PTPN6	1,20	0,01
Nucleolar MIF4G domain-containing protein 1	NOM1	1,20	0,10
Condensin complex subunit 3	NCAPG	1,19	0,16
Protein YIPF5	YIPF5	1,19	N.D.
Mitochondrial import inner membrane translocase subunit Tim17-B	TIMM17B	1,19	0,21
E3 ubiquitin-protein ligase UHRF2	UHRF2	1,19	N.D.
Transmembrane protein 33	TMEM33	1,19	0,06
Filamin-C	FLNC	1,18	N.D.
Protein PRRC2C	PRRC2C	1,18	0,06
Ovarian cancer-associated gene 2 protein	OVCA2	1,18	0,03
Zinc transporter 6	SLC30A6	1,18	N.D.
HAUS augmin-like complex subunit 2	HAUS2	1,17	0,21
Lactoylglutathione lyase	GLO1	1,17	0,01
Probable tRNA pseudouridine synthase 1	TRUB1	1,17	N.D.
F-box/LRR-repeat protein 12	FBXL12	1,17	N.D.
Sodium/potassium-transporting ATPase subunit alpha-1	ATP1A1	1,17	0,14
DNA mismatch repair protein Mlh1	MLH1	1,17	0,27
Inositol polyphosphate 1-phosphatase	INPP1	1,16	0,35
Protein transport protein Sec61 subunit gamma	SEC61G	1,16	0,14
Obg-like ATPase 1	OLA1	1,16	0,00
2,3-cyclic-nucleotide 3-phosphodiesterase	CNP	1,16	0,11
Nucleoporin NDC1	NDC1	1,16	0,16
Tyrosine-protein phosphatase non-receptor type 9	PTPN9	1,16	0,01
NudC domain-containing protein 3	NUDCD3	1,16	0,30
3-ketoacyl-CoA thiolase, mitochondrial	ACAA2	1,16	0,17
Peptidyl-prolyl cis-trans isomerase A	PPIA	1,15	0,07
ATP-dependent DNA helicase Q4	RECQL4	1,15	N.D.
Kinetochore protein Spc25	SPC25	1,15	0,15
Cytochrome c	CYCS	1,15	0,17
SEC23-interacting protein	SEC23IP	1,15	0,02
Ribonuclease P protein subunit p14	RPP14	1,15	0,05
Annexin A11	ANXA11	1,15	0,17
Nicotinamide/nicotinic acid mononucleotide adenylyltransferase 1	NMNAT1	1,15	N.D.
Nuclear cap-binding protein subunit 2	NCBP2	1,15	0,17
ADP-ribosylation factor 4	ARF4	1,14	0,21
Calcium-binding mitochondrial carrier protein Aralar1	SLC25A12	1,14	0,00
Ganglioside-induced differentiation-associated protein 2	GDAP2	1,14	N.D.
Methionine synthase	MTR	1,14	0,04
Microtubule-associated protein 4	MAP4	1,14	0,14
[Protein ADP-ribosylarginine] hydrolase	ADPRH	1,13	0,37
Fructose-bisphosphate aldolase A	ALDOA	1,13	0,04
Ras-related protein Rab-3D	RAB3D	1,13	0,04
Vesicle transport protein GOT1B	GOLT1B	1,13	0,14
Cyclin-dependent kinase 1	CDK1	1,13	0,24

Elongation factor G, mitochondrial	GFM1	1,13	0,00
ETS-related transcription factor Elf-1	ELF1	1,13	0,36
DmX-like protein 2	DMXL2	1,12	N.D.
Mitochondrial chaperone BCS1	BCS1L	1,12	0,25
Actin-related protein 2	ACTR2	1,12	0,02
Proteasome activator complex subunit 2	PSME2	1,12	0,06
Renin receptor	ATP6AP2	1,12	0,01
Reactive oxygen species modulator 1	ROMO1	1,12	0,07
WD repeat domain-containing protein 83	WDR83	1,12	N.D.
Dolichyl-diphosphooligosaccharide--protein glycosyltransferase subunit DAD1	DAD1	1,12	0,02
DNA mismatch repair protein Msh6	MSH6	1,12	0,02
Prefoldin subunit 1	PFDN1	1,12	0,03
Kynureninase	KYNU	1,12	0,01
Omega-amidase NIT2	NIT2	1,12	0,17
Regulation of nuclear pre-mRNA domain-containing protein 2	RPRD2	1,12	0,11
Crk-like protein	CRKL	1,11	1,00
(3R)-hydroxyacyl-CoA dehydrogenase	HSD17B4	1,11	0,19
Ribonuclease UK114	HRSP12	1,11	0,12
Protein kinase C-binding protein 1	ZMYND8	1,11	N.D.
Spectrin beta chain, non-erythrocytic 1	SPTBN1	1,11	0,15
Plastin-2	LCP1	1,11	0,04
Ubiquitin-like modifier-activating enzyme 5	UBA5	1,10	0,14
BUB3-interacting and GLEBS motif-containing protein ZNF207	ZNF207	1,10	0,18
Torsin-1A-interacting protein 2	TOR1AIP2	1,10	N.D.
Protein transport protein Sec24D	SEC24D	1,10	0,34
Cancer-related nucleoside-triphosphatase	NTPCR	1,10	0,11
Costars family protein ABRACL	ABRACL	1,10	0,05
Protein misato homolog 1	MSTO1	1,09	0,01
Probable ATP-dependent RNA helicase DHX35	DHX35	1,09	0,17
BET1-like protein	BET1L	1,09	0,62
Tyrosine-protein kinase SYK	SYK	1,09	0,03
ADP-ribosylation factor 5	ARF5	1,09	0,19
Kanadaptin	SLC4A1AP	1,09	0,28
Ras-related protein Rab-21	RAB21	1,08	0,12
Toll-interacting protein	TOLLIP	1,08	2,13
Ras association domain-containing protein 2	RASSF2	1,08	N.D.
Pyridoxal kinase	PDXK	1,08	0,15
DNA replication licensing factor MCM6	MCM6	1,08	0,26
Glutaredoxin-1	GLRX	1,08	0,04
V-type proton ATPase 116 kDa subunit a isoform 1	ATP6V0A1	1,08	0,16
Phosphoserine aminotransferase	PSAT1	1,07	0,08
MAP kinase-activated protein kinase 3	MAPKAPK3	1,07	0,17
Pachytene checkpoint protein 2 homolog	TRIP13	1,07	0,02
Tyrosine-protein phosphatase non-receptor type 23	PTPN23	1,07	0,38
Protein transport protein Sec24A	SEC24A	1,07	0,49
Stress-70 protein, mitochondrial	HSPA9	1,07	0,02
Major facilitator superfamily domain-containing protein 10	MFSD10	1,07	N.D.
Thymosin beta-4;Hematopoietic system regulatory peptide	TMSB4X	1,07	N.D.
Minor histocompatibility antigen H13	HM13	1,07	0,03
Vesicle-fusing ATPase	NSF	1,07	0,07
Polypeptide N-acetylgalactosaminyltransferase 6	GALNT6	1,07	N.D.
Adipocyte plasma membrane-associated protein	APMAP	1,06	0,23
Coiled-coil domain-containing protein 6	CCDC6	1,06	0,07
Beta-mannosidase	MANBA	1,06	N.D.
HIG1 domain family member 1A, mitochondrial	HIGD1A	1,06	0,07
Vitamin K epoxide reductase complex subunit 1-like protein 1	VKORC1L1	1,06	0,08
Dehydrogenase/reductase SDR family member 4	DHRS4	1,06	0,10
Mitochondrial carrier homolog 1	MTCH1	1,06	0,98
Cyclin-dependent-like kinase 5	CDK5	1,06	0,08
Vesicle-associated membrane protein 7	VAMP7	1,05	0,26
Helicase ARIP4	RAD54L2	1,05	N.D.
Peptidyl-prolyl cis-trans isomerase-like 3	PPIL3	1,05	0,06
Syntaxin-binding protein 2	STXBP2	1,05	0,16
Peroxisomal biogenesis factor 3	PEX3	1,05	N.D.
Translocation protein SEC62	SEC62	1,05	0,13
Genetic suppressor element 1	GSE1	1,05	N.D.
DNA replication licensing factor MCM4	MCM4	1,05	0,01
Trafficking protein particle complex subunit 8	TRAPPC8	1,04	0,20
Conserved oligomeric Golgi complex subunit 3	COG3	1,04	N.D.
Amyloid beta A4 protein	APP	1,04	0,46
Receptor-type tyrosine-protein phosphatase epsilon	PTPRE	1,04	1,57
Autophagy-related protein 101	ATG101	1,04	N.D.
Tricarboxylate transport protein, mitochondrial	SLC25A1	1,04	0,07
Cytochrome b5 type B	CYB5B	1,04	0,15
SH3 domain-containing kinase-binding protein 1	SH3KBP1	1,04	0,50
Elongation of very long chain fatty acids protein 1	ELOVL1	1,04	0,06
Very-long-chain 3-oxoacyl-CoA reductase	HSD17B12	1,04	0,02
Clathrin light chain B	CLTB	1,04	N.D.
Lipase maturation factor 2	LMF2	1,04	0,23
Vacuolar protein sorting-associated protein 45	VPS45	1,03	0,00

Protein transport protein Sec61 subunit alpha isoform 1	SEC61A1	1,03	0,06
Target of EGR1 protein 1	TOE1	1,03	0,17
HLA class I histocompatibility antigen, Cw-3 alpha chain	HLA-C	1,03	N.D.
60 kDa heat shock protein, mitochondrial	HSPD1	1,03	0,03
Protein RER1	RER1	1,03	0,08
Probable ATP-dependent RNA helicase DDX41	DDX41	1,03	0,28
Golgin subfamily A member 4	GOLGA4	1,03	N.D.
Prefoldin subunit 4	PFDN4	1,03	0,27
Lys-63-specific deubiquitinase BRCC36	BRCC3	1,03	0,00
Protein jagunal homolog 1	JAGN1	1,03	0,03
Tonsoku-like protein	TONSL	1,02	0,02
NHL repeat-containing protein 3	NHLRC3	1,02	N.D.
Methylcrotonoyl-CoA carboxylase beta chain, mitochondrial	MCCC2	1,02	0,04
E3 SUMO-protein ligase RanBP2	RANBP2	1,02	0,21
Mitochondrial import receptor subunit TOM6 homolog	TOMM6	1,02	N.D.
G-protein-signaling modulator 3	GPSM3	1,01	N.D.
Coiled-coil-helix-coiled-coil-helix domain-containing protein 5	CHCHD5	1,01	N.D.
Lactoperoxidase	LPO	1,01	N.D.
LIM and SH3 domain protein 1	LASP1	1,01	0,02
Probable cation-transporting ATPase 13A3	ATP13A3	1,01	N.D.
Endoplasmic reticulum-Golgi intermediate compartment protein 1	ERGIC1	1,01	0,03
Sepiapterin reductase	SPR	1,01	0,07
Methylated-DNA--protein-cysteine methyltransferase	MGMT	1,01	0,25
Programmed cell death 6-interacting protein	PDCD6IP	1,01	0,21
Alpha-actinin-1	ACTN1	1,01	0,04
Dolichol-phosphate mannosyltransferase subunit 3	DPM3	1,01	0,04
Eukaryotic initiation factor 4A-II	EIF4A2	1,01	0,09
Beta-hexosaminidase subunit beta	HEXB	1,01	0,04
Filamin-A	FLNA	1,01	0,04
Condensin complex subunit 1	NCAPD2	1,00	0,07
Protein kish-B	TMEM167B	1,00	N.D.
Protein YIF1B	YIF1B	1,00	0,34
Ataxin-2-like protein	ATXN2L	1,00	0,24
Dehydrodolichyl diphosphate syntase complex subunit NUS1	NUS1	1,00	N.D.
Rab3 GTPase-activating protein catalytic subunit	RAB3GAP1	1,00	0,11
Tumor necrosis factor alpha-induced protein 8-like protein 2	TNFAIP8L2	0,99	0,35
Endoplasmin	HSP90B1	0,99	0,10
AP-3 complex subunit mu-1	AP3M1	0,99	0,31
Ras GTPase-activating-like protein IQGAP1	IQGAP1	0,99	0,12
Transmembrane 9 superfamily member 3	TM9SF3	0,99	0,09
Anoctamin-10	ANO10	0,99	0,04
Uridine 5-monophosphate synthase	UMPS	0,98	0,21
Eukaryotic translation initiation factor 3 subunit K	EIF3K	0,98	0,15
Membrane-associated progesterone receptor component 1	PGRMC1	0,98	0,18
Single-stranded DNA-binding protein, mitochondrial	SSBP1	0,98	0,01
Protein transport protein Sec24C	SEC24C	0,98	0,06
Retinoid-inducible serine carboxypeptidase	SCPEP1	0,98	0,02
Myosin-14	MYH14	0,98	0,03
FUN14 domain-containing protein 2	FUNDC2	0,98	0,07
von Willebrand factor A domain-containing protein 8	VWA8	0,98	0,23
Calcium-binding mitochondrial carrier protein Aralar2	SLC25A13	0,98	0,04
Zinc finger CCCH-type antiviral protein 1-like	ZC3HAV1L	0,98	0,31
GTPase-activating protein and VPS9 domain-containing protein 1	GAPVD1	0,98	0,04
Ubiquitin-fold modifier-conjugating enzyme 1	UFC1	0,98	0,24
Importin-7	IPO7	0,97	0,02
14-3-3 protein beta/alpha	YWHAB	0,97	0,07
Kinetochore protein NDC80 homolog	NDC80	0,97	N.D.
2,5-phosphodiesterase 12	PDE12	0,97	0,15
Succinate dehydrogenase cytochrome b560 subunit, mitochondrial	SDHC	0,97	0,13
DNA replication licensing factor MCM5	MCM5	0,97	0,02
Mitochondrial import receptor subunit TOM40B	TOMM40L	0,97	N.D.
DNA replication licensing factor MCM2	MCM2	0,97	0,01
Ubiquitin-conjugating enzyme E2 C	UBE2C	0,97	N.D.
Protein disulfide-isomerase A5	PDIA5	0,97	0,15
Caspase recruitment domain-containing protein 8	CARD8	0,97	0,08
Syntaxin-18	STX18	0,96	0,15
Ubiquitin-conjugating enzyme E2 A	UBE2A	0,96	0,12
Alpha-1,6-mannosyl-glycoprotein 2-beta-N-acetylglucosaminyltransferase	MGAT2	0,96	N.D.
Signal recognition particle receptor subunit beta	SRPRB	0,96	0,10
Tapasin	TAPBP	0,96	0,16
Succinate dehydrogenase [ubiquinone] cytochrome b small subunit, mitochondrial	SDHD	0,96	0,11
Delta(3,5)-Delta(2,4)-dienoyl-CoA isomerase, mitochondrial	ECH1	0,96	0,07
Probable methyltransferase TARBP1	TARBP1	0,96	0,04
ADP-ribosylation factor-like protein 2-binding protein	ARL2BP	0,96	N.D.
Fucose-1-phosphate guanylyltransferase	FPGT	0,96	N.D.
B-cell receptor-associated protein 31	BCAP31	0,96	0,10
Histone deacetylase complex subunit SAP130	SAP130	0,96	N.D.
1,2-dihydroxy-3-keto-5-methylthiopentene dioxygenase	ADI1	0,95	0,08
Signal transducer and activator of transcription 6	STAT6	0,95	0,48
	SLC35A4	0,95	0,02

Unconventional myosin-Ig;Minor histocompatibility antigen HA-2	MYO1G	0,95	0,05
Ubiquitin-conjugating enzyme E2 R2	UBE2R2	0,95	N.D.
Receptor-type tyrosine-protein phosphatase beta	PTPRB	0,95	N.D.
DnaJ homolog subfamily C member 10	DNAJC10	0,95	0,21
BRCA1-A complex subunit BRE	BRE	0,95	N.D.
Enoyl-CoA hydratase, mitochondrial	ECHS1	0,95	0,04
AP-1 complex subunit sigma-1A	AP1S1	0,95	0,14
Protein FAM208A	FAM208A	0,95	N.D.
Zinc finger protein 598	ZNF598	0,94	N.D.
Peroxisomal acyl-coenzyme A oxidase 3	ACOX3	0,94	N.D.
mRNA-decapping enzyme 1A	DCP1A	0,94	0,37
Rho GTPase-activating protein 30	ARHGAP30	0,94	1,30
Huntingtin-interacting protein K	HYPK	0,94	1,40
Tubulin-specific chaperone A	TBCA	0,94	0,21
Dynamin-like 120 kDa protein, mitochondrial	OPA1	0,94	0,22
Transmembrane emp24 domain-containing protein 3	TMED3	0,94	0,12
Opioid growth factor receptor	OGFR	0,93	0,10
ATP-dependent RNA helicase DDX19B	DDX19B	0,93	N.D.
Actin, cytoplasmic 2;Actin, cytoplasmic 2, N-terminally processed	ACTG1	0,93	0,00
Mesoderm-specific transcript homolog protein	MEST	0,93	0,08
Signal peptidase complex subunit 3	SPCS3	0,93	0,05
BolA-like protein 1	BOLA1	0,93	N.D.
CWF19-like protein 1	CWF19L1	0,93	0,04
Calcium/calmodulin-dependent protein kinase type II subunit delta	CAMK2D	0,93	N.D.
Adenylate kinase 2, mitochondrial	AK2	0,93	0,00
Presenilin-1	PSEN1	0,93	0,69
Nesprin-1	SYNE1	0,93	N.D.
Phosducin-like protein 3	PDCL3	0,92	0,03
Plasminogen receptor (KT)	PLGRKT	0,92	0,44
Exportin-T	XPOT	0,92	0,05
Nucleolar RNA helicase 2	DDX21	0,92	0,16
Disintegrin and metalloproteinase domain-containing protein 10	ADAM10	0,92	0,29
Activating transcription factor 7-interacting protein 1	ATF7IP	0,92	N.D.
Very-long-chain (3R)-3-hydroxyacyl-CoA dehydratase 2	HACD2	0,92	0,24
Thymidylate kinase	DTYMK	0,92	0,19
Lactation elevated protein 1	LACE1	0,92	N.D.
Heterogeneous nuclear ribonucleoprotein L-like	HNRNPLL	0,92	0,29
FAST kinase domain-containing protein 1	FASTKD1	0,92	0,14
Leucyl-cystinyl aminopeptidas	LNPEP	0,92	0,06
Golgi-specific brefeldin A-resistance guanine nucleotide exchange factor 1	GBF1	0,91	0,33
Clathrin interactor 1	CLINT1	0,91	0,69
Calpain-2 catalytic subunit	CAPN2	0,91	0,13
Calumenin	CALU	0,91	0,51
Rap guanine nucleotide exchange factor 6	RAPGEF6	0,91	N.D.
Serine/threonine-protein kinase TAO1	TAOK1	0,91	0,15
ADAMTS-like protein 4	ADAMTSL4	0,91	N.D.
Torsin-2A	TOR2A	0,91	N.D.
Transcription initiation factor TFIID subunit 6	TAF6	0,91	0,13
ADP-ribosylation factor-related protein 1	ARFRP1	0,90	0,54
Nuclear cap-binding protein subunit 1	NCBP1	0,90	0,02
Histone-lysine N-methyltransferase 2A	KMT2A	0,90	3,86
Signal recognition particle 19 kDa protein	SRP19	0,90	0,29
HAUS augmin-like complex subunit 8	HAUS8	0,90	0,89
Mitochondrial import inner membrane translocase subunit Tim23	TIMM23;TIMM23B	0,90	0,12
Sodium/potassium-transporting ATPase subunit beta-3	ATP1B3	0,90	0,03
Catalase	CAT	0,90	0,14
Protein zwilch homolog	ZWILCH	0,90	N.D.
U6 snRNA-associated Sm-like protein LSm8	LSM8	0,90	0,07
Emerin	EMD	0,90	0,27
V-type proton ATPase subunit E 1	ATP6V1E1	0,89	0,07
UDP-glucose 6-dehydrogenase	UGDH	0,89	0,71
Malectin	MLEC	0,89	0,03
Transforming growth factor beta-1	TGFB1	0,89	N.D.
RNA 3-terminal phosphate cyclase	RTCA	0,89	0,06
Antigen KI-67	MKI67	0,89	0,02
Dolichyl-diphosphooligosaccharide--protein glycosyltransferase subunit 2	RPN2	0,89	0,10
V-type proton ATPase subunit G 1	ATP6V1G1	0,89	0,02
Exportin-2	CSE1L	0,89	0,09
F-box/LRR-repeat protein 18	FBXL18	0,89	N.D.
Collagen type IV alpha-3-binding protein	COL4A3BP	0,88	0,41
Zinc transporter 7	SLC30A7	0,88	0,40
E1A-binding protein p400	EP400	0,88	0,08
Zinc finger CCHC domain-containing protein 8	ZCCHC8	0,88	0,16
Oxysterol-binding protein-related protein 1	OSBPL1A	0,88	0,39
Dolichyl-diphosphooligosaccharide--protein glycosyltransferase 48 kDa subunit	DDOST	0,88	0,11
4F2 cell-surface antigen heavy chain	SLC3A2	0,88	0,49
UPF0538 protein C2orf76	C2orf76	0,88	N.D.
Tetratricopeptide repeat protein 1	TTC1	0,88	0,46
Signal transducer and activator of transcription 1-alpha/beta	STAT1	0,88	0,25
Myeloid-derived growth factor	MYDGF	0,87	0,03

Actin, cytoplasmic 1	ACTB	0,87	N.D.
Myotubularin-related protein 14	MTMR14	0,87	0,38
Mannose-1-phosphate guanyltransferase alpha	GMPPA	0,87	0,11
Cyclin-dependent kinase 6	CDK6	0,87	0,23
Cyclin-dependent kinase 2	CDK2	0,87	0,07
Golgi phosphoprotein 3	GOLPH3	0,87	0,05
Cytosolic 5-nucleotidase 3A	NT5C3A	0,87	N.D.
F-box-like/WD repeat-containing protein TBL1XR1	TBL1XR1	0,87	0,17
Alpha-N-acetylgalactosaminidase	NAGA	0,87	0,02
Structural maintenance of chromosomes protein 3	SMC3	0,87	0,03
Methyltransferase-like protein 5	METTL5	0,87	0,38
DNA ligase 1	LIG1	0,87	0,09
THO complex subunit 7 homolog	THOC7	0,87	0,21
Actin, alpha cardiac muscle 1	ACTC1	0,86	0,09
ADP-ribosylation factor-like protein 3	ARL3	0,86	0,16
Probable 28S rRNA (cytosine-C(5))-methyltransferase	NSUN5	0,86	0,34
DNA mismatch repair protein Msh2	MSH2	0,86	0,08
Coatomer subunit gamma-1	COPG1	0,86	0,02
Myotubularin-related protein 10	MTMR10	0,86	0,07
PDZ and LIM domain protein 1	PDLIM1	0,86	0,43
Selenocysteine lyase	SCLY	0,86	0,91
Gamma-aminobutyric acid receptor-associated protein-like 2	GABARAPL2	0,86	0,18
Alanine--tRNA ligase, cytoplasmic	AARS	0,86	0,02
Serine/threonine-protein kinase Nek9	NEK9	0,85	0,00
Extended synaptotagmin-1	ESYT1	0,85	0,10
Phosphorylated adapter RNA export protein	PHAX	0,85	0,21
GH3 domain-containing protein	GHDC	0,85	0,20
TIP41-like protein	TIPRL	0,85	0,22
Malate dehydrogenase, mitochondrial	MDH2	0,85	0,06
Nuclease-sensitive element-binding protein 1	YBX1	0,85	0,02
DNA-binding protein RFX5	RFX5	0,85	N.D.
ADP-ribosylation factor GTPase-activating protein 1	ARFGAP1	0,85	N.D.
V-type proton ATPase subunit F	ATP6V1F	0,85	0,08
Chitobiosyldiphosphodolichol beta-mannosyltransferase	ALG1	0,84	1,81
Surfeit locus protein 4	SURF4	0,84	0,05
Signal peptidase complex catalytic subunit SEC11A	SEC11A	0,84	0,14
Protein-tyrosine kinase 2-beta	PTK2B	0,84	0,39
ATP synthase subunit d, mitochondrial	ATP5H	0,84	0,21
Prefoldin subunit 5	PFDN5	0,84	0,22
Voltage-dependent anion-selective channel protein 1	VDAC1	0,84	0,09
Alpha-1,3/1,6-mannosyltransferase ALG2	ALG2	0,84	N.D.
Coatomer subunit zeta-1	COPZ1	0,84	0,11
Probable ATP-dependent RNA helicase DDX20	DDX20	0,84	0,07
Translin	TSN	0,84	0,04
Aspartyl aminopeptidase	DNPEP	0,83	0,07
ADP-ribose pyrophosphatase, mitochondrial	NUDT9	0,83	N.D.
Probable E3 ubiquitin-protein ligase HERC1	HERC1	0,83	0,10
Malate dehydrogenase, cytoplasmic	MDH1	0,83	0,15
Histone H2B type 2-E	HIST2H2BE	0,83	0,09
Glycogen phosphorylase, brain form	PYGB	0,83	0,22
Interferon-induced 35 kDa protein	IFI35	0,83	0,01
Rho GTPase-activating protein 17	ARHGAP17	0,83	0,05
DNA replication licensing factor MCM3	MCM3	0,83	0,06
Probable ATP-dependent RNA helicase DDX56	DDX56	0,83	0,03
V-type proton ATPase subunit d 1	ATP6V0D1	0,82	0,60
WD repeat-containing protein 76	WDR76	0,82	N.D.
D-3-phosphoglycerate dehydrogenase	PHGDH	0,82	0,03
Nucleobindin-2;Nesfatin-1	NUCB2	0,82	0,22
ATP synthase-coupling factor 6, mitochondrial	ATP5J	0,82	0,03
Transmembrane emp24 domain-containing protein 7	TMED7	0,82	0,13
ATP synthase subunit e, mitochondrial	ATP5I	0,82	0,03
Annexin A5	ANXA5	0,82	0,02
Chloride intracellular channel protein 1	CLIC1	0,82	0,02
Transmembrane protein 205	TMEM205	0,82	0,26
Aladin	AAAS	0,81	0,06
Sorting nexin-6;Sorting nexin-6, N-terminally processed	SNX6	0,81	0,17
ATP synthase subunit f, mitochondrial	ATP5J2	0,81	0,19
Manganese-transporting ATPase 13A1	ATP13A1	0,81	0,14
Epoxide hydrolase 1	EPHX1	0,81	0,00
Oligosaccharyltransferase complex subunit OSTC	OSTC	0,81	0,11
DnaJ homolog subfamily C member 2	DNAJC2	0,81	0,29
Ubiquitin thioesterase otulin	OTULIN	0,81	N.D.
Procollagen galactosyltransferase 1	COLGALT1	0,80	0,09
Glyceraldehyde-3-phosphate dehydrogenase	GAPDH	0,80	0,05
NIF3-like protein 1	NIF3L1	0,80	0,09
Nucleoside diphosphate kinase B	NME2	0,80	0,06
Glutathione S-transferase P	GSTP1	0,80	0,02
Ribonuclease P protein subunit p30	RPP30	0,80	0,02
Succinate dehydrogenase [ubiquinone] iron-sulfur subunit, mitochondrial	SDHB	0,80	0,11
Mini-chromosome maintenance complex-binding protein	MCMBP	0,80	0,12

Sec1 family domain-containing protein 1	SCFD1	0,80	0,08
TBC1 domain family member 15	TBC1D15	0,80	0,01
Bifunctional methylenetetrahydrofolate dehydrogenase/cyclohydrolase, mito	MTHFD2	0,80	0,05
NF-kappa-B essential modulator	IKBKG	0,80	N.D.
Twinfilin-2	TWF2	0,79	0,26
Large neutral amino acids transporter small subunit 1	SLC7A5/LAT1	0,79	0,20
ER membrane protein complex subunit 1	EMC1	0,79	0,02
Serine/threonine-protein kinase PAK 2;PAK-2p27;PAK-2p34	PAK2	0,79	0,15
Isocitrate dehydrogenase [NAD] subunit beta, mitochondrial	IDH3B	0,79	0,81
Tumor suppressor p53-binding protein 1	TP53BP1	0,79	0,19
Protein BRICK1	BRK1	0,79	0,08
Gamma-glutamylcyclotransferase	GGCT	0,79	0,22
Cell cycle checkpoint protein RAD1	RAD1	0,79	N.D.
DnaJ homolog subfamily A member 2	DNAJA2	0,79	0,18
ATP-dependent RNA helicase DHX36	DHX36	0,79	0,07
Threonine--tRNA ligase, cytoplasmic	TARS	0,79	0,10
Rho guanine nucleotide exchange factor 2	ARHGEF2	0,78	0,19
Methylcrotonoyl-CoA carboxylase subunit alpha, mitochondrial	MCCC1	0,78	0,02
Protein SAAL1	SAAL1	0,78	N.D.
Vinculin	VCL	0,78	0,04
Signal transducing adapter molecule 2	STAM2	0,78	0,58
Xaa-Pro aminopeptidase 1	XPNPEP1	0,78	0,05
Thioredoxin domain-containing protein 9	TXNDC9	0,78	0,13
DNA replication licensing factor MCM7	MCM7	0,78	0,05
2-oxoglutarate dehydrogenase, mitochondrial	OGDH	0,78	0,02
Zinc finger protein 217	ZNF217	0,78	N.D.
Inhibitor of nuclear factor kappa-B kinase subunit alpha	CHUK	0,78	0,38
Dolichol-phosphate mannosyltransferase subunit 1	DPM1	0,78	0,02
Cytochrome c oxidase assembly factor 3 homolog, mitochondrial	COA3	0,78	0,19
Protein CDV3 homolog	CDV3	0,78	0,07
Ras-related protein Rab-24	RAB24	0,78	N.D.
Serpin H1	SERPINH1	0,78	0,31
Basic leucine zipper and W2 domain-containing protein 1	BZW1	0,78	0,29
Rab5 GDP/GTP exchange factor	RABGEF1	0,77	N.D.
Alpha- and gamma-adaptin-binding protein p34	AAGAB	0,77	N.D.
Myosin regulatory light chain 12A;Myosin regulatory light chain 12B	MYL12A;MYL12B	0,77	0,03
General transcription factor 3C polypeptide 2	GTF3C2	0,77	N.D.
Probable leucine--tRNA ligase, mitochondrial	LARS2	0,77	0,03
ATP synthase subunit epsilon, mitochondrial	ATP5E	0,77	0,03
Vacuolar fusion protein CCZ1 homolog and homolog B	CCZ1;CCZ1B	0,77	0,18
Signal peptidase complex subunit 2	SPCS2	0,77	0,01
Ras-related protein Rab-5C	RAB5C	0,77	0,06
Ubiquitin-associated protein 2-like	UBAP2L	0,77	1,18
Ras and Rab interactor-like protein	RINL	0,77	N.D.
Multifunctional methyltransferase subunit TRM112-like protein	TRMT112	0,77	0,21
Thymidine kinase 2, mitochondrial	TK2	0,77	N.D.
Coatomer subunit epsilon	COPE	0,77	0,13
ATP synthase subunit O, mitochondrial	ATP5O	0,77	0,02
Regulation of nuclear pre-mRNA domain-containing protein 1B	RPRD1B	0,76	0,09
ADP/ATP translocase 2;ADP/ATP translocase 2, N-terminally processed	SLC25A5	0,76	0,16
Small integral membrane protein 7	SMIM7	0,76	0,23
Eukaryotic translation initiation factor 4B	EIF4B	0,76	0,19
Transcription initiation factor TFIID subunit 1	TAF1	0,76	0,40
Ceroid-lipofuscinosis neuronal protein 6	CLN6	0,76	0,03
MAX gene-associated protein	MGA	0,76	N.D.
CMP-sialic acid transporter	SLC35A1	0,76	N.D.
ATP synthase F(0) complex subunit B1, mitochondrial	ATP5F1	0,76	0,09
PEST proteolytic signal-containing nuclear protein	PCNP	0,76	0,66
3-beta-hydroxysteroid-Delta(8),Delta(7)-isomerase	EBP	0,76	0,29
Nucleoside diphosphate kinase A	NME1	0,75	0,19
Protein AAR2 homolog	AAR2	0,75	N.D.
Cyclin-dependent kinases regulatory subunit 1	CKS1B	0,75	0,00
Up-regulated during skeletal muscle growth protein 5	USMG5	0,75	0,12
Protein sel-1 homolog 1	SEL1L	0,75	0,48
Myosin-9	MYH9	0,75	0,01
Ras-related C3 botulinum toxin substrate 1	RAC1	0,75	0,33
RUN and FYVE domain-containing protein 1	RUFY1	0,74	0,08
Phosphoinositide 3-kinase regulatory subunit 4	PIK3R4	0,74	0,10
E3 ubiquitin-protein ligase RNF31	RNF31	0,74	0,41
Vigilin	HDLBP	0,74	0,09
Rho GTPase-activating protein 27	ARHGAP27	0,74	N.D.
ADP-sugar pyrophosphatase	NUDT5	0,74	0,12
Phosphomannomutase 2	PMM2	0,74	N.D.
Protein ERGIC-53	LMAN1	0,74	0,22
COX assembly mitochondrial protein homolog	CMC1	0,74	0,18
Target of Myb protein 1	TOM1	0,74	N.D.
Non-histone chromosomal protein HMG-17 and 3	HMGN2;HMGN3	0,73	N.D.
Alpha/beta hydrolase domain-containing protein 11	ABHD11	0,73	0,30
DNA replication complex GINS protein PSF3	GINS3	0,73	0,03
Uncharacterized protein C18orf8	C18orf8	0,73	0,59

Alpha-soluble NSF attachment protein	NAPA	0,73	0,05
Coiled-coil and C2 domain-containing protein 1B	CC2D1B	0,73	0,12
Charged multivesicular body protein 5	CHMP5	0,73	0,52
Mismatch repair endonuclease PMS2	PMS2	0,73	N.D.
Treacle protein	TCOF1	0,73	0,21
Mannosyl-oligosaccharide glucosidase	MOGS	0,72	0,04
1-phosphatidylinositol 3-phosphate 5-kinase	PIKFYVE	0,72	N.D.
High mobility group protein HMG-I/HMG-Y	HMGA1	0,72	N.D.
Adenosine 3-phospho 5-phosphosulfate transporter 1	SLC35B2	0,72	0,05
Cyclin-dependent kinase 4 inhibitor C	CDKN2C	0,72	0,19
Dihydropteridine reductase	QDPR	0,72	0,07
14-3-3 protein gamma	YWHAG	0,72	0,13
Prosaposin	PSAP	0,72	0,11
Protein MEMO1	MEMO1	0,72	0,09
Protein DPCD	DPCD	0,72	0,06
Probable global transcription activator SNF2L2	SMARCA2	0,72	0,57
Transportin-3	TNPO3	0,72	0,22
Transcriptional activator protein Pur-beta	PURB	0,72	N.D.
BRISC complex subunit Abro1	FAM175B	0,72	N.D.
Peptidyl-prolyl cis-trans isomerase FKBP3	FKBP3	0,72	0,06
Filamin-B	FLNB	0,72	0,17
Protein YIF1A	YIF1A	0,72	0,25
Spermidine synthase	SRM	0,72	0,06
Signal recognition particle 14 kDa protein	SRP14	0,72	0,11
Transmembrane 9 superfamily member 2	TM9SF2	0,72	0,20
TBC1 domain family member 5	TBC1D5	0,71	0,24
UPF0489 protein C5orf22	C5orf22	0,71	N.D.
Ras-related protein Rap-1b	RAP1B	0,71	0,04
Mitochondrial pyruvate carrier 1	MPC1	0,71	0,16
Transmembrane emp24 domain-containing protein 5	TMED5	0,71	N.D.
Mitochondrial intermembrane space import and assembly protein 40	CHCHD4	0,71	N.D.
Homeobox protein cut-like 1	CUX1	0,71	0,28
KDEL motif-containing protein 2	KDELC2	0,71	N.D.
Clathrin light chain A	CLTA	0,71	0,09
ATP synthase subunit gamma, mitochondrial	ATP5C1	0,71	0,06
UTP--glucose-1-phosphate uridylyltransferase	UGP2	0,71	0,03
Ribosome biogenesis protein WDR12	WDR12	0,71	0,28
Protein tyrosine phosphatase type IVA 2	PTP4A2	0,71	1,96
Integrin beta-1	ITGB1	0,71	0,04
Transmembrane protein 87A	TMEM87A	0,71	0,06
Ras GTPase-activating protein 2	RASA2	0,71	0,41
Ubiquitin-conjugating enzyme E2 L3	UBE2L3	0,70	0,15
Prefoldin subunit 3	VBP1	0,70	0,16
U6 snRNA-associated Sm-like protein LSm7	LSM7	0,70	0,19
Interleukin-1 receptor-associated kinase 3	IRAK3	0,70	0,19
Histone-lysine N-methyltransferase SETD7	SETD7	0,70	N.D.
Cystatin-C	CST3	0,70	0,64
GEM-interacting protein	GMIP	0,70	0,28
tRNA (cytosine(34)-C(5))-methyltransferase	NSUN2	0,70	0,01
CCR4-NOT transcription complex subunit 10	CNOT10	0,70	0,17
Cytochrome c oxidase protein 20 homolog	COX20	0,70	0,12
WD repeat-containing protein 55	WDR55	0,70	N.D.
PC4 and SFRS1-interacting protein	PSIP1	0,70	0,19
Rab GDP dissociation inhibitor beta	GDI2	0,70	0,05
Aconitate hydratase, mitochondrial	ACO2	0,70	0,02
Signal recognition particle 54 kDa protein	SRP54	0,70	0,08
Antigen peptide transporter 1	TAP1	0,69	0,12
Protein SON	SON	0,69	0,35
Polyribonucleotide nucleotidyltransferase 1, mitochondrial	PNPT1	0,69	0,05
ATP synthase subunit g, mitochondrial	ATP5L	0,69	0,05
Origin recognition complex subunit 2	ORC2	0,69	0,09
POTE ankyrin domain family member J	POTEJ	0,69	N.D.
Symplekin	SYMPK	0,68	0,04
ATP-dependent RNA helicase DHX8	DHX8	0,68	0,18
Calcyclin-binding protein	CACYBP	0,68	0,02
Kinesin-like protein KIF2C	KIF2C	0,68	N.D.
mRNA-decapping enzyme 1B	DCP1B	0,68	N.D.
Septin-6	SEPT6	0,68	0,56
Activated RNA polymerase II transcriptional coactivator p15	SUB1	0,68	0,05
Ras-related protein Rap-2c	RAP2C	0,68	0,31
Leucine-rich repeat flightless-interacting protein 1	LRRFIP1	0,68	0,14
Diphthine--ammonia ligase	DPH6	0,68	0,21
AP-4 complex subunit beta-1	AP4B1	0,68	0,04
Probable ATP-dependent RNA helicase DDX46	DDX46	0,68	0,02
Succinate dehydrogenase [ubiquinone] flavoprotein subunit, mitochondrial	SDHA	0,68	0,13
Integrin alpha-5;Integrin alpha-5 heavy chain;Integrin alpha-5 light chain	ITGA5	0,68	0,25
Histone H1.3;Histone H1.4	HIST1H1D;HIST1H1E	0,68	0,43
Peptidyl-prolyl cis-trans isomerase G	PPIG	0,68	N.D.
Mannose-1-phosphate guanyltransferase beta	GMPPB	0,67	0,03
Glomulin	GLMN	0,67	0,00

Protein-lysine N-methyltransferase METTL10	METTL10	0,67	0,18
Citrate synthase, mitochondrial	CS	0,67	0,23
Mitochondrial fission process protein 1	MTFP1	0,67	0,24
Cell cycle control protein 50A	TMEM30A	0,67	N.D.
Leucine-rich repeat serine/threonine-protein kinase 1	LRRK1	0,67	N.D.
THO complex subunit 1	THOC1	0,67	0,04
Calcium/calmodulin-dependent protein kinase type 1D	CAMK1D	0,67	N.D.
28S ribosomal protein S36, mitochondrial	MRPS36	0,67	0,19
E3 ubiquitin-protein ligase RBX1	RBX1	0,67	0,08
Rab-like protein 3	RABL3	0,67	0,03
Rho GDP-dissociation inhibitor 2	ARHGDIB	0,67	0,07
UPF0693 protein C10orf32	C10orf32	0,67	0,06
Anaphase-promoting complex subunit 16	ANAPC16	0,67	0,30
6.8 kDa mitochondrial proteolipid	MP68	0,66	0,08
N(G),N(G)-dimethylarginine dimethylaminohydrolase 1	DDAH1	0,66	N.D.
Ras-related C3 botulinum toxin substrate 2	RAC2	0,66	0,09
Guanine nucleotide-binding protein G(I)/G(S)/G(T) subunit beta-2	GNB2	0,66	0,22
Telomeric repeat-binding factor 2	TERF2	0,66	N.D.
5-3 exoribonuclease 1	XRN1	0,66	0,31
Gamma-soluble NSF attachment protein	NAPG	0,66	0,11
HCLS1-associated protein X-1	HAX1	0,66	N.D.
RNA-binding protein 47	RBM47	0,66	N.D.
Myotrophin	MTPN	0,66	0,08
DNA replication complex GINS protein PSF1	GINS1	0,66	N.D.
N-myc-interactor	NMI	0,66	N.D.
Ribonuclease P protein subunit p29	POP4	0,65	0,03
Enoyl-CoA delta isomerase 1, mitochondrial	ECI1	0,65	0,09
DENN domain-containing protein 4B	DENND4B	0,65	0,16
Transmembrane emp24 domain-containing protein 10	TMED10	0,65	0,13
Protein disulfide-isomerase TMX3	TMX3	0,65	0,58
V-type proton ATPase subunit D	ATP6V1D	0,65	0,10
Mitochondrial import receptor subunit TOM40 homolog	TOMM40	0,65	0,17
Cathepsin D	CTSD	0,65	0,25
Transketolase	TKT	0,65	0,08
Solute carrier family 35 member E1	SLC35E1	0,65	0,10
THO complex subunit 5 homolog	THOC5	0,65	0,35
6-phosphogluconolactonase	PGLS	0,65	0,09
Glutathione synthetase	GSS	0,65	0,03
Nuclear export mediator factor NEMF	NEMF	0,65	0,17
Vacuole membrane protein 1	VMP1	0,65	N.D.
Kinesin-like protein KIF2A	KIF2A	0,64	0,24
WD repeat-containing protein mio	MIOS	0,64	N.D.
Ubiquitin carboxyl-terminal hydrolase 19	USP19	0,64	0,05
Protein ELYS	AHCTF1	0,64	0,02
Uncharacterized protein KIAA2013	KIAA2013	0,64	0,11
Partner of Y14 and mago	WIBG	0,64	0,07
Activity-dependent neuroprotector homeobox protein	ADNP	0,64	0,59
ADP-ribosylation factor 1	ARF1	0,64	0,12
DNA repair protein complementing XP-G cells	ERCC5	0,64	0,12
Heat shock protein 105 kDa	HSPH1	0,63	0,06
BCL2/adenovirus E1B 19 kDa protein-interacting protein 2;Caytaxin	BNIP2;ATCAY	0,63	0,07
Ribosomal RNA small subunit methyltransferase NEP1	EMG1	0,63	0,02
AP-1 complex subunit mu-1	AP1M1	0,63	0,16
Dihydrolipoyl dehydrogenase, mitochondrial	DLD	0,63	0,03
Bcl-2-like protein 13	BCL2L13	0,63	0,03
THO complex subunit 3	THOC3	0,63	0,04
Tudor domain-containing protein 7	TDRD7	0,63	N.D.
5-nucleotidase domain-containing protein 3	NT5DC3	0,63	N.D.
Dehydrogenase/reductase SDR family member 2, mitochondrial	DHRS2	0,63	N.D.
Glycogen [starch] synthase, muscle	GYS1	0,63	0,10
14 kDa phosphohistidine phosphatase	PHPT1	0,62	0,01
E3 ubiquitin-protein ligase synoviolin	SYVN1	0,62	0,07
Isopentenyl-diphosphate Delta-isomerase 1	IDI1	0,62	0,14
Iron-responsive element-binding protein 2	IREB2	0,62	0,22
CGG triplet repeat-binding protein 1	CGGBP1	0,62	0,15
SS18-like protein 2	SS18L2	0,62	0,25
Deoxyribose-phosphate aldolase	DERA	0,62	0,07
Synaptobrevin homolog YKT6	YKT6	0,62	0,08
High affinity cationic amino acid transporter 1	SLC7A1	0,62	0,01
RNA polymerase II subunit A C-terminal domain phosphatase	CTDP1	0,62	0,23
Low-density lipoprotein receptor	LDLR	0,62	N.D.
Inositol monophosphatase 3	IMPAD1	0,62	0,05
ER membrane protein complex subunit 2	EMC2	0,62	N.D.
Rab GDP dissociation inhibitor alpha	GDI1	0,62	0,05
Pre-mRNA-splicing factor SYF1	XAB2	0,62	0,24
BolA-like protein 3	BOLA3	0,62	0,16
Protein FAM195A	FAM195A	0,62	N.D.
2-5A-dependent ribonuclease	RNASEL	0,62	N.D.
Dynein light chain roadblock-type 1	DYNLRB1	0,62	0,05
Dolichyl-diphosphooligosaccharide--protein glycosyltransferase subunit STT3A	STT3A	0,61	0,00

Schlafen family member 11	SLFN11	0,61	0,34
Copine-1	CPNE1	0,61	0,16
Conserved oligomeric Golgi complex subunit 1	COG1	0,61	0,08
Mitochondrial import receptor subunit TOM34	TOMM34	0,61	0,22
COP9 signalosome complex subunit 8	COPS8	0,61	0,08
AP-1 complex subunit gamma-1	AP1G1	0,61	0,10
NADPH--cytochrome P450 reductase	POR	0,61	0,15
Rabankyrin-5	ANKFY1	0,61	0,06
General transcription factor 3C polypeptide 1	GTF3C1	0,61	0,01
UHRF1-binding protein 1	UHRF1BP1	0,61	N.D.
Heat shock protein 75 kDa, mitochondrial	TRAP1	0,61	0,03
Proteasome subunit beta type-1	PSMB1	0,61	0,07
Double-strand-break repair protein rad21 homolog	RAD21	0,61	0,08
3-hydroxyisobutyrate dehydrogenase, mitochondrial	HIBADH	0,61	0,02
Geranylgeranyl transferase type-2 subunit beta	RABGGTB	0,61	0,09
Multiple coagulation factor deficiency protein 2	MCFD2	0,61	N.D.
DnaJ homolog subfamily C member 3	DNAJC3	0,61	0,20
60S acidic ribosomal protein P2	RPLP2	0,61	0,59
Cytoplasmic protein NCK1	NCK1	0,61	N.D.
Inverted formin-2	INF2	0,61	N.D.
Protein N-lysine methyltransferase METTL21A	METTL21A	0,61	0,67
E3 ubiquitin-protein ligase LRSAM1	LRSAM1	0,61	N.D.
Tyrosyl-DNA phosphodiesterase 1	TDP1	0,60	N.D.
Dual specificity protein phosphatase 12	DUSP12	0,60	0,14
Heat shock 70 kDa protein 4	HSPA4	0,60	0,02
Inosine-5-monophosphate dehydrogenase 1	IMPDH1	0,60	0,23
cAMP-dependent protein kinase type II-alpha regulatory subunit	PRKAR2A	0,60	0,36
Putative nucleoside diphosphate kinase	NME2P1	0,60	0,48
DNA repair endonuclease XPF	ERCC4	0,60	N.D.
Nascent polypeptide-associated complex subunit alpha, muscle-specific form	NACA	0,59	0,10
Very-long-chain enoyl-CoA reductase	TECR	0,59	0,11
THO complex subunit 6 homolog	THOC6	0,59	0,11
DNA replication complex GINS protein SLD5	GINS4	0,59	0,06
ATP synthase protein 8	MT-ATP8	0,59	0,04
Dehydrodolichyl diphosphate syntase complex subunit DHDDS	DHDDS	0,59	N.D.

Table 1 Upregulated proteins in KU812 ImaR compared to KU812 P cells under normoxia. Proteomic profiling (SILAC) data were used. Significant upregulated proteins were calculated using the fold difference threshold of 1.5 (log_2 fold change=0.58). Mean±SD for n=2 replicates. Non-detected (N.D.) means less than 2 replicates detected for one protein measured.

DOWNREGULATED PROTEINS IN KU812 ImaR VS. KU812 P			
Protein names	**Gene names**	**Mean Log_2 fold change**	**SD Log_2 fold change**
Cellular tumor antigen p53	TP53	-7.22	N.D.
Carboxymethylenebutenolidase homolog	CMBL	-6.31	0.19
Prolactin-inducible protein	PIP	-5.71	N.D.
Myosin-10	MYH10	-5.42	0.05
Hemoglobin subunit theta-1	HBQ1	-5.33	N.D.
Serpin B9	SERPINB9	-5.21	0.04
Tyrosine-protein kinase transmembrane receptor ROR2	ROR2	-5.08	N.D.
Protein-glutamine gamma-glutamyltransferase 2	TGM2	-5.05	0.41
GRB2-related adapter protein 2	GRAP2	-4.88	1.21
Acid ceramidase	ASAH1	-4.88	0.21
Flavin reductase (NADPH)	BLVRB	-4.80	0.01
OCIA domain-containing protein 2	OCIAD2	-4.78	0.84
CB1 cannabinoid receptor-interacting protein 1	CNRIP1	-4.78	2.37
O-acetyl-ADP-ribose deacetylase MACROD1	MACROD1	-4.73	0.51
Guanine nucleotide-binding protein G(I)/G(S)/G(O) subunit gamma-2	GNG2	-4.71	1.10
Tropomyosin alpha-1 chain	TPM1	-4.70	N.D.
Hemoglobin subunit beta;LVV-hemorphin-7;Spinorphin	HBB	-4.60	0.67
Myosin light chain 4	MYL4	-4.53	N.D.
Apolipoprotein C-I;Truncated apolipoprotein C-I	APOC1	-4.40	N.D.
Estradiol 17-beta-dehydrogenase 8	HSD17B8	-4.35	N.D.
PDZ and LIM domain protein 5	PDLIM5	-4.26	1.46
Amine oxidase [flavin-containing] B	MAOB	-4.25	N.D.
Thiosulfate sulfurtransferase/rhodanese-like domain-containing protein 1	TSTD1	-4.23	N.D.
Dematin	DMTN	-4.20	N.D.
Latexin	LXN	-4.18	N.D.
Signal transducer and activator of transcription 5A	STAT5A	-4.15	0.22
Delta-1-pyrroline-5-carboxylate dehydrogenase, mitochondrial	ALDH4A1/P5CDH	-4.14	1.06
Agmatinase, mitochondrial	AGMAT	-4.07	N.D.
Alanine aminotransferase 1	GPT	-4.00	N.D.
Protoporphyrinogen oxidase	PPOX	-4.00	0.25
Ankyrin-1	ANK1	-4.00	0.13
Carbonic anhydrase 2	CA2	-3.97	0.12
Receptor-interacting serine/threonine-protein kinase 1	RIPK1	-3.93	0.50
Calretinin	CALB2	-3.93	N.D.
Galectin-3	LGALS3	-3.90	0.06
2-amino-3-ketobutyrate coenzyme A ligase, mitochondrial	GCAT	-3.86	N.D.
Porphobilinogen deaminase	HMBS	-3.86	0.43
von Willebrand factor A domain-containing protein 5A	VWA5A	-3.85	0.14
Hemoglobin subunit alpha	HBA1	-3.82	0.09
Transferrin receptor protein 1	TFRC	-3.82	0.03
Desmoplakin	DSP	-3.81	N.D.
Protein phosphatase 1 regulatory subunit 14A	PPP1R14A	-3.81	N.D.
NF-kappa-B inhibitor beta	NFKBIB	-3.79	N.D.
Cadherin-1	CDH1	-3.79	0.82
Carbonic anhydrase-related protein	CA8	-3.77	1.10
Carbonic anhydrase 1	CA1	-3.76	0.14
RNA-binding protein 38 and 24	RBM38;RBM24	-3.75	N.D.
Junction plakoglobin	JUP	-3.75	0.48
Aldo-keto reductase family 1 member C1	AKR1C1	-3.74	0.94
Retinal dehydrogenase 1	ALDH1A1	-3.73	0.21
Annexin A1	ANXA1	-3.73	0.59
Bis(5-adenosyl)-triphosphatase	FHIT	-3.71	N.D.
Catenin alpha-2	CTNNA2	-3.71	N.D.
Pleckstrin homology domain-containing family A member 2	PLEKHA2	-3.66	N.D.
Mucin-1	MUC1	-3.64	N.D.
Ubiquitin thioesterase OTU1	YOD1	-3.60	N.D.
Hemoglobin subunit gamma-1	HBG1	-3.60	1.16
Metastasis suppressor protein 1	MTSS1	-3.56	0.02
Ferritin heavy chain;Ferritin heavy chain, N-terminally processed	FTH1	-3.55	0.09
Hemoglobin subunit gamma-2	HBG2	-3.53	0.50
Uroporphyrinogen decarboxylase	UROD	-3.49	0.09
Transmembrane protein 14C	TMEM14C	-3.48	0.14
Tyrosine-protein kinase Lyn	LYN	-3.46	0.04
Acyl-coenzyme A thioesterase 13	ACOT13	-3.45	0.01
Spectrin beta chain, non-erythrocytic 2	SPTBN2	-3.41	0.50
Spectrin alpha chain, erythrocytic 1	SPTA1	-3.39	0.30
Carbonyl reductase family member 4	CBR4	-3.36	0.66
Chloride intracellular channel protein 2	CLIC2	-3.36	0.47
Nicotinamide/nicotinic acid mononucleotide adenylyltransferase 3	NMNAT3	-3.35	N.D.
SAM domain-containing protein SAMSN-1	SAMSN1	-3.35	N.D.

UBX domain-containing protein 6	UBXN6	-3,35	0,75
Signal transducer and activator of transcription 5B	STAT5B	-3,34	0,13
15-hydroxyprostaglandin dehydrogenase [NAD(+)]	HPGD	-3,33	0,29
Protein S100-A6	S100A6	-3,32	0,07
Thiopurine S-methyltransferase	TPMT	-3,31	0,38
TBC1 domain family member 4	TBC1D4	-3,31	1,05
S-methyl-5-thioadenosine phosphorylase	MTAP	-3,28	0,60
Interferon-induced guanylate-binding protein 2 and 1	GBP2;GBP1	-3,27	N.D.
55 kDa erythrocyte membrane protein	MPP1	-3,27	2,27
Mitochondrial 2-oxodicarboxylate carrier	SLC25A21	-3,26	1,86
Multidrug resistance-associated protein 4	ABCC4	-3,26	0,09
Protein-glutamine gamma-glutamyltransferase K	TGM1	-3,24	N.D.
Putative RRN3-like protein RRN3P2	RRN3P2	-3,24	N.D.
Niban-like protein 1	FAM129B	-3,22	0,40
Ectonucleotide pyrophosphatase/phosphodiesterase family member 3	ENPP3	-3,20	0,28
Bifunctional polynucleotide phosphatase/kinase	PNKP	-3,20	0,22
Nck-associated protein 1	NCKAP1	-3,20	1,01
cAMP-dependent protein kinase type I-alpha regulatory subunit	PRKAR1A	-3,19	0,78
Oxysterol-binding protein-related protein 3	OSBPL3	-3,19	N.D.
Complement receptor type 1	CR1	-3,18	N.D.
Pirin	PIR	-3,18	N.D.
Glutamate--cysteine ligase catalytic subunit	GCLC	-3,18	0,23
Spectrin beta chain, erythrocytic	SPTB	-3,18	0,11
ATPase WRNIP1	WRNIP1	-3,17	0,19
UPF0598 protein C8orf82	C8orf82	-3,17	0,13
Keratinocyte proline-rich protein	KPRP	-3,16	N.D.
Kynurenine--oxoglutarate transaminase 3	CCBL2	-3,16	0,61
Selenium-binding protein 1	SELENBP1	-3,15	1,41
Caspase-6	CASP6	-3,13	0,89
Tight junction protein ZO-2	TJP2	-3,13	N.D.
Alpha-synuclein	SNCA	-3,12	N.D.
Flotillin-1	FLOT1	-3,12	0,50
Tyrosine-protein kinase Yes	YES1	-3,12	1,25
Pyruvate carboxylase, mitochondrial	PC	-3,12	0,15
Bcl-2-like protein 1	BCL2L1	-3,12	0,04
Solute carrier family 2, facilitated glucose transporter member 3	SLC2A3/GLUT3	-3,11	0,30
Caspase-10	CASP10	-3,11	N.D.
Eukaryotic translation initiation factor 2D	EIF2D	-3,09	N.D.
Branched-chain-amino-acid aminotransferase, mitochondrial	BCAT2	-3,08	0,35
Intelectin-1	ITLN1	-3,08	0,94
Sorting nexin-9	SNX9	-3,08	0,18
Integrin alpha-IIb;Integrin alpha-IIb heavy chain	ITGA2B	-3,07	0,02
Multiple inositol polyphosphate phosphatase 1	MINPP1	-3,06	0,16
Nuclear factor 1 A-type	NFIA	-3,03	1,66
Mast/stem cell growth factor receptor Kit	KIT	-3,03	0,56
Mannosyl-oligosaccharide 1,2-alpha-mannosidase IA	MAN1A1	-3,02	1,40
Fatty acid desaturase 2	FADS2	-3,01	0,60
Ammonium transporter Rh type A	RHAG	-3,01	1,22
GMP reductase 1	GMPR	-3,01	0,22
Ferrochelatase, mitochondrial	FECH	-3,00	0,17
ATP-binding cassette sub-family B member 10, mitochondrial	ABCB10	-2,98	0,10
Sulfotransferase 1A4 and 1A3	SULT1A4;SULT1A3	-2,98	0,11
Stonin-2	STON2	-2,98	0,27
1-phosphatidylinositol 4,5-bisphosphate phosphodiesterase beta-3	PLCB3	-2,98	0,10
Oligoribonuclease, mitochondrial	REXO2	-2,97	0,35
Ras-related protein Rab-6B	RAB6B	-2,96	N.D.
Solute carrier family 12 member 6	SLC12A6	-2,95	0,85
Rho GTPase-activating protein 18	ARHGAP18	-2,94	0,18
Inosine triphosphate pyrophosphatase	ITPA	-2,93	0,16
Nucleus accumbens-associated protein 1	NACC1	-2,90	N.D.
Protein PML	PML	-2,89	0,38
Valacyclovir hydrolase	BPHL	-2,88	N.D.
Heterogeneous nuclear ribonucleoprotein U-like protein 2	HNRNPUL2	-2,87	0,05
Tetratricopeptide repeat protein 7B	TTC7B	-2,87	N.D.
Glucosamine-6-phosphate isomerase 2	GNPDA2	-2,86	0,11
Pyruvate kinase PKLR	PKLR	-2,86	1,44
Band 3 anion transport protein	SLC4A1	-2,82	0,86
Caspase-3;Caspase-3 subunit p17;Caspase-3 subunit p12	CASP3	-2,81	0,39
Inositol-tetrakisphosphate 1-kinase	ITPK1	-2,80	N.D.
SEC14-like protein 2	SEC14L2	-2,79	N.D.
Rap guanine nucleotide exchange factor 2	RAPGEF2	-2,78	1,23
Zinc finger Ran-binding domain-containing protein 2	ZRANB2	-2,77	N.D.
WD repeat-containing protein 74	WDR74	-2,75	0,56
HLA class I histocompatibility antigen, B-41 alpha chain	HLA-B	-2,75	N.D.
Sentrin-specific protease 6	SENP6	-2,75	N.D.
Probable asparagine--tRNA ligase, mitochondrial	NARS2	-2,72	0,12
CD2-associated protein	CD2AP	-2,72	0,08
Succinate-semialdehyde dehydrogenase, mitochondrial	ALDH5A1	-2,72	0,10
Platelet glycoprotein 4	CD36	-2,71	0,38
UPF0696 protein C11orf68	C11orf68	-2,70	0,59

Chromatin complexes subunit BAP18	BAP18	-2,68	0,02
Valine--tRNA ligase, mitochondrial	VARS2	-2,68	0,14
Catenin beta-1	CTNNB1	-2,67	0,69
Kinase suppressor of Ras 1	KSR1	-2,66	N.D.
Annexin A2;Putative annexin A2-like protein	ANXA2;ANXA2P2	-2,66	0,08
Serine/threonine-protein kinase MRCK alpha	CDC42BPA	-2,66	0,19
Protein unc-13 homolog D	UNC13D	-2,66	0,80
Neogenin	NEO1	-2,66	0,59
Tyrosine-protein phosphatase non-receptor type 7	PTPN7	-2,64	0,27
Probable ATP-dependent RNA helicase DDX28	DDX28	-2,64	N.D.
Dedicator of cytokinesis protein 9	DOCK9	-2,63	2,43
Catenin alpha-1	CTNNA1	-2,62	0,23
Neuroblast differentiation-associated protein AHNAK	AHNAK	-2,62	0,52
Serine/threonine-protein kinase 38	STK38	-2,62	N.D.
Glutamate-rich WD repeat-containing protein 1	GRWD1	-2,61	0,37
Leukocyte elastase inhibitor	SERPINB1	-2,61	0,15
Chloride channel CLIC-like protein 1	CLCC1	-2,58	N.D.
Sulfiredoxin-1	SRXN1	-2,55	0,19
Ethanolamine-phosphate cytidylyltransferase	PCYT2	-2,55	0,01
1-acyl-sn-glycerol-3-phosphate acyltransferase epsilon	AGPAT5	-2,54	0,12
Destrin	DSTN	-2,54	0,34
Ribosomal protein S6 kinase alpha-4	RPS6KA4	-2,54	0,68
Ubiquitin-associated and SH3 domain-containing protein B	UBASH3B	-2,54	0,35
Syntaxin-binding protein 5	STXBP5	-2,54	0,96
Desmoglein-1	DSG1	-2,53	N.D.
Protein THEMIS2	THEMIS2	-2,52	0,39
UMP-CMP kinase 2, mitochondrial	CMPK2	-2,52	1,38
Catenin delta-1	CTNND1	-2,50	0,21
Pleckstrin homology domain-containing family F member 2	PLEKHF2	-2,49	N.D.
Calcineurin B homologous protein 3	TESC	-2,49	0,46
Methyltransferase-like protein 7A	METTL7A	-2,47	2,08
Tripartite motif-containing protein 16	TRIM16	-2,47	0,67
Apolipoprotein B-100;Apolipoprotein B-48	APOB	-2,46	N.D.
Beta-adducin	ADD2	-2,46	0,71
Focal adhesion kinase 1	PTK2	-2,45	N.D.
DNA-directed RNA polymerase III subunit RPC7	POLR3G	-2,45	N.D.
Nesprin-2	SYNE2	-2,45	0,42
LIM domain-binding protein 1	LDB1	-2,44	N.D.
Phenylalanine--tRNA ligase, mitochondrial	FARS2	-2,44	0,08
Ubiquitin carboxyl-terminal hydrolase 25	USP25	-2,44	0,73
Lymphocyte cytosolic protein 2	LCP2	-2,44	0,78
Dual specificity mitogen-activated protein kinase kinase 3	MAP2K3	-2,43	1,11
Inactive serine/threonine-protein kinase VRK3	VRK3	-2,41	N.D.
SH3 domain-binding glutamic acid-rich-like protein 2	SH3BGRL2	-2,40	0,19
Arf-GAP with coiled-coil, ANK repeat and PH domain-containing protein 1	ACAP1	-2,40	N.D.
NF-kappa-B inhibitor epsilon	NFKBIE	-2,40	N.D.
Ribosomal protein S6 kinase beta-1	RPS6KB1	-2,39	N.D.
Alpha-mannosidase 2x	MAN2A2	-2,39	0,53
Inositol 1,4,5-trisphosphate receptor type 2	ITPR2	-2,38	0,57
Cyclin-Y	CCNY	-2,38	N.D.
N-acetylgalactosamine kinase	GALK2	-2,38	0,07
Dual specificity mitogen-activated protein kinase kinase 7	MAP2K7	-2,38	N.D.
Src substrate cortactin	CTTN	-2,37	0,17
Apolipoprotein E	APOE	-2,37	1,08
Serine/threonine-protein kinase 25	STK25	-2,36	N.D.
HBS1-like protein	HBS1L	-2,36	0,08
Ribosomal protein S6 kinase alpha-3	RPS6KA3	-2,35	0,39
Dehydrogenase/reductase SDR family member 11	DHRS11	-2,34	0,50
Stabilin-1	STAB1	-2,33	1,21
Hematopoietic prostaglandin D synthase	HPGDS	-2,33	0,50
Protein scribble homolog	SCRIB	-2,33	0,19
3-5 exoribonuclease 1	ERI1	-2,32	N.D.
Acyl-CoA-binding domain-containing protein 6	ACBD6	-2,31	N.D.
Hexokinase-1	HK1	-2,31	0,11
F-box/LRR-repeat protein 8	FBXL8	-2,30	N.D.
Amyloid-like protein 2	APLP2	-2,30	N.D.
Charged multivesicular body protein 1b	CHMP1B	-2,30	N.D.
GDP-L-fucose synthase	TSTA3	-2,30	0,05
Keratin, type II cytoskeletal 6B	KRT6B	-2,28	N.D.
Ribosome biogenesis protein BMS1 homolog	BMS1	-2,28	0,62
Protein NDRG1	NDRG1	-2,27	N.D.
Alsin	ALS2	-2,26	N.D.
Heme-binding protein 1	HEBP1	-2,26	0,02
Alpha-(1,6)-fucosyltransferase	FUT8	-2,26	0,30
Enoyl-CoA delta isomerase 2, mitochondrial	ECI2	-2,25	0,40
Transportin-2	TNPO2	-2,25	0,13
Oxygen-dependent coproporphyrinogen-III oxidase, mitochondrial	CPOX	-2,24	0,16
Vacuolar protein sorting-associated protein 37B	VPS37B	-2,23	N.D.
Pyrroline-5-carboxylate reductase 1, mitochondrial	PYCR1	-2,23	0,32
Putative tyrosine-protein phosphatase auxilin	DNAJC6	-2,23	N.D.

Arf-GAP with SH3 domain, ANK repeat and PH domain-containing protein 1	ASAP1	-2,23	0,33
Ribosome production factor 2 homolog	RPF2	-2,23	0,21
Hsp70-binding protein 1	HSPBP1	-2,22	0,29
Bifunctional ATP-dependent dihydroxyacetone kinase/FAD-AMP lyase (cyclizing)	DAK	-2,22	0,36
Trafficking protein particle complex subunit 9	TRAPPC9	-2,21	N.D.
Roundabout homolog 2	ROBO2	-2,21	N.D.
Diphosphoinositol polyphosphate phosphohydrolase 2	NUDT4	-2,21	0,14
Mitochondrial genome maintenance exonuclease 1	MGME1	-2,21	N.D.
Translation factor GUF1, mitochondrial	GUF1	-2,21	0,38
Biliverdin reductase A	BLVRA	-2,20	0,18
Alpha-adducin	ADD1	-2,20	0,03
TATA box-binding protein-like protein 1	TBPL1	-2,20	0,49
Piezo-type mechanosensitive ion channel component 1	PIEZO1	-2,19	0,19
ATP-binding cassette sub-family F member 1	ABCF1	-2,19	0,09
Bifunctional lysine-specific demethylase and histidyl-hydroxylase MINA	MINA	-2,19	N.D.
Serine/threonine-protein phosphatase 2A 65 kDa regulatory subunit A beta isoform	PPP2R1B	-2,19	0,83
60 kDa SS-A/Ro ribonucleoprotein	TROVE2	-2,18	0,03
NADPH:adrenodoxin oxidoreductase, mitochondrial	FDXR	-2,18	0,08
Eukaryotic translation initiation factor 1A, Y-chromosomal	EIF1AY	-2,18	0,13
GDP-mannose 4,6 dehydratase	GMDS	-2,18	0,22
Digestive organ expansion factor homolog	DIEXF	-2,17	1,13
Transmembrane protein 2	TMEM2	-2,17	0,32
Methionine aminopeptidase 2	METAP2	-2,16	0,98
Coiled-coil domain-containing protein 25	CCDC25	-2,16	0,29
Haloacid dehalogenase-like hydrolase domain-containing protein 3	HDHD3	-2,15	0,07
Septin-8	SEPT8	-2,14	N.D.
Cyclin-dependent kinase 4	CDK4	-2,14	0,69
Threonine synthase-like 1	THNSL1	-2,13	N.D.
Myotubularin-related protein 5	SBF1	-2,13	N.D.
Ras-related C3 botulinum toxin substrate 3	RAC3	-2,12	0,22
Ubiquitin carboxyl-terminal hydrolase isozyme L5	UCHL5	-2,12	0,22
Protein kinase C theta type	PRKCQ	-2,12	0,74
Proteasome inhibitor PI31 subunit	PSMF1	-2,12	0,14
Protein FAM195B	FAM195B	-2,12	0,10
Endoplasmic reticulum aminopeptidase 2	ERAP2	-2,12	0,28
Nitric oxide synthase-interacting protein	NOSIP	-2,11	0,06
Cullin-5	CUL5	-2,11	0,06
Ras-related protein R-Ras	RRAS	-2,11	0,46
Uroporphyrinogen-III synthase	UROS	-2,11	0,10
Ribosome biogenesis regulatory protein homolog	RRS1	-2,10	0,06
Charged multivesicular body protein 7	CHMP7	-2,10	0,30
Phosphofurin acidic cluster sorting protein 1	PACS1	-2,10	N.D.
Retinol dehydrogenase 14	RDH14	-2,09	N.D.
Testis-expressed sequence 2 protein	TEX2	-2,09	N.D.
Pro-cathepsin H	CTSH	-2,09	0,04
cAMP-dependent protein kinase catalytic subunit beta	PRKACB	-2,08	0,23
Probable ATP-dependent RNA helicase DDX10	DDX10	-2,08	0,42
Zinc finger protein 451	ZNF451	-2,07	0,01
Remodeling and spacing factor 1	RSF1	-2,07	N.D.
Protein MAK16 homolog	MAK16	-2,06	N.D.
Inhibitor of Bruton tyrosine kinase	IBTK	-2,05	N.D.
Atypical kinase ADCK3, mitochondrial	ADCK3	-2,05	0,18
Coiled-coil domain-containing protein 90B, mitochondrial	CCDC90B	-2,05	0,26
Protein arginine N-methyltransferase 1	PRMT1	-2,05	0,18
LIM domain-containing protein 2	LIMD2	-2,05	0,17
Ubiquitin-associated domain-containing protein 1	UBAC1	-2,05	0,50
Kinase D-interacting substrate of 220 kDa	KIDINS220	-2,04	0,12
Interferon-induced transmembrane protein 2, 1 and 3	IFITM2;IFITM1;IFITM3	-2,04	0,18
UDP-glucose 4-epimerase	GALE	-2,03	0,32
Breakpoint cluster region protein	BCR	-2,02	0,08
Protein phosphatase 1 regulatory subunit 14B	PPP1R14B	-2,02	0,10
Acylphosphatase-1	ACYP1	-2,02	0,06
MOB kinase activator 2	MOB2	-2,02	0,01
Thioredoxin domain-containing protein 5	TXNDC5	-2,01	0,38
pre-rRNA processing protein FTSJ3	FTSJ3	-2,01	0,17
Electron transfer flavoprotein subunit beta	ETFB	-2,01	0,01
Formin-like protein 2	FMNL2	-2,01	N.D.
Interferon regulatory factor 2-binding protein-like	IRF2BPL	-2,01	N.D.
Ribosomal RNA processing protein 1 homolog B	RRP1B	-2,00	0,33
DBIRD complex subunit ZNF326	ZNF326	-2,00	0,23
Copper chaperone for superoxide dismutase	CCS	-2,00	0,31
DIS3-like exonuclease 1	DIS3L	-1,99	0,58
Ran-binding protein 9	RANBP9	-1,98	0,10
Chromatin assembly factor 1 subunit A	CHAF1A	-1,97	N.D.
Probable E3 ubiquitin-protein ligase HECTD4	HECTD4	-1,96	0,38
Protein Jumonji	JARID2	-1,96	0,10
Protein phosphatase 1A	PPM1A	-1,96	0,33
PITH domain-containing protein 1	PITHD1	-1,95	0,03
Suppressor of cytokine signaling 2	SOCS2	-1,95	0,84
Fructosamine-3-kinase	FN3K	-1,95	N.D.

Serine/threonine-protein phosphatase 2A 55 kDa regulatory subunit B alpha isoform	PPP2R2A	-1,94	0,16
Double-stranded RNA-binding protein Staufen homolog 1	STAU1	-1,94	N.D.
Exportin-7	XPO7	-1,92	0,06
Small integral membrane protein 12	SMIM12	-1,92	0,11
Semaphorin-7A	SEMA7A	-1,91	N.D.
DNA polymerase subunit gamma-1	POLG	-1,91	0,20
Cathepsin B;Cathepsin B light chain;Cathepsin B heavy chain	CTSB	-1,90	0,01
Ubiquitin carboxyl-terminal hydrolase 48	USP48	-1,90	0,00
Kynurenine--oxoglutarate transaminase 1	CCBL1	-1,90	N.D.
Kelch-like ECH-associated protein 1	KEAP1	-1,90	0,06
Guanine nucleotide-binding protein subunit beta-like protein 1	GNB1L	-1,90	N.D.
Protein argonaute-3	AGO3	-1,90	N.D.
Probable 8-oxo-dGTP diphosphatase NUDT15	NUDT15	-1,90	N.D.
Putative ataxin-7-like protein 3B	ATXN7L3B	-1,90	0,08
Guanine nucleotide-binding protein subunit alpha-15	GNA15	-1,90	N.D.
7-dehydrocholesterol reductase	DHCR7	-1,90	0,61
F-box only protein 7	FBXO7	-1,89	0,07
CD109 antigen	CD109	-1,89	1,29
Cystathionine gamma-lyase	CTH	-1,89	0,31
ESF1 homolog	ESF1	-1,88	0,01
Death-associated protein kinase 1	DAPK1	-1,88	N.D.
Plastin-1	PLS1	-1,88	0,68
Transcription factor p65	RELA	-1,88	0,48
Protein pelota homolog	PELO	-1,87	0,14
CDKN2A-interacting protein	CDKN2AIP	-1,87	0,32
Sorcin	SRI	-1,87	0,03
Carnitine O-acetyltransferase	CRAT	-1,87	N.D.
DNA-directed RNA polymerase III subunit RPC2	POLR3B	-1,87	0,26
Interferon regulatory factor 3	IRF3	-1,86	N.D.
Serine--tRNA ligase, mitochondrial	SARS2	-1,86	0,49
Endophilin-B1	SH3GLB1	-1,86	0,00
Y-box-binding protein 3	YBX3	-1,85	0,04
Acetyl-CoA acetyltransferase, mitochondrial	ACAT1	-1,85	0,03
Casein kinase I isoform delta;Casein kinase I isoform epsilon	CSNK1D;CSNK1E	-1,85	N.D.
Mitochondrial calcium uniporter regulator 1	MCUR1	-1,85	0,30
Centromere protein F	CENPF	-1,84	0,10
Lysophospholipid acyltransferase 7	MBOAT7	-1,84	0,18
Short-chain dehydrogenase/reductase 3	DHRS3	-1,84	N.D.
Histone-arginine methyltransferase CARM1	CARM1	-1,84	0,11
Suppressor of SWI4 1 homolog	PPAN	-1,83	0,14
Unconventional myosin-Id	MYO1D	-1,83	0,22
Serine/arginine-rich splicing factor 4	SRSF4	-1,83	N.D.
Isoprenoid synthase domain-containing protein	ISPD	-1,82	N.D.
2,4-dienoyl-CoA reductase, mitochondrial	DECR1	-1,82	0,00
p21-activated protein kinase-interacting protein 1	PAK1IP1	-1,82	0,21
Single-stranded DNA-binding protein 2;Single-stranded DNA-binding protein 3	SSBP2;SSBP3	-1,82	0,32
Uridine diphosphate glucose pyrophosphatase	NUDT14	-1,82	0,17
Plasma membrane calcium-transporting ATPase 4	ATP2B4	-1,82	0,06
Superoxide dismutase [Mn], mitochondrial	SOD2	-1,81	0,10
Prelamin-A/C;Lamin-A/C	LMNA	-1,81	0,35
Cytosolic acyl coenzyme A thioester hydrolase	ACOT7	-1,81	0,07
Protein Daple	CCDC88C	-1,80	N.D.
Sacsin	SACS	-1,80	0,03
Cell cycle and apoptosis regulator protein 2	CCAR2	-1,79	0,19
Serine/threonine-protein phosphatase PGAM5, mitochondrial	PGAM5	-1,79	0,74
Epidermal growth factor receptor substrate 15	EPS15	-1,79	0,18
Sec1 family domain-containing protein 2	SCFD2	-1,78	0,21
Protein kinase C beta type	PRKCB	-1,78	1,12
NADH dehydrogenase (ubiquinone) complex I, assembly factor 6	NDUFAF6	-1,77	N.D.
Phosphatidylinositol-binding clathrin assembly protein	PICALM	-1,77	0,40
Autophagy-related protein 2 homolog B	ATG2B	-1,77	N.D.
DNA-directed RNA polymerases I and III subunit RPAC1	POLR1C	-1,77	0,23
Guanine nucleotide-binding protein G(q) subunit alpha	GNAQ	-1,76	0,26
Unconventional prefoldin RPB5 interactor 1	URI1	-1,76	0,28
Nucleolar transcription factor 1	UBTF	-1,76	0,24
Arginase-1	ARG1	-1,76	N.D.
Zinc finger protein 706	ZNF706	-1,76	1,02
SCY1-like protein 2	SCYL2	-1,75	0,08
Very long-chain acyl-CoA synthetase	SLC27A2	-1,75	0,68
Erythrocyte band 7 integral membrane protein	STOM	-1,74	0,06
CD44 antigen	CD44	-1,74	0,77
Sin3 histone deacetylase corepressor complex component SDS3	SUDS3	-1,74	N.D.
Pseudouridylate synthase 7 homolog	PUS7	-1,74	0,13
Maestro heat-like repeat-containing protein family member 1	MROH1	-1,74	0,77
Endophilin-B2	SH3GLB2	-1,74	0,03
Proline-rich AKT1 substrate 1	AKT1S1	-1,74	0,07
Voltage-dependent anion-selective channel protein 3	VDAC3	-1,74	0,10
A-kinase anchor protein 2	AKAP2	-1,74	N.D.
Ras GTPase-activating-like protein IQGAP2	IQGAP2	-1,73	0,07
Deubiquitinating protein VCIP135	VCPIP1	-1,73	0,03

Lamina-associated polypeptide 2, isoforms beta/gamma	TMPO	-1,73	0,88
DNA-directed RNA polymerase III subunit RPC5	POLR3E	-1,73	0,07
RNA polymerase II elongation factor ELL	ELL	-1,73	N.D.
E3 ubiquitin-protein ligase UBR5	UBR5	-1,73	0,04
Cytoplasmic aconitate hydratase	ACO1	-1,73	0,02
Copine-3	CPNE3	-1,73	0,04
Formin-like protein 1	FMNL1	-1,72	0,15
Something about silencing protein 10	UTP3	-1,72	N.D.
Barrier-to-autointegration factor	BANF1	-1,72	0,00
Terminal uridylyltransferase 7	ZCCHC6	-1,72	0,41
Protein NipSnap homolog 3A	NIPSNAP3A	-1,72	0,09
Serine/threonine-protein phosphatase CPPED1	CPPED1	-1,71	0,01
Guanosine-3,5-bis(diphosphate) 3-pyrophosphohydrolase MESH1	HDDC3	-1,71	0,12
5-oxoprolinase	OPLAH	-1,71	0,82
RNA-binding protein 12B	RBM12B	-1,71	0,02
Oxysterol-binding protein-related protein 6	OSBPL6	-1,70	0,37
Neuroguidin	NGDN	-1,70	N.D.
Guanylate-binding protein 4	GBP4	-1,70	N.D.
Nucleolar protein 9	NOP9	-1,70	0,49
Sarcoplasmic/endoplasmic reticulum calcium ATPase 3	ATP2A3	-1,70	0,09
O-acetyl-ADP-ribose deacetylase 1	OARD1	-1,70	0,22
Son of sevenless homolog 1	SOS1	-1,69	2,25
Calcium and integrin-binding protein 1	CIB1	-1,69	0,31
Tyrosine-protein kinase Tec	TEC	-1,69	N.D.
Phosphatidylinositol 4,5-bisphosphate 3-kinase catalytic subunit alpha isoform	PIK3CA	-1,68	0,56
CDC42 small effector protein 2	CDC42SE2	-1,68	0,31
NudC domain-containing protein 1	NUDCD1	-1,68	0,17
Nucleoside diphosphate kinase 7	NME7	-1,68	N.D.
Cytochrome b5 reductase 4	CYB5R4	-1,68	N.D.
PHD finger protein 14	PHF14	-1,67	N.D.
Na(+)/H(+) exchange regulatory cofactor NHE-RF1	SLC9A3R1	-1,67	N.D.
Hematological and neurological expressed 1 protein	HN1	-1,67	N.D.
Serine/threonine-protein kinase PRP4 homolog	PRPF4B	-1,67	0,14
Protein Smaug homolog 2	SAMD4B	-1,67	N.D.
UDP-N-acetylglucosamine--dolichyl-phosphate N-acetylglucosaminephosphotransferase	DPAGT1	-1,67	0,60
40S ribosomal protein S27-like	RPS27L	-1,66	0,02
Transcription initiation factor IIE subunit beta	GTF2E2	-1,66	0,37
N-acylneuraminate cytidylyltransferase	CMAS	-1,66	0,02
Four and a half LIM domains protein 2	FHL2	-1,66	N.D.
GTPase Era, mitochondrial	ERAL1	-1,65	N.D.
Serine/threonine-protein kinase RIO1	RIOK1	-1,65	N.D.
NLR family member X1	NLRX1	-1,65	0,19
Serine/threonine-protein kinase 19	STK19	-1,65	N.D.
Protein RMD5 homolog A	RMND5A	-1,65	N.D.
Receptor-type tyrosine-protein phosphatase alpha	PTPRA	-1,65	0,32
UPF0687 protein C20orf27	C20orf27	-1,64	0,22
Chromodomain-helicase-DNA-binding protein 7	CHD7	-1,64	0,56
Sorting nexin-15	SNX15	-1,64	N.D.
RNA-binding protein 4	RBM4	-1,64	0,06
52 kDa repressor of the inhibitor of the protein kinase	PRKRIR	-1,64	0,28
28S ribosomal protein S31, mitochondrial	MRPS31	-1,64	0,97
Phosducin-like protein	PDCL	-1,63	1,53
Isochorismatase domain-containing protein 1	ISOC1	-1,63	0,19
ADP/ATP translocase 1	SLC25A4	-1,63	0,18
Elongation of very long chain fatty acids protein 5	ELOVL5	-1,62	0,06
Uncharacterized protein C15orf57	C15orf57	-1,62	N.D.
Nicotinate phosphoribosyltransferase	NAPRT	-1,61	0,18
ATP-binding cassette sub-family B member 6, mitochondrial	ABCB6	-1,61	N.D.
Protein NEDD1	NEDD1	-1,61	N.D.
Synaptosomal-associated protein 23	SNAP23	-1,61	0,05
Dipeptidyl peptidase 3	DPP3	-1,61	0,06
Caspase-4	CASP4	-1,60	0,02
Spermine synthase	SMS	-1,60	0,27
Glucose 1,6-bisphosphate synthase	PGM2L1	-1,60	1,01
Small integral membrane protein 13	SMIM13	-1,60	0,67
Histone deacetylase 6	HDAC6	-1,60	0,29
Protein FAM76B	FAM76B	-1,60	N.D.
Axin interactor, dorsalization-associated protein	AIDA	-1,59	0,11
Serine--tRNA ligase, cytoplasmic	SARS	-1,59	0,02
Sialate O-acetylesterase	SIAE	-1,59	0,43
Molybdopterin synthase sulfur carrier subunit	MOCS2	-1,58	0,56
Electron transfer flavoprotein subunit alpha, mitochondrial	ETFA	-1,58	0,04
Repressor of RNA polymerase III transcription MAF1 homolog	MAF1	-1,58	N.D.
Protein DDI1 homolog 2	DDI2	-1,58	0,04
Lipid phosphate phosphohydrolase 1	PPAP2A	-1,58	N.D.
Serine-protein kinase ATM	ATM	-1,58	0,05
Protein-L-isoaspartate(D-aspartate) O-methyltransferase	PCMT1	-1,57	0,04
Microtubule-actin cross-linking factor 1, isoforms 1/2/3/5	MACF1	-1,57	0,09
Grancalcin	GCA	-1,57	0,07
Zinc finger protein 30	ZNF30	-1,57	N.D.

BAG family molecular chaperone regulator 2	BAG2	-1,57	0,03
Tumor susceptibility gene 101 protein	TSG101	-1,57	N.D.
ARF GTPase-activating protein GIT1	GIT1	-1,57	0,53
TRMT1-like protein	TRMT1L	-1,57	0,47
Uncharacterized protein C1orf109	C1orf109	-1,57	N.D.
C-terminal-binding protein 2	CTBP2	-1,57	N.D.
Rho GTPase-activating protein 15	ARHGAP15	-1,56	0,09
Protein THEM6	THEM6	-1,56	0,34
Serine protease HTRA2, mitochondrial	HTRA2	-1,56	0,16
Peroxiredoxin-2	PRDX2	-1,56	0,16
Ubiquitin carboxyl-terminal hydrolase 7	USP7	-1,56	0,07
Pyrroline-5-carboxylate reductase 3	PYCRL	-1,56	N.D.
Zinc finger HIT domain-containing protein 2	ZNHIT2	-1,56	N.D.
Uncharacterized protein C7orf50	C7orf50	-1,56	0,25
Golgi integral membrane protein 4	GOLIM4	-1,55	0,50
Receptor expression-enhancing protein 4	REEP4	-1,55	N.D.
EH domain-containing protein 1	EHD1	-1,55	0,05
Hydroxymethylglutaryl-CoA lyase, mitochondrial	HMGCL	-1,55	0,04
Vacuolar protein sorting-associated protein 28 homolog	VPS28	-1,55	0,06
Choline transporter-like protein 1	SLC44A1	-1,55	N.D.
1-phosphatidylinositol 4,5-bisphosphate phosphodiesterase beta-2	PLCB2	-1,54	0,02
Periodic tryptophan protein 1 homolog	PWP1	-1,54	0,12
Dual specificity mitogen-activated protein kinase kinase 2	MAP2K2	-1,54	0,40
Beta-catenin-like protein 1	CTNNBL1	-1,54	0,18
Protein phosphatase 1 regulatory subunit 11	PPP1R11	-1,53	N.D.
TATA-binding protein-associated factor 2N	TAF15	-1,53	0,32
Isovaleryl-CoA dehydrogenase, mitochondrial	IVD	-1,53	0,06
Uncharacterized protein KIAA1211	KIAA1211	-1,53	N.D.
TBC1 domain family member 17	TBC1D17	-1,53	N.D.
Spartin	SPG20	-1,52	0,47
Perilipin-2	PLIN2	-1,52	0,01
Brain-specific angiogenesis inhibitor 1-associated protein 2	BAIAP2	-1,52	0,16
Ankyrin repeat domain-containing protein 17	ANKRD17	-1,52	0,19
TFIIH basal transcription factor complex helicase XPB subunit	ERCC3	-1,52	0,05
Myeloid cell surface antigen CD33	CD33	-1,52	0,12
Gamma-glutamyl hydrolase	GGH	-1,52	0,01
Serine/threonine-protein kinase 26	STK26	-1,52	0,29
Eukaryotic translation initiation factor 2-alpha kinase 4	EIF2AK4	-1,52	0,66
Dynamin-3	DNM3	-1,51	N.D.
Solute carrier family 43 member 3	SLC43A3	-1,51	0,19
Dimethyladenosine transferase 1, mitochondrial	TFB1M	-1,51	0,45
RAC-alpha serine/threonine-protein kinase	AKT1	-1,51	0,46
Cystathionine beta-synthase	CBS	-1,51	0,20
Ubiquitin carboxyl-terminal hydrolase 28	USP28	-1,51	1,14
Ubiquitin/ISG15-conjugating enzyme E2 L6	UBE2L6	-1,50	0,44
tRNA (guanine(26)-N(2))-dimethyltransferase	TRMT1	-1,50	0,38
FAS-associated death domain protein	FADD	-1,49	0,25
RNA-binding protein Musashi homolog 2	MSI2	-1,49	0,60
Coronin-1C	CORO1C	-1,49	0,10
Superoxide dismutase [Cu-Zn]	SOD1	-1,48	0,27
Transmembrane protein 50A	TMEM50A	-1,48	0,34
Dedicator of cytokinesis protein 7	DOCK7	-1,48	0,57
Spermatogenesis-associated protein 5	SPATA5	-1,48	0,13
Ribosyldihydronicotinamide dehydrogenase [quinone]	NQO2	-1,48	0,09
Tyrosyl-DNA phosphodiesterase 2	TDP2	-1,48	0,66
Syntaxin-7	STX7	-1,48	0,07
Chromodomain-helicase-DNA-binding protein 2	CHD2	-1,47	0,23
Protein-glutamine gamma-glutamyltransferase E	TGM3	-1,47	N.D.
DNA polymerase beta	POLB	-1,46	N.D.
Aspartate--tRNA ligase, mitochondrial	DARS2	-1,46	0,05
Lamin-B receptor	LBR	-1,46	0,06
Transient receptor potential cation channel subfamily V member 2	TRPV2	-1,46	N.D.
Guanine nucleotide-binding protein G(I)/G(S)/G(O) subunit gamma-7	GNG7	-1,46	0,27
Hepatoma-derived growth factor-related protein 2	HDGFRP2	-1,46	0,31
Werner syndrome ATP-dependent helicase	WRN	-1,46	0,31
Helicase-like transcription factor	HLTF	-1,45	0,32
Active regulator of SIRT1	RPS19BP1	-1,45	0,35
Oxidation resistance protein 1	OXR1	-1,45	N.D.
Serine/threonine-protein kinase MRCK beta	CDC42BPB	-1,45	0,82
Rab11 family-interacting protein 1	RAB11FIP1	-1,45	0,29
Golgi-associated PDZ and coiled-coil motif-containing protein	GOPC	-1,44	N.D.
RB1-inducible coiled-coil protein 1	RB1CC1	-1,44	0,31
Zinc finger protein ZPR1	ZPR1	-1,44	0,11
Echinoderm microtubule-associated protein-like 3	EML3	-1,44	0,47
Myotubularin-related protein 12	MTMR12	-1,44	0,56
Guanine nucleotide-binding protein-like 1	GNL1	-1,43	0,02
Ras-related protein R-Ras2	RRAS2	-1,43	N.D.
Rho guanine nucleotide exchange factor 12	ARHGEF12	-1,43	1,47
Glucosamine 6-phosphate N-acetyltransferase	GNPNAT1	-1,43	0,19
ADP-ribosylation factor-like protein 8A	ARL8A	-1,43	0,62

Protein LTV1 homolog	LTV1	-1,42	0,25
N-alpha-acetyltransferase 25, NatB auxiliary subunit	NAA25	-1,42	0,03
Kinesin-like protein KIF13B	KIF13B	-1,42	1,03
Apoptosis-inducing factor 2	AIFM2	-1,42	N.D.
Protein SCO1 homolog, mitochondrial	SCO1	-1,42	0,07
Zinc finger CCCH domain-containing protein 18	ZC3H18	-1,42	0,85
Phosphatidylinositol 4-kinase type 2-alpha	PI4K2A	-1,42	0,31
Tropomyosin alpha-4 chain	TPM4	-1,42	0,46
Serpin B6	SERPINB6	-1,41	0,02
Acyl-coenzyme A thioesterase 9, mitochondrial	ACOT9	-1,41	1,95
Cold-inducible RNA-binding protein	CIRBP	-1,41	0,38
Unconventional myosin-Ic	MYO1C	-1,41	0,16
WW domain-binding protein 2	WBP2	-1,41	0,85
NAD-dependent protein deacylase sirtuin-5, mitochondrial	SIRT5	-1,41	N.D.
Protein CBFA2T3	CBFA2T3	-1,41	N.D.
Transmembrane protein 223	TMEM223	-1,40	0,09
Transmembrane protein 109	TMEM109	-1,40	0,41
Probable ubiquitin carboxyl-terminal hydrolase FAF-X	USP9X	-1,40	0,17
Quinone oxidoreductase	CRYZ	-1,40	0,02
Nuclear pore complex protein Nup50	NUP50	-1,40	0,23
Glycerol-3-phosphate acyltransferase 4	AGPAT6	-1,39	0,52
Cytohesin-1	CYTH1	-1,39	N.D.
Probable RNA-binding protein 19	RBM19	-1,39	0,09
Glutamate--cysteine ligase regulatory subunit	GCLM	-1,39	0,03
Protein zyg-11 homolog B	ZYG11B	-1,39	N.D.
Threonylcarbamoyladenosine tRNA methylthiotransferase	CDKAL1	-1,39	N.D.
Proline-, glutamic acid- and leucine-rich protein 1	PELP1	-1,39	0,03
Vacuolar protein sorting-associated protein 51 homolog	VPS51	-1,39	0,11
Merlin	NF2	-1,39	N.D.
ERO1-like protein alpha	ERO1L	-1,38	0,02
Mitofusin-1	MFN1	-1,38	N.D.
Basement membrane-specific heparan sulfate proteoglycan core protein	HSPG2	-1,38	0,17
Macrophage erythroblast attacher	MAEA	-1,38	N.D.
Ras-related protein Rap-2b	RAP2B	-1,38	0,23
Vam6/Vps39-like protein	VPS39	-1,37	0,44
Dedicator of cytokinesis protein 5	DOCK5	-1,37	0,27
Coiled-coil domain-containing protein 124	CCDC124	-1,37	0,21
N-alpha-acetyltransferase 20	NAA20	-1,37	0,46
Activating signal cointegrator 1 complex subunit 2	ASCC2	-1,37	0,77
Acylpyruvase FAHD1, mitochondrial	FAHD1	-1,37	0,02
cAMP-dependent protein kinase type II-beta regulatory subunit	PRKAR2B	-1,37	N.D.
Carboxypeptidase Q	CPQ	-1,36	0,42
Methylenetetrahydrofolate reductase	MTHFR	-1,36	0,97
ATPase ASNA1	ASNA1	-1,36	0,14
Uveal autoantigen with coiled-coil domains and ankyrin repeats	UACA	-1,36	1,10
Poly [ADP-ribose] polymerase 10	PARP10	-1,36	0,69
A-kinase anchor protein 8	AKAP8	-1,36	0,14
Aminopeptidase N	ANPEP	-1,35	0,16
Ubiquinol-cytochrome-c reductase complex assembly factor 3	UQCC3	-1,35	0,07
Ubiquitin carboxyl-terminal hydrolase 11	USP11	-1,35	0,58
Integrin alpha-M	ITGAM	-1,35	0,19
Ferritin light chain	FTL	-1,35	0,21
Multivesicular body subunit 12A	MVB12A	-1,35	N.D.
Heterochromatin protein 1-binding protein 3	HP1BP3	-1,34	0,14
Galectin-9	LGALS9	-1,34	0,86
Prostaglandin G/H synthase 1	PTGS1	-1,34	N.D.
Propionyl-CoA carboxylase beta chain, mitochondrial	PCCB	-1,34	0,04
Poly [ADP-ribose] polymerase 14	PARP14	-1,34	0,17
RWD domain-containing protein 4	RWDD4	-1,33	0,18
Branched-chain-amino-acid aminotransferase, cytosolic	BCAT1	-1,33	0,30
Tetratricopeptide repeat protein 9C	TTC9C	-1,33	0,42
Oxysterol-binding protein-related protein 11 and 10	OSBPL11;OSBPL10	-1,33	0,40
Diphthine synthase	DPH5	-1,33	0,28
Phosphoacetylglucosamine mutase	PGM3	-1,33	0,09
3-mercaptopyruvate sulfurtransferase	MPST	-1,33	0,22
Mitogen-activated protein kinase kinase kinase kinase 4	MAP4K4	-1,32	0,05
Cysteine and histidine-rich domain-containing protein 1	CHORDC1	-1,32	0,08
Ribonuclease P protein subunit p25-like protein	RPP25L	-1,32	0,40
Nucleoside diphosphate-linked moiety X motif 19, mitochondrial	NUDT19	-1,32	0,74
Ester hydrolase C11orf54	C11orf54	-1,32	0,18
NADH-cytochrome b5 reductase 1	CYB5R1	-1,32	N.D.
Probable ATP-dependent RNA helicase DDX6	DDX6	-1,32	0,24
ATP-dependent RNA helicase DDX3Y	DDX3Y	-1,32	0,39
tRNA-dihydrouridine(20) synthase [NAD(P)+]-like	DUS2	-1,31	N.D.
Nuclear mitotic apparatus protein 1	NUMA1	-1,31	0,01
Microfibrillar-associated protein 1	MFAP1	-1,31	N.D.
Phosphatidylinositol 5-phosphate 4-kinase type-2 alpha	PIP4K2A	-1,30	0,57
Serine/threonine-protein kinase MARK2	MARK2	-1,30	N.D.
RNA-binding protein 42	RBM42	-1,30	0,38
Plasma alpha-L-fucosidase	FUCA2	-1,30	N.D.

Membrane-associated guanylate kinase, WW and PDZ domain-containing protein 1	MAGI1	-1,29	1,53
Transmembrane protein 126A	TMEM126A	-1,29	0,24
Methylmalonate-semialdehyde dehydrogenase [acylating], mitochondrial	ALDH6A1	-1,29	N.D.
DDB1- and CUL4-associated factor 7	DCAF7	-1,29	N.D.
Tetratricopeptide repeat protein 27	TTC27	-1,29	0,00
Poly(ADP-ribose) glycohydrolase ARH3	ADPRHL2	-1,29	0,07
Calpain-1 catalytic subunit	CAPN1	-1,29	0,07
Aminopeptidase B	RNPEP	-1,29	0,04
Tripartite motif-containing protein 65	TRIM65	-1,29	0,18
Biogenesis of lysosome-related organelles complex 1 subunit 5	BLOC1S5	-1,29	0,44
Proteasomal ATPase-associated factor 1	PAAF1	-1,29	0,28
Ragulator complex protein LAMTOR1	LAMTOR1	-1,28	0,07
Glutathione reductase, mitochondrial	GSR	-1,28	0,09
FACT complex subunit SPT16	SUPT16H	-1,28	0,22
Multidrug resistance-associated protein 1	ABCC1	-1,28	0,18
Platelet-activating factor acetylhydrolase IB subunit beta	PAFAH1B2	-1,28	0,04
Beta-arrestin-1	ARRB1	-1,28	0,30
Vesicle-associated membrane protein 3	VAMP3;VAMP2	-1,28	0,29
Microtubule-associated protein 1S	MAP1S	-1,27	0,01
RNA-binding protein 14	RBM14	-1,27	0,73
PDZ domain-containing protein 8	PDZD8	-1,27	N.D.
AH receptor-interacting protein	AIP	-1,27	0,13
Crossover junction endonuclease MUS81	MUS81	-1,27	N.D.
Zinc finger protein 574	ZNF574	-1,27	0,44
Proline-rich protein PRCC	PRCC	-1,27	N.D.
Calcineurin B homologous protein 1	CHP1	-1,27	0,08
Transferrin receptor protein 2	TFR2	-1,27	N.D.
Nucleolar protein 56	NOP56	-1,26	0,23
Signal transducing adapter molecule 1	STAM	-1,26	0,47
Aldo-keto reductase family 1 member C3	AKR1C3	-1,26	N.D.
Peflin	PEF1	-1,26	0,13
ATP-dependent RNA helicase DDX55	DDX55	-1,26	0,54
Di-N-acetylchitobiase	CTBS	-1,26	N.D.
Epiplakin	EPPK1	-1,26	N.D.
Protein diaphanous homolog 1	DIAPH1	-1,25	0,13
Fermitin family homolog 3	FERMT3	-1,25	0,05
Lysosomal Pro-X carboxypeptidase	PRCP	-1,25	0,03
Testis-expressed sequence 10 protein	TEX10	-1,25	0,12
Protein SDA1 homolog	SDAD1	-1,25	0,29
YTH domain-containing family protein 3	YTHDF3	-1,25	0,60
Spermatid perinuclear RNA-binding protein	STRBP	-1,25	0,61
E3 ubiquitin-protein ligase UBR3	UBR3	-1,25	N.D.
Golgi SNAP receptor complex member 2	GOSR2	-1,24	0,09
Polypyrimidine tract-binding protein 3	PTBP3	-1,24	1,17
Leukosialin	SPN	-1,24	0,23
Neuropathy target esterase	PNPLA6	-1,24	0,08
Pre-mRNA-splicing factor 38A	PRPF38A	-1,24	0,28
Transmembrane emp24 domain-containing protein 1	TMED1	-1,24	0,32
NADH dehydrogenase [ubiquinone] 1 alpha subcomplex assembly factor 5	NDUFAF5	-1,24	N.D.
Peptidyl-prolyl cis-trans isomerase FKBP1A	FKBP1A	-1,23	0,06
RRP15-like protein	RRP15	-1,23	N.D.
Ragulator complex protein LAMTOR3	LAMTOR3	-1,23	0,04
rRNA/tRNA 2-O-methyltransferase fibrillarin-like protein 1	FBLL1	-1,23	N.D.
tRNA-dihydrouridine(47) synthase [NAD(P)(+)]-like	DUS3L	-1,23	0,22
Zinc finger protein 512	ZNF512	-1,23	N.D.
Lymphokine-activated killer T-cell-originated protein kinase	PBK	-1,23	0,08
Vacuolar protein sorting-associated protein 13B	VPS13B	-1,23	0,18
DNA-directed RNA polymerase III subunit RPC6	POLR3F	-1,22	N.D.
Ribonucleoprotein PTB-binding 1	RAVER1	-1,22	0,44
Transmembrane protein 68	TMEM68	-1,22	N.D.
U1 small nuclear ribonucleoprotein 70 kDa	SNRNP70	-1,22	0,38
Actin-related protein 6	ACTR6	-1,22	N.D.
Ribonucleoside-diphosphate reductase subunit M2	RRM2	-1,22	N.D.
Coiled-coil domain-containing protein 9	CCDC9	-1,22	0,79
Cytochrome c oxidase assembly protein COX19	COX19	-1,22	N.D.
SURP and G-patch domain-containing protein 1	SUGP1	-1,22	N.D.
Chromobox protein homolog 1	CBX1	-1,22	0,07
Putative pre-mRNA-splicing factor ATP-dependent RNA helicase DHX16	DHX16	-1,22	0,18
Retinol dehydrogenase 10	RDH10	-1,22	N.D.
Prostaglandin reductase 2	PTGR2	-1,21	N.D.
Intercellular adhesion molecule 1	ICAM1	-1,21	0,64
Septin-9	SEPT9	-1,21	0,13
Non-syndromic hearing impairment protein 5	DFNA5	-1,21	N.D.
Mannose-P-dolichol utilization defect 1 protein	MPDU1	-1,21	0,03
Peptidyl-prolyl cis-trans isomerase D	PPID	-1,21	0,10
Serine/threonine-protein phosphatase 6 regulatory subunit 3	PPP6R3	-1,21	0,08
RING finger protein 214	RNF214	-1,21	0,29
Protein-methionine sulfoxide oxidase MICAL3	MICAL3	-1,21	N.D.
SWI/SNF-related matrix-associated actin-dependent regulator of chromatin subfamily D member 1	SMARCD1	-1,21	0,10
DNA-directed RNA polymerase III subunit RPC1	POLR3A	-1,21	0,13

Mitochondrial ribonuclease P protein 3	KIAA0391	-1,21	N.D.
Protein O-mannose kinase	POMK	-1,21	N.D.
Protein-associating with the carboxyl-terminal domain of ezrin	SCYL3	-1,20	N.D.
Protein yippee-like 5	YPEL5	-1,20	0,06
U3 small nucleolar ribonucleoprotein protein MPP10	MPHOSPH10	-1,20	N.D.
Alcohol dehydrogenase class-3	ADH5	-1,20	0,05
Intermediate conductance calcium-activated potassium channel protein 4	KCNN4	-1,20	N.D.
Dedicator of cytokinesis protein 6	DOCK6	-1,20	0,44
General transcription factor IIH subunit 3	GTF2H3	-1,20	N.D.
UPF0462 protein C4orf33	C4orf33	-1,20	N.D.
Leukotriene A-4 hydrolase	LTA4H	-1,20	0,13
UPF0428 protein CXorf56	CXorf56	-1,20	N.D.
Guanine nucleotide-binding protein-like 3-like protein	GNL3L	-1,19	N.D.
DDB1- and CUL4-associated factor 8	DCAF8	-1,19	0,57
Pre-mRNA-processing factor 19	PRPF19	-1,19	0,21
PHD finger protein 6	PHF6	-1,19	0,11
WD repeat-containing protein 18	WDR18	-1,19	0,17
Lamin-B2	LMNB2	-1,18	0,04
Menin	MEN1	-1,18	0,58
Phosphoribosyl pyrophosphate synthase-associated protein 2	PRPSAP2	-1,18	0,37
Guanine nucleotide-binding protein subunit alpha-11	GNA11	-1,18	0,48
A-kinase anchor protein 8-like	AKAP8L	-1,18	0,07
Ubiquitin carboxyl-terminal hydrolase 24	USP24	-1,17	0,30
Adapter molecule crk	CRK	-1,17	0,66
Tether containing UBX domain for GLUT4	ASPSCR1	-1,17	0,26
Leucine-rich repeat-containing protein 47	LRRC47	-1,17	0,04
Peptidyl-tRNA hydrolase 2, mitochondrial	PTRH2	-1,17	0,23
Lysosomal acid lipase/cholesteryl ester hydrolase	LIPA	-1,17	N.D.
Diphthamide biosynthesis protein 1	DPH1	-1,17	0,29
Probable methyltransferase-like protein 15	METTL15	-1,17	N.D.
Trafficking protein particle complex subunit 10	TRAPPC10	-1,17	0,10
Kinesin-like protein KIFC1	KIFC1	-1,17	N.D.
Vacuolar protein sorting-associated protein 53 homolog	VPS53	-1,16	0,51
Retinoblastoma-binding protein 5	RBBP5	-1,16	0,20
FACT complex subunit SSRP1	SSRP1	-1,16	1,07
Mitochondrial import inner membrane translocase subunit Tim10 B	TIMM10B	-1,16	0,08
Lipopolysaccharide-responsive and beige-like anchor protein	LRBA	-1,16	0,19
Adaptin ear-binding coat-associated protein 2	NECAP2	-1,16	0,09
SET and MYND domain-containing protein 5	SMYD5	-1,16	0,70
AP-1 complex subunit gamma-like 2	AP1G2	-1,16	0,34
COX assembly mitochondrial protein 2 homolog	CMC2	-1,16	0,31
Enolase-phosphatase E1	ENOPH1	-1,15	0,13
Diphosphoinositol polyphosphate phosphohydrolase 1	NUDT3	-1,15	0,47
RNA-binding protein 10	RBM10	-1,15	0,26
General transcription factor IIE subunit 1	GTF2E1	-1,15	N.D.
LYR motif-containing protein 4	LYRM4	-1,15	0,47
[3-methyl-2-oxobutanoate dehydrogenase [lipoamide]] kinase, mitochondrial	BCKDK	-1,15	N.D.
Receptor-type tyrosine-protein phosphatase gamma	PTPRG	-1,15	N.D.
Tumor necrosis factor receptor type 1-associated DEATH domain protein	TRADD	-1,14	0,33
Heterogeneous nuclear ribonucleoprotein R	HNRNPR	-1,14	0,12
UPF0585 protein C16orf13	C16orf13	-1,14	0,15
Histone deacetylase 2	HDAC2	-1,14	0,19
Nucleoredoxin	NXN	-1,14	N.D.
Cytoplasmic tRNA 2-thiolation protein 1	CTU1	-1,14	N.D.
Nuclear RNA export factor 1	NXF1	-1,13	0,71
Transcriptional repressor CTCF	CTCF	-1,13	0,12
Dihydrolipoyllysine-residue acetyltransferase component of pyruvate dehydrogenase complex, mitochondrial	DLAT	-1,13	0,01
Triple functional domain protein	TRIO	-1,13	0,36
UV excision repair protein RAD23 homolog B	RAD23B	-1,13	0,85
General transcription factor IIH subunit 4	GTF2H4	-1,12	N.D.
Bcl-2-associated transcription factor 1	BCLAF1	-1,12	0,17
Kinectin	KTN1	-1,12	0,00
Glucose-induced degradation protein 8 homolog	GID8	-1,12	0,08
U6 snRNA-associated Sm-like protein LSm1	LSM1	-1,12	0,22
Nuclear factor NF-kappa-B p105 subunit;Nuclear factor NF-kappa-B p50 subunit	NFKB1	-1,12	0,14
Zinc finger and BTB domain-containing protein 40	ZBTB40	-1,12	0,16
Dual specificity mitogen-activated protein kinase kinase 1	MAP2K1	-1,11	N.D.
Armadillo repeat-containing protein 6	ARMC6	-1,11	0,49
Scaffold attachment factor B2	SAFB2	-1,11	0,13
Calcineurin subunit B type 1	PPP3R1	-1,11	0,10
Armadillo repeat-containing protein 10	ARMC10	-1,11	0,04
Spermatogenesis-associated protein 5-like protein 1	SPATA5L1	-1,10	0,47
UBX domain-containing protein 1	UBXN1	-1,10	0,30
Craniofacial development protein 1	CFDP1	-1,10	N.D.
tRNA pseudouridine synthase A, mitochondrial	PUS1	-1,10	0,32
Nuclear protein localization protein 4 homolog	NPLOC4	-1,10	0,03
General transcription factor IIH subunit 1	GTF2H1	-1,10	N.D.
Protein phosphatase methylesterase 1	PPME1	-1,10	0,01
Cyclic AMP-dependent transcription factor ATF-1	ATF1	-1,10	N.D.
WD repeat-containing protein 89	WDR89	-1,09	N.D.

Mitochondrial import inner membrane translocase subunit Tim22	TIMM22	-1,09	N.D.
Lysine-specific demethylase 6A;Histone demethylase UTY	KDM6A;UTY	-1,09	N.D.
Thyroid hormone receptor-associated protein 3	THRAP3	-1,09	0,14
Fascin	FSCN1	-1,09	0,02
rRNA methyltransferase 1, mitochondrial	MRM1	-1,09	N.D.
Mitogen-activated protein kinase kinase kinase 5	MAP3K5	-1,08	0,32
Protein DEK	DEK	-1,08	N.D.
Lanosterol synthase	LSS	-1,08	0,05
Propionyl-CoA carboxylase alpha chain, mitochondrial	PCCA	-1,08	0,13
SRSF protein kinase 1	SRPK1	-1,08	0,03
Thymocyte nuclear protein 1	THYN1	-1,08	0,25
Charged multivesicular body protein 2a	CHMP2A	-1,08	N.D.
Serine/threonine-protein phosphatase 1 regulatory subunit 10	PPP1R10	-1,07	0,08
Transcriptional regulator ATRX	ATRX	-1,07	0,38
ATPase inhibitor, mitochondrial	ATPIF1	-1,07	0,28
Transcription activator BRG1	SMARCA4	-1,07	0,19
Protein farnesyltransferase subunit beta	FNTB	-1,07	0,29
Nucleolysin TIA-1 isoform p40	TIA1	-1,07	N.D.
Protein asunder homolog	ASUN	-1,07	N.D.
5-nucleotidase domain-containing protein 1	NT5DC1	-1,06	2,07
Interferon-induced, double-stranded RNA-activated protein kinase	EIF2AK2	-1,06	0,17
Mothers against decapentaplegic homolog 5 and 1	SMAD5;SMAD1	-1,06	0,18
YTH domain-containing protein 1	YTHDC1	-1,06	0,75
Ribosomal RNA processing protein 1 homolog A	RRP1	-1,05	0,39
Exosome complex component RRP45	EXOSC9	-1,05	0,09
Mitofusin-2	MFN2	-1,05	N.D.
AP-2 complex subunit alpha-1	AP2A1	-1,05	0,00
Ragulator complex protein LAMTOR2	LAMTOR2	-1,05	0,13
NAD-dependent protein deacetylase sirtuin-2	SIRT2	-1,05	N.D.
Protein Hikeshi	C11orf73	-1,05	0,33
14-3-3 protein zeta/delta	YWHAZ	-1,04	0,01
Activator of basal transcription 1	ABT1	-1,04	0,55
Germinal-center associated nuclear protein	MCM3AP	-1,04	0,28
Mevalonate kinase	MVK	-1,04	N.D.
Glutamine-dependent NAD(+) synthetase	NADSYN1	-1,04	0,01
Alpha-ketoglutarate-dependent dioxygenase FTO	FTO	-1,04	0,19
Putative ribonuclease	YBEY	-1,04	1,07
Proline synthase co-transcribed bacterial homolog protein	PROSC	-1,04	0,04
Pericentriolar material 1 protein	PCM1	-1,04	0,48
Mitochondrial antiviral-signaling protein	MAVS	-1,04	0,13
Nuclear factor NF-kappa-B p100 subunit;Nuclear factor NF-kappa-B p52 subunit	NFKB2	-1,03	0,00
WD repeat-containing protein 26	WDR26	-1,03	0,71
Phosphoribosyl pyrophosphate synthase-associated protein 1	PRPSAP1	-1,03	0,15
Poly(rC)-binding protein 1	PCBP1	-1,03	0,06
Serine/threonine-protein phosphatase 2A activator	PPP2R4	-1,03	0,04
Pyrroline-5-carboxylate reductase 2	PYCR2	-1,03	0,16
Serine/threonine-protein kinase RIO2	RIOK2	-1,03	N.D.
SAP domain-containing ribonucleoprotein	SARNP	-1,03	N.D.
Nuclear receptor 2C2-associated protein	NR2C2AP	-1,02	0,25
Amino-terminal enhancer of split	AES	-1,02	0,60
Selenide, water dikinase 2	SEPHS2	-1,02	N.D.
BMP-2-inducible protein kinase	BMP2K	-1,02	0,13
Synembryn-A	RIC8A	-1,02	0,12
Galactocerebrosidase	GALC	-1,02	0,51
Translation machinery-associated protein 16	TMA16	-1,02	0,14
Adenylate kinase 4, mitochondrial	AK4	-1,02	0,00
	SMCR7L	-1,02	0,43
Ragulator complex protein LAMTOR5	LAMTOR5	-1,02	0,08
Endophilin-A2	SH3GL1	-1,01	N.D.
Ubiquitin conjugation factor E4 B	UBE4B	-1,01	0,28
Epidermal growth factor receptor substrate 15-like 1	EPS15L1	-1,01	0,56
Serine/arginine-rich splicing factor 11	SRSF11	-1,01	0,06
Serine/threonine-protein phosphatase 2A 56 kDa regulatory subunit delta isoform	PPP2R5D	-1,01	0,10
Pre-rRNA-processing protein TSR1 homolog	TSR1	-1,01	0,26
Zinc finger protein 579	ZNF579	-1,01	N.D.
F-BAR domain only protein 2	FCHO2	-1,01	N.D.
Putative transferase CAF17, mitochondrial	IBA57	-1,01	0,07
Complement factor H	CFH	-1,01	N.D.
Protein LSM14 homolog A	LSM14A	-1,01	0,09
Thiosulfate sulfurtransferase	TST	-1,01	0,00
Serine/threonine-protein kinase Nek7	NEK7	-1,01	N.D.
Solute carrier family 35 member F2	SLC35F2	-1,01	N.D.
Armadillo repeat-containing protein 1	ARMC1	-1,01	N.D.
Ataxin-2	ATXN2	-1,00	0,14
Ribonuclease inhibitor	RNH1	-1,00	0,15
Scaffold attachment factor B1	SAFB	-1,00	0,08
Methyl-CpG-binding protein 2	MECP2	-1,00	N.D.
Peptidyl-prolyl cis-trans isomerase FKBP2	FKBP2	-1,00	0,03
Methionine aminopeptidase 1	METAP1	-1,00	0,27
Small subunit processome component 20 homolog	UTP20	-1,00	0,09

Squalene monooxygenase	SQLE	-1,00	1,15
Nuclear receptor corepressor 1	NCOR1	-1,00	0,13
Ig gamma-1 chain C region	IGHG1	-1,00	N.D.
Tubulin alpha-1C chain	TUBA1C	-1,00	0,20
ATP-dependent DNA helicase Q5	RECQL5	-1,00	N.D.
cAMP-dependent protein kinase catalytic subunit alpha	PRKACA	-1,00	0,29
CD82 antigen	CD82	-1,00	1,51
Splicing factor, arginine/serine-rich 19	SCAF1	-0,99	0,63
KH domain-containing, RNA-binding, signal transduction-associated protein 1	KHDRBS1	-0,99	0,01
Ribosomal L1 domain-containing protein 1	RSL1D1	-0,99	0,07
ATP-dependent RNA helicase DDX54	DDX54	-0,99	0,49
AN1-type zinc finger protein 1	ZFAND1	-0,99	0,11
GA-binding protein subunit beta-1	GABPB1	-0,99	N.D.
G patch domain-containing protein 4	GPATCH4	-0,99	0,52
Putative RNA-binding protein 15	RBM15	-0,99	0,04
Tryptophan--tRNA ligase, cytoplasmic;T1-TrpRS;T2-TrpRS	WARS	-0,99	0,53
Collagen alpha-1(XVIII) chain;Endostatin	COL18A1	-0,99	1,68
Protein argonaute-1	AGO1	-0,99	N.D.
NADH dehydrogenase [ubiquinone] complex I, assembly factor 7	NDUFAF7	-0,98	2,02
Serine/threonine-protein phosphatase 2B catalytic subunit alpha isoform	PPP3CA	-0,98	0,00
Cyclin-dependent kinase 11B;Cyclin-dependent kinase 11A	CDK11B;CDK11A	-0,98	N.D.
28S ribosomal protein S22, mitochondrial	MRPS22	-0,98	0,32
Lanosterol 14-alpha demethylase	CYP51A1	-0,98	N.D.
Fumarylacetoacetase	FAH	-0,98	0,14
Gamma-tubulin complex component 4	TUBGCP4	-0,97	0,59
Deoxyhypusine hydroxylase	DOHH	-0,97	0,49
Decaprenyl-diphosphate synthase subunit 2	PDSS2	-0,97	N.D.
Ras-related GTP-binding protein C	RRAGC	-0,97	0,45
Frataxin, mitochondrial	FXN	-0,97	0,09
DNA polymerase subunit gamma-2, mitochondrial	POLG2	-0,97	N.D.
Thymosin beta-10	TMSB10	-0,97	0,11
THAP domain-containing protein 11	THAP11	-0,97	N.D.
Phosphatidate cytidylyltransferase, mitochondrial	TAMM41	-0,96	N.D.
ATP-dependent RNA helicase A	DHX9	-0,96	0,04
FAST kinase domain-containing protein 5	FASTKD5	-0,96	0,27
Multiple myeloma tumor-associated protein 2	MMTAG2	-0,96	0,38
Casein kinase I isoform alpha;Casein kinase I isoform alpha-like	CSNK1A1;CSNK1A1L	-0,96	0,26
Mediator of RNA polymerase II transcription subunit 16	MED16	-0,96	0,04
Ras GTPase-activating protein 3	RASA3	-0,96	0,31
Protein LAP2	ERBB2IP	-0,96	0,03
Guanine nucleotide-binding protein G(k) subunit alpha	GNAI3	-0,96	0,09
Protein Dr1	DR1	-0,96	0,20
Activating signal cointegrator 1 complex subunit 1	ASCC1	-0,96	N.D.
Replication protein A 32 kDa subunit	RPA2	-0,96	0,16
S-formylglutathione hydrolase	ESD	-0,96	0,04
Selenoprotein H	SELH	-0,95	0,04
Epididymal secretory protein E1	NPC2	-0,95	0,27
Protein S100-A10	S100A10	-0,95	0,13
Phosphatidylinositol transfer protein alpha isoform	PITPNA	-0,95	0,09
Replication protein A 70 kDa DNA-binding subunit	RPA1	-0,95	0,14
Platelet-activating factor acetylhydrolase IB subunit gamma	PAFAH1B3	-0,95	0,05
Xaa-Pro dipeptidase	PEPD	-0,95	0,09
Exocyst complex component 7	EXOC7	-0,95	0,20
Endothelin-converting enzyme 1	ECE1	-0,95	0,23
28S ribosomal protein S35, mitochondrial	MRPS35	-0,95	0,03
Glutathione S-transferase omega-1	GSTO1	-0,95	0,03
Interleukin enhancer-binding factor 3	ILF3	-0,95	0,04
E3 ubiquitin-protein ligase HECTD3	HECTD3	-0,95	N.D.
1-acyl-sn-glycerol-3-phosphate acyltransferase alpha	AGPAT1	-0,95	0,40
Krueppel-like factor 16	KLF16	-0,94	N.D.
Mannose-6-phosphate isomerase	MPI	-0,94	0,40
SRSF protein kinase 2	SRPK2	-0,94	0,75
DNA topoisomerase 3-beta-1	TOP3B	-0,94	N.D.
Heterogeneous nuclear ribonucleoprotein H2	HNRNPH2	-0,94	0,07
H/ACA ribonucleoprotein complex subunit 1	GAR1	-0,94	0,13
N-acetyltransferase 10	NAT10	-0,94	0,34
Methionine--tRNA ligase, cytoplasmic	MARS	-0,94	0,03
DNA-directed RNA polymerase, mitochondrial	POLRMT	-0,94	0,08
MOB kinase activator 1B	MOB1B	-0,94	0,38
	ASNSD1	-0,94	N.D.
UV excision repair protein RAD23 homolog A	RAD23A	-0,94	0,01
Epsin-1	EPN1	-0,93	0,22
Thioredoxin-interacting protein	TXNIP	-0,93	0,22
Diacylglycerol O-acyltransferase 1	DGAT1	-0,93	N.D.
H/ACA ribonucleoprotein complex subunit 4	DKC1	-0,93	0,37
Zinc finger protein 316	ZNF316	-0,93	0,13
Phosphorylase b kinase regulatory subunit beta	PHKB	-0,93	0,12
Transformer-2 protein homolog beta	TRA2B	-0,93	0,01
Polyadenylate-binding protein 1	PABPC1	-0,93	0,63
Snurportin-1	SNUPN	-0,92	0,06

DNA-directed RNA polymerase III subunit RPC3	POLR3C	-0,92	0,57
Tyrosine-protein phosphatase non-receptor type 11	PTPN11	-0,92	0,07
MORC family CW-type zinc finger protein 2	MORC2	-0,92	0,11
AMP deaminase 2	AMPD2	-0,92	0,68
Thimet oligopeptidase	THOP1	-0,92	0,04
Nuclear receptor coactivator 7	NCOA7	-0,91	0,19
Tubulin-specific chaperone D	TBCD	-0,91	0,06
Erlin-2	ERLIN2	-0,91	0,47
Alpha-endosulfine	ENSA	-0,91	0,77
Zinc finger FYVE domain-containing protein 1	ZFYVE1	-0,91	0,29
DNA repair protein RAD50	RAD50	-0,91	0,04
Protein KRI1 homolog	KRI1	-0,91	0,49
Heat shock factor protein 1	HSF1	-0,91	N.D.
ATP-dependent RNA helicase DDX51	DDX51	-0,91	0,21
Serine/threonine-protein phosphatase 2A 65 kDa regulatory subunit A alpha isoform	PPP2R1A	-0,91	0,18
La-related protein 7	LARP7	-0,91	0,19
Probable RNA-binding protein EIF1AD	EIF1AD	-0,91	0,08
Retinoic acid receptor RXR-beta	RXRB	-0,90	N.D.
Acyl-protein thioesterase 2	LYPLA2	-0,90	0,01
Sarcoplasmic/endoplasmic reticulum calcium ATPase 2	ATP2A2	-0,90	0,18
Sorting nexin-1	SNX1	-0,90	0,13
Cyclin-dependent kinases regulatory subunit 2	CKS2	-0,90	N.D.
Mothers against decapentaplegic homolog 3	SMAD3;SMAD2;SMAD9	-0,90	0,46
Cactin	CACTIN	-0,90	0,19
Transcription elongation factor B polypeptide 3	TCEB3	-0,90	N.D.
Serine palmitoyltransferase 2	SPTLC2	-0,89	0,05
Heterogeneous nuclear ribonucleoprotein D0	HNRNPD	-0,89	0,00
U3 small nucleolar ribonucleoprotein protein IMP3	IMP3	-0,89	0,07
Complement component 1 Q subcomponent-binding protein, mitochondrial	C1QBP	-0,89	0,06
Vitamin K-dependent protein S	PROS1	-0,89	0,27
General transcription factor IIH subunit 2-like protein	GTF2H2C;GTF2H2	-0,89	0,08
Transmembrane protein 261	TMEM261	-0,89	N.D.
Pre-mRNA-splicing factor SPF27	BCAS2	-0,89	0,08
Transmembrane protein 256	TMEM256	-0,88	0,04
Zinc finger CCHC domain-containing protein 3	ZCCHC3	-0,88	N.D.
Eukaryotic translation elongation factor 1 epsilon-1	EEF1E1	-0,88	0,35
Calmegin	CLGN	-0,88	0,10
Transcription initiation factor IIA subunit 2	GTF2A2	-0,88	0,24
Protein phosphatase 1 regulatory subunit 12A	PPP1R12A	-0,88	0,05
Translation initiation factor eIF-2B subunit beta	EIF2B2	-0,88	0,07
Myb-binding protein 1A	MYBBP1A	-0,88	0,04
Probable 28S rRNA (cytosine(4447)-C(5))-methyltransferase	NOP2	-0,88	0,10
Transcription and mRNA export factor ENY2	ENY2	-0,88	0,04
DNA dC->dU-editing enzyme APOBEC-3C	APOBEC3C	-0,88	0,11
Ragulator complex protein LAMTOR4	LAMTOR4	-0,87	0,05
Protein TANC1	TANC1	-0,87	0,66
Methyltransferase-like protein 17, mitochondrial	METTL17	-0,87	N.D.
DNA-binding protein SMUBP-2	IGHMBP2	-0,87	1,01
U4/U6 small nuclear ribonucleoprotein Prp31	PRPF31	-0,87	0,03
Breast cancer metastasis-suppressor 1	BRMS1	-0,87	0,16
Integrator complex subunit 8	INTS8	-0,87	0,18
Ubiquitin-like modifier-activating enzyme 1	UBA1	-0,87	0,13
Mitogen-activated protein kinase kinase kinase 7	MAP3K7	-0,87	N.D.
Ankyrin repeat domain-containing protein 27	ANKRD27	-0,87	N.D.
Armadillo repeat-containing X-linked protein 3	ARMCX3	-0,86	N.D.
Non-POU domain-containing octamer-binding protein	NONO	-0,86	0,10
TAR DNA-binding protein 43	TARDBP	-0,86	0,18
Uncharacterized protein C12orf43	C12orf43	-0,86	N.D.
Eukaryotic translation initiation factor 5A-1	EIF5A;EIF5AL1	-0,86	0,21
Pericentrin	PCNT	-0,86	0,05
Mimitin, mitochondrial	NDUFAF2	-0,86	0,01
Nibrin	NBN	-0,86	N.D.
N-terminal Xaa-Pro-Lys N-methyltransferase 1	NTMT1	-0,86	0,25
Ribosomal protein S6 kinase alpha-5	RPS6KA5	-0,85	N.D.
Putative deoxyribonuclease TATDN1	TATDN1	-0,85	0,29
Ribosomal biogenesis protein LAS1L	LAS1L	-0,85	0,22
General transcription factor IIF subunit 1	GTF2F1	-0,85	0,10
Uncharacterized protein NCBP2-AS2	NCBP2-AS2	-0,85	N.D.
Nucleolar protein 10	NOL10	-0,85	0,70
CD59 glycoprotein	CD59	-0,85	0,89
Annexin A3	ANXA3	-0,85	0,07
Set1/Ash2 histone methyltransferase complex subunit ASH2	ASH2L	-0,85	0,46
MORC family CW-type zinc finger protein 3	MORC3	-0,85	0,17
Chromobox protein homolog 8	CBX8	-0,85	N.D.
Transmembrane protein 70, mitochondrial	TMEM70	-0,85	0,17
G protein-coupled receptor kinase 6	GRK6	-0,85	N.D.
Stress-induced-phosphoprotein 1	STIP1	-0,85	0,00
Uncharacterized protein KIAA0825	KIAA0825	-0,85	N.D.
Probable dimethyladenosine transferase	DIMT1	-0,85	0,11
Inhibitor of nuclear factor kappa-B kinase subunit beta	IKBKB	-0,84	0,32

Pre-mRNA-splicing regulator WTAP	WTAP	-0,84	N.D.
Cytosol aminopeptidase	LAP3	-0,84	0,24
D-tyrosyl-tRNA(Tyr) deacylase 1	DTD1	-0,84	0,07
Spliceosome RNA helicase DDX39B	DDX39B	-0,84	0,06
Heat shock 70 kDa protein 1B;Heat shock 70 kDa protein 1A	HSPA1B;HSPA1A	-0,84	0,06
A-kinase anchor protein 17A	AKAP17A	-0,84	0,34
Regulator of microtubule dynamics protein 3	RMDN3	-0,84	0,38
28S ribosomal protein S29, mitochondrial	DAP3	-0,84	0,01
Proteasome subunit beta type-5	PSMB5	-0,84	0,07
60S ribosomal protein L7-like 1	RPL7L1	-0,84	0,22
Tetraspanin-14	TSPAN14	-0,84	N.D.
Flotillin-2	FLOT2	-0,84	0,09
Splicing factor 1	SF1	-0,84	0,11
E3 ubiquitin-protein ligase HUWE1	HUWE1	-0,84	0,00
Ras-related protein Rab-37	RAB37	-0,83	1,29
Probable ATP-dependent RNA helicase DHX37	DHX37	-0,83	0,32
Pentatricopeptide repeat-containing protein 1, mitochondrial	PTCD1	-0,83	N.D.
Protein HGH1 homolog	HGH1	-0,83	0,06
Nucleolar protein 58	NOP58	-0,83	0,20
Notchless protein homolog 1	NLE1	-0,83	0,30
Engulfment and cell motility protein 1	ELMO1	-0,83	0,21
Phosphatidylinositol 3-kinase regulatory subunit beta	PIK3R2	-0,83	0,07
Mitochondrial assembly of ribosomal large subunit protein 1	MALSU1	-0,83	0,34
Mitochondrial Rho GTPase 2	RHOT2	-0,83	0,15
Serine/threonine-protein phosphatase PP1-gamma catalytic subunit	PPP1CC	-0,83	0,16
Mitotic spindle assembly checkpoint protein MAD2A	MAD2L1	-0,82	0,35
Histone H1.0;Histone H1.0, N-terminally processed	H1F0	-0,82	0,34
Tyrosine-protein phosphatase non-receptor type 1	PTPN1	-0,82	0,08
Kelch domain-containing protein 4	KLHDC4	-0,82	0,07
Coiled-coil and C2 domain-containing protein 1A	CC2D1A	-0,82	0,04
L-aminoadipate-semialdehyde dehydrogenase-phosphopantetheinyl transferase	AASDHPPT	-0,82	0,02
Nuclear valosin-containing protein-like	NVL	-0,82	0,20
Presequence protease, mitochondrial	PITRM1	-0,82	0,11
Uncharacterized protein C6orf203	C6orf203	-0,82	N.D.
Histone-lysine N-methyltransferase EHMT2	EHMT2	-0,82	N.D.
Polypeptide N-acetylgalactosaminyltransferase 2	GALNT2	-0,82	0,01
Ubiquitin fusion degradation protein 1 homolog	UFD1L	-0,82	0,25
Zinc finger protein 22	ZNF22	-0,82	N.D.
Protein argonaute-2	AGO2	-0,82	0,16
Rho guanine nucleotide exchange factor 10	ARHGEF10	-0,82	0,45
TNF receptor-associated factor 2	TRAF2	-0,82	0,16
N-terminal kinase-like protein	SCYL1	-0,82	0,12
Carnitine O-palmitoyltransferase 1, liver isoform	CPT1A	-0,81	0,04
Serine/threonine-protein phosphatase 6 regulatory ankyrin repeat subunit A	ANKRD28	-0,81	0,02
Ubiquitin-conjugating enzyme E2 variant 2	UBE2V2	-0,81	0,15
Cell division cycle 5-like protein	CDC5L	-0,81	0,08
Exosome complex component RRP40	EXOSC3	-0,81	0,30
Transformer-2 protein homolog alpha	TRA2A	-0,81	N.D.
Platelet-activating factor acetylhydrolase IB subunit alpha	PAFAH1B1	-0,81	0,01
ATP-dependent RNA helicase DDX39A	DDX39A	-0,81	0,32
Ras-related protein Rab-11A	RAB11A	-0,81	N.D.
Protein PAT1 homolog 1	PATL1	-0,81	0,92
Hexokinase-2	HK2	-0,81	0,28
Prolow-density lipoprotein receptor-related protein 1	LRP1	-0,81	0,79
Transitional endoplasmic reticulum ATPase	VCP	-0,81	0,05
Mitochondrial import inner membrane translocase subunit Tim10	TIMM10	-0,80	0,09
Probable ATP-dependent RNA helicase DHX40	DHX40	-0,80	0,17
Phosphopantothenoylcysteine decarboxylase	PPCDC	-0,80	0,05
Mitochondrial import inner membrane translocase subunit Tim9	TIMM9	-0,80	0,02
Vacuolar protein sorting-associated protein 11 homolog	VPS11	-0,80	0,35
RAS protein activator like-3	RASAL3	-0,80	0,13
Protein SMG9	SMG9	-0,80	0,37
HEAT repeat-containing protein 6	HEATR6	-0,80	0,08
Dehydrogenase/reductase SDR family member 7B	DHRS7B	-0,80	0,78
Unhealthy ribosome biogenesis protein 2 homolog	URB2	-0,80	0,10
Cat eye syndrome critical region protein 5	CECR5	-0,80	0,17
Mediator of RNA polymerase II transcription subunit 14	MED14	-0,79	0,15
E2/E3 hybrid ubiquitin-protein ligase UBE2O	UBE2O	-0,79	0,05
Integrator complex subunit 11	CPSF3L	-0,79	0,15
Transaldolase	TALDO1	-0,79	0,05
THUMP domain-containing protein 1	THUMPD1	-0,79	0,06
Coiled-coil domain-containing protein 47	CCDC47	-0,79	0,08
Cysteine desulfurase, mitochondrial	NFS1	-0,79	N.D.
Heterogeneous nuclear ribonucleoprotein F	HNRNPF	-0,79	0,42
CTP synthase 2	CTPS2	-0,79	0,03
Codanin-1	CDAN1	-0,79	0,43
Aspartyl/asparaginyl beta-hydroxylase	ASPH	-0,79	0,29
Transforming growth factor-beta receptor-associated protein 1	TGFBRAP1	-0,79	N.D.
Polynucleotide 5-hydroxyl-kinase NOL9	NOL9	-0,79	0,15
Ras-related protein Rab-35	RAB35	-0,79	0,22

Fatty acid-binding protein, epidermal	FABP5	-0,78	0,22
Pleiotropic regulator 1	PLRG1	-0,78	0,07
Cullin-9	CUL9	-0,78	0,62
Protein virilizer homolog	KIAA1429	-0,78	0,33
Methyltransferase-like protein 13	METTL13	-0,78	0,01
M-phase phosphoprotein 6	MPHOSPH6	-0,78	0,58
Surfeit locus protein 1	SURF1	-0,78	0,72
tRNA (adenine(58)-N(1))-methyltransferase catalytic subunit TRMT61A	TRMT61A	-0,77	0,18
NSFL1 cofactor p47	NSFL1C	-0,77	0,19
Iron-sulfur cluster assembly enzyme ISCU, mitochondrial	ISCU	-0,77	N.D.
Amidophosphoribosyltransferase	PPAT	-0,77	0,14
Plasminogen activator inhibitor 1 RNA-binding protein	SERBP1	-0,77	0,29
TFIIH basal transcription factor complex helicase XPD subunit	ERCC2	-0,77	0,04
N6-adenosine-methyltransferase 70 kDa subunit	METTL3	-0,77	0,01
Alanyl-tRNA editing protein Aarsd1	AARSD1	-0,77	0,17
Oxysterol-binding protein 1	OSBP	-0,77	0,08
2-oxoisovalerate dehydrogenase subunit beta, mitochondrial	BCKDHB	-0,77	0,05
Fructose-bisphosphate aldolase C	ALDOC	-0,76	0,07
Serine/threonine-protein phosphatase 2A 56 kDa regulatory subunit epsilon isoform	PPP2R5E	-0,76	0,09
Equilibrative nucleoside transporter 1	SLC29A1	-0,76	0,44
ELMO domain-containing protein 2	ELMOD2	-0,76	N.D.
Uncharacterized protein C19orf52	C19orf52	-0,76	0,65
1-acyl-sn-glycerol-3-phosphate acyltransferase gamma	AGPAT3	-0,76	0,66
Glutaminase kidney isoform, mitochondrial	GLS	-0,76	0,33
RNA-binding protein 34	RBM34	-0,76	N.D.
Deoxynucleotidyltransferase terminal-interacting protein 1	DNTTIP1	-0,75	N.D.
Protein transport protein Sec23A	SEC23A	-0,75	0,23
Phosphoenolpyruvate carboxykinase [GTP], mitochondrial	PCK2	-0,75	0,04
GTP cyclohydrolase 1 feedback regulatory protein	GCHFR	-0,75	0,19
m7GpppX diphosphatase	DCPS	-0,75	0,06
Nuclear inhibitor of protein phosphatase 1;Activator of RNA decay	PPP1R8	-0,75	0,01
Programmed cell death protein 10	PDCD10	-0,75	0,02
Chromodomain-helicase-DNA-binding protein 1-like	CHD1L	-0,75	0,00
Non-homologous end-joining factor 1	NHEJ1	-0,75	N.D.
Acyl-protein thioesterase 1	LYPLA1	-0,74	0,06
UDP-N-acetylhexosamine pyrophosphorylase	UAP1	-0,74	0,71
tRNA (adenine(58)-N(1))-methyltransferase non-catalytic subunit TRM6	TRMT6	-0,74	0,25
Ubiquitin carboxyl-terminal hydrolase 34	USP34	-0,74	0,06
Double-strand break repair protein MRE11A	MRE11A	-0,74	0,24
Ubiquitin-like protein 7	UBL7	-0,74	0,29
Reticulocalbin-2	RCN2	-0,74	0,14
Mitochondrial fission 1 protein	FIS1	-0,74	0,28
Isobutyryl-CoA dehydrogenase, mitochondrial	ACAD8	-0,74	1,24
Heterogeneous nuclear ribonucleoprotein H3	HNRNPH3	-0,74	0,18
Methyltransferase-like protein 16	METTL16	-0,74	0,04
Serine/threonine-protein kinase A-Raf	ARAF	-0,74	N.D.
Coiled-coil domain-containing protein 127	CCDC127	-0,74	N.D.
Regulation of nuclear pre-mRNA domain-containing protein 1A	RPRD1A	-0,74	0,20
Syntaxin-8	STX8	-0,74	0,04
Ubiquitin carboxyl-terminal hydrolase 14	USP14	-0,74	0,06
Trafficking protein particle complex subunit 4	TRAPPC4	-0,73	0,41
Ubiquitin-like protein 5	UBL5	-0,73	0,07
Mitochondrial import inner membrane translocase subunit TIM44	TIMM44	-0,73	0,09
Zinc finger MYM-type protein 3	ZMYM3	-0,73	0,44
Core histone macro-H2A.1	H2AFY	-0,73	0,10
Melanoma-associated antigen G1	NDNL2	-0,73	N.D.
Stomatin-like protein 2, mitochondrial	STOML2	-0,73	0,18
Mitochondrial glutamate carrier 1	SLC25A22	-0,73	0,19
Elongation factor Tu GTP-binding domain-containing protein 1	EFTUD1	-0,73	0,07
von Willebrand factor A domain-containing protein 9	VWA9	-0,73	0,63
Sorting nexin-5	SNX5	-0,73	0,09
Importin-9	IPO9	-0,73	0,12
Alpha-1,2-mannosyltransferase ALG9	ALG9	-0,73	0,03
Trafficking protein particle complex subunit 6B	TRAPPC6B	-0,73	0,18
Zinc finger protein ubi-d4	DPF2	-0,73	0,33
Amine oxidase [flavin-containing] A	MAOA	-0,72	1,57
POTE ankyrin domain family member I	POTEI	-0,72	N.D.
Zinc finger CCCH domain-containing protein 13	ZC3H13	-0,72	0,11
Protein VAC14 homolog	VAC14	-0,72	0,30
2-oxoisovalerate dehydrogenase subunit alpha, mitochondrial	BCKDHA	-0,72	0,18
Multifunctional protein ADE2	PAICS	-0,72	0,09
Stathmin	STMN1	-0,72	0,22
Probable ATP-dependent RNA helicase DDX52	DDX52	-0,72	0,13
BolA-like protein 2	BOLA2	-0,72	0,02
Glyoxalase domain-containing protein 4	GLOD4	-0,72	0,04
Retinol dehydrogenase 11	RDH11	-0,72	0,24
Eukaryotic translation initiation factor 4E	EIF4E	-0,72	0,10
Neuroblastoma-amplified sequence	NBAS	-0,72	0,06
Heparan sulfate 2-O-sulfotransferase 1	HS2ST1	-0,72	0,24
Galactose-1-phosphate uridylyltransferase	GALT	-0,72	N.D.

Biogenesis of lysosome-related organelles complex 1 subunit 1	BLOC1S1	-0,72	N.D.
p53 and DNA damage-regulated protein 1	PDRG1	-0,71	N.D.
SAP30-binding protein	SAP30BP	-0,71	N.D.
Signal transducer and activator of transcription 3	STAT3	-0,71	0,03
Sorting nexin-12	SNX12	-0,71	0,11
Transmembrane protein 161A	TMEM161A	-0,71	0,45
Cap-specific mRNA (nucleoside-2-O-)-methyltransferase 1	CMTR1	-0,71	0,85
Methylmalonyl-CoA mutase, mitochondrial	MUT	-0,71	0,11
Transcription intermediary factor 1-beta	TRIM28	-0,71	0,07
WD repeat-containing protein 92	WDR92	-0,71	0,07
28S ribosomal protein S27, mitochondrial	MRPS27	-0,71	0,17
Calpain small subunit 1	CAPNS1	-0,71	0,10
AP-2 complex subunit beta	AP2B1	-0,71	0,17
Mitogen-activated protein kinase 14	MAPK14	-0,70	0,04
Proteasome assembly chaperone 4	PSMG4	-0,70	0,14
Tyrosine--tRNA ligase, cytoplasmic	YARS	-0,70	0,02
E3 ubiquitin-protein ligase MARCH5	MARCH5	-0,70	0,05
Hydroxyacylglutathione hydrolase, mitochondrial	HAGH	-0,70	N.D.
Acyl-coenzyme A thioesterase 1	ACOT1	-0,70	0,20
Trans-3-hydroxy-L-proline dehydratase	L3HYPDH	-0,70	0,43
Ribosome biogenesis protein BOP1	BOP1	-0,70	0,01
Intercellular adhesion molecule 3	ICAM3	-0,70	2,22
Methylmalonic aciduria and homocystinuria type C protein	MMACHC	-0,70	N.D.
Probable histidine--tRNA ligase, mitochondrial	HARS2	-0,70	N.D.
rRNA-processing protein UTP23 homolog	UTP23	-0,70	N.D.
Valine--tRNA ligase	VARS	-0,69	0,02
Armadillo repeat-containing protein 8	ARMC8	-0,69	0,06
Cleavage and polyadenylation specificity factor subunit 6	CPSF6	-0,69	0,29
Translation initiation factor eIF-2B subunit delta	EIF2B4	-0,69	0,14
GTPase KRas;GTPase KRas, N-terminally processed	KRAS	-0,69	N.D.
mRNA-capping enzyme;Polynucleotide 5-triphosphatase	RNGTT	-0,69	0,03
NEDD4-like E3 ubiquitin-protein ligase WWP2	WWP2	-0,69	N.D.
Nodal modulator 1	NOMO1	-0,69	0,03
45 kDa calcium-binding protein	SDF4	-0,69	N.D.
Activating signal cointegrator 1 complex subunit 3	ASCC3	-0,69	0,02
Pentatricopeptide repeat domain-containing protein 3, mitochondrial	PTCD3	-0,69	0,10
Mediator of RNA polymerase II transcription subunit 1	MED1	-0,69	0,36
SURP and G-patch domain-containing protein 2	SUGP2	-0,69	0,16
Transcriptional repressor protein YY1	YY1	-0,69	0,21
Protein S100-A4	S100A4	-0,69	0,11
Abnormal spindle-like microcephaly-associated protein	ASPM	-0,69	N.D.
ATP-dependent zinc metalloprotease YME1L1	YME1L1	-0,69	0,15
Serine/threonine-protein kinase OSR1	OXSR1	-0,69	0,34
Polyglutamine-binding protein 1	PQBP1	-0,68	N.D.
Heterogeneous nuclear ribonucleoprotein U-like protein 1	HNRNPUL1	-0,68	0,18
DnaJ homolog subfamily C member 11	DNAJC11	-0,68	0,14
Peptidyl-prolyl cis-trans isomerase FKBP5	FKBP5	-0,68	0,04
Isochorismatase domain-containing protein 2, mitochondrial	ISOC2	-0,68	0,17
DnaJ homolog subfamily A member 4	DNAJA4	-0,68	N.D.
Programmed cell death protein 4	PDCD4	-0,68	0,19
AP-2 complex subunit mu	AP2M1	-0,68	0,17
Eukaryotic translation initiation factor 4E-binding protein 1	EIF4EBP1	-0,68	N.D.
Cytochrome c oxidase assembly factor 6 homolog	COA6	-0,68	N.D.
Peptidyl-prolyl cis-trans isomerase NIMA-interacting 1	PIN1	-0,68	0,22
AP-5 complex subunit sigma-1	AP5S1	-0,68	N.D.
28S ribosomal protein S23, mitochondrial	MRPS23	-0,68	0,12
Nucleoporin p54	NUP54	-0,67	0,16
Septin-2	SEPT2	-0,67	0,18
Probable ATP-dependent RNA helicase DDX47	DDX47	-0,67	0,09
Chromodomain-helicase-DNA-binding protein 1	CHD1	-0,67	N.D.
Integrator complex subunit 4	INTS4	-0,67	0,07
Neurochondrin	NCDN	-0,67	1,17
Translation initiation factor eIF-2B subunit gamma	EIF2B3	-0,67	0,14
Methionine aminopeptidase 1D, mitochondrial	METAP1D	-0,67	N.D.
Heat shock 70 kDa protein 4L	HSPA4L	-0,67	0,12
Guanine nucleotide-binding protein subunit alpha-13	GNA13	-0,67	0,06
Zinc finger C3H1 domain-containing protein	ZFC3H1	-0,67	0,36
Vacuolar protein sorting-associated protein 52 homolog	VPS52	-0,67	0,01
Metastasis-associated protein MTA1	MTA1	-0,67	0,04
Ubiquitin carboxyl-terminal hydrolase 36	USP36	-0,66	0,29
Nucleoplasmin-3	NPM3	-0,66	0,03
Speckle targeted PIP5K1A-regulated poly(A) polymerase	TUT1	-0,66	N.D.
Heterogeneous nuclear ribonucleoproteins C1/C2	HNRNPC	-0,66	0,14
ATP-binding cassette sub-family E member 1	ABCE1	-0,66	0,03
PCNA-associated factor	KIAA0101	-0,66	N.D.
Protein FAM98B	FAM98B	-0,66	0,49
Large subunit GTPase 1 homolog	LSG1	-0,66	0,23
Serine/threonine-protein phosphatase PP1-alpha catalytic subunit	PPP1CA	-0,66	0,11
Ornithine aminotransferase, mitochondrial	OAT	-0,66	0,02
Lysosome membrane protein 2	SCARB2	-0,66	0,04

Malonyl-CoA-acyl carrier protein transacylase, mitochondrial	MCAT	-0,66	0,05
Nucleoporin Nup43	NUP43	-0,66	0,07
28S ribosomal protein S26, mitochondrial	MRPS26	-0,66	0,32
28 kDa heat- and acid-stable phosphoprotein	PDAP1	-0,65	0,16
28S ribosomal protein S15, mitochondrial	MRPS15	-0,65	0,07
Eukaryotic peptide chain release factor GTP-binding subunit ERF3A	GSPT1	-0,65	0,10
Serine/threonine-protein phosphatase 4 regulatory subunit 3A	SMEK1	-0,65	0,06
Flap endonuclease 1	FEN1	-0,65	0,24
28S ribosomal protein S18b, mitochondrial	MRPS18B	-0,65	0,06
28S ribosomal protein S6, mitochondrial	MRPS6	-0,65	0,01
Vacuolar protein sorting-associated protein 26B	VPS26B	-0,65	N.D.
Chromodomain-helicase-DNA-binding protein 3	CHD3	-0,65	0,34
SAFB-like transcription modulator	SLTM	-0,65	0,02
Cytochrome c oxidase assembly factor 4 homolog, mitochondrial	COA4	-0,65	0,17
Protein phosphatase 1F	PPM1F	-0,65	0,02
Nucleolar complex protein 2 homolog	NOC2L	-0,65	0,02
ADP-ribosylation factor-like protein 2	ARL2	-0,64	0,18
Ribosomal protein S6 kinase alpha-1	RPS6KA1	-0,64	0,43
Septin-11	SEPT11	-0,64	0,09
Ankyrin repeat domain-containing protein 13D	ANKRD13D	-0,64	N.D.
RNA polymerase-associated protein CTR9 homolog	CTR9	-0,64	0,05
Coiled-coil domain-containing protein 97	CCDC97	-0,64	0,28
RNA polymerase II-associated factor 1 homolog	PAF1	-0,64	0,02
Torsin-1A-interacting protein 1	TOR1AIP1	-0,64	0,02
ADP-ribosylation factor-like protein 5A	ARL5A	-0,64	N.D.
Sequestosome-1	SQSTM1	-0,64	0,20
Lysine-specific demethylase 5B	KDM5B	-0,64	N.D.
Serine/arginine-rich splicing factor 7	SRSF7	-0,64	0,02
Liprin-alpha-1	PPFIA1	-0,64	0,12
Ribonucleases P/MRP protein subunit POP1	POP1	-0,64	0,12
Eukaryotic translation initiation factor 1A, X-chromosomal	EIF1AX	-0,63	0,09
ATP-dependent (S)-NAD(P)H-hydrate dehydratase	CARKD	-0,63	N.D.
Heterogeneous nuclear ribonucleoprotein Q	SYNCRIP	-0,63	0,04
Histone H2A type 1-C	HIST1H2AC	-0,63	N.D.
28S ribosomal protein S7, mitochondrial	MRPS7	-0,63	0,02
TGF-beta-activated kinase 1 and MAP3K7-binding protein 1	TAB1	-0,63	0,38
Cytoskeleton-associated protein 5	CKAP5	-0,63	0,16
Histone H1.5	HIST1H1B	-0,63	0,37
ATP-dependent Clp protease ATP-binding subunit clpX-like, mitochondrial	CLPX	-0,63	0,32
E3 ubiquitin-protein ligase NEDD4-like	NEDD4L	-0,63	0,45
Transmembrane protein 245	TMEM245	-0,63	0,20
rRNA 2-O-methyltransferase fibrillarin	FBL	-0,63	0,12
Glutaryl-CoA dehydrogenase, mitochondrial	GCDH	-0,63	0,30
Mitogen-activated protein kinase kinase kinase 4	MAP3K4	-0,62	0,32
THO complex subunit 4	ALYREF	-0,62	0,36
Zinc finger CCCH domain-containing protein 7B	ZC3H7B	-0,62	0,04
Down syndrome critical region protein 3	DSCR3	-0,62	0,30
Ran-binding protein 3	RANBP3	-0,62	0,34
Cleavage stimulation factor subunit 3	CSTF3	-0,62	0,08
ATP synthase subunit s, mitochondrial	ATP5S	-0,62	0,09
Zinc finger MIZ domain-containing protein 1	ZMIZ1	-0,62	N.D.
PRA1 family protein 2	PRAF2	-0,62	N.D.
Etoposide-induced protein 2.4 homolog	EI24	-0,62	0,09
39S ribosomal protein L49, mitochondrial	MRPL49	-0,62	0,17
Eukaryotic peptide chain release factor GTP-binding subunit ERF3B	GSPT2	-0,62	N.D.
Girdin	CCDC88A	-0,62	0,75
Nucleolar protein 8	NOL8	-0,62	0,00
Inositol-3-phosphate synthase 1	ISYNA1	-0,62	0,13
Dual specificity protein phosphatase 23	DUSP23	-0,62	0,05
AP-3 complex subunit sigma-2	AP3S2	-0,61	N.D.
Short/branched chain specific acyl-CoA dehydrogenase, mitochondrial	ACADSB	-0,61	0,20
Dynamin-2	DNM2	-0,61	0,03
28S ribosomal protein S28, mitochondrial	MRPS28	-0,61	0,01
AT-rich interactive domain-containing protein 4B	ARID4B	-0,61	N.D.
Arylamine N-acetyltransferase 1	NAT1	-0,61	0,31
Polymerase delta-interacting protein 2	POLDIP2	-0,61	0,15
Uncharacterized protein C14orf119	C14orf119	-0,61	N.D.
Golgin subfamily A member 7	GOLGA7	-0,61	0,02
SHC-transforming protein 1	SHC1	-0,61	N.D.
Squamous cell carcinoma antigen recognized by T-cells 3	SART3	-0,61	0,05
CDK5 regulatory subunit-associated protein 3	CDK5RAP3	-0,61	0,19
Cytosolic non-specific dipeptidase	CNDP2	-0,60	0,03
Translation initiation factor eIF-2B subunit epsilon	EIF2B5	-0,60	0,08
Replication initiator 1	REPIN1	-0,60	0,32
Leucine-rich repeat-containing protein 40	LRRC40	-0,60	0,17
RNA-binding protein 5	RBM5	-0,60	N.D.
Serine/threonine-protein kinase D2	PRKD2	-0,60	N.D.
Protein FRG1	FRG1	-0,60	0,82
Hepatoma-derived growth factor	HDGF	-0,60	0,07
Atlastin-3	ATL3	-0,59	0,18

Zinc finger protein 687	ZNF687	-0,59	0,48
Cytochrome b reductase 1	CYBRD1	-0,59	N.D.
Protein UXT	UXT	-0,59	0,39
Membrane-associated progesterone receptor component 2	PGRMC2	-0,59	0,09
E3 ubiquitin-protein ligase UBR2	UBR2	-0,59	0,04
Protein AATF	AATF	-0,59	0,20
WD repeat-containing protein 81	WDR81	-0,59	0,26
Interferon regulatory factor 2-binding protein 2	IRF2BP2	-0,59	0,41

Table 2 Downregulated proteins in KU812 ImaR compared to KU812 P cells under normoxia. Proteomic profiling (SILAC) data were used. Significant downregulated proteins were calculated using the fold difference threshold of 0.7 (log_2 fold change=-0.58). Mean±SD for n=2 replicates. Non-detected (N.D.) means less than 2 replicates detected for one protein measured.

EXTRACELLULAR FLUXES NORMOXIA					
Kpc (nmol*millioncell-1*h-1)					
	KU812 Parental		KU812 ImaR		
	Amino acids				
	Mean	SD	Mean	SD	pvalue
Ala	5.02	0.92	3.72	0.52	0.101
Arg	-0.65	0.25	-3.87	4.05	0.365
Asn	-0.26	0.02	-0.61	0.49	0.394
Asp	0.02	0.12	-0.41	0.13	0.013
Cit	0.01	0.00	-0.10	0.04	0.006
Gln	-9.12	0.24	-22.44	4.79	0.034
Glu	2.63	0.65	3.97	0.38	0.036
Gly	0.25	0.19	0.39	0.28	0.492
His	-0.21	0.10	-0.46	0.20	0.128
Ile	-1.43	0.09	-2.86	0.39	0.003
Leu	-1.93	0.13	-4.13	0.68	0.005
Lys	-1.25	0.12	-2.52	0.58	0.020
Met	-0.32	0.01	-0.92	0.17	0.004
Orn	0.61	0.09	1.80	0.60	0.028
Phe	-0.45	0.04	-1.11	0.23	0.008
Pro	0.20	0.15	2.47	0.27	0.000
Ser	-1.79	0.11	-5.05	0.89	0.003
Thr	-0.52	0.02	-1.91	0.68	0.025
Trp	-0.12	0.01	-0.25	0.09	0.062
Tyr	-0.38	0.06	-1.01	0.09	0.001
Val	-1.17	0.11	-2.56	0.47	0.007
Polyamines					
Putrescine	-4E-05	4E-05	-5E-04	2E-04	0.010
Spermidine	-7E-06	2E-05	2E-05	4E-05	0.362
Spermine	-7E-05	2E-05	-8E-04	1E-03	0.409

Table 3. Extracellular fluxes result of KU812 Parental and KU812 ImaR cell lines under normoxia. Amino acids and polyamines results are represented.

EXTRACELLULAR FLUXES HYPOXIA					
Kpc (nmol*millioncell-1*h-1)					
	KU812 Parental		KU812 ImaR		
	Amino acids				
	Mean	SD	Mean	SD	pvalue
Ala	3.19	0.51	1.85	0.63	0.045
Arg	-1.95	0.03	10.68	6.07	0.099
Asn	-0.86	0.88	0.32	0.57	0.308
Asp	-0.36	0.30	1.06	1.07	0.091
Cit	-0.02	0.00	0.09	0.18	0.356
Gln	-6.39	1.10	6.54	15.92	0.358
Glu	0.90	0.71	7.01	3.50	0.041
Gly	1.32	0.31	3.44	1.29	0.359
His	-0.02	0.09	0.41	0.68	0.336
Ile	-0.42	0.33	-1.00	1.10	0.433
Leu	-0.83	0.22	-1.97	1.02	0.130
Lys	-0.24	0.64	-1.49	0.87	0.115
Met	0.08	0.01	-0.01	0.73	0.871
Orn	2.15	0.51	1.90	0.66	0.639
Phe	0.09	0.25	-0.54	0.30	0.049
Pro	0.46	0.22	1.47	0.44	0.023
Ser	-1.58	0.26	-8.33	0.95	0.000
Thr	-0.25	0.37	0.13	1.51	0.695
Trp	0.02	0.02	-0.25	0.18	0.054
Tyr	0.13	0.29	-0.93	0.31	0.012
Val	0.03	0.53	-1.51	0.81	0.051
Polyamines					
Putrescine	4E-04	2E-04	-2E-03	3E-04	0.001
Spermidine	-1E-06	2E-05	5E-05	2E-04	0.739
Spermine	-3E-05	3E-05	1E-04	2E-04	0.315

Table 4. Extracellular fluxes result of KU812 Parental and KU812 ImaR cell lines under hypoxia. Amino acids and polyamines results are represented.

INTRACELLULAR CONTENT NORMOXIA					
nmol/mg protein					
	KU812 Parental		KU812 ImaR		
	Amino acids				
	Mean	SD	Mean	SD	pvalue
Ala	271.86	130.35	448.71	198.69	0.267
Arg	89.71	14.48	96.74	48.08	0.820
Asn	253.43	14.36	500.37	178.44	0.075
Asp	180.60	72.28	222.23	39.51	0.523
Cit	D	D	D	D	D
Gln	1162.32	500.57	2141.94	847.04	0.160
Glu	D	D	D	D	D
Gly	275.13	142.35	768.70	235.22	0.057
His	26.28	3.18	47.00	28.66	0.281
Ile	67.55	13.16	138.49	32.39	0.025
Leu	55.69	8.21	170.55	50.71	0.018
Lys	23.24	4.06	20.24	1.44	0.295
Met	19.15	3.70	52.75	28.28	0.111
Orn	6.84	0.59	38.37	11.96	0.010
Phe	18.59	1.46	34.06	6.78	0.018
Pro	43.54	1.65	D	D	D
Ser	39.94	14.85	81.03	69.67	0.374
Thr	65.16	10.89	134.42	19.08	0.005
Trp	3.42	1.48	8.04	1.58	0.021
Tyr	30.27	3.48	60.51	21.60	0.075
Val	22.63	5.55	21.91	10.02	0.918
Polyamines					
Putrescine	23.63	7.46	4.22	0.90	0.011
Spermidine	31.66	2.06	26.32	7.98	0.324
Spermine	15.49	0.66	9.63	2.82	0.025

Table 5. Intracellular content fluxes result of KU812 Parental and KU812 ImaR cells under normoxia. Non-detected amino acids or polyamines or amino acids and polyamines whose replicates were not reproducible are named as discarded (D).

INTRACELLULAR CONTENT HYPOXIA					
nmol/mg protein					
	KU812 Parental		KU812 ImaR		
	Amino acids				
	Mean	SD	Mean	SD	pvalue
Ala	196.81	70.77	555.71	205.39	0.267
Arg	124.89	82.72	168.62	8.77	0.820
Asn	374.27	155.35	584.22	159.18	0.075
Asp	41.06	15.07	176.95	111.59	0.523
Cit	D	D	D	D	D
Gln	2102.55	122.34	2939.16	475.32	0.160
Glu	D	D	D	D	D
Gly	341.37	25.92	1847.53	898.01	0.057
His	50.56	17.24	85.98	22.96	0.281
Ile	124.73	37.62	306.43	65.23	0.025
Leu	138.61	18.59	352.46	29.64	0.018
Lys	68.98	24.70	89.94	44.29	0.295
Met	36.54	14.07	84.08	35.11	0.111
Orn	60.62	32.88	52.32	16.46	0.010
Phe	33.73	3.72	75.25	11.72	0.018
Pro	223.72	47.62	D	D	D
Ser	99.18	67.01	107.43	8.54	0.374
Thr	98.19	10.44	247.54	98.36	0.005
Trp	8.06	1.54	14.28	5.59	0.021
Tyr	55.90	13.18	113.93	32.12	0.075
Val	66.16	32.79	104.60	37.65	0.918
Polyamines					
Putrescine	22.53	9.31	1.05	0.19	0.011
Spermidine	41.91	0.44	59.18	36.97	0.324
Spermine	19.49	6.13	25.64	13.60	0.025

Table 6. Intracellular content fluxes result of KU812 Parental and KU812 ImaR cells under hypoxia. Non-detected amino acids or polyamines or amino acids and polyamines whose replicates were not reproducible are named as discarded (D).

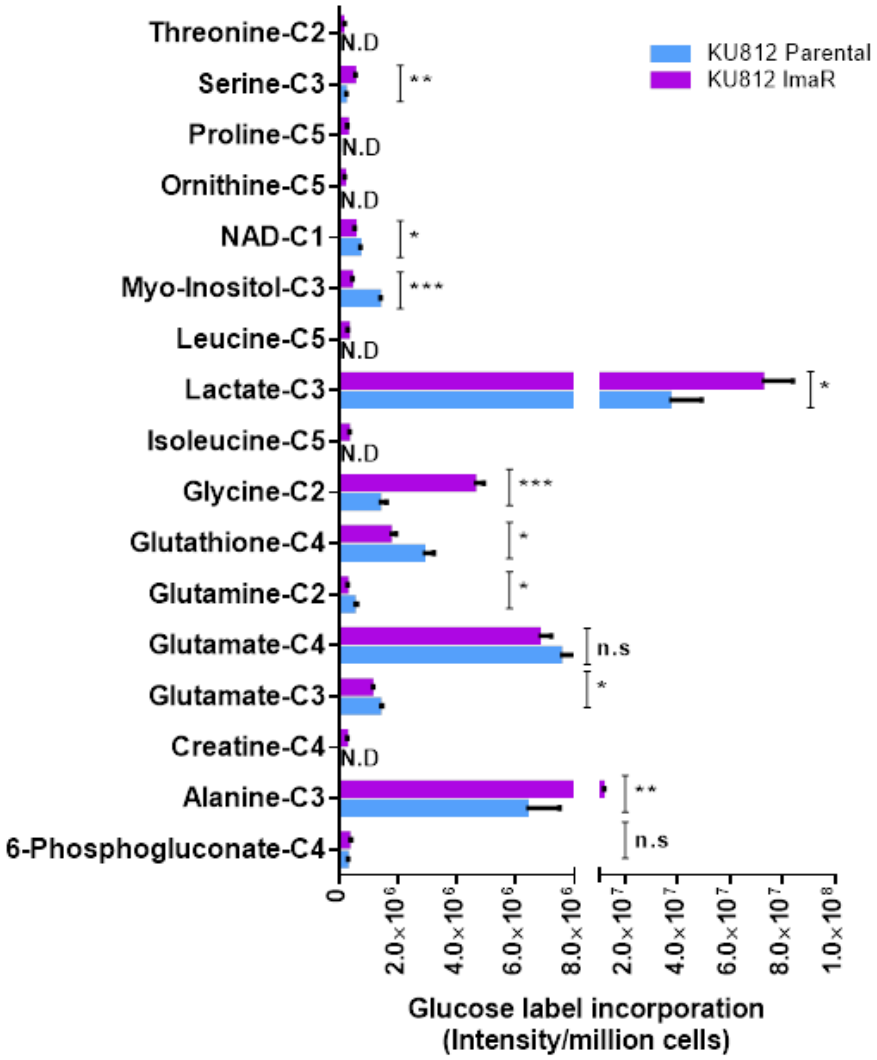

Figure 1. ^{13}C Glucose label incorporation in KU812 Parental and ImaR cells under normoxia measured by NMR.

^{13}C Glucose label incorporation					
Intensity/million cells					
	KU812 Parental		KU812 ImaR		
	Amino acids				
	Mean	SD	Mean	SD	pvalue
6-Phosphogluconate-C4	2.55E+05	5.59E+04	3.11E+05	1.06E+05	4.64E-01
Alanine-C3	6.37E+06	1.13E+06	1.12E+07	6.99E+05	3.16E-03
Creatine-C4	N.D.	N.D.	2.38E+05	4.95E+04	N.D.
Glutamate-C3	1.36E+06	1.13E+05	1.09E+06	7.63E+04	2.64E-02
Glutamate-C4	7.51E+06	6.82E+05	6.78E+06	4.32E+05	1.94E-01
Glutamine-C2	4.95E+05	1.16E+05	2.45E+05	5.73E+04	2.85E-02
Glutathione-C4	2.86E+06	3.69E+05	1.72E+06	2.22E+05	1.01E-02
Glycine-C2	1.35E+06	2.66E+05	4.59E+06	3.34E+05	1.95E-04
Isoleucine-C5	N.D.	N.D.	3.06E+05	6.72E+04	N.D.
Lactate-C3	3.68E+07	1.24E+07	7.21E+07	1.19E+07	2.34E-02
Leucine-C5	N.D.	N.D.	2.91E+05	1.36E+04	N.D.
Myo-Inositol-C3	1.35E+06	7.06E+04	4.09E+05	5.11E+04	4.79E-05
NAD-C1	6.75E+05	6.29E+04	5.16E+05	2.08E+04	1.44E-02
Ornithine-C5	N.D.	N.D.	1.61E+05	3.97E+04	N.D.
Proline-C5	N.D.	N.D.	2.67E+05	1.59E+04	N.D.
Serine-C3	1.96E+05	6.33E+04	5.12E+05	5.88E+04	3.19E-03
Threonine-C2	N.D.	N.D.	1.09E+05	9.26E+04	N.D.

Table 6 Values of ^{13}C Glucose label incorporation in KU812 Parental and ImaR cells under normoxia measured by NMR. Metabolites without ^{13}C Glucose label incorporation are indicated as non -detected (N.D).

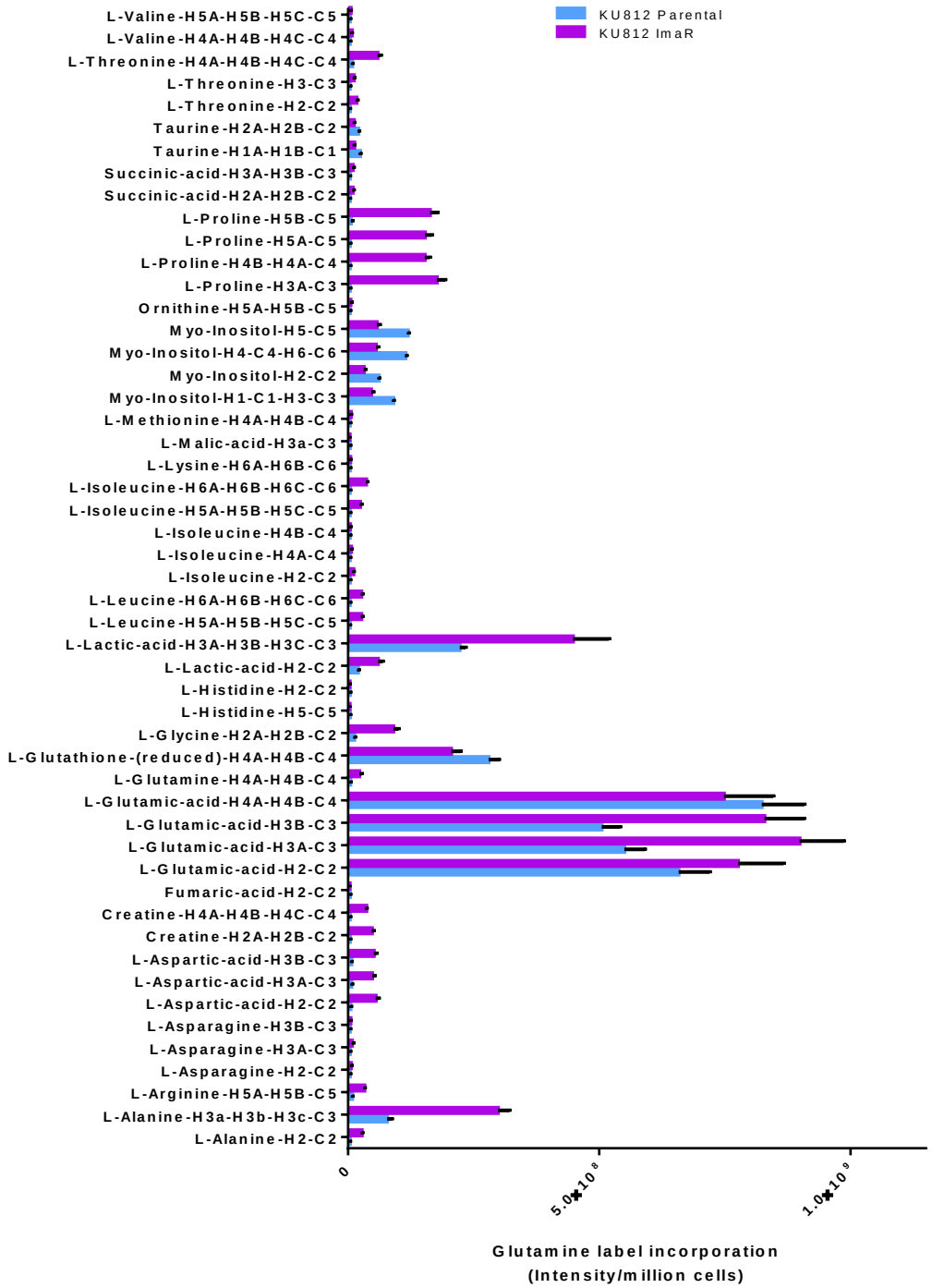

Figure 2. ^{13}C Glutamine label incorporation in KU812 Parental and ImaR cells under normoxia measured by NMR.

^{13}C Glutamine label incorporation					
Intensity/million cells					
	KU812 Parental		KU812 ImaR		
	Amino acids				
	Mean	SD	Mean	SD	pvalue
L-Alanine-H2-C2	4.09E+06	3.82E+05	2.75E+07	1.12E+06	4.39E-06
L-Alanine-H3a-H3b-H3c-C3	7.80E+07	9.34E+06	2.99E+08	2.28E+07	1.01E-04
L-Arginine-H5A-H5B-C5	8.32E+06	8.06E+05	3.30E+07	6.14E+05	1.89E-06
L-Asparagine-H2-C2	3.94E+06	6.25E+05	6.07E+06	1.54E+06	9.07E-02
L-Asparagine-H3A-C3	3.94E+06	6.25E+05	7.88E+06	2.99E+06	8.90E-02
L-Asparagine-H3B-C3	3.94E+06	6.25E+05	5.09E+06	6.22E+05	8.69E-02
L-Aspartic-acid-H2-C2	5.24E+06	1.15E+06	5.53E+07	6.17E+06	1.58E-04
L-Aspartic-acid-H3A-C3	6.86E+06	1.43E+06	4.82E+07	5.02E+06	1.64E-04
L-Aspartic-acid-H3B-C3	6.87E+06	9.74E+05	5.15E+07	5.93E+06	2.10E-04
Creatine-H2A-H2B-C2	3.94E+06	6.25E+05	4.79E+07	3.51E+06	2.84E-05
Creatine-H4A-H4B-H4C-C4	3.94E+06	6.25E+05	3.64E+07	1.04E+06	1.28E-06
Fumaric-acid-H2-C2	3.94E+06	6.25E+05	3.43E+06	2.37E+05	2.61E-01
L-Glutamic-acid-H2-C2	6.58E+08	6.21E+07	7.76E+08	9.09E+07	1.36E-01
L-Glutamic-acid-H3A-C3	5.50E+08	4.10E+07	8.99E+08	8.80E+07	3.40E-03
L-Glutamic-acid-H3B-C3	5.05E+08	3.70E+07	8.29E+08	7.88E+07	2.97E-03
L-Glutamic-acid-H4A-H4B-C4	8.24E+08	8.51E+07	7.48E+08	9.83E+07	3.72E-01
L-Glutamine-H4A-H4B-C4	1.73E+12	2.99E+12	2.24E+07	5.61E+06	3.74E-01
L-Glutathione-(reduced)-H4A-H4B-C4	2.80E+08	2.10E+07	2.05E+08	1.93E+07	1.06E-02
L-Glycine-H2A-H2B-C2	1.27E+07	1.56E+06	9.04E+07	1.02E+07	2.03E-04
L-Histidine-H5-C5	3.94E+06	6.25E+05	3.43E+06	2.37E+05	2.61E-01
L-Histidine-H2-C2	3.94E+06	6.25E+05	3.63E+06	4.48E+05	5.24E-01
L-Lactic-acid-H2-C2	2.01E+07	1.60E+06	5.99E+07	9.49E+06	2.00E-03
L-Lactic-acid-H3A-H3B-H3C-C3	2.22E+08	1.19E+07	4.48E+08	7.20E+07	5.90E-03
L-Leucine-H5A-H5B-H5C-C5	4.09E+06	3.77E+05	2.66E+07	2.44E+06	9.36E-05
L-Leucine-H6A-H6B-H6C-C6	3.94E+06	6.25E+05	2.65E+07	2.87E+06	1.84E-04
L-Isoleucine-H2-C2	3.94E+06	6.25E+05	1.10E+07	6.21E+05	1.56E-04
L-Isoleucine-H4A-C4	3.94E+06	6.25E+05	6.30E+06	1.19E+06	3.80E-02
L-Isoleucine-H4B-C4	3.94E+06	6.25E+05	4.48E+06	5.83E+05	3.32E-01
L-Isoleucine-H5A-H5B-H5C-C5	3.94E+06	6.25E+05	2.44E+07	2.63E+06	1.96E-04
L-Isoleucine-H6A-H6B-H6C-C6	3.94E+06	6.25E+05	3.62E+07	2.65E+06	3.30E-05
L-Lysine-H6A-H6B-C6	3.94E+06	6.25E+05	4.95E+06	4.21E+05	7.97E-02
L-Malic-acid-H3a-C3	3.94E+06	6.25E+05	3.43E+06	2.37E+05	2.61E-01
L-Methionine-H4A-H4B-C4	3.94E+06	6.25E+05	5.86E+06	7.27E+05	2.53E-02
Myo-Inositol-H1-C1-H3-C3	9.02E+07	9.35E+05	4.60E+07	4.66E+06	8.70E-05
Myo-Inositol-H2-C2	6.15E+07	8.09E+05	3.17E+07	3.31E+06	1.10E-04
Myo-Inositol-H4-C4-H6-C6	1.15E+08	2.19E+06	5.57E+07	4.91E+06	4.57E-05
Myo-Inositol-H5-C5	1.19E+08	1.65E+06	5.74E+07	5.99E+06	6.67E-05
Ornithine-H5A-H5B-C5	3.94E+06	6.25E+05	5.27E+06	2.51E+06	4.22E-01
L-Proline-H3A-C3	3.94E+06	6.25E+05	1.77E+08	1.69E+07	6.02E-05
L-Proline-H4B-H4A-C4	3.94E+06	6.25E+05	1.53E+08	1.03E+07	1.52E-05
L-Proline-H5A-C5	3.94E+06	6.25E+05	1.53E+08	1.42E+07	5.38E-05
L-Proline-H5B-C5	5.89E+06	3.58E+06	1.63E+08	1.53E+07	6.51E-05
Succinic-acid-H2A-H2B-C2	4.06E+06	4.31E+05	9.73E+06	2.08E+06	9.86E-03
Succinic-acid-H3A-H3B-C3	4.06E+06	4.31E+05	9.73E+06	2.08E+06	9.86E-03
Taurine-H1A-H1B-C1	2.44E+07	6.62E+05	1.25E+07	6.73E+05	2.66E-05
Taurine-H2A-H2B-C2	2.03E+07	2.21E+06	1.17E+07	1.33E+06	4.59E-03
L-Threonine-H2-C2	3.98E+06	5.45E+05	1.70E+07	2.25E+06	6.32E-04
L-Threonine-H3-C3	3.94E+06	6.25E+05	1.20E+07	1.19E+06	4.93E-04
L-Threonine-H4A-H4B-H4C-C4	8.59E+06	7.85E+05	5.91E+07	6.66E+06	1.99E-04
L-Valine-H4A-H4B-H4C-C4	3.94E+06	6.25E+05	7.61E+06	3.90E+05	9.88E-04
L-Valine-H5A-H5B-H5C-C5	3.94E+06	6.25E+05	5.47E+06	5.71E+05	3.50E-02

Table 7. Values of ^{13}C Glutamine label incorporation in KU812 Parental and ImaR cells under normoxia measured by NMR.

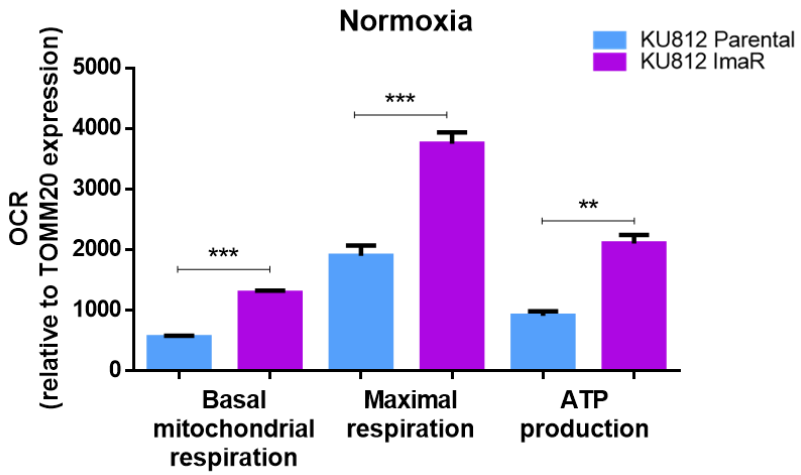

Figure 3. Basal and maximal mitochondrial respiration of KU812 imatinib-resistant vs. KU812 Parental cells after the normalisation with a parameter reflecting the mitochondrial content. Cells were first incubated with KHB Buffer in the presence of glucose and glutamine under normoxic incubation conditions. OCR values were measured during sequential injection of oligomycin, CCCP, and Rot+Ama in KU812 Parental (P) and imatinib-resistant (ImaR) cells under normoxia. Basal and maximal respiration were calculated as described in **section 4.12.** Data were initially normalised to protein content. Data from KU812 ImaR cells were further normalised by dividing the OCR value by the FD of the translocase of outer mitochondrial membrane 20 (TOMM20) obtained in the protein profiles. Data are provided as mean ± SD of n=3**.** Significance was determined by two-tailed independent sample Student's t-test. Statistically significant differences between KU812 P and ImaR cells are indicated as $p<0.01$(**), and $p<0.001$(***).